The aerodynamic control of the v-type vertical axis wind turbine

Thesis

THE AERODYNAMIC CONTROL OF THE V-TYPE VERTICAL AXIS WIND TURBINE

by

A. J. ROBOTHAM, B. Sc., A. M. I. Mech. E.

A thesis submitted for the degree of Doctor of Philosophy
The Open University, April 1989

Author's number: M7021586
Date of submission: 13 March 1989
Date of award: 22 June 1989

EX12

HIGHER DEGREES OFFICE

LIBRARY AUTHORISATION FORM

STUDENT: ANTONY JOHN ROBOTHAM SERIAL NO: M7021586

DEGREE: PHD

TITLE OF THESIS: THE AERODYNAMIC CONTROL OF THE V-TYPE VERTICAL AXIS WIND TURBINE

I confirm that I am willing that my thesis be made available to readers and maybe photocopied, subject to the discretion of the Librarian.

SIGNED:  DATE: 7/2/89

Abstract of Thesis

The V-type vertical axis wind turbine (V-VAWT) is of simple design and construction, has a low aerodynamic efficiency, yet its originators consider that it will be a cost effective configuration in electricity generation applications. However, the quality and reliability of its power output must be ensured; this necessarily requires continual control of rotor speed and power.

The initial V-VAWT investigations of Sharpe and Taylor, and methods of wind turbine control are reviewed. Partial-span pitch angle variation is considered the most promising option, and the systematic investigation of this control method in V-VAWT applications is reported. This work includes the design, construction and performance testing of a small V-VAWT with pitching blade tips. The tests showed that rotor power can be regulated with small blade tip areas, however, correlation between the measured and theoretical results was not good. Wind tunnel test were undertaken to determine the characteristics of the NACA0025 aerofoil used for the model blades. Performance predictions using this data showed better correlation between experimental and theoretical results. This has allowed the theoretical model to be used with confidence for predicting the performance of larger V-VAWTs with partial-span pitch control. A theoretical model of the dynamic behaviour of a V-VAWT generator integrated with an electricity supply network has been developed and embodied in the computer program DYNVAWT. This program has allowed the dynamic behaviour of a 5kW sized V-VAWT to be simulated, and an active control strategy developed. The simulation studies show that active partial-span pitch control ensures the quality and reliability of the electricity supply can be maintained even when the V-VAWT is operating in turbulent wind conditions.

Acknowledgements

My thanks must go to the past members of the Appropriate Technology Group at The Open University for their encouragement and support in the early years of this project. Special thanks to Dr Derek Taylor for allowing me access to his vast source of wind energy information and data, Godfrey Boyle for his patient supervision, Scott Forrest for his tireless efforts in making the experimental models, and David Sharpe for providing much food for thought, arranging for my use of the wind tunnel test facilities at Queen Mary College, and for tutoring me in the use and operation of VAWTTAY. Thanks must also go to my colleagues and students at Portsmouth Polytechnic for displaying tolerance and understanding in the latter stages of the project.

Above all, my love and sincerest gratitude go to my wife Jill for her endless support throughout the project, her single-minded dedication to my completion of the task, and as thanks for the countless hours lost to "the PhD" during the last five years.

Ellen Wallace Robotham has been the inspiration of it all.

Contents

Colour Plate: The model V-VAWT with pitching tips erected in wind tunnel test facility at Queen Mary College, London

Chapter One: Introduction

1.1: Background

In the U.K., the Department of Energy (DEn) considers wind energy technology to be "promising, but uncertain" [1]. This does not mean to say that the DEn considers wind turbines to be unproven in their ability to achieve high levels of energy capture and generate useful power from the wind, but that present day machines have yet to prove that such energy can be generated reliably and cost effectively.

The cost of energy from modern electricity generating wind turbines is evaluated by distributing the capital and maintenance costs of the installation over the total energy predicted to be generated in its useful life. The British Wind Energy Association (BWEA) have recently predicted wind energy costs to be as little as 2 pence/kWh [2] for U.K. based machines. This figure has been derived from costings experienced by two major British manufacturers supplying large numbers of medium sized wind turbines to the American market in 1985 and 1986, and amongst the many assumptions made, the design life of a wind turbine system is expected to be 30 years. Since none of the modern wind turbines have operated more than 10 years (the 1MW Tvind wind turbine celebrated 10 years of operation in early 1988 [3]), the reality of the BWEA's predicted wind energy costs is yet to be proven. For this reason the DEn is sceptical of such low energy costings, and hence their placement of wind energy technology in the "promising, but uncertain" category.

In March 1988, despite this uncertainty, a £30 million wind power programme [4] was announced by the Chairman of the Central Electricity Generating Board (CEGB), Lord

Marshall, and the Energy Minister, Michael Spicer. Of this sum, £28 million will be jointly funded by the DEn and the CEGB for the development of three demonstration wind parks, each with 25 wind turbines. The remaining £2 million will be funded by the DEn, the CEGB, and other collaborators for developing an offshore wind turbine. The success of this wind power programme is central to the future acceptance of wind energy by these two institutions as a reliable and cost effective energy source. These projects clearly show that the emphasis of current wind energy research, development and manufacturing effort in the U.K. is directed towards the use of wind power in electricity generation systems.

While the announcement of the wind parks programme has provided a welcome boost to the wind power industry in the U.K., abroad the rapid development of wind powered electricity supply systems is far more advanced. The maturing of the wind energy industry worldwide can be identified in two ways: firstly, the progress made in the development and understanding of the technology itself, and secondly, the increasing reliability and cost effectiveness of wind energy systems.

The progress made in the development and understanding of the technology is best illustrated by the increasing numbers of large sized wind turbines (rated at 500kW and above) erected worldwide. Large wind turbine development programmes are currently underway in Canada, Denmark, Germany, Italy, Netherlands, Spain, Sweden, U.K. and the U.S.A. [5]. The erection of these machines clearly demonstrates the increased knowledge, experience and confidence that has been gained in the design, manufacture and operation of wind turbine systems. In all cases, the wind turbine systems have been designed for electricty generation purposes.

The increasing reliability and cost effectiveness of wind energy systems is best illustrated by considering the continued expansion of wind powered electricity generating capacity in California, U.S.A. [6]. Initially, tax credit incentives were required to promote and develop wind parks in California, but by 1985 over 1000 MW of wind powered generating capacity had been installed in this area alone. In 1987 this figure had risen to over 1400 MW, despite the loss of the tax incentives after 1985, showing the willingness of investors to continue financial support of the wind parks scheme. During this period, annual wind energy production rose from 642 GWh to 1700 GWh. In the same period, the annual wind energy production per wind turbine increased from 75,000 kWh to 112,00 kWh. This was due, in part, to the increased capacity of each new wind turbine, but also to the increased reliability and availability of the wind turbines installed.

These figures present a rosy picture of the wind energy industry in California, but Lynette [7] observes that many wind power stations are in financial trouble because of a shortfall in energy production. Lynette considers that these shortfalls are due to technological reasons, and are:

> "a result of attempts to accelerate the commercialization of an emerging, but immature technology."

The early wind energy programmes of a number of countries have included the building of large wind turbines, some of which were of mega-watt capacity. Many of these larger projects have floundered because of technical problems, and some wind turbines have even been dismantled after the repeated occurence of operating problems. Although a number of large wind turbines are currently operating satisfactorily, and as implied above the numbers of such

machines is increasing, the average installed capacity of the 16,000 wind turbines operating in California is only 114 kW. The confidence and knowledge gained to develop and erect the large wind turbines is the direct result of successful development and operation of smaller scale machines. The BWEA's predicted cost of wind generated electricity is based upon the experience gained by manufacturing, installing and operating medium sized machines. Therefore the significant contribution made by such machines should not be under estimated, especially in light of the push towards larger sized machines. Lynette's assessment of the Californian experience is pertinent to wind energy programmes worldwide. The BWEA, similarly, state [2]:

> "Small wind turbines can provide sensible stepping stones to the larger sizes."

The DEn acknowledges [8] that land-based wind turbines could by 2025, in theory, annually produce 45 TWh of electricity in the U.K. This could be further increased with offshore wind turbines by as much as 140 TWh per annum. The development of wind power systems on such a scale, however, will only come about when the predicted low energy costs are proven to be accurate and reliable.

The cost of wind generated electricity is sensitive to a number of controlling parameters. These include the mean speed of the wind at the turbine site, the availability of the machine, and the ratio of the capital cost of the turbine system to its rated power output capacity. Of these parameters, wind speed has the most influence on wind energy costs, indicating that windy sites are essential for a cost effective wind powered electricity supply system. Simplicity of machine design and planned maintenance schedules will ensure reliable operation and

high availability. Availabilities of 95% have already been reported, leaving little scope for improvement. The capital cost to rated power output ratio of a wind turbine system is crucially dependent upon the selection of an effective wind turbine configuration. In the competitive Californian market, horizontal axis wind turbines are currently being offered by manufacturers, ex-works, for between $800 and $900 per kilowatt output capacity. Operational windfarms are being offered for between $1000 and $1200 per kilowatt. The "cost per kilowatt" of a wind turbine system is used as an indicator to compare its commercial merits with other wind turbine systems.

However, when comparing wind turbine systems on technical merits, it is more usual to consider the efficiency of the system as an aerodynamic device for extracting energy from the wind and converting it to useful energy. Whether the wind turbine rotor be of horizontal axis or vertical axis configuration, techniques for improving the efficiency of the system are continually being sought.

While the selection of a particular wind turbine rotor configuration will immediately determine the likely conversion efficiences achievable, a complex design with a good conversion efficiency may be less cost effective than a simple design with a poorer conversion efficiency. The V-type vertical axis wind turbine (V-VAWT) is known to have a low aerodynamic efficiency [9], but it is claimed that its simple construction will ensure a low capital cost, easy maintenance, and high reliability. It is, therefore, expected that this configuration will be commercially competitive with other wind turbine designs, despite its low aerodynamic efficiency.

The current institutional interest in wind energy technology in the U.K. is dominated by its application for

electricty generation. While research funds are being allocated for studies of stand-alone systems, the DEn and CEGB are primarily interested in the operation of wind turbine systems as an integral part of the national electricty supply network. The grid connected application of a wind turbine poses many problems, so it was considered appropriate that any further investigation of the V-type vertical axis wind turbine concept should concentrate on the specific needs of this highly commercial application. Such an investigation is the focus of the study reported here, and while the cost effectiveness of this novel wind turbine design is still unproven, the work presented here does clearly demonstrate that electricity generation using this turbine concept is technically feasible, provided the turbine is suitably controlled.

1.2: Wind Energy Technology

The systematic development of the modern electricity generating wind turbine can be traced back to 1891 when the Danish government established a windmill experimental station at Askov. Professor P. La Cour was in charge of a research programme with the specific aim of improving windmill performance, and developing a type that could be economically constructed for the generation of electricity for agricultural applications. La Cour was the first to undertake a systematic investigation of electricty generation using wind power, and his work led to guiding principles for the design and construction of the "ideal windmill". By 1908, several hundred windmills that embodied these design principles had been built and constructed in Denmark.

The development of the windmill as an electricity generating machine continued in both Europe and North America. A small number of large scale projects were undertaken by national governments and private companies are described by Golding [10]. During the 1950s, wind turbines rated at 100 kW or more were erected in Great Britain, France and Germany. All were experimental machines designed to allow systematic study of the technology. Research programmes continued in some countries into the 1960s, but it was the "energy crisis" of October 1973 that stimulated the current international interest shown in wind power, and its use for electricity generation.

The government sponsored research, development and demonstration programmes of many countries show initial interest has been directed towards developing large, multi-megawatt machines, while privately funded development has centred on the small to medium sized wind turbines. The recent developments in wind energy technology are well documented, but reference in this report to particular projects will only be made as appropriate.

Not suprisingly, the development of wind energy technology has been accompanied by the development of an associated technical language and knowledge base. The terminology and technical definitions in common usage allow different wind turbine systems to be readily compared, and these are briefly discussed below.

1.2.1: Wind Resource

Wind turbines extract kinetic energy from the wind. The amount of electrical energy extracted from the wind by a wind turbine system depends upon:

(a) windspeed at the wind turbine site

(b) the cross-sectional area of the wind swept by the blades of the wind turbine rotor

(c) the height of the wind turbine rotor above the ground or sea level

(d) the efficiency of the wind turbine system at converting wind energy to electrical energy

The power available in the wind passing through a cross-sectional area A, is given by:

$$\text{power} = \tfrac{1}{2}\rho A V^3 \qquad (1.1)$$

where

ρ = air density, kg/m^3

V = windspeed, m/s

A = cross-sectional area, m^2

As equation (1.1) shows, the power available in the wind is proportional to the cube of its speed, so the energy that a wind turbine generates is significantly affected by windspeed changes. A site with an average annual windspeed of 6.3 m/s will have twice as much energy available as one with an average annual windspeed of 5.0 m/s. Even small differences in the average annual windspeed can clearly affect the energy available at a potential site. It has been shown [11] that the average annual power per unit cross-sectional area, known as the power density, is equal to $0.95\rho V_M^3$ W/m^2, where V_M is the average annual windspeed of the site. This expression assumes a Rayleigh distribution (see below) of windspeeds throughout the year, but if $\rho = 1.225$ kg/m^3, then for a site with an average annual windspeed $V_M = 5.0$ m/s, the average power density will be 145 W/m^2, corresponding to 1275 kWh/m^2 per annum.

Wind is highly variable. Its speed varies with geographic location, local terrain, height, time of the day and the seasons. At a particular wind turbine site, the long term wind energy availability can be estimated from knowledge of the average annual windspeed. Its value is best determined by short term, on-site measurements made at the standard height of ten metres. Correlation of these measurements with those made over the same period of time at a local weather station, will allow the first estimate of the average annual windspeed to be validated with long term measurements.

Although published data and computer based models [12] now enable potential wind turbine locations to be readily indentified, local variations of terrain and land form ensure that on-site windspeed measurement is still the most effective and reliable means of evaluating the wind resource of a particular site.

It is usual to consider the windspeed "seen" by a wind turbine to be that blowing at the height of the rotor hub. Wind turbines operate in the planetary boundary layer, in which a variation of horizontal windspeed occurs with height. Therefore, the average annual windspeed seen by the wind turbine will differ with changes of hub height. The variation of windspeed with hub height can be estimated using the logarithmic relationship [13]:

$$\frac{V(z)}{V(z_R)} = \frac{\ln(z/z_o)}{\ln(z_R/z_o)} \qquad (1.2)$$

where

$V(z)$ = horizontal windspeed at height z, m/s

z_o = the surface roughness, m

z_R = reference height, m

The reference height is usually z_r = 10 m, and the surface roughness z_o varies with terrain. For open terrain with short grass z_o = 0.03 m, but for rough terrain with low woods z_o = 0.25 m [13]. This relationship can be used to evaluate the average annual windspeed seen at the rotor hub from windspeed measurements made at the standard height. If z_o = 0.03, it is readily demonstrated that the average power density at a hub height of 75 m is twice that at a hub height of only 15 m.

The statistical variation of windspeed throughout the year can be described mathematically using a probability density function such as the Weibull function. The two shape parameters of this function can be evaluated by short term windspeed measurement on site. The Rayleigh distribution is a special case of the Weibull function, and is representative of windspeed distributions in the U.K. [14].

The Weibull probability density function allows the number of hours per year for which the windspeed equals or exceeds a specified value to be readily calculated. The characteristic windspeed frequency distribution of the site, where the windspeed domain is divided into "bins" of one metre per second width, gives for each bin the number of hours per year which the windspeed is within the interval of the bin width. The wind turbine system is unable to extract all the energy available in the wind, and each system will have a "power output versus windspeed" characteristic, allowing the power developed by the system for each windspeed bin to be evaluated. Integration of the product of "number of hours" and "power output" for each bin for all windspeeds, will yield the total energy output of the system in one year at the site.

Musgrove [15] shows that the average power output, P_M, of a well designed wind turbine system is given by

$$P_M = 0.25\rho A V_M^3 \qquad (1.3)$$

For V_M = 5.0 m/s this gives an average power output density of P_M = 38 W/m^2, corresponding to 335 kWh/m^2 per annum. The efficiency with which a wind turbine system converts wind energy to electricity energy is highly dependent on the design and operating characteristics of the system, so the expression (1.3) for evaluating average power output of a wind turbine system is unsuitable for all but the most general discussions of the wind energy resource.

1.2.2: Wind Turbine Configurations

The majority of commercial wind turbines are of a horizontal axis configuration (HAWT). In this design configuration the wind turbine rotor revolves about an axis that is, essentially, parallel to the ground. The blades of the rotor sweep out a circular disc through which the wind passes. Rotor power is transmitted through a gearbox to the generator for conversion to electrical energy. The speed of the wind turbine rotor is determined by its overall size, and the number and design of the blades. Large rotors will operate at low rotational speeds, and require large speed increasing gearboxes to drive the generator at its operating speed. The low speed transmission elements of the drive train system carry large torques, and require specialist components to be designed. The rotational speed of the rotor can be increased, for its size, by reducing the number of blades. Two and three bladed rotor configurations are popular, and provide a good compromise between aerodynamic performance and power

transmission design, but single and multi-bladed options have their advocates.

The rotor blades use the aerodynamic lift force characteristics of aerofoil sections to develop mechanical torque at the rotor hub. The choice of aerofoil type, the blade planform design, and the geometry of the blade across it span, are all crucial factors in determining the aerodynamic performance of the blade. The structural design of the blade must consider the aerodynamic, gravitational and centrifugal forces that act across the whole blade. Of these forces, gravitational force varies cyclically, a complete reversal of its vector sign with respect to the blade once per revolution. The final blade design is the result of balancing good aerodynamic characteristics against good structural characteristics. A compromise is inevitable, but the use of well established, and proven, design procedures and analysis techniques, enables HAWT blade design to be completed with effective engineering solutions being generated.

The HAWT rotor is supported by a tall tower, and it is usual to house all the mechanical and electrical power transmission elements in a nacelle at, or near, its top. The rotor and nacelle must rotate about the tower to ensure the disc of the rotor faces the wind. The rotor may be free to yaw, or driven by some drive mechanism. The tower has to be designed to support the weight of the rotor, the drive train system, electrical generator, and other ancillary equipment. The tower structure not only influences the response of the wind turbine to external forces acting on the rotor, but affects the aerodynamic efficiency of the rotor as each blade passes by.

The characteristics of horizontal axis configurations have been comprehensively studied and reported for many machine

designs, rotor sizes and operating conditions. It is the configuration that has been developed with most success by industrial organisations and national research programmes. The current interest in wind energy technology, as a cost-effective energy source, is based upon the successful commercial operation of many HAWTs in both North America and Europe. The development of the vertical axis wind turbine (VAWT), by contrast, is less well advanced commercially, in part due to the additional technical complexity of this configuration, and in part due to the diversity of VAWT configurations currently being developed.

Vertical axis wind turbine configurations have rotors that revolve about an axis that is perpendicular to the ground, and therefore are always facing the wind. The blades of the rotor sweep out a volume through which the wind must pass. Each blade cuts through a stream of air twice every revolution; once on the upwind pass, and once on the downwind pass. Like HAWTs, the rotor blades use aerodynamic lift force to develop mechanical torque at the rotor hub. Again, the choice of aerofoil type, the blade planform design, and the geometry of the blade across its span, are crucial factors in determining the aerodynamic performance of the blade. The blade design, however, must achieve a balance between its aerodynamic effectiveness on the upwind half of the cycle and that on the downwind half. The structural design must consider aerodynamic, gravitational and centrifugal forces, but, unlike HAWTs, it is the aerodynamic force that varies cyclically with VAWTs. In the final blade design, a compromise must be struck between good aerodynamic performance characteristics and good structural performance characteristics. This has resulted in a diversity of VAWT configurations being evolved, some of which have been developed to commercial maturity. The various VAWT configurations can

be broadly categorised by blade type, e.g. curved or straight blade types.

The Darrieus VAWT uses curved blades which are attached at both ends to a rotating torque tube. The torque tube transmits rotor torque to a gearbox and generator system that is placed at the base of the rotor in a short tower. The curve of the blade can take many forms, but the troposkein blade geometry has the most structural advantage. Its "skipping rope" shape ensures all centrifugal forces are reacted by tensile forces around the blade, and that the bending loads in the blade are due to aerodynamic and gravitational forces alone. The Darrieus machines can be designed to rotate at high rotational speeds, reducing the torque developed by the rotor for a given power rating. This type of VAWT has been extensively developed in North America, where power conversion efficiencies comparable to those of well designed HAWTs have been achieved.

Straight blade designs have centred on variations of the H-VAWT configuration, in which the rotor blades are set parallel to the axis of rotation, sweeping a cylinderical path through the air. The blades are connected to the rotor hub by single or multiple crossarms, so giving the rotor its characteristic aitch shape. The rotor is supported by a tall tower, and like HAWTs, it is usual to house all mechanical and electrical equipment at, or near, its top. This design allows the whole span of the blade to operate at the largest moment arm about the axis of rotation, ensuring the maximum rotor torque is developed from the aerodynamic forces acting on the blades. Variable geometry versions of the H-VAWT have been developed for control purposes, but these variations will be discussed in Chapter Three.

The V-VAWT is a straight bladed configuration in which the rotor blades are set at an angle to the axis of rotation, sweeping out a conical path through the air. The blades are connected to the rotor hub at their root, so giving the rotor its characteristic vee shape. The rotor is supported by a short tower, allowing all the mechanical and electrical equipment to be close to the ground. Although the blades may be supported close to their tip by cables, large bending loads occur in the blade at its root. The length of the moment arm about the axis of rotation varies across the span of the blades, so the aerodynamic forces are less effectively developed into rotor torque. Although this configuration has a relatively low power conversion efficiency, its simple construction is considered by its originators to make it a worthy VAWT configuration to develop further.

The initial design and subsequent development of the V-VAWT configuration is discussed in Chapter Two.

1.2.3: Wind Turbine Characteristics

The power, torque and speed characteristics of a wind turbine can be conveniently considered using the following non-dimensional terms:

$$\text{power coefficient} \quad C_P = \frac{P}{\frac{1}{2}\rho A V^3} \tag{1.4}$$

$$\text{torque coefficient} \quad C_Q = \frac{Q}{\frac{1}{2}\rho A V^2 R} \tag{1.5}$$

$$\text{tip speed ratio} \quad \lambda = \frac{R\Omega}{V} \tag{1.6}$$

where

P = power developed by rotor, W

Q = torque developed by rotor, Nm

A = swept area of wind turbine rotor, m^2

Ω = rotational speed of rotor, rad/s

R = maximum radius of rotor, m

The power-rotational speed and torque-rotational speed characteristics of a wind turbine rotor vary with windspeed, rotor size, and even the density of the air. Whilst it is possible to determine a series of power-speed and torque-speed curves for different windspeeds, rotor sizes, and air densities, the use of the above non-dimensional terms enables the wind turbine characteristics to be described by just two curves: C_P-λ and C_Q-λ. It should be noted that since $P = Q.\Omega$, then:

$$C_P = C_Q.\lambda \qquad (1.7)$$

The power coefficient, C_P, of a wind turbine is a measure of its effectiveness at extracting the kinetic energy of the wind which would normally pass through the area swept by the rotor if it was not there. In 1927, Betz used simple momentum theory to show that the maximum fraction of the available power in the wind that can be extracted by an ideal wind turbine was $^{16}/_{27}$, or 59.3%. This theoretical maximum value of power coefficient is known as the Betz limit. Golding [10] discusses the many early studies of wind turbine theory that have suggested modifying the value of the Betz limit for maximum C_P. There is, however, little proof that power outputs in excess of the Betz limit are achievable, and further discussion would be of little value.

Modern wind turbine designs are achieving power coefficients of C_P = 0.40 to 0.45, but its actual value is a

function of the rotor configuration, its detailed design, and the tip speed ratio at which it is operating.

Tip speed ratio, λ, is the ratio of the peripheral speed of the rotor to the windspeed. The peripheral speed of the rotor is a function of its size and rotational speed. Since, however, power coefficient, torque coefficient, and tip speed ratio are dimensionless parameters, the C_P-λ and C_Q-λ characteristics of different wind turbine configurations can be readily compared. These characteristics should only be used to describe the behaviour of the rotor, and not the wind turbine system as a whole. The conversion of the power developed by the rotor into electricity inevitably incurs additional mechanical and electrical losses, further reducing the overall efficiency of the whole system.

Typical C_P-λ characteristics of different wind turbine configurations are shown in Figure 1.1. In all cases the optimum value of C_P occurs at a single value of λ. To ensure maximum energy capture is achieved, the wind turbine must operate at a constant tip speed ratio, so the rotational speed of the rotor must change if any windspeed change occurs. Variable speed operation is favoured by manufacturers of small and medium sized wind turbines, though large wind turbines connected to national electricty supply networks generally operate at a constant rotational speed, sacrificing maximum energy capture efficiency. The merits of each mode of operation will be discussed at length later in this report, but suffice to say, in either situation the rotor must be carefully and accurately controlled to ensure the safe and reliable operation of the whole wind turbine system.

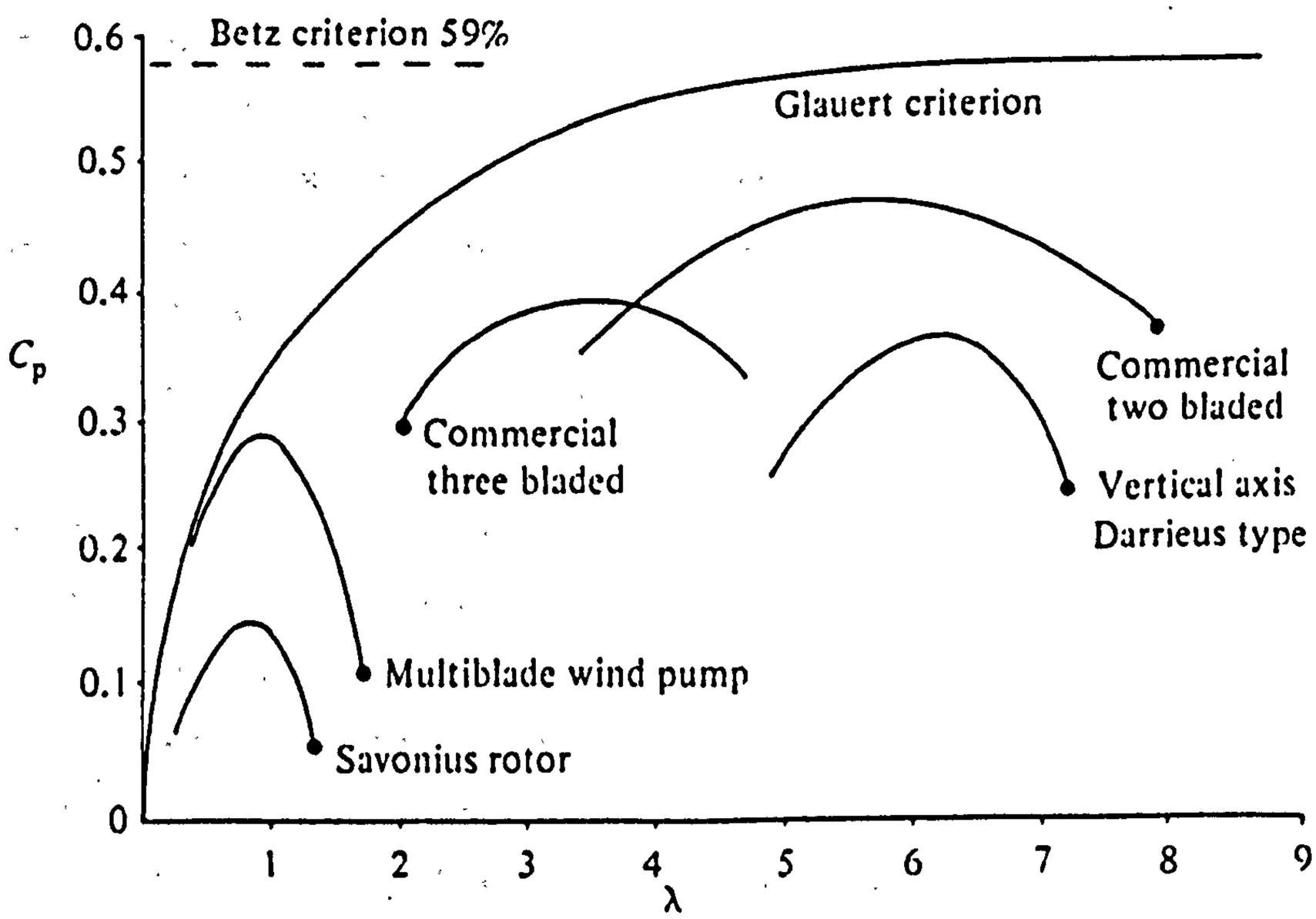

Figure 1.1: Typical C_p-λ characteristics of various wind turbine configurations

The performance of an electricty generating wind turbine system is, regardless of its configuration, characterised by the following parameters:

(a) Rated power output, P_R
(b) Rated windspeed, V_R
(c) Cut-in windspeed, V_{IN}
(d) Cut-out windspeed, V_{OUT}
(e) Survival windspeed, V_S

The rated power output is the maximum power that the wind turbine system will deliver in constant windspeed conditions. The rated windspeed is the lowest windspeed at which the system will deliver its rated power output. Below this windspeed, the power output will be less than rated. The cut-in windspeed is the lowest windspeed at which the system is able to deliver any useful electrical power, typically V_{IN} = 5 m/s. When the windspeed is greater than or equal to the cut-out windspeed, the wind turbine is disconnected from the supply system and the rotor stopped. Wind turbine systems do not to operate in winds greater than the cut-out windspeed because large structural loads would occur in this operating regime, typically V_{OUT} = 25 m/s. With the rotor stationary, the wind turbine is designed to withstand the structural loads that would occur in very high windspeeds upto the survival windspeeds of V_S = 60 m/s.

The power output of the system below V_{IN} is zero, not because the wind turbine rotor is unable to capture any wind energy at such low windspeeds, but because the system is unable to run quickly enough for the electrical generator to operate at the required frequency. Above V_{IN}, the power output from the system will rise rapidly as the windspeed increases to V_R, at which windspeed the power output will equal P_R. If the windspeed increases

further, the power that could be delivered would continue to rise, however, the electrical generator has a limited capacity, so restricting the power that may be delivered by the system. Consequently for windspeeds above V_{rr}, the mechanical power from the rotor is modulated to ensure that the electrical output of the system is no greater than rated. Various methods of controlling the mechanical power developed by a wind turbine rotor have been used, and these are briefly reviewed in Chapter Three. One such method is selected for use with the V-VAWT, and to test its suitability for this configuration a wind tunnel sized model wind turbine has been designed and tested. Chapter Four describes its design and construction. Chapter Five describes the test procedures, data analysis techniques, and presents the experimental results that were obtained.

Analytical methods have been developed to predict the aerodynamic performance of both horizontal and vertical axis machines. These theoretical mathematical models of wind turbine behaviour are generally considered accurate and reliable, though their verification and improvement continue. These mathematical models enable the aerodynamic performance of a wind turbine system to be predicted without a detailed knowledge of the specific application. They are used extensively in design to determine the likely power-windspeed characteristic of the system. Such a tool has already been developed for predicting the behaviour of the V-VAWT. The basis of the prediction model is described in Chapter Two, but to ensure that good predictions were obtained for the wind tunnel V-VAWT model, it has been necessary to measure the aerodynamic characteristics of the aerofoil section used for the model blades. The experimental test procedure, data analysis and experimental results that were obtained are presented in Chapter Six.

The aerodynamic performance prediction model is used in Chapter Seven to determine the likely effects of using the selected power modulation method on free-air V-VAWTs. In the free-air fluctuations in the windspeed occur continuously. These fluctuations will affect the instantaneous power output of the wind turbine system, so the wind turbine must be either passively or actively controlled to ensure the system does not respond to the windspeed change in a manner that is detrimental to its output quality or safety. To predict the reponse of a system to continuous windspeed fluctuations, however, requires a more detailed approach that is specific for each application. Any mathematical model of the system will require the dynamic characteristics of both the mechanical and electrical components to be described and evaluated. Chapter Eight descibes the development of such a mathematical model specific to the V-VAWT. This model has allowed methods for controlling the wind turbine system during such disturbances to be simulated.

The aerodynamic control of the V-VAWT rotor not only has to modulate the power output of the system in high speed and gusty winds, but must ensure that many other tasks can be completed satisfactorily. These tasks are described in detail later, but this study clearly shows that aerodynamic control of the V-VAWT rotor using a fast acting blade tip pitch control system, will enable electricity supply to a large supply network to be successfully and reliably acomplished.

1.3: Scope of this Research Report

The investigations into the aerodynamic control of the V-VAWT reported here were carried out by the author as a member of the Appropriate Technology Group of the Open

University between November 1983 and September 1986, and subsequently continued to the present in the Department of Mechanical Engineering of Portsmouth Polytechnic. All the wind tunnel based experimental work was carried out at the Department of Aeronautical Engineering of Queen Mary College, London.

During this period the author attended a number of wind energy conferences, and prepared a small number of technical papers in which the intermediate results of the work were presented. Copies of these papers are included in the Appendix. In the programme of study described and reported here, the following tasks were undertaken by the author:

(a) Technical review of wind technology and wind turbine control methods.
(b) Appraisal of control method suitable for the V-VAWT configuration.
(c) Design and analysis of wind tunnel V-VAWT model.
(d) Performance testing of V-VAWT model and analysis of experimental results.
(e) Further development of computer based aerodynamic performance prediction model, enhancing its speed of execution and ease of use.
(f) Aerodynamic testing of aerofoil section used for V-VAWT model blades, analysis of experimental results, and application of data to validate the modifications to the aerodynamic performance prediction model.
(g) Determine suitable control methods and strategies for larger V-VAWT designs.
(h) Develop a mathematical model of the dynamic behaviour of a V-VAWT system, simulate its response to typical disturbances, and so verify the suitability of the adopted control system.

Chapter Two: The V-Type Vertical Axis Wind Turbine

2.1: The Initial Concept and Early Development Work of Sharpe and Taylor

The first systematic appraisal of the V-type VAWT configuration was reported by Sharpe and Taylor [9] in 1983. Earlier descriptions of this concept by Park [16] and Ljungstrom [17] are acknowledged by Sharpe and Taylor, but neither of these other authors presented detailed studies of this VAWT configuration. A variety of designs had been conceived by Taylor, Figure 2.1, including an X-VAWT, but it was the multiple and single blade configurations with fixed or variable geometry that were considered to be most promising. Sharpe and Taylor considered the concept to have the following advantages:

"(a) A very short tower requirement for any size of rotor. This can be as little as 3 or 4 metres tall, which helps to minimize capital costs and allows for easy access to generator, transmission and the rotor itself, so reducing installation , operation and maintenance costs.

(b) The use of simple, straight blades attached directly to the shaft avoids the heavy rigid support arms or cumbersome curved blades that characterise other Darrieus-type VAWTs.

(c) The greater portion of the swept area is located in the higher wind speed zone.

(d) Proven self-starting capability, due to high starting torque - at least for the 2 blade version. This feature means that the turbine may be suitable for water pumping applications as well as electricity generation.

(e) Simple, straight, untwisted blades that are relatively easy to manufacture and to transport can be used.

(f) In the case of variable geometry versions, the swept area can be varied much like the Musgrove-type "H" Darrieus VAWT. The turbine is maintained at its optimum angle of inclination θ_D until the windspeed approaches the maximum normal operating value. When this is exceeded the blade tilts further so that the angle of inclination θ increases until in very high winds the blades are horizontal and can be parked in that position. This feature is not shared by any other current VAWT.

(g) In the case of the cantilevered single-blade, variable-geometry version, the blade of which can be a strong beam, tower shadow and tower induced turbulence effects on the

blade are non existent; in addition, the blade can be parked horizontally in high winds and allowed to "weather vane" downwind of the tower, so reducing considerably the loads on both blade and tower.

(h) As with any other straight-bladed VAWT, the blades of this design are subject to high bending loads induced when rotating due to the centrifugal force acting on the blades. However, for this type of turbine these loads can be taken by cable bracing and/or the blades themselves, rather than the heavy crossarms - though the cables may have to be faired to reduce drag.

(i) in the constant speed mode, these loads can be kept under control by the use of spoilers, flaps or variable pitch tips of the type similar to those currently in use on HAWTs. Alternatively active or passive variable geometry control systems can be employed."

Some of these statements require further qualification and justification of their validity, however, Sharpe and Taylor's reasoning will be borne out by the discussion below.

Of the configurations conceived, the two-bladed fixed geometry V-VAWT was the subject of Sharpe and Taylor's preliminary investigations. In this configuration each blade is attached to the rotor hub at their root at a fixed angle to the vertical. The blade is braced using cables attached near to the blade tip, giving the rotor a greater rigidity. The study included both theoretical and experimental evaluations of the aerodynamic performance of this configuration, concentrating on the behaviour of the rotor itself.

2.1.1: Theoretical Predictions of V-VAWT Aerodynamic Performance

To determine the aerodynamic performance of the V-VAWT concept, a computer based prediction model known as VAWTTAY was developed by Sharpe based upon the his refined version of the multiple streamtube theory [18] suitable

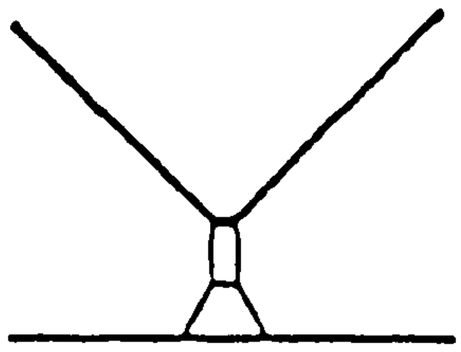

(a)

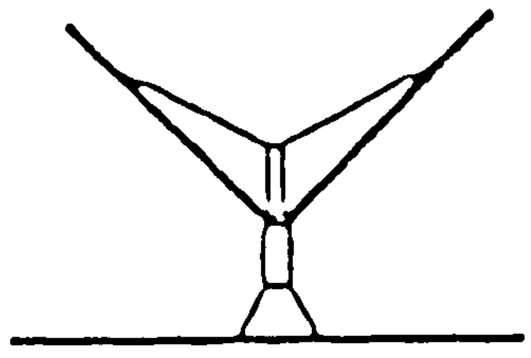

(b)

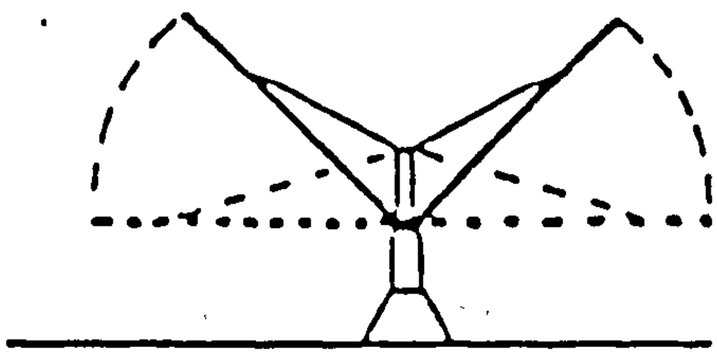

(c)

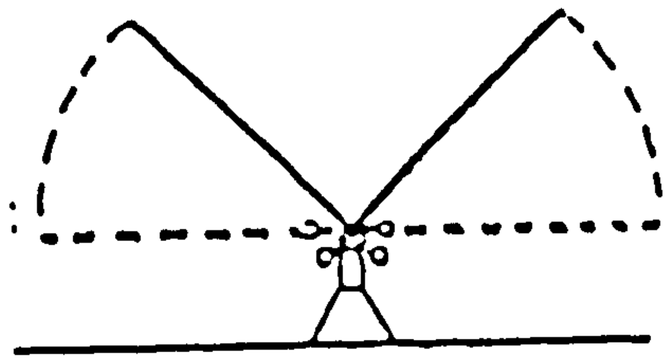

(d)

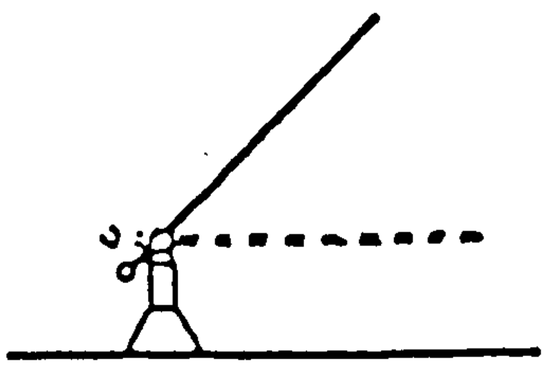

(e)

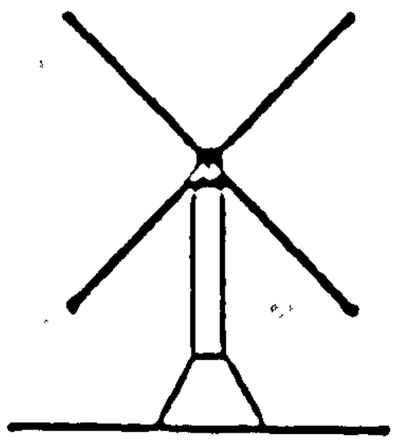

(f)

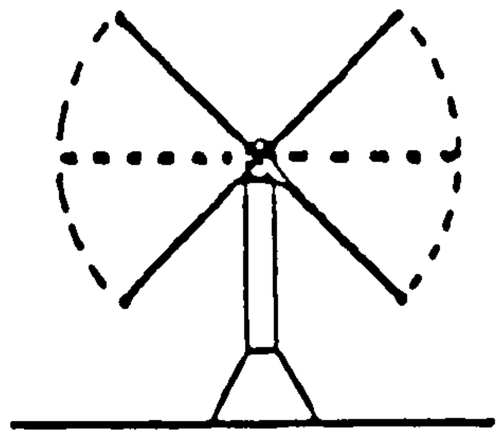

(g)

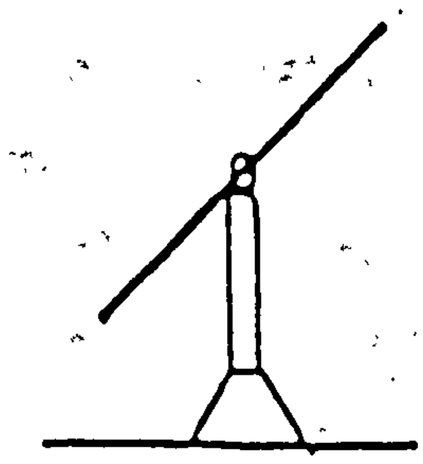

(h)

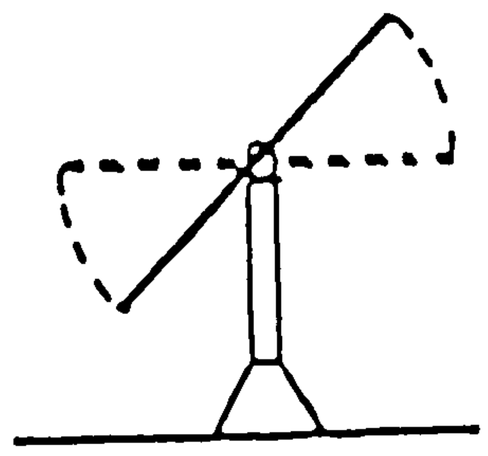

(i)

Figure 2.1: Various fixed and variable geometry V-VAWT and X-VAWT configurations concieved by Taylor [9]

for all vertical axis configurations. This theory, and its development as a computer based model is discussed in detail later, but suffice to say the validity of the results from the model had been proven with known data from experiments performed on other VAWT types, and is considered a reliable analysis tool.

The computer model VAWTTAY allows the blade shape, aerofoil section and rotor geometry to be uniquely defined, enabling both small and large scale rotor configurations to be evaluated. However, to enable the performance of these configurations to be compared, the following non-dimensional terms are defined:

$$\text{aspect ratio} \qquad AR = \frac{L}{c} \tag{2.1}$$

$$\text{tip radius} \qquad R = L.\sin\theta \tag{2.2}$$

$$\text{solidity} \qquad \sigma = \frac{Nc}{R} \tag{2.3}$$

$$\text{wind Reynolds Number} \qquad WRe = \frac{Vc}{\nu} \tag{2.4}$$

where

L = blade length, m

c = mean blade chord, m

θ = angle of blade inclination to the vertical, deg

N = number of blades

V = undisturbed windspeed, m/s

ν = kinematic viscosity of air, m^2/s

A wind tunnel sized V-VAWT model with straight blades of length 750 mm and chord 63 mm, i.e. AR = 11.9, was used as the basis for initial parametric studies of the V-VAWT. Sharpe and Taylor presented the results of predicted C_{p_w}-λ

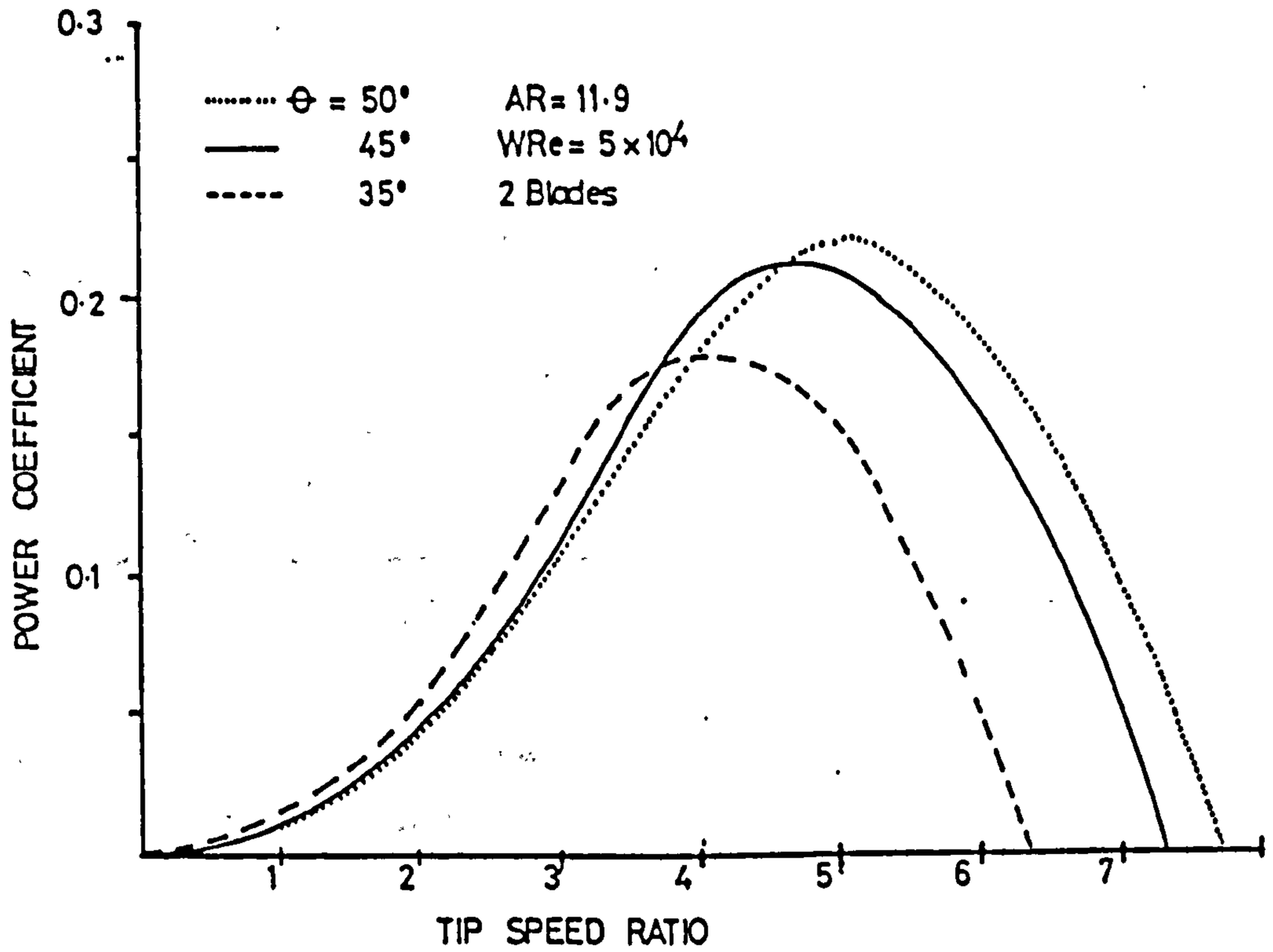

Figure 2.2: Effect of blade inclination angle on V-VAWT C_p-λ characteristic [9]

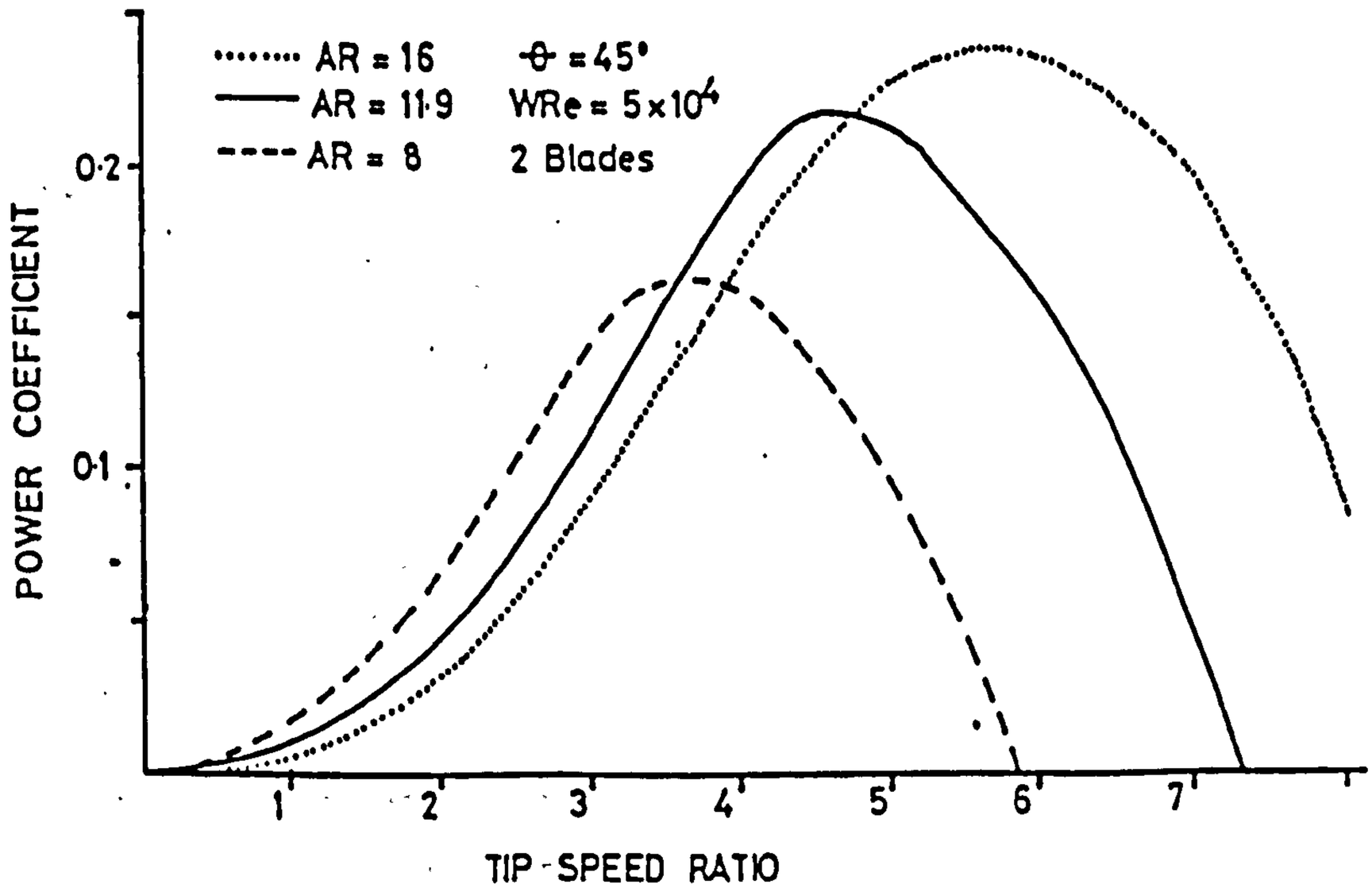

Figure 2.3: Effect of aspect ratio on V-VAWT C_p-λ characteristic [9]

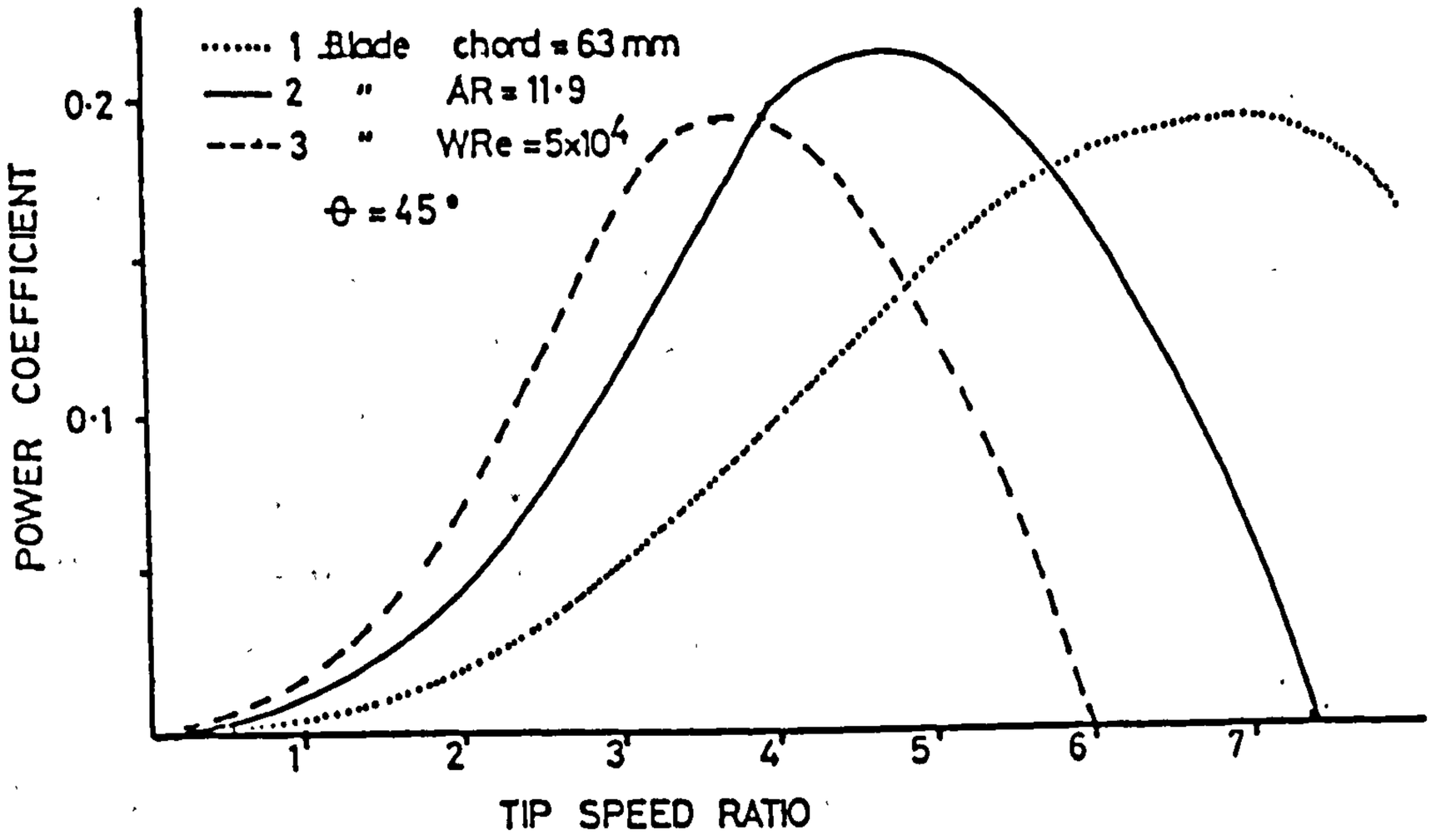

Figure 2.4: Effect of blade number angle on V-VAWT C_{p_m}-λ characteristic [9]

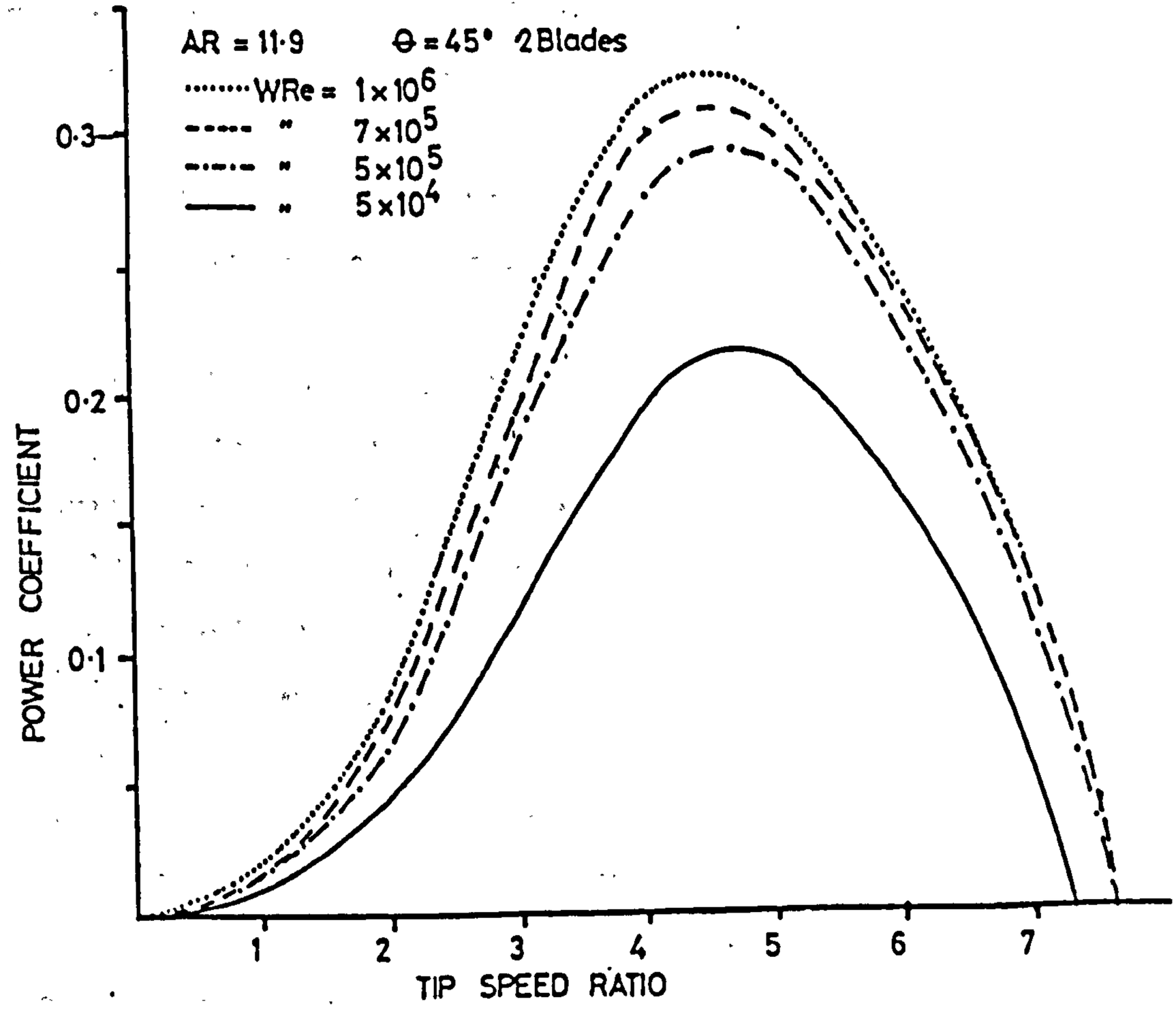

Figure 2.5: Effect of wind Reynolds Number on V-VAWT C_{p_m}-λ characteristic [9]

characteristics for different angles of inclination, aspect ratio, and blade number, Figures 2.2 to 2.4. These results showed that a maximum power coefficient would be achieved using high aspect ratio blades, and two-bladed rotor configurations. Although an angle of inclination of $\theta = 50°$ yielded the best maximum C_{P_m}, subsequent rotor designs have all used $\theta = 45°$. Although not explicitly shown, the high starting torque that is developed by the V-VAWT is represented by the slope of the C_{P_m}-λ curve at $\lambda = 0$. In all cases this is clearly seen to be positive.

Full-sized wind turbine configurations can be studied by increasing the wind Reynolds Number. The effects of this change are shown in Figure 2.5, which clearly shows the improvement made by increasing the size of the rotor. In all cases the windspeed is constant, so the results for WRe = 500,000 are for a rotor of approximately 13 m diameter, and those at WRe = 1,000,000 are for a rotor of approximately 28 m diameter.

Design schemes for practical, full-sized V-VAWTs were prepared; these are shown in Figures 2.6 and 2.7.

Sharpe and Taylor continued their theoretical work of the fixed geometry V-VAWT with a parametric study of a 5kW configuration [19]. Blade number, aspect ratio, and angle of inclination were considered once again, but the study was extended to consider blade taper, the attachment position of the blade to the rotor hub, and bracing cable drag losses, Figures 2.8 to 2.10. Earlier experiments by Sharpe [20] on small Darrieus VAWTs had showed the effects of blade thickness on aerodynamic performance. From these results an optimum 5kW design was specified: each blade has an aspect ratio of 16, a taper ratio of 2:1, a blade length of 5.5 m, and a symmetrical 18% thickness to chord ratio aerofoil is used for its construction. The maximum

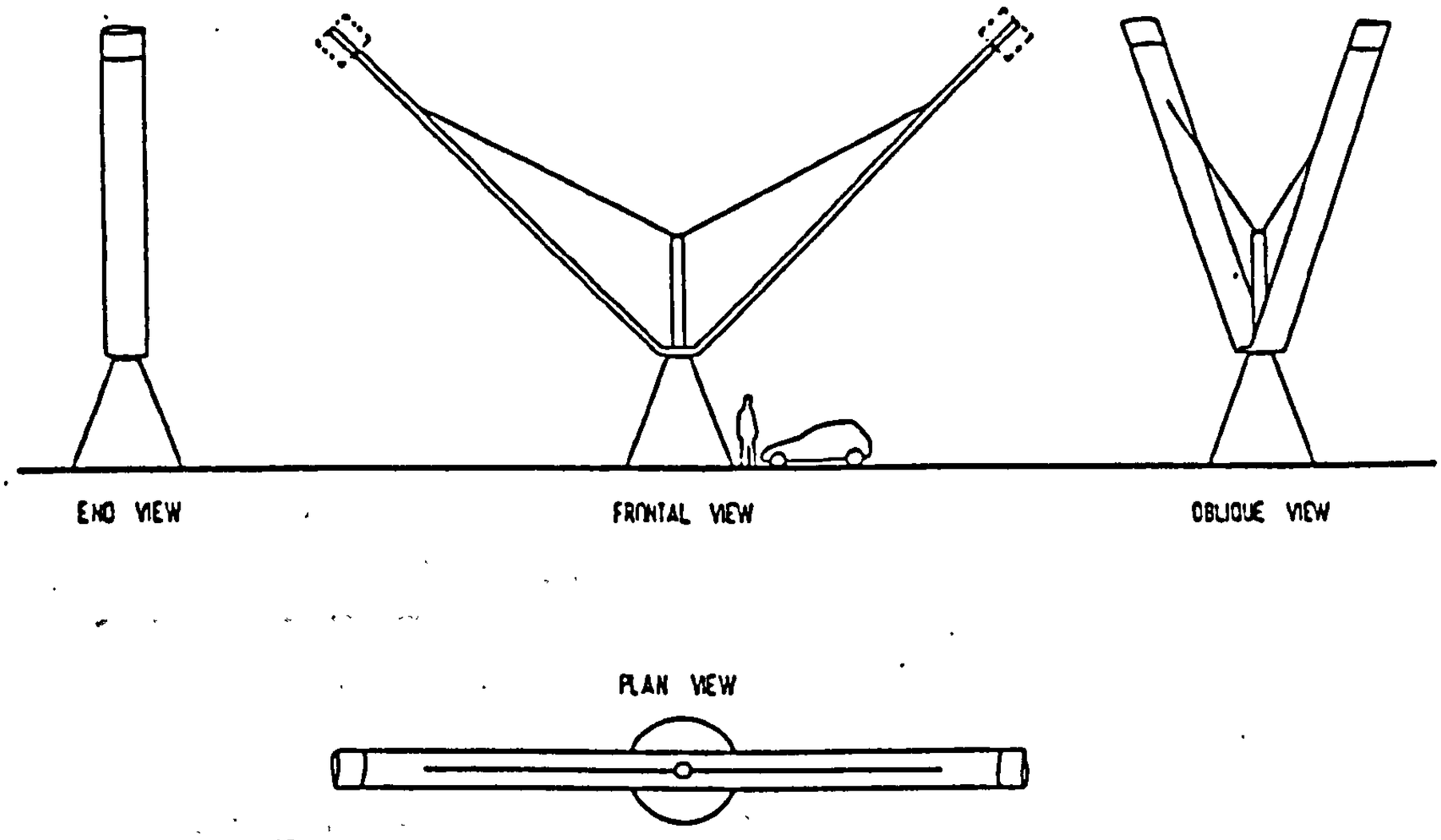

Figure 2.6: 20 kW fixed geometry V-VAWT

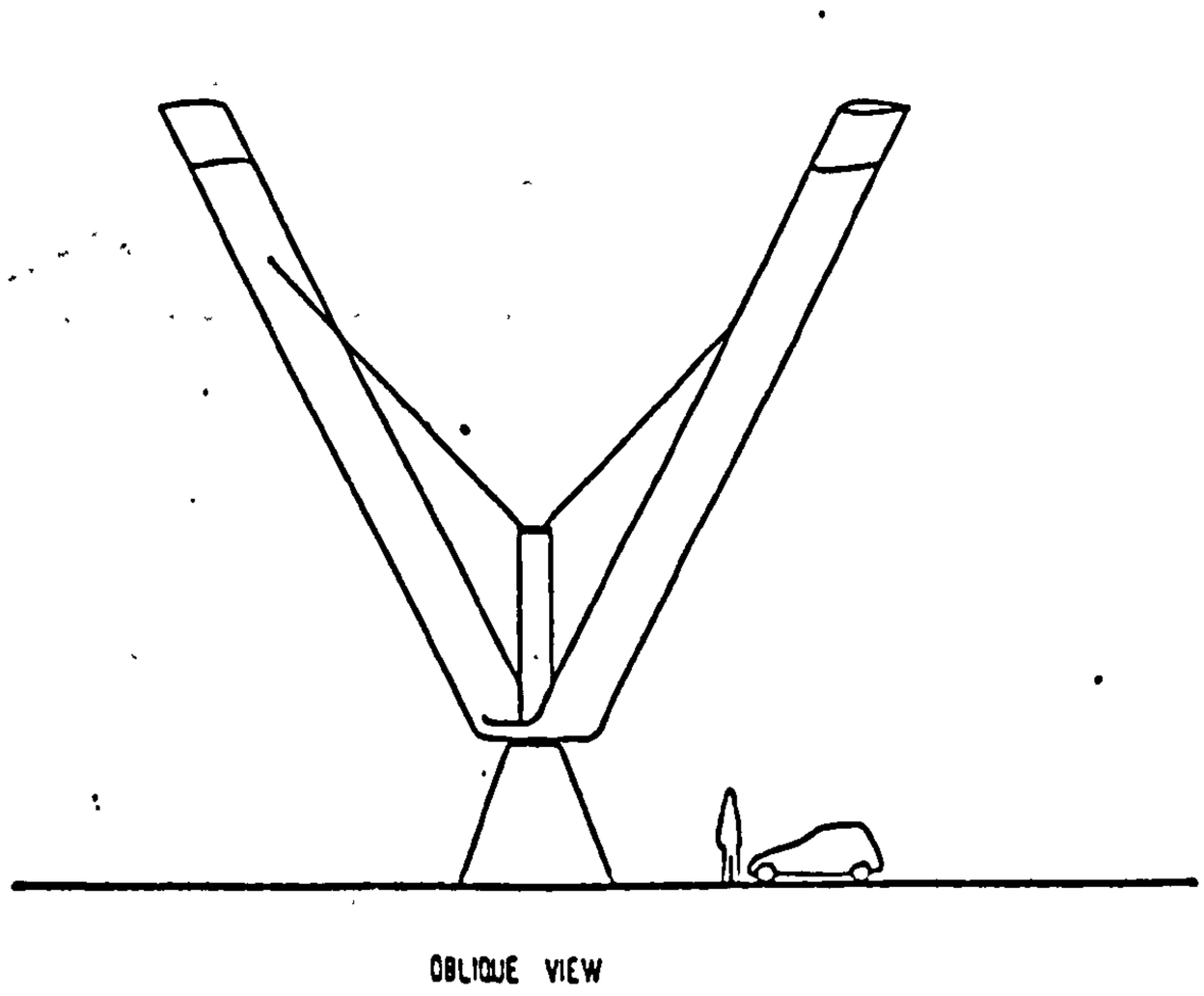

Figure 2.7: 50 kW fixed geometry V-VAWT

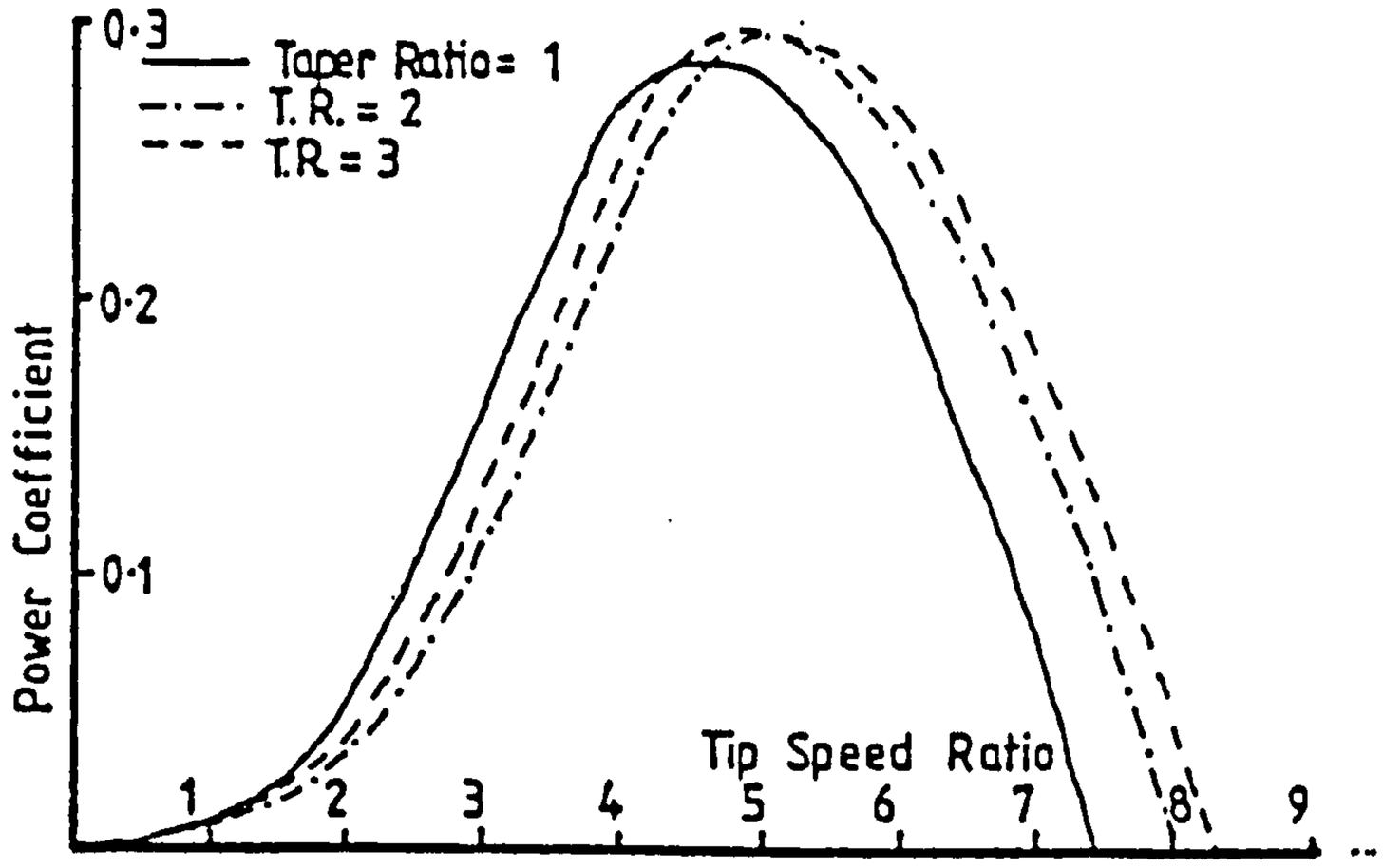

Figure 2.8: Effect of blade taper on 5 kW V-VAWT [19]

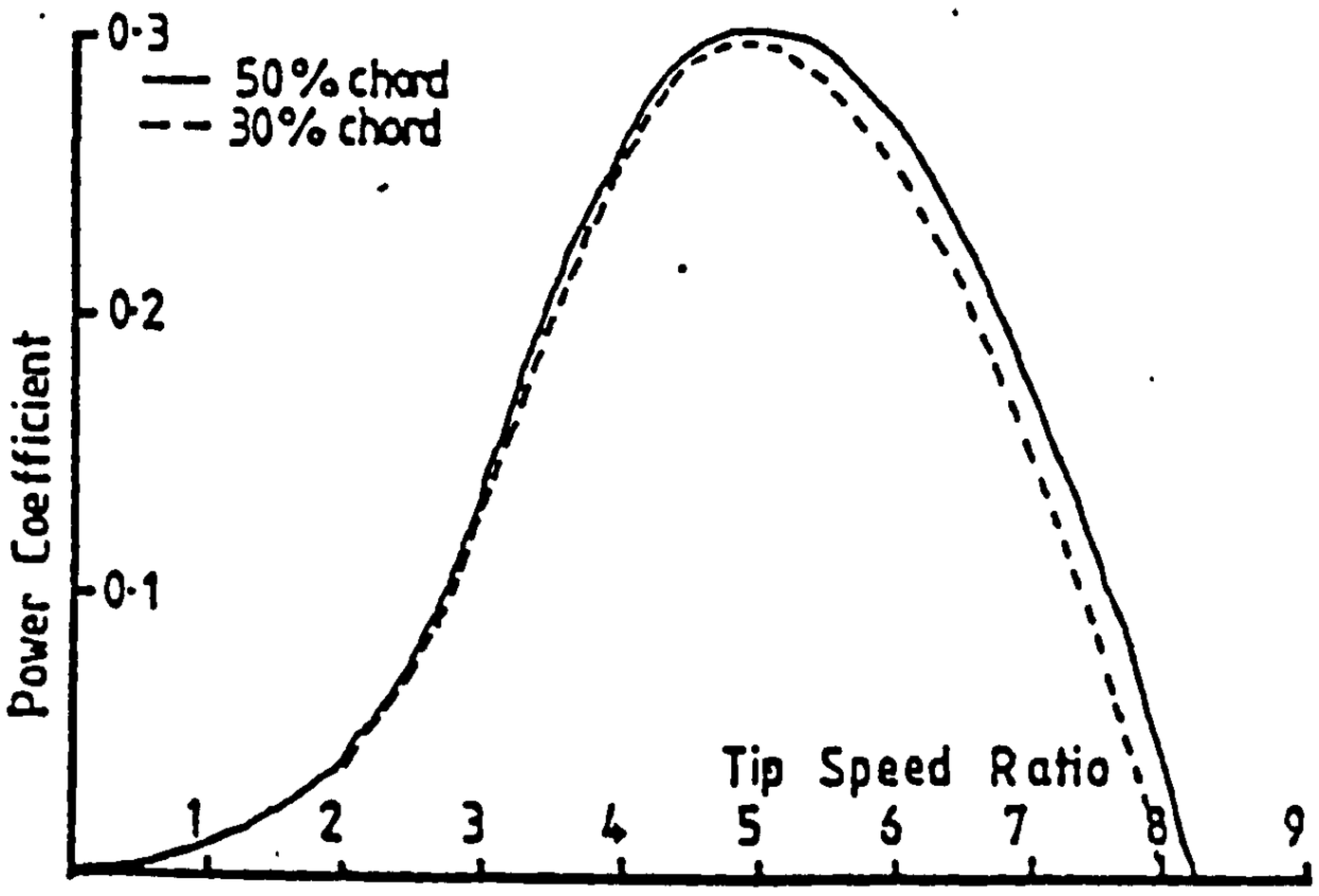

Figure 2.9: Effect of blade offset on 5 kW V-VAWT [19]

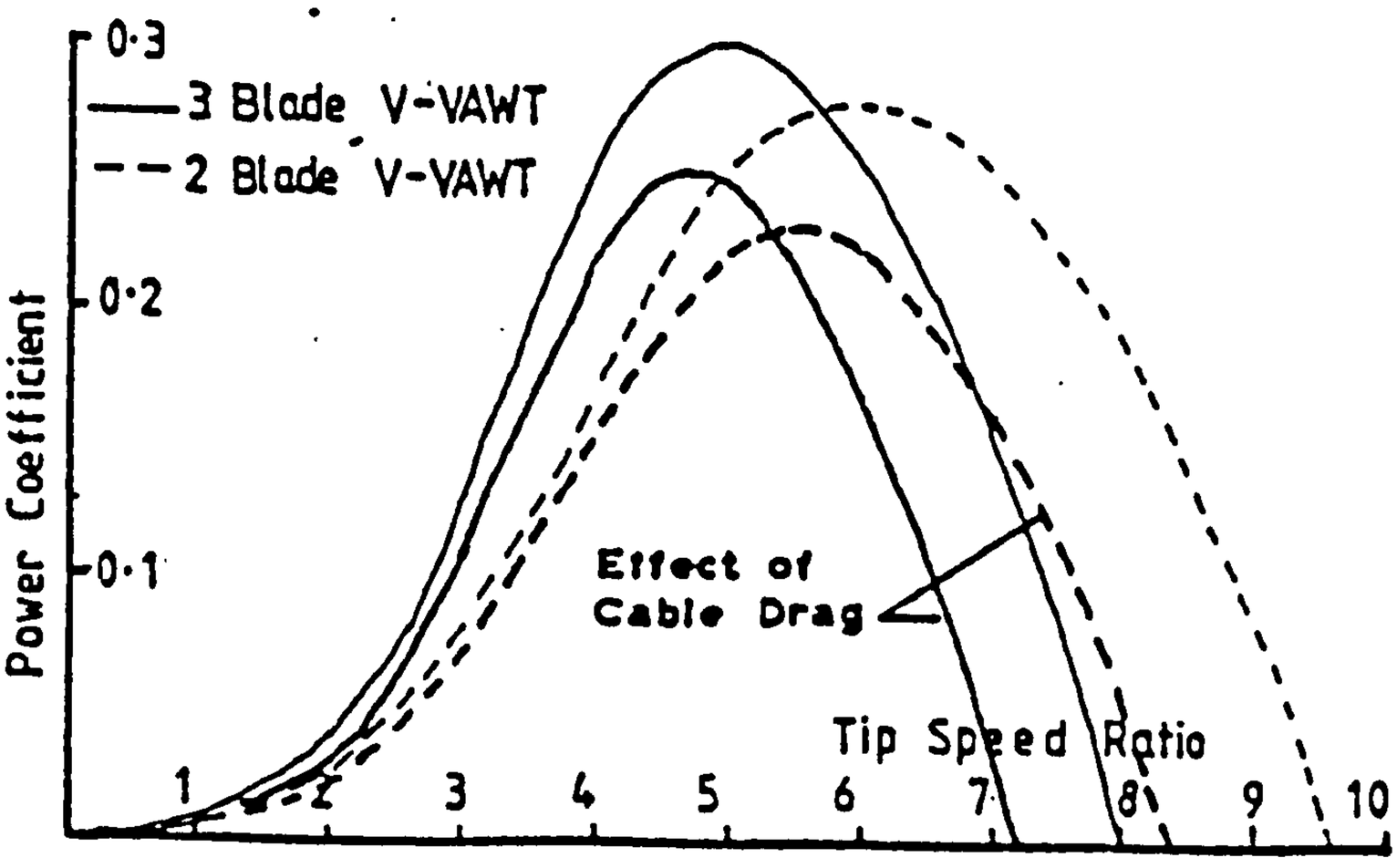

Figure 2.10: Effect of cable drag on 5 kW V-VAWT [19]

power coefficient for this design is predicted to be in excess of 0.3, which is lower than other VAWT configurations, but [19]:

> "... the primary objective is to design a turbine which produces energy at a lower cost than existing designs: it is anticipated that this would be obtained from the simplicity of the structure."

The 5kW V-VAWT design is rated at a windspeed of 12 m/s, and has since been erected on the free-air test facility at the Open University [21]. The wind turbine has been designed so that both two-bladed and three-bladed options can be evaluated. Initial test results have been encouraging [22], but a consistent dataset over a large range of operating conditions has not, as yet, been generated. The validity of the predicted performance figures lies in both the known accuracy of the computer model VAWTTAY, and the results of small scale wind tunnel tests.

2.1.2: Wind Tunnel Tests of Small V-VAWT Models

Small scale models of the V-VAWT were constructed by Sharpe and Taylor to verify the predicted performance results of VAWTTAY [9]. The first model was made using two straight blades, each of length 750 mm and chord 63 mm. The blades were of wood construction and had to be braced using faired fibre packing tape for additional support. The blades were attached to a steel shaft that was free to rotate in a rigid tubular steel framework. The rotor was placed at the outlet to a blowdown wind tunnel at Queen Mary College, London. A simple test technique devised by Sharpe [23], and fully described in Chapter Five, was used to determine the complete C_{P}-λ characteristic of the model.

A maximum $C_{p_{max}}$ of 0.21 at a λ of 7.2 was predicted for this model, but initial test results fell considerably short of these values. Inspection during operation showed that the blades were twisting due to the high centrifugal loading on the model. The blades were shortened to 560 mm in length, and the angle of inclination adjusted to $\theta = 40°$. Sharpe and Taylor note that some improvement in performance was achieved with this modification, but the results were still considered poor. The angle of blade twisting was observed and assesed to be equivalent to 7.5° nose-in at the tip, for a tip speed ratio of $\lambda = 3.2$. The assumptions of the aerodynamic predictions were modified to accomodate the twisting effect; these showed better correlation to the experimental results, Figure 2.11, however, it was concluded that the tests were [9]:

> "...inconclusive in terms of indicating true aerodynamic performance."

Despite their poor overall performance, both the models were observed to develop a high starting torque and readily self-start. This capability is, amongst vertical axis configurations, unique to the V-VAWT.

A third model V-VAWT was constructed and tested [19] with greater success. This model had two straight blades of length 550 mm, chord 60 mm, and angle of inclination 45°. Each blade was supported by *two* cables in tandem, fixed at a point 120 mm from the blade tip. The cables straddled the flexural centre of the 18% thick aerofoil, ensuring the blade did not twist at high rotational speed. The wind tunnel test results showed a marked improvement of the C_p-λ characteristic, Figure 2.12. The theoretical predictions could not be matched exactly, because the computer predictions considered the blades to have a 12% thick aerofoil, however, Sharpe and Taylor concluded [19]:

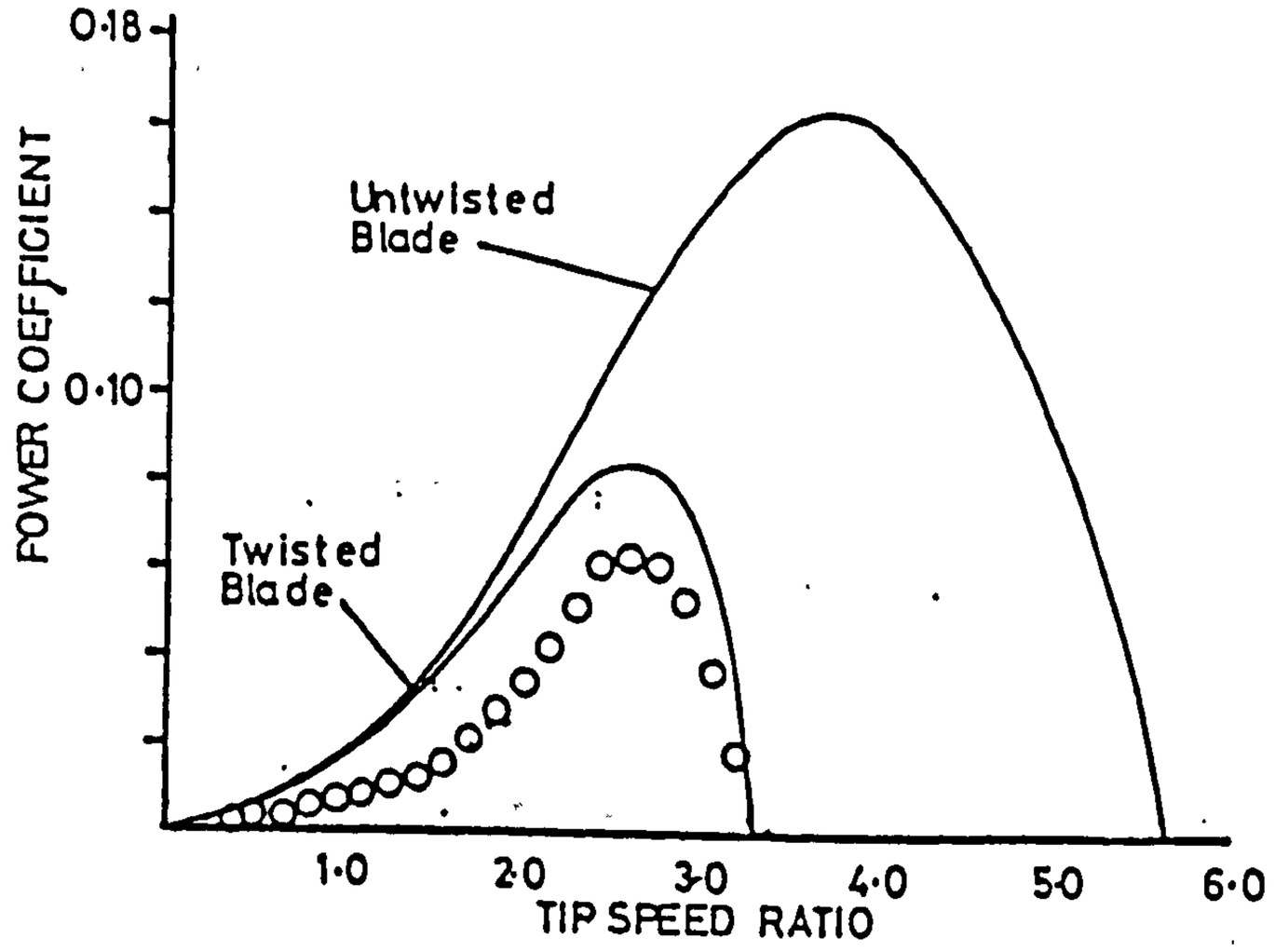

Figure 2.11: Comparison of theoretical results and experimental results of original model V-VAWT with twisting blade [9]

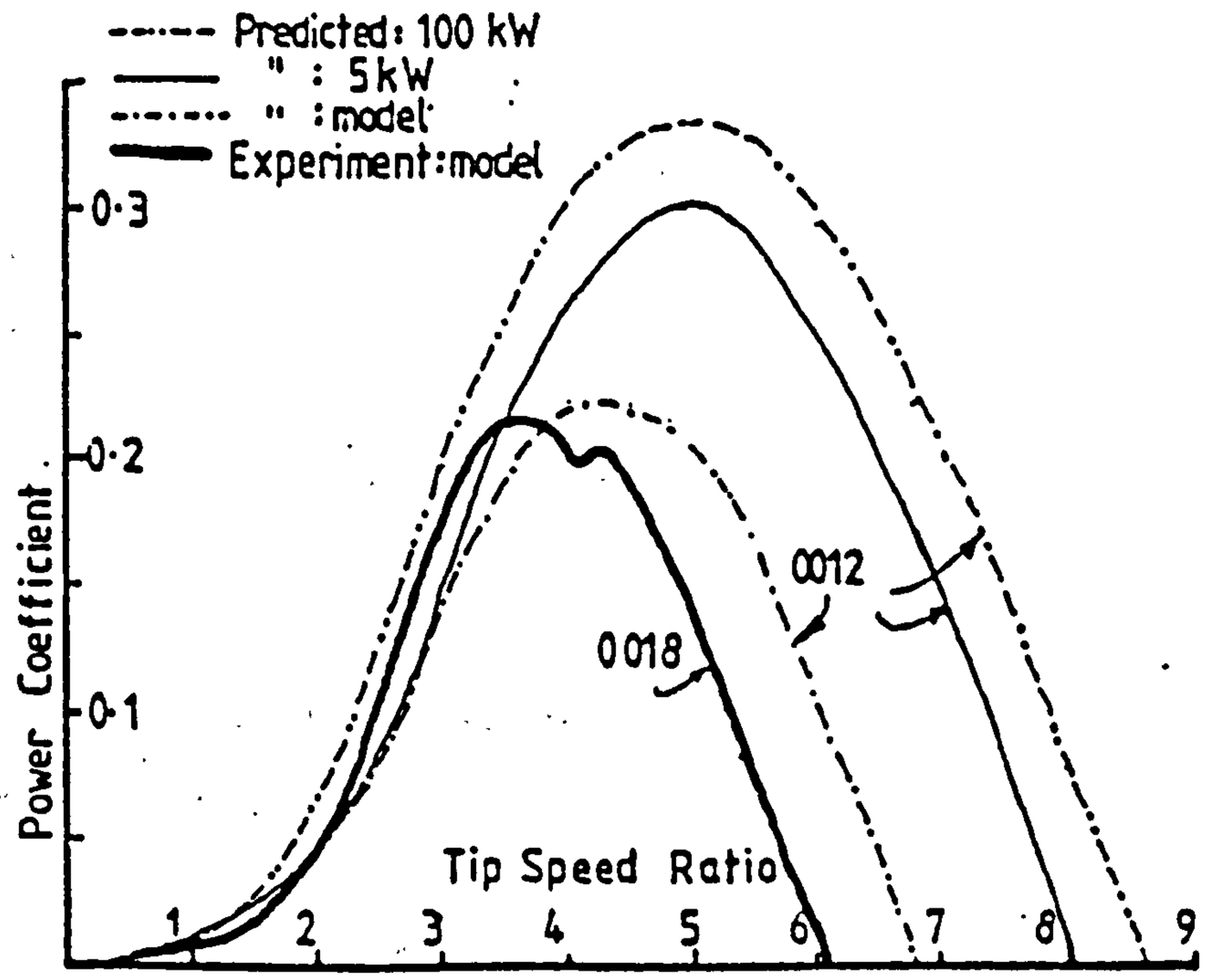

Figure 2.12: Comparison of theoretical results of 100 kW, 5 kW and model V-VAWT with experimental results [19]

"The wind tunnel test results were regarded as encouraging, and confirmed the use of the theoretical model as a design tool."

A consequence of the improved wind tunnel test results was the confidence to use the aerodynamic prediction model for developing the 5kW design previously mentioned, and a 100 kW design. The C_p-λ characteristics of these two wind turbines are also shown in Figure 2.12. In both cases the cable drag losses are ignored, though their effect on the 5kW version is clearly seen in Figure 2.10.

2.1.3: Conclusions from the Preliminary Studies of Sharpe and Taylor

Sharpe and Taylor's preliminary studies of the V-VAWT configuration have covered many aspects of this novel VAWT concept. They have demonstrated that the aerodynamic performance prediction model VAWTTAY can be used with some confidence for V-VAWT design studies, and that despite its low overall aerodynamic efficiency, careful blade design can ensure optimum performance is achieved. The self-starting capability has been proven by experiment and predicted using VAWTTAY.

Methods of power regulation, however, were not systematically investigated, though possible control devices have been offered, nor has the use of the V-VAWT specifically for electricity generation been considered in detail. It is these aspects of the V-VAWT configuration that have been specifically considered in the study reported here. The principles of operation of the V-VAWT are embodied in the theoretical model used as the basis of VAWTTAY, and the author has used this computer model throughout the study period. It is, therefore, appropriate to consider this aerodynamic prediction model in greater depth.

2.2: The Aerodynamic Performance Prediction Model VAWTTAY

The aerodynamic performance prediction model VAWTTAY is a computer based embodiment of Sharpe's refined multiple streamtube theory [18]. The multiple streamtube theory is applicable to all VAWT configurations, and has resulted from many years of development and refinement by Sharpe and other authors. The computer model VAWTTAY was written by Sharpe specifically for the V-VAWT, and first ran on a Commodore PET microcomputer. Later versions of VAWTTAY were adapted for the IBM-PC computer, but these were considered inadequate by the author for extensive use because of the long program execution times involved.

A significant proportion of the author's time has been spent adapting Sharpe's original BASIC computer code to a FORTRAN based computer code suitable for use on mini-computers such as the VAX 11/750 and 11/780 series. The subsequent development and verification of the FORTRAN program now allows the author to complete the theoretical analysis of a V-VAWT design with greater accuracy and in more detail in minutes rather than hours. The significant saving in computational time made by transferring VAWTTAY to a minicomputer, has contributed significantly to the author's understanding and comprehension of both the theoretical model and the behaviour of the V-VAWT itself.

2.2.1: Multiple Streamtube Theory

The multiple streamtube theory is based upon equating the change in streamwise momentum through the wind turbine rotor to the aerodynamic forces acting on the rotor blades. It is strictly a two dimensional analysis, but the three dimensional geometry of the V-VAWT configuration can be accomodated by considering a number of horizontal

slices, analysed independently of each other. For each slice, the Bernoulli equation and momentum equation are applied to a number of streamtubes that are bounded by straight streamlines which flow through the turbine. The streamlines are characterised by the parameter β, as shown in Figure 2.13, and $\beta + \delta\beta$. Each blade passes through the streamtube twice in every revolution, and by application of the continuity equation to the flow in the streamtube, the upwind and downwind passes cannot be treated independently. Expansion of the streamtube is included and, by using suitable aerofoil data, the variation of blade forces with blade position can be predicted. The following summary of the fundamentals of the theory is based upon refs. [18, 24, 25].

The theory considers a horizontal, two dimensional slice of the rotor of unit height. The rotor comprises of a large number N of blades, each of chord c, that sweep out an actuator circle of radius R. The solidity is $\sigma = Nc/R$. The far upstream wind has a constant speed V_∞, and if the angular speed of the rotor is Ω, then the tip speed ratio is $\lambda = \Omega R/V_\infty$. Its is assumed that atmospheric pressure p_∞ occurs in the far upstream and far downstream parts of the streamtube, and that at some point inside the turbine p_∞ is attained on each streamline. The streamtube velocity at that point V_∞ is taken to be the "wake" velocity for the upstream blades, and the "freestream" velocity for the downstream blades. The velocity in the far wake is V_w, and the flow is assumed to be incompressible.

Applying Bernoulli's equation and the momentum equation to the streamtube, as if the velocities were parallel to the direction of V_∞, yields the following expressions for the forces in the streamtube:

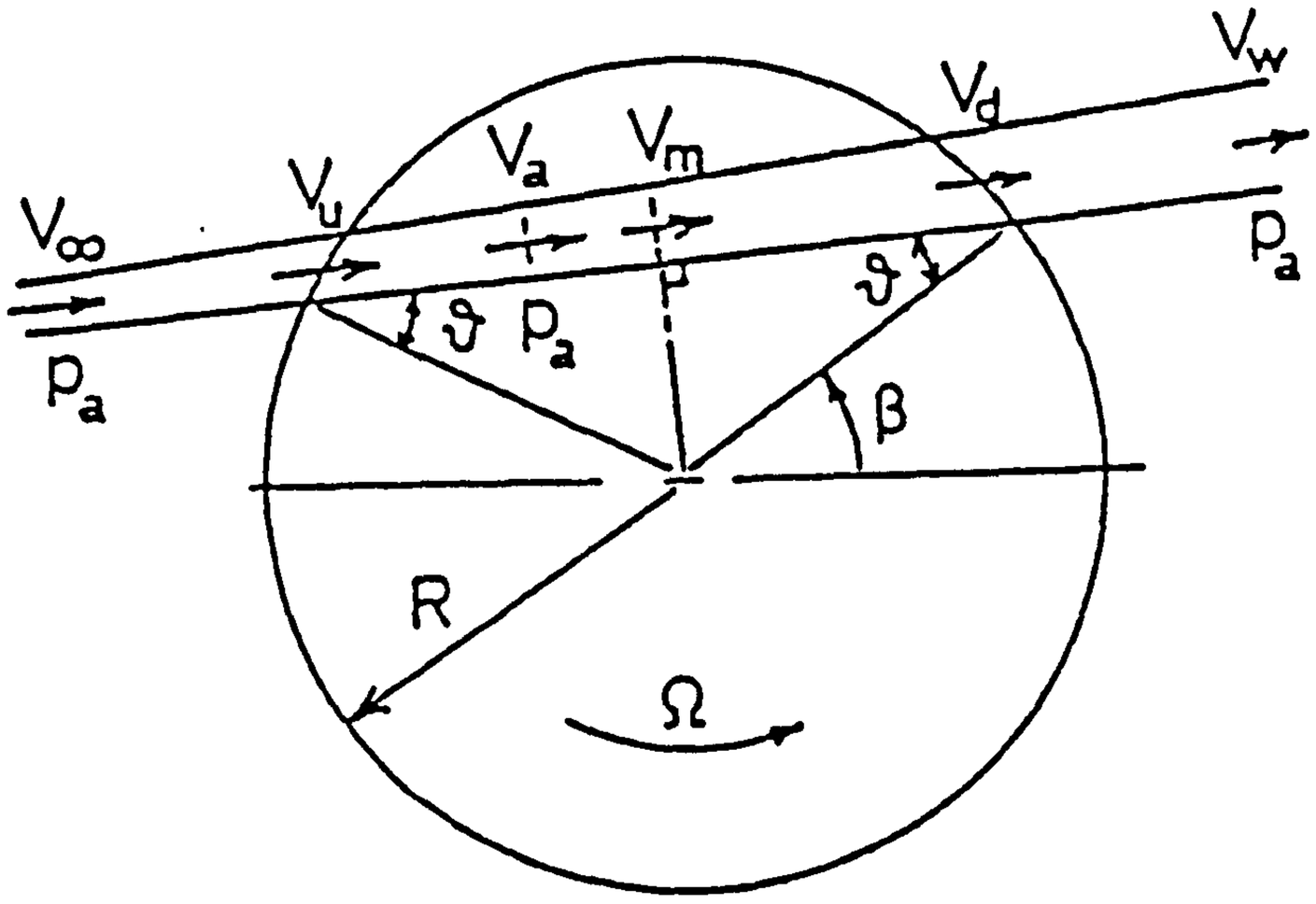

Figure 2.13: Characterisation of VAWT streamtube [18]

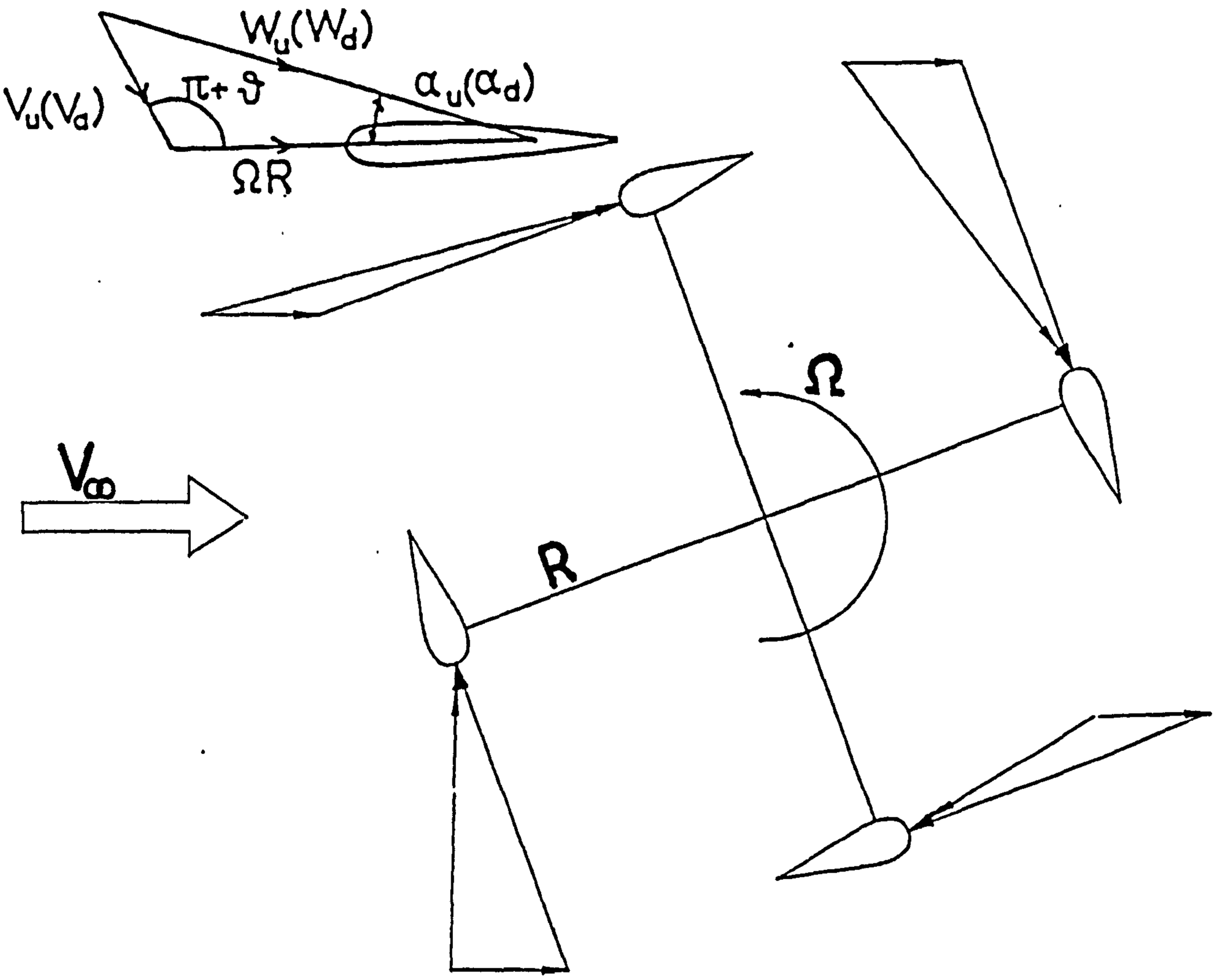

Figure 2.14: Relative velocity triangle acting on VAWT blade element

$$\delta F_U = 2V_U \rho \delta A_U (V_\infty - V_U) \tag{2.5a}$$

$$\delta F_D = 2V_D \rho \delta A_D (V_A - V_D) \tag{2.5b}$$

where

$$V_U = (V_\infty + V_A)/2 \tag{2.6a}$$

$$V_D = (V_A + V_w)/2 \tag{2.6b}$$

Here δF_U and δF_D are respectively the incremental upstream and downstream streamwise forces exerted by the blades in the streamtube, and δA_U and δA_D are the respective incremental cross sections. Note that subtracting (2.6b) from (2.6a) gives:

$$V_U - V_D = \tfrac{1}{2}(V_\infty - V_w) \tag{2.7}$$

implying that half the retardation of the flow across the streamline occurs across the wind turbine rotor. The velocities V_U and V_D are termed the "induced velocities".

Figure 2.14 shows the relative velocity triangle acting on the blade element. The local resultant velocity W is dependent upon the local induced velocity V, the peripheral speed of the blade element ΩR, its angle of inclination θ to the vertical, and the parameter β. Blade element theory yields the following streamwise blade element forces:

$$\delta F_U = \tfrac{1}{2}\rho W_U^2 \frac{\sigma}{2\pi} \delta A_U (C_N - C_T \tan\beta \sec\theta) \tag{2.8a}$$

$$\delta F_D = \tfrac{1}{2}\rho W_D^2 \frac{\sigma}{2\pi} \delta A_D (C_N - C_T \tan\beta \sec\theta) \tag{2.8b}$$

The resolved aerodynamic forces induced on the blade are given by the coefficients of normal and thrust force, C_N and C_T, which can be evaluated at the appropriate angle of

attack α and local Reynold Number Wc/ν for the aerofoil section used to model the blade. The chord c is replaced by the effective chord length within the streamtube $(\sigma/2\pi)\delta A.\sec\beta$. The $\sec\theta$ term ensures the induced velocity components are resolved in a plane normal to the blade span.

Using eqns. (2.5) and (2.8) gives:

$$\frac{V_U}{V_\infty}\left(1 - \frac{V_U}{V_\infty}\right) = \frac{\sigma}{8\pi}\frac{W_U^2}{V_\infty}(C_{NU} - C_{TU}\tan\beta\sec\theta) \qquad (2.9a)$$

and

$$\frac{V_D}{V_A}\left(1 - \frac{V_D}{V_A}\right) = \frac{\sigma}{8\pi}\frac{W_D^2}{V_\infty}(C_{ND} - C_{TD}\tan\beta\sec\theta) \qquad (2.9b)$$

These equations cannot be solved explicitly, so an iterative approach must be adopted. First both sides of eqn. (2.12) are balanced to determine V_U, then eqn. (2.7) is used to determine V_A, and finally eqn. (2.13) is balanced to determine V_D. This technique is highly suited to computer based solution, allowing the values of V_U and V_D to be readily determined for specific rotor geometries.

The torque contribution per streamtube is:

$$\delta Q = \tfrac{1}{2}\rho\frac{\sigma}{2\pi}R^2\left(\frac{W_U^2}{V_U}C_{TU} + \frac{W_D^2}{V_D}C_{TD}\right)V_M\sec\theta\,d\beta\,dh \qquad (2.10)$$

where

$$V_M = \frac{2V_UV_D}{(V_U + V_D)} \qquad (2.11)$$

and dh is the vertical depth of the streamtube.

The normal and tangential forces per unit length of the blade are given by:

$$F_N = \tfrac{1}{2}\rho W^2 c C_N \qquad (2.12a)$$

$$F_T = \tfrac{1}{2}\rho W^2 c C_T \qquad (2.12b)$$

The expression for torque can be numerically integrated around the actuator circle to give the torque for a complete revolution. Similarly, numerical integration across the blade span will yield the total torque for the rotor. Local variations of blade geometry can be accomodated by the theory, and by using tabulated data for C_N and C_T over a variety of Reynolds Number, allowances for local Reynolds Number variations can be made. Angles of attack, windwise force and crosswind force, and their variation with rotational position can all be predicted using this theory.

Sharpe's refined multiple streamtube theory [18] includes corrections for flow curvature, dynamic stall and blade tip losses. The incorporation of these effects into the aerodynamic performance theory is discussed at length by Sharpe, and to assess the validity of the "composite" theory, he has compared its predictions to the experimental results of other authors. Good correlation has been demostrated, provided dynamic stall is included in the theory only for normal blade forces, and only on the upstream pass. While the mechanism of dynamic stall is not completely understood, Sharpe considers that the level of turbulence generated by the upstream blade pass accounts for there being no evidence of dynamic stall on the downstream blade pass. This refined theory is currently the most comprehensive multiple streamtube theory proposed for VAWTs, and therefore is considered a highly valuable analytical tool for V-VAWT development.

2.2.2: Aerodynamic Peformance Prediction Computer Programs

The computer based aerodynamic performance prediction model consists of a suite of programs. The FORTRAN based programs developed by the author are a direct descendent of Sharpe's original BASIC programs. The current suite consists of three discrete programs:

(a) WRITEBLADE
(b) VAWTTAY
(c) READVAWTTAY

WRITEBLADE is used to numerically model the blade geometry of the V-VAWT rotor. The blade is split into a number of small elements, the local characteristics of each being determined from the overall planform dimensions and geometrical attributes of the blade, including its angle of inclination to the vertical. The program allows local chord length and pitch angle for each element, and the root positions of the attachment point, taper axis and pitch axis to be defined. In this way a unique numerical description of the blade can be generated. The program generates a blade geometry datafile that is used in the two other programs.

VAWTTAY embodies the multiple streamtube theory described above and is, therefore, the core program of the suite. The program utilises the WRITEBLADE blade geometry file to retrieve specific blade descriptions. The rotor is fully described by the number of blades, the aerofoil section, and the type of operation (constant rotational speed or constant windspeed) to be analysed. The program executes a calculation sequence that analyses the aerodynamic performance characteristics of the V-VAWT over a range of operating conditions determined by tip speed ratio. The aerodynamic forces acting on the rotor are calculated for

each blade element at a number of azimuth positions around the actuator circle. The application of the multiple streamtube theory requires the normal and tangential force coefficients of the aerofoil to be repeatedly used in the iterative process required to determine the upstream and downstream induced velocities. The C_N and C_T values of the aerofoil are contained in a "look-up" table of coefficients held in the computer memory. The aerofoil data must represent a large range of Reynolds Number, and angles of attack upto 180°. Suitable data in a format taht can readily be transferred to the computer is scarce. Reliable datasets for the NACA series of symmetrical aerofoil sections have, however, been presented in [23, 26, 27]. Of these datasets, that developed by Sharpe for the NACA0012 aerofoil [23] was used in the initial analysis of the V-VAWT concept.

VAWTTAY generates the angle of attack, local induced velocity, elemental blade forces, and elemental torque at each azimuth position and blade element. Integration of torque across the blade span and around the actutaor circle will generate the total torque developed by the rotor as a whole. The program prints out a performance summary once the analysis at each tip speed ratio is complete. The summary table includes the calculated power and torque coefficients of the rotor. All elemental data can be stored in a performance datafile for further analysis using READVAWTTAY.

READVAWTTAY is a post-processor for VAWTTAY. It uses data from the blade geometry and performance datafiles to create additional information about the behaviour of the V-VAWT rotor. The program presents the elemental data in a tabular form, calculates the variation of torque with azimuth angle, and calculates the torque distribution across the blade span. The aerodynamically induced forces

and bending loads on the blade are calculated, and the worst loading cases identified. All the information is presented in a numerical form, as routines for the graphical output of data have not yet been created.

All three programs have been written in standard FORTRAN and have been validated by comparing predicted results with those generated by the proven BASIC versions. The author chose to develop minicomputer forms of the microcomputer programs because of the long program execution times required for determining rotor characteristics. The present suite of programs run on a VAX 11/750 minicomputer at Portsmouth Polytechnic. To determine the C_p-λ characteristic for, say, ten tip speed ratio settings currently takes approximately two minutes, compared to the two and half hours required by the microcomputer. Time saving alone justified the effort, but the flexibility and size of the larger computer has many other benefits that has allowed the scope and application of the programs to be expanded. Some of the modifications and developments made by the author to the programs will be discussed later, however, the reliability and suitability of these programs now allows them to be quickly and effectively used in the design and development of the V-VAWT concept.

2.3: Aerodynamic Characteristics and Power Control of the V-VAWT Rotor for Electricity Generation

The fundamental aerodynamic principles of operation of the V-VAWT are little different to other VAWT configurations, however, the behaviour specific to this turbine is the result of its characteristic rotor geometry. Consider a three-bladed V-VAWT, each blade having an aspect ratio of 16 and a taper ratio of 2:1. The C_{p_m}-λ characteristic of this rotor geometry, predicted with VAWTTAY using NACA0012

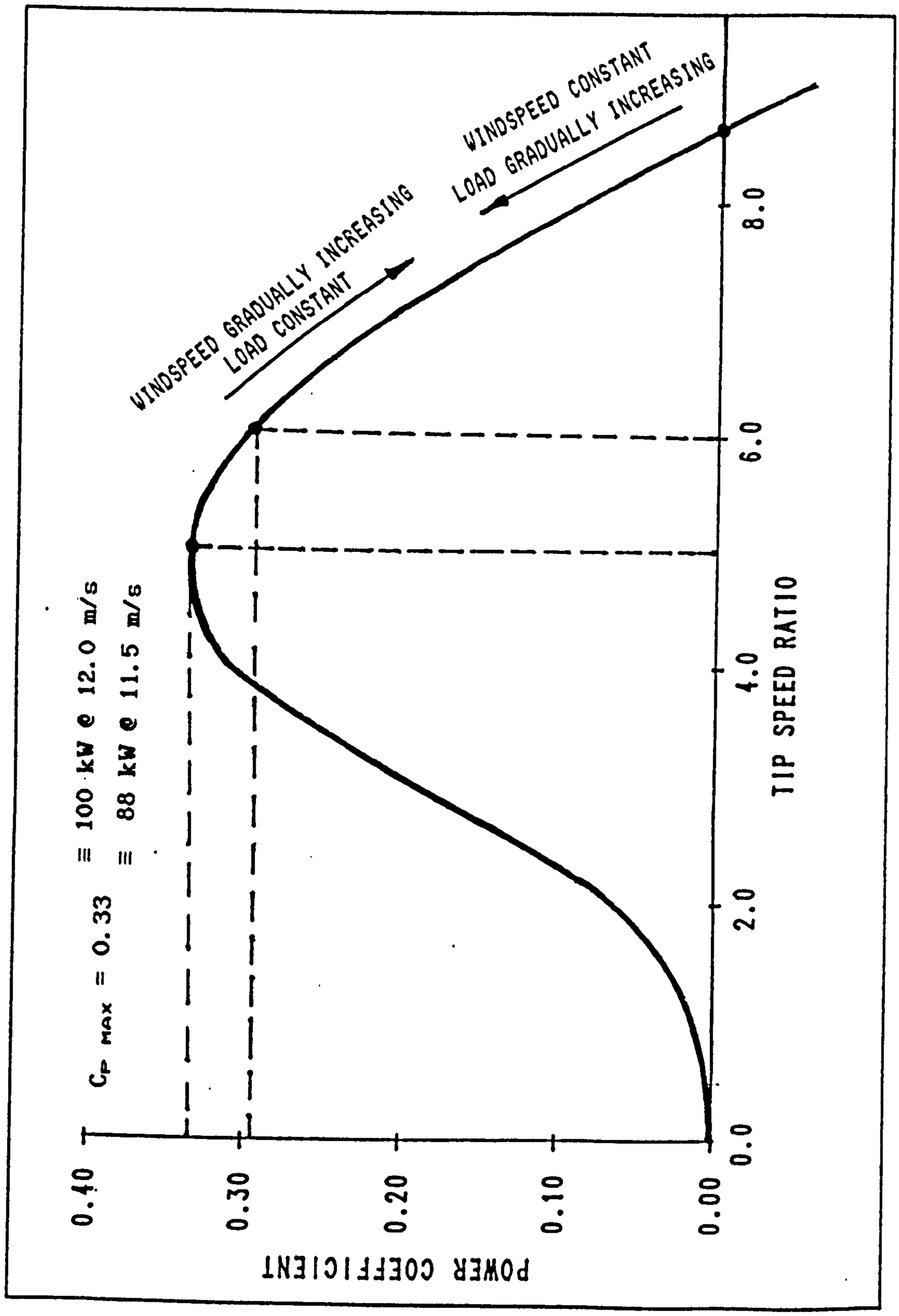

Figure 2.15: Theoretical C_P-λ characteristic of a 100 kW V-VAWT predicted using VAWTTAY and NACA0012 aerofoil data

aerofoil data, is shown in Figure 2.15. The peak value of power coefficient occurs at $\lambda = 5$ and is $C_{P\ MAX} = 0.33$. As tip speed ratio increases, it can be seen that C_P diminishes to zero at $\lambda = 8.5$. This condition is known as "runaway" and, ignoring all parasitic losses, is the tip speed ratio to which the rotor will accelerate if it is unloaded.

If the rotor radius is R = 17.5 m, the rated windspeed is V_R = 12 m/s, and the rotor was operating at $C_{P\ MAX}$, it would be rated at 100 kW and its rotational speed would be 33 rpm; its runaway rotational speed would be 56 rpm.

Operating in a 12 m/s windspeed, an unloaded V-VAWT rotor would accelerate to a speed of 56 rpm, at which condition the aerodynamic power output of the rotor is zero. If, while the windspeed remains constant, a small external load was applied to the rotor, the rotor would slow until a new equilibrium state was achieved where the magnitude of the aerodynamic power developed by the rotor equalled that of the load. Such a state could exist at $\lambda = 6$, where $C_P = 0.29$. Here a load of 88 kW could be supplied with the rotor operating at 40 rpm. If the windspeed continues to remain constant, then the external load could be slowly increased further until an output of 100 kW was demanded of the rotor. At the new equilibrium state, the rotational speed of the rotor would be 33 rpm, $\lambda = 5$ and $C_P = 0.33$. A further increase in the load on the rotor would cause the speed of the rotor to decrease even further, in which case C_P would start to fall and the rotor power output would not be able to supply the demand. Increasing the load above 100 kW would cause the rotor to slow to a complete stop.

Essentially, while the windspeed remains constant and whilst the operating condition on the C_P-λ curve continues

to be to the right of $C_{P\ max}$, the V-VAWT rotor will respond in a stable manner to any small fluctuations of external load. Conversely, moving the operating point to the left of $C_{P\ max}$ will result in an unstable response to any small load fluctuations.

Now consider the situation where the load on the rotor remains constant, and it is the windspeed that fluctuates. If in the initial state the windspeed is 12 m/s and the load is 88 kW, then, as above, the rotor speed would be 40 rpm, $\lambda = 6$ and $C_P = 0.29$. If the windspeed gradually increases from 12 m/s, then the excess power available will cause the rotor to accelerate until a new equilibrium position is attained. If the windspeed were to increase to 13.5 m/s, then at $\lambda = 7$ where $C_P = 0.20$ equilibrium would be restored. At this condition the power output of the rotor would be 88 kW, as required, and the rotor speed would be 52 rpm. If the windspeed continues to increase gradually, the rotor speed would continue to increase whilst the rotor load remained constant. This is potentially very dangerous because the rotor speed may eventually exceed its safe operating limit, and a catastrophic failure of a component part may be provoked by the overspeeding rotor.

Conversely, if the windspeed falls gradually, the rotor speed will decrease as the available power diminishes. In this example, C_P will initially rise, but the rapid reduction of power in the wind with changing windspeed would soon overcome the small C_P gain. If the windspeed falls to only 11.5 m/s then equilibrium is attained at $\lambda = 5$, where $C_P = 0.33$. The new rotor speed would be 32 rpm and its power output would be 88 kW, as required. Gradually decreasing the windspeed further would create an unstable situation in which the load would be in excess of

any power that might be developed by the rotor, resulting in the rotor slowing until its stops.

Again operational stability is only achieved for small windspeed fluctuations whilst the rotor continues to operate to the right of $C_{P\ max}$, though overspeeding can be considered as a system instability, since it would be an undesirable event. Moving the operating point to the left of $C_{P\ max}$ will provoke the rotor to stop, as before.

In both these cases, the changes in windspeed or load are small or gradual. Clearly operating at $\lambda = 5$, where $C_P = C_{P\ max}$, the system will be at the limit of stability to these external changes. Rapid changes, such as wind gusting or sudden load losses, will provoke different events and the effect of these larger perturbations on the system will be discussed later.

If the rotor is to operate at maximum efficiency at all times, then it must operate at a constant tip speed ratio i.e. $\lambda = 5$. The speed of the rotor must, therefore, vary as changes in windspeed occur. For instance, if the windspeed rises from 12 m/s to 14 m/s, then the rotational speed of the rotor must increase from 33 rpm to 38.5 rpm to ensure this condition is met. At the new operating condition, the power developed by the rotor would have increased from 100 kW to 160 kW. A 17% increase in windspeed has led to a 60% increase in available power due to the cubic wind power law, however, penalities for this gain must be tolerated. The 17% windspeed increase will induce a 37% increase in the aerodynamic forces acting on the rotor, and the necessary 17% increase in rotational speed, to maintain a constant tip speed ratio, results in the centrifugal forces acting on the rotor increasing by 37%. The 60% increase in power and 17% increase in

rotational speed will result in a 37% increase of torque developed by the rotor.

Alternatively, if the windspeed gradually falls from 12 m/s to 10 m/s, then the speed of the rotor must decrease to 27.5 r.p.m. to ensure constant tip speed ratio operation is maintained. At the new operating condition, the power developed would only be 60 kW. Although there has been a fall in output power, the V-VAWT is still operating at its optimum tip speed ratio, so that the maximum power is being developed by the rotor.

Operating at a constant tip speed ratio clearly presents major design problems to accomodate even small windspeed increases above rated. Power output would be maximised, but large variations would occur as the windspeed changed. Also, it is uneconomic to design the wind turbine to sustain the structural loads on the rotor and to select suitable torque transmission elements for operation at windspeeds significantly larger than rated.

Alternatively, if the rotor operates at constant rotational speed, then it is tip speed ratio that will change with changes in windspeed. Changes in λ result in changes of C_P, so the rotor will no longer operate at maximum efficiency at all times. If the windspeed rises from 12 m/s to 14 m/s, the tip speed ratio drops from $\lambda = 5$ to $\lambda = 4.3$, the power coefficient would drop from 0.33 to 0.32, and the power developed by the rotor would be 155 kW. Increases in power, torque and aerodynamic forces will still be significant, but the amount of change will be dependent upon the characteristics of the wind turbine itself. Centrifugal forces acting on the rotor will not change, as the speed of rotation is constant.

If the windspeed drops to 10 m/s, then the tip speed ratio needs to rise to $\lambda = 6$, the power coefficient would drop to 0.29, and the power developed by the rotor would only be 53 kW.

Clearly operating at constant rotational speed is less effective in terms of energy capture than operating at a constant tip speed ratio, however, the structural loading on the rotor and mechanical transmission elements is less demanding with this option. In both cases there is a clear need to regulate energy capture efficiency to ensure that the power, torque and forces developed by or acting on the rotor do not exceed acceptable design limits.

Using wind turbines for electricity generation purposes poses a number of other problems. The prime movers of conventional electricity generating systems operate at constant speed to ensure the frequency of the supply is fixed. Large electricity supply utilities use high speed steam turbines, gas turbines or diesel engines to drive synchronous generators at a fixed synchronous speed. In all cases the speed of the system is regulated by controlling the flow of fuel to the prime mover. If wind turbine generators are to make significant contributions to the supply networks of large utilities, then electricity from these sources must be supplied at a fixed frequency. The wind turbine system must be designed to ensure that the frequency of the electricity output is controlled to meet this requirement, and that the power demanded of the system can be met.

Cooper and Law [28] are amongst many authors who have reviewed the various options for the control of wind turbine generators used specifically with the public supply network. Whilst mention is made of some methods of rotor speed and power control, their review concentrates

on the choice of electrical generator, and the problems of maintaining the quality of the electrical power output of the system.

Firstly, though, they identify the two major differences between wind turbines and other prime movers:

> "(a) The variability of the 'fuel'. Whereas in a conventional generating set the available input energy flow is fixed and may be varied by a simple valve or throttle to set the output power, with an aerogenerator this input is variable. Thus to deliver a sensibly constant power output requires either some form of short term energy storage or the rejection of a large proportion of the available input energy ...
>
> (b) The aerodynamic characteristics of the machine require that, for maximum efficiency, it operates at a constant tip speed ratio ... thus for maximum efficiency the rotor speed must vary with wind velocity and since the machine is normally generating into a constant frequency supply network some form of frequency or speed conversion equipment is necessary."

These two statements succinctly summarise the problems associated with designing a wind turbine generator system, especially in light of the operating characteristics discussed above. Cooper and Law identified the need for the power and speed of a wind turbine generator to be controlled, since they considered that as wind turbine size increases (an "undoubted trend" of the future) and penetration of wind turbine generated capacity increases, then:

> "...aerogenerators must be capable of operation in the same manner as conventional generating plant having automatic load sharing to follow load variations and scheduled on an economic basis. This implies local controls on the machine on a basis of speed with the power control as a system input."

The power developed by the wind turbine must be regulated, whether the wind turbine operates as a constant speed or variable speed generating system, to ensure the output

power does not rise above rated power, and that the speed of the rotor remains within it operating limits. In addition to the needs of normal running, the control needs for system start-up, synchronisation and shutdown must be considered if autonomous operation is to be achieved. Power and speed control is again required during these particular phases of wind turbine generator operation.

In summary, the control of wind turbine power and speed is a need inherent in all configurations used in electricity generating applications; the V-VAWT is no different. Consequently, the power developed by a V-VAWT rotor must be regulated, and its speed maintained within safe operating limits. Control methods that ensure that both rotor power and rotor speed can be controlled are sought for use with V-VAWT applications. The options that have been considered are briefly reviewed in the following chapter.

Chapter Three: Review of Control Options for V-VAWT

3.1: Introduction

In this chapter control options for the V-VAWT will be briefly reviewed and suitable methods identified. Before, however, considering available options in any detail, the scope of the control need must be clarified. This is best achieved by specification of the control needs. Such a specification will identify both the primary and secondary functional requirements of a control method; primary functional requirements *must* be satisfied to ensure the desired performance needs are fulfilled, whereas secondary requirements do not have to be necessarily satisfied to ensure the success of the adopted control method.

3.1.1: Specification V-VAWT Control Needs

In striving to identify suitable control methods for the V-VAWT, its application for the generation of electricity as part of a large utility network is considered most important, as argued in Chapter One. Such an application will require individual machines to operate autonomously, requiring speed and power control of the rotor during start-up, synchronisation, normal running and shutdown phases of the operation cycle, whilst ensuring the quality of the electrical output is satisfactorily maintained. Thus, as identified in Chapter Two, the control of both rotor power and speed during these operational phases is a primary requirement of any control method.

Bossanyi and Anderson [29] estimate that a wind turbine will undergo several thousand low windspeed starts, and a number of high windspeed shutdowns per annum. A wind turbine will, therefore, experience many more start-up and synchronisation cycles during its lifetime than any

conventional electricity generating system. With the continual, and often rapid, variation of windspeed, the control requirements for this phase of wind turbine operation alone are far more onerous than for other prime movers. In designing a wind turbine, the good use of materials and well established technologies can go a long way to prolonging service life; increasing wind turbine availability; decreasing the probability of component failure; and minimising service and maintenance, yet the structural loading; wind turbine performance; energy output; and economic viability of a wind turbine system can be crucially dependent upon the form of the control method. Mets and Hermansson [30] state, for example, that the essential design objectives of Swedish wind turbine design includes:

(a) 30 year service life
(b) one in 100,000 probability of failure for primary structural components
(c) 90% availability
(d) proven technology to be used when possible
(e) minimum service and maintenance

The consideration of these design objectives here will ensure that the control method adopted for the V-VAWT will fulfil the broader design aims and objectives of the whole system as stated above. Features of a particular control method that assist or detract from the overall achievement of these design objectives, must be considered on merit.

With these basic design requirements in mind, it is now possible to objectively review the control options considered most suitable for adaptation to the V-VAWT configuration.

3.2: Review of control options

In discussing wind turbine control options, it is usual to define the system boundary as encompassing the whole machine, as shown for a typical horizontal axis machine in Figure 3.1. Such a system will include within its boundary the folowing major components:

(a) rotor blades
(b) rotor hub
(c) low speed shaft
(d) brake
(e) transmission elements, including gearbox and high speed shaft
(f) electrical generator
(g) yaw drive (HAWT only)
(h) tower

The system inputs are:

(a) windspeed
(b) wind direction
(c) electrical frequency and power demand

and the system outputs are:

(a) electrical frequency and power
(b) vibration
(c) noise

Within the system boundary, the autonomous control system will utilise the signals measuring windspeed; wind direction; shaft speed; shaft torque; generator voltage, current, frequency and synchronisation to control any aerodynamic control surfaces; the yaw drive (HAWT only); generator field current and synchronisation; and the rotor

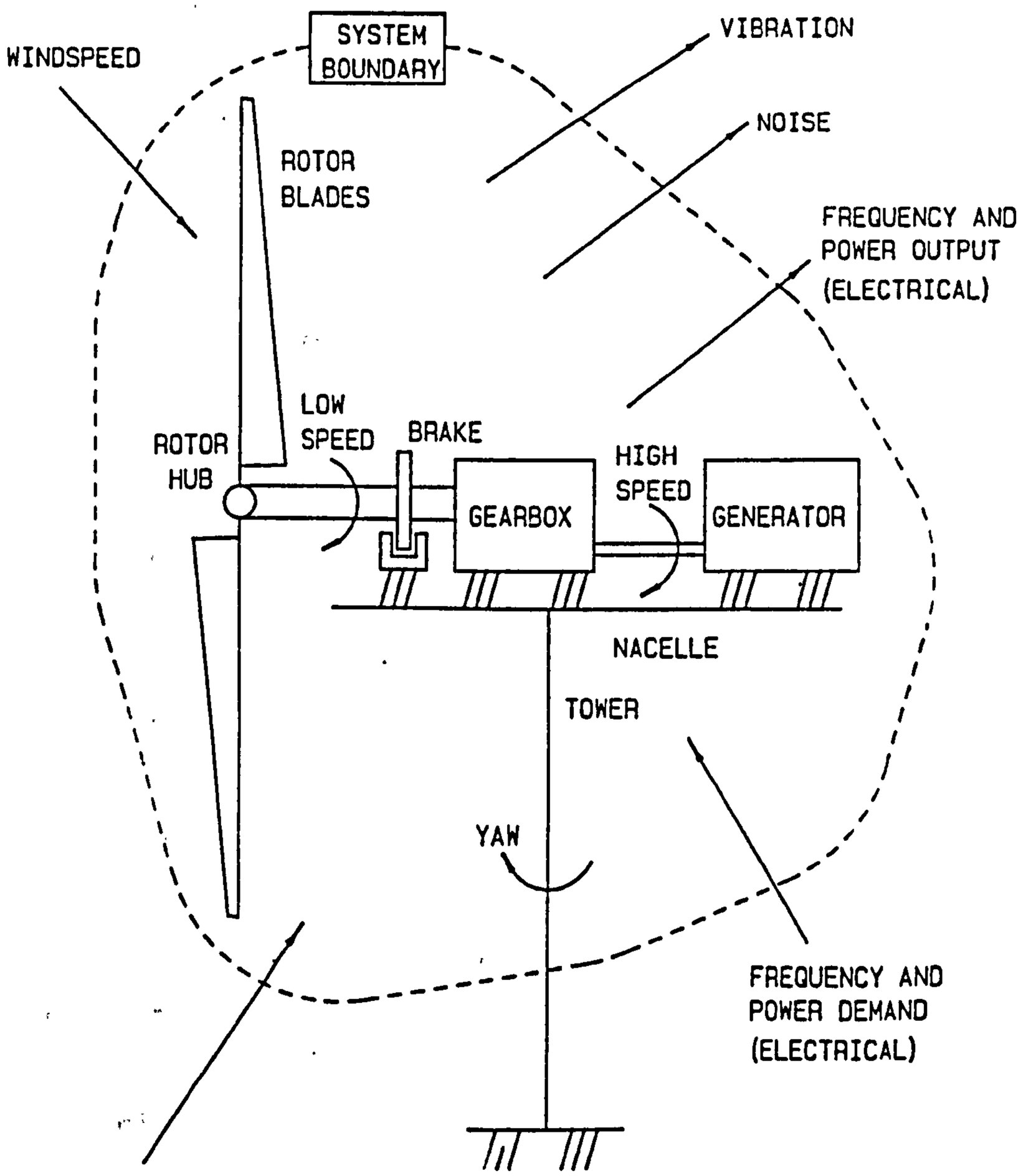

Figure 3.1: Elements of a wind turbine system

brake. Other 'out-of-limits' signals, would be used to maintain fail-safe operation of the system.

Cooper and Law, in their review of wind turbine control options [28], concentrate on the choice of electrical generator, and the problems of maintaining the quality of the electrical power output. The electrical control options they considered were:

(a) constant rotor speed operation
    synchronous generator
    induction generator
(b) variable rotor speed operation
    rectifier-invertor
    double-fed induction generator
    hydraulic transmission
(c) mulitple rotor speed operation
    dual generators
    P.A.M. wound generator

Electrical generators and alternative approaches to wind energy electricity generation are also succinctly reviewed by Freris [31]. The salient points of both these reviews are summarised below.

A wind turbine must operate at constant speed to drive a synchronous generator. Since a wind turbine needs to operate at a constant tip speed ratio to achieve optimum power output, a constant speed rotor will generally perform below optimum. Synchronous generators must operate at the frequency of the electricity supply network, so that synchronisation of the generator with the network, and ensuring the stability of the connection in gusty wind conditions are significant control problems. At windspeeds below rated, low efficiency means that energy capture losses will be incurred. Above rated windspeed,

energy capture must be reduced to ensure the wind turbine operates within its rated design limits. Induction generators accomodate small changes in speed, but with only 0.5% - 5.0% full speed slip allowable, the range of operating speeds is limited.

Variable speed operation enables the rotor to operate at its optimum tip speed ratio, ensuring maximum energy will be extracted in the low windspeed regimes. For variable speed operation, there are two commonly used generator systems that allow the constant frequency electrical output of the system to be maintained. The ac-dc-ac rectifier inverter system rectifies the variable frequency output from a variable speed synchronous generator to give dc output which in turn is fed to a synchronous converter to give a fixed frequency output. Alternatively, a double fed induction generator that has a variable frequency excitation supply, will output a fixed frequency supply over a large range of operating speeds. A hydraulic transmission system using a fixed displacement pump and variable displacement motor would allow the equivalent gear ratio of the transmission between the rotor and the generator to the constantly changed.

Multi-speed operation is a compromise between fixed and fully variable speed operation, allowing the wind turbine to operate at a finite number of fixed speeds. Two generators allow operation at two different rotational speeds; an excellent method for increasing low windspeed energy capture. A single P.A.M. generator allows operation at two speeds, but the operating range is limited by the dependency of one speed on the other.

The reviews of electrical generator choice [28,31] show that provided rotor speed and power can be controlled, any of these generator schemes can be adopted. Therefore,

while the interaction of the wind turbine and the generator is crucial to the dynamic response of the wind turbine system to input changes, for the purposes of the control option review, the choice of generator can be ignored, and the wind turbine rotor regarded as any other conventional prime mover. Simplifying the system reduces the number of elements within the system boundary, Figure 3.2. The modified system now only includes:

(a) rotor blades
(b) rotor hub
(c) low speed shaft
(d) brake
(e) yaw drive (HAWT only)
(h) tower

The system inputs are:

(a) windspeed
(b) wind direction
(c) rotor speed and mechanical power demand
(d) transmission and generator reaction torque

and the system outputs are:

(a) rotor speed and power
(b) vibration
(c) noise

In this way, the wind turbine generator system has been simplified to include only those elements directly influencing the behaviour of the wind turbine rotor itself. A consequence of this approach is that electrical control options are ignored, so that only aerodynamic or mechanical options need be considered.

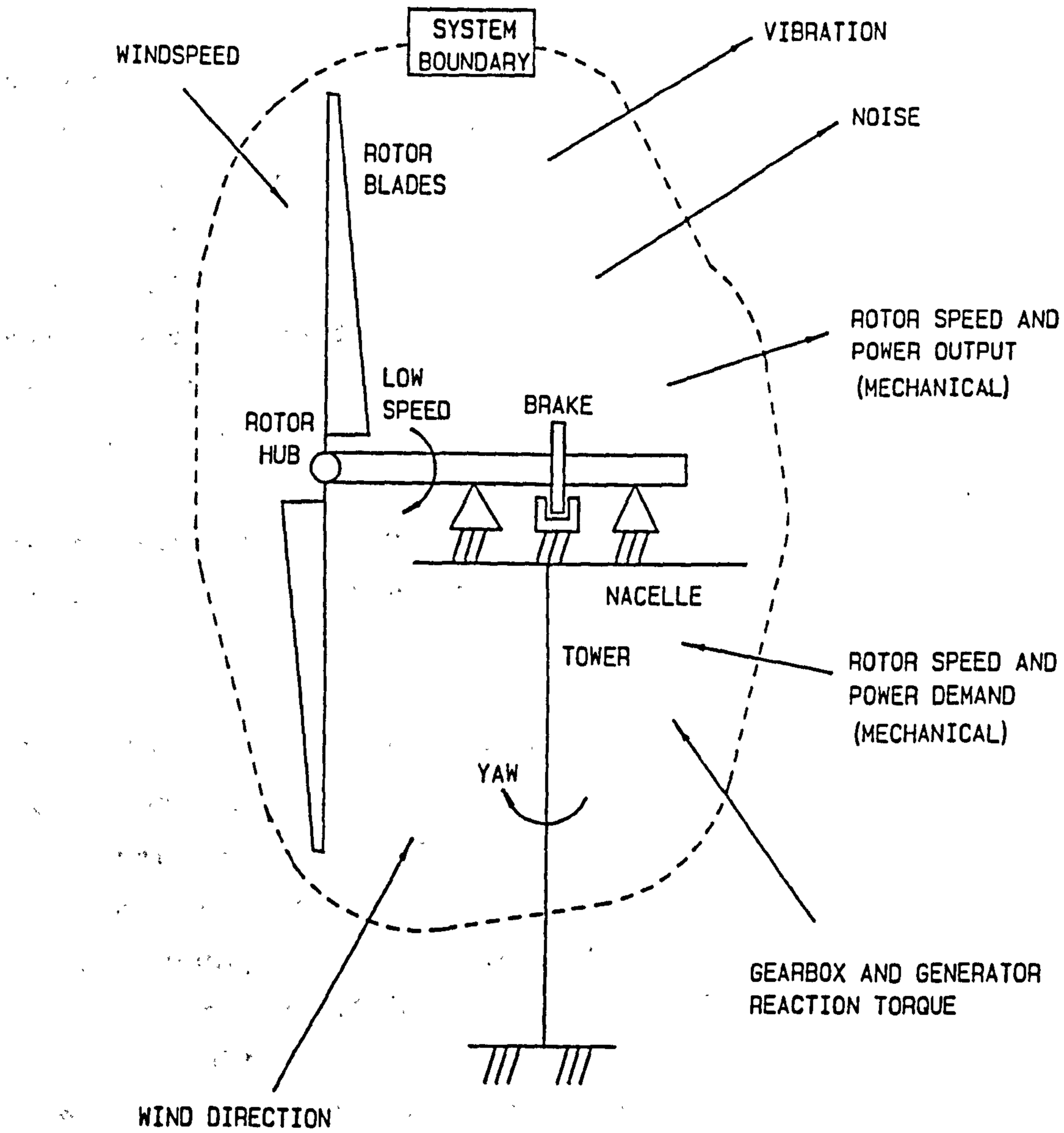

Figure 3.2: Elements of a reduced wind turbine system

Control methods for both HAWTs and VAWTs were considered in a literature search that included many technical papers and journal publications. When considering vertical-axis configurations specifically, it is noted that the angle of attack of the relative flow incidence on the blade varies cyclically. Even when the upstream windspeed and rotor speed remain constant, the angle of attack of the relative flow will oscillate about the blade chord as it rotates from the upstream pass of its cycle to the downstream pass, and vice versa. For an H-VAWT, where the blades are set parallel to the axis of rotation, the magnitude of the peak-to-peak variation of angle of attack decreases as tip speed ratio increases. This variation is essentially similar across the whole span of the blade (ignoring tip effects and spanwise flows). As the rotor speed decreases, the magnitude of the variation will increase, until complete reversal will be experienced in some parts of the cycle when the tip speed ratio is less than unity.

The blades of the V-VAWT are inclined to the axis of rotation, and as such the local speed ratio varies across the span of the blade. Consequently, the magnitude of the cyclic variation of angle of attack varies across the blade span. In contrast, there is no such cyclic variation of angle of attack with HAWTs. Fluctuations that do occur result from local variations of windspeed within the swept area of the wind turbine. However, this difference does not prevent the aerodynamaic control methods utilised on HAWTs to be considered for use with the V-VAWT. The upstream pass of a VAWT rotor has more energy available for capture than the downstream pass, and during each half of the rotation the sign of the angle of attack remains constant. Essentially, provided a greater control effect can be achieved on the upstream pass than on the downstream pass, a net effect can be gained using HAWT control methods for VAWT applications. The straight blade

configuration of the V-VAWT lends itself to HAWT type control surfaces and actuators being fitted. These can be operated in much the same manner as they would be on a HAWT, but the detail design would obviously differ because of the different rotor configurations.

With this in mind, it was convenient to commence the literature search by initially considering current HAWT control methods. The search was then broadened to consider VAWT control options, and to assess the possibility of sucessfully adapting any of these control methods to V-VAWT applications. In the review presented here, each control method will be considered in turn. A more detailed review can be found in the author's interim report [32], which was the basis of a seminar prepared and presented by the author at the Open University.

3.2.1: Full-span Pitch Control

Full-span pitch control is being used on HAWTs of all sizes for both speed and power regulation. The pitch of the blade of the blade is the angle between the chord line of the aerofoil and the plane of the rotor disc. To achieve good aerodynamic efficiencies, the blade of a HAWT is designed with preset pitch (twist) that varies acros the blade span. However, if the rotational speed of the rotor and the upstream windspeed remain constant, then changing the pitch of the blade during operation will change the angle of attack of the wind at all points along the span of the blade. In this way, the induced aerodynamic lift and drag forces acting on the blade can be modified, and a resultant change in rotor power can be effected. The change in blade pitch may be actively or passively controlled, and can be towards either the feather or stall directions.

In the feather option, the blade is rotated into wind, reducing the angle of attack of the resultant wind vector on the blade. Aerodynamic lift force will be reduced and a net reduction in the aerodynamic loads on the blade will result. The torque developed by the rotor will be reduced as the loss of lift across the whole blade is effected.

In the stall option, the blade is rotated away from the wind and aerodynamic stalling of the blade invoked. Small variations in lift force will occur, but the drag forces induced by moving towards and beyond the stall condition of the aerofoil are significantly greater than for the feather option. The rapid increase in drag force results in an overall increase in the aerodynamic load on the blade. The large increase in drag serves to counteract the lift forces still being induced, resulting in a rapid reduction in the torque developed by the rotor.

Since the aerodynamic forces are varied across the whole blade span, the torque developed by the rotor is sensitive to small blade pitch changes, allowing a rapid response to any control need. This feature ensures that full-span variable pitch is suitable for power and speed control purposes. The advantages and disadvantages of the approach are summarised by Ketley and Quarton [33], and illustrated in Figure 3.3.

Full-span pitch control requires the whole blade to be free to rotate about its spanwise axis. The blade must, therefore, be fully supported at its root by the hub bearing. The blades are effectively cantilevered, with no additional support or bracing attached. The design of these blades requires careful attention to detail at the blade root and hub fixings, but have un-interrupted surfaces that will give good aerodynamic performance.

VARIABLE PITCH-REDUCING INCIDENCE

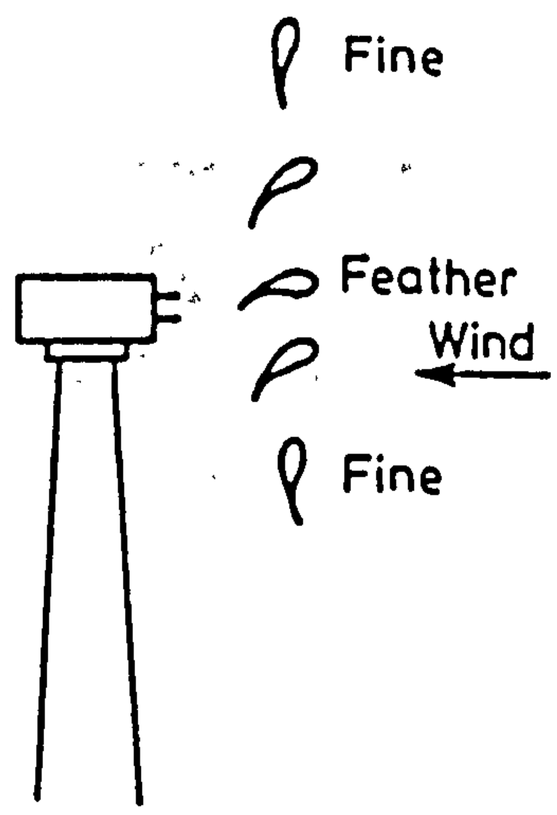

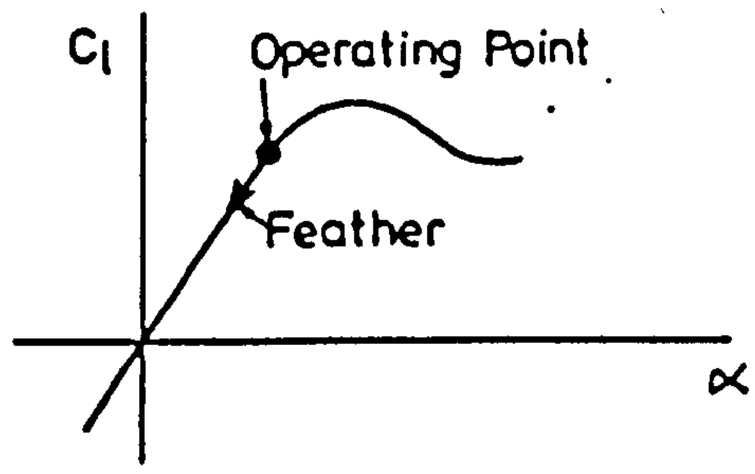

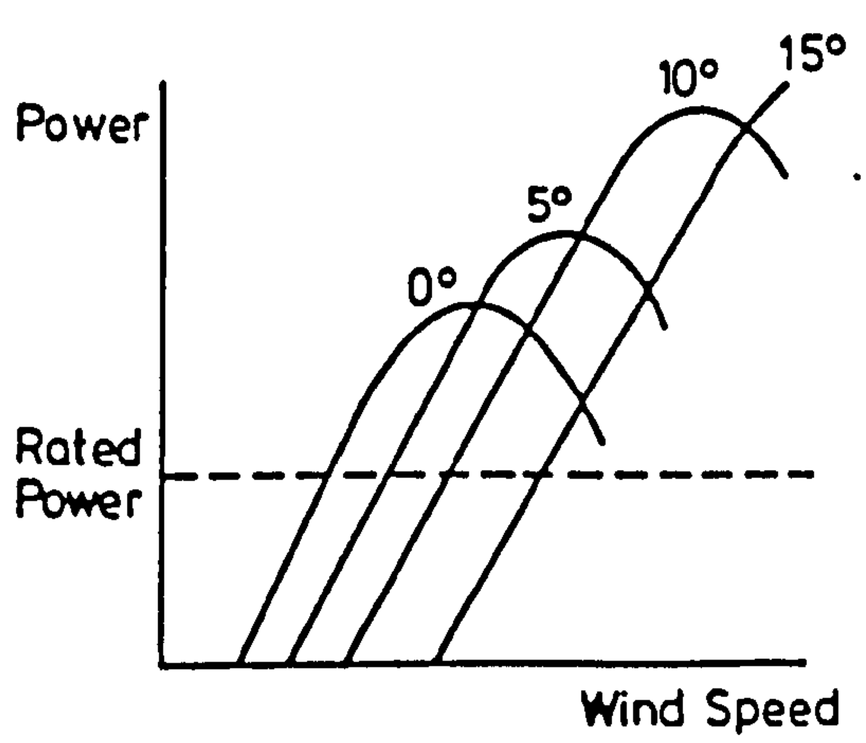

PROS
Good Power Control
Aero Damping
Reducing Loads
Off Loaded Stationary
Assisted Start-Up
Built-In Braking

CONS
Cost of Pitch Mechanism
Extra Complexity

Figure 3.3a: Full-span pitch control, feather option [33]

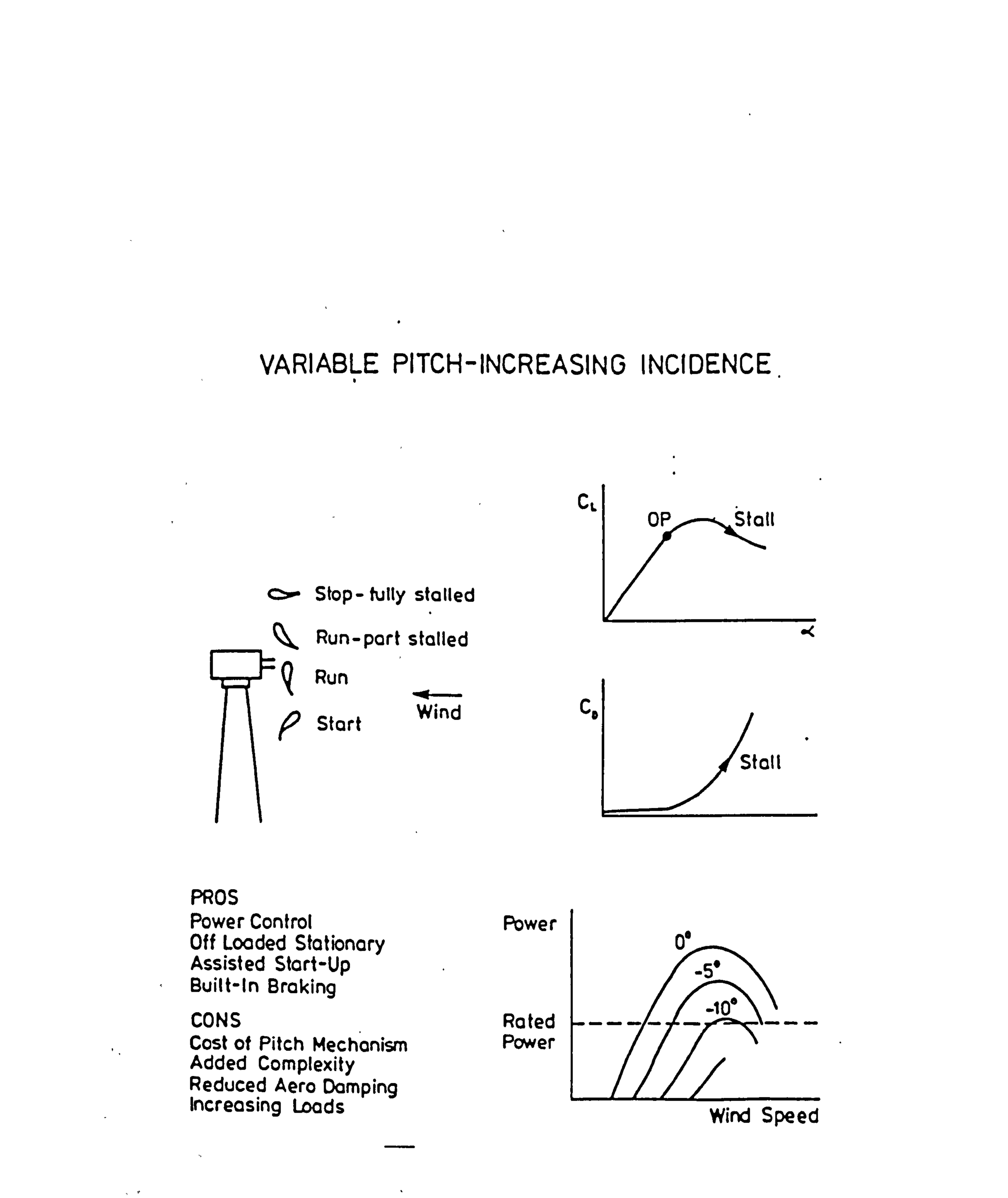

Figure 3.3b: Full-span pitch control, stall option [33]

Pitching mechanisms for medium and large sized machines are incorporated into the hub itself, allowing simplified blade root fixings to be used. The nature of the pitch mechanism and actuator are, however, dependent on the size of machine and the accuracy of control required. Localised pitch mechanisms act on one blade only, enabling each blade to be independently controlled and its pitch adjusted to suit local variations of windspeed. There is a possibility that each blade will change its pitch at a different time or different rate to the others, which could result in the rotor becoming unbalanced. Centralisation of the pitch mechanism requires each blade to be linked to a common actuator, but ensures that each blade is operating in the same manner as the others. Failure of the link may result in complete loss of pitch control, so it is good practice to include other 'fail-safe' features.

The actuation of the pitch mechanism may be passive or active. Passive actuation utilises the forces that normally act on the wind turbine to activate the pitch mechanism, whereas active control requires some evaluation of the state of the rotor to be made, usually by measurement, and the control action determined accordingly by, say, a computer controller. The pitch mechanism is then activated by some auxillary force.

Centrifugal and aerodynamic moment forces can be used on small machines to passively control blade pitch. The famous Jacobs wind turbine, first patented in 1929 [34], used a flyball governor placed in the rotor hub to control blade pitch using centrifugal force. Internal linkages and gears ensured actuation of each blade was centralised. The Flexbeam concept developed by United Technologies for a 8 kW HAWT [35] utilises a flexible spar to connect each blade to the rotor hub. This allows the blade to be structurally stiff, and the root/hub connection to be

rigid. Each blade is allowed to pitch by twisting about the flexible spar. Flyball governors control the pitching movement. This technique was adopted by Windtech for an 80 kW HAWT, which suggests the device is suitable for small and medium sized machines. Similarly, the natural tendency of a blade to twist due the offset between the aerodynamic pressure centre and the flexural centre of the aerofoil can be used to invoke blade pitching. The Bergey Powerflex wind turbine range [36] is designed with torsionally elastic blades that are designed to twist about the root fixing, thereby modifying the blade pitch. Finally an FDO/Holec/Fokker HAWT design proposal [37] uses aerodynamic forces to twist in pitch the blades of a large 2.5 MW wind turbine.

The utilisation of these passive actuators is limited by the ability of the designer to ensure the behaviour of the pitch mechanism can be guaranteed. Once the actuator and pitch mechanism have been designed, there is little scope for modification of the control effect that is now embodied in the rotor. Where the power and speed control characteristics are required to be modified, and control of the speed and accuracy of the pitch response is required, active control is necessary. The use of pneumatic, hydraulic or electrical devices to apply the required actuating forces to the pitch mechanism, offers the designer great scope for controlling the blade pitch angle and the response of the system to external changes. This is especially true where computer controllers are used. Active control, however, requires some evaluation of the state of the wind turbine to be made. Monitoring the performance of the machine and the state of the environment will enable the optimum pitch angle of the blades to be specified by the controller. The response of the control system can, therefore, be accurately and reliably controlled, ensuring good power and speed

characteristics. The majority of current medium and large sized HAWTs using full-span pitch control, such as the WEG MS-2 250 kW and KaMeWa 2 MW HAWTs, utilise active control to ensure the desired control effect is guaranteed.

In assessing the suitability of full-span pitch control for VAWTs, only those machines with straight blades, such as the H-VAWT and V-VAWT, can be seriously considered. The curved blades of the troposkein Darrieus VAWTs are generally fixed at the blade ends and cannot be twisted or rotated in pitch during operation. Klimas has, however, reported upto 25% changes in peak efficiency and peak power output for a Darrieus VAWT with preset pitch [38]. The range of pitch angle settings was only ±5° and full power control cannot be achieved within this range.

The principles of the control method are the same for VAWT applications as for HAWTs, however, the cyclic variation of angle of attack on the blades results in a different overall effect. The angle of attack of the resultant velocity vector varies cyclically as the blade moves around its axis and makes upwind and downwind passes. In conventional VAWT configurations, the blade extracts more energy from the upwind pass than from the downwind pass, therefore, a power regulation effect can be gained using full-span pitching if the pitch angle change is suited to upwind blade passes. For instance, the feather option would require a 'nose-out' rotation of the blade. Small pitch angle changes in this direction, would generally reduce the angle of attack on the upwind pass but increase it on the downwind pass. Alternatively, the stall option would require a 'nose-in' rotation of the blade which, for small pitch angle changes, would generally increase the angle of attack on the upwind pass and reduce it on the downwind pass of the cycle. To ensure an overall power regulation effect is achieved, any energy gains made

around the cycle must be countered by greater energy losses elsewhere. Since the energy available on the upwind pass is greater than on the downwind pass, modifying the blade pitch to ensure reduced energy capture on the upwind pass will generally give an overall reduction in energy capture.

Small 'nose-out' pitch changes can actually increase the energy capture of the rotor. Since the resultant wind vector acting on the VAWT blade continually moves from one side of the blade to the other, the blade is positioned with its chord set tangentially to its circular path of movement. This position ensures a good compromise is achieved between upwind and downwind passes. However, Stacey and Musgrove [39], have observed that small full-span pitch offsets in the 'nose-out' direction increased the overall power output of an H-VAWT. The pitch offset was fixed and a maximum offset of 3½° gave best results. Clearly, this small change increased the effectiveness of the upwind pass without significantly reducing that of the downwind pass. It must be noted, though, that the pitch offset was preset, and that no variation of blade pitch was possible during operation.

The author is aware of only a few instances of H-VAWTs being constructed with variable pitch blades, most notably the VAWTs constructed by Evans at St. Andrews University and by Grylls and Dale at Exeter University, Figure 3.4a. At low rotational speeds, the Evans VAWT allowed the the blades to pitch passively under the influence of aerodynamic forces. However, as rotational speed increased, the pitch of the blade became effectively fixed as centrifugal forces overcame the aerodynamic forces and "locked" the blade in its normal operating position. The Exeter University machine was used for the cyclic pitch studies reported by Grylls and Dale [40].

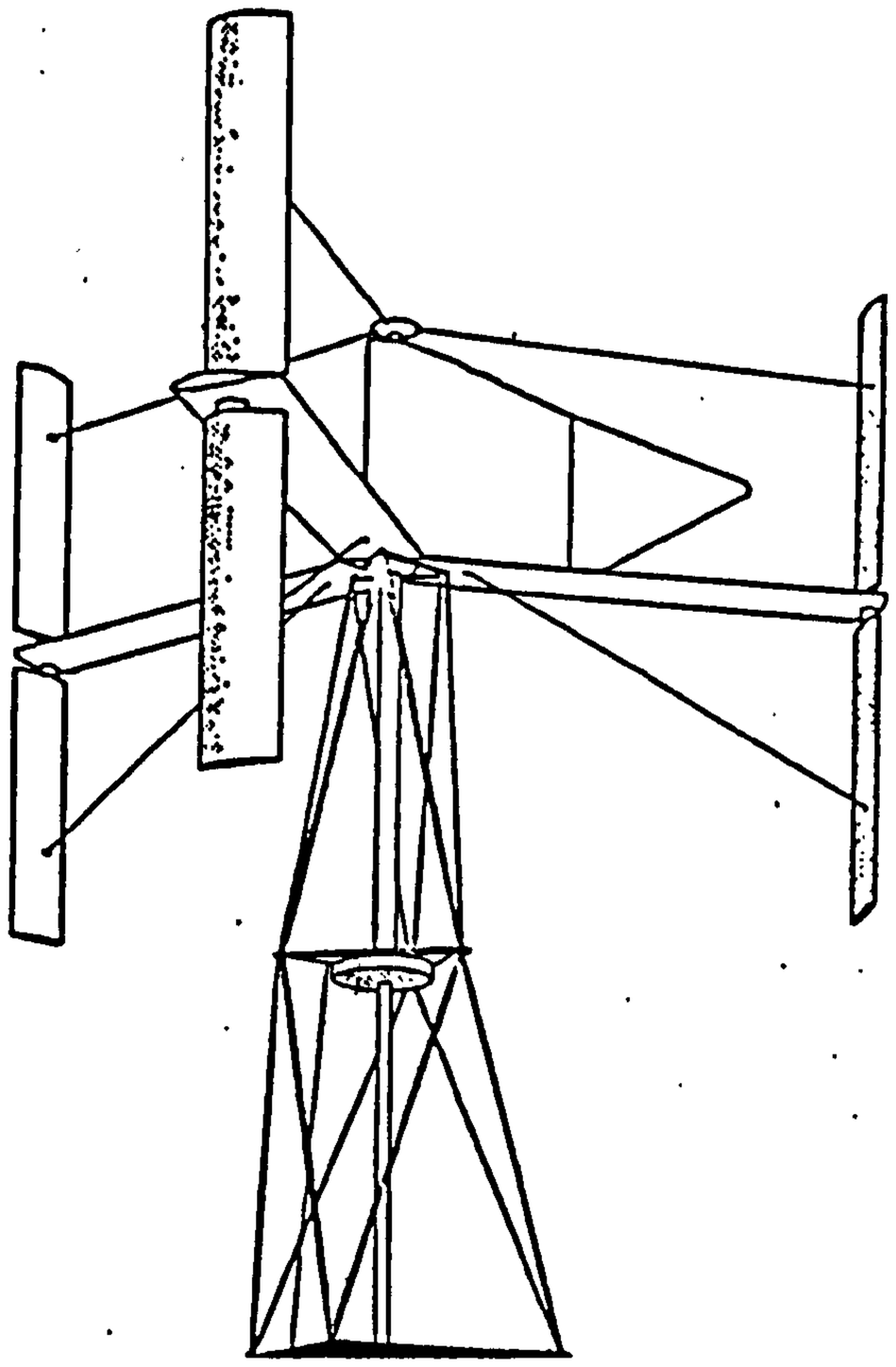

Figure 3.4a: Exeter University's Variable Pitch VAWT [40]

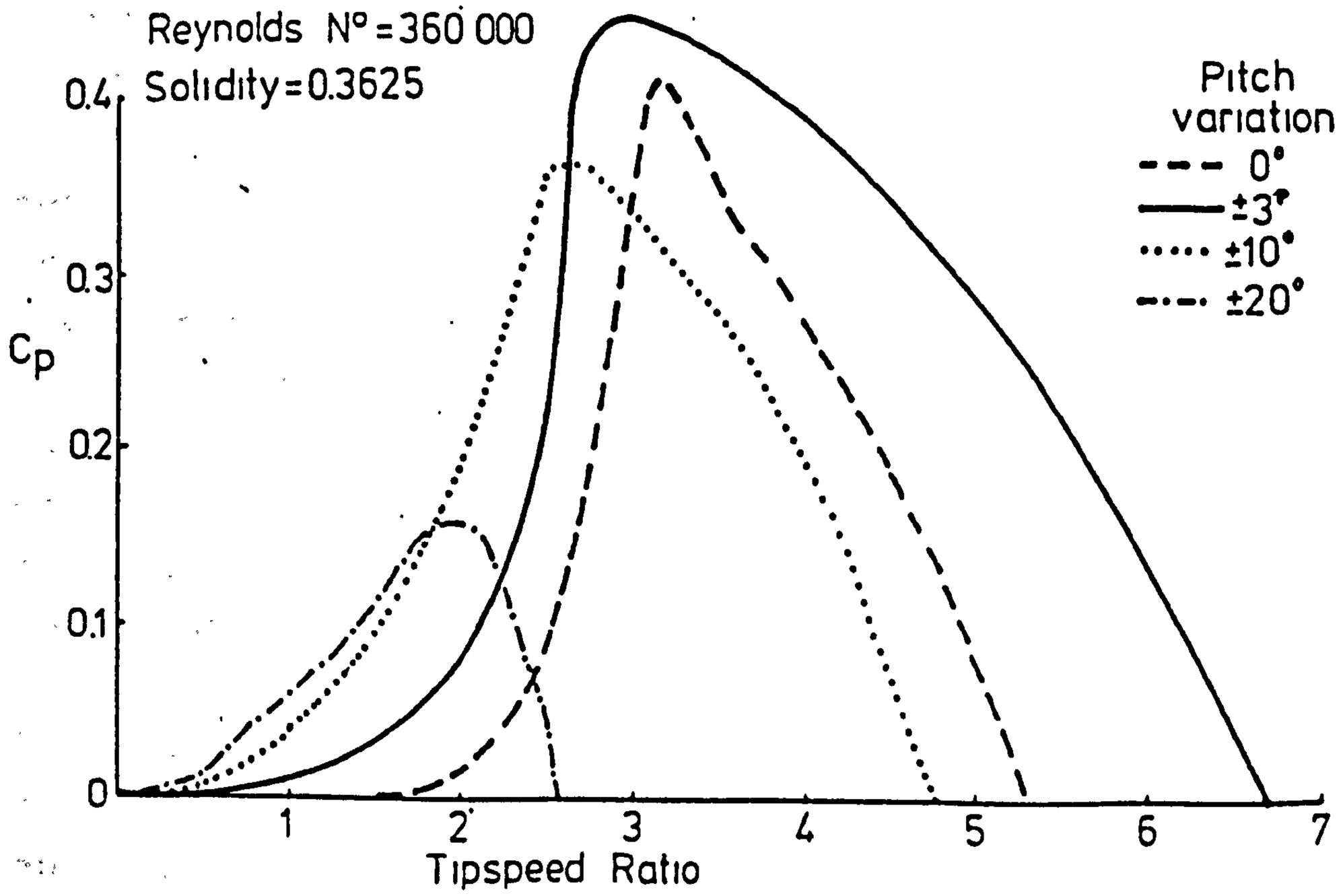

Figure 3.4b: C_{p_m} versus λ for a variety of pitch half amplitudes of Exeter University's VAWT [40]

The Exeter VAWT did not use blade pitch to regulate power output or provide overspeed control, but instead varied the pitch of the VAWT continuously to optimise the angle of attack of the relative flow to the blades through the rotation cycle. The aim was to minimise the variation of both the torque and aerodynamic loads of the rotor, and so maximise the efficiency of the VAWT by extracting as much energy as possible throughout its cycle. Torque smoothing is highly desirable, especially with two-bladed VAWTs that are used for electricity generation. Unless damped, the variation of torque from a VAWT results in an undesirable ripple in electrical output.

The Exeter H-VAWT used a wind vane to sense the direction of the wind and a cam to control the pitch of each blade through the rotation cycle. The wind vane would ensure that optimum cyclic pitch variation was achieved even if the wind direction changed. The variation of pitch angle was sinusoidal, and wind tunnel tests showed that power output could be significantly enhanced with only small pitch angle changes, Figure 3.4b. A sinusoidal variation with an amplitude of ±3° gave best results. A 9% improvement of peak C_P was observed, and a general improvement of torque at low tip speed ratios noted. Larger pitch amplitudes gave even better results at low tip speed ratios, but were detrimental to performance at the higher rotational speeds. The amplitude of the cyclic pitch variation could not be altered during operation, so it was not possible to optimise the machine performance for each tip speed ratio.

It should be noted that the mid-span blade fixing to the crossarm bearing posed particular technical difficulties, and that such difficulties will be manifest in any H-VAWT configuration that uses full-span pitch control. To allow the blades freedom to rotate in pitch, does not enable

additional support or bracing devices to be attached, requiring all loads to be supported at the blade bearing.

Full-span pitch control offers both power regulation and speed control for VAWTs, but its application is limited to straight bladed machines. Activation can be active or passive, though aerodynamic moment actuation would not be suitable because of the cyclic variation of aerodynamic forces on the blade. The response of the rotor to any control action can be rapid, as the torque developed by the rotor results from aerodynamic force changes along the whole blade.

To conclude, full-span pitch control has the following advantages:

(a) suitable for all machine sizes
(b) suitable for power regulation during normal running
(c) suitable for overspeed protection
(d) active or passive actuation
(e) rapid power changes for any given pitch change
(f) possible to optimise rotor efficiency including cyclic pitch control

and disadvantages:

(a) highly loaded blade bearings
(b) large actuating forces required to move blades accurately and quickly
(c) pitch mechanism potential source of failure
(d) additional cost of pitch mechanism and control system
(e) unsuitable for curve bladed Darrieus VAWTs

3.2.2: Partial-span Pitch Control

Partial-span pitch control utilises the same principles of operation as full-span pitch control, in that changing the pitch of the blade alters the aerodynamic force characteristics of the blade. However, rather than change the pitch of the whole blade, only a small portion of the blade is moved. If the blade tip section is used as the control surface, then the inner portion of the blade can be rigidly fixed at the blade root/hub bearing, simplifying this aspect of rotor design.

The significance of the power and speed regulation effect will depend upon the relative size of the moveable tip portion to the fixed pitch portion of the blade, but utilising the outer 20% to 30% of the blade seems to give acceptable control performance in most cases. Feather or stall options are used on HAWTs, for example the 2.5 MW MOD-2 HAWT moves the tip towards the feather position, while the Howden HWP 300 HAWT moves the tips to the stall position. However, since the inner portion of the blade is fixed in pitch, this area will continue to produce useful lift even when the tips have been deployed. The reduction in power at the tips must overcome any increase in power developed by the fixed blade portion. This necessarily requires larger pitch angle changes than for full-span pitch control, but the smaller inertial mass of the tip section allows pitch changes to be far quicker and pitch mechanisms to be smaller.

A structural advantage gained is that the blade may be rigidly fixed to the hub at its root and supported near to the tip by some bracing structure. The tip section bearing and pitching mechanism, however, must now be placed at some outboard position. The pitching mechanism may be carried either in the fixed inner portion of the

blade or in the tip section itself. In either case the mass of the blade is increased and larger structural loads will be imposed at the blade root by placing the mechanism away from the it. Moving the pitching mechanism inboard will reduce such loads, but cables or linkages must be used to control the tip section.

The actuator may be centrally of locally placed, and in essence the same devices considered for full-span pitch control can be used. Centralised operation of the tips requires some linkage or connection to be made to local pitch mechanisms, and in general local actuation is preferred. Active control is a weakness of any wind turbine system because if they fail, the safety of the rotor is jeopardised. The first of the MOD 2 wind turbines experienced such a failure during a routine overspeed test. A hydraulic tip pitch actuator failed to feather one of the tips during this test, consequently when the electrical load was disconnected, the rotor accelerated from 17.5 rpm to 29.5 rpm before the tip was eventually feathered. Extensive damage to the low speed shaft and generator was caused by this failure. Modifications to the control circuit and controller logic had to be made before operation of the wind turbine resumed. Good design demands 'fail-safe' operation of the control system.

The use of partial-span pitch control to regulate VAWTs has received little or no interest. To date, only one H-VAWT, the Westwind 75 kW VAWT, is known to have operated with this control option, Figure 3.5a. Little is known by the author of this machine, but Sharpe has recently estimated the effect of variable pitch on its performance [41], Figure 3.5b. Sharpe observes that the tip pitch control allows the Westwind VAWT to operate in windspeeds upto 36 m/s while maintaining a constant power output of

Figure 3.5a: Westwind 75 kW VAWT

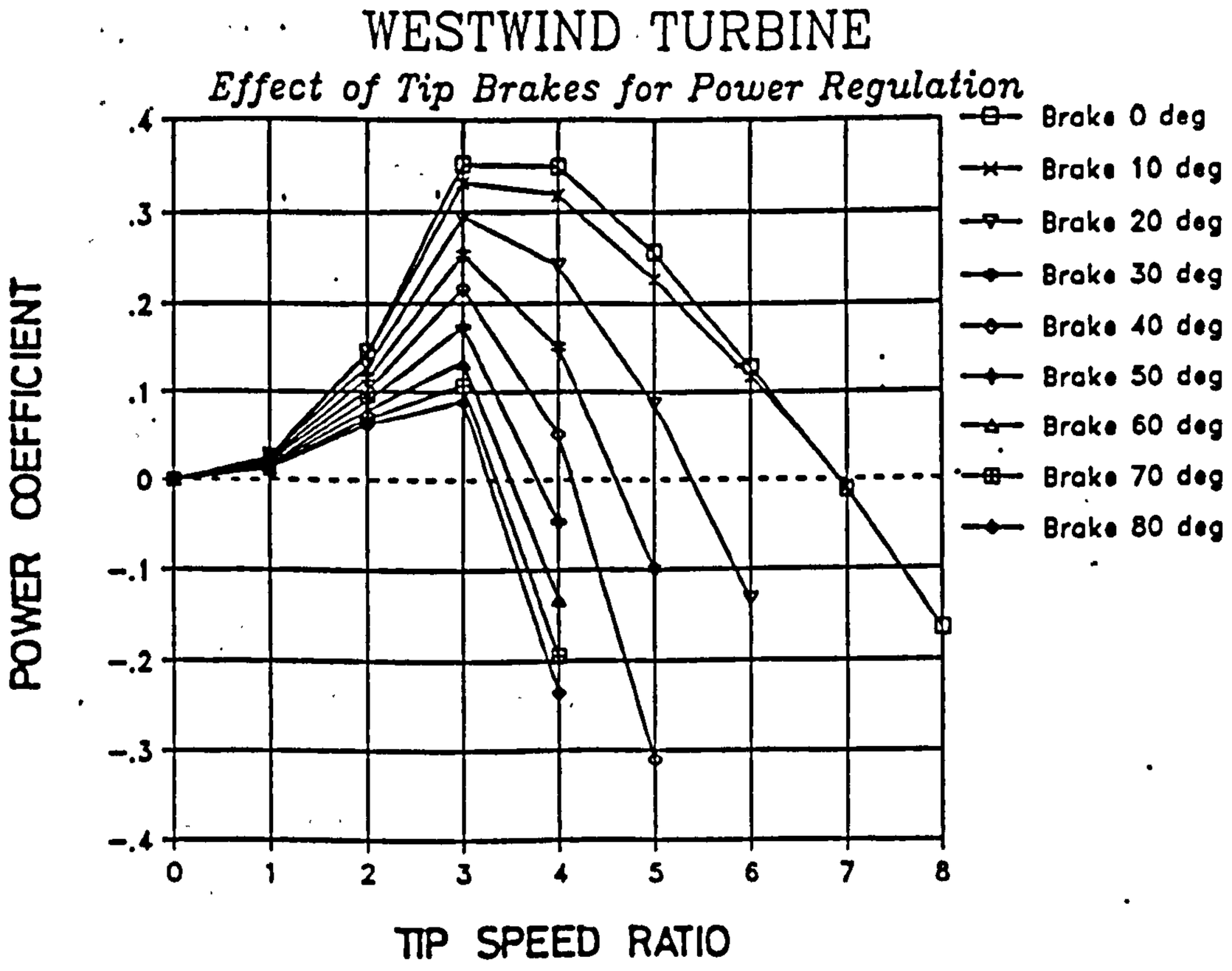

Figure 3.5b: C_{pm} - λ characteristic of Westwind VAWT for various tip pitch angles [41]

75 kW at a rotor speed of 40 rpm. However, since the total area of the tip section is only 6% of the total blade area, the power output of the rotor cannot be reduced to less than zero in high windspeeds, so the tip pitch control is unsuitable for high windspeed shutdown.

Considering that some studies of VAWT performance have been made using full-span pitch control, the author is surprised that the partial-span pitch control option has not been considered further. In their original description of the V-VAWT [9], Sharpe and Taylor suggest variable tip pitch as a possible control option, and the design proposals shown in the previous chapter illustrate their use.

Structurally the advantages and disadvantages of the approach are the same for VAWTs as for HAWTs, and provided the aerodynamic effectiveness of partial-span pitch control for the V-VAWT can be demonstrated, it seems a highly suitable control option.

To conclude, partial span pitch control has the following advantages:

(a) suitable for all machine sizes
(b) suitable for power regulation during normal running
(c) suitable for overspeed protection
(d) active or passive actuation
(e) rapid power changes for any given pitch change
(f) possible to optimise rotor efficiency
(g) simple blade/hub connection
(h) small activation forces required

and disadvantages:

(a) reduces power only at tip section
(b) complicated blade construction with pitching mechanism located near blade tip
(c) pitch mechanism potential source of failure
(d) additional cost of pitch mechanism and control system
(e) unsuitable for curve-bladed Darrieus VAWTs

3.2.3: Shaft Brakes

Shaft brakes for all but the smallest HAWTs, can only be considered suitable for the prevention of overspeed when other control devices have failed, and for stopping the rotor from low rotational speeds during a controlled shut-down. All commercial HAWTs have shaft brakes fitted for this purpose, and use other means to regulate rotor power and speed.

Friction brakes are wholly unsuitable for rotor speed regulation during normal operation, because prolonged activation while highly loaded would lead to overheating and eventual failure. Shaft brakes are used only for low rotational speed activation, but are designed with a capacity to stop the rotor overspeeding when all other control means have failed. Emergency action may render the brake unservicable, but if its prevents the rotor from being damaged, then it is a cost-effective solution.

Good design practice is to place a high torque brake on the low speed shaft where its braking torque can be applied directly to the rotor. Disc brakes are commonly used, but need to be overly large to achieve the high torque capacity required in this application. Placing the brake on the high speed shaft allows smaller, low torque brakes to be used. In this case, the braking torque must

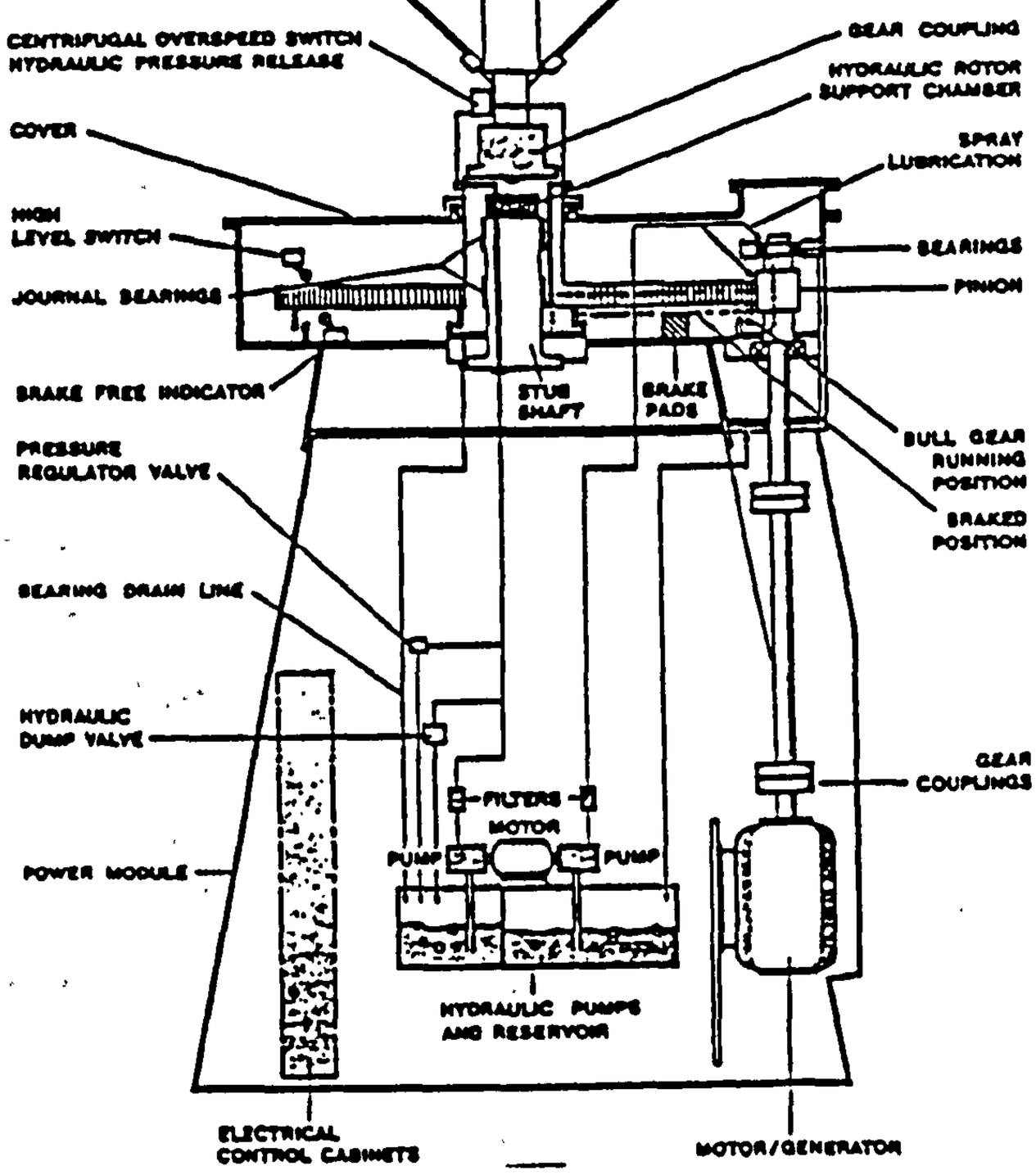

Figure 3.6: DAF-Indal 50 kW VAWT hydraulically released stationary pad rotor brake

be applied to the rotor via the transmission system. This layout may damage the coupling and gearbox elements of the transmission, especially during emergency shutdowns.

The author is unaware of any HAWT currently using shaft brakes as a power and speed control device. Similarly, the use of shaft brakes for VAWTs has the same limitations as discussed above, and again the author is unaware of any VAWT currently using shaft brakes for control.

As a fail-safe device, stationary disc pad brakes have been used by DAF-Indal for curve-bladed VAWTs in an elegant and effective way, Figure 3.6. The approach is described fully by Templin and Rangi [42], but briefly, the system utilises the weight of the rotor and the tension in the guy cables supporting the rotor to engage the bull gear at the base of the rotor with four stationary brake pads. During normal operation, the rotor is raised off the pads by the hydraulic pressure of the externally pressurised rotor bearing. When the pressure in the system is released, the rotor will descend and contact is made between the gear and the pads.

To conclude, shaft brakes have the following advantages:

(a) existing element of wind turbine systems
(b) active or passive actuation
(c) prevents self-starting
(d) acts directly onto low-speed shaft

and disadvantages:

(a) unsuitable for accurate power regulation
(b) limited to low speed use, except in emergencies
(c) aerodynamic loads on blades are not reduced
(d) no power augmentation

3.2.4: Rotor Yaw

The yaw angle is the angle of mis-alignment between the rotor axis of rotation and the direction of the oncoming wind. To ensure maximum energy capture, a HAWT rotor must face directly into wind so that the yaw angle is zero. As the rotor is turned away from the wind, the component of the windspeed vector perpendicular to the rotor disc will vary with the cosine of the yaw angle. Consequently, varying the yaw angle would enable the power and speed of the rotor to be regulated.

All HAWTs are equipped with yaw drives of somekind, however, these devices are primarily used to turn the rotor into wind should the wind direction change. The fantail of the Traditional Windmill has been adopted by many European manufacturers as a passive yaw drive for medium sized machines. This device is, however, unsuitable as an actuator for power and speed control. Larger machines require active yaw control systems but, for power or speed control, these systems are unsuitable because of their slow response to change. Only the tailvanes fitted to small machines provide suitable power control characteristics, because these devices respond directly to the strength of the wind.

Moving the rotor in yaw while it is operating will invoke gyroscopic forces that are proportional to both the rate of change of yaw angle and the inertia of the rotor itself. Rapid yaw angle changes in response to, say, gusting, could invoke large gyroscopic forces with potentially dangerous results if utilised on anything but the smallest of rotor sizes. It is more common on medium and large scale HAWTs to use the yaw drive to park the rotor obliquely to the wind during shutdown; this ensures

minimal aerodynamic forces act on the rotor during these periods.

When considering VAWTs, the equivalent of HAWT yaw may, at first, be considered as a movement of the rotor about its axis of rotation. This movement is more commonly termed azimuthal movement, since the axis of rotation is vertical to the ground. Clearly, controlling azimuth angle during normal operation is not feasible, but, like HAWTs, the aerodynamic forces on the VAWT rotor can be significantly reduced during shutdown by parking the rotor at some oblique azimuth angle to the wind.

A better analogy to HAWT yaw in the VAWT case, would be that of tilting the rotor about the root of the tower. However, this is impracticable during normal operation and need not be considered further.

To conclude, yaw control for VAWTs i.e. azimuth angle control, has the following advantages:

(a) minimise aerodynamic forces on whole rotor during shutdown periods

and disadvantages:

(a) unsuitable for power and speed control during normal operation since azimuthal angle continually changes

3.2.5: Rotor Tilt

Tilting the rotor, usually upwards, has the same effect as rotor yaw, and the characteristics of this control method are the same. Little advantage, if any, is gained in the

control characteristic, but a major disadvantage is that the HAWT must now be allowed an additional degree of freedom to the movement of the rotor. As with yaw control, the rotor can be parked during shutdown in a position of minimum aerodynamic load.

Tilting the rotor of a VAWT is only possible on small machines where the rotor would be mounted off the ground, and the blades would not foul the ground when tilted. To ensure effective power regulation during tilting, the tilt axis must be set perpendicular to the wind direction. To achieve this, the tilt axis itself must be able to yaw, consequently VAWT tilt requires two additional degrees of freedom of movement of the rotor. Clearly, the complexity of this approach makes this control option impracticable, even for the smallest VAWTs.

To conclude, rotor tilt is considered highly unsuitable for VAWT applications.

3.2.6: Blade Coning

Blade coning requires each blade to be hinged at its root to allow spanwise rotation into or out of wind. The power developed by the rotor is reduced in three ways. Firstly, the swept area of the rotor is reduced, secondly the magnitude of the windspeed component normal to blades is reduced, and finally the moment arm of the aerodynamic chordwise forces on the blade about the axis of rotation is reduced. The combined effect of these actions is that significant power output changes can be quickly made with only small coning angle displacements, which is highly suitable for the alleviation of gust loads. Flexible blade root mountings allow small coning movements to occur passively as increasing wind forces act on the rotor.

Small coning movements would not allow complete power control at high windspeeds, because large coning angles are required to give the necessary power reductions in these conditions. The blades must, therefore, be hinged to give freedom of movement through larger cone angles. Complete rolling of the blades to a horizontal position cannot be practically achieved, so rotor power cannot be reduced completely to zero. The addition of a centrifugal actuator would ensure that rotor overspeeding is prevented using the coning action, however, the forces from the actuator must overcome the centrifugal forces on the blade resisting such movement. In this way, both power and speed control can be passively controlled.

In reality, full blade coning is only viable on small machines where the large blade movements can more easily be tolerated. However, many large HAWTs include some flexibility in either the blade/hub or hub/low-speed shaft connection. Teetering of the large blades significantly reduces the structural loads experienced at the blade root during a gust, extending the life in service of the rotor.

The principles of blade coning can be applied to straight bladed VAWTs. The early versions of the Variable Geometry VAWT (VG-VAWT) first described by Musgrove [43], and then by Stacey [44], allowed full blade rolling about the blade/crossarm connection in the flapwise direction for this particular H-VAWT design, Figure 3.7. This movement of the blade can be considered as a VAWT equivalent of HAWT coning. The blade angle to the vertical was changed by the action of centrifugal force, allowing the speed and power of the rotor to be regulated. This control method was adopted by P.I. Specialists for a commercial 6 m VAWT in which the blade rolling was restrained by spring loaded cables, Figure 3.8

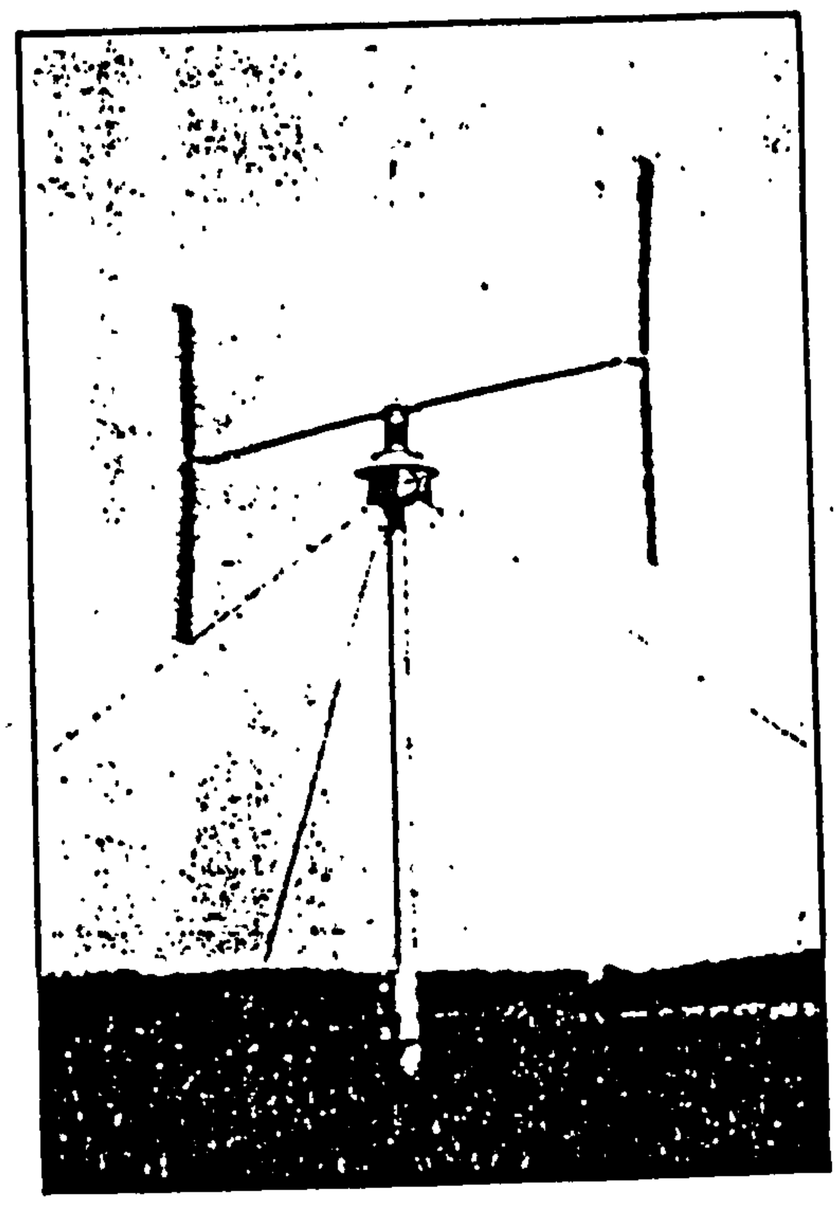

Figure 3.7: Musgrove 4.5 m diameter prototype VG-VAWT

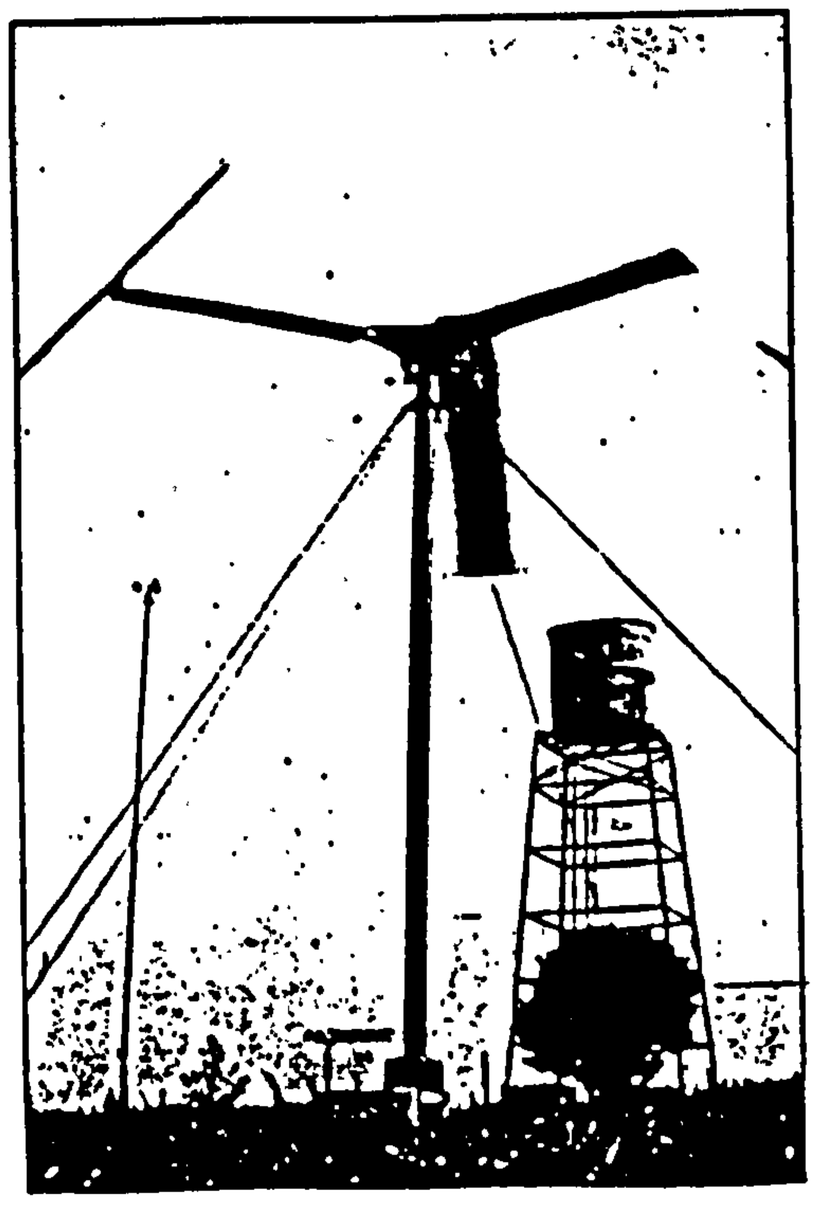

Figure 3.8: P.I. Specialists 6 m diameter VG-VAWT

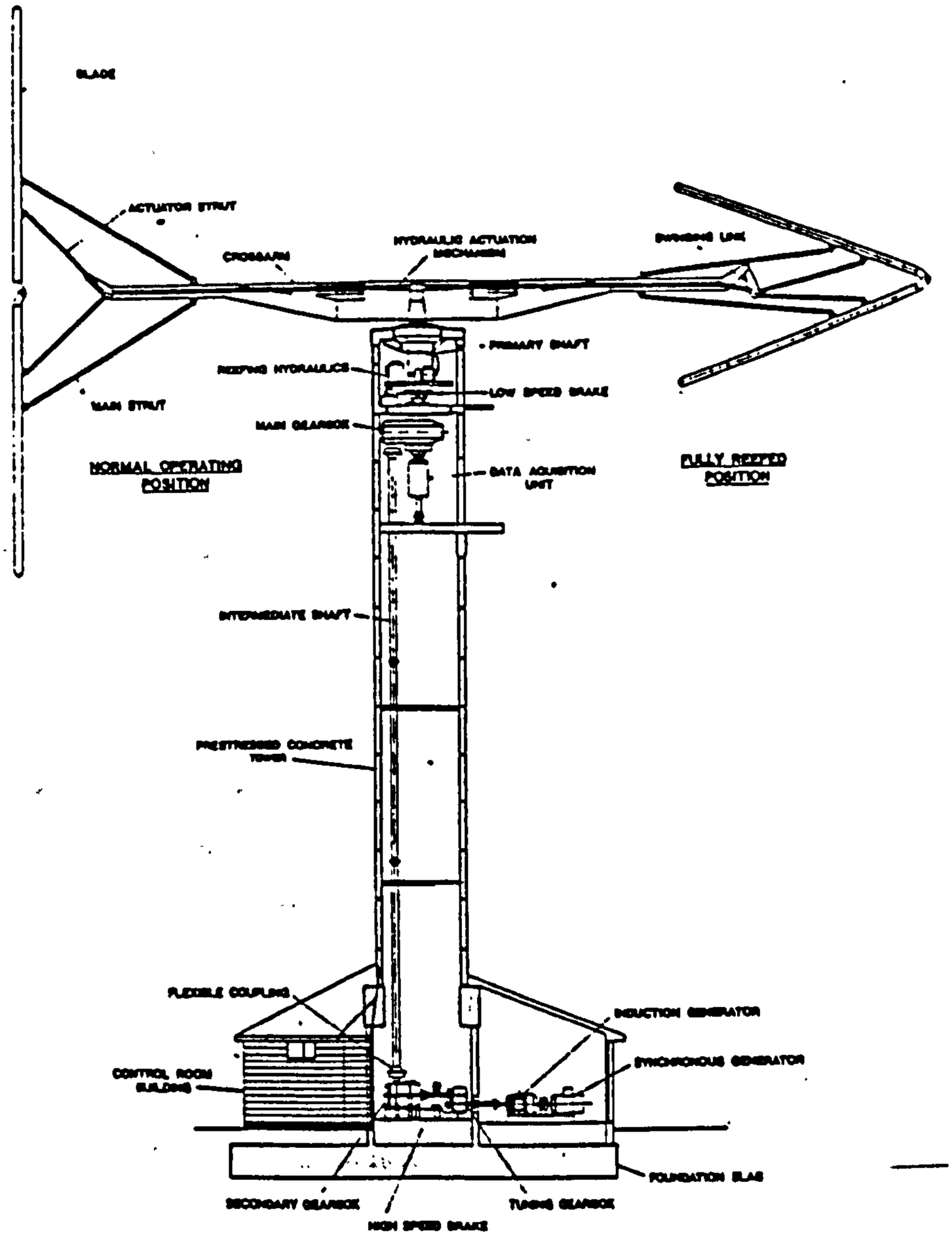

Figure 3.9a: Carmarthen Bay 25 m diameter VG-VAWT

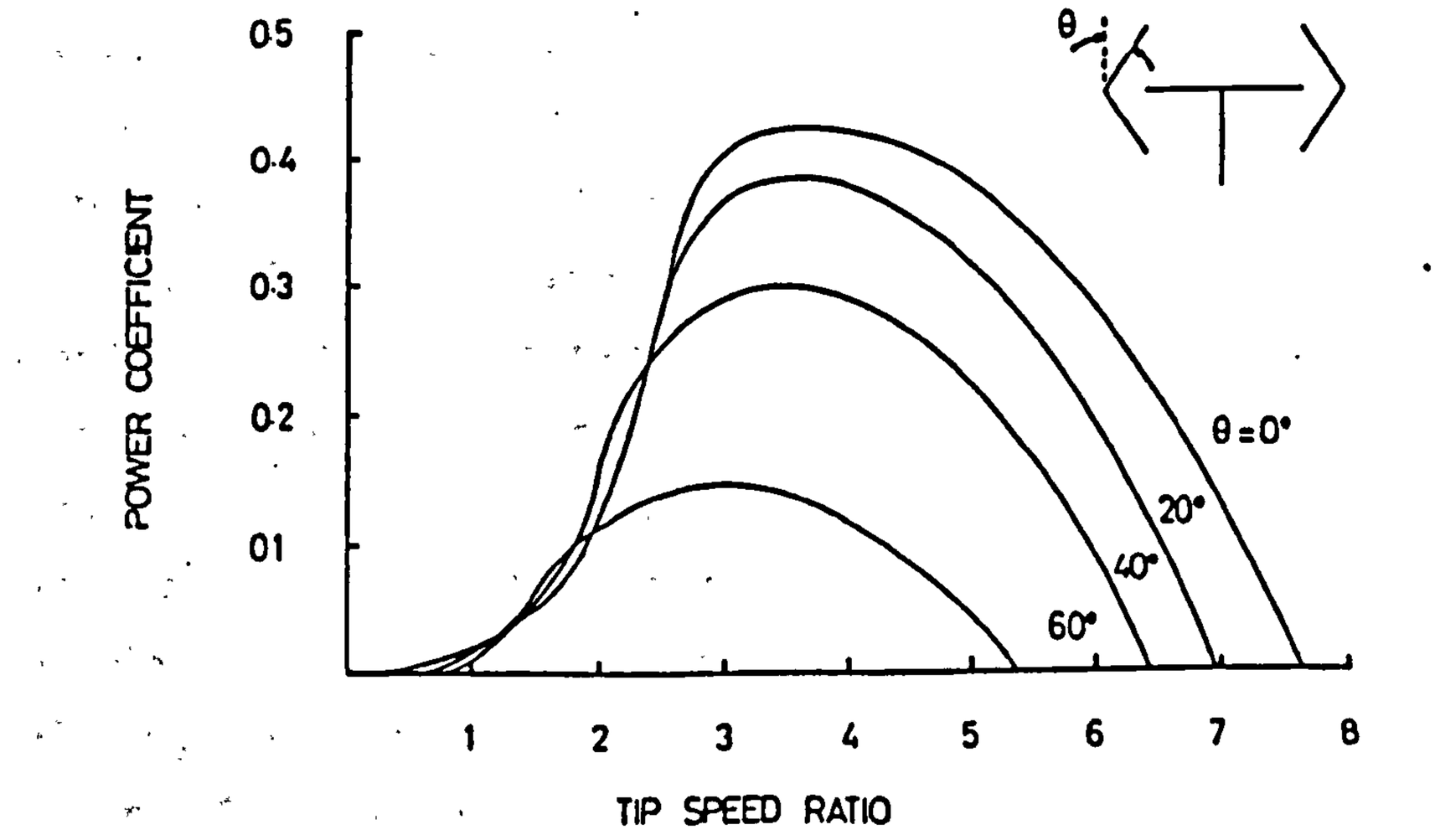

Figure 3.9b: C_{pm}-λ characteristic of 25 m diameter VG-VAWT for various coning angles

The further development of the variable geometry concept is well documented and currently ongoing, as Mays et al recently described [45]. The construction of the 125 kW Carmarthen Bay machine by VAWT, Figure 3.9a, demonstrates the suitability of this method for power and speed regulation for medium and large sized applications. However, the simplicity of the original blade rolling scheme, has in the opinion of the author been lost in the larger VG-VAWT. The Carmarthen Bay machine has each blade split in two, with each half being supported by a main strut and an actuator strut. A centrally controlled hydraulic actuator controls the "reefing" angle of all blade sections. This design was primarily developed as a research prototype, but the subsequent commercial derivatives once again show a greater simplicity in construction and design.

As with HAWT coning, the power of the VG-VAWT can never be completely reduced to zero, because of the limitations of the reefing movement (maximum reefing angle is 60° to the vertical). However, the method does satisfy most power and speed control requirements, Figure 3.9b.

The variable geometry concept was originally considered by Sharpe and Taylor [9] for V-VAWT applications, though primarily stowage and shutdown safety options were being considered. Essentially, there is no reason why reefing of the V-VAWT blades cannot provide a suitable means of controlling the power and speed of the rotor. Since the blades would be hinged at their root, the blades could be moved to lie a the horizontal plane, a position in which no power could be developed. In this way, the reefing blades would ensure complete power and speed regulation in all operating conditions. Alternatively, the blades could be reefed to a vertical position, however, the reduction in rotor inertia as the blades fold inward, will make it very responsive to any windspeed fluctuations.

To conclude, blade coning offers the following advantages:

(a) suitable for power regulation
(b) suitable for speed control
(c) alleviates gust loads
(d) passive or active actuation
(e) reduces aerodynamic forces across the whole blade

and disadvantages:

(a) unsuitable for curve-bladed VAWTs
(b) blade/hub bearing is additional to basic needs
(c) blade/hub bearing is a structural weakness
(d) additional blade supports required where full reefing required
(e) large reefing angles required to greatly reduce power output
(f) large actuating forces on both blades and support structures

3.2.7: Aerodynamic Stall

The lift force on an aerofoil is dependent upon the state of the boundary layer that surrounds its surface. If the angle of attack of the aerofoil to the oncoming air increases, the circulation around the aerofoil will also increase. The resulting lift force induced by the section will be increased too. The pressure difference between the upper surface close to the leading edge, where large suction pressures develop (see Chapter Six), and the trailing edge will also increase. The pressure gradient on the rear part of the aerofoil will continue to increase as the angle of attack increases, until such time as the difference is so great that it causes separation of the boundary layer from the upper surface, and a turbulent

wake will form. The separation point of the boundary layer will move towards the leading edge as the angle of attack continues to increase, until complete separation across the upper surface is achieved. With the boundary layer completely separated, the lift force will have decreased, but more significantly the drag force will have risen rapidly. The aerofoil is said to be in a condition of aerodynamic stall. The angle of attack at which lift force is at its maximum is known as the stall angle. The lift and drag force coefficient characteristics of an aerofoil are dependent upon the shape of the section and the Reynolds Number describing its operating condition.

Reducing the angle of attack will allow the boundary layer to re-attach itself to the upper surface of the aerofoil to restore the induced lift and drag forces.

Aerodynamic stall is a convenient method of controlling wind turbines of all sizes. Full and partial span pitch control methods rely upon either the feather or stall characteristics of the blade to regulate power output. By increasing the angle of attack of the wind onto the blades, aerodynamic stall can be actively encouraged. The subsequent reduction in lift force and increase in drag force result in a reduced power output from the rotor.

If the pitch of the blades is fixed, aerodynamic stall can occur naturally as windspeed increases occur. Sudden windspeed increases due to, say, gusting will cause the angle of attack of the relative flow to increase. The operating point of the blade on the characteristic lift and drag coefficient curves of the aerofoil section will climb to new values. Despite more wind energy being available, the angle of attack increase may be so great that the blade stalls and no significant change in power output occurs.

The characteristic behaviour of a wind turbine operating in stall conditions can be seen on the low tip speed ratio part of the C_P-λ curve. If the curve to the left of $C_{P\ max}$ falls rapidly, the rotor can be stall regulated. If this part of the curve falls gently, the rotor will be unsuitable for stall regulation. Better still, a stall regulated rotor will display a distinct peak power output on the power versus windspeed characteristic curve.

Many Danish manufacturers have adopted this simple and reliable approach to power control, but it does present the designer with a number of additional problems. Fixed pitch blades are structurally advantageous, and since stall occurs passively, no control actuator mechanism is required. However, the stall regulated wind turbine requires an additional brake to prevent rotor overspeed. It must also be designed so that its peak power output is within the limits of the machine rating, which means at low windspeeds it has a low energy capture efficiency. Also, little is known about operating in the stalled regime of an aerofoil, and there is a distinct lack of good characteristic post stall aerofoil data to assist designing such wind turbines. Ketley and Quarton [33] have summarised the advantages and disadvantages of this approach for HAWTs, as illustrated in Figure 3.10.

The cyclic variation of the angle of attack of the relative flow to a VAWT blade, means that aerodynamic stall is a feature of VAWT operation. Figure 3.11 shows the angle of attack time histories of a typical VAWT at two different speed ratios. At low speed ratios the angle of attack often exceeds the stall angle of the aerofoil, whereas at high speed ratios this is not the case. Since the angle of attack is continually changing, dynamic stall is known to occur on the upwind blade pass. During dynamic stall, the oscillation of the aerofoil causes a delay in the

FIXED PITCH-STALL REGULATED

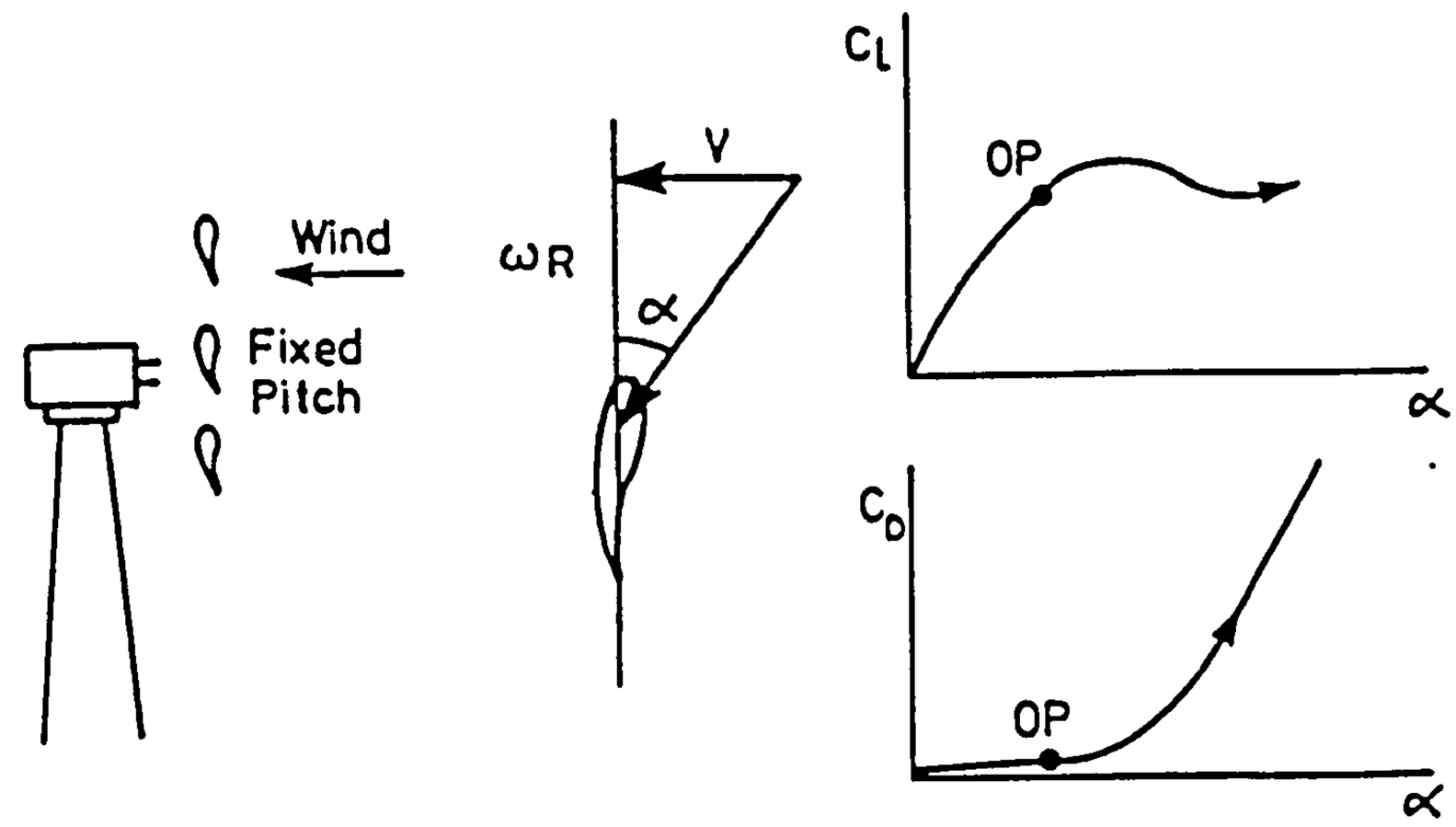

PROS
Simple
Cheap
Reliable

CONS
Some Loss of Energy
Reduced Aero Damping
Poor Knowledge of Post-Stall Behaviour
Loaded Stationary
No Assisted Start
Separate Rotor Brake Required

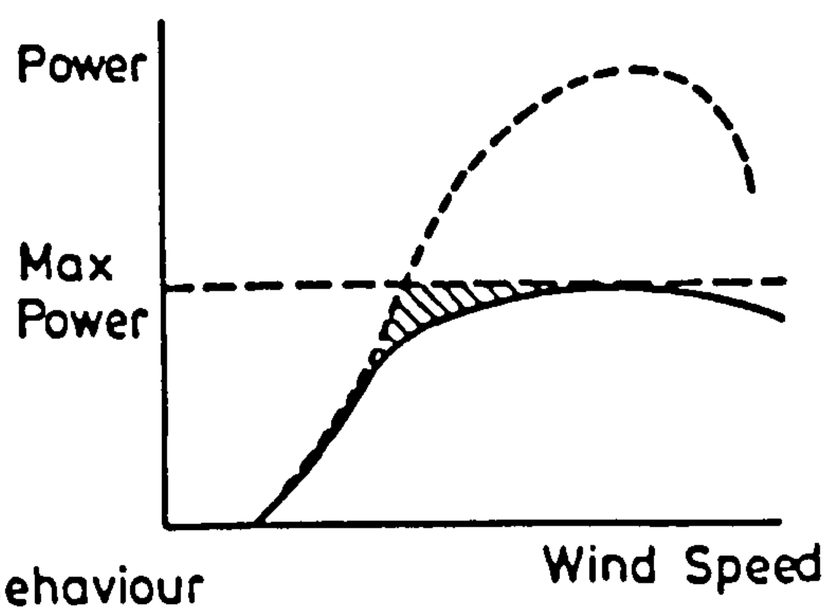

Figure 3.10: Stall regulated HAWT characteristics [33]

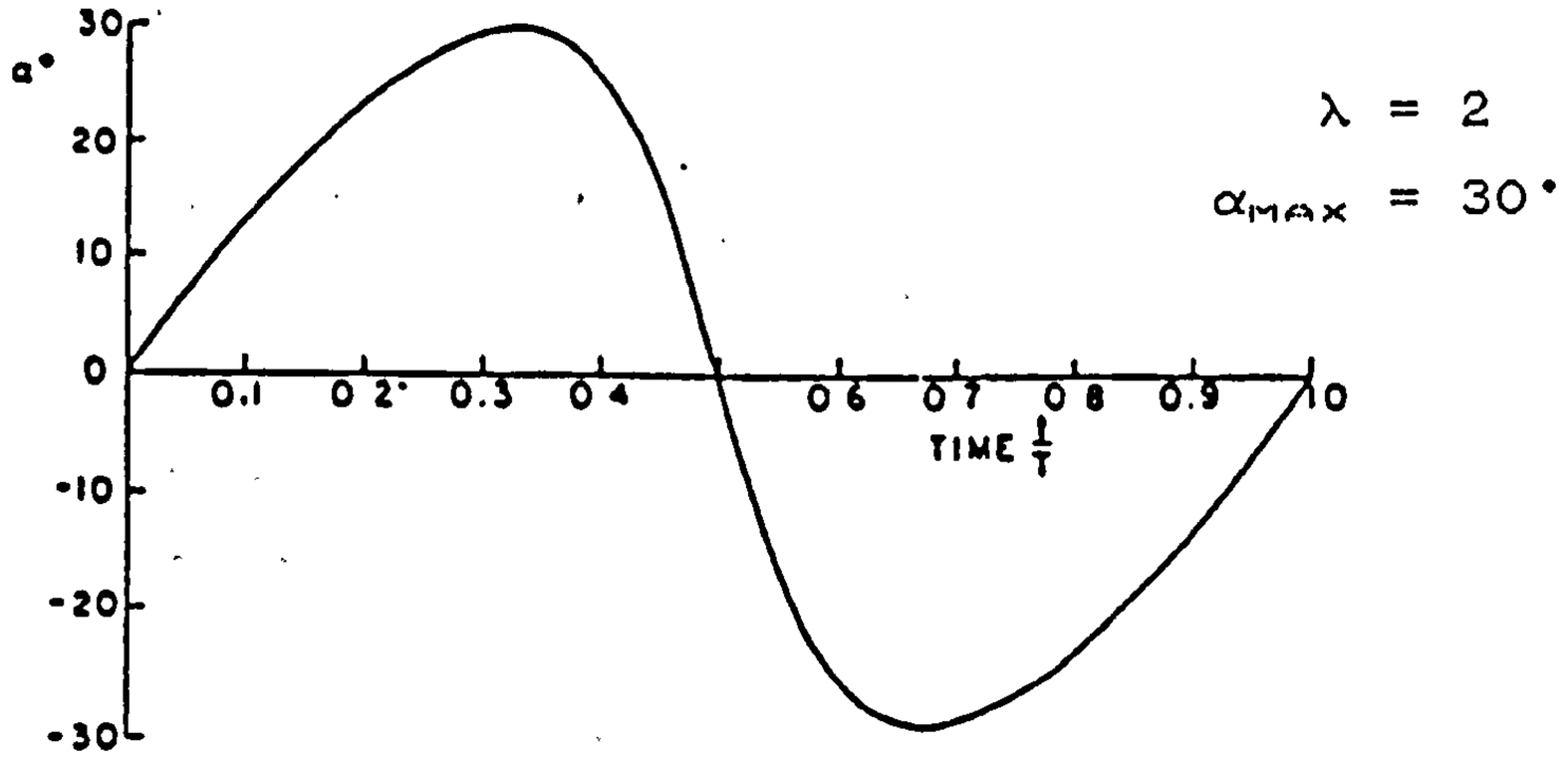

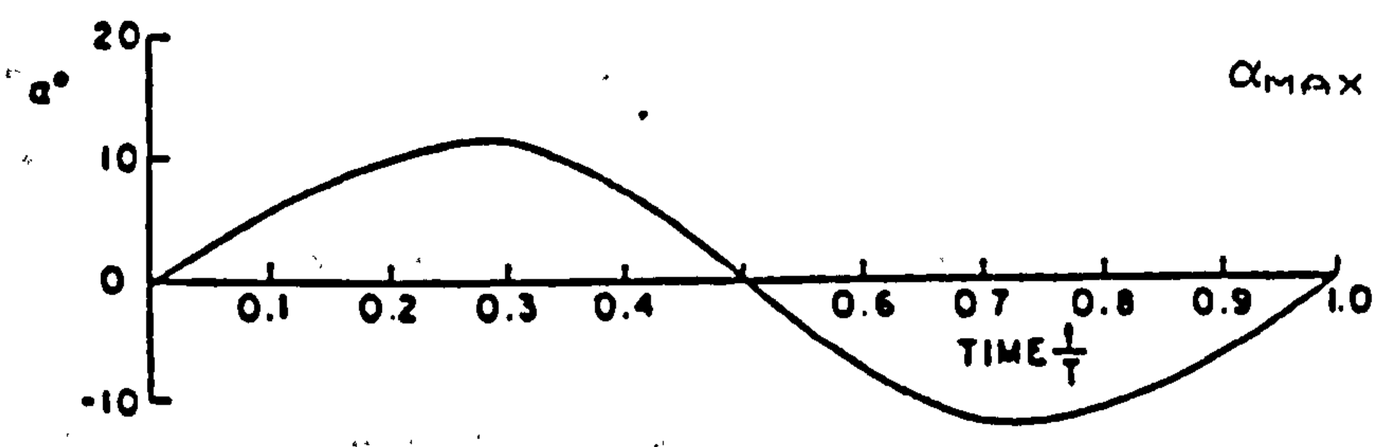

Figure 3.11: Cyclic variation of angle of attack for a VAWT operating at two different speed ratios

separation of the boundary layer. The delay enables lift forces to be induced at higher angles of attack than normal before stall occurs at the dynamic stall angle. Dynamic stall accounts for small increases in power output from the rotor, but in essence does not affect the overall stall regulation characteristics of the VAWT.

Most of the curved-bladed Darrieus VAWTs operate as stall regulated machines, but require additional means of overspeed control. Very recently it was reported that the 125 kW Carmarthen Bay VG-VAWT was displaying good stall regulation characteristics [45], and that fixed geometry designs were being considered. Again, the simplicity of construction and the lack of any control actuator mechanism is highly attractive, and leads to simple elegant designs. However, the difficulty arises in developing suitable power versus windspeed characteristics that are within the limits of the machine rating.

Sharpe and Taylor's studies of the V-VAWT have demonstrated the good starting torque characteristics of this VAWT configuration, and it appear that it does not have a suitable C_p-λ performance characteristic to operate as a stall regulated wind turbine. The high torque developed at low tip speed ratios indicate that operating in this regime in high windspeeds would not produce significant power reductions. The high solidity of the rotor, especially near the blade roots, seems to enhance the low tip speed ratio performance of the V-VAWT and give it superior power output than its "rival" VAWTs. Unfortunately, this does not allow it to operate as a stall regulated machine, because significant power would be produced even when operating at very low tip speed ratios.

To conclude, aerodynamic stall offers the following advantages:

(a) suitable for all wind turbine types
(b) simplicity of rotor construction
(c) no control actuator mechanism
(d) passive operation

and disadvantages:

(a) additional overspeed control required
(b) low energy capture in low windspeeds
(c) peak power to be within limits of machine rating
(d) post-stall behaviour difficult to predict
(e) poor self-starting characteristic required

3.2.8: Boundary Layer Control

The performance of an aerofoil is greatly affected by the state of the boundary layer surrounding the aerofoil surface. Aircraft utilise a number of devices to control the state of the boundary layer, some which will be considered for wind turbine use.

The state of the flow within the boundary layer is laminar near the leading edge, but as the flow moves towards the trailing edge, the boundary layer becomes thicker and the flow becomes turbulent. Boundary layer thickness affects skin friction, so the larger the boundary layer thickness the greater the form drag of the aerofoil section. Aircraft are designed to ensure that the boundary layer remains laminar as long as possible, thereby minimising the drag of the body. However, a turbulent boundary layer delays separation, allowing the aerofoil to operate at higher angles of attack before stall occurs.

Boundary layer control techniques seek to control the state of the boundary layer, either to delay separation or to promote it.

Separation may be delayed by injecting kinetic energy into the laminar flow to excite it to a turbulent state, or else by extracting slow moving air from the boundary layer to give it greater resistance to the separating pressure gradient on the upper aerofoil surface. Roughening the aerofoil surface will increase turbulence to some degree, but using slots to inject air into or remove it from the boundary layer is more effective. The movement of air may be assisted by a blower or pump, or else the pressure differences around the aerofoil may be utilised to move it un-aided. Delaying separation will improve the lift characteristics of the aerofoil, which will be beneficial to the wind turbine designer in increasing power output.

Alternatively, separation may be promoted by reversing the principles considered above. Power regulation might be achieved if stall can be encouraged by controlling the state of the boundary layer.

Consideration has been given to boundary layer control for use with VAWTs by only a few authors. These studies were recently discussed by Bannister [46], who concludes from his own investigations that it is possible to control the boundary layer by blowing through perforations on the upper surface of the aerofoil, and that boundary layer control could be used for governing wind turbines. The most notable of recent studies is that of Klimas and Sladky [47], who have used the natural centrifugal pumping action of a rotating wind turbine to inject air into the boundary layer close to leading edge of the rotor blades. Figure 3.12 shows the measured reduction in power output of a 5 m Sandia National Laboratories (SNL) Darrieus VAWT.

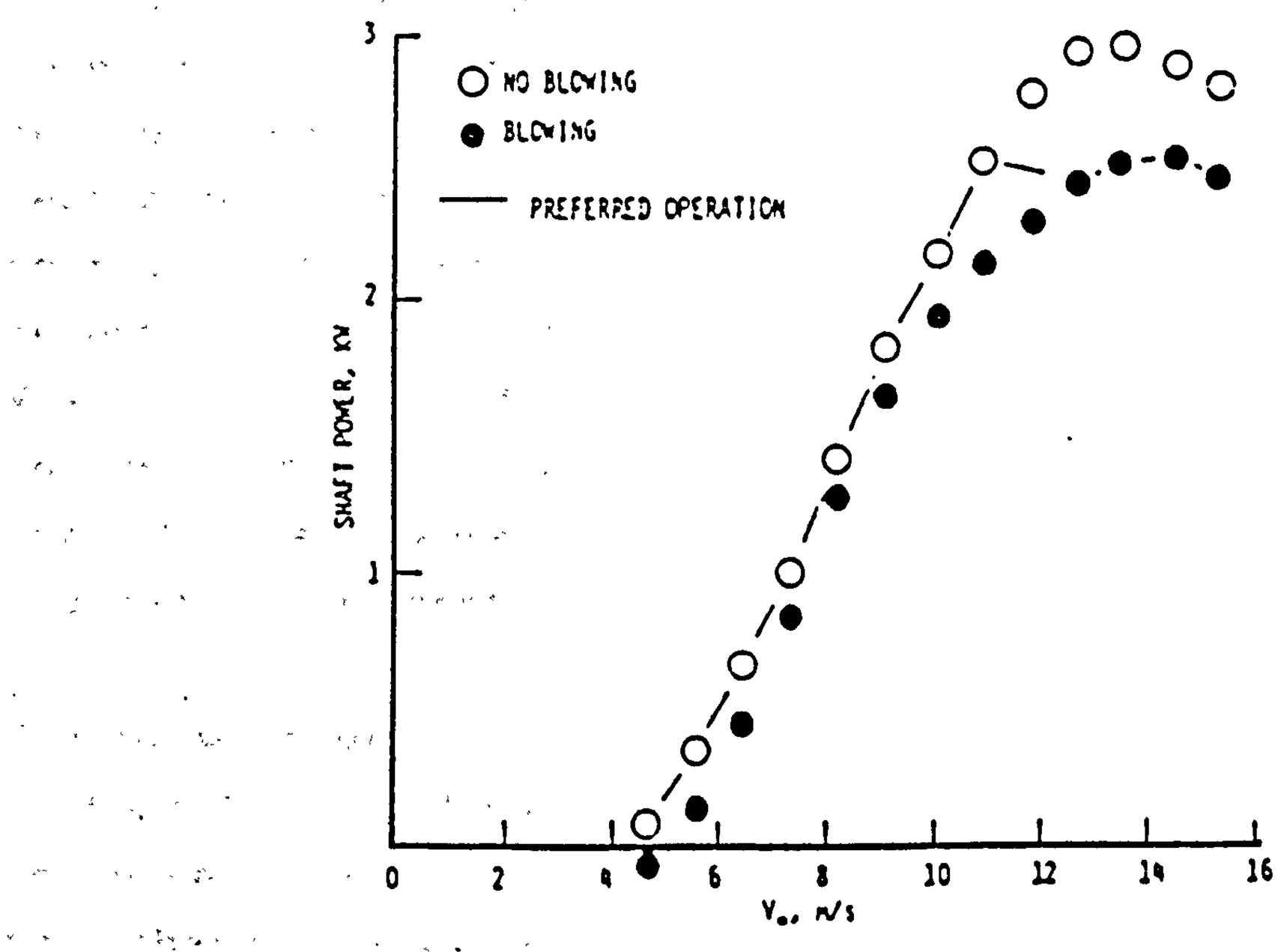

Figure 3.12: Power output versus windspeed of SNL 5 m diameter VAWT with and without centrifugal blowing [47]

While this method does not provide shutdown and speed control, the moderation of the peak power output can be clearly seen. The preferred operation is indicated, showing that blowing can be used at windspeeds greater than rated to maintain the power within the limits of the machine rating.

Klimas has also investigated the use of "tailored" aerofoils for VAWTs [27]. The tailored aerofoil sections were designed to have laminar boundary layers, with subsequent lower profile drag characteristics than the conventional aerofoil sections used on Sandia VAWTs. Wind tunnel measurements of the aerofoils proved that lower drag coefficients were achieved, however, Sharpe [41] has recently observed that, when fitted to a 17 m Darrieus VAWT, these aerofoils showed *larger* drag force characteristics than the standard aerofoil. This suggests that in the turbulent working environment of the free-air VAWT, boundary layer control is limited with these aerofoils.

The blowing of air into the boundary layer requires small perforations or holes to be made in the blade. Not only do these holes create a weakness in the blade, but that in the "harsh" environment in which wind turbine operate, these holes may be easily blocked by debris in the air. The natural "pumping" action of hollow blades can be used to assist with the boundary layer control process.

Similarly, it is unrealistic to conceive that the good surface finish required for a laminar boundary layer flow can be maintained when the tailored aerofoils are operated in a free-air environment. The superior performance of the tailored aerofoils has been proven in the clean environment of a wind tunnel, but its successful application in the real world has yet to be demonstrated.

To conclude, boundary layer control has the following advantages:

(a) suitable for all wind turbine sizes
(b) aerodynamic forces controlled across whole blade
(c) passive or active control
(d) little or no actuator mechanisms
(e) fixed blade rotor

and disadvantages:

(a) difficult to predict state of boundary layer
(b) small holes create structural weakness
(c) debris and dirt affect boundary layer performance
(d) not proven in free-air wind turbine environment

3.2.9: Flaps, Slats and Slots

Flaps, slats and slots are all devices currently in extensive use on aircraft as a means of enhancing the lift force characteristics of an aerofoil. Some of these devices may assist the wind turbine designer to increase the power output of a wind turbine, but their use as power and speed regulation devices is somewhat limited.

The major disadvantages with all these devices are that structurally the blade section is less stiff, hinges and internal attachment points are highly loaded, and significant drag losses will be created by the discontinuites on the surface of the blade.

Detailed lift and drag characteristics of various flaps, slats and slots were obtained from McCormick [48] and Abbott and Von Doenhoff [49], but only the following devices are considered here:

(a) Plain flaps (ailerons)

(b) Split flaps

(c) Slotted flaps

(d) Slats

(e) Slots

(f) Leading edge flaps

Trailing edge plain flaps are formed by hinging the rear-most part of the aerofoil section about a point within the section itself. Downward deflections of the trailing edge are termed positive, while upward deflections are termed negative. Where there is no gap between the flap and the main body of the aerofoil, the deflections effectively changes the camber of the aerofoil, and changes in its aerodynamic characteristics occur. Large flap deflections almost certainly trigger separation.

Negative flap deflection decreases the lift created by the aerofoil, but increases the static stall angle of the section. Conversely, positive flap deflections increase lift forces, but decrease the static stall angle. Since plain flaps are able to actively increase or decrease lift, they are extensively used on aircraft where they are more commonly referred to as ailerons.

Clearly, plain flaps offer the wind turbine designer the ability to both enhance and regulate the power output of a rotor. Active or passive actuating control mechanisms could be used, but large pitching forces are generally required to activate such devices.

To date the author is only aware of the NASA/DOE sponsored studies of aileron control for the MOD wind turbines. The initial feasibility study by Wentz et al [50] concluded that ailerons would provide control of both rotor speed and power output. Additionally, the starting torque of

the machine could be increased with full positive deflection, and deploying the aileron 5° when the windspeed was lower than rated would lead to a 1.8% increase in annual energy capture.

More recently, Miller and Sirocky [51] reported the results of full-scale rotor tests for various aileron types. The test programme included both power regulation and loss-of-load overspeed tests, from which the authors concluded:

> "...aileron control is a viable rotor control method for an intermediate size wind turbine like the MOD-0. The 38 percent chord aileron control rotor provided loss-of-load overspeed protection; as well as effective power regulation on the MOD-0 wind turbine."

The authors went on to recommend further development work and consideration of aileron control for large HAWTs, such as the MOD-2 wind turbine.

The split flap is a simple device, formed by deflecting the rearward portion of the lower surface about a hinge point on the forward edge of the flap itself. A variation of the simple flap has the hinge located slightly forward of the flap, thereby leaving a gap between the deflected flap and the aerofoil. The leading edge of the flap sometimes moves rearward as it is deployed, either with or without the gap.

The effectiveness of the split flap is derived from the large increase in camber of the aerofoil, and in some cases an increase in blade area. Their effectiveness is greatest for thicker rather than thinner aerofoil sections. While large increases in drag will occur when they are deployed, the change in lift characteristics results in a net increase of the lift to drag ratio of the aerofoil. With the hinge forward, the split offers no lift

reducing capability and is unsuitable for wind turbine overspeed control. Power augmentation is clearly a possibility, but since lift characteristics are generally enhanced, regulating power in high windspeeds does not seem feasible. The usefulness of such a device is clearly limited for wind turbine applications.

If the flap hinge is mounted on the trailing edge, the flap is deployed by moving downward and backward, creating a large bluff body. Such a device is often termed a "dive brake" and will be considered in greater length in the next section.

Slotted flaps provide one or more slots between the main portion of the aerofoil section and the deflected flap. The subsequent increase of lift is due to increasing the effective camber and, in some cases, increasing the effective chord length of the section. The slots duct high energy air from the lower surface to the upper surface and provide a degree of boundary layer control that delays separation.

There are many variations of the slotted flap with classification by the number of slots. Typical geometries include:

(a) single-slotted flap
(b) double-slotted flap
(c) venetian blind flap
(d) external aerofoil flap

The slotted flap is primarily designed to enhance the lift characteristics of an aerofoil, and in some cases delay separation to achieve higher angles of attack. However, these devices do not offer the wind turbine designer much

scope for power or speed control, and generally increase the complexity of blade construction.

Slats are leading edge aerofoils that are mounted forward of the leading edge of the main aerofoil, and may be fixed or retractable. Slats are positioned to allow fluid to pass from the lower to upper surface of the aerofoil to provide some degree of boundary layer control. Slats are used to delay leading edge stall at high angles of attack, and significant increases in both lift and stall angles have been observed.

Slats provide the wind turbine designer with a simple method of increasing low windspeed performance of the blade, and if used with, say, ailerons would enhance the performance of these devices too. Used on their own, however, slats do not appear to be suitable for either power regulation or speed control.

Leading edge slots allow control of the boundary layer to delay separation. The most common form of slot is the slotted flap which, when located near to the leading edge, is not much different from a slat. The effectiveness of a slot on an aerofoil has been shown to decrease as it is moved away from the leading edge. Multiple slots (three being optimum) are only effective if all are located close to the leading edge.

Slots increase profile drag, and for wind turbines such losses would be detrimental to output efficiency unless the gains are significant. There is little scope for the use of slots in wind turbines unless enhancement of starting characteristics is a real need. Slots alone would not provide adequate power or speed control characteristics.

A leading edge flap is formed either by moving a forward portion of the aerofoil or by extending a surface forward or downward from the leading edge. The flap may be extended from the upper surface or hinged from the lower surface. They are used to delay separation at high angle of attack, so extending the useful operating range of the aerofoil. The effectiveness of a leading edge flap increases with smaller leading edge radii. Therefore these flaps are most effective when used with thin aerofoil sections. The performance of the flap is unaffected by trailing edge devices, and may provide a means of enhancing the low windspeed output of a wind turbine.

When considering the use of flaps, slats or slots for VAWT applications, only ailerons can be seriously considered with the information presently available. The information available for the other devices that have been considered here, does not include any data on their performance with negative angles of attack. It is, therefore, not possible to assess their behaviour in such conditions. It is only the aileron that can be deployed in two directions and performance data is available for both cases.

The cyclic variation of angle of attack experienced by a VAWT blade means that an aileron deployed with its trailing edge moved outward, would be acting with a positive deflection, augmenting lift, on the upwind pass and a negative deflection, reducing lift, on the downwind pass. Since a greater proportion of the total energy capture of the cycle is achieved on the upwind pass, it is reasonable to assume that, in this particular case, an overall net gain in lift will be achieved over the complete cycle when using an aileron.

As yet no VAWT known to the author has been built using ailerons, so a great deal more work is required before it

is possible to determine the effectiveness of this device for VAWT power and speed control. The aileron does allow a rigid blade construction across the whole span, with only a small proportion of the trailing edge section being free to move. But the pitching forces required to deploy the aileron are large, creating significant structural difficulties at bearing and support features.

To conclude, ailerons have the following advantages:

(a) relatively simple devices
(b) active or passive actuation
(c) suitable for power and speed regulation
(d) suitable for overspeed control
(e) low windspeed power enhancement

and disadvantages:

(a) large actuator forces required
(b) highly loaded bearings and supports
(c) aerodynamic loads controlled only at position of aileron

3.2.10: Airbrakes

Airbrakes may be defined as any device that reduce the aerodynamic performance of a rotor by increasing the drag of the aerofoil. A consequence of its deployment may also be the reduction of lift if separation is invoked. Air-brake devices include:

(a) ailerons and flaps
(b) spoilers
(c) drag flaps and parachutes

Ailerons and flaps have been considered previously, but in this context it is their ability to reduce performance by aerodynamic braking that is of interest.

Spoilers can be defined as airbrakes that operate within the swept area of the blade and, when not deployed, either form part of the blade surface or are retained within the blade section. Plug or plate types are described by Wentz et al [50].

Spoilers primarily interfere with the boundary layer flow over the aerofoil surface, and when fully deployed destroy the lift forces induced by the section, provided they protude beyond the depth of the boundary layer. The spoiler is also a bluff body that increases the projected frontal area of the blade. Drag forces increase proportionally to the area of the spoiler, and it is this effect that dominates the torque change experienced by a blade.

The effectiveness of spoilers to control a HAWT has been successfully demonstrated by Wentz et al [50], amongst others [52,53]. Wentz et al compared the performance of spoilers to ailerons for use on the MOD-0 wind turbine. The study concluded that spoilers were suitable for providing overspeed protection, and they could be used for power regulation at higher than rated windspeeds. However Wilmshurst [52] observes:

> "...that for use as brakes, spoilers must be fully retractable. The least protuberance remaining when they are not in use is likely to have a severe impact on the performance (of the HAWT)."

Drag flaps can be considered as any surface that when deployed operate outside the swept area of the rotor, so not directly affecting the blades themselves. The drag developed by such an airbrake is proportional to its

frontal area, and like spoilers, relatively small devices can be used to control a wind turbine rotor.

Drag flaps are most effective if placed at the blade tips. This allows the blade to be of simple construction without any discontinuities in the surface, but most importantly, the drag flap will operate in the region where the relative windspeed to the blade is greatest. Since drag flaps do not directly interfere with the lift characteristics of the blade, the flap must be sized to overcome the torque of the whole rotor.

Drag flaps can be fitted to any part of the rotor, and fitting them to the low speed shaft connection does have benefits. The retardation forces are transmitted directly to the rotor hub, alleviating the blade of the drag forces and bending loads that would be applied if fitted at the tip. However, the flap operates in a low relative windspeed region and the flap size must be enlarged to give the same braking effect. The Windco Windcharger is a small HAWT that uses drag flaps in this way, and the centrifugally activated brake offers complete overspeed control.

Drag flaps are in common use on small HAWTs because of their simple construction. Unlike spoilers, they do not interfere directly with the performance of the rotor and offer good overspeed protection where the rotor is normally stall regulated, a combination greatly favoured by Dutch wind turbine manufacturers.

Parachutes can only be realistically considered for overspeed protection in the event of all other control devices failing, because once deployed they require repacking before use again. Pedersen [53] used data from experimental tests to predict the performance of HAWTs fitted

with parachutes. He concluded that suitably sized parachutes could bring a rotor to near rest, at which point the parachute is likely to collapse and become ineffective. Only the Tvind 1 MW wind turbine is known to the author to be fitted with parachutes. These are folded and packed inside each blade tip and are deployed for emergency overspeed control.

Airbrakes are the most commonly used control devices on the curve-bladed Darrieus VAWTs, as they offer overspeed protection and some degree of power regulation. Their usage on VAWTs can be as effective as with HAWTs, especially where the circulation around the aerofoil is greatly interrupted. Drag flaps and parachutes can operate during the whole cycle of operation and show little sensitivity to variations in angle of attack. Pederseen's experimental work with parachutes was carried out using a small Darrieus VAWT.

The Canadian VAWT development programme has relied heavily on the use of spoilers to complement the stall regulated power control that is characteristic to these low solidity machines. Templin and South [54] have demonstrated the effectiveness of spoilers from tests on 1.83 m and 2.29 m diameter wind tunnel sized VAWTs. The results of these tests are reproduced in Figure 3.13, from which Templin and South were able to show that the effective drag coefficient of the spoilers was $C_{DS} = 1.5$. They identified the design condition for which spoilers must be sized to prevent positive shaft power being developed by the rotor, and derived a non-dimensional relationship for determining the effective spoiler area to swept area ratio to satisfy this requirement. Confidence in airbrake control was somewhat reduced, however, when the 230 kW Magdalen Islands VAWT suffered a severe overspeed accident when the airbrake failed to deploy [42].

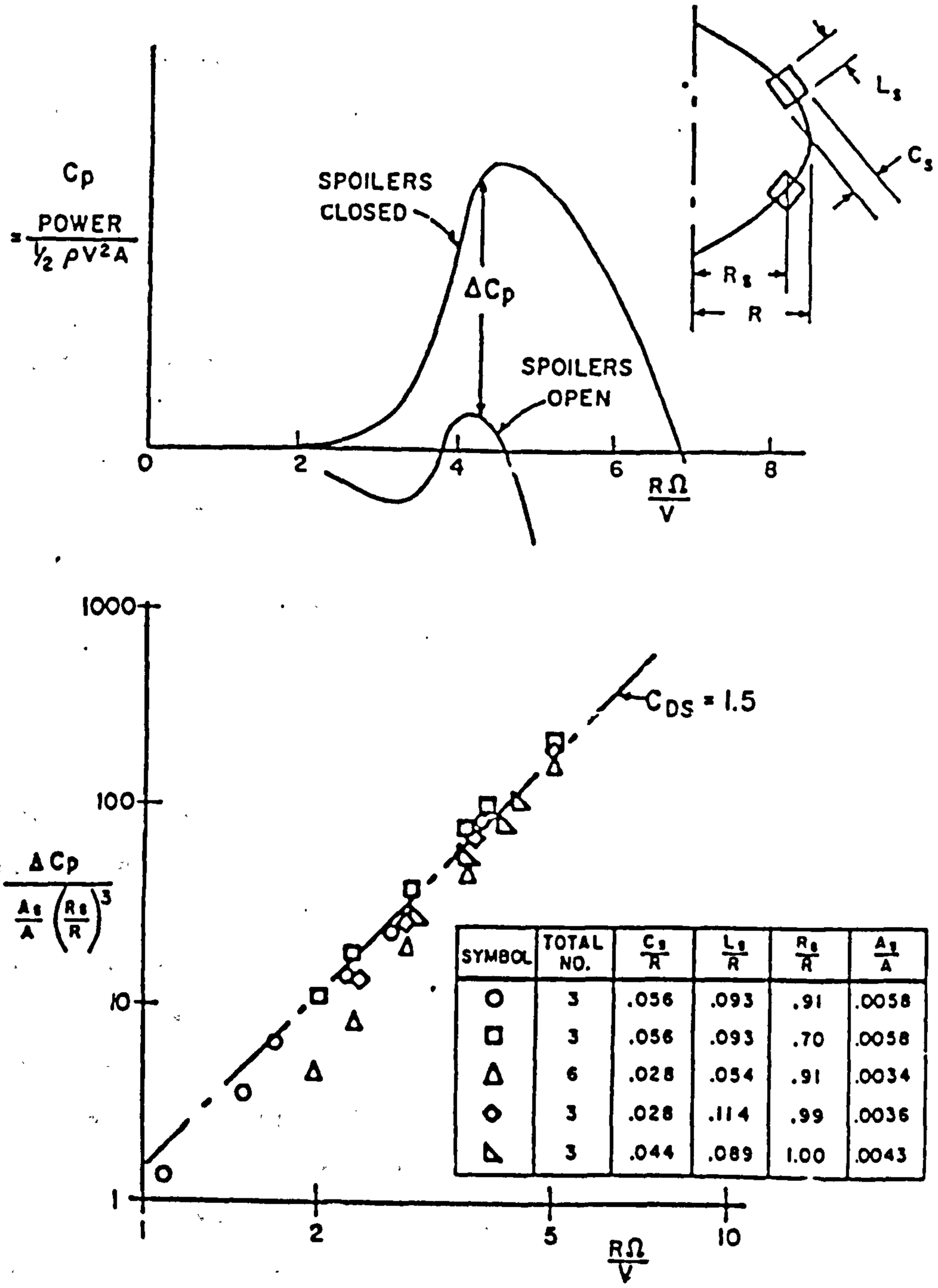

Figure 3.13: Measured effectiveness of spoilers on curve bladed VAWT [54]

To conclude, airbrakes have the following advantages:

(a) suitable for all wind turbine sizes
(b) suitable for overspeed control
(c) suitable for power regulation, if controlled
(d) active or passive actuation
(e) large drag forces developed by relatively small devices
(f) simple blade construction achievable

and disadvantages:

(a) does not reduce lift of blades
(b) large additional aerodynamic forces applied to rotor
(c) variable deployment difficult to achieve
(d) co-ordination of deployment difficult to achieve

3.3: Evaluation and Selection of a suitable Control Method for the V-VAWT.

When the review of control options was complete, the author had gained a much better understanding of the control problem itself and a greater insight of what might be achieved with the devices available. A re-evaluation of the requirements of a control system was made, and a revision of the broad specification of section 3.1.1 considered. In light of the information retrieved by the review, the specific requirements that must be satisfied by the V-VAWT control system for electricity generation can be re-defined as follows:

(a) Regulate power output of rotor to specified limit during normal operation in all operational wind-speeds

opinion of the author, considered worthy of further investigation:

(a) Aerodynamic stall regulation with airbrakes
(b) Partial-span pitch control
(c) Ailerons

The most promising control option, and the simplest, is the combination of stall regulation for power control and airbrakes for overspeed protection. This option is suitable for all machine sizes, and the blades can be of a simple construction, rigidly mounted at the root to the hub. The airbrakes can be assembled onto the blades after manufacture, and if mounted at the blade tips, small drag flaps will provide adequate speed control and overspeed protection. Stall regulation is passive, and centrifugal actuation of the airbrakes will ensure the control is both simple and reliable. Stall regulation of both HAWTs and VAWTs is tried and tested and considered to be highly reliable. The low windspeed energy capture of stall regulated wind turbines is less than the that of variable pitch wind turbines of equivalent rating, but the stall regulated machines are smaller, maximising their cost effectiveness at higher windspeeds.

Further consideration of this control option with respect to the V-VAWT revealed that stall regulation is unlikely to be manifest in this VAWT configuration. The high starting torque that is characteristic of the V-VAWTs considered to date give the V-VAWT a useful self-starting capability. However, the large positive torques developed at low tip speed ratios by this configuration suggest that the rotor will not automatically stall as the windspeed increases above rated. The predicted performance curves of Chapter Seven confirm this notion, and therefore stall regulation is not considered further.

(b) Regulate speed of rotor to specified limit during normal operation in all operational windspeeds

(c) Ensure unloaded rotor can be shutdown and brought to rest, or near rest, in all operational windspeeds

(d) Regulate unloaded rotor speed during synchronisation of generator with supply network in all operational windspeeds

In addition to these primary requirements, some secondary needs can be defined. These will include increasing low windspeed energy capture; enhancing starting torque; reduce structural loads on rotor; minimise cyclic torque variation; simplify blade construction; minimal actuation and deployment equipment; established or proven technology; passive actuation; fail-safe operation.

Without repeating the description of the control methods reviewed, or the summary of advantages and disadvantages given in each section, the author was able to eliminate a number of options simply by their inability to satisfy the primary requirements stated above. The criteria that is most difficult to satisfy is (c), since this demands that the C_p-λ characteristic curve is less than or equal to zero for all tip speed ratios. Satisfying this characteristic demonstrates that positive retardation of the rotor can be ensured, regardless of windspeed, rotor speed or rotor loading. This elimination procedure left the author with four options that included variable geometry. However, the initial development programme for the V-VAWT was concentrating on fixed geometry configurations, and it is for these V-VAWTs that control methods were being sought here. Variable geometry options (including full-span pitching) were, therefore, inappropriate and dismissed, leaving the following options that were, in the

The electricity generation application of the V-VAWT provides a number of challenges, and if constant speed operation is required active control of the wind turbine must be seriously considered. HAWTs currently generating electricity that is supplied directly to the grid use active microprocessor control to maintain a reliable, good quality power output. The use of a centrally controlled partial-span pitch control satisfies all the primary needs as stated above. This technique is well proven in HAWT applications, and is used for all power and speed regulation requirements. The partial-span variable pitch option is ideally suited for fixed geometry V-VAWT configurations where the blade is rigidly fixed at its root, supported by cables near to the blade tips, and only the outer portion of the blades are free to move in pitch. Variable pitch tips will also regulate the aerodynamic performance of the part of the rotor that does the most work. The high local speed ratios and swept area means that the blade tips are the most effective part of the V-VAWT rotor, and capture more energy than the blade root portions.

This control option allows the main blades to be relatively simple in construction, with the tip and actuator mechanism fixed to the blade end as a "bolt-on" module (see Howden HWP 330 HAWT). Power and speed regulation can be achieved by ensuring the positive control effect on the upwind pass of the VAWT overcomes any negative control effects on the downwind pass to give a net regulation effect over the complete cycle. Preliminary performance prediction suggest either nose-in or nose-out pitch deflections will provide the power regulation required, and that some power augmentation is achievable.

The added complexity and cost of actuator mechanisms, and the need to ensure greater structural strength around a

highly load tip bearing, detract from the simplicity of the original V-VAWT concept. However, by mounting the equipment inboard, the structural penalties of the additional equipment can be reduced. The active control of the blade tips means that tried and tested actuator mechanisms can be used, but since the tip will be used for all control tasks, it must be designed for fail-safe operation, so in the event of a failure of the controller or actuating mechanism, the blade tips will deploy automatically to the shutdown position.

The justification and limitations of using partial-span pitch control apply equally well to the use of ailerons. Ailerons offer, at first sight, some structural advantage over tip control, in that the leading edge and forward portion of the whole blade can be manufactured as one. Only a small chordwise section of the blade need be free to move to control the aerodynamic characteristics of the section. However, the aileron bearings are highly loaded and the blade will need additional support structures in the trailing edge section. Wind turbine blades are manufactured with the minimum of material in the trailing edge. The composite construction of most blades uses only foam, or its equivalent, to give shape to the outer skin of the blade. Additional structures are required, therefore, in this application.

The partial-span pitch control option is an established method of HAWT control, and its application to VAWTs has been limited, whereas comparatively little work has been directed towards ailerons. The choice of control method for a novel VAWT in its early development stages needed to be conservative to ensure its application to the V-VAWT configuration would be successful. For this reason partial-span pitch control was chosen as the control method to which further work would be devoted.

When the author first made this decision, it was considered that utilising partial-span pitch control on the V-VAWT would be the first instance of this control method being adapted for VAWT use. The Westwind VAWT was not known about at the time, and its existence only came to light after Derek Taylor's trip to the Windpower '85 wind energy conference at San Francisco in August 1985. At this time the results of the wind tunnel tests reported in Chapter Five had already been presented by the author at the ISES Intersol solar energy conference at Montreal in June 1985.

In March 1985 at the British Wind Energy Conference, Sharpe and Taylor proposed controlling the free-air 5 kW V-VAWT that has been subsequently erected at the Open University with a device they called the 'T' brake' [19]. The T-brake is a control surface set across the tip of the blade for which they claim:

> "This control device is capable of acting as an overspeed brake and as a power regulator in both the passive and active modes of operation."

The effectiveness of this device was not demonstrated by measurement nor prediction, and it was this author's own experimental work on partial-span pitch control that has been subsequently utilised to predict the performance of this device.

The 'T' brake has a number advantages over the actively controlled tip pitch option, however, the research and development work reported here concentrates on the author's original control choice that was made in the early months of 1984. The theoretical and experimental work that is the subject of the following chapters centres around the measurement and prediction of the effectiveness of partial-span pitch control in V-VAWT applications.

Chapter Four: The Design and Construction of a V-VAWT Wind Tunnel Model with Pitching Blade Tips

4.1: Introduction

In the previous chapter the use of partial-span blade pitching was identified as a suitable method for controlling the aerodynamic performance of the V-VAWT, and as such warrants further investigation. The initial performance predictions using the author's modified version of the computer program VAWTTAY showed that power regulation and overspeed control may be adequately achieved using this control method. However, there is no suitable experimental evidence available that either confirms the suitability of the control method for use with a V-type wind turbine, or verifies the validity of the modified version of VAWTTAY. The adoption of tip pitch control for the V-VAWT has been made on technical merits and in anticipation of a control effect being observed in reality.

Clearly, though, at this stage of the project, the need had arisen for experimental evidence to confirm the suitability of this V-VAWT control concept, and validate the accuracy and reliability of the modified version of VAWTTAY.

The development of the V-type wind turbine by Taylor and Sharpe, had included experimental work using small wind tunnel sized models. However, since all these models were of a simple construction and built using straight, fixed pitch blades, a specialist model of the V-VAWT was needed for this project. This chapter describes the design and construction of such a V-VAWT model. The model was designed to allow the effects of blade tip pitching to be experimentally observed in the blowdown wind tunnel at Queen Mary College, London. This test facility has

subsequently enabled the aerodynamic performance of the "controlled" V-VAWT model to be measured with good accuracy and high reliability.

Testing of the control concept alone is not satisfactory. The results of the experimental work using the specialist V-VAWT model must be used to validate the modifications made to the computer program VAWTTAY. As discussed previously, VAWTTAY is used as a design tool, so its accuracy and reliability must be verified if it is to be used for designing larger V-VAWTs. Similarly, validation of VAWTTAY will allow the suitability of tip pitch control to be assessed for these larger configurations, without necessarily building and testing full-size prototypes. However, these issues will be discussed in more detail in Chapter Seven.

The development of the specialist model of the V-VAWT underwent many repetitive phases of design, analysis and modification before a final solution was evolved that was suitable for manufacture and test. A computer based static structural analysis of the blades was developed by the author to assist the iterative design and analysis process followed. And while no formal product design specification was ever prepared, the initial functional requirements of the model had to often be modified in response to the changing constraints imposed upon the designer.

The V-VAWT model that was eventually developed, and that is described fully in this chapter, has two constant chord blades, each with three equi-sized, tip sections that are moveable in pitch. This configuration allows the effect on aerodynamic performance of three different sizes of blade tip area to be studied over a ±30° range of pitch angle deflection. The pitch angle of each tip section is

fixed during operation, and can only be changed when the model is not running. The blades are generally constructed from English Ash that is bonded to an aluminium alloy spar. Each blade is rigidly attached at its root to the lower hub, and simply supported close to its tip by two wire cables connected to the upper hub. Both hubs are assembled onto the freely rotating, central shaft of the Queen Mary College test facility space frame.

The mechanical components of the final design solution were all manufactured and assembled into their final form in the workshop facilities of the Open University by Scott Forrest, with assistance from the author as appropriate.

The author prepared detailed drawings of all components and photographically recorded the various stages of manufacture.

4.2: Initial Design Objectives and Technical Constraints

The primary objective of designing a specialist V-VAWT model for wind tunnel testing, was to develop a small wind turbine that would allow the effect of blade tip pitch control on the performance of the machine to be empirically evaluated. The specialist model must, therefore, allow the effect of *both* blade tip pitch *and* blade tip size to be studied.

The range of pitch angle displacements or blade tip sizes, over which measurements are required to be made, cannot be specified explicitly. However, initially it was considered that blade tip areas upto 20% of total blade area and pitch angles upto ±90° would provide suitable design objectives.

The initial dimensions of the V-VAWT model were constrained by the size of the wind tunnel itself. The exit of the wind tunnel is rectangular, and its dimensions are 1.26 x 1.00 m. If the blades are inclined at 45° to the axis of rotation, the blade length must be limited to a maximum of 0.7 m. The rotor diameter is therefore limited to a maximum of about one metre. This limit ensures that there would be adequate clearance between the rotor and the support frame, and that the rotor would operate in the middle of the airstream coming from the wind tunnel exit. A blade aspect ratio of ten would provide geometric similarity with previous V-VAWT models, and implies that the chordlength of the blades would be only 70mm.

With these initial dimensions, VAWTTAY was used to predict the aerodynamic performance of a two-bladed version of the V-VAWT model. A runaway tip speed ratio in excess of six was initially predicted, which, for wind tunnel speeds of 14 m/s, would be equivalent to a rotational speed of 1600 rpm. Even though the predictions did not include parasitic drag losses, a maximum operational speed of 1800 rpm was considered appropriate. This would allow the rotor to be safely "driven" to speeds in excess of its predicted runaway speed, so allowing measurements to made at speeds where drag losses are larger than aerodynamic lift gains. The survival design speed of the model rotor was subsequently specified to be 2500 rpm. This design constraint was imposed on the author to ensure that access to the wind tunnel facilities at Queen Mary College would be granted.

The need to design a wind tunnel model to "operate" at such a high rotational speed proved to be a challenge, especially since the blade tips were to be moveable in pitch and of variable size. However, the a final solution

was eventually determined that met the survival speed requirements, though the range of blade tip sizes and pitch displacements at which the model could operate was somewhat restricted.

4.3: Blade Design and Structural Analysis

All the V-VAWT models developed by Taylor and Sharpe were of a simple construction and adapted for use with the space frame structure that was available at Queen Mary College test facility. The blades for these models were straight, untwisted, and were of constant chord across their span. This allowed the blades to made from solid wood, which was accurately crafted into shape using hand-tools. The simplicity of the blade design, and the adoption of the NACA0018 aerofoil section, enabled lightweight blades to be manufactured for these models. The choice aerofoil section enabled a good compromise between aerodynamic and structural performance to be successfully achieved, especially since all the blades were small in size. Each blade was supported by two cables attached near to the blade tip. Two cables are used to prevent the blade twisting under the passive influence of aerodynamic and centrifugal forces, a problem initially encountered with the first V-VAWT model [9]. The blades were connected to the rotating shaft by sheet aluminium that was wrapped around the root area of the blade, clamped securely together to sandwich the wood of the blade, and screwed directly to a small hub on the shaft. This provided a robust fitting, provided the thickness of the blade was not so large that the aluminium became overly distorted. The angle of blade inclination was fixed at 45° in all cases.

The design and construction methods of these simple blades cannot be readily adapted to the case of the specialist V-VAWT model, where each blade must be fitted with pitching tips. A new approach was required. The need for pitching tips significantly complicates the design of the blades. The blade tips must be secured to the root section of the blade and locked at the required pitch angle, yet be free to rotate about their pitch axis for adjustment of this angle. The size of the blade tip must also be variable, to allow the effect of blade tip size to be compared.

The problem of adjusting the size of the blade tip area was crucial to the design and construction of the blade. The solution concept chosen requires the blade to be constructed with a small number of tip sections, each tip section being moveable in pitch, and a fixed root section. The tip sections are all similar in size, and can be fixed either in-line with the root section or in-line with each other. In this way, a large tip area can be created by moving all tip sections together as one. Alternatively a small tip area can be created by moving the outermost tip section by itself, leaving all the other tip sections in-line with the root section. This concept ensures that the geometric properties of the wind turbine model, such as blade aspect ratio, rotor radius, rotor inertia, blade shape, etc..., remain constant throughout the test period. The only variable between tests will be the size and pitch angle of the blade tip. The test results can then be directly compared with each other. Differences between experimental results will be due to either changes of blade tip size or pitch angle, and not differences in the rotor configuration.

The discontinuity between the root section and adjacent tip section is a structural weakness inherent of wind

turbine blades constructed with pitchable blade tips. Here the problem is much worse, since a number of tip sections are proposed. Adopting an internal blade spar becomes very attractive, because continuity of material is created throughout the blade. The blade spar becomes the backbone of the blade, and all other blade material is merely used to create the cross-sectional profile of the aerofoil. This material will add rigidity to the root section, but at the tips all the loads on the tip sections must be supported by the spar alone.

The design of a composite blade, using an internal spar and outer skin material, requires a subtle compromise between material selection and component dimensions to ensure that an effective solution is determined, and that the blade is structurally sound at the survival rotational speed of 2500 rpm. To assist in the process of evaluating proposed design solutions, a structural analysis of the composite blade was developed. The analysis, which is detailed in Appendix 1, assumes the blade to be a stiff, rigid beam. The blade root is modelled either as a simple support or as a built-in support, and the cable support close to the blade tip as a simple support. The blade is straight, and is considered to have a constant chordlength with uniform mass distribution across its span.

The blade is acted upon by three forces:

(a) Aerodynamic
(b) Gravitational
(c) Centrifugal

Aerodynamic forces cannot be explicitly determined and are excluded from the analysis. In the general case, gravitational and centrifugal forces are included. Superposition of forces is assumed, and expressions developed

for shear force, bending moment, axial force, displacement and material stress have distinct centrifugal and gravitational force terms. Here, however, the centrifugal forces are very much larger than the gravitational forces, due the high rotational speed used for design purposes, so the gravitational terms may be ignored.

The structural analysis equations developed in Appendix 1 have been embodied into two computer programs written and developed by the author on a BBC-B microcomputer. The first program, TAYVAWT, is used to initialise all the blade dimensions and material properties. The second program, STAVAWT, performs the static analysis of the blade by evaluating the expressions of Appendix 1 for shear force, bending moment, axial force, displacement and material stresses. This process is repeated at various spanwise ordinates so that results across the whole blade are determined. The numerical results are tabulated on the screen, printed on an attached printer, or graphically displayed on the terminal screen using the graphics facilities of the computer. A summary of forces and bending moments at the root and cable support is supplied, and the position of maximum material stresses is identified.

The details of the programs or their structure are not considered further, since the programs only embody the equations developed in Appendix 1. In their present form, the two programs only provide a general overview of the structural behaviour of a given blade design. They provide sufficient information to assess the likely success of a design and its ability to satisfy the survival speed criterion.

The initial dimensions were, as discussed above, determined by the size of the wind tunnel. The angle of

inclination to the rotation axis was set at 45°, so the blade length was restricted to 700mm. A blade aspect ratio of ten, gives an initial chordlength of 70mm. The cable attachment was set to be in proximity to the 80% spanwise position, and for superior strength the NACA0025 aerofoil section was selected for the blade profile. Thus the maximum thickness of the blade was 17.5mm at the 30% chordwise position. Since the tip sections must be able to rotate about the pitch axis, the spar was initially conceived as being of circular cross section. For bench-mark purposes, the spar material was originally chosen as mild steel, and the skin material as spruce wood.

The maximum stresses calculated for the initial blade design at a rotational speed of 2500 rpm were far greater than the ultimate tensile strength of the materials selected. The repeated use of the analysis programs enabled the design of the V-VAWT model blades to progress quickly to satisfactory overall solution.

Aluminium alloy replaced steel as the spar material because of its superior strength to weight qualities, especially the B.S. 1471 HT30TF grade which immediately gave more promising results. However, initial designs were still too highly stressed and a number of more fundamental changes were made.

The overall blade length was reduced to 665mm, but the cable attachment position was unchanged. This reduced the maximum possible size of the blade tip to 15% of the total blade area. However, the bending moment at the cable attachment point was reduced by approximately 45% by this change.

The blade chord length was increased to 80mm, with the consequential increase in section thickness to 20mm. This

allowed the major dimension of the internal spar to be increased, increasing the stiffness of this member. Typically, the outer diameter of a circular tube spar could be increased from 15.5mm to 18mm, so reducing the maximum stresses in the blade by 35%.

Spar stiffness could also be changed by using different cross-sectional geometries. Hollow sections reduce the overall weight of the blade and so reduce the body forces acting on it, yet the stiffness of the spar need not be greatly affected. Rectangular box sections are stiffer in the direction of the major dimension than a circular section having the same major dimensions, but the availability of small extruded aluminium alloy box sections was somewhat limiting. However, circular tube section was readily available in a number sizes with various wall thicknesses. In order to achieve a good compromise, the blade spar was constructed from circular tube, machined to size to give a rectangular outer geometry. Thus the spar was rectangular in profile, but had a circular bore. This proved to be an effective solution, giving the author the flexibility to accurately control the dimensions of the spar, yet allowing the raw material to be ordered directly from the suppliers in a stock bar form. The tubular section allowed the spindles, on which the tip sections would be positioned, to be readily machined.

The blade skin material was always considered to be solid and made of wood. This would enable the profile of the blades to be hand-crafted to the shape of the NACA0025 aerofoil. Initially spruce was considered suitable, and though a number of different woods were considered, their different structural properties did not significantly affect the stress levels in the blade. Finally, English Ash was selected as the skin material because on inspection of the raw material itself at the suppliers, a

sample of this wood was found to be closely grained, dry and inherently stable. It proved to be more than adequate for this V-VAWT model.

The results of the computer based analysis of the final design concept are summarised in Table 4.1, and the spanwise distributions of shear force, bending moment and flapwise displacement at 2500 rpm for this blade are graphically displayed in Figure 4.1. Having finally determined overall dimensions of the blade and selected suitable materials, the detail design of the blade and other rotor components could begin.

In the final design, the available blade tip area was approximately 15% of the total blade area. Three tip sections, each with an area equivalent to 5% of the total blade area, was considered to give sufficient scope for changing of the total blade tip area during tests. Each section would be positioned on circular spindles machined from the blade spar. The diameter of the spindles reduces from 18mm to 15mm to 12mm for each section, minimising the bending moment acting on the spar at the cable attachment point. The fillet radius between sections is 5mm to ensure low stress levels in these areas. Grubscrews in each tip section secure the pitch angle of the tip, while dowel pins restrain axial movement. The dowel pins require holes to be drilled through the neutral axis of the spar. Although these holes act as stress raisers, this solution was the best of those considered, and the levels of stress were found to be acceptable.

The cable attachment position and method of attachment requires careful consideration. As discussed above, a single cable cannot prevent the blade twisting under the influence of aerodynamic and body forces, primarily centrifugal force here. Using two cables alleviates the

T.ALUM16 BS1471_HT30TF Ash

M = 5.976E-1 kg
N = 2.500E3 rpm
pw = 6.890E2 kg/m^3
ps = 2.705E3 kg/m^3
d = 1.400E-2 m
L = 6.650E-1 m
T = 4.500E1 deg
Iw = 2.208E-8 m^4
Is = 2.344E-9 m^4
b = 1.200E-2 m
A = 5.500E-1 m
EI = 4.269E2 Nm^2
Ew = 1.190E10 N/m^2
Es = 7.000E10 N/m^2
Di = 9.500E-3 m

Do you wish to continue (Y or N)
Rotational Speed =2500.00 rpm

	Z	SF	BM	PF	V	SIGwcm	SIGstm
	mm	N	Nm	N	mm	Nmm^2	Nmm^2
0.00	0.00	1750.06	-235.29	-6805.30	0.00	61.03	296.86
1.00	35.00	1730.98	-174.26	-6786.65	0.31	44.03	226.74
2.00	70.00	1674.17	-114.56	-6730.28	1.12	27.43	157.99
3.00	105.00	1579.64	-57.51	-6636.19	2.26	11.59	92.14
4.00	140.00	1447.39	-4.43	-6504.36	3.56	-3.12	30.69
5.00	175.00	1277.40	43.37	-6334.82	4.88	7.85	74.71
6.00	210.00	1069.69	84.55	-6127.55	6.07	19.47	121.17
7.00	244.00	824.26	117.80	-5882.55	7.03	28.90	158.37
8.00	280.00	541.10	141.81	-5599.83	7.65	35.78	184.81
9.00	315.00	220.22	155.24	-5279.38	7.86	39.74	198.97
10.00	350.00	-138.39	156.78	-4921.21	7.63	40.41	199.33
11.00	385.00	-534.73	145.11	-4525.31	6.96	37.42	184.37
12.00	420.00	-968.79	118.91	-4091.68	5.87	30.41	152.59
13.00	455.00	-1440.57	76.86	-3620.33	4.44	19.00	102.47
14.00	489.00	-1950.09	17.63	-3111.26	2.80	2.83	32.49
15.00	525.00	-2497.32	-60.09	-2564.46	1.11	15.03	79.06
	550.00	-2911.30	-127.66	-2150.79	-0.00	34.14	154.99
	550.00	2152.22	-127.66	-2150.79	-0.00	34.14	154.99
16.00	560.00	1981.24	-106.99	-1979.93	-0.40	28.50	130.59
17.00	595.00	1358.55	-48.43	-1357.68	-1.63	12.59	60.93
18.00	630.00	698.14	-12.33	-697.70	-2.72	2.97	16.90
19.00	665.00	0.00	0.00	0.00	-3.77	0.00	0.00

Ra = 1750.06 Ma = -235.29 Pa = -6805.30

Rb = 5063.52 Mb = -127.66 Pb = -2150.79
Shear Force at Z= 336.00 mm is Zero
Bending Moment at this point = 157.68 Nm
Displacement at this point = 7.77 mm
Compressive Stress in Ash is = 40.57 N/mm^2
Tensile Stress in BS1471_HT30TF is = 200.90 N/mm^2
Do you wish to continue (Y or N)

Table 4.1: Summarised output of computer based structural analysis of the finalised model V-VAWT design operating at 2500 rpm

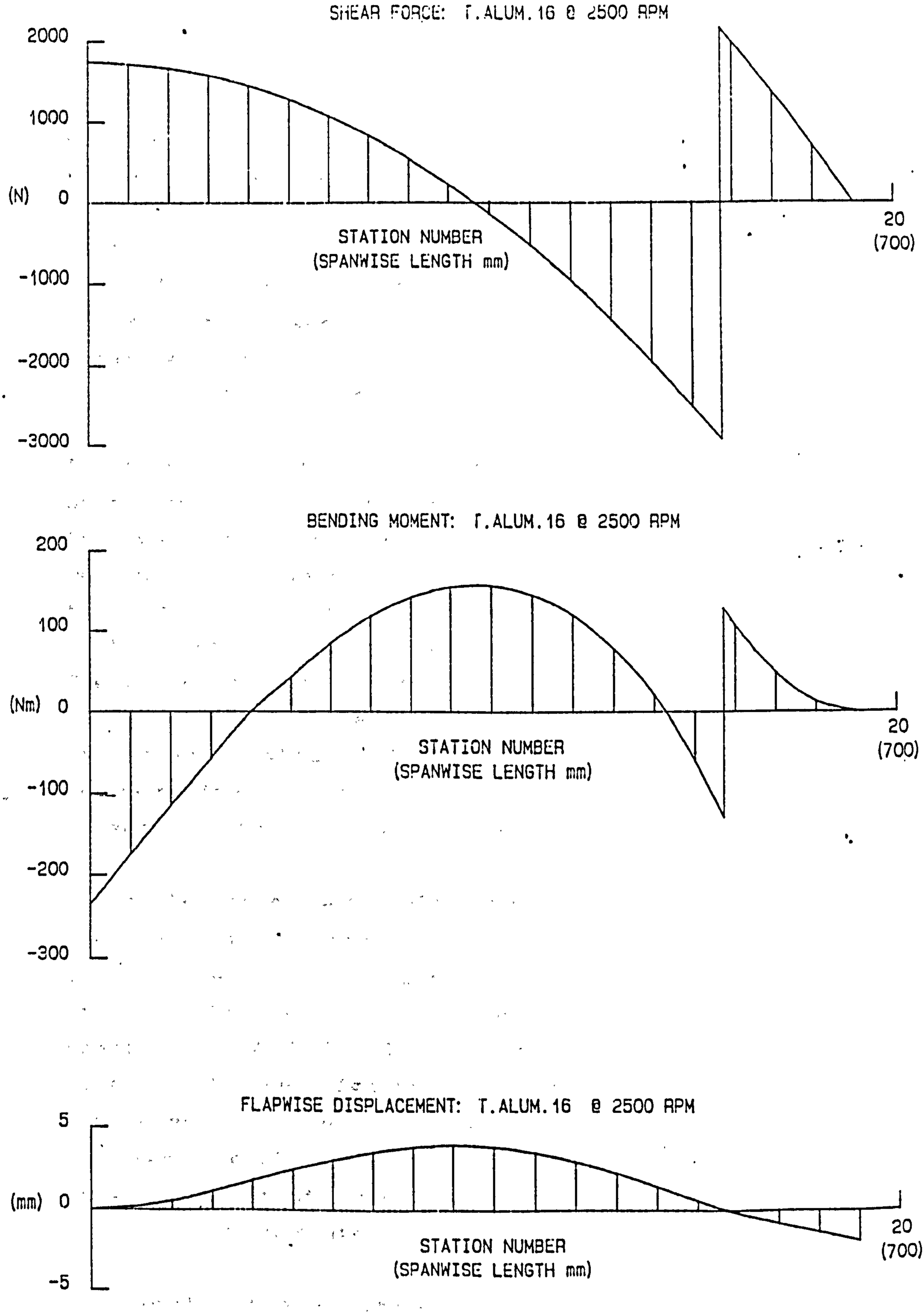

Figure 4.1: Spanwise distributions of shear force, bending moment and displacement for the finalised model V-VAWT design operating at 2500 rpm

problem of blade twist due to centrifugal force, provided the chordwise positions of the blade mass and flexure centres fall between the two cables. The spar is placed at the 30% chordwise position because this is the position of maximum blade thickness. In this design, the centres of mass and flexure very close to each other. The cable attachments were chosen to be at 20% and 40% chordwise positions, thus ensuring no blade twisting would occur.

A number of methods for attaching the cables to the blades were considered, and most were rejected because they involved drilling holes through the blade spar, thus weakening this member at a highly stressed position. the final solution involves using a single, continuous cable that is looped around the spar at the attachment point. The cable rests in a small groove machined into the spar. The groove distributes the cable loading over a large area of the spar, while ensuring a maximum material condition is maintained at this location. The groove is a stress raiser, so its fillet radius is made as large as possible.

The cable forces were calculated to be in excess of 2000N, therefore 2mm diameter, 7 x 7 round strand steel wire had to be selected to support this design load. The wire diameter is much larger than the piano wire used on previous V-VAWT models, therefore the parasitic drag losses will be significantly larger. However, these losses are measured in the wind tunnel and corrections to the test results applied as appropriate. It was not possible to obtain smaller diameter wire that would have its strength guaranteed to the limits required here.

The length of each cable had to be adjustable to ensure that each is equally tensioned. The cable adjusting screws are assembled onto the wire rope before the cable

endings are attached at the rope suppliers. The screws are fitted directly into the aluminium alloy cable hub.

The blades were much thicker than previous V-VAWT models, so that the usual blade root attachment method was unsuitable here. The method devised requires the blade spar to be rigidly attached to a U-shaped root component. This allows the blades to be screwed directly to the aluminium alloy root hub. The blade spar root is effectively wider across its chord, allowing space for six high tensile, hub fixing screws that are sized appropriately. The modification to the blade spar is completely contained within the blade section, and so provides a neat, unobtrusive blade attachment.

The forces and bending moments calculated using STAVAWT were used as the basis of detailed analysis of all the features of the design that were of special interest. However the use of standard data sheets and simple hand calculations gave the author an unrivalled appreciation of the problems involved in designing a reliable and structurally sound wind turbine model. The detailed analysis was required to ensure the correct sizing and selection of components was maintained throughout the design.

Detailed stress analysis was carried out for the following features of the design:

(a) tip section dowel holes
(b) tip section dowel pins
(c) spindle fillet radii
(d) cable attachment groove
(e) sizing of cable adjustment screws
(f) cable hub dimensions
(g) blade root component dimensions
(h) blade spar

(i) root/spar attachment

(j) root/hub attachment

(k) sizing of root/hub securing screws

(l) root hub dimensions

The results of the analysis are not presented here, but the extensive analysis of the design led to a final solution that was complete in every detail as reported by the author in an interim report [55].

The author prepared detail drawings of all components and was responsible for overseeing the procurement of all raw materials and manufacture of all specialist parts. A computer based three dimensional solid model was also prepared using GEOMOD, a commercial quality CAD applications package. The solid model enabled the complete assembly of parts to be simulated, and has allowed the author to visualise the final solution *before* authorising manufacture, Figure 4.2. By specifying the mechanical properties of the component parts, it was possible to estimate the moment of inertia of the wind turbine model. The computer estimate compared favourably with that actually measured (Chapter Five).

4.4: Manufacture and Assembly of the Model V-VAWT

The manufacture of the model V-VAWT was carried out in the workshop facilities of The Open University by Mr Scott Forrest. The aluminium alloy was specially bought in with its mechanical properties certified by the suppliers. It is easily machinable and the manufacture of the blade spars and support hubs was carried out using conventional machine tools. The blade spar and root components were completely manufactured in accordance with the detail drawings as prepared, before being assembled as one.

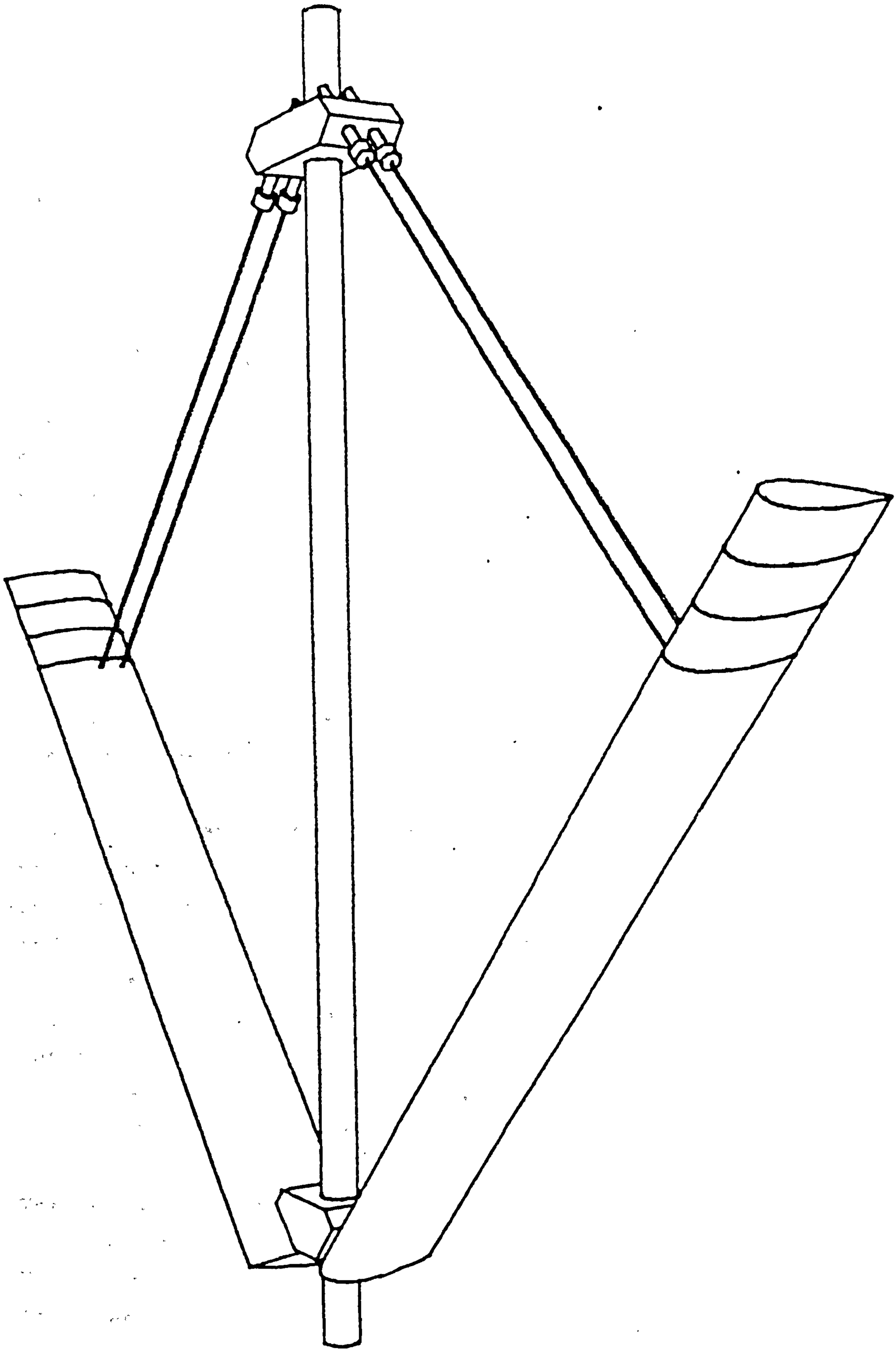

Figure 4.2: Computer based 3D solid model of model V-VAWT with pitching tips

The root section of the blade was made from leading edge and trailing edge sections. A slot was routed out in each section to provide a cavity for the blade spar; Figure 4.3 shows the blade spars and skin material before joining.

The blade spar and root were then enclosed between the leading edge and trailing edge sections, which were firmly joined together with glue resin. With the composite blade complete, the skin material was rough planed before hand finishing to a NACA0025 aerofoil section profile. A brass template was used to check the accuracy of the blade to this profile. Where the root of the spar was widened, a large amount of wood had to be removed to ensure a good fit between the skin and spar was achieved. The material lost was made good using epoxy filler. Once hard set, the filler was easy to work. The blade profile could be restored without creating any discontinuities between the wood and the filler, Figure 4.4.

The cables came from a specialist wire rope supplier with the adjusting screws ready fitted. The rope supplier was able to guarantee the reliability of the cable fittings and ensure the specified mechanical properties of the rope. A small slot at the end of the root section of the blade allowed the cables to be looped around blade spar, before being secured in position with epoxy filler. The filler allowed the blade profile around the cable attachment to be made good as shown in Figure 4.5.

The blade tips were made from solid wood and hand-crafted to the aerofoil profile using the template as a guide. Each tip section was drilled through, and brass plates inserted into a small slot. The dowel pins bear against

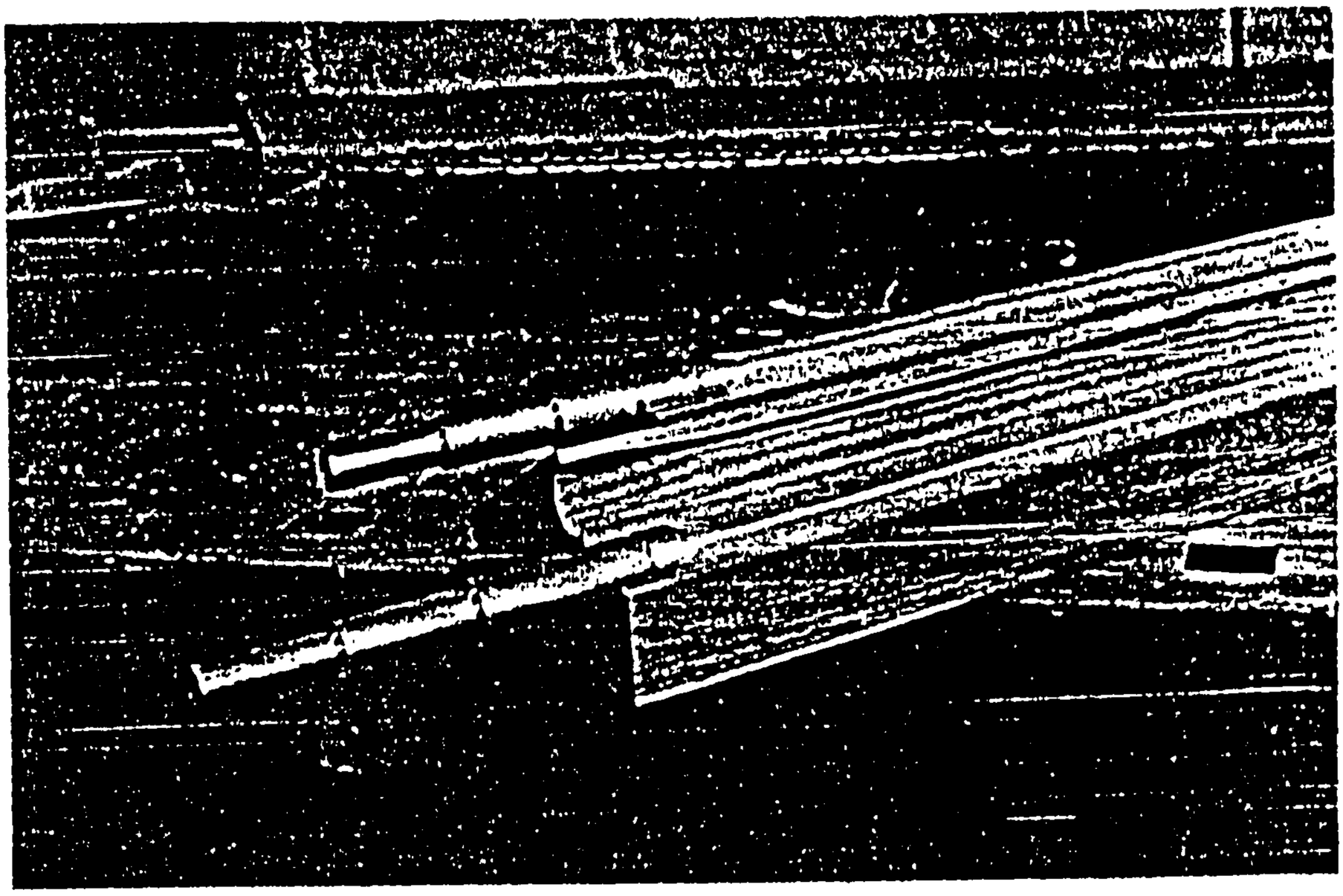

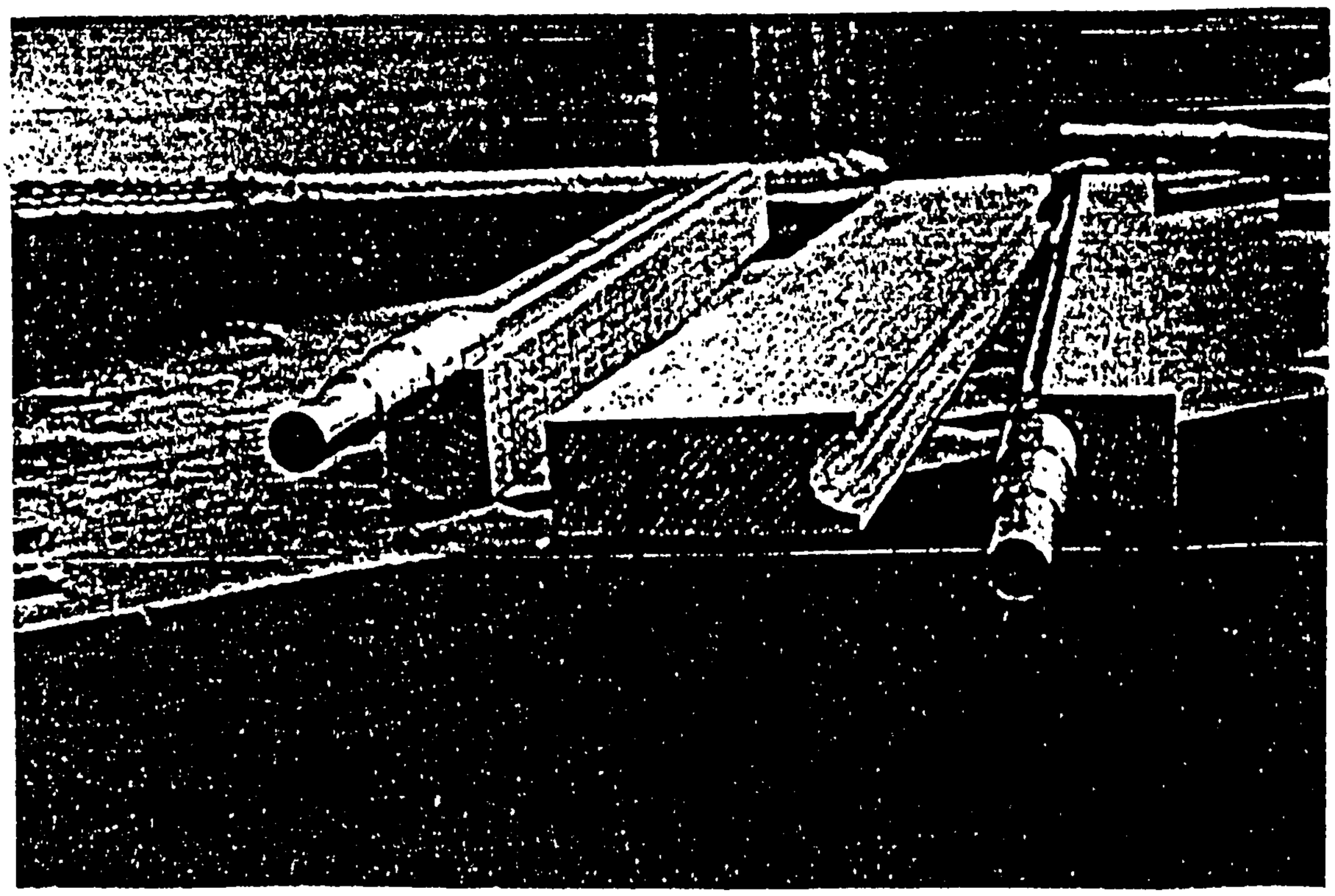

Figure 4.3: Blade spars and skin material before joining

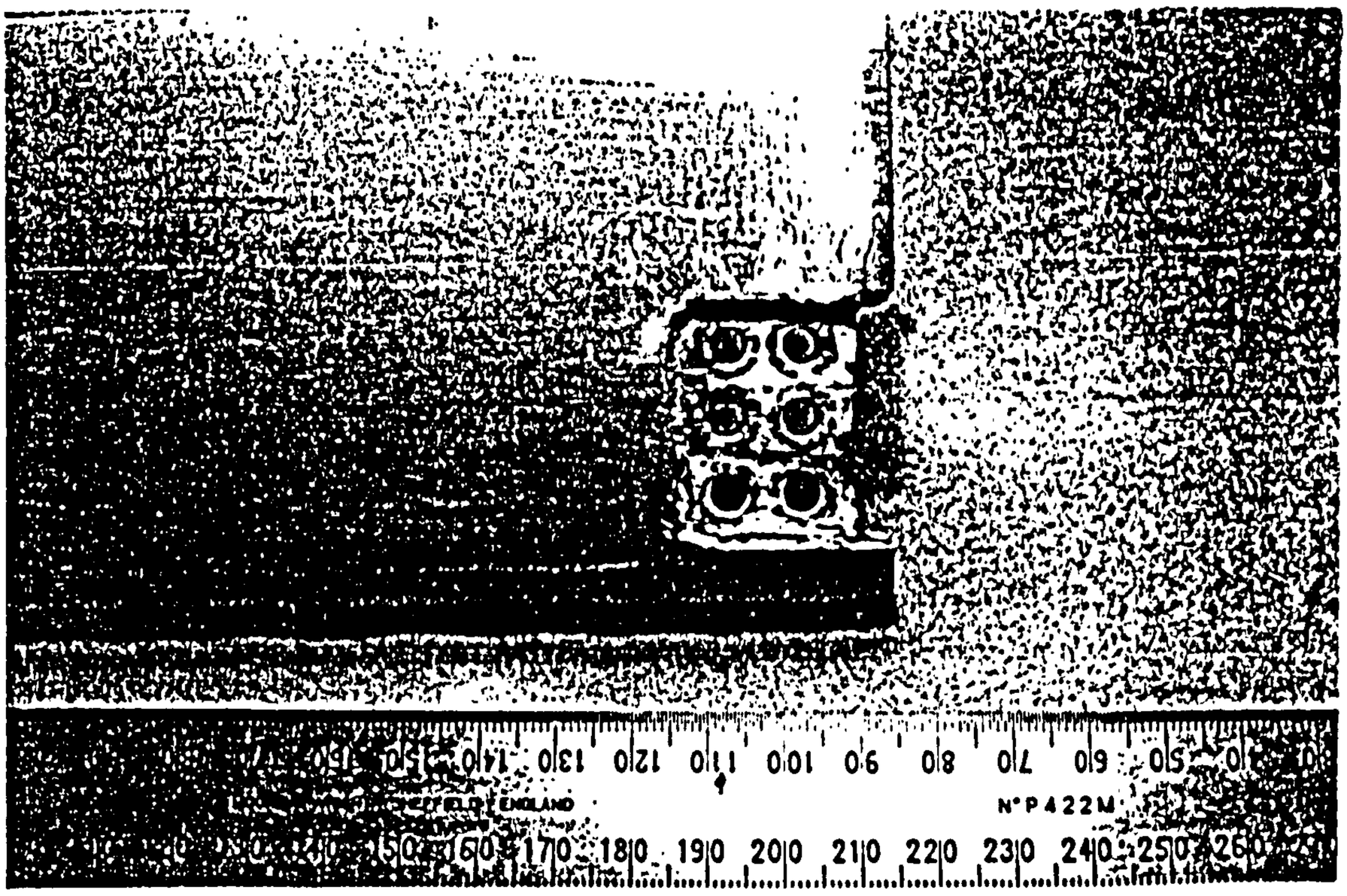

Figure 4.4: Blade root showing hub attachment

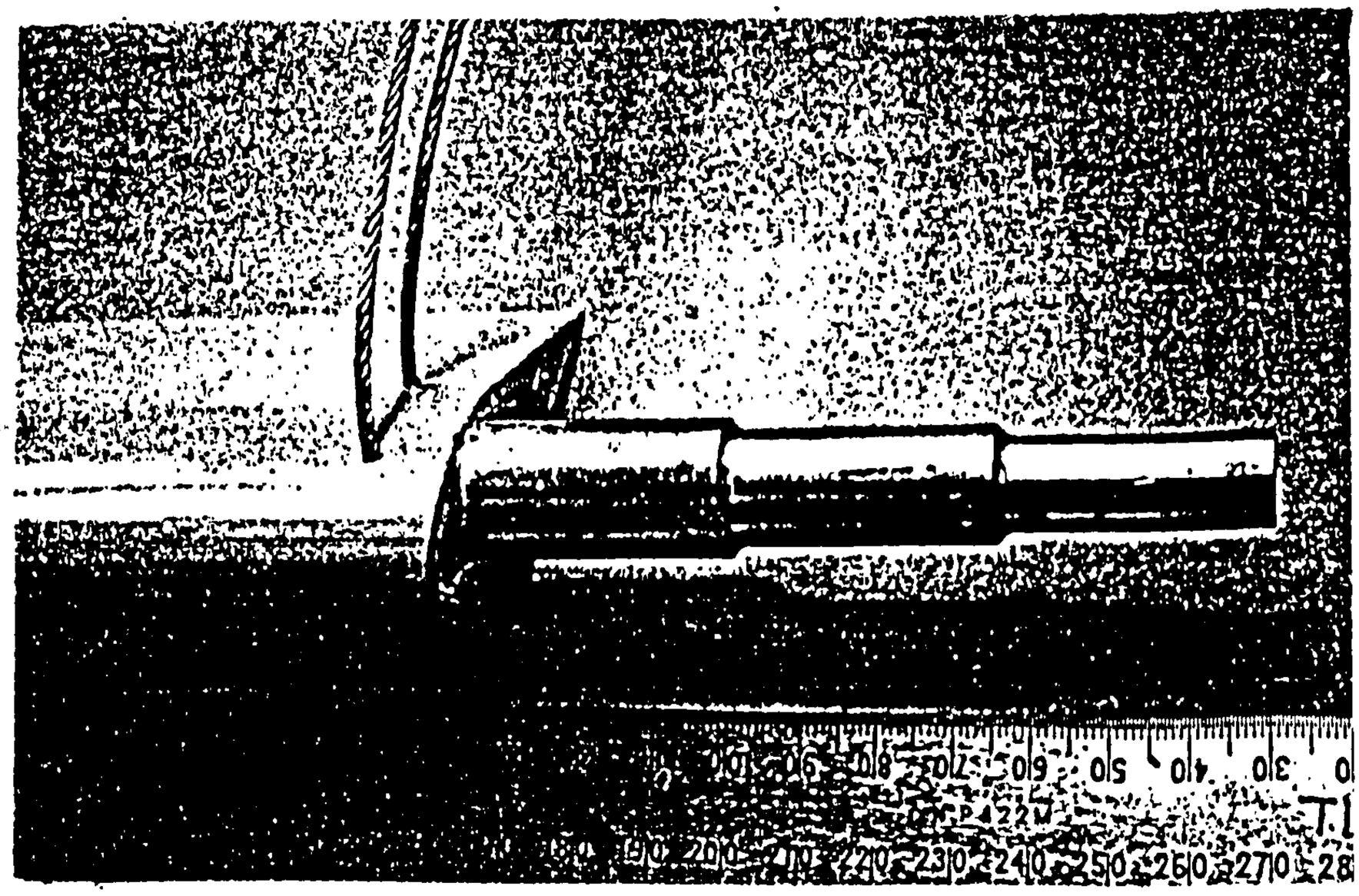

Figure 4.5: Blade tip showing cable support and spindles for tip sections

the brass plates to restrain the tip sections axially. The pitch locking grubscrews are supported by a small brass tube inserted into the leading edge. The grubscrews are adjusted from holes drilled in the leading edge of the tip section, and act directly onto the spindle supporting the tip. During testing, the holes are filled with soft wax which allows the leading edge profile to be restored for the duration of the test. Figures 4.6 and 4.7 show the finished tip sections as described.

Once the blades and tip sections were fully assembled and the profile finished, numerous coats of paint primer and topcoat were applied to the wood. Each coat of paint was allowed to harden, before being cut back with fine emery cloth and another coat of paint applied. This process was repeated many times, until a smooth, glossy surface finish was achieved.

The tip sections were then sequentially assembled onto the blade spar spindles. Each section is secured by the dowel pin which is inserted into the dowel hole through a small hole in the leading edge of the tip. Once secured, the hole in the tip was made good with wax and the leading edge profile restored.

The two blades were now complete and could be assembled in the workshop with the root hub and cable hub. The success of the variable tip area concept could now be judged and Figures 4.8 to 4.11 show the blade tip with 5%, 10% and 15% tip areas locked in pitch. Once complete, only the size of the locking grubscrews needed modification, since it was not possible to "feel" the locking torque being applied.

In general, few problems were encountered in the manufacture of the wind turbine and the components assembled

easily together in the workshop. Once satisfied all was complete, the components were transported to Queen Mary College where they were assembled into the spaceframe, see the Colour Plate on page (vii).

4.5: Conclusions

The design of a specialist V-VAWT model with pitching tips proved to be an interesting and stimulating exercise in engineering design. The constraints imposed upon the author has led to a robust design that has a potential survival speed of 2500 rpm. A consequence of this has been that the wind turbine model is significantly larger than any previous V-VAWT model, and is much more complicated in its construction. Extensive structural analysis was required to ensure that the final design solution would satisfy the survival speed criterion. However, the author is satisfied that an effective design solution has been prepared, and that a worthy wind tunnel V-VAWT model has been constructed.

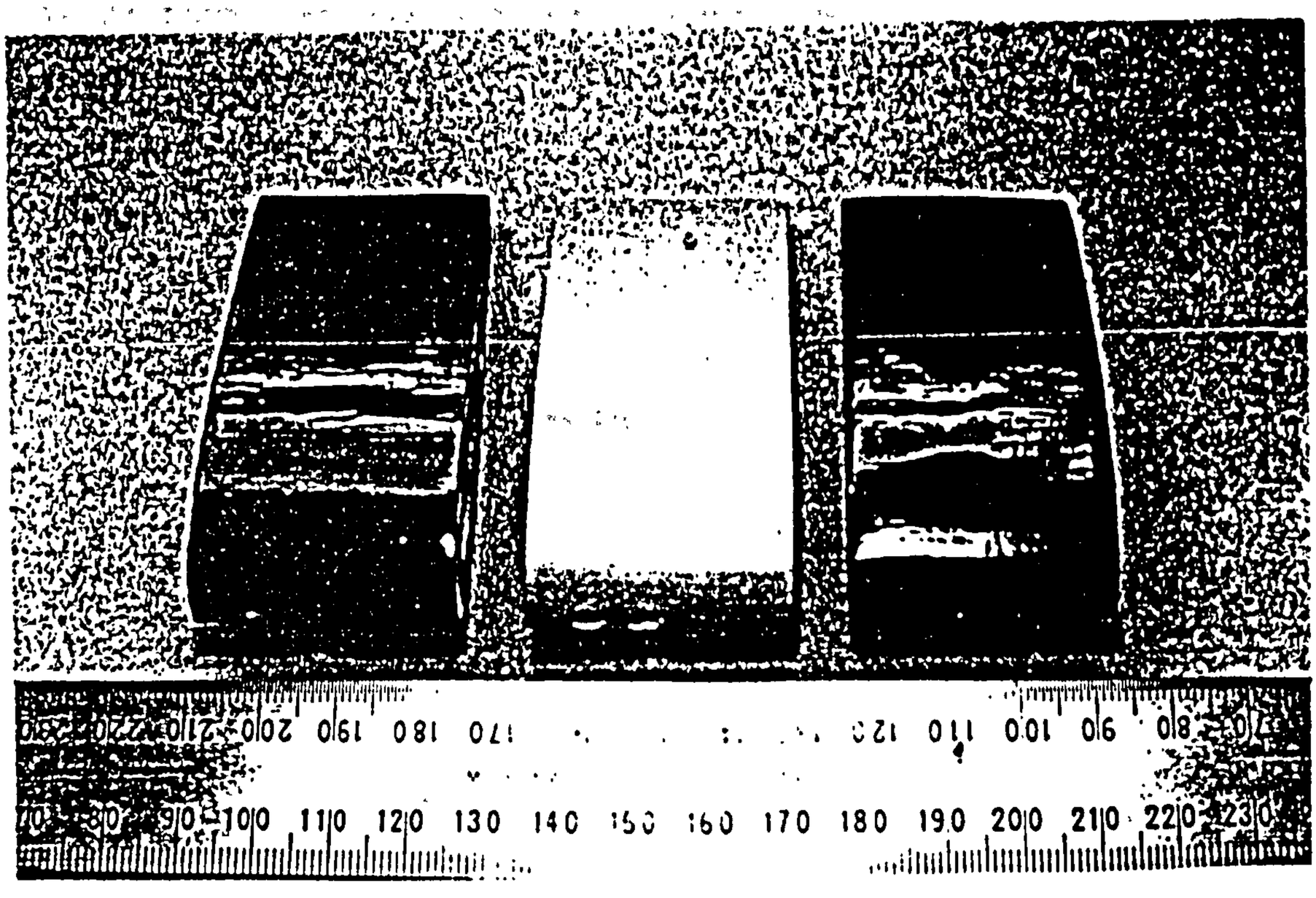

Figure 4.6: Frontal view of tip sections showing leading edge grubscrew access holes

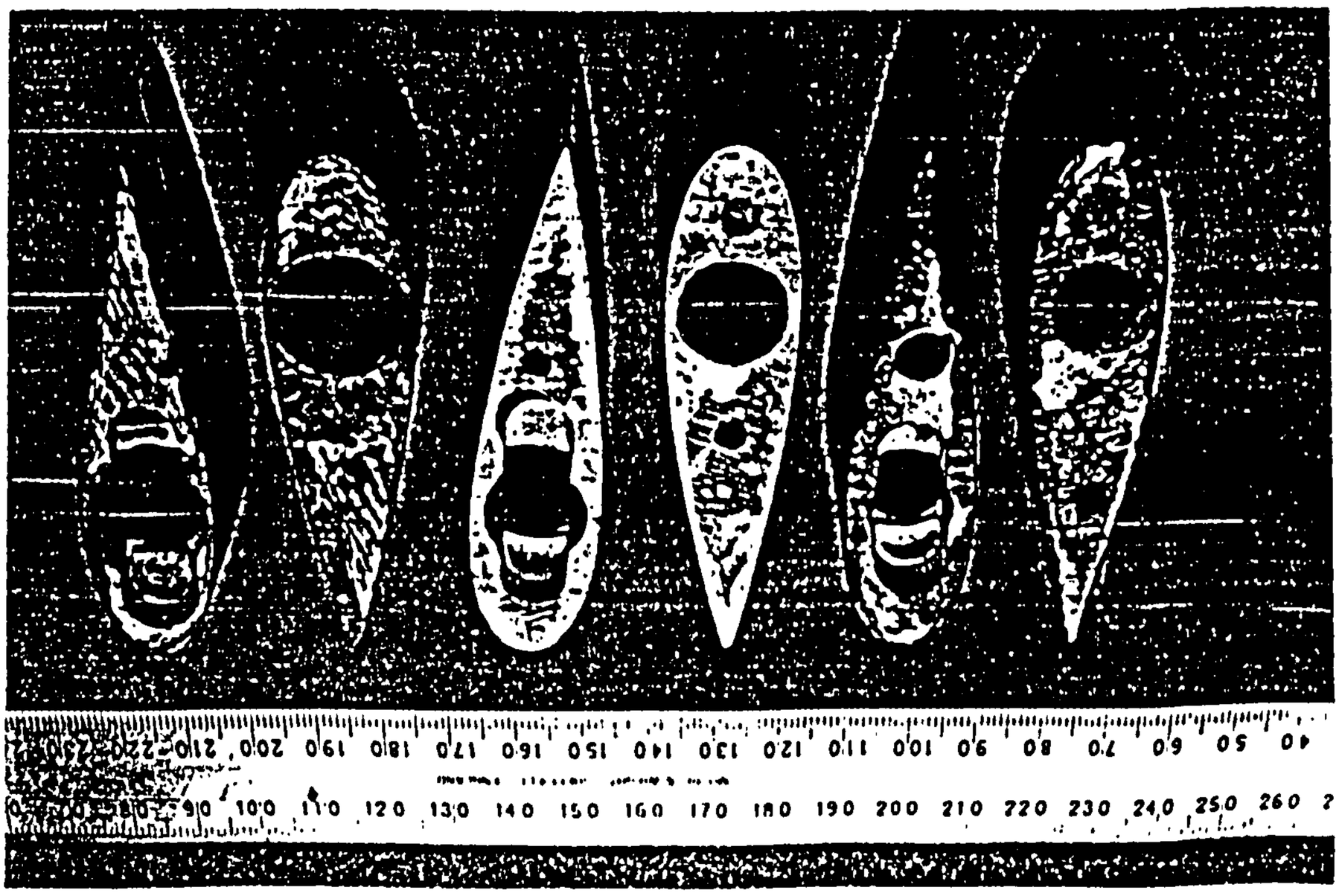

Figure 4.7: End view of tip sections showing variation of bearing diameter and brass plate inserts

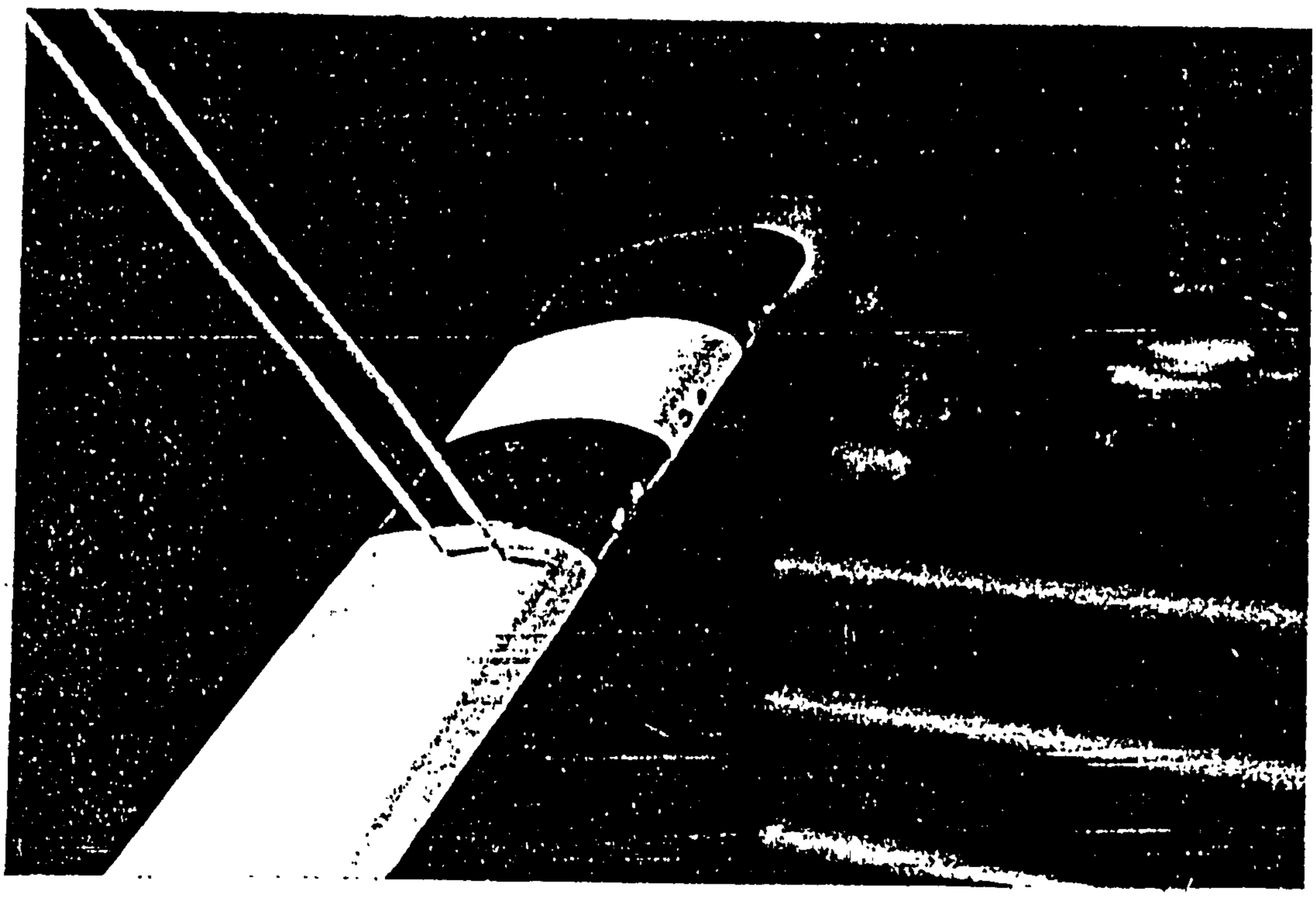

Figure 4.8: Blade tip area showing normal running condition with zero tip pitch offset

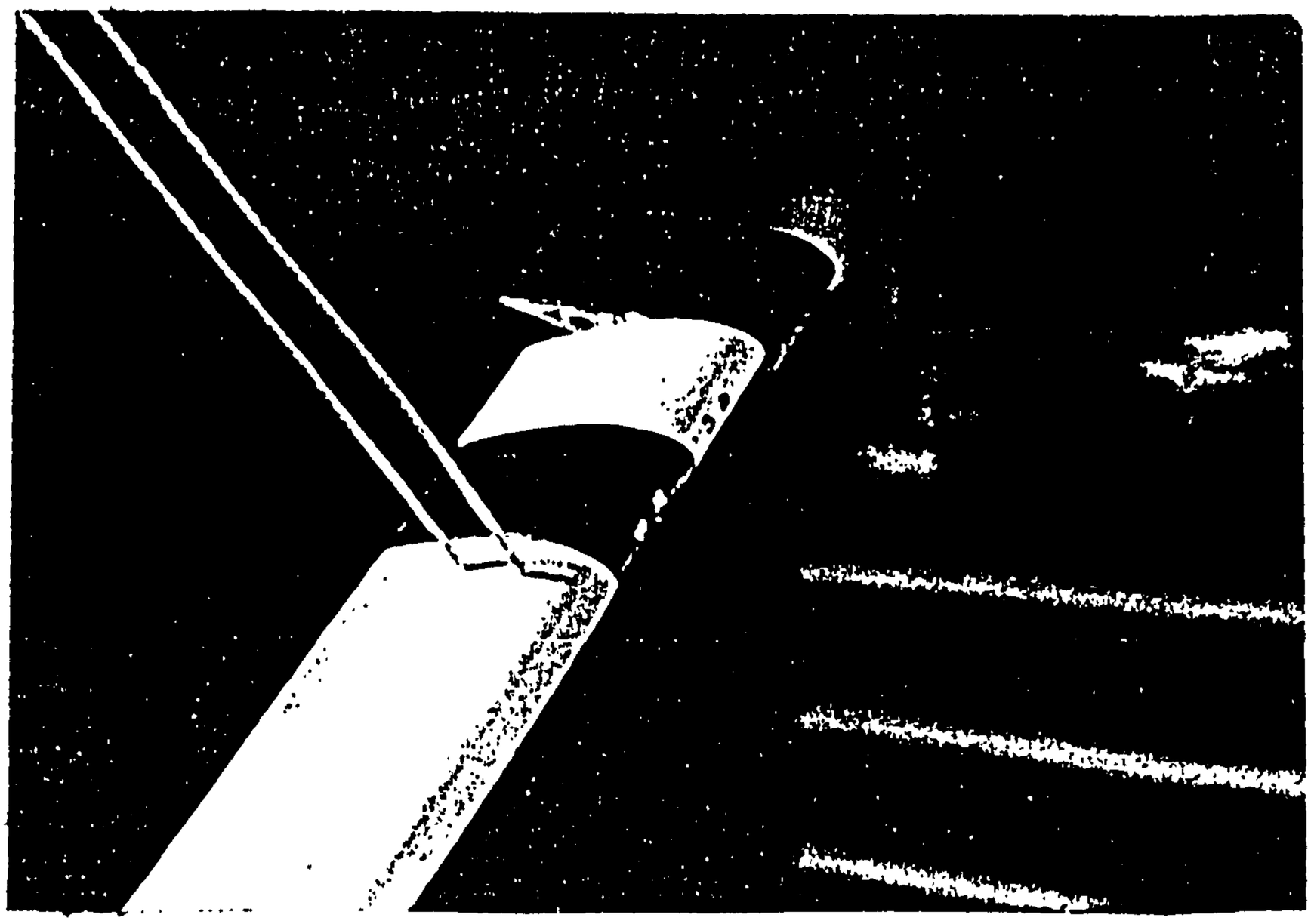

Figure 4.9: Blade tip area showing 5% tip area and small nose-out pitch offset

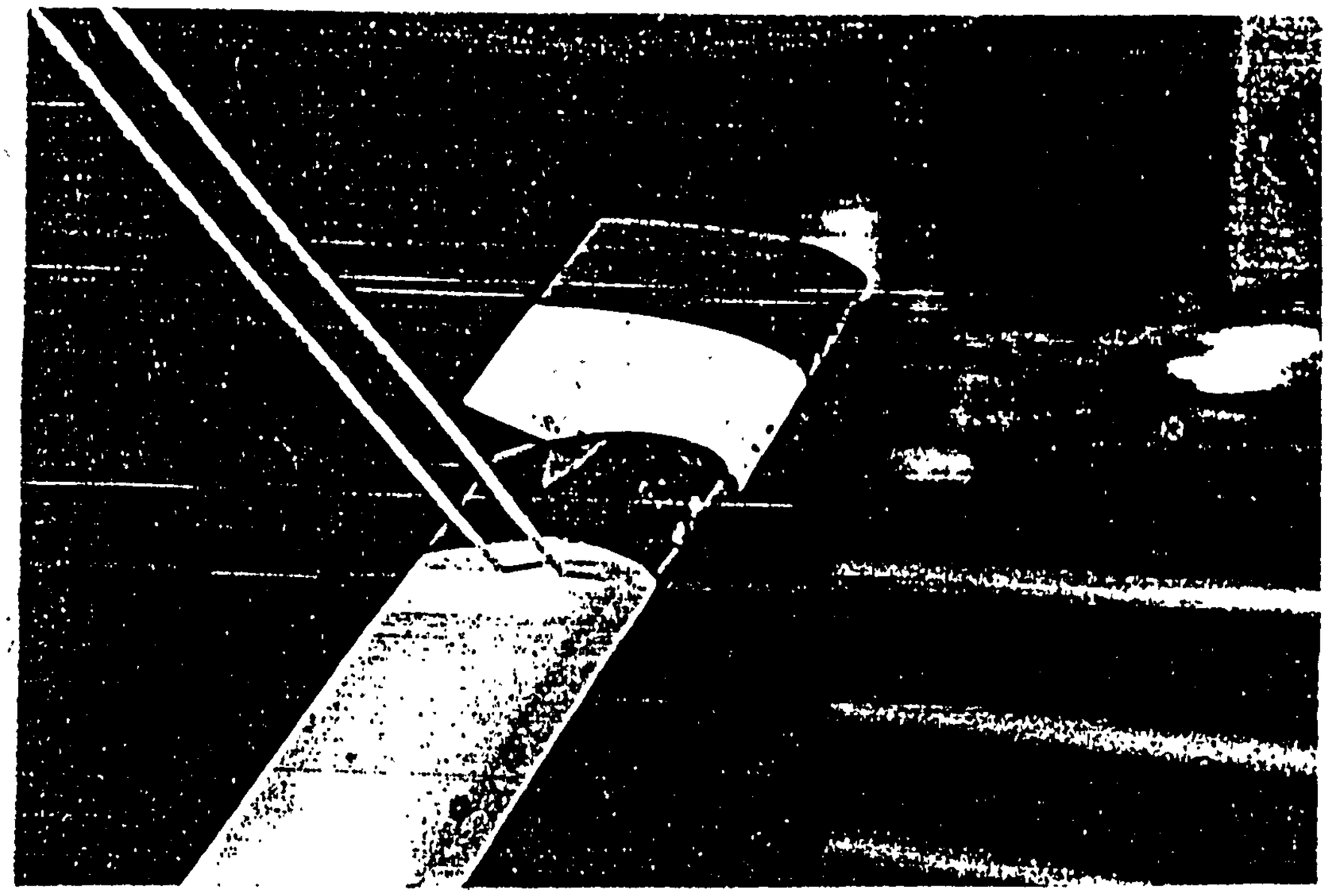

Figure 4.10: Blade tip area showing 10% tip area and small nose-out pitch offset

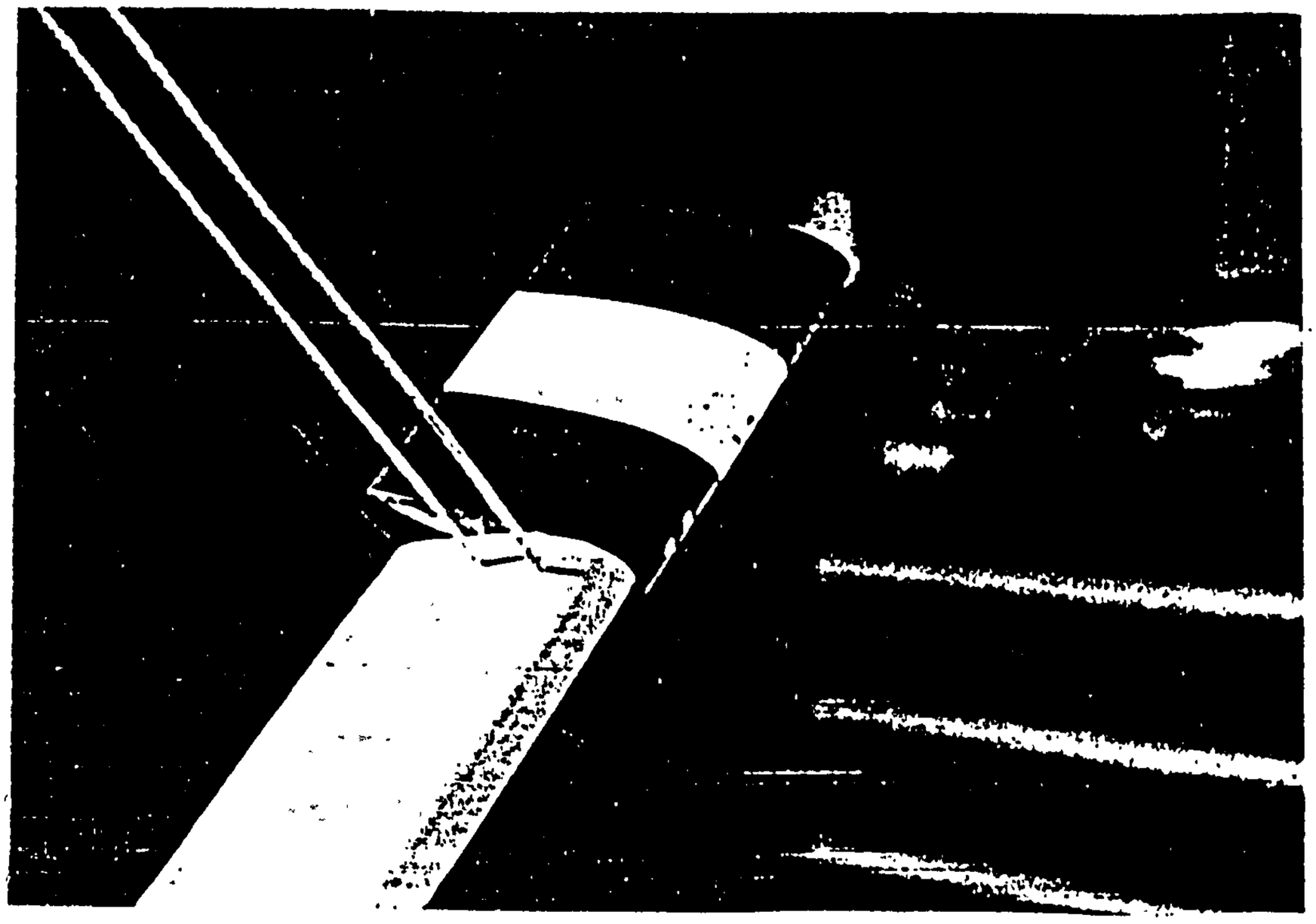

Figure 4.11: Blade tip area showing 15% tip area and small nose-out pitch offset

Chapter Five: Performance Testing of the Model V-VAWT

5.1: Performance Test Objectives

The objectives of the performance testing of the model V-VAWT described in the previous chapter were twofold:

(a) to measure the effect of the variation of blade tip pitch and blade tip area on the performance of the model V-VAWT, and so determine whether pitch tip control is a suitable aerodynamic control method for the V-VAWT.

(b) to provide further wind turbine performance data for the verification of the performance prediction program VAWTTAY.

These were considered to be only modest objectives for the test program, but the wind tunnel was only available for a short period of time and all experimentation had to be completed within two weeks. During the course of the work a number of interesting effects were observed, but it was not possible to examine these effects in any detail in the time available. However, these passing observations will be discussed later.

The blowdown wind tunnel in the Department of Aeronautical Engineering, Queen Mary College, London was used for this experimental work . This facility had been previously used by Sharpe to conduct the first performance measurements of model V-VAWTs. For convenience the equipment and experimental techniques developed for those tests were used for the experimental work presented here.

The wind turbine model was rigidly attached to a vertical steel shaft which was simply supported by two bearings

mounted in a tubular steel space frame. The space frame was free-standing, allowing it to be moved around the laboratory.

During the performance evaluation tests, the space frame was positioned so that the axis of rotation of the model V-VAWT was approximately one metre downstream of the wind tunnel diffuser. In this position the wind turbine was able to rotate freely, airflow around the turbine was unimpeded and measurement of the upstream windspeed could be made with some confidence. A coarse wire mesh was hung between the space frame and the wind tunnel diffuser for safety purposes. It is believed that the mesh did not restrict the air movement around the turbine.

The acceleration method developed by Sharpe [23], and subsequently used by other experimentors, was adopted for the measurement of the model V-VAWT performance. This technique is a simple and quick method for determining the complete C_{pm}-λ characteristic of a wind turbine operating in constant windspeed conditions. However, it is not sufficiently sensitive to allow for the measurement of cyclic torque variation.

The acceleration method requires that the wind turbine model be allowed to accelerate from near rest until it reaches a constant rotational speed. The rate of acceleration is dependent upon the net torque being developed by turbine at any instant and the moment of inertia of all rotating parts. When the wind turbine reaches a constant rotational speed, the net torque acting on the turbine is zero. At this rotational speed the magnitude of aerodynamic torque being developed by the blades is equal to sum of parasitic losses due to friction in the bearings and aerodynamic drag on the blade support cables and other rotating components. Since the

aerodynamic performance predictions of VAWTTAY do not account for parasitic losses, these losses had to measured separately and the test results corrected as appropriate.

The rotational speed at which the aerodynamic torque and parasitic losses were in equilibrium, was the maximum speed at which the wind turbine would operate without assistance. In order to obtain performance data for higher rotational speeds, it was necessary to drive the wind turbine via a friction contact with a small electric motor. At the higher rotational speeds the parasitic losses are greater than the aerodynamic torque being developed by the blades, so that when the motive power was released, the wind turbine would deccelerate until it reached the equilibrium speed once more.

Whenever the wind turbine was accelerating or retarding unaided, the rotational speed of the turbine was measured and recorded by a microcomputer at regular time intervals. From these measurements it is possible to calculate the instantaneous acceleration of the turbine at a particular rotational speed, and given the moment of inertia of all the rotating parts, the net torque can be calculated.

The acceleration tests were carried out with the wind tunnel exit speed constant. Generally the exit speed was 4 m/s which, for this particular wind turbine model, was equivalent to a wind Reynold's Number WRe ≃ 70,000. The implications of operating at a low WRe will be discussed below.

From the measurements of torque and windspeed it is possible to calculate the non-dimensional coefficients of torque C_Q and power C_P for various Tip Speed Ratios λ. The results of the all measurements will be presented in both these forms.

Since the wind tunnel model was designed with three moveable tip portions on each blade, the C_{r_2}-λ and $C_{p_{max}}$-λ characteristics were determined for tip areas of 5%, 10% and 15% of the blade area, with pitch angles of ±30°. The pitch angle of the tip portion of each blade was preset before each test and could not be altered dynamically during the test period. In all some forty pitch angle/tip area combinations were evaluated, and the results from these tests are presented below. Before, however, considering the experimental results, the experimental methods and procedures are discussed in greater detail.

5.2: Description of Test Facilities and Equipment

All previous wind tunnel testing of model V-VAWTs had been at Queen Mary College, London where Mr David Sharpe has established a suitable test facility in the Department of Aeronautical Engineering. This facility was used for the wind tunnel investigations as described here.

The model V-VAWT was placed near the exit of a blowdown wind tunnel capable of producing exit windspeeds in excess of 14 m/s. The exit of the wind tunnel is rectangular, 1.26 m wide by 1.00 m high, and the model was positioned approximately one metre downwind of the exit. The diameter of the rotor was measured as D = 0.96 m, and its height H = 0.47 m.

The windspeed at the wind tunnel exit is calculated from the measurement of the dynamic head of the air passing through an upstrean contraction in the wind tunnel. The pressure difference is measured using a Betz Manometer. This manometer uses water as the working fluid and had a vernier scale with a resolution of ±0.05 mm with which to measure the water column height. Typically a measured

water height of 23.5 mm would be equivalent to a tunnel exit windspeed of V = 14 m/s.

The contraction is immediately upstream of the enclosed working section of the wind tunnel, and the Betz Manometer measurement is usually used to calculate the windspeed in the working section. To use the same measurement for calculating the windspeed at the tunnel exit, a correction is applied to account for the difference in the cross-sectional areas of the working section and the rectangular exit. This correction factor is automatically included in the microcomputer calculation of exit windspeed.

The validity of the windspeed measurement was not checked since the wind tunnel is frequently used by staff and students of Queen Mary College for experimental work, and the calibration factor given was accepted as accurate.

The model V-VAWT was held in a free-standing tubular steel frame with the vertical shaft supported in two bearings allowing free and easy rotation. The steel frame was positioned approximately one metre downstream of the wind tunnel exit, and for safety purposes a coarse wire gauze was suspended between the frame and the tunnel walls. The area of the laboratory immediately behind the model V-VAWT was clear, and the rear wall of the room was some 5 to 6 m downstream of the turbine. A cloth backdrop was suspended from the ceiling of the laboratory to absorb wind energy and reduce the turbulence around the test environment.

Essentially, the model V-VAWT operated in an open jet tunnel. In these operating conditions, corrections for wind tunnel blockage, which in this case would be solid-blockage, need not be applied. Sharpe has applied, on previous occasions, wind tunnel blockage corrections to V-VAWT power measurements [19]. The validity of using

blockage corrections in open jet testing is in doubt, so none have been applied to the measurements made here.

The acceleration method is a simple technique for determining the torque being developed by the model V-VAWT. It requires only the variation of the angular velocity of the wind turbine to be measured with respect to time as the rotor accelerates against its own inertia. The angular velocity of the wind turbine was measured with a d.c. tachometer that was coupled directly to the wind turbine shaft. The analogue output voltage from the tachometer was converted by an analogue-to-digital converter into a 12-bit digital signal which could be recorded by a PET microcomputer. The digital signal was used to calulate the angular velocity of the wind turbine. The accuracy of this measurement had been previously verified by observing the frequency of rotation of the rotor using a variable frequency stroboscope. In this way, a suitable angular velocity calibration factor was determined. The internal clock of the microcomputer was used to record time. The microcomputer enabled rapid and accurate measurements of the wind turbine angular velocity to be recorded.

The ambient conditions of air pressure and air temperature were measured with a mercury barometer and mercury thermometer respectively. These measurements were used to calculate the air density.

Since all the angular velocity measurements were recorded by the microcomputer, the analysis of the measurements was carried out using the PET microcomputer. The computer programs used throughout the wind tunnel testing period were all written by Sharpe, and modifications were only made for convenience. Since the computer programs, test facilities and test techniques were all well developed,

only a short amount of time was needed to set-up the equipment before the initial measurements could be made.

5.3: The Acceleration Method

The acceleration method for determining the torque characteristics of model wind turbines was devised by Sharpe for his wind tunnel investigations of model Darrieus wind turbines [20,23]. Subsequently, many other experimentors have adopted this simple technique for determining the power characteristics of other wind turbines operating both in wind tunnel and the free-air environments.

The acceleration method is a simple and quick method for determining the power characteristics of a wind turbine since it only requires that the wind turbine accelerates against its own inertia, and that during this acceleration period the angular velocity of the rotor be recorded with respect to time. The wind tunnel air speed during the acceleration period is not altered. From the measurements of angular velocity ω and time, at any instance during the acceleration period, the instantaneous angular acceleration $\dot{\omega}$ is determined by numerical differentiation using the Taylor Series. Given the moment of inertia J of the rotor, the instantaneous net shaft torque Q_s being developed is calculated.

The instantaneous torque developed by the rotor is:

$$Q_s = J\dot{\omega} \tag{5.1}$$

The use of numerical differentiation to calculate instantaneous angular acceleration is not ideal, since it is possible to introduce large calculation errors especially when the rate of change of angular velocity is small.

However, it was not possible to measure angular acceleration directly, so the sensitivity of this calculation using the Taylor Series numerical differentiation technique was thoroughly investigated to ensure the method could be used with confidence. This investigation is discussed in Appendix 2.

The acceleration method is used throughout this experimental test programme to measure the torque being developed by any rotating body, not just that developed by the wind turbine.

5.4: The Measurement of Moment of Inertia

The measurement of the moment of inertia of the rotating system is essential for the calculation of instantaneous shaft torque, as shown above, and is carried out before any other tests are made. The method adopted for determining the moment of inertia J of a rotating system is as follows:

A chord, of diameter d, is wrapped around the shaft, of diameter D, a number of times and tensioned at each end by two springs, of stiffness k. The shaft is given a small initial angular displacement and released. As the shaft gently oscillates, the angular velocity of the shaft ω is recorded with respect to time using the PET microcomputer, and from these measurements the period of motion τ is calculated. The procedure is repeated a number of times for accuracy.

The calculation of the moment of inertia considers the free body motion of the rotating parts. If the instantaneous angular position of the body is θ, then the torque, q, imparted on the body by the springs is given by:

$$q = 2r^2k\theta \tag{5.2}$$

where the moment arm, r, is:

$$r = \frac{(D + d)}{2} \tag{5.3}$$

The free body motion by D'Alembert's Rule gives:

$$q = - J\ddot{\theta} \tag{5.4}$$

substituting for q and rearranging gives:

$$\ddot{\theta} + \frac{2r^2k\theta}{J} = 0 \tag{5.5}$$

compare this with the general equation of motion of an undamped rotating free body:

$$\ddot{\theta} + \omega_n^2\theta = 0 \tag{5.6}$$

where the natural frequency, ω_n, of oscillation of the body is:

$$\omega_n = \frac{2\pi}{\tau} \tag{5.7}$$

Hence the moment of inertia of the free body is:

$$J = \frac{r^2k\tau^2}{2\pi^2} \tag{5.8}$$

The method described above is used to measure the moment of inertia of all rotating bodies as required. The constants of equation (5.8) were measured as r = 12.77 mm

and k = 192.8 N/m. These values were used in all subsequent calculations of moment of inertia.

5.5: The Measurement of Bearing Friction

The bearing friction is measured without the blades attached to the rotor, leaving only the blade hub and cable hub attached to the vertical shaft. This allowed the measurement of bearing friction to be made independent of the windage losses that would be induced if the blades were attached.

Firstly the moment of inertia of this system was measured using the technique described above. With the air still, the shaft was driven to the highest possible rotational speed using the friction drive, released, and the retardation of the rotor monitored using the PET microcomputer. This was repeated a number of times so that the range of measurements of angular velocity included all likely operating speeds of the model V-VAWT. The measurements were recorded in the datafile "DRAGTESTSHAFT2".

The retardation of the rotor was due entirely to friction torque generated by losses in the shaft bearings and still-air rotor windage losses. The acceleration method was used to analyse the angular velocity measurements to determine the variation of friction torque, Q_F, with angular velocity, ω. For speed of friction loss correction in subsequent calculations, the relationship between Q_F and ω is fitted to a second-order polynomial such that:

$$Q_F = a3\omega^2 + a2\omega + a1 \qquad (5.9)$$

The coefficients a1, a2 and a3 were determined by analysing the measurements using a Least Squares Fit.

Since the maximum rotational speed, at which retardation measurements were made, was in excess of 150 rad/s, torque corrections for bearing friction losses using equation (5.9) and the measured coefficients a1, a2 and a3 can be applied with confidence over the entire range of angular velocities at which the model V-VAWT operated.

5.6: The Measurement of Cable Drag

Cable drag losses are by far the most significant of all the losses experienced by the model V-VAWT. Each blade of the model wind turbine is supported by two 2 mm diameter cables attached 115 mm from the blade tip. It was not possible to design the wind turbine using cantilevered blades for operation at the high rotational speeds of the experiments; each blade had to be simply supported at some spanwise position by cables . Two cables are required for each blade to prevent the blade dynamically twisting during operation. Twisting was observed by Sharpe and Taylor during the testing of the first model V-VAWT [9], the blades of which were supported by only one cable. Using two cables prevents the blade twisting during performance testing. Unfortunately, the use of cables incurs a high drag penalty which in practice is difficult to reduce on the model-sized V-VAWTs. Experience from previous model V-VAWT tests suggested that it was better experimental practice to leave the cables uncovered, measure the cable drag in isolation, and include corrections in the performance test results in the same manner as the corrections for bearing friction are applied.

Unlike the bearing friction measurements, the measurement of cable drag had to be made after the performance testing of the model V-VAWT had been completed and the wind tunnel was free for use again. During performance testing the

cable drag was estimated from the corrections applied to previous model V-VAWTs. However, the estimated value of cable drag was significantly smaller than that actually measured. This demonstrates the clear need to determine corrections for the parasitic losses of each experimental configuration; it is not satisfactory to rely upon measurements from previous experiments for determining these corrections.

Cable drag corrections are determined from two sets of experimental data. The first test configuration consists of a spacer bar attached at the mid-point of the vertical shaft. In a diamond geometry around the spacer bar are stretched four cables similar to those fitted to the model V-VAWT. These cables are attached to the shaft using two cable support hubs such that the angle to the vertical, the maximum diameter and the spacing between pairs is similar to the cables on the model. The diamond configuration provides twice the cable area as used for the model V-VAWT, so allowing cable drag to be measured accurately using the acceleration.

The moment of inertia of this test configuration was determined as described above. With the wind speed constant, the shaft was driven to as high a rotational speed as possible using the friction drive, released and the decceleration of the rotor monitored using the PET microcomputer. This method is identical to that used to measure bearing friction. However, since cable drag losses are due to the aerodynamic forces acting on the wires, unlike bearing friction these losses are windspeed dependent so the test procedure was repeated a number of times for various windspeed settings.

For each windspeed setting, the acceleration method was used to determine the variation of drag torque with

respect to angular velocity. Using these calculated values of torque, the coefficients of equation (5.10) were determined using a Least Squares Fit algorithm. Equation (5.10) is a two-dimensional, second-order relationship between drag torque Q_c, angular velocity ω, and windspeed V:

$$Q_c = c3\omega + c6\omega^2 + V(c1+c4\omega+c7\omega^2) + V^2(c2+c5\omega+c8\omega^2) \qquad (5.10)$$

This is a convenient form in which to summarise all the cable drag measurements, and subsequently allows drag torque corrections to be easily calculated.

The coefficients c1, c2, c3 etc.. determined from the measurements made using the above test configuration included the drag penalaties incurred by fitting the cross-arm to the shaft. Consequently the drag losses due to the cross-arm alone had to be determined. The cables and cable support hubs were removed leaving only the cross-arm attached to the shaft. The moment of inertia of this test configuration was determined and the test procedure described above repeated. A second set of coefficients c1, c2, c3 etc.. were determined from these measurements.

The measurements made using both test configurations resulted in two sets of coefficients for equation (6.4). The drag of the cables alone could be calculated using a third set of coefficients, these being the difference between those derived by measurement. However, since the cable area was twice that of the cables used for the model V-VAWT, the final set of coefficients were halved so that cable losses on the model V-VAWT could be simply calculated using equation (5.10), where Q_c is the cable drag torque.

The cable drag coefficients were determined from measurements made in windspeeds upto 15.8 m/s. However, when the windspeed was greater than 10 m/s, the friction drive motor was not powerful enough to drive the cable diamond configuration at angular velocities much in excess of 75 rad/s. Thus for windspeeds greater than 10 m/s, the measured values of Q_c should be treated with caution at angular velocities greater than 75 rad/s, because only a small number of measurements were made. Equation (5.10), therefore, can only be used with confidence for calculating cable drag losses when the model V-VAWT operates within the range of windspeeds and angular velocities given above.

All the performance tests were carried out at a windspeed of $V \simeq 14$ m/s, where $V < 15.8$ m/s. For most tests, however, the rotational speed of the model V-VAWT exceeded 75 rad/s (approximately equivalent to $\lambda = 2.5$), and therefore the model V-VAWT operated outside the range of conditions for which cable drag measurements were made. Despite this, equation (5.10) was initially used to calculate cable drag corrections for all the performance tests. To calculate Q_c often required extrapolation beyond the range of angular velocities for which the cable drag coefficients were valid.

The initial analysis of the model V-VAWT performance tests included corrections for cable drag using equation (6.4) and the cable drag coefficients as measured. However, since present V-VAWT designs all include cable supports for the blades, there is a real need for cable drag losses to be accurately predicted in order to assess the true net torque that the wind turbine would develop. A mathematical model of cable drag loss is required. The measurements made here would allow such a model to be validatedd, and enable cable drag corrections for the

model V-VAWT performance tests to be made with greater confidence for angular velocities exceeding 75 rad/s.

5.7: The Prediction of Cable Drag

The accurate prediction of cable drag is essential for future V-VAWT designs which include cable supports for the blades. Cable drag losses are the most significant parasitic loss with small scale wind tunnel V-VAWTs, and while these losses may be proportionally smaller for larger, free-air sized V-VAWTs it is essential that they be accurately assessed to enable the overall performance of the wind turbine to be predicted with confidence.

The prediction model below has been developed using simple two-dimensional, steady state flow theory and ignores any dynamic effects. At any instant, the local velocity vector on a small element of the cable is only dependent upon the cable geometry, upstream windspeed and the angular velocity of the cable. Streamwise momentum losses are ignored. Local elemental forces are calculated using coefficients of lift and drag force taken from Hoerner who has summarised the results of many experimentors [56].

Predicting cable drag is best achieved by considerationg of a small elemental length of one cable. The geometrical features of the element are shown in Figure 5.1a using the following nomenclature:

z = spanwise ordinate of element, m

e = chordwise offset of the cable from the axis of rotation, m

r = radial distance between the axis of rotation and the element, m

FRONT VIEW

PLAN VIEW

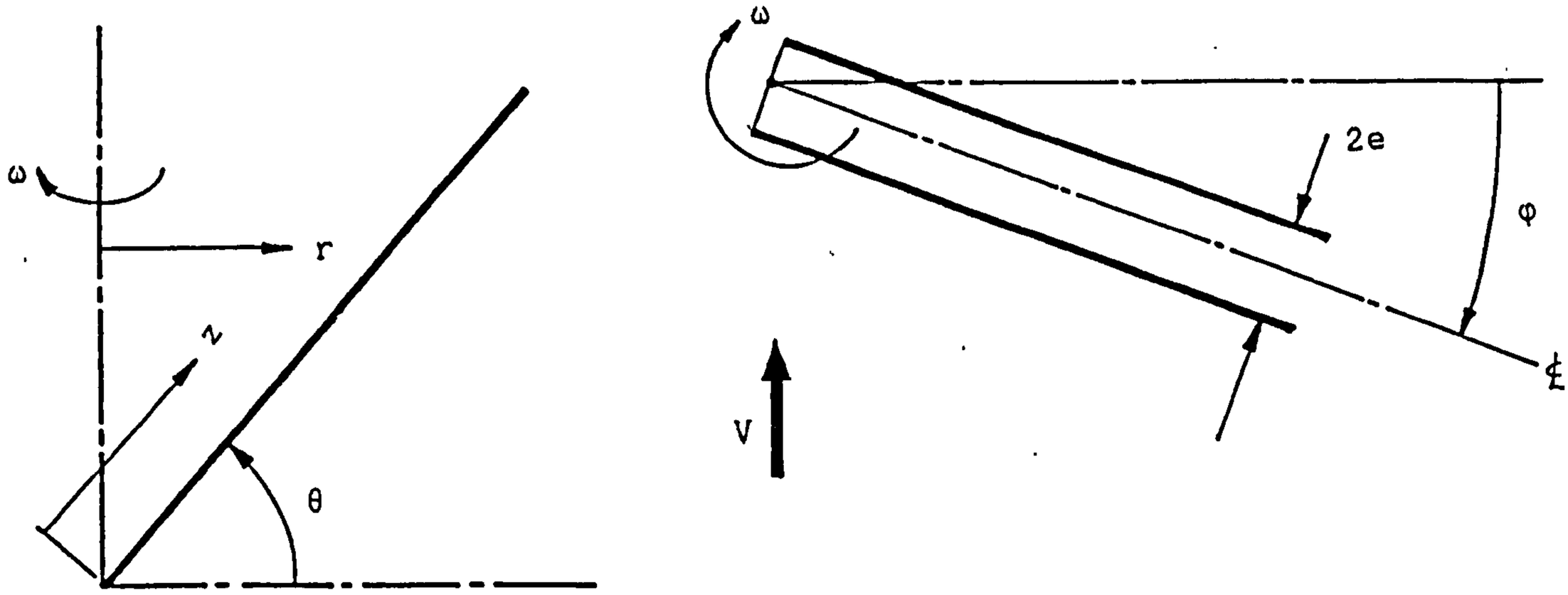

Figure 5.1a: Cable geometry for prediction purposes

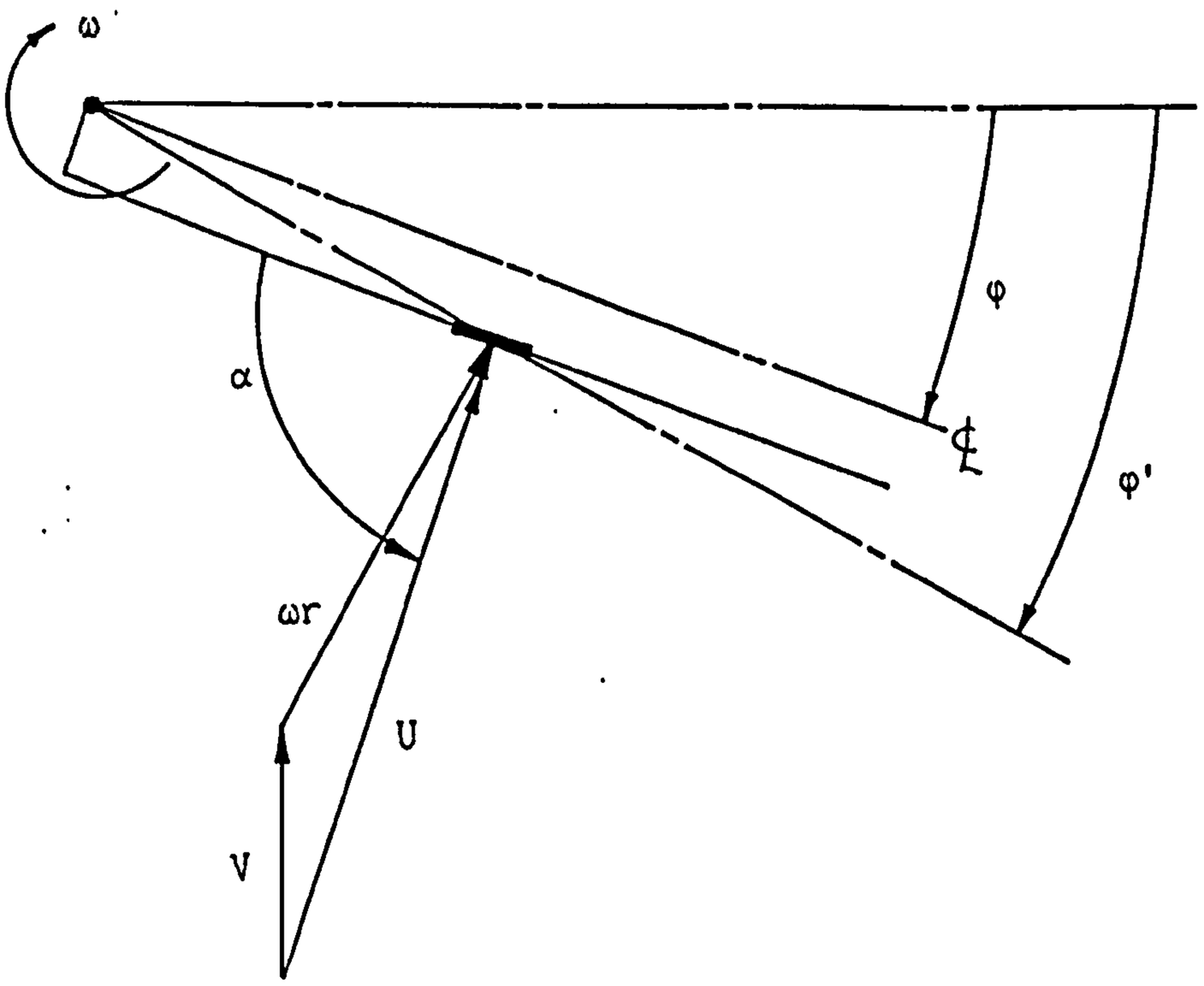

Figure 5.1b: Localised flow velocity and angle of attack

θ = angle of cable inclination to horizon, °

φ = azimuthal angle of cable, °

d = cable diameter, m

V = upstream windspeed, m/s

ω = angular velocity, rad/s

The radial distance between the element and the axis of rotation is:

$$r = \sqrt{(z\cos\theta)^2 + e^2} \tag{5.11}$$

and the modified azimuthal angle of the element φ' is given by:

$$\varphi' = \varphi + \tan^{-1}\left(\frac{e}{z\cos\theta}\right) \tag{5.12}$$

The local velocity U that acts on the element which is rotating at a constant angular velocity ω, Figure 5.1b, is given by:

$$U = \sqrt{(\omega r)^2 + V^2 + 2V\omega r\cos\varphi'} \tag{5.13}$$

The angle of attack α of the velocity vector to the span-wise axis of the cable is:

$$\alpha = \frac{\pi}{2} - (\varphi' - \varphi) + \tan^{-1}\left(\frac{V\sin\varphi'}{\omega r + V\cos\varphi'}\right) \qquad -\pi \leq \alpha \leq \pi \tag{5.14}$$

The local Reynold's Number Re is:

$$Re = \frac{\rho U d}{\mu} \tag{5.15}$$

where ρ is the density of air and μ its viscocity.

The forces on a circular cylinder inclined to the flow are considered by Hoerner [56], who presents expressions for the coefficient of lift C_L, and coefficient of drag C_D, acting on a cylinder inclined at an angle, α, to the fluid flow. These two force coefficients are both dependent upon the coefficient of chordwise force C_C, whose value was determined by Hoerner from the results of a number of tests on wires, cables and circular cylinders. The expressions derived by Hoerner for the coefficients of lift and drag are:

$$C_L = C_C \sin^2\alpha\cos\alpha \qquad (5.16a)$$

$$C_D = C_C \sin^3\alpha + 0.02 \qquad (5.16b)$$

The coefficients of tangential force C_T, and normal force C_N, can be derived by resolving C_L and C_D with respect to α, such that:

$$C_T = C_L \sin\alpha - C_D \cos\alpha \qquad (5.17a)$$

$$C_N = C_L \cos\alpha + C_D \sin\alpha \qquad (5.17b)$$

Substituting for C_L and C_D gives

$$C_T = -0.02\cos\alpha \qquad (5.18a)$$

$$C_N = C_C \sin^2\alpha + 0.02\sin\alpha \qquad (5.18b)$$

The value of the coefficient of chordwise force C_C, is known to be Reynold's Number dependent. Table 5.1 shows the values for C_C that Hoerner had derived from the experimental results he considered. The model V-VAWT cables were made from 2mm diameter wire so that the local Reynold's Number even at the highest rotational speeds would not have greatly exceeded 10,000. Even the blade

Reynold's No.	C_c
$< 2x10^5$	1.1 - 1.2
$2x10^5 - 4x10^5$	0.7
$> 4x10^5$	0.3

Table 5.1: Coefficients of chordwise force for a range of Reynolds Number [56]

support cables of free-air machines using wires of larger diameters would operate at Reynold's Numbers well below the critical number of 200,000. Initially a value of $C_c = 1.2$ was used, but this was later modified when the predicted cable drag was found to be different to that actually measured.

The local force coefficients C_T and C_N are calculated with respect to the local cable geometry, and they can be further resolved into coefficients of radial force C_{RAD}, and tangential force C_{TAN}, which act repectively radially and tangentially to the axis between the vertical axis of rotation and the local cable element. These coefficients are given by:

$$C_{RAD} = C_N\sin(\varphi'-\varphi) + C_T\cos(\varphi'-\varphi) \qquad (5.19a)$$

$$C_{TAN} = C_N\cos(\varphi'-\varphi) - C_T\sin(\varphi'-\varphi) \qquad (5.19b)$$

If the spanwise length of the cable element being considered is δz, then the elemental drag torque δQ, is given by

$$\delta Q = \tfrac{1}{2}\rho U^2 dC_{TAN}\delta z \qquad (5.20)$$

For any given windspeed, angular velocity and azimuthal position, the total drag acting on the cable is

$$Q_C = \int_{z=z_1}^{z_o} \tfrac{1}{2}\rho U^2 dC_{TAN}\delta z \qquad (5.21)$$

where z_1 is the innermost spanwise ordinate of the cable and z_o the outermost spanwise ordinate. Since it is not possible to measure the azimuthal variation of cable drag torque on the test equipment described above, the mean torque must be calculated over one rotation so that values of Q_C can be derived only in terms of windspeed and angular velocity, i.e.:

$$Q_C = f(V, \omega) \qquad (5.22)$$

In order to calculate the variation of cable drag torque with windspeed and angular velocity, these equations have been embodied in the computer program CABLEDRAG, which was written and developed in FORTRAN by the author. The program essentially considers each cable as a series of small elements for which the elemental drag torque δQ, is calculated at a finite number of azimuthal positions. The mean elemental drag torque for one full rotation is calculated from the values of δQ. The total drag torque for each cable is then calculated by numerical integration of all the elemental torque values. This calculation is made for each blade cable with the overall drag torque being the sum of all the cable drag torque values. The program CABLEDRAG repeats these calculations over a range of angular velocities for a constant upstream windspeed.

Initially the chordwise force coefficient C_c was set to Hoerner's value of $C_c = 1.2$ for local Reynold's Number below 200,000. However, when the predicted cable drag torque for the model V-VAWT support cables was compared to the measured drag torque, as calculated using equation (5.10), it is found that the correlation of torque values was not good. Since most performance tests of the model V-VAWT were conducted at windspeeds of V = 14 m/s, a value of C_c was best established by comparison of predicted drag torque with the actual values of cable drag measured at V = 14 m/s. This comparison yielded a value of $C_c = 1.3$, which gives good correlation for angular velocities upto 75 rad/s, as is shown in Figure 5.2. This value of C_c is higher than that given by Hoerner and may be due to the cable having a rough surface due to its stranded wire construction, and/or may be due to a high level of turbulence around the cables on the downstream pass caused by operating in the wake of cables on the upstream pass.

While it may be possible to establish a value of C_c that may better fit the measured drag torque values, it must be remembered that the variation of C_c with Reynold's number maybe significantly more complex that assumed here. The variation of C_c for circular cylinders with respect to Reynold's Number is well documented, and is by no means constant for Reynold's Numbers less than 200,000 as it is assumed in this simple prediction model.

However, since a good correlation between measured and predicted values of cable drag torque can be established for angular velocities upto 75 rad/s using a constant value of C_c, it is believed that this prediction model can be used with confidence at the higher angular velocities where equation (5.10) is being extrapolated well beyond the range of valid cable drag measurements. At the higher rotational velocities the predicted drag torque is sign

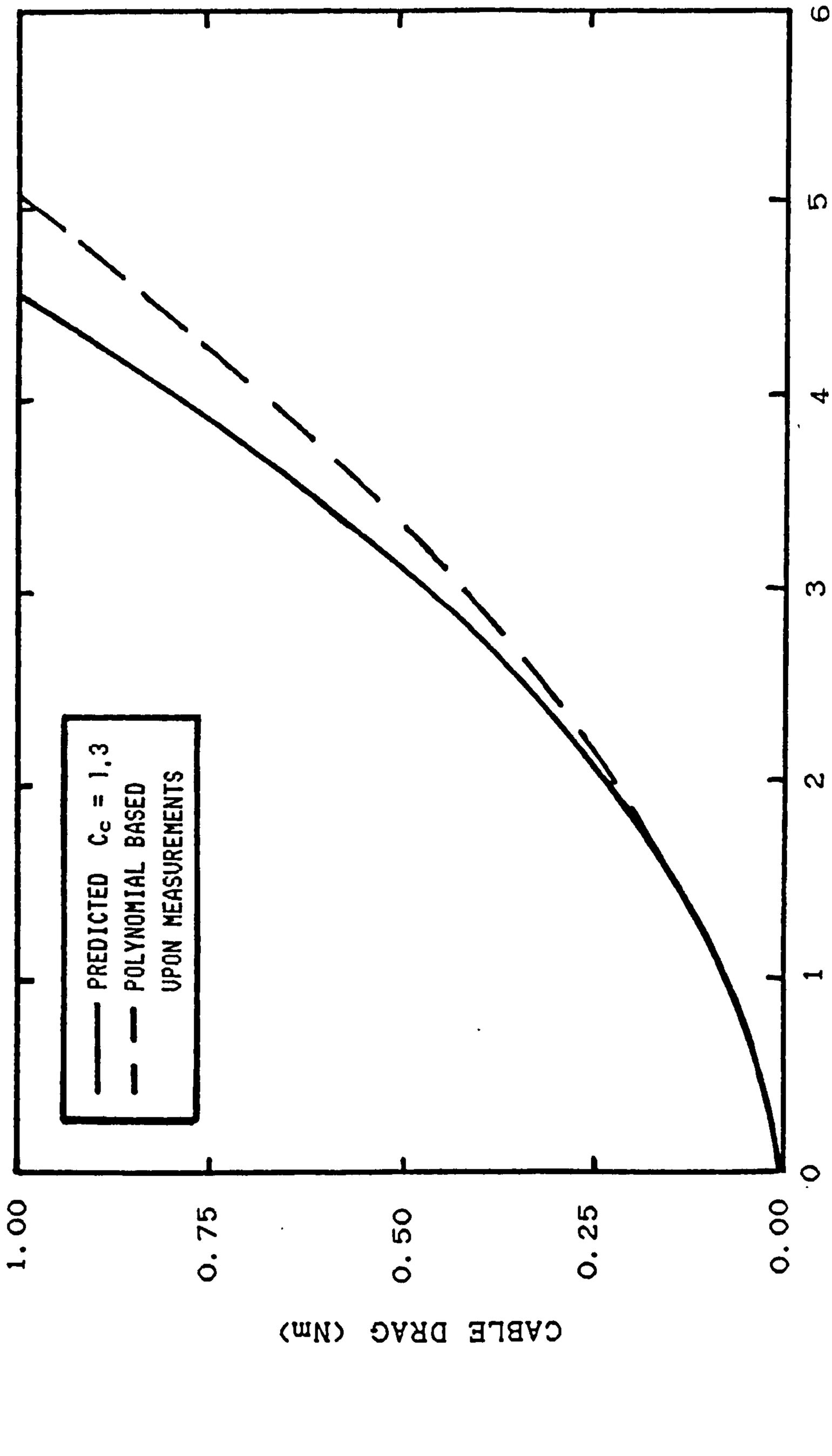

Figure 5.2: Comparison of measured and predicted cable drag losses at a windspeed of V = 14 m/s

ificantly greater than that calculated using equation (5.10), and therefore the corrections for cable drag losses will be much greater if the prediction model results are used.

5.8: The Measurement of the Coefficients of Torque and Power

The ultimate aim of the performance tests was to determine the torque and power characteristics of the model V-VAWT, and the effect that both tip pitch and tip area has on these characteristics. The variation of wind turbine power and torque with respect to angular velocity is best expressed in terms of the non-dimensional quantities coefficient of power C_P, coefficient of torque C_Q, and tip speed ratio λ. These non-dimensional units allow the wind turbine engineer some means of comparing the performances of different wind turbines or wind turbine geometries. However, when making such comparisons, the effect of Reynold's Number must always be considered as C_P and C_Q are both Reynold's Number dependent.

The torque and power characteristcs of the model V-VAWT are determined by use of the acceleration method. The moment of inertia of the model V-VAWT is determined with the blades fixed and all tip sections positioned at zero pitch. With the moment of inertia determined it is possible to commence performance testing of the wind turbine.

The wind tunnel speed is set constant, usually at about 14 m/s, and remains unchanged throughout the test period. The ambient air temperature and pressure are recorded to ensure accurate calculation of the upstream windspeed. The model wind turbine is then allowed to accelerate from

near rest, during which period its changing angular velocity is monitored and recorded with respect to time by the PET microcomputer. This procedure is repeated a number of times to ensure consistency and reliability in the recorded dataset.

As previously discussed, the model V-VAWT will accelerate to an angular velocity at which the net torque acting on the wind turbine is zero. At this operating condition, the aerodynamic torque being developed by the wind turbine is equal in magnitude to the parasitic drag losses due to bearing friction and cable drag. The model wind turbine cannot accelerate beyond or operate above this "equilibrium speed" without assistance, and therefore to obtain torque characteristics for the model V-VAWT above this angular velocity, the turbine had to be driven to higher speeds using the friction drive. At these higher speeds the aerodynamic torque that is developed by the wind turbine is smaller in magnitude than the losses due to friction and aerodynamic drag; if the turbine was running freely, it would tend to retard. So, once the turbine is spinning at as high a rotational speed as possible, the friction drive is released and the retardation of the rotor monitored, remembering that it is only during the period of free-running that the changing wind turbine angular velocity should be monitored. This high speed testing is repeated to ensure confidence in the dataset recorded by the microcomputer.

Whether the wind turbine is accelerating from low speed or deccelerating from high speed, the analysis of the angular velocity with respect to time measurements, in order to determine the C_m-λ and C_ω-λ characteristics of the wind turbine, is identical. The data-capture and analysis program CP-LAMDA, written by David Sharpe, was used to perform this analysis based upon the principles of the

acceleration method as previously discussed. This program has three major sections each of which can be considered in isolation.

The initialisation sequence, amongst other activities, is used to record experimental constants, some of these being:

(a) Test Name
(b) Ambient air temperature
(c) Ambient air pressure
(d) Betz manometer water head

The test name is an alphanumeric string of characters that uniquely identifies the filename in which all measured data is to be recorded on magnetic floppy disk. A typical test name is "T2+153" which would be the third datafile of measurements for two tip sections (i.e. 10% tip area) set at a pitch angle of +15 degrees. The sign of the pitch angle is dependent upon the pitch direction and, for consistency, the same sign convention of VAWTTAY, which uses a positive sign for nose-in tip pitch, was used for these experiments.

The ambient air temperature and pressure were measured and recorded and used to calculate the air density, ρ. The Betz manometer water head was recorded and used to calculate the wind tunnel exit windspeed, V. As previously discussed, no blockage corrections have been included in the analysis of the measurements since the model V-VAWT operates in an open-jet tunnel, consequently the upstream windspeed is taken as being equal to V. It was not possible to monitor the Betz manometer during testing, so the water head measurement was checked at the end of each test to ensure that it had not changed; if it had the test would be repeated.

The datafile is opened on floppy disk, all the test constants are recorded, and the data capture routine entered. When the wind turbine model is running freely, either accelerating from rest or deccelerating from high speed, the data capture sequence is activated by the experimentor. The PET microcomputer immediately enters a loop in which measurements of angular velocity ω, and time t, are continuously made and stored in the memory of the computer. This sequence can be either terminated by the experimentor, or else is automatically terminated by the computer if 500 angular velocity and time measurements have been made. The program CP-LAMDA then immediately enters the analysis sequence.

Using equations (A2.3) and (A2.4), the angular acceleration ω, and the angular velocity ω, of the rotor is systematically calculated at nearly all the time increments at which a measurement was made. Using an index number stepwidth of 30, from a dataset of 500 measurements a total of 470 instantaneous values of ω and ω can be calculated. The instantaneous net shaft torque $Q_{s,i}$, is calculated using equation (5.1), and by addition of corrections for cable drag torque Q_c, and bearing friction torque Q_f, the magnitude of each being calculated using equations (5.21) and (5.9) respectively, the instantaneous aerodynamic torque Q_A is determined:

$$Q_A = Q_s + Q_C + Q_F \qquad (5.23)$$

The instantaneous tip speed ratio λ_i, is given by:

$$\lambda_i = \frac{\omega R}{V} \qquad (5.24)$$

and the instantaneous torque coefficient $C_{q,i}$, is given by:

$$C_{Q1} = \frac{Q_n}{\frac{1}{2}\rho V^2 A R} \qquad (5.25)$$

Since upto 470 instantaneous values of C_{Q1} and λ_1 may be determined from one dataset, the C_Q-λ characteristic of the wind turbine is summarised by binning all instantenous measurements with respect to discrete values of λ. The value of C_Q for each tip speed ratio bin being the mean of the instantaneous C_{Q1} values calculated for all λ_1 within the width of the bin. The results presented here have been summarised into tip speed ratio bins of width 0.125, consequently the value of C_Q is the mean of often in excess of fifty instantaneous C_{Q1} values.

The analysis sequence includes the recording of all measured values of ω and t to floppy disk and the plotting of the C_P-λ characteristic on the screen of the computer monitor, where the power coefficient C_P is given by:

$$C_P = C_Q\lambda \qquad (5.26)$$

The visual plot of C_P-λ enables the progress with which the complete C_P-λ characteristic is being established to be monitored, and allows the validity of the measurements to be continuously checked.

Once the analysis of the dataset is complete, the option to terminate testing is given. However, if testing is to be continued, the data capture and analysis sequences are repeated. The binned values of C_Q are further modified by the addition of more instantaneous measurements and the number of measurements for each bin increases. When the C_P-λ characteristic is considered to be complete, the testing program can be terminated. At this time, all the binned values of C_Q are recorded to floppy diskette and the datafile closed.

The final screen plot of C_{p_m}-λ can be recorded on paper using a screen dump facility which transmits a pixel-image of the screen to a dot matrix printer. A tabulated summary of the results is also produced and recorded on paper by the printer.

The test sequence would generally take half an hour to complete, most of this time being used to record on floppy diskette the measurements of ω and t, and to complete the C_{p_m}-λ analysis. In retrospect, the analysis need not be undertaken at the time of experimentation, since valuable wind tunnel time is being lost while the computer undertakes the numerous calculations involved. However, the validity of all the measurements was constantly being assessed by observation of the C_{p_m}-λ screen plot, and therefore it was usually easy to identify when experimental errors had occurred. Typical errors included:

(a) Shutdown of the wind tunnel during Data Capture
(b) Starting Data Capture while the rotor was still being accelerated using the friction drive
(c) Movement of the tips in pitch because of inadequate securing of the grubscrews

All these errors were easily identified by observation of the C_{p_m}-λ screen plot, and while one dataset of measurements may be invalid, it was often possible to continue using the previously recorded datasets with confidence.

With the C_{p_m}-λ characteristic completely determined, the geometry of the rotor was altered and the test sequence repeated for the new tip area/tip pitch setting. Some forty tip pitch angle/tip pitch area combinations were investigated during the two week period of wind tunnel testing of the model V-VAWT. The data for some of these rotor geometries is incomplete, as a number of minor

experimental problems were encountered during the first few days of the test programme, the most significant being the degradation until eventual failure of the friction drive mechanism, which initially was not designed for the continuous usage required here. The consequence of this failure was that during early tests, the model V-VAWT could not be driven to high speed when tip pitch angles were significantly large. When the friction drive mechanism was eventually upgraded and replaced, the rotor could be driven to high rotational speeds even with large tip pitch angles and tip areas. Unfortunately, there was little time at the end of the test program to repeat the measurements for the tip pitch/tip area combinations affected by the failure of the friction drive.

For some tip pitch angle/tip area combinations the aerodynamic torque was so low that the rotor acceleration was very small and that in the short time available it was not possible to ensure that measurements had been made at all possible tip speed ratios. The CP-LAMDA computer program was modified slightly to help overcome this problem, but there are still some gaps in the dataset where measurements were not made.

In a two-week period during January to February 1985, some forty performance tests of the model V-VAWT were completed at Queen Mary College, London. Little or no time was available to repeat tests or verify results, but to ensure that the model V-VAWT performance was not degraded during the experimental period, the measurement of its C_m-λ characteristic for a zero-pitch angle geometry was performed both at the start and repeated at the end of the two-week test programme.

Table 5.2a: Measured Variation of Power Coefficient for Model V-VAWT with 5% Blade Tip Area

TSR	PITCH ANGLE (degrees) 0	+5	+10	+15	+20	+25	+30	-5	-10	-15	-20	-25	-30	TSR
0.125	0.0016	------	------	------	------	------	------	------	------	------	------	------	------	0.125
0.250	0.0022	------	------	------	------	-0.0004	-0.0005	------	------	------	------	------	0.0031	0.250
0.375	0.0035	------	------	------	------	-0.0006	-0.0011	------	------	------	0.0045	------	0.0038	0.375
0.500	0.0051	0.0046	0.0028	------	0.0003	-0.0012	-0.0022	------	------	------	0.0059	0.0055	0.0045	0.500
0.625	0.0073	0.0056	0.0031	------	0.0001	-0.0023	-0.0043	0.0083	------	------	0.0071	0.0061	0.0049	0.625
0.750	0.0092	0.0076	0.0055	------	0.0001	-0.0035	-0.0062	0.0096	0.0107	0.0101	0.0087	0.0073	0.0053	0.750
0.875	0.0122	0.0103	0.0071	------	0.0009	-0.0039	-0.0074	0.0129	0.0129	0.0132	0.0110	0.0092	0.0060	0.875
1.000	0.0165	0.0143	0.0114	------	0.0018	-0.0041	-0.0090	0.0167	0.0172	0.0173	0.0144	0.0116	0.0072	1.000
1.125	0.0212	0.0185	0.0137	------	0.0036	-0.0044	-0.0109	0.0222	0.0218	0.0214	0.0176	0.0133	0.0079	1.125
1.250	0.0271	0.0238	0.0183	0.0132	0.0051	-0.0043	-0.0126	0.0278	0.0274	0.0261	0.0210	0.0150	0.0078	1.250
1.375	0.0340	0.0299	0.0231	0.0154	0.0071	-0.0045	-0.0153	0.0342	0.0337	0.0323	0.0249	0.0164	0.0078	1.375
1.500	0.0411	0.0372	0.0291	0.0226	0.0093	-0.0047	-0.0180	0.0416	0.0411	0.0383	0.0288	0.0200	0.0078	1.500
1.625	0.0500	0.0450	0.0370	0.0248	0.0133	-0.0037	-0.0210	0.0505	0.0494	0.0455	0.0330	0.0223	0.0086	1.625
1.750	0.0614	0.0558	0.0467	0.0381	0.0190	-0.0021	-0.0238	0.0616	0.0595	0.0546	0.0403	0.0294	0.0102	1.750
1.875	0.0733	0.0667	0.0575	0.0444	0.0249	-0.0013	-0.0261	0.0743	0.0722	0.0649	0.0482	0.0345	0.0118	1.875
2.000	0.0870	0.0826	0.0672	0.0532	0.0314	0.0006	-0.0308	0.0884	0.0858	0.0790	0.0590	0.0384	0.0126	2.000
2.125	0.1007	0.0935	0.0788	0.0620	0.0361	-0.0017	-0.0359	0.1020	0.0997	0.0918	0.0699	0.0425	0.0123	2.125
2.250	0.1145	0.1062	0.0902	0.0688	0.0393	-0.0043	-0.0475	0.1172	0.1139	0.1042	0.0812	0.0457	0.0108	2.250
2.375	0.1273	0.1163	0.0985	0.0752	0.0420	-0.0100	-0.0629	0.1290	0.1264	0.1161	0.0893	0.0504	0.0083	2.375
2.500	0.1387	0.1290	0.1067	0.0807	0.0437	-0.0175	------	0.1410	0.1388	0.1280	0.0960	0.0540	0.0045	2.500
2.625	0.1483	0.1380	0.1131	0.0837	0.0422	-0.0284	------	0.1528	0.1504	0.1376	0.1013	0.0564	-0.0008	2.625
2.750	0.1567	0.1457	0.1182	0.0841	0.0396	-0.0435	------	0.1614	0.1595	0.1460	0.1048	0.0528	-0.0069	2.750
2.875	0.1647	0.1509	0.1198	0.0819	------	-0.0581	------	0.1693	0.1665	0.1512	0.1061	0.0463	------	2.875
3.000	0.1695	0.1551	0.1170	0.0762	------	-0.0744	------	0.1740	0.1728	0.1542	0.1029	0.0432	------	3.000
3.125	0.1734	0.1562	0.1134	0.0678	------	------	------	0.1784	0.1763	0.1553	0.1003	0.0363	------	3.125
3.250	0.1725	0.1511	0.1079	0.0555	------	------	------	0.1784	0.1765	0.1557	0.0962	0.0273	------	3.250
3.375	0.1663	0.1444	0.0968	0.0401	------	------	------	0.1748	0.1731	0.1559	0.0898	------	------	3.375
3.500	0.1571	0.1298	0.0826	0.0245	------	------	------	0.1715	0.1652	0.1516	0.0781	------	------	3.500
3.625	0.1453	0.1170	0.0725	------	------	------	------	0.1606	0.1537	0.1414	0.0656	------	------	3.625
3.750	0.1357	0.1050	------	------	------	------	------	0.1519	0.1444	0.1324	0.0649	------	------	3.750
3.875	0.1274	0.0937	------	------	------	------	------	0.1449	0.1387	0.1232	------	------	------	3.875
4.000	0.1180	0.0780	------	------	------	------	------	0.1368	0.1308	0.1128	------	------	------	4.000
4.125	0.1039	0.0672	------	------	------	------	------	0.1394	0.1196	0.1040	------	------	------	4.125
4.250	0.0841	------	------	------	------	------	------	------	0.1118	0.0948	------	------	------	4.250
4.375	0.0621	------	------	------	------	------	------	------	------	------	------	------	------	4.375
4.500	------	------	------	------	------	------	------	------	------	------	------	------	------	4.500

Table 5.2b: Measured Variation of Torque Coefficient for Model V-VAWT with 5% Blade Tip Area

TSR	PITCH ANGLE (degrees) 0	+5	+10	+15	+20	+25	+30	-5	-10	-15	-20	-25	-30	TSR
0.125	0.0130	------	------	------	------	------	------	------	------	------	------	------	------	0.125
0.250	0.0089	------	------	------	------	-0.0014	-0.0020	------	------	------	------	------	0.0123	0.250
0.375	0.0092	------	------	------	------	-0.0015	-0.0029	------	------	------	0.0121	------	0.0102	0.375
0.500	0.0102	0.0091	0.0056	------	0.0005	-0.0023	-0.0043	------	------	------	0.0117	0.0109	0.0090	0.500
0.625	0.0116	0.0090	0.0049	------	0.0001	-0.0036	-0.0068	0.0133	------	------	0.0113	0.0098	0.0078	0.625
0.750	0.0123	0.0101	0.0073	------	0.0001	-0.0046	-0.0082	0.0128	0.0143	0.0134	0.0116	0.0097	0.0070	0.750
0.875	0.0139	0.0118	0.0082	------	0.0010	-0.0045	-0.0084	0.0147	0.0147	0.0151	0.0126	0.0105	0.0069	0.875
1.000	0.0165	0.0143	0.0114	------	0.0018	-0.0041	-0.0090	0.0167	0.0172	0.0173	0.0144	0.0116	0.0072	1.000
1.125	0.0188	0.0165	0.0122	------	0.0032	-0.0039	-0.0097	0.0197	0.0194	0.0190	0.0156	0.0118	0.0070	1.125
1.250	0.0217	0.0191	0.0147	0.0106	0.0041	-0.0034	-0.0101	0.0222	0.0219	0.0209	0.0168	0.0120	0.0062	1.250
1.375	0.0247	0.0218	0.0168	0.0112	0.0052	-0.0033	-0.0111	0.0249	0.0245	0.0235	0.0181	0.0119	0.0057	1.375
1.500	0.0274	0.0248	0.0194	0.0151	0.0062	-0.0031	-0.0120	0.0277	0.0274	0.0255	0.0192	0.0133	0.0052	1.500
1.625	0.0308	0.0277	0.0228	0.0153	0.0082	-0.0023	-0.0129	0.0311	0.0304	0.0280	0.0203	0.0137	0.0053	1.625
1.750	0.0351	0.0319	0.0267	0.0218	0.0109	-0.0012	-0.0136	0.0352	0.0340	0.0312	0.0230	0.0168	0.0058	1.750
1.875	0.0391	0.0356	0.0307	0.0237	0.0133	-0.0007	-0.0139	0.0396	0.0385	0.0346	0.0257	0.0184	0.0063	1.875
2.000	0.0435	0.0413	0.0336	0.0266	0.0157	0.0003	-0.0154	0.0442	0.0429	0.0395	0.0295	0.0192	0.0063	2.000
2.125	0.0474	0.0440	0.0371	0.0292	0.0170	-0.0008	-0.0169	0.0480	0.0469	0.0432	0.0329	0.0200	0.0058	2.125
2.250	0.0509	0.0472	0.0401	0.0306	0.0175	-0.0019	-0.0211	0.0521	0.0506	0.0463	0.0361	0.0203	0.0048	2.250
2.375	0.0536	0.0490	0.0415	0.0317	0.0177	-0.0042	-0.0265	0.0543	0.0532	0.0489	0.0376	0.0212	0.0035	2.375
2.500	0.0555	0.0516	0.0427	0.0323	0.0175	-0.0070	------	0.0564	0.0555	0.0512	0.0384	0.0216	0.0018	2.500
2.625	0.0565	0.0526	0.0431	0.0319	0.0161	-0.0108	------	0.0582	0.0573	0.0524	0.0386	0.0215	-0.0003	2.625
2.750	0.0570	0.0530	0.0430	0.0306	0.0144	-0.0158	------	0.0587	0.0580	0.0531	0.0381	0.0192	-0.0025	2.750
2.875	0.0573	0.0525	0.0417	0.0285	------	-0.0202	------	0.0589	0.0579	0.0526	0.0369	0.0161	------	2.875
3.000	0.0565	0.0517	0.0390	0.0254	------	-0.0248	------	0.0580	0.0576	0.0514	0.0343	0.0144	------	3.000
3.125	0.0555	0.0500	0.0363	0.0217	------	------	------	0.0571	0.0564	0.0497	0.0321	0.0116	------	3.125
3.250	0.0531	0.0465	0.0332	0.0171	------	------	------	0.0549	0.0543	0.0479	0.0296	0.0084	------	3.250
3.375	0.0493	0.0428	0.0287	0.0119	------	------	------	0.0518	0.0513	0.0462	0.0266	------	------	3.375
3.500	0.0449	0.0371	0.0236	0.0070	------	------	------	0.0490	0.0472	0.0433	0.0223	------	------	3.500
3.625	0.0401	0.0323	0.0200	------	------	------	------	0.0443	0.0424	0.0390	0.0181	------	------	3.625
3.750	0.0362	0.0280	------	------	------	------	------	0.0405	0.0385	0.0353	0.0173	------	------	3.750
3.875	0.0329	0.0242	------	------	------	------	------	0.0374	0.0358	0.0318	------	------	------	3.875
4.000	0.0295	0.0195	------	------	------	------	------	0.0342	0.0327	0.0282	------	------	------	4.000
4.125	0.0252	0.0163	------	------	------	------	------	0.0338	0.0290	0.0252	------	------	------	4.125
4.250	0.0198	------	------	------	------	------	------	------	0.0263	0.0223	------	------	------	4.250
4.375	0.0142	------	------	------	------	------	------	------	------	------	------	------	------	4.375
4.500	------	------	------	------	------	------	------	------	------	------	------	------	------	4.500

TSR	PITCH ANGLE (degrees)																							
	0	+3	+5	+7	+10	+12	+15	+17	+20	+25	-5	-10	-12	-15	-17	-20	-25	TSR
0,125	0,0016	-----	-----	-----	-----	-----	-----	-----	-----	-0,0005	-----	-----	-----	-----	-----	-----	-----	0,125
0,250	0,0022	-----	0,0012	0,0008	-----	0,0001	-0,0007	-----	-0,0003	-0,0014	-----	-----	-----	-----	-----	0,0040	0,0037	0,250
0,375	0,0035	0,0027	0,0017	0,0012	-----	-0,0001	-0,0012	0,0009	-0,0009	-0,0029	0,0050	-----	-----	-----	0,0050	0,0045	0,0039	0,375
0,500	0,0051	0,0038	0,0025	0,0016	-0,0002	-----	-0,0024	0,0020	-0,0020	-0,0052	0,0060	0,0066	0,0047	-0,0041	0,0057	0,0054	0,0041	0,500
0,625	0,0073	0,0053	0,0034	-----	0,0002	0,0000	-0,0034	0,0036	-0,0056	-0,0083	0,0079	0,0085	0,0064	-0,0061	0,0069	0,0061	0,0040	0,625
0,750	0,0092	0,0067	0,0050	0,0035	0,0002	-0,0005	-0,0044	0,0077	-0,0088	-0,0121	0,0102	0,0104	0,0086	-0,0070	0,0088	0,0070	0,0033	0,750
0,875	0,0122	0,0089	0,0076	0,0044	0,0004	-----	-0,0045	0,0101	-0,0108	-0,0157	0,0134	0,0132	0,0107	-0,0080	0,0108	0,0080	0,0026	0,875
1,000	0,0165	0,0119	0,0086	0,0058	-0,0005	-----	-0,0052	0,0119	-0,0127	-0,0194	0,0174	0,0165	0,0136	-0,0084	0,0127	0,0084	0,0013	1,000
1,125	0,0212	0,0161	0,0132	0,0087	0,0003	0,0008	-0,0061	0,0144	-0,0153	-0,0243	0,0219	0,0206	0,0169	-0,0097	0,0153	0,0097	-0,0008	1,125
1,250	0,0271	0,0209	0,0183	0,0130	-0,0015	0,0020	-0,0061	0,0161	-0,0159	-0,0269	0,0269	0,0246	0,0201	-0,0089	0,0159	0,0089	-0,0035	1,250
1,375	0,0340	0,0263	0,0231	0,0158	-0,0103	0,0041	-0,0062	0,0183	-0,0162	-0,0296	0,0333	0,0296	0,0240	-0,0072	0,0162	0,0072	-0,0072	1,375
1,500	0,0411	0,0338	0,0300	0,0237	0,0054	0,0078	-0,0050	0,0231	-0,0189	-0,0364	0,0413	0,0357	0,0283	-0,0084	0,0189	0,0068	-0,0113	1,500
1,625	0,0500	0,0408	0,0385	0,0293	0,0138	0,0112	-0,0034	0,0300	-0,0221	-0,0440	0,0512	0,0444	0,0341	-0,0098	0,0221	0,0060	-0,0167	1,625
1,750	0,0614	0,0515	0,0485	0,0373	0,0242	0,0165	-0,0005	0,0385	-0,0270	-0,0525	0,0621	0,0543	0,0411	-0,0110	0,0270	0,0054	-0,0228	1,750
1,875	0,0733	0,0630	0,0602	0,0473	0,0296	0,0221	0,0013	0,0485	-0,0294	-0,0614	0,0737	0,0662	0,0501	-0,0137	0,0294	0,0049	-0,0289	1,875
2,000	0,0870	0,0750	0,0718	0,0572	0,0402	0,0280	0,0034	0,0602	-0,0344	-0,0729	0,0872	0,0782	0,0596	-0,0163	0,0344	0,0054	-0,0358	2,000
2,125	0,1007	0,0867	0,0842	0,0665	0,0485	0,0342	0,0055	0,0718	-0,0404	-0,0884	0,1009	0,0918	0,0696	-0,0188	0,0404	0,0038	-0,0446	2,125
2,250	0,1145	0,0988	0,0952	0,0767	0,0531	0,0387	0,0052	0,0842	-0,0473	-0,1056	0,1161	0,1053	0,0941	-0,0208	0,0473	0,0041	-0,0563	2,250
2,375	0,1273	0,1074	0,1047	0,0834	-----	0,0428	0,0067	0,0952	-0,0553	-----	0,1275	0,1195	0,1038	-0,0262	0,0553	0,0055	-0,0686	2,375
2,500	0,1387	0,1158	0,1135	0,0883	0,0643	0,0448	0,0028	0,1047	-0,0698	-----	0,1410	0,1315	0,1140	-0,0305	0,0698	0,0033	-0,0798	2,500
2,625	0,1483	0,1231	0,1202	0,0927	0,0659	0,0449	-----	0,1135	-----	-----	0,1509	0,1425	0,1234	-0,0369	-----	0,0003	-0,0982	2,625
2,750	0,1567	0,1282	0,1246	0,0941	0,0657	0,0435	-----	0,1202	-----	-----	0,1592	0,1513	0,1290	-0,0436	-----	-0,0080	-0,1183	2,750
2,875	0,1647	0,1311	0,1279	0,0932	0,0612	0,0382	-----	0,1246	-----	-----	0,1653	0,1561	0,1323	-0,0502	-----	-0,0173	-----	2,875
3,000	0,1695	0,1317	0,1284	0,0915	0,0534	0,0270	-----	0,1279	-----	-----	0,1713	0,1605	0,1350	-0,0566	-----	-0,0297	-----	3,000
3,125	0,1734	0,1231	0,1247	0,0838	0,0431	0,0147	-----	0,1284	-----	-----	0,1747	0,1644	0,1413	-0,0625	-----	-0,0384	-----	3,125
3,250	0,1725	0,1177	0,1180	0,0735	0,0309	-0,0052	-----	0,1247	-----	-----	0,1749	0,1635	0,1433	-0,0677	-----	-0,0504	-----	3,250
3,375	0,1663	0,1053	0,1090	0,0577	-----	-0,0429	-----	0,1180	-----	-----	0,1735	0,1637	0,1401	-0,0722	-----	-0,0527	-----	3,375
3,500	0,1571	0,0966	0,0952	0,0399	-----	-----	-----	0,1090	-----	-----	0,1705	0,1631	0,1327	-0,0757	-----	-----	-----	3,500
3,625	0,1453	0,0779	0,0834	0,0239	-----	-----	-----	0,0952	-----	-----	0,1628	0,1562	0,1240	-0,0778	-----	-----	-----	3,625
3,750	0,1357	0,0596	-----	-0,0094	-----	-----	-----	0,0834	-----	-----	0,1568	0,1504	0,1140	-0,0786	-----	-----	-----	3,750
3,875	0,1274	0,0457	-----	-----	-----	-----	-----	-----	-----	-----	0,1500	0,1442	0,1062	-0,0779	-----	-----	-----	3,875
4,000	0,1180	0,0168	-----	-----	-----	-----	-----	-----	-----	-----	0,1404	0,1364	0,0940	-----	-----	-----	-----	4,000
4,125	0,1039	-----	-----	-----	-----	-----	-----	-----	-----	-----	0,1320	0,1262	0,0842	-----	-----	-----	-----	4,125
4,250	0,0841	-----	-----	-----	-----	-----	-----	-----	-----	-----	0,1233	0,1165	0,0659	-----	-----	-----	-----	4,250
4,375	0,0621	-----	-----	-----	-----	-----	-----	-----	-----	-----	0,1120	0,1129	-----	-----	-----	-----	-----	4,375
4,500	-----	-----	-----	-----	-----	-----	-----	-----	-----	-----	0,1062	-----	-----	-----	-----	-----	-----	4,500

Table 5.3a: Measured Variation of Power Coefficient for Model V-VAWT with 10% Blade Tip Area

Table 5.3b: Measured Variation of Torque Coefficient for Model V-VAWT with 10% Blade Tip Area

TSR	PITCH ANGLE (degrees) 0	+3	+5	+7	+10	+12	+15	+20	+25	-5	-10	-12	-15	-17	-20	-25	TSR
0.125	0.0130	------	------	------	------	------	------	-0.0020	-0.0038	------	------	------	------	------	------	------	0.125
0.250	0.0089	------	0.0049	0.0033	------	0.0003	-0.0026	-0.0034	-0.0056	------	------	0.0165	------	------	0.0160	0.0147	0.250
0.375	0.0092	0.0071	0.0045	0.0031	------	-0.0003	-0.0033	-0.0053	-0.0078	0.0132	------	0.0124	------	0.0134	0.0121	0.0103	0.375
0.500	0.0102	0.0076	0.0049	0.0032	-0.0003	------	-0.0048	-0.0072	-0.0103	0.0119	0.0131	0.0128	0.0141	0.0114	0.0107	0.0082	0.500
0.625	0.0116	0.0084	0.0054	------	0.0003	0.0000	-0.0054	-0.0089	-0.0132	0.0127	0.0136	0.0138	0.0124	0.0111	0.0097	0.0064	0.625
0.750	0.0123	0.0089	0.0067	0.0046	0.0002	-0.0006	-0.0059	-0.0103	-0.0161	0.0136	0.0139	0.0142	0.0130	0.0117	0.0093	0.0044	0.750
0.875	0.0139	0.0102	0.0087	0.0050	0.0004	------	-0.0051	-0.0115	-0.0179	0.0153	0.0151	0.0155	0.0126	0.0123	0.0091	0.0030	0.875
1.000	0.0165	0.0119	0.0086	0.0058	-0.0005	------	-0.0052	-0.0119	-0.0194	0.0174	0.0165	0.0169	0.0137	0.0127	0.0084	0.0013	1.000
1.125	0.0188	0.0143	0.0117	0.0077	0.0003	0.0007	-0.0054	-0.0128	-0.0216	0.0195	0.0183	0.0179	0.0145	0.0136	0.0086	-0.0007	1.125
1.250	0.0217	0.0167	0.0146	0.0104	-0.0012	0.0016	-0.0049	-0.0129	-0.0237	0.0215	0.0197	0.0192	0.0150	0.0127	0.0071	-0.0028	1.250
1.375	0.0247	0.0191	0.0168	0.0115	-0.0075	0.0030	-0.0045	-0.0138	-0.0265	0.0242	0.0215	0.0206	0.0151	0.0118	0.0052	-0.0052	1.375
1.500	0.0274	0.0225	0.0200	0.0158	0.0036	0.0052	-0.0033	-0.0140	-0.0293	0.0275	0.0238	0.0227	0.0155	0.0126	0.0045	-0.0075	1.500
1.625	0.0308	0.0251	0.0237	0.0180	0.0085	0.0069	-0.0021	-0.0140	-0.0323	0.0315	0.0273	0.0253	0.0161	0.0136	0.0037	-0.0103	1.625
1.750	0.0351	0.0294	0.0277	0.0213	0.0138	0.0094	-0.0003	-0.0139	-0.0351	0.0355	0.0310	0.0286	0.0186	0.0154	0.0031	-0.0130	1.750
1.875	0.0391	0.0336	0.0321	0.0252	0.0158	0.0118	0.0007	-0.0143	-0.0389	0.0393	0.0353	0.0318	0.0204	0.0157	0.0026	-0.0154	1.875
2.000	0.0435	0.0375	0.0359	0.0286	0.0201	0.0140	0.0017	-0.0155	-0.0442	0.0436	0.0391	0.0348	0.0233	0.0172	0.0027	-0.0179	2.000
2.125	0.0474	0.0408	0.0396	0.0313	0.0228	0.0161	0.0026	-0.0174	-0.0497	0.0475	0.0432	0.0386	0.0252	0.0190	0.0018	-0.0210	2.125
2.250	0.0509	0.0439	0.0423	0.0341	0.0236	0.0172	0.0023	-0.0203	------	0.0516	0.0468	0.0418	0.0271	0.0210	0.0018	-0.0250	2.250
2.375	0.0536	0.0452	0.0441	0.0351	------	0.0180	0.0028	-0.0233	------	0.0537	0.0503	0.0436	0.0297	0.0240	0.0023	-0.0289	2.375
2.500	0.0555	0.0463	0.0454	0.0353	0.0257	0.0179	0.0011	-0.0279	------	0.0564	0.0526	0.0456	0.0340	0.0257	0.0013	-0.0319	2.500
2.625	0.0565	0.0469	0.0458	0.0353	0.0251	0.0171	------	------	------	0.0575	0.0543	0.0470	0.0369	0.0256	-0.0001	-0.0374	2.625
2.750	0.0570	0.0466	0.0453	0.0342	0.0239	0.0158	------	------	------	0.0579	0.0550	0.0469	0.0387	0.0257	-0.0029	-0.0430	2.750
2.875	0.0573	0.0456	0.0445	0.0324	0.0213	0.0133	------	------	------	0.0575	0.0543	0.0460	0.0386	0.0233	-0.0060	------	2.875
3.000	0.0565	0.0439	0.0428	0.0305	0.0178	0.0090	------	------	------	0.0571	0.0535	0.0450	0.0369	0.0206	-0.0099	------	3.000
3.125	0.0555	0.0394	0.0399	0.0268	0.0138	0.0047	------	------	------	0.0559	0.0526	0.0452	0.0371	0.0184	-0.0123	------	3.125
3.250	0.0531	0.0362	0.0363	0.0226	0.0095	-0.0016	------	------	------	0.0538	0.0503	0.0441	0.0351	0.0158	-0.0155	------	3.250
3.375	0.0493	0.0312	0.0323	0.0171	------	-0.0127	------	------	------	0.0514	0.0485	0.0415	0.0332	0.0141	-0.0156	------	3.375
3.500	0.0449	0.0276	0.0272	0.0114	------	------	------	------	------	0.0487	0.0466	0.0379	0.0309	0.0125	------	------	3.500
3.625	0.0401	0.0215	0.0230	0.0066	------	------	------	------	------	0.0449	0.0431	0.0342	0.0272	0.0077	------	------	3.625
3.750	0.0362	0.0159	------	-0.0025	------	------	------	------	------	0.0418	0.0401	0.0304	0.0238	------	------	------	3.750
3.875	0.0329	0.0118	------	------	------	------	------	------	------	0.0387	0.0372	0.0274	0.0201	------	------	------	3.875
4.000	0.0295	0.0042	------	------	------	------	------	------	------	0.0351	0.0341	0.0235	------	------	------	------	4.000
4.125	0.0252	------	------	------	------	------	------	------	------	0.0320	0.0306	0.0204	------	------	------	------	4.125
4.250	0.0198	------	------	------	------	------	------	------	------	0.0290	0.0274	0.0155	------	------	------	------	4.250
4.375	0.0142	------	------	------	------	------	------	------	------	0.0256	0.0258	------	------	------	------	------	4.375
4.500	------	------	------	------	------	------	------	------	------	0.0236	------	------	------	------	------	------	4.500

Table 5.4a: Measured Variation of Power Coefficient for Model V-VAWT with 15% Blade Tip Area

TSR	PITCH ANGLE (degrees) 0	+3	+5	+7	+10	+15	+20	-3	-5	-10	-15	-20	TSR
0.125	0.0016	------	------	------	------	-0.0002	-0.0004	------	------	------	------	------	0.125
0.250	0.0022	0.0017	0.0012	------	------	-0.0007	-0.0013	0.0035	0.0039	------	------	------	0.250
0.375	0.0035	0.0024	0.0017	0.0012	0.0004	-0.0014	-0.0029	0.0048	0.0048	0.0063	0.0056	0.0053	0.375
0.500	0.0051	0.0036	0.0024	0.0015	0.0002	-0.0027	-0.0054	0.0068	0.0066	0.0073	0.0071	0.0063	0.500
0.625	0.0073	0.0050	0.0031	0.0024	0.0001	-0.0041	-0.0081	0.0090	0.0088	0.0096	0.0088	0.0073	0.625
0.750	0.0092	0.0069	0.0048	0.0030	0.0004	-0.0053	-0.0116	0.0115	0.0116	0.0131	0.0106	0.0078	0.750
0.875	0.0122	0.0092	0.0069	0.0038	0.0007	-0.0069	-0.0158	0.0147	0.0149	0.0159	0.0120	0.0081	0.875
1.000	0.0165	0.0129	0.0084	0.0044	0.0005	-0.0085	-0.0204	0.0193	0.0196	0.0193	0.0135	0.0084	1.000
1.125	0.0212	0.0167	0.0109	0.0063	0.0011	-0.0107	-0.0254	0.0241	0.0242	0.0230	0.0153	0.0078	1.125
1.250	0.0271	0.0216	0.0148	0.0091	0.0015	-0.0135	-0.0314	0.0299	0.0295	0.0269	0.0161	0.0064	1.250
1.375	0.0340	0.0281	0.0190	0.0125	0.0034	-0.0151	-0.0385	0.0367	0.0360	0.0309	0.0162	0.0033	1.375
1.500	0.0411	0.0342	0.0240	0.0173	0.0056	-0.0170	-0.0464	0.0438	0.0438	0.0357	0.0177	-0.0009	1.500
1.625	0.0500	0.0421	0.0307	0.0247	0.0091	-0.0185	-0.0566	0.0530	0.0512	0.0427	0.0190	-0.0057	1.625
1.750	0.0614	0.0525	0.0406	0.0319	0.0142	-0.0207	-0.0665	0.0642	0.0611	0.0506	0.0205	-0.0103	1.750
1.875	0.0733	0.0641	0.0504	0.0401	0.0199	-0.0223	-0.0788	0.0767	0.0735	0.0594	0.0238	-0.0146	1.875
2.000	0.0870	0.0772	0.0612	0.0502	0.0258	-0.0254	-0.0960	0.0898	0.0872	0.0708	0.0260	-0.0200	2.000
2.125	0.1007	0.0886	0.0712	0.0584	0.0310	-0.0276	------	0.1024	0.1012	0.0842	0.0281	-0.0259	2.125
2.250	0.1145	0.0999	0.0803	0.0666	0.0362	-0.0322	------	0.1175	0.1163	0.0970	0.0347	-0.0306	2.250
2.375	0.1273	0.1112	0.0912	0.0741	0.0399	-0.0382	------	0.1309	0.1297	0.1095	0.0430	-0.0354	2.375
2.500	0.1387	0.1205	0.0970	0.0793	0.0410	-0.0470	------	0.1415	0.1410	0.1253	0.0518	-0.0403	2.500
2.625	0.1483	0.1265	0.1016	0.0816	0.0394	-0.0567	------	0.1515	0.1512	0.1347	0.0711	-0.0488	2.625
2.750	0.1567	0.1326	0.1053	0.0806	0.0382	-0.0712	------	0.1598	0.1603	0.1427	0.0765	-0.0580	2.750
2.875	0.1647	0.1351	0.1058	0.0799	0.0339	------	------	0.1662	0.1659	0.1489	0.0802	-0.0690	2.875
3.000	0.1695	0.1359	0.1014	0.0747	0.0252	------	------	0.1713	0.1710	0.1524	0.0846	-0.0756	3.000
3.125	0.1734	0.1366	0.0972	0.0666	0.0116	------	------	0.1763	0.1741	0.1525	0.0834	------	3.125
3.250	0.1725	0.1287	0.0884	0.0540	-0.0059	------	------	0.1765	0.1758	0.1541	0.0770	------	3.250
3.375	0.1663	0.1208	0.0753	0.0381	------	------	------	0.1748	0.1745	0.1546	0.0689	------	3.375
3.500	0.1571	0.1085	0.0585	0.0186	------	------	------	0.1638	0.1663	0.1526	0.0592	------	3.500
3.625	0.1453	0.0939	0.0395	------	------	------	------	0.1555	0.1620	0.1472	0.0468	------	3.625
3.750	0.1357	0.0791	------	------	------	------	------	0.1470	0.1534	0.1406	0.0428	------	3.750
3.875	0.1274	0.0670	------	------	------	------	------	0.1407	0.1492	0.1349	------	------	3.875
4.000	0.1180	------	------	------	------	------	------	0.1320	0.1396	0.1268	------	------	4.000
4.125	0.1039	------	------	------	------	------	------	0.1209	0.1328	0.1167	------	------	4.125
4.250	0.0841	------	------	------	------	------	------	0.1118	0.1216	0.1067	------	------	4.250
4.375	0.0621	------	------	------	------	------	------	0.0958	0.1142	0.0932	------	------	4.375
4.500	------	------	------	------	------	------	------	------	0.1008	0.0842	------	------	4.500

Table 5.4b: Measured Variation of Torque Coefficient for Model V-VAWT with 15% Blade Tip Area

TSR	PITCH ANGLE (degrees) 0	+3	+5	+7	+10	+15	+20	-3	-5	-10	-15	-20	TSR
0.125	0.0130	------	------	------	------	-0.0014	-0.0030	------	------	------	------	------	0.125
0.250	0.0089	0.0069	0.0046	------	------	-0.0026	-0.0050	0.0138	0.0156	------	------	------	0.250
0.375	0.0092	0.0065	0.0044	0.0033	0.0010	-0.0037	-0.0078	0.0129	0.0127	0.0169	0.0150	0.0141	0.375
0.500	0.0102	0.0071	0.0048	0.0029	0.0004	-0.0053	-0.0107	0.0135	0.0131	0.0146	0.0142	0.0125	0.500
0.625	0.0116	0.0080	0.0049	0.0038	0.0002	-0.0065	-0.0130	0.0144	0.0141	0.0154	0.0140	0.0116	0.625
0.750	0.0123	0.0092	0.0064	0.0040	0.0005	-0.0071	-0.0154	0.0153	0.0154	0.0175	0.0141	0.0104	0.750
0.875	0.0139	0.0105	0.0079	0.0043	0.0008	-0.0079	-0.0181	0.0168	0.0170	0.0182	0.0137	0.0093	0.875
1.000	0.0165	0.0129	0.0084	0.0044	0.0005	-0.0085	-0.0204	0.0193	0.0196	0.0193	0.0135	0.0084	1.000
1.125	0.0188	0.0148	0.0097	0.0056	0.0010	-0.0095	-0.0226	0.0214	0.0215	0.0204	0.0136	0.0069	1.125
1.250	0.0217	0.0173	0.0118	0.0073	0.0012	-0.0108	-0.0251	0.0239	0.0236	0.0215	0.0129	0.0051	1.250
1.375	0.0247	0.0204	0.0138	0.0091	0.0025	-0.0110	-0.0280	0.0267	0.0262	0.0225	0.0118	0.0024	1.375
1.500	0.0274	0.0228	0.0160	0.0115	0.0037	-0.0113	-0.0309	0.0292	0.0292	0.0238	0.0118	-0.0006	1.500
1.625	0.0308	0.0259	0.0189	0.0152	0.0056	-0.0114	-0.0348	0.0326	0.0315	0.0263	0.0117	-0.0035	1.625
1.750	0.0351	0.0300	0.0232	0.0182	0.0081	-0.0118	-0.0380	0.0367	0.0349	0.0289	0.0117	-0.0059	1.750
1.875	0.0391	0.0342	0.0269	0.0214	0.0106	-0.0119	-0.0420	0.0409	0.0392	0.0317	0.0127	-0.0078	1.875
2.000	0.0435	0.0386	0.0306	0.0251	0.0129	-0.0127	-0.0480	0.0449	0.0436	0.0354	0.0130	-0.0100	2.000
2.125	0.0474	0.0417	0.0335	0.0275	0.0146	-0.0130	------	0.0482	0.0476	0.0396	0.0132	-0.0122	2.125
2.250	0.0509	0.0444	0.0357	0.0296	0.0161	-0.0143	------	0.0522	0.0517	0.0431	0.0154	-0.0136	2.250
2.375	0.0536	0.0468	0.0384	0.0312	0.0168	-0.0161	------	0.0551	0.0546	0.0461	0.0181	-0.0149	2.375
2.500	0.0555	0.0482	0.0388	0.0317	0.0164	-0.0188	------	0.0566	0.0564	0.0501	0.0207	-0.0161	2.500
2.625	0.0565	0.0482	0.0387	0.0311	0.0150	-0.0216	------	0.0577	0.0576	0.0513	0.0271	-0.0186	2.625
2.750	0.0570	0.0482	0.0383	0.0293	0.0139	-0.0259	------	0.0581	0.0583	0.0519	0.0278	-0.0211	2.750
2.875	0.0573	0.0470	0.0368	0.0278	0.0118	------	------	0.0578	0.0577	0.0518	0.0279	-0.0240	2.875
3.000	0.0565	0.0453	0.0338	0.0249	0.0084	------	------	0.0571	0.0570	0.0508	0.0282	-0.0252	3.000
3.125	0.0555	0.0437	0.0311	0.0213	0.0037	------	------	0.0564	0.0557	0.0488	0.0267	------	3.125
3.250	0.0531	0.0396	0.0272	0.0166	-0.0018	------	------	0.0543	0.0541	0.0474	0.0237	------	3.250
3.375	0.0493	0.0358	0.0223	0.0113	------	------	------	0.0518	0.0517	0.0458	0.0204	------	3.375
3.500	0.0449	0.0310	0.0167	0.0053	------	------	------	0.0468	0.0475	0.0436	0.0169	------	3.500
3.625	0.0401	0.0259	0.0109	------	------	------	------	0.0429	0.0447	0.0406	0.0129	------	3.625
3.750	0.0362	0.0211	------	------	------	------	------	0.0392	0.0409	0.0375	0.0114	------	3.750
3.875	0.0329	0.0173	------	------	------	------	------	0.0363	0.0385	0.0348	------	------	3.875
4.000	0.0295	------	------	------	------	------	------	0.0330	0.0349	0.0317	------	------	4.000
4.125	0.0252	------	------	------	------	------	------	0.0293	0.0322	0.0283	------	------	4.125
4.250	0.0198	------	------	------	------	------	------	0.0263	0.0286	0.0251	------	------	4.250
4.375	0.0142	------	------	------	------	------	------	0.0219	0.0261	0.0213	------	------	4.375
4.500	------	------	------	------	------	------	------	------	0.0224	0.0187	------	------	4.500

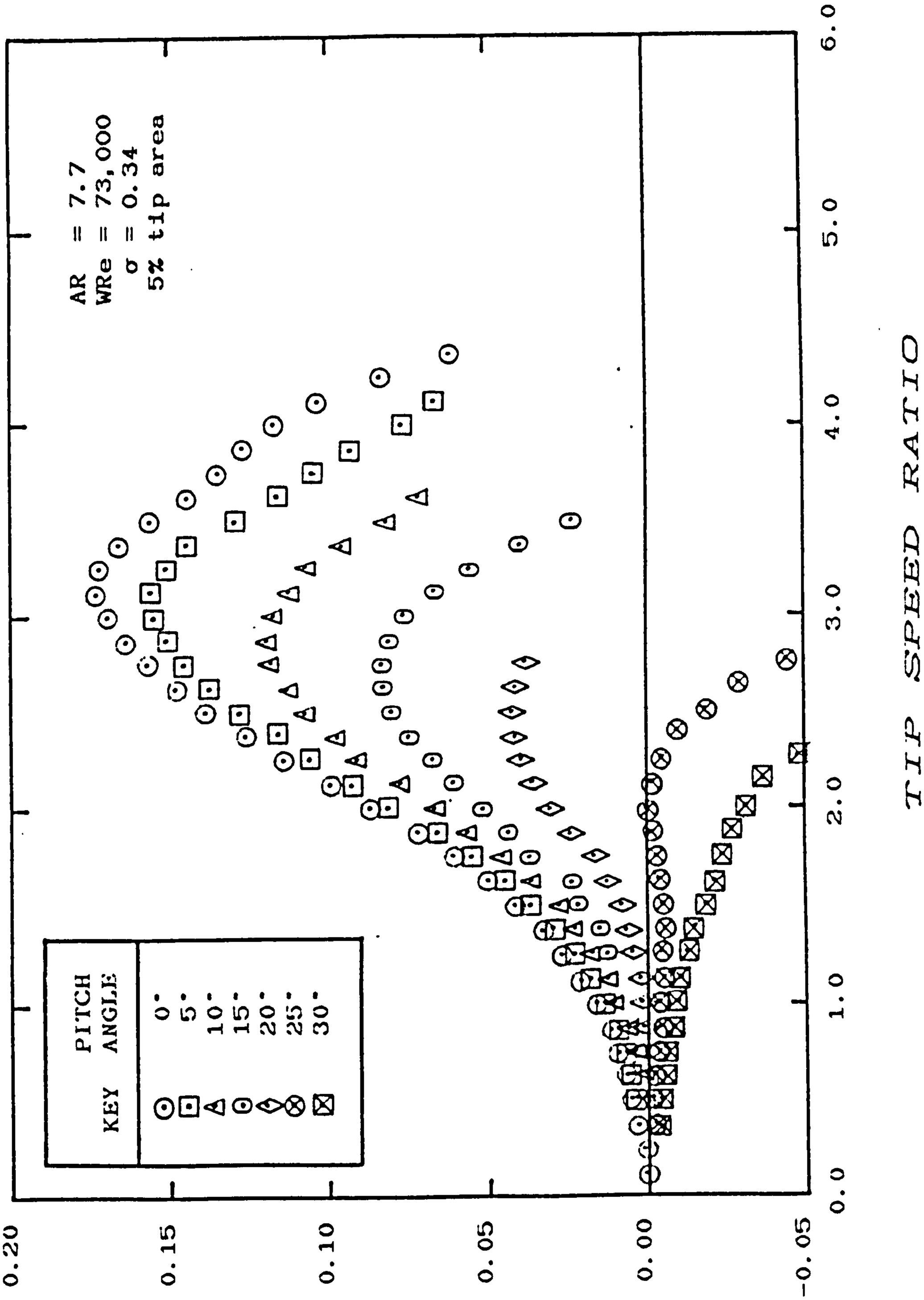

Figure 5.3a: Measured C_{pm}-λ characteristic for model V-VAWT with 5% tip area and positive pitch angles

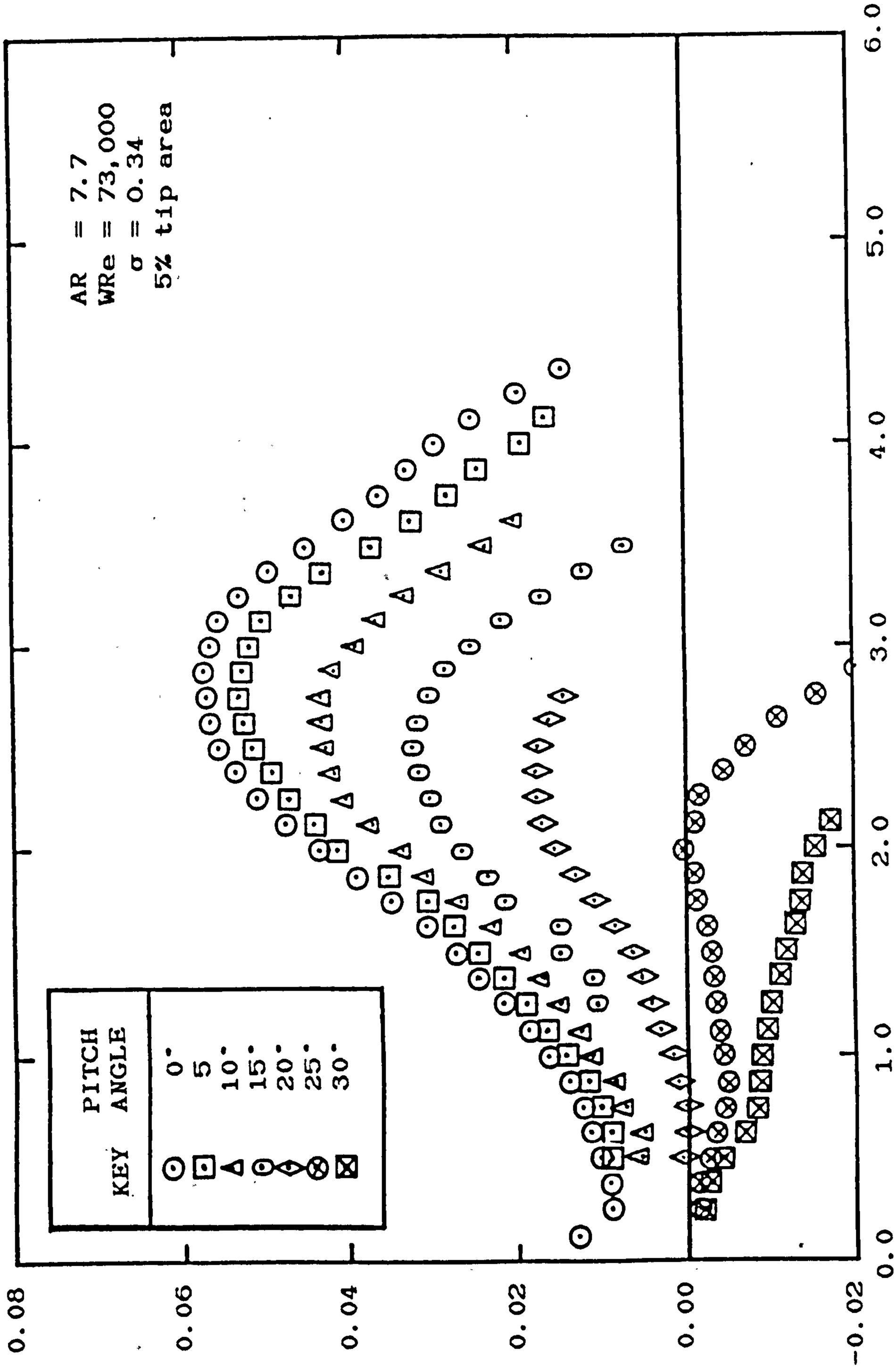

Figure 5.3b: Measured C_{Q}-λ characteristic for model V-VAWT with 5% tip area and positive pitch angles

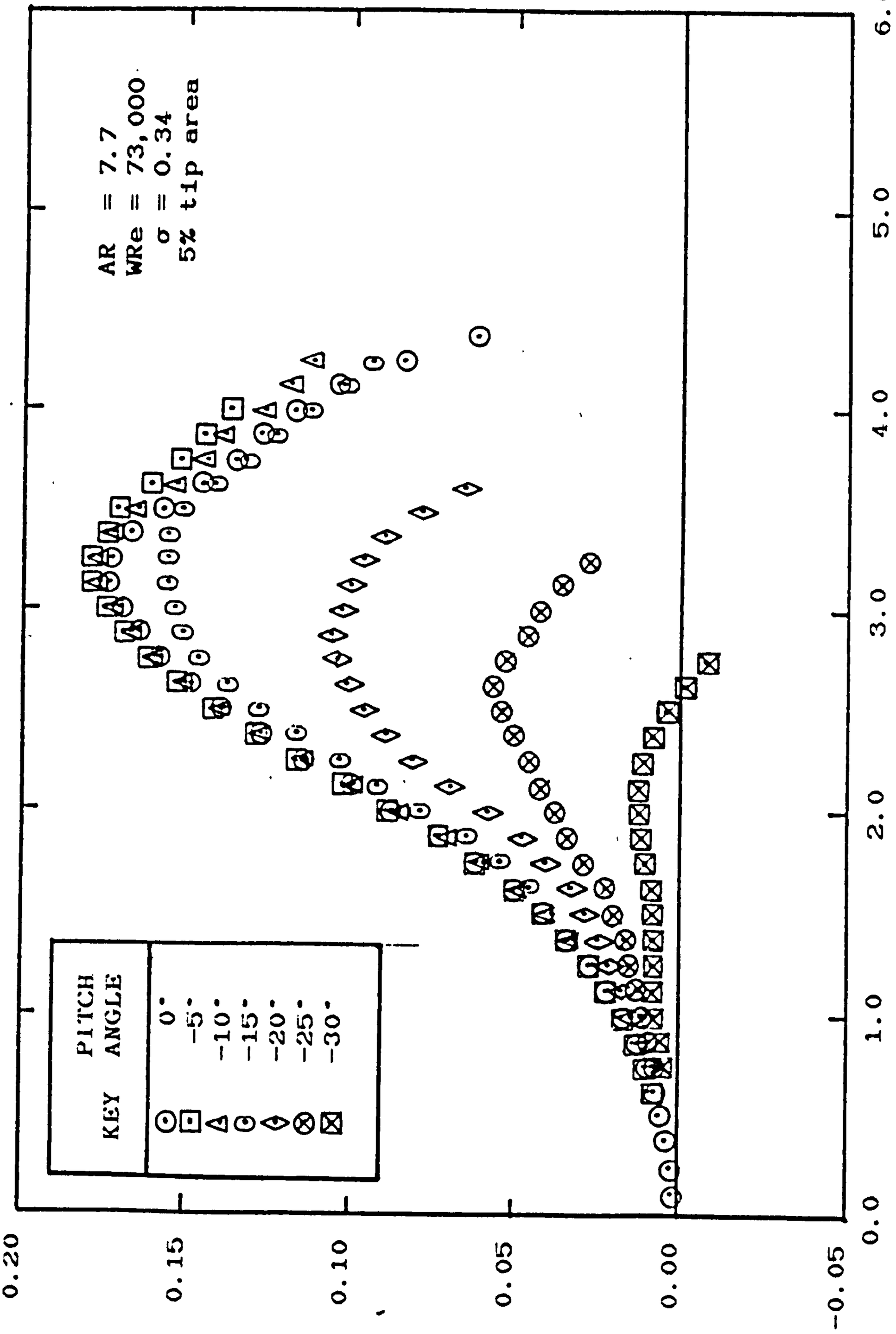

Figure 5.3c: Measured C_{P_m}-λ characteristic for model V-VAWT with 5% tip area and negative pitch angles

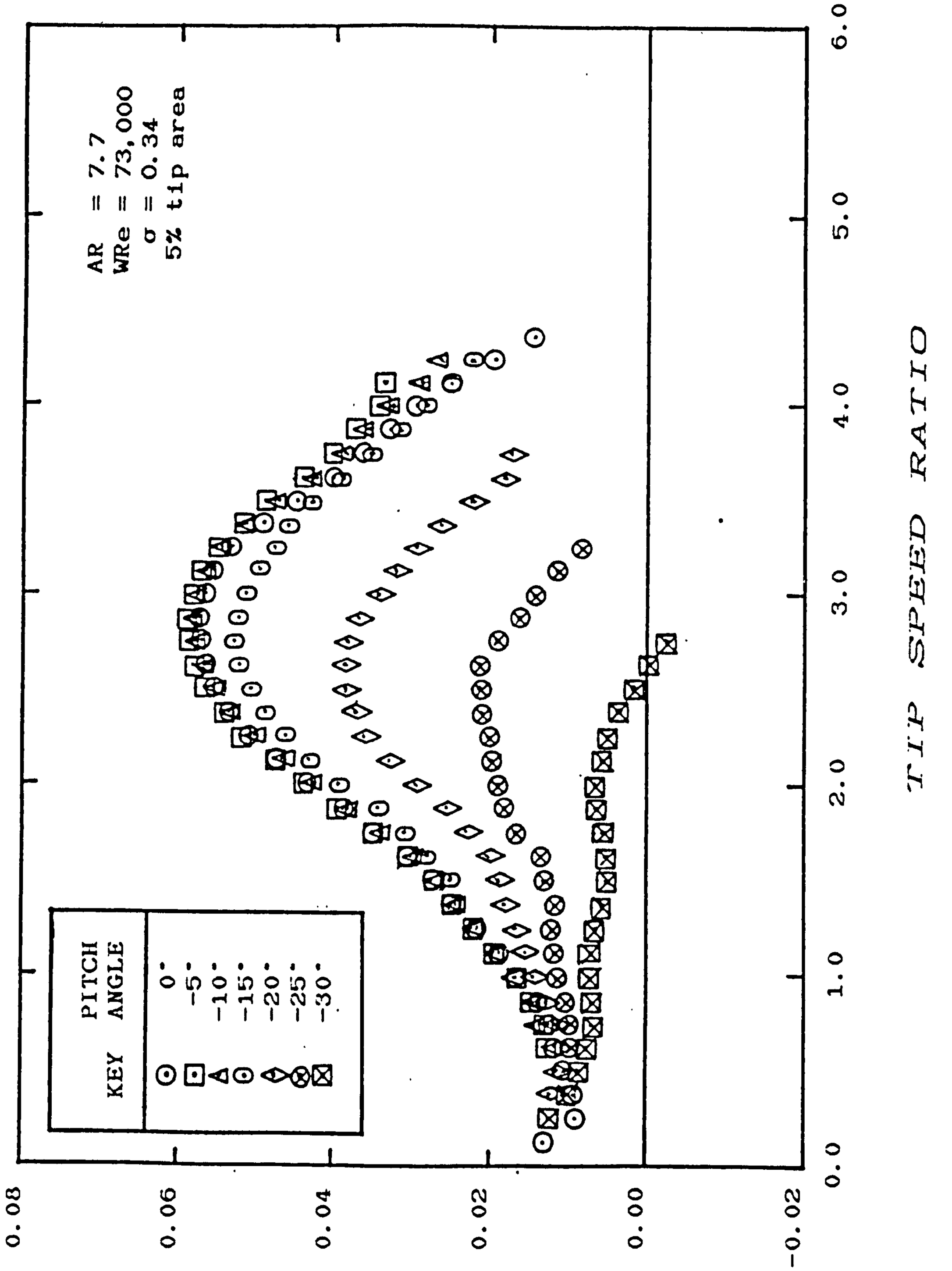

Figure 5.3d: Measured C_m-λ characteristic for model V-VAWT with 5% tip area and negative pitch angles

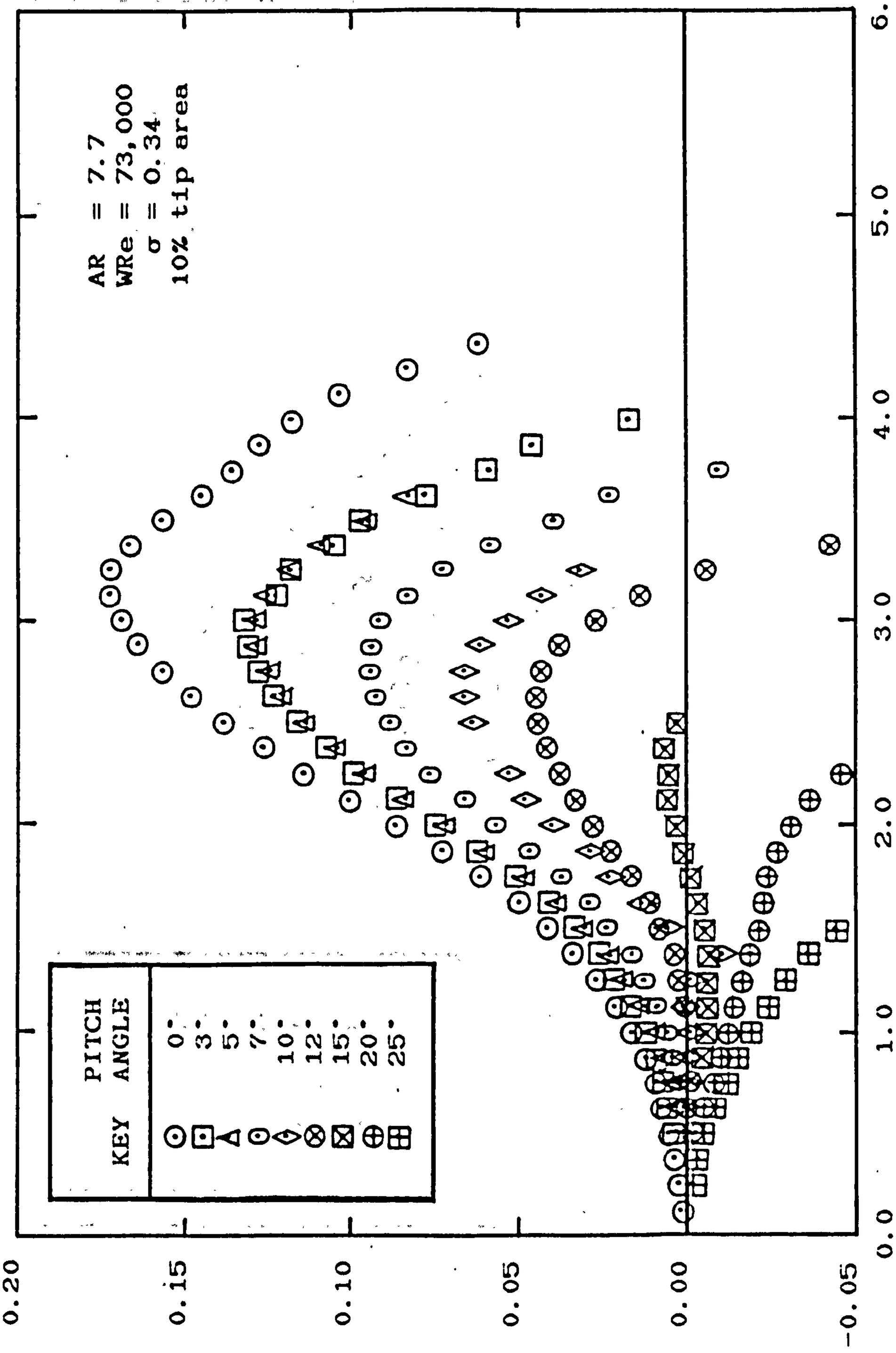

Figure 5.4a: Measured C_{P_m}-λ characteristic for model V-VAWT with 10% tip area and positive pitch angles

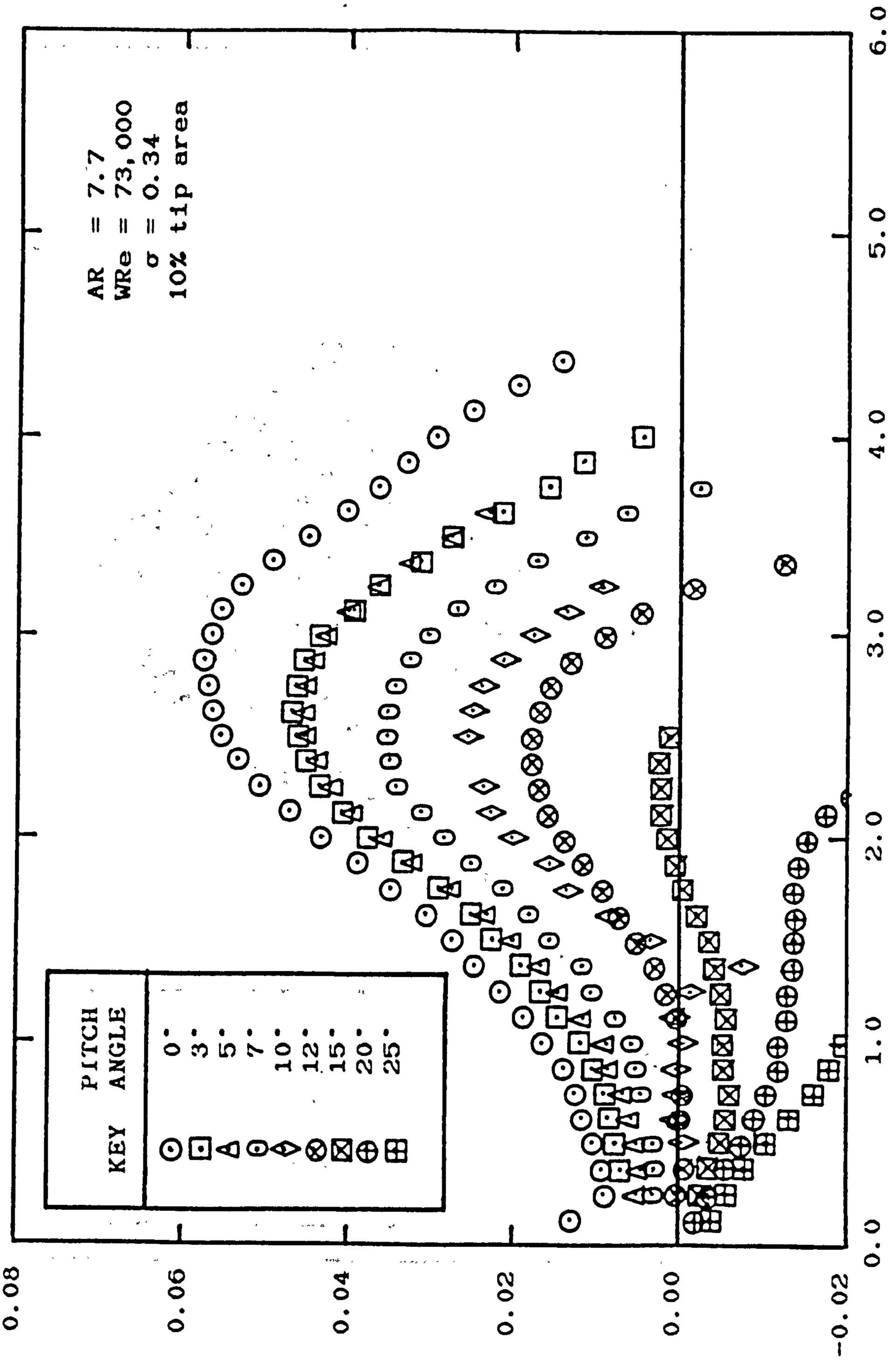

Figure 5.4b: Measured C_{Q_2}-λ characteristic for model V-VAWT with 10% tip area and positive pitch angles

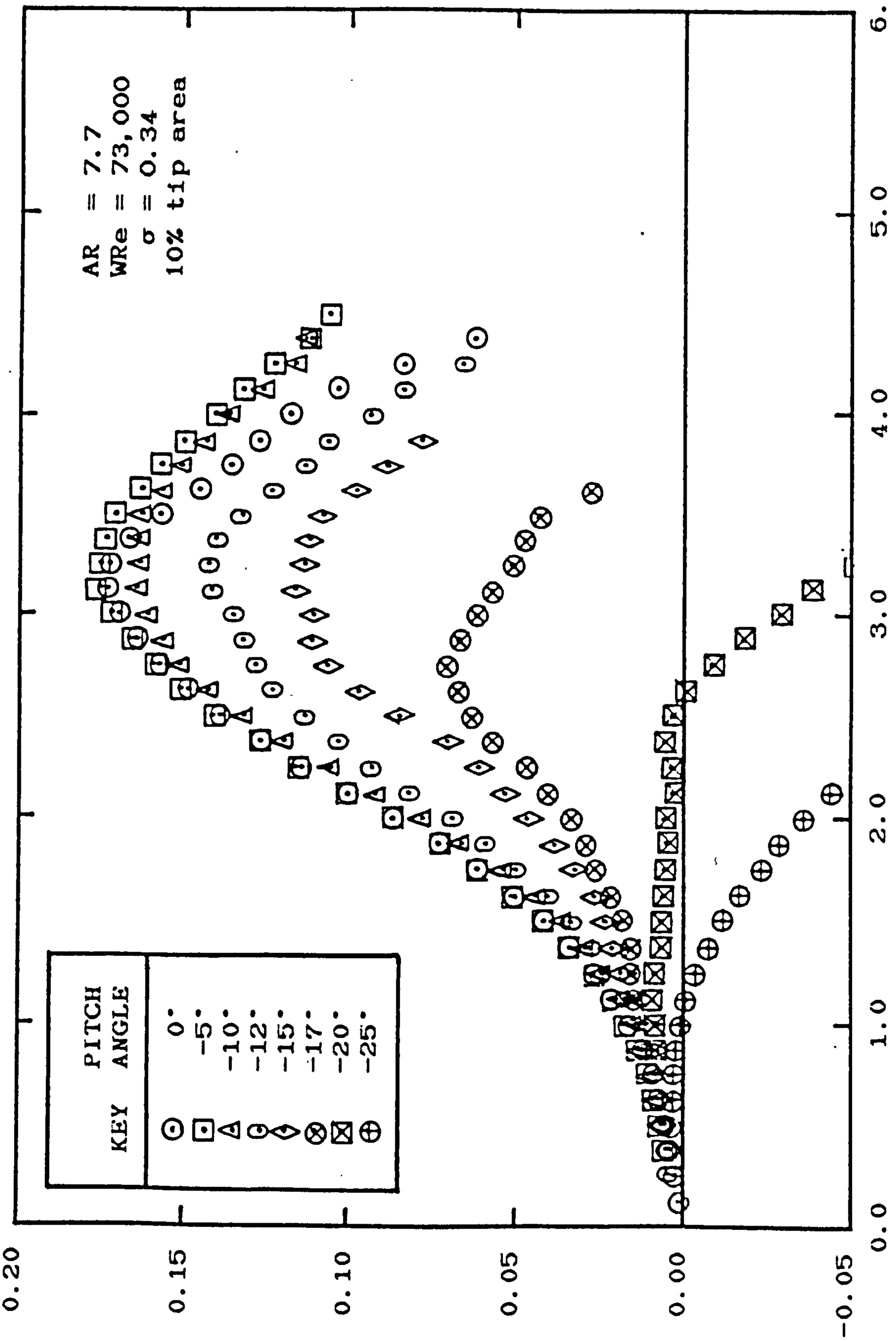

Figure 5.4c: Measured C_{P_m}-λ characteristic for model V-VAWT with 10% tip area and negative pitch angles

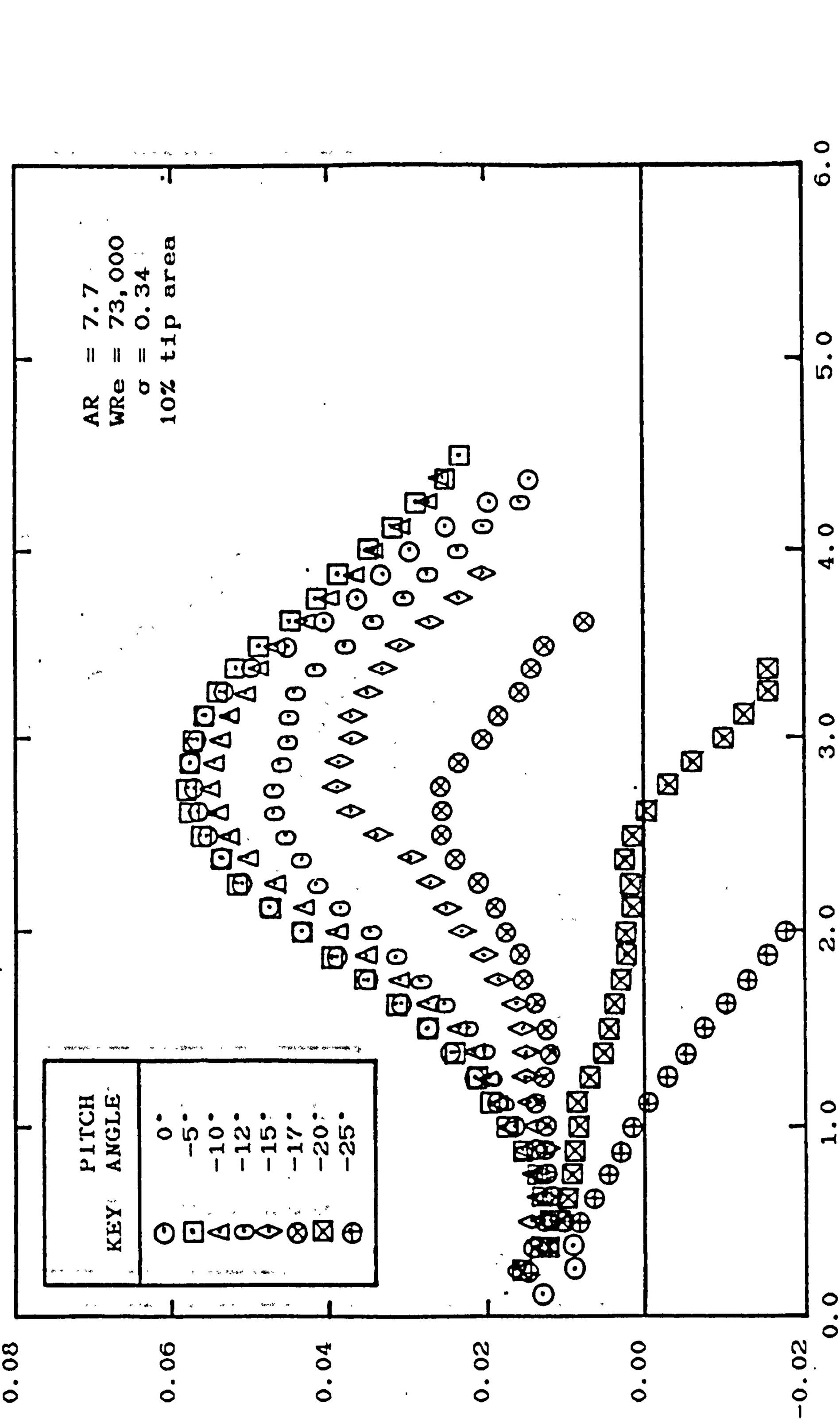

Figure 5.4d: Measured C_{rq}-λ characteristic for model V-VAWT with 10% tip area and negative pitch angles

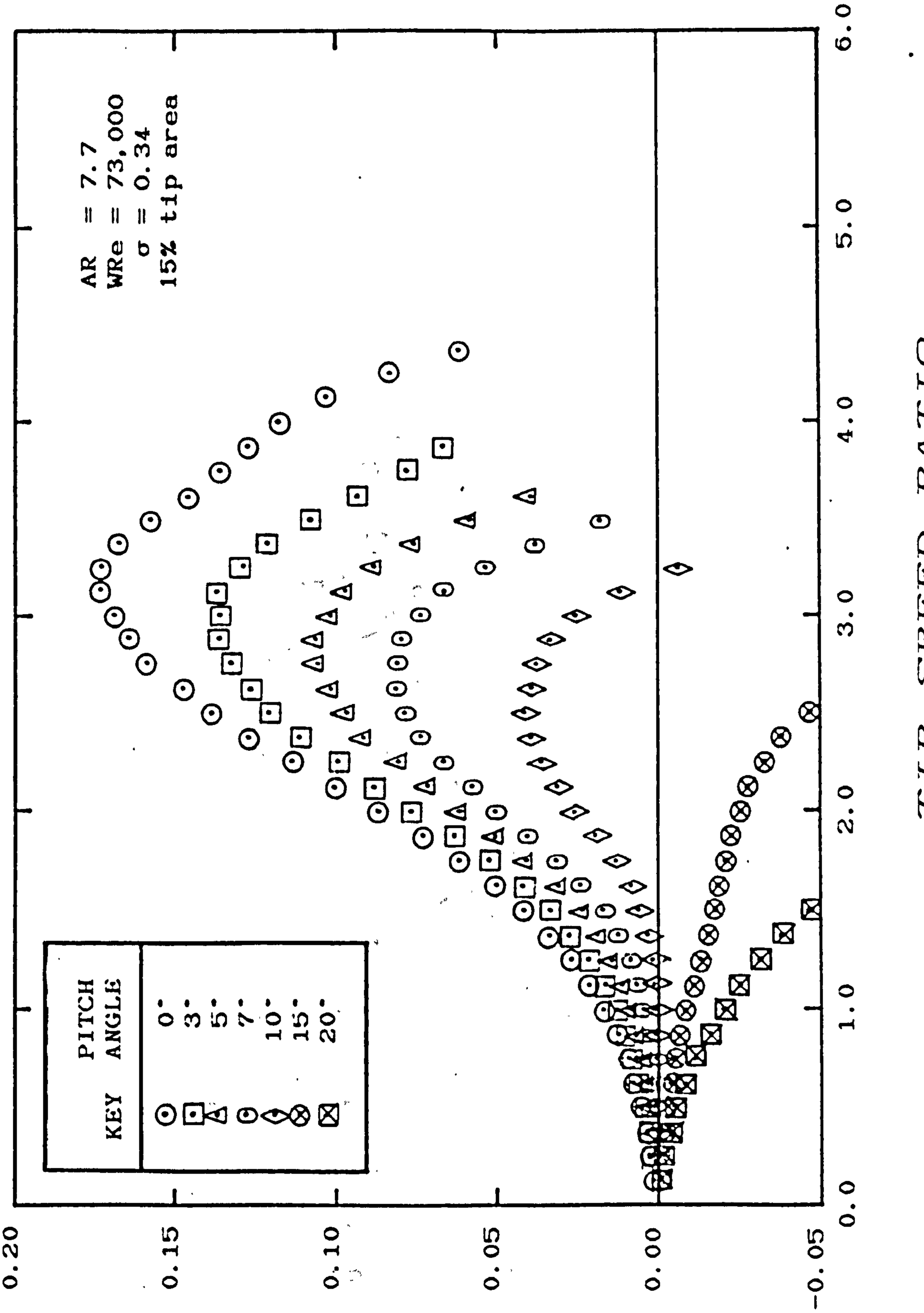

Figure 5.5a: Measured C_{P_m}-λ characteristic for model V-VAWT with 15% tip area and positive pitch angles

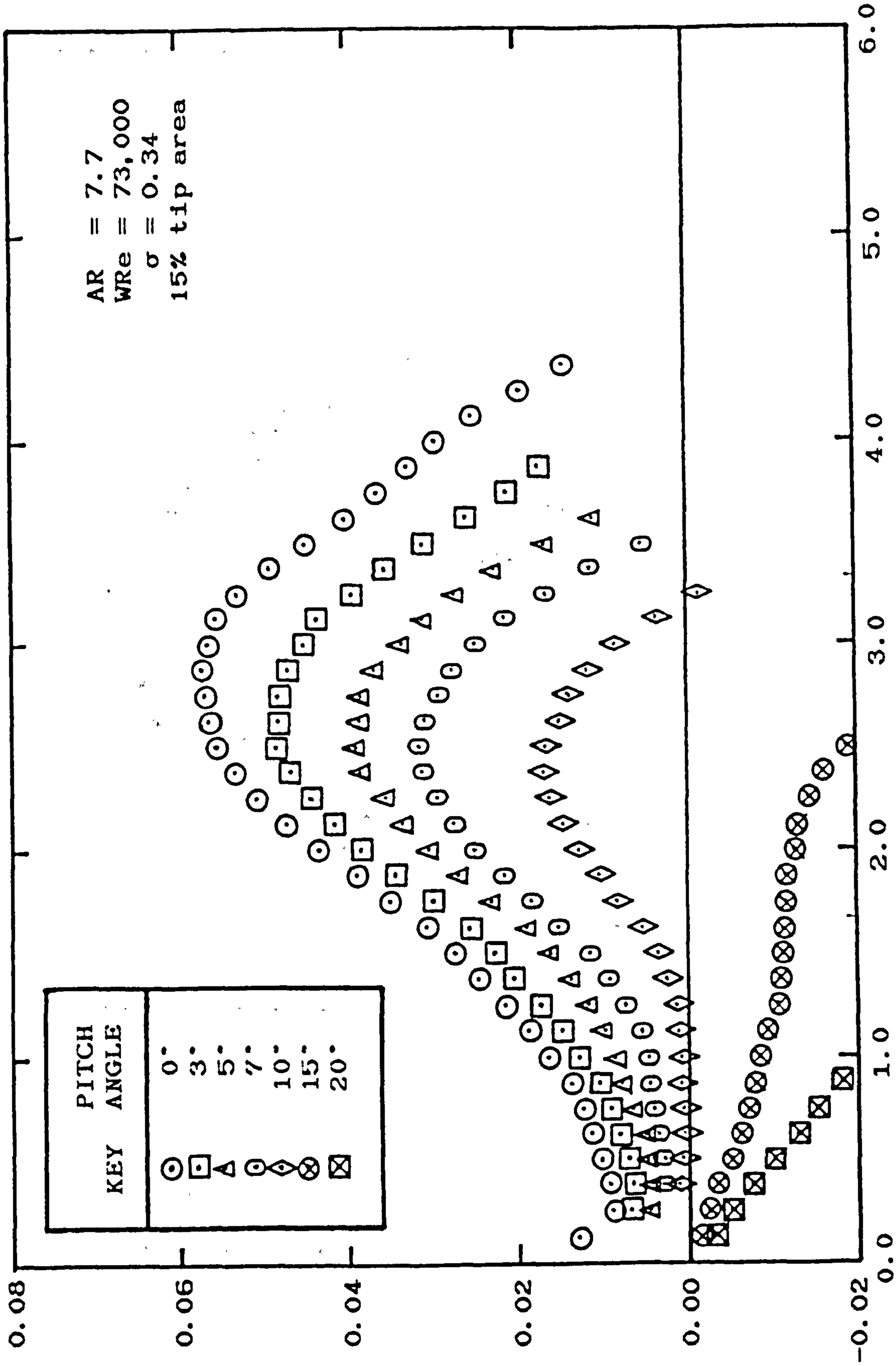

Figure 5.5b: Measured C_{ω}-λ characteristic for model V-VAWT with 15% tip area and positive pitch angles

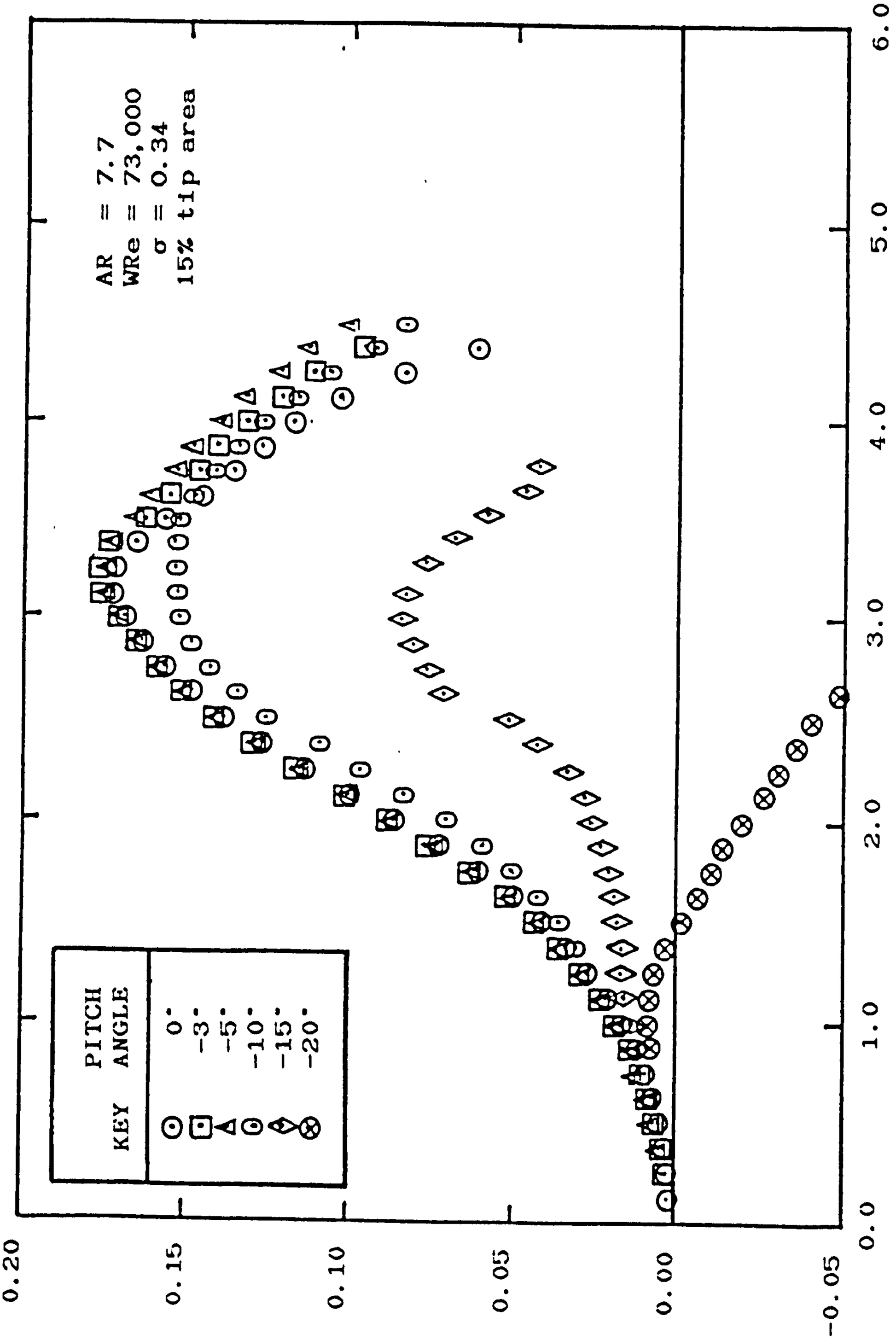

Figure 5.5c: Measured C_{P_m}-λ characteristic for model V-VAWT with 15% tip area and negative pitch angles

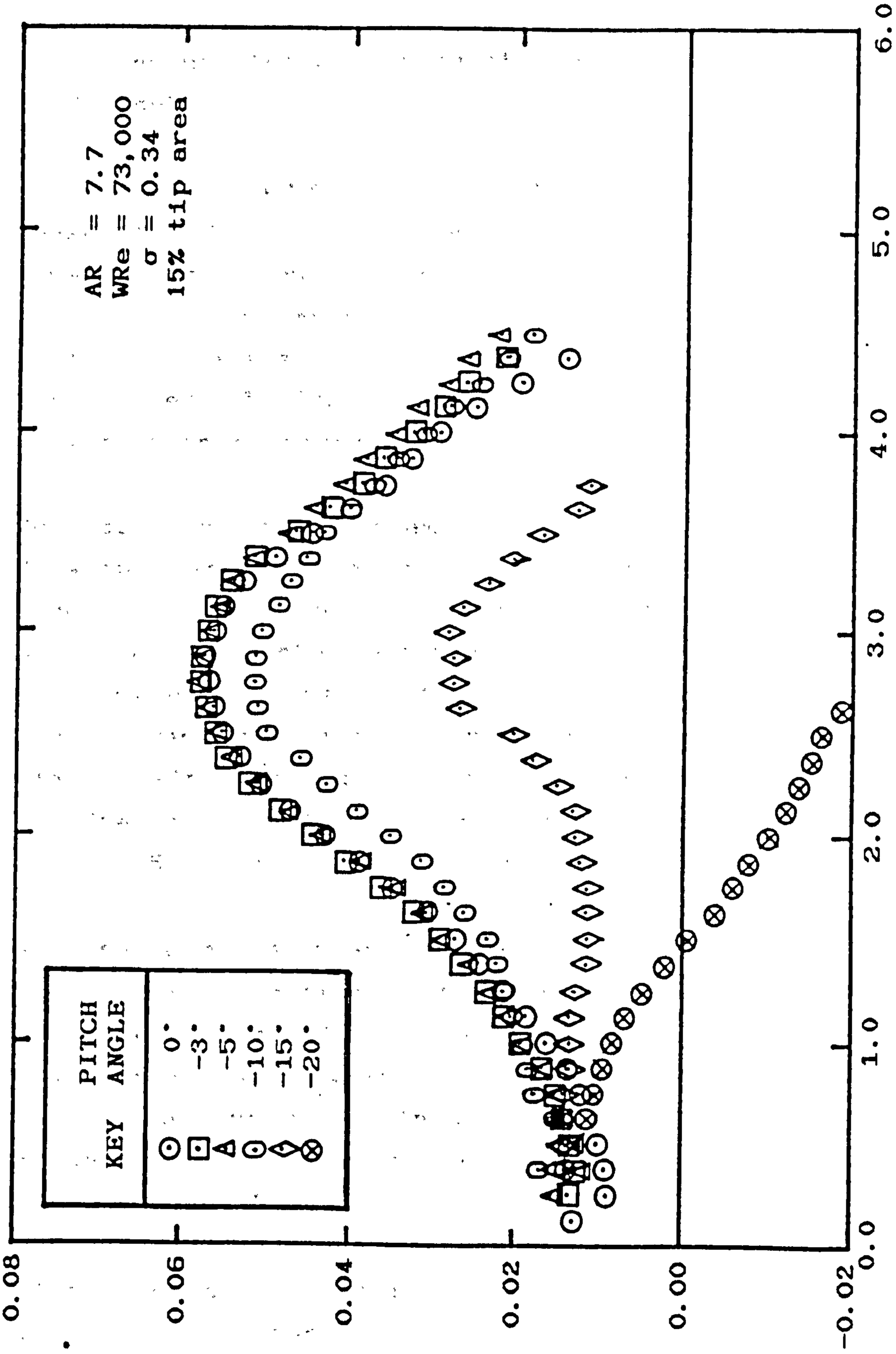

Figure 5.5d: Measured C_{Q_s}-λ characteristic for model V-VAWT with 15% tip area and negative pitch angles

5.9: Presentation and Discussion of the Performance Test Results

The initial analysis of the experimental results used the measured cable drag corrections to determine the aerodynamic performance of the V-VAWT rotor. The experimental results were promising and so a sample were presented in technical papers at a number of wind and solar energy conferences [57,58,59]. These papers are included for reference in Appendix 3.

Subsequently, the mathematical model of cable drag was developed and validated by the author. The cable drag model indicated that cable drag losses were larger than would be calculated using equation (5.10) at high rotational speeds. Consequently, all the measured values of C_m and C_q were modified to include cable drag losses calculated using the computer program CABLEDRAG. It is these modified results that are presented in full in Tables 5.2, 5.3 and 5.4, and plotted in Figures 5.3, 5.4 and 5.5.

All performance measurements were made with the wind tunnel speed constant. It was not possible to ensure that each test was carried out at exactly the same windspeed as previous tests, however, the speed of the tunnel fan was varied to try and maintain a similarity of windspeeds between tests. The tunnel exit velocity was generally measured as V = 14 m/s. At this windspeed, the wind Reynolds Number of the model V-VAWT is WRe ≃ 73,000. Since the results are presented in a non-dimensional form, they can be compared with each other without consideration of Reynold's Number changes. However, the influence of Reynolds Number must be considered when these performance results are compared with those of larger configurations.

The results of the tests made with zero blade tip pitch offset are shown in all figures. These results allow comparison of the effects of variable pitch and tip area on the performance of the model V-VAWT to be made. The results of measurements made with zero blade tip pitch offset also allow the performance of the model V-VAWT to be compared with the characteristics of previous V-VAWT models and other VAWT configurations. Therefore, the performance characteristics with zero blade tip pitch offset require detailed consideration before continuing with the discussion of the other test results.

5.9.1: Discussion of the Performance Test Results with Zero Blade Tip Pitch Offset

The performance characteristics for the model V-VAWT with zero blade tip pitch offset are recorded in Tables 5.2, 5.3 and 5.4, and illustrated in Figures 5.3, 5.4 and 5.5.

These results show the power and torque curves steadily rising to and falling from respective peak values, with the torque curve showing a small, but distinct, plateau in the range $\lambda = 2.50$ to $\lambda = 3.125$. In this tip speed ratio range, the maximum power and torque coefficients are observed to be:

$$C_{P\ MAX} = 0.173 \quad @ \quad \lambda = 3.125 \qquad (5.27a)$$

$$C_{Q\ MAX} = 0.057 \quad @ \quad \lambda = 2.875 \qquad (5.27b)$$

The test measurements do not extend beyond a tip speed ratio of $\lambda = 4.5$, at which speed ratio the model V-VAWT is still developing a positive torque. The runaway tip speed ratio must be estimated by extrapolation of the torque coefficient results beyond $\lambda = 4.5$ until $C_Q = 0$, and its value is determined to be $\lambda_{RUN} = 4.7$.

At low tip speed ratios the high torque developed by the model V-VAWT is clearly seen. The validity of the high torque measurement at $\lambda = 0.125$ is in doubt because its value is derived from only twelve measurements that fell into this tip speed ratio bin. However, all the other low tip speed ratio measurements are considered valid, and show a rising torque characteristic that remains positive. The value of the torque coefficient at zero tip speed ratio is estimated by extrapolation to be:

$$C_Q = 0.080 \quad @ \quad \lambda = 0 \tag{5.28}$$

The high torque characteristic of the V-VAWT configuration gives the turbine its excellent self-starting capability. This was observed throughout the testing of the V-VAWT model, as mechanical assistance was not required to accelerate it from rest to its normal operating speed.

When these results are compared with those presented by Sharpe and Taylor [19] for a previous model V-VAWT tested in the same wind tunnel, the maximum power coefficient, torque coefficient and runaway tip speed ratio measured here are observed to be significantly smaller in magnitude. The considerable difference between the performance of the two model V-VAWTs is clearly seen in Figure 5.6. Conversely, the performance of the model tested here shows the torque developed in the low tip speed ratio operating regime to be larger in magnitude. It is unfair to compare the results of these two V-VAWT models directly because their geometries differ in many ways. The variation in performance characteristics are due to the different aerofoil sections used for the turbine blades, and the difference in both turbine solidity and blade aspect ratio.

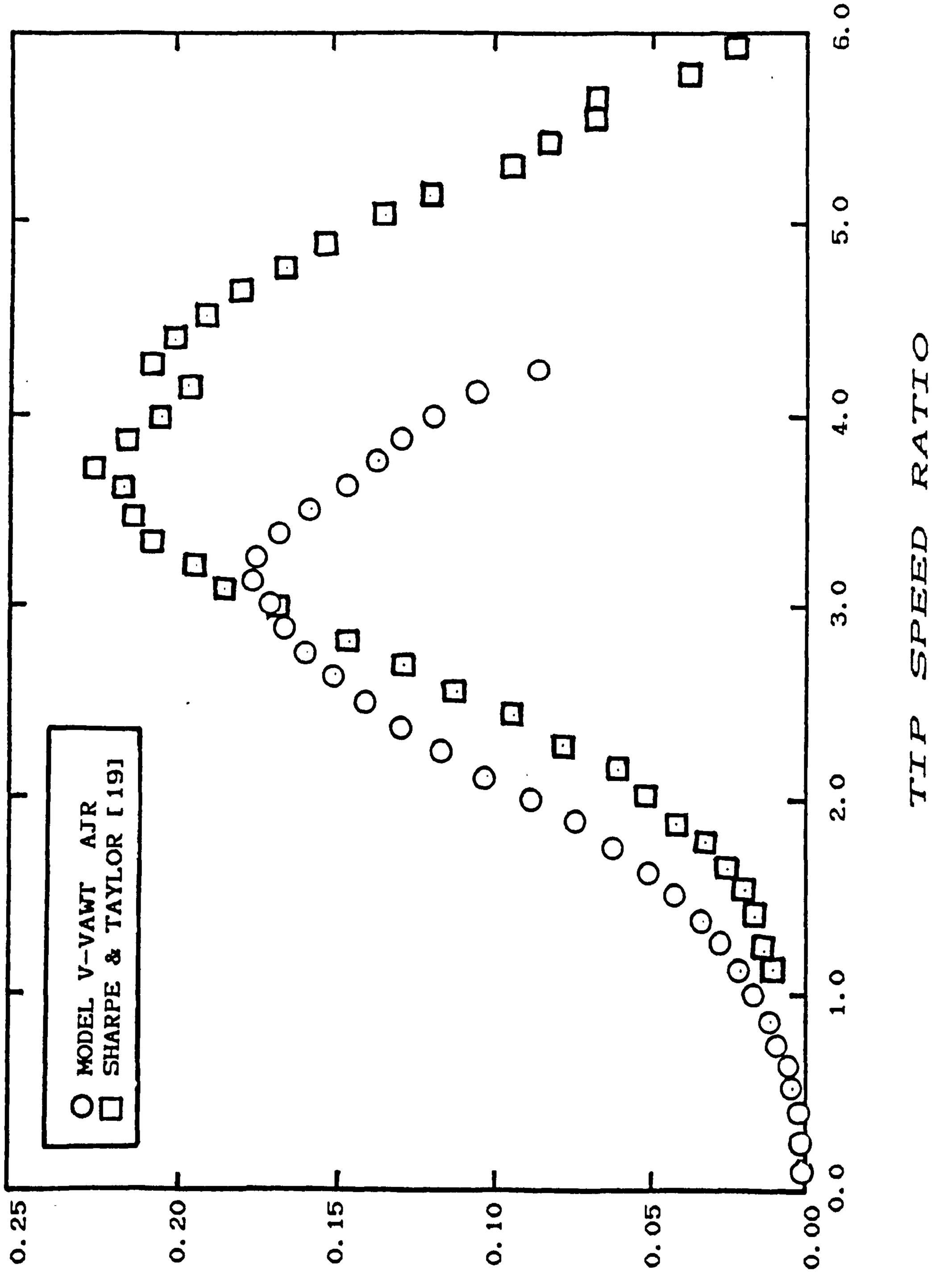

Figure 5.6a: Comparison of C_p-λ characteristics of two model V-VAWTs

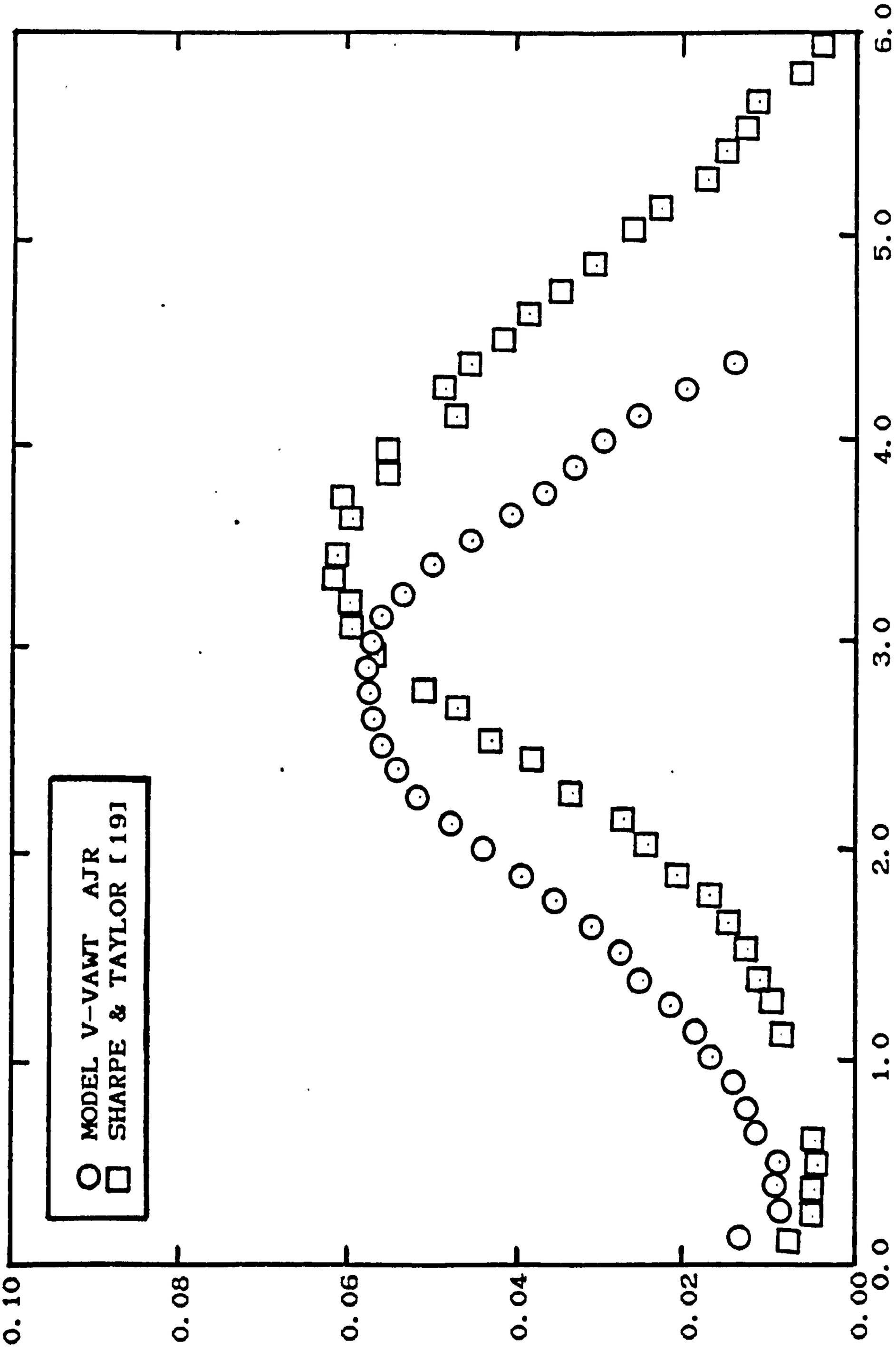

Figure 5.6b: Comparison of C_{rq}-λ characteristics of two model V-VAWTs

The NACA0025 section used here generally incurs a larger aerodynamic drag penalty than the NACA0018 used by Sharpe and Taylor, thus the torque developed in the higher tip speed ratio range is considerably smaller for the thicker blade section. A similar observation can be made from the experimental results of tests performed on small curve bladed Darrieus VAWTs by Sharpe [20], Figure 5.7. Four model VAWTs, each geometrically similar, but with blades of different thicknesses were tested. These tests showed the peak power coefficient for the NACA0018 section to be larger than that for the thicker NACA0021 section, so the similar difference between the two model V-VAWT test results is not suprising.

The larger solidity of $\sigma = 0.34$ for the model V-VAWT tested here contributes to both its superior starting torque performance and to the peak power coefficient occuring at a lower tip speed ratio when compared to Sharpe and Taylor's model V-VAWT, which has a solidity of only $\sigma = 0.28$. The superior starting torque characteristics of high solidity VAWTs has been adequately demonstrated by both Sharpe [23] and Sarre [60], though the effect of blade thickness on starting torque is inconclusive.

Small aspect ratio blades severely affect the peak power coefficient achievable for a particular configuration and reduces the runaway tip speed ratio, again clearly demonstrated for H-VAWTs by Sarre [60]. Sharpe and Taylor's study of the V-VAWT concept shows that both blade aspect ratio to a larger, and blade tangential offset to a lesser degree affect the overall performance of the V-VAWT. The model used here has blades of aspect ratio AR = 7.7 which are attached to the hub at the 30% chord position at their root. Sharpe and Taylor's model had blades with AR = 9.2 attached at the 50% chord position.

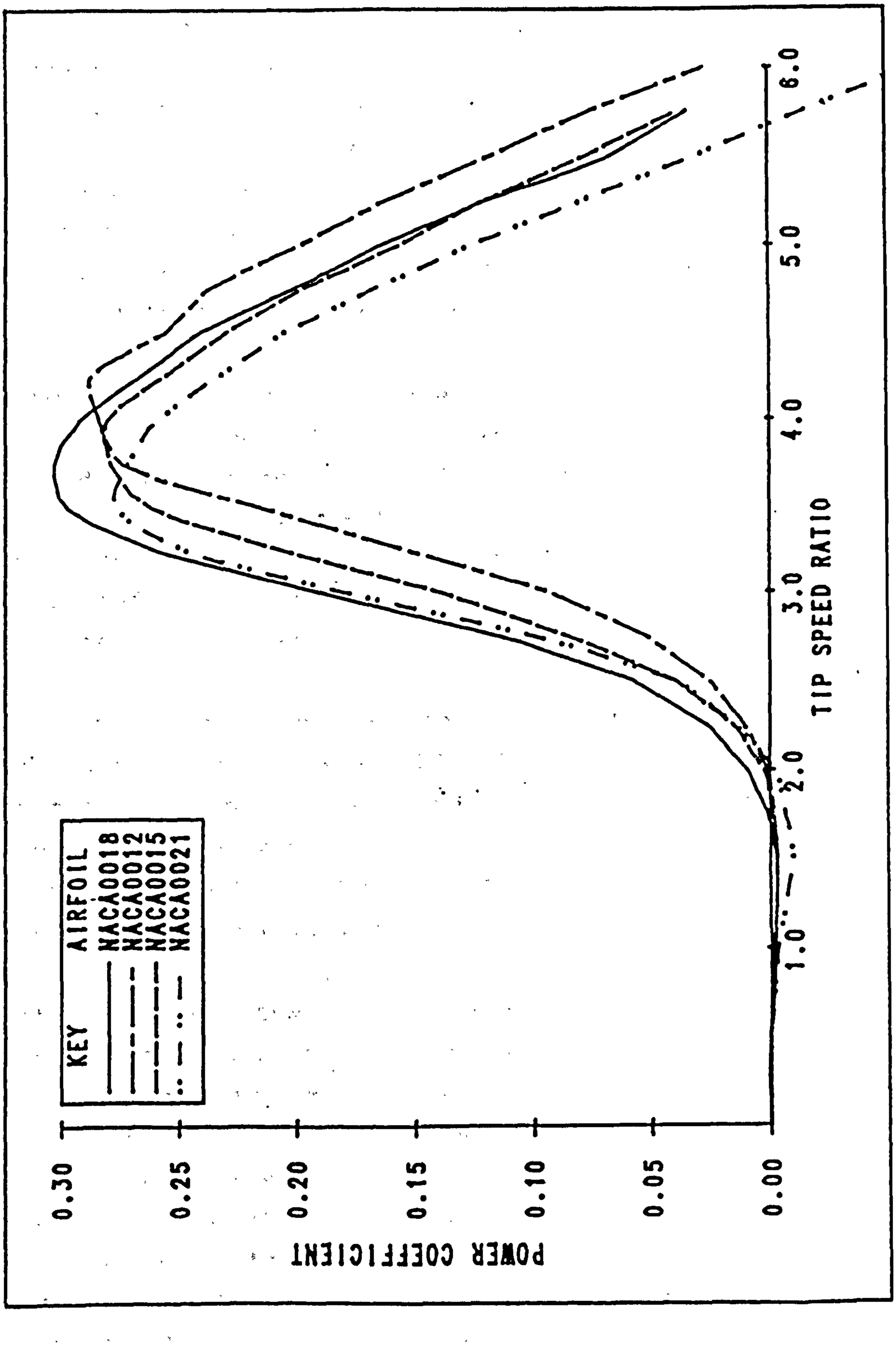

Figure 5.7: Effect of blade thickness on C_{p_m}-λ characteristics of model Darrieus VAWTs [20]

Since the model V-VAWTs differ in many ways, further comparison of the test results for these two models is meaningless unless the effects of each describing parameter can be isolated. The above comparison merely attempts to show that the performance test results of the model V-VAWT tested here are not unreasonable, especially in light of the previous V-VAWT test results and generally observed VAWT operating characteristics.

Notwithstanding the differences in performance discussed above, the values of peak power and torque coefficient are considerably lower than would be expected of larger, free-air machines. The greater efficiency of larger V-VAWTs is due essentially to Reynolds Number effects which cannot be accounted for in the non-dimensional power coefficient and tip speed ratio terms.

All the tests reported here were conducted at a wind Reynolds Number of WRe ≃ 73,000. The free-air 5kW V-VAWT operating in a similar windspeed of V = 14 m/s would be running with a wind Reynolds Number of WRe ≃ 315,000, and a 100kW V-VAWT of WRe ≃ 1,250,000. Sharpe and Taylor demonstrated the effect of Reynolds Number by comparing predictions of their model test results (WRe = 60,000) with 5kW and 100kW V-VAWT configurations (WRe = 250,000 and WRe = 1,000,000 respectively), reproduced in Figure 2.12. The rotor geometries of the latter two configurations are exactly the same, therefore it is only the influence of WRe that determines the differences in the prediction results. Consequently, the low aerodynamic efficiency of the model tested here should not prevent the test results being "extrapolated" to larger sized machines provided the differences in WRe are considered.

5.9.2: Discussion of the Performance Test Results with Variable Blade Tip Pitch Offset

The experimental test results plotted in Figures 5.3, 5.4 and 5.5 clearly show the effects of positive pitch, negative pitch, and blade tip size on the overall perfomance of the model V-VAWT. It is worth remarking that the author considers the results to be of excellent quality both in reliability and accuracy. This is due to each "measurement" being averaged from many instantaneous measurements falling into the appropriate tip speed ratio bin, and the careful use of numerical methods in the angular acceleration calculations. All C_{P}-λ and C_{Q}-λ curves are smooth and show few invalid measurements.

Considering the positive pitch angle results first, it is clear to see that progressive increases of nose-in pitch reduces the power and torque output of the rotor across the whole tip speed ratio range. The effectiveness of the tip increases with tip area, as seen by the larger power reductions evident for the large tip area results. The power output of model V-VAWT is highly sensitive to variations of pitch angle, even for the smallest tip area. More importantly, the torque developed by the rotor can be completely killed off across the whole tip speed ratio range with pitch angles of 25°, 20° and 15° for the 5%, 10% and 15% tip areas respectively. This condition holds true for starting torque, where negative torque coefficients are observed for the low tip speed ratio results. This characteristic ensures that overspeeding of the rotor can be controlled and aerodynamic braking to a standstill can be effected at any windspeed. Positive pitch angle variations, clearly offer the V-VAWT designer complete power and speed control capability with relatively small tip areas.

The negative pitch angle results show some interesting effects, notably that nose-out pitch offsets can actually *increase* power output. The increase in power output is most notable at the high speed end of the tip speed ratio range where the runaway tip speed ratio is much higher for small nose-out pitch offsets of -3°, -5° and -10°. Power output increases of approximately 18% are observed at $\lambda = 4.0$ for pitch offsets of -5°, though the best increase in peak power output observed is only 2%. If the nose-out pitch is increased beyond -10°, a decrease in power and torque output becomes apparent. Unlike the nose-in pitch results, the reduction in power output only occurs at high tip speed ratios. As tip speed ratio decreases, the power regulation effect diminishes such that the starting torque of the rotor is actually *enhanced* by large negative pitch offsets. Unfortunately, the experimental data is sporadic at the very low tip speed ratios and it is difficult to determine which pitch angle offsets maximise starting torque. These experimental results indicate that energy capture gains can be made by operating the blade tips with small nose-out offsets. Aerodynamic braking is, however, limited, and considering the evidence, complete braking to a standstill cannot be achieved. Enhancement of starting torque is clearly possible, though it is difficult to assess the gains made at the very lowest tip speed ratios.

The variable pitch experimental results have clearly demonstrated the suitability of partial-span pitch control for both power and speed control of the V-VAWT. For the model tested here, it has been demonstrated that complete control can be achieved with a tip area of only 5% of the total blade area. Positive, nose-in pitch angles provide complete power regulation at all rotor speeds, while small nose-out pitch angles can be used to enhance power output at high rotor speeds; low speed power enhancement has also been demonstrated. While the overall power regulation

effect is not suprising, the author had not considered that the rotor power output would be so sensitive to small tip pitch angle changes as has been observed. Increases of power with small nose-out pitch offsets had already been observed by Stacey and Musgrove [39], so it was not unexpected to see this effect here, but the enhancement of starting torque with larger nose-out pitch offsets had not been previously observed.

The effectiveness of variable pitch tip control for larger V-VAWT configurations requires the influence of Reynolds Number to be considered. As with the zero pitch performance, there will be a general increase in the power output of the V-VAWT rotor as wind Reynolds Number increases. In this event, it is unlikely that 5% tip areas will be able to provide complete power and speed regulation as achieved here. The Westwind VAWT has been shown to have inadequate control capability with small tip areas [41], so for V-VAWT applications larger tip areas will be required. The range of tip pitch angles evaluated was limited to a maximum of ±30°; the effect of pitching the tips beyond this range has not been demonstrated, but it is assumed that the reductions in power output at high tip speed ratios would continue. The speculation about the effectiveness of variable tip pitch control on larger V-VAWTs can only be continued with any worth if evidence of its control effect can be presented. One approach is to use VAWTTAY for predicting the effect of variable tip pitch control on full scale V-VAWTs. However, before proceeding to the analysis of larger V-VAWTs, the validity of VAWTTAY predictions of tip pitch control effects must be verified. Therefore a theoretical analysis of the model V-VAWT is required, and a comparison between the theoretical results and the experimental results presented here to be made. Only when satisfactory correlation is achieved may VAWTTAY be used for design studies of full scale V-VAWTs.

5.10: Theoretical Predictions of Model V-VAWT Performance

The aerodynamic performance prediction model VAWTTAY enables theoretical C_P-λ and C_Q-λ characteristics of V-VAWT configurations to be determined. Whilst the blade geometry program WRITEBLADE allows preset blade pitch to be defined i.e. twist, in the original version of the program, variation of blade pitch was not accomodated in any way. To predict the effect of tip pitch variation on the performance of a V-VAWT rotor, a tedious but effective approach to the analysis was adopted.

To predict tip pitch effects for each tip area, each pitch angle variant had to be defined in a separate blade tip geometry file. The fixed pitch portion of the blade was also modelled, but in a separate file. The prediction program VAWTTAY was run for each blade geometry file, and the theoretical C_P-λ and C_Q-λ results for each geometry stored in separate results files. The results for the fixed pitch portion of the blade and the results for a particular tip area and pitch angle were numerically combined to give an overall C_P-λ and C_Q-λ performance characteristic for that particular tip variant. This process was repeated for all pitch areas and pitch angles considered. This required numerous executions of the programs which was tedious and repetitive to undertake. Subsequent to this initial analysis, the author has made some significant changes to the modus operandi of the computer programs WRITEBLADE and VAWTTAY. A considerable improvement in both time and resources has been achieved, allowing theoretical studies of tip pitch variation to be completed with greater effectiveness. These changes will be considered further in Chapter Seven.

The results of the initial theoretical study of the model V-VAWT are shown in Figures 5.8, 5.9, 5.10 and 5.11.

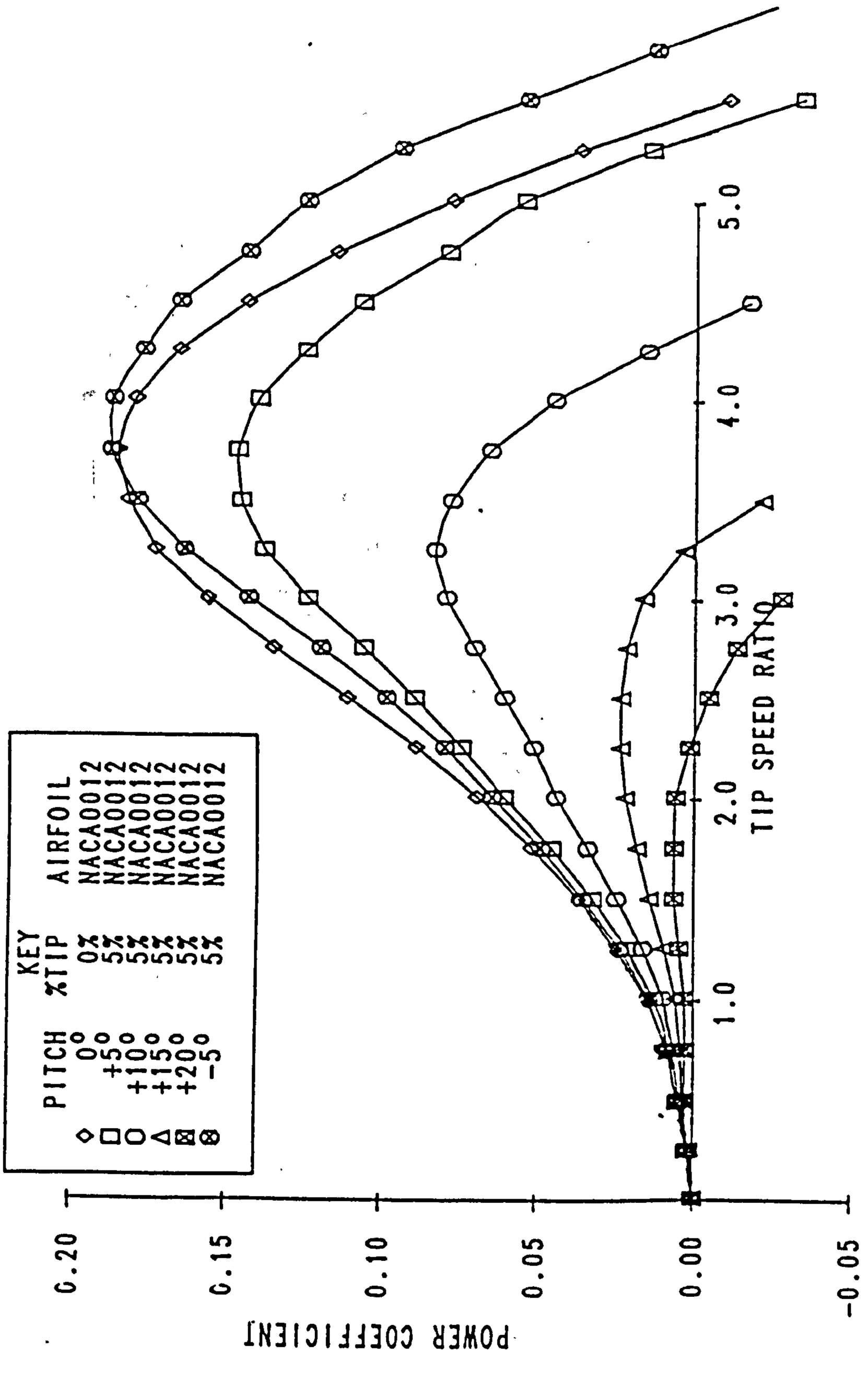

Figure 5.8: Theoretical C_{pm}-λ characteristic for model V-VAWT with 5% tip area

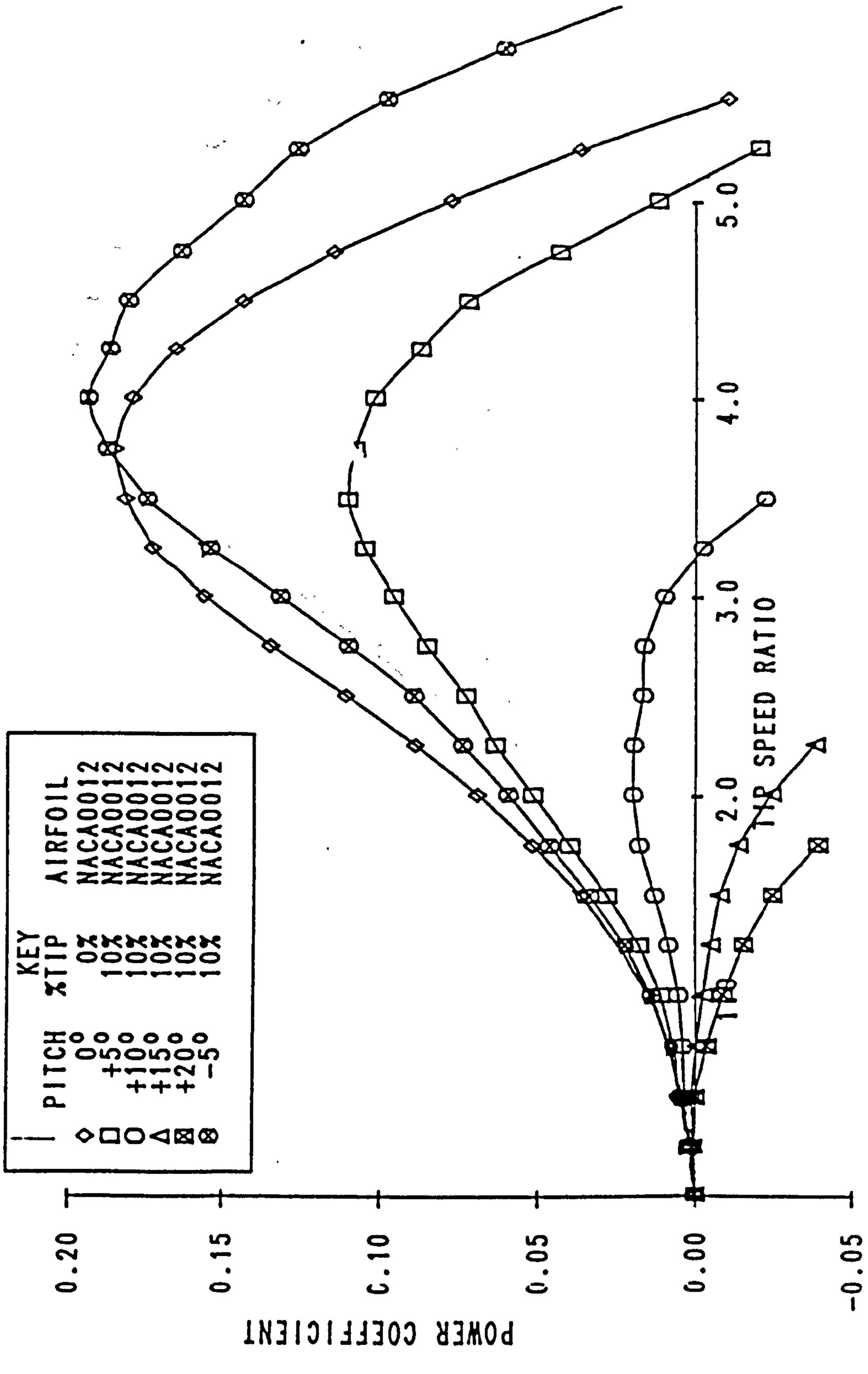

Figure 5.9: Theoretical C_{pm}-λ characteristic for model V-VAWT with 10% tip area

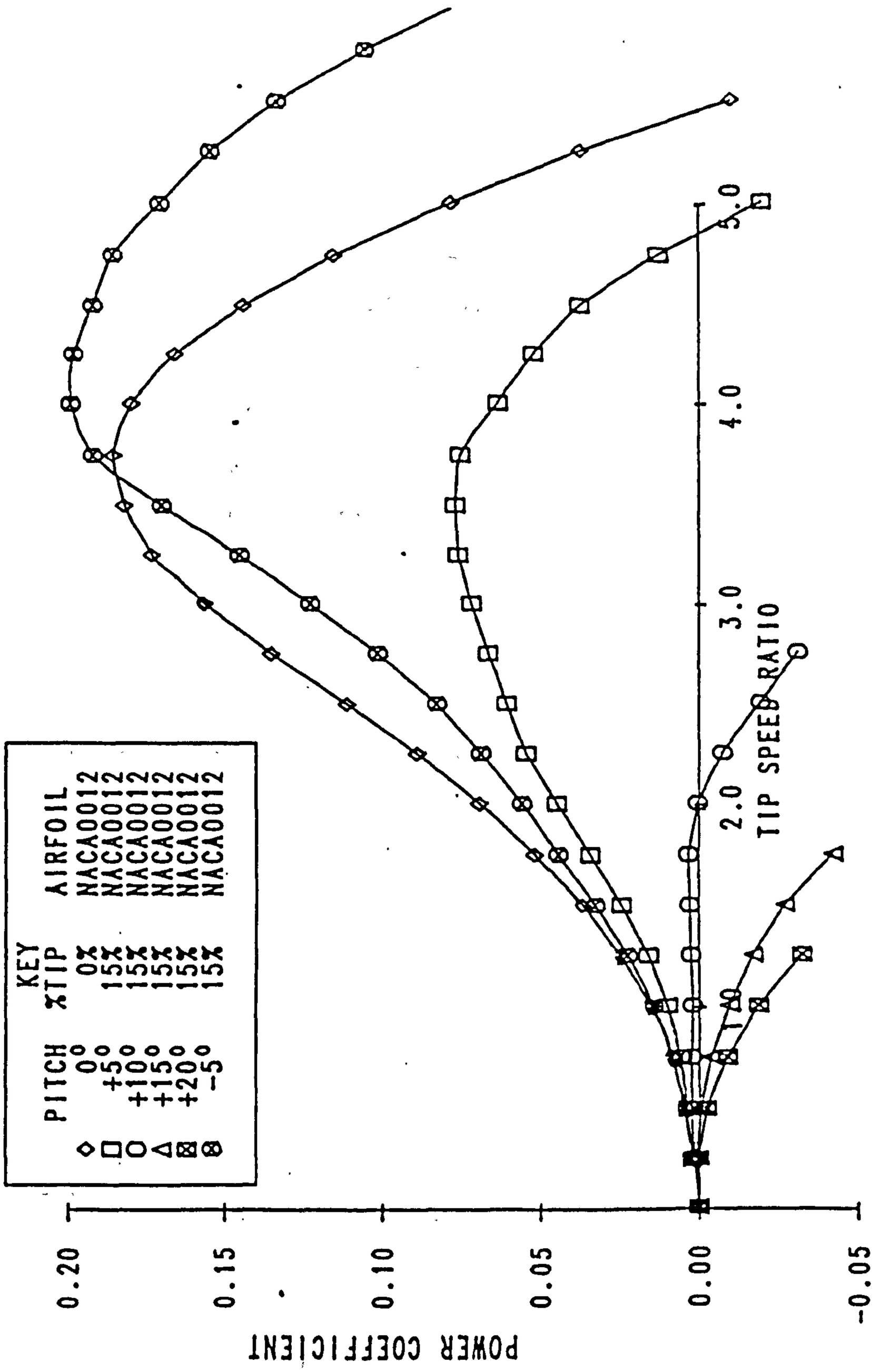

Figure 5.10: Theoretical C_{P_m}-λ characteristic for model V-VAWT with 15% tip area

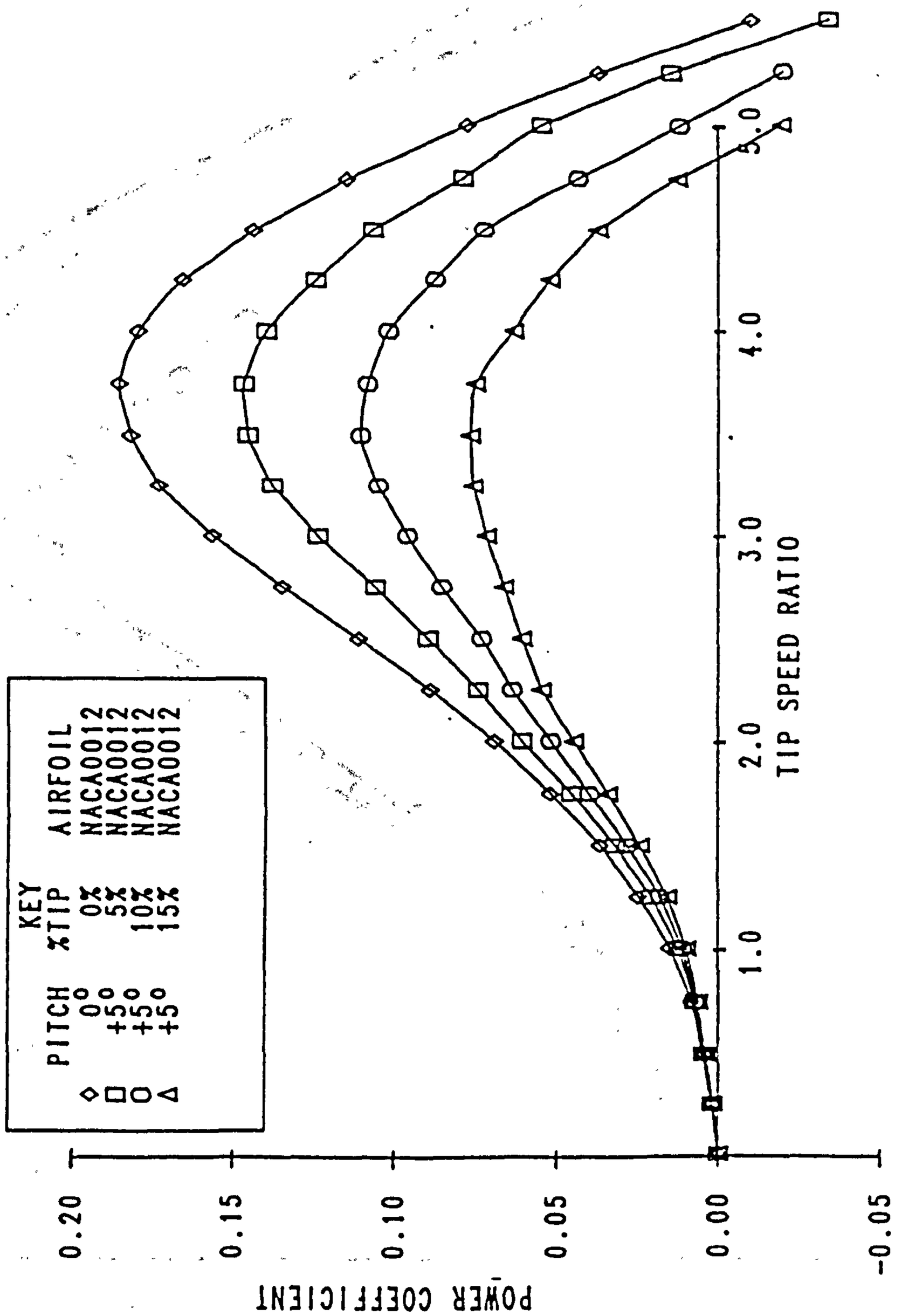

Figure 5.11: Theoretical C_{P_m}-λ characteristic for model V-VAWT with 5° pre-set pitch and 5%, 10% and 15% tip areas

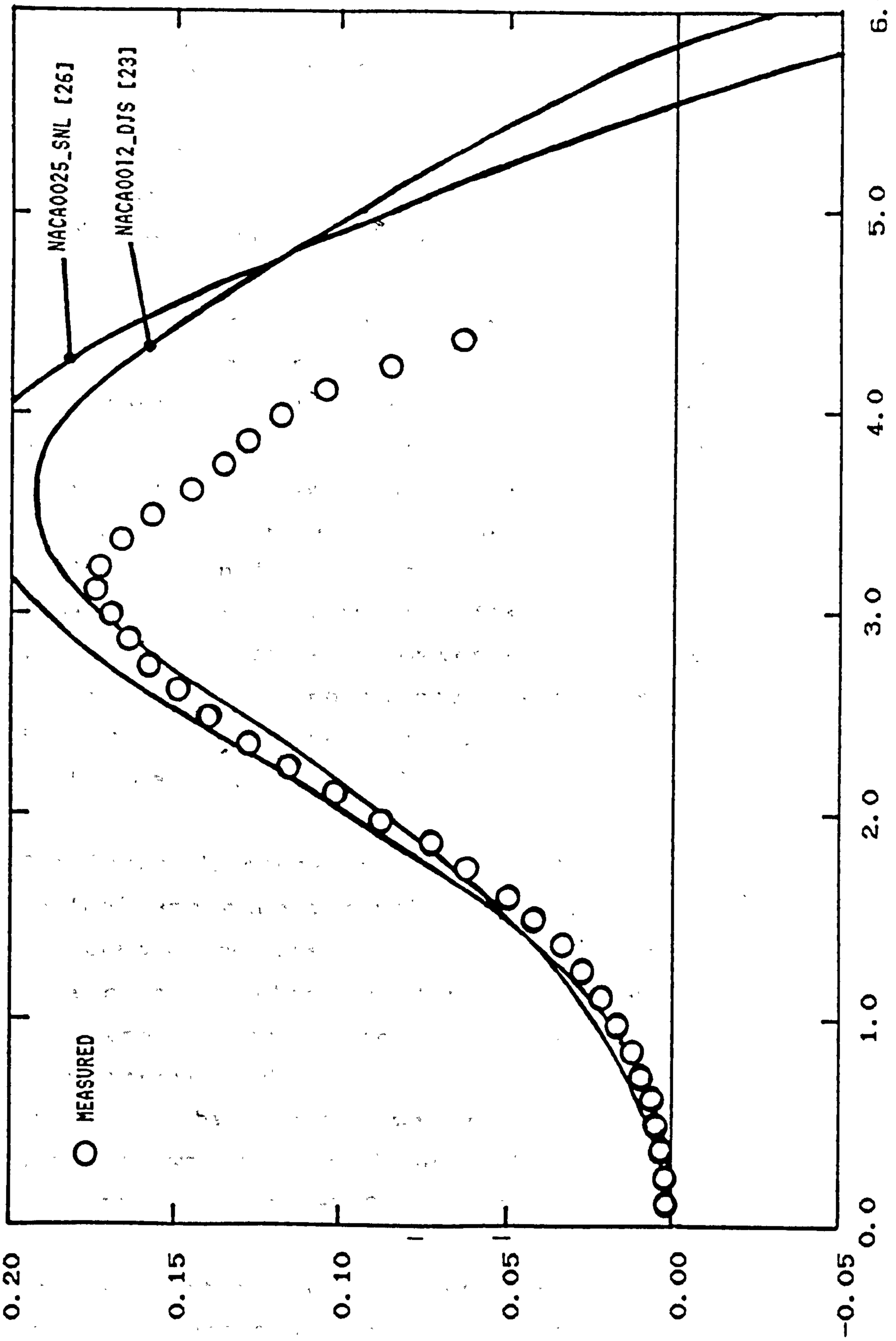

Figure 5.12: Comparison between measured and theoretical C_{P_m}-λ characteristic for model V-VAWT

The C_{p_w}-λ characteristics have been determined for constant windspeed operation, with a wind Reynolds Number corresponding to the test conditions of WRe ≈ 73,000. The blade tip geometries for 5%, 10% and 15% tip areas with pitch angle variations in increments of 5° have been considered.

The theoretical results are encouraging at first sight, because the moderation of power output with nose-in pitch is clearly observed, as is the enhancement of power output at high tip speed ratios with small nose-out pitch. The enhancement of power at lower tip speed ratios, however, is not demonstrated. These results, when considered in isolation, indicate that the prediction program VAWTTAY is capable of predicting the effect of tip pitch variation on V-VAWT performance. However, the accuracy and validity of the predictions are in doubt when the theoretical results for zero pitch are compared to the corresponding experimental results, Figure 5.12.

The large discrepancy that can be seen between the theoretical and experimental results at high tip speed ratios was considered unacceptable. It is due to the differences in aerofoil section used for the theoretical analysis and that used in the construction of the model V-VAWT. The only aerofoil data suitable for use with VAWTTAY at his stage of the project was that for the NACA0012 aerofoil section, whereas the blades of the model V-VAWT were made with the thicker NACA0025 section.

To ensure that the prediction model VAWTTAY could be used with confidence for predicting the performance of larger V-VAWT configurations, it was vital to prove that the discrepancy between the theoretical and experimental results is due to the aerofoil data alone, and not to some error in the analysis program itself.

The theoretical results for the 5%, 10% and 15% tip areas show trends that are consistent with the experimental evidence. The discrepancy between the two sets of results is largely due to differences in the numerical values of the C_{p_m}-λ curves. This suggested that the prediction program VAWTTAY itself is reliable, and that the discrepancy is due to the inappropriate use of NACA0012 aerofoil data.

At high tip speed ratios, the reduction in C_{p_m} from $C_{p_{m\,max}}$ as λ increases is due to the drag losses incurred at low angles of attack on the blade. The inferior performance of the model V-VAWT to that predicted is due to the larger drag penalties incurred by using the thicker NACA0025 section in preference to the NACA0012 section. The influence of blade thickness on VAWT performance can be seen in Figure 5.7. If the predictions are to show better correlation to the measured results, then there is a clear need for NACA0025 aerofoil data in a format suitable for use with VAWTTAY. However, the availability of good aerofoil data for use with VAWT performance prediction programs is limited, and is a problem familiar to VAWT experimentors and designers.

The most popular source of aerofoil data suitable for VAWT applications is that compiled by Sheldahl and Klimas [26] at Sandia National Laboratories. This data includes aerofoil characteristics of seven NACA00XX sections for angles of attack upto 180° over a wide range of Reynolds Number; the set includes data for the NACA0025 section. This data was used to generate a NACA0025 look-up table of aerodynamic force coeeficients that was suitable for use with VAWTTAY. The predictions using the Sandia NACA0025 are also shown in Figure 5.12. Again the discrepancy between theoretical predictions and experimental results is clear to see at the higher tip speed ratios.

The disappointment of being unable to validate the prediction model by correlating the theoretical results to the experimental results was somewhat alleviated when it was realised that the NACA0025 data compiled by Sheldahl and Klimas had been theoretically generated. The aerofoil characteristics for this thick section had not been verified by experiment, though some of the sections considered in [26] had been wind tunnel tested. Since no other NACA0025 data could be found to verify the Sandia data across the broad range of Reynolds Number that it covers, the author had no means of evaluating its validity. Since VAWTTAY overpredicts the power output of the model V-VAWT at high tip speed ratios when using the Sandia data, the aerodynamic characteristics of this dataset are clearly unrepresentative of the characteristics of the model V-VAWT blades themselves. If the theoretical predictions using VAWTTAY are to be matched with the experimental results presented here, the aerodynamic characteristics of the blade section must be determined, and a dataset suitable for use with VAWTTAY derived. This task was duly undertaken by the author and is reported in the following chapter.

5.11: Conclusions

The experimental results presented here have clearly demonstrated the suitability of partial-span pitch control as a means of regulating the power output the V-VAWT. The results show that full aerodynamic braking can be achieved with only small tip areas; a 5% tip area being adequate for the model V-VAWT. Whether such small tip areas will provide similar results will depend upon the sensitivity of the V-VAWT to Reynolds Number effects. The experimental results also indicate that small nose-out tip pitch offsets may increase the power output of the rotor.

The aerodynamic performance prediction model VAWTTAY has been shown to be, in principle, suitable for predicting the effects of partial span pitch control. However, a discrepancy between measured and theoretical results is observed at high tip speed ratios; this was considered unacceptable by author. A possible cause of the difference is the shortage of good aerofoil characteristic data for use with VAWTTAY. It has, therefore, been identified that additional characteristic aerofoil data is required. Only when the correlation between measured and theoretical results is better, can VAWTTAY be considered seriously for tip pitch design studies of larger V-VAWT configurations.

Chapter Six: Determination of the Aerodynamic Characteristics of a NACA0025 Aerofoil Section

6.1: Introduction

The aerodynamic prediction model VAWTTAY uses two-dimensional static aerofoil data to calculate the local aerodynamic forces acting on a blade element. The local angle of attack of the relative flow to the blade element and the local Reynolds Number are crucial in determining the magnitude of the local aerodynamic forces from a look-up table of coefficients of chordwise force C_T, and normal force C_N. While a number of dynamic effects must be accounted for in predicting the behaviour of a vertical-axis wind turbine, the use of two-dimensional aerofoil data for such predictions has been reasonably successful as Sharpe has demonstrated [18]. The prediction model VAWTTAY has been developed using two-dimensional data for the NACA0012 aerofoil section which Sharpe compiled from various sources for his initial studies of Darrieus type vertical-axis wind turbines [23]. This data is relevant for angles of attack of ±180° for a range of Reynolds Numbers from 40,000 to 2,760,000. This broad range of characteristics is suitable for the operating conditions of most vertical-axis wind turbines.

Until recently, the NACA0012 data continued to be used for all aerodynamic performance predictions of the V-VAWT using VAWTTAY, even though the wind tunnel models have all been made with thicker aerofoil sections. Consequently, it has never been possible to exactly match experimental results to predicted results derived using VAWTTAY. The continued use of the NACA0012 data, despite the discrepancy between predicted and measured results, is due to the short supply of two-dimensional aerofoil data for the other blade sections. The most commonly used aerofoil

sections for vertical axis wind turbine blades are those of the symmetric four-digit NACA series, with special interest being directed towards the NACA0015 and NACA0018 sections. These two sections combine good aerodynamic characteristics with good structural properties, which is necessary in wind turbine design.

Major studies of the symmetric four-digit NACA series aerofoil sections were restricted, until more recently, to those made at the Langley Memorial Aeronautical Laboratory in 1937 by Jacobs and Sherman [61]. The lift and drag characteristics for a number of symmetric sections was derived by experiment by these authors. The range of results is restricted to small angles of attack, with few measurements being made beyond stall, but the data does cover a wide range of Reynolds Number. In deriving his NACA0012 data for use with his early versions of VAWTTAY, Sharpe encountered a number of difficulties when using the Jacobs and Sherman data [23]. In order to derive the a consistent look-up table of coefficients of normal force and thrust force for the NACA0012 section, Sharpe had to cross-correlate more recentlt derived aerofoil data with that Jacobs and Sherman's original data.

The more recent studies of the symmetrical four-digit NACA have concentrated on the NACA0012, NACA0015 and NACA0018 sections, though Sheldahl and Klimas [26] also present performance data for the thicker NACA0021 and NACA0025 sections. Other than data presented by Bullivant [62], this is the only source known to the author of aerofoil data for the NACA0025 section. Bullivant's experimental data is restricted to small angles of incidence at high Reynolds Number, whereas the Sheldahl and Klimas data is tabulated for angles of incidence upto 30° over a wide range of Reynolds Number. It also includes a single set of data for the post stall characteristics of the section

upto angles of attack of $\alpha = 180°$. Only one such set of data is provided since it is generally accepted that the post stall behaviour of an aerofoil is independent of Reynolds Number.

The NACA0025 data presented by Sheldahl and Klimas, however, is synthesize using the Sandia National Laboratories computer code based upon the Eppler model. This computer code is used for the linear and early non-linear portions of the C_L-α curves but none of the data for the NACA0025 section has been verified by experimental measurement. The computer code has been used to generate data for the finer sections reported, but in most cases the data includes experimental results from wind tunnel tests of the aerofoil sections. Since the NACA0025 dataset covers a wide range of Reynolds Number and angles of attack upto 180° it is highly suitable for use with VAWTTAY, though the performance predictions using this data should be treated with caution until such time as the aerofoil characteristics have been verified by experimentation.

Since no experimental data could be found for the NACA0025 section for low Reynolds Numbers experienced by the model V-VAWT, nor for angles of attack upto $\alpha = 180°$, the theoretical performance predictions of the model V-VAWT using this data has not been considered particularly valid. The discrepancies between theoretical and experimental results were illustrated in the previous chapter. The considerable difference between results observed at high tip speed ratios identified the need for the aerodynamic characteristics of the NACA0025 section to be determined by experimentation. This chapter describes the implementation of such an experimental programme including the presentation of the test results and the discussion of their validity.

6.2: Construction of a NACA0025 Aerofoil Section

The primary objective of the experimental programme was to determine the static aerodynamic characteristics of a NACA0025 aerofoil for a range of operating conditions similar to those experienced by the blades of the model V-VAWT. The blades were of 80mm chord and operated over a range of tip speed ratios upto a maximum of $\lambda = 4.5$ in windspeeds of V = 14 m/s. Consequently the local angle of attack could vary to $\alpha = \pm 180°$ but the local Reynolds number would not exceed Re = 300,000.

The blades of the model V-VAWT were made from English Ash and encapsulated a high tensile strength aluminium alloy spar. This construction was essential for the dynamic operating conditions in which the blades were designed to perform. However, for the determination of the aerodynamic characteristics of a NACA0025 section, the blade need only be designed to withstand the aerodynamic forces that would act upon it in the wind tunnel. So the blade was simply constructed from mature English Ash that had been in storage for some years. The wood was closely grained and dry which meant the blade was dimensionally stable even after the NACA0025 profile had been formed.

The wind tunnel used for these tests was the Nº 2 closed-return wind tunnel in the Department of Aeronautical Engineering, Queen Mary College, London. The working section has dimensions 1016 mm by 762 mm (40 inches by 30 inches), and the maximum windspeed in this section that can be achieved is V = 40 m/s. Ideally at least two blades of different chordlengths were needed to ensure that the measurements would cover the range of Reynolds Number experienced by the model V-VAWT. However, the limited availability of wind tunnel time for these tests would only allow measurements to be made on one aerofoil

section. The choice of chordlength was crucial in determining the range of Reynolds number that could be investigated. The choice of an 80 mm chordlength allowed measurements to be made for Reynolds numbers between 80,000 and 250,000, and since this is the same chordlength as the blades of the model V-VAWT, the same profile template could be used during blade manufacture. Since all the blades have been made by hand, using the same template, the blade for these tests will be of similar quality in profile shape and surface finish to the model V-VAWT blades. The aerodynamic data derived from these tests will therefore be particularly appropriate for the prediction of the model V-VAWT performance using VAWTTAY.

Two methods of measuring the aerodynamic characteristics of an aerofoil section were considered, these being:

(a) two-dimensional, pressure measurements

(b) three-dimensional, balance measurements

The first method involves measuring the pressure distribution around the blade surface and, by integration of the pressure with respect to chord and thickness, the coefficients of normal and tangential force can be determined. This method is highly suitable for all angles of attack, including those beyond stall. However, since it is not a direct measurement of the aerodynamic forces acting on the aerofoil, profile drag has to be measured separately and all tangential forces modified as appropriate. The accuracy of the C_N and C_T results is highly dependent upon the number of pressure measurements made around the blade surface, the accuracy of each measurement, the accuracy of the pressure integration method, and the accuracy of the profile drag corrections. This method is considered to be two-dimensional since the blade extends across the working section and intersects the section walls.

The second method involves supporting the blade on a force balance from which direct measurements of lift and drag forces can be made. The measured forces are those acting on the whole blade and therefore are considered as three-dimensional measurements. Since the blade must be free from support, other than that of the balance, three-dimensional flow is experienced as air passes between the lower and upper blade surfaces around the blade tips. Corrections for this effect must be considered when determining values of C_L and C_D. These measurements can be resolved with respect to the angle of incidence to determine values of C_N and C_T, however, since direct measurements have been made of the forces acting on the blade, the value of C_T will include both pressure force and profile drag. The range of angles of attack which the balance can operate is usually restricted to approximately $\alpha = 40°$. If measurements were to be made for angles of attack upto $\alpha = 180°$, the blade would have to fixed to the balance with preset pitch to enable measurements to be made for the high angles of incidence.

The two-dimensional, pressure measurement method was considered most suitable because it is more reliable for measurements at high angles of attack where the corrections for blade tip effects on three-dimensional testing become more difficult to evaluate as flow separation and stall occur. It was, however, intended that three-dimensional, balance measurements would be made to confirm the pre-stall characteristics of the blade as determined by the two-dimensional method.

The pressure measurement method requires as large a number as possible of static pressure tappings be located on the blade surface. Since the blade was relatively small and constructed with a solid cross-section, the simplest method of incorporating surface pressure tappings into the

blade was by laying many small-bore brass tubes into spanwise slots cut into the blade surface. The tubes were retained in the slots with epoxy filler and the NACA0025 profile restored to its original dimensions and finish. Into each tube was drilled a small pressure tapping, and in all twenty such tappings were able to be made in the blade surface. The distribution of these tappings was severely restricted by the size of the brass tubes with most of the tubes being placed closely around the leading edge and mid-chord positions; it was extremely difficult to place a tapping any closer to the trailing edge than at the 80% chord position. Each tube ran from an approximate mid-span position in a spanwise direction to extend 100mm beyond the blade edge. The open tubes at the blade endings could be conveniently connected to the pressure measurement device using small-bore rubber tubes.

Once the blade had been constructed in the manner described, the aerofoil profile was checked and a wax finish applied to the blade surface. All the pressure tappings were cleaned and the the brass tubes blown clear of debris from the drilling operation. A steel dowel was inserted at one blade end at the 50% chord position. This pin was for the location and support of the blade in the working section of the wind tunnel.

6.3: The Wind Tunnel and Pressure Measurement Equipment

The wind tunnel tests to determine the characteristics of the NACA0025 blade were all performed in a closed-return wind tunnel at Queen Mary College, London. The maximum windspeed in the working section is approximately 40 m/s. The turbulence factor was not determined but is considered to be low since the wind tunnel is specifically designed for aerofoil testing and research.

The NACA0025 blade was placed in the working section with its spanwise axis vertical. The blade passed through a supportive collar which was located to a rotating floor panel. The dowel pin in the end of the blade was used to position the blade on the rotation axis of the turntable. The blade was firmly secured to the collar with epoxy filler so that the blade end was flush with the ceiling panel, thereby ensuring that tip effects were negligble and that only two-dimensional flow occurred. The twenty brass tubes all protuded from the support collar and were all connected to a water manometer bank with small-bore rubber tubing. The turntable was rotated by a worm gear that was driven by a hand crank. The angle of rotation was measured by a trip counter which was incremented for every tenth of a degree of rotation. To check the accuracy of the counter the turntable was rotated through one complete revolution until two bench-marks were aligned once more. It was noted that the counter accurately recorded this rotation as being 360.0°.

At first, the measurement of static pressure was to be carried out automatically using a system controlled by a BBC-B microcomputer. This equipment included a pressure selecting device to which all twenty static pressure tappings were connected using the rubber tubes. The selector switch allowed a single pressure measurement to be made with an electronic pressure transducer. The analogue output from this transducer was transmitted to the microcomputer via an A/D converter. The pressure measurement was recorded by the computer from fifty samples of the output from the pressure transducer. Once the measurement was complete, the pressure selector switch was turned by a stepper motor to the next pressure outlet and the measurement cycle repeated. The complete action was controlled by the microcomputer so that measurement

and recording of static pressure around the blade section could be performed automatically.

This system initially appeared to be highly suitable for the programme of tests that were planned, however, during preliminary tests, the equipment proved unreliable. The stepper motor drive system had no positional feedback from the pressure selector, consequently the computer control system was not able to detect whether the desired rotation of the selector had been completed when the power to the motor was switched off. The control system relied upon the time that power was being supplied to the motor as its means of controlling the angle of rotation of the pressure selector. Whilst this was adequate for only a small number of movements, the culmulative error following a few complete revolutions was such that the static pressure measurement could not be relied upon. Occasionally the pressure selector could not be moved by the motor so that the synchronisation of the actual static pressure being measured and the static pressure which the computer considered to be measuring would break down and the recorded dataset would be in error. After such an occurrence, the equipment would have to be reset and the measurement sequence repeated. A trouble-free data capture sequence took approximately five minutes to complete and required no human intervention, however, if an error occurred a significantly longer time was required to complete the measurement sequence with satisfaction.

After using this method of data capture for a short period with various degrees of sucess, the pressure selector switch and sundry equipment was discarded in favour of more traditional measurement devices. All the static pressure tubes were connected to a water manometr bank. The manometer columns were each over one metre in length and covered by a glass panel that had a graduated scale

etched on its surface. The graduation scale was marked in tenths of an inch over its complete length. The angle of the manometer bank to the horizon could be altered and the angle was measured using a graduated scale close to the pivot axis. The angle of the manometr bank could be measured to ±0.5° and, with experience, the height of a water column could be measured by eye to an accuracy of ±0.02 inches. By suitable adjustment of the angle of inclination of the manometer bank, the height of the water columns could be maximised to ensure the accuracy of the pressure measurements was as high as possible.

The measurements of water column height were recorded using the BBC-B microcomputer with the computer program "NACATST" which was written and developed specially for this experimental programme by the author. The program is described more fully later, but measurement data was entered via the keyboard, stored in memory and when validated, recorded on floppy disk in a datafile uniquely named for the operating conditions being observed. This method required the observer to make some twenty-two measurements for each operating condition tested and for the appropriate measurements to typed into the computer, therefore, it could be considered that human errors were highly likely to occur during the "manual" transfer of pressure measurements to the computer. However, the program was devised to give a visual check of all recorded data before the it was stored permanently on floppy disk, consequently, significant human errors could be observed immediately and corrected before proceeding to the next test condition. The program NACATST included many other features to reduce the likelihood of human error during data capture, and its success is reflected in the quality of the measurements made throughout the experimental programme.

It was found that the manual method required approximately five minutes for a complete dataset to be measured, recorded and stored to disk. This time was similar to that of the automatic method, but it was repeatable and rarely varied during the course of the experimental programme. The reliabilty with which this data capture cycle time could be maintained enabled the allocated time in the wind tunnel to be used to good advantage. However, a useful feature that the manual system afforded, was that the water columns in the manometer bank presented a visual representation of the pressure distribution around the aerofoil. Consequently the author was able to gain a valuable insight into the behaviour of the aerofoil as operating conditions changed merely by observation of the manometer bank alone. The onset of stall could be indentified, allowing the stall angle to be recorded before analysis of the measurements had been completed.

6.4: The Measurement of Wind Speed in the Working Section

The wind tunnel air speed was controlled by the fan speed which could only operate at ten finite speed settings. The fan motor was operated from a control console sited near to the working section and among the controls were ten speed selection switches which were nominated 0-9. Since it was not possible to control the wind speed in the tunnel by any other means, the ten speed settings effectively dictated the range of windspeeds at which measurements could be made.

The working section windspeed was measured by recording the static pressure difference over the upstream contraction section. The static pressure difference was measured using the water manometer and verified with measurements taken from a Betz manometer. This ensured that even the

smallest pressure difference could be measured with a high degree of confidence. The ratio of cross-sectional areas at inlet and outlet of the contraction section was 5.2:1. By application of the Bernoulli and continuity equations, the static pressure difference can be used to determine the working section windspeed. However, such a method relies upon ideal fluid flow conditions and does not anticipate energy losses due to the construction of the wind tunnel itself. If accurate analysis of the measured data was to be achieved, it was essential that the true velocity of the air entering the working section be known. This required that the calculated value of windspeed be verified by measurement of the true windspeed in the working section. A set calibration factors were determined that ensured the calculation of windspeed from the pressure difference across the contraction yielded accurate values.

The calibration of the tunnel was simple and quick, but required the test blade to be removed and the wind tunnel empty. Using a pitot-static tube, the total head was measured at a number positions across the width of the working section for a given fan speed setting. The static pressures at each traverse position and at the inlet and outlet of the contraction section were also measured. All the measurements were recorded using the BBC-B microcomputer and stored on floppy disk in datafiles named "VTi", where i was the fan speed index number. Twenty-eight total head measurements were made at equally spaced positions across the tunnel at the working section mid-height. These measurements were repeated for all fan speed settings and appropriate calibration factors determined for each tunnel speed. The angle of inclination of the manometer bank was not changed for these measurements, so that the water column levels were directly proportional to the pressure heads for each measurement.

The theoretical relationships between the working section windspeed and pressure difference across the contraction section can be determined by application of the Bernoulli and Continuity equations using the following nomeclature:

H = Total head, m H_2O

p = Static pressure, N/m^2

V = Windspeed, m/s

A = Cross-sectional area of the tunnel, m^2

z = Piezometric height, m

and the following suffices:

A Outlet of contraction/inlet of working section

B Inlet of contraction

3 Pitot-static tube position

∞ Working section

Figure 6.1 is a schematic view of the wind tunnel contraction and working section, and shows the pitot-static tube and static pressure measurement positions.

If the flow in the wind tunnel is in a state of static equilibrium, then Bernoulli's equation gives:

$$p_A + \tfrac{1}{2}\rho V_A^2 + \rho g z_A = p_B + \tfrac{1}{2}\rho V_B^2 + \rho g z_B \qquad (6.1)$$

and Continuity gives

$$\rho A_A V_A = \rho A_B V_B = \rho A_3 V_\infty \qquad (6.2)$$

Since the piezometric height can be considered to be invarient at all positions in the contraction and working section, then equation (6.1) can be rearranged to give

$$p_B - p_A = \tfrac{1}{2}\rho (V_A^2 - V_B^2) \qquad (6.3)$$

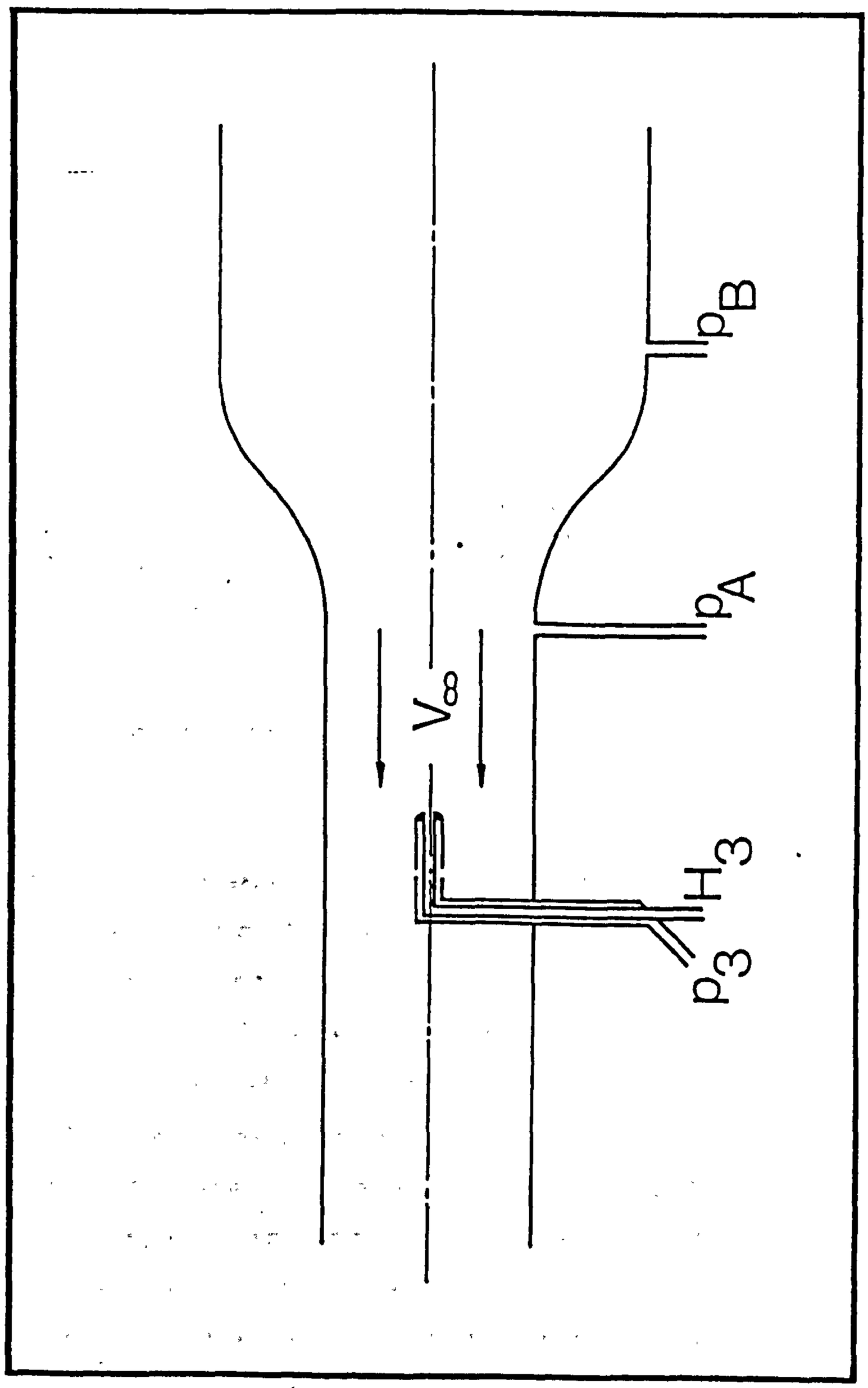

Figure 6.1: Schematic diagram of working section of the wind tunnel, showing pitot-static tube and static pressure measurement positions

and equation (6.2) can be rearranged such that

$$V_B = \left(\frac{A_A}{A_B}\right) V_A \qquad (6.4)$$

and substituting for V_B in (6.3) gives

$$p_B - p_A = \tfrac{1}{2}\rho V_A^2 \left(1 - \left(\frac{A_A}{A_B}\right)^2\right) \qquad (6.5)$$

However, the cross-sectional area of the outlet of the contraction is the same as the working section, so $A_A = A_B$, implying $V_A = V_\infty$. Substituting for V_A in (6.5) and rearranging gives,

$$\tfrac{1}{2}\rho V_\infty^2 = \frac{(p_B - p_A)}{\left(1 - \left(\frac{A_A}{A_B}\right)^2\right)} \qquad (6.6)$$

The ratio of areas at inlet to outlet of the contraction section was known to be 5.2:1. This ratio is used with measurements of static pressure across the contraction to calculate V_∞. However, small friction losses cause the static pressure at the contraction outlet to be smaller than would be measured for an ideal fluid. Therefore the pressure difference across the contraction would be slightly larger, and the use of equation (6.6) would yield high values of windspeed in the working section. The efficiency of the contraction must be determined to ensure accurate evaluations of V_∞ can made using the two static pressure measurements. It is common practice to evaluate the oefficient of discharge C_d of the contraction. This coefficient can be used to modify equation (6.6) such that:

$$\tfrac{1}{2}\rho V_\infty^2 = \frac{(p_B - p_A)}{\left(1 - \left(\frac{A_A}{A_B}\right)^2\right)} C_d^2 \qquad C_d < 1.0 \qquad (6.7)$$

To determine C_d for each fan speed setting, average measurements of total head and static pressure in the working section were made using a pitot-static tube traverse. The static pressures p_A and p_B were also measured. The quantity $\frac{1}{2}\rho V_\infty^2$ is known as the "dynamic head" and can be determined from the pitot-static tube measurements, such that:

$$\frac{1}{2}\rho V_\infty^2 = H_3 - p_3 \qquad (6.8)$$

Rearranging equations (6.7) and (6.8) gives:

$$C_d = \sqrt{\frac{(H_3 - p_3)}{(p_B - p_A)}\left(1 - \left(\frac{A_3}{A_B}\right)^2\right)} \qquad (6.9)$$

Table 6.1 shows the values of C_d that were calculated from the pitot-static tube traverse measurements.

Fan speed index number	Coefficient of Discharge C_d
0	0.995
1	0.966
2	0.942
3	0.934
4	0.921
5	0.920
6	0.918
7	0.918
8	0.929
9	0.938

Table 5.1: Coefficient of discharge C_d at each fan speed setting

Equation (6.7) is used to calculate the freestream windspeed in the working section. When the aerofoil is positioned in the working section the presence of the tunnel walls interferes with the flow around the aerofoil, creating a small increase in the actual windspeed in the working section. Tunnel interference is considered at length by Pankhurst and Holder [63], and of the effects discussed, those due to solid blockage, wake blockage and lift effect are the most significant here. Pankhurst and Holder make the observation that at low windspeed, blockage effects are usually small and it is lift effect that is usually the most significant. In all cases, corrections for these tunnel interference effects can be applied to the force coefficients after they have been calculated using the uncorrected freestream speed, V_∞. Consequently, the results will be initially presented without any interference corrections applied. The estimation of interference effects will be discussed in detail later, and only then will corrections be applied to the measured results.

6.5: The Measurement of Blade Surface Pressure at Various Angles of Attack and Reynolds Number

The major part of the test programme was the measurement of static pressure variation on the surface of the test blade when inclined at various angles of attackand windspeeds. The test procedure adopted for this experimental work was straightforward and requires little explanation, however, the analysis of the measurements to determine the various components of aerodynamic force acting upon the blade is complex and time consuming. Since the wind tunnel was only available for a short period of time, the analysis of the measurements was not undertaken until the test programme had been completed. Only a handful of

measured datasets were analysed during the test period. To ensure that the measurements would yield meaningful and reliable results, it was imperitive to ensure that all measurements were verified by some means at the time of testing before the recorded data was stored on floppy disk and the test conditions altered. If, during analysis, the measured data was found to be in error or yielding unusual results, there would be no opportunity to verify or repeat the static pressure measurements around the blade.

The test programme required that the pressure distribution around the NACA0025 test blade be measured for angles of attack upto 180° over a range of Reynolds Number between 40,000 and 400,000, however it was only possible to make measurements for Reynolds Numbers between 80,000 and 250,000 with the single test blade used. At all but the lower fan speed settings the pressure distribution around the aerofoil was measured for angles of attack upto and including 20° at 1° intervals. The post-stall behaviour of an aerofoil section is generally regarded as being independent of Reynolds Number, so it was not necessary to make measurements much beyond the stall angle for each fan speed setting. Measurements of the aerofoil behaviour for angles of attack greater than 20° were made at only one fan speed setting, with the angle of attack being changed in 5° increments to a maximum of 180°. At this angle of attack, the trailing edge of the aerofoil is directly incident with the wind. The angle of attack was nominally based upon the geometric postion of the chordwise axis of the blade to the longitudinal axis of the working section. As will be discussed later the actual angle of attack was determined from the calculations of C_N and the geometric angle of attack modified as appropriate.

As discussed above all pressure measurements were manually transferred to a BBC-B microcomputer using the program

NACATST. This program was used to record, display for verification and store the pressure measurements and provided the experimentor with the appropriate prompts at each stage of the test procedure which was as follows:

(a) Activate computer program NACATST
(b) Set test blade at zero angle of attack
(c) Start wind tunnel fan motor
(d) Select required fan speed and allow time for working conditions to settle
(e) Input initial data as requested
(f) Measure and record static pressures
(g) Verify static pressure measurements
(h) Store static pressure measurements
(i) Change angle of attack or fan speed
(j) Repeat measurement sequence.

For each series of measurements where either the angle of attack or the fan speed had been changed, the following initial data was recorded:

(a) Test date
(b) Ambient air temperature, °C
(c) Ambient air pressure, mm Hg
(d) Angle of inclination of the manometer bank, °
(e) Nominal angle of attack of the test blade, °
(f) Data filename
(g) Betz manometer measurement, mm H_2O

The ambient air temperature and pressure were measured using a mercury thermometer and mercury barometer sited in the laboratory. These measurements were used to calculate the ambient air density to enable the operational Reynolds Number Re to be calculated:

$$Re = \frac{\rho V_\infty c}{\mu} \qquad (6.10)$$

where c is the blade chord, μ the static viscosity of air and V_∞ the frestream windspeed of the working section, calculated using equation (6.7).

The angle of inclination of the manometer bank and the nominal angle of attack are recorded for reference only; the true angle of attack was determined following the analysis of the measurements and the calculation of C_N.

The data filename was a unique seven character string that identified the test measurements with respect to both the fan speed setting and the nominal angle of attack. A typical data filename was "RE4+007" indicating the measurements were taken with fan speed set at index 4 and the nominal angle of attack being +7°. If measurements were repeated for similar operating conditions, the "RE" prefix to the data filename would be changed. In this manner each dataset could be stored with a unique filename that indicated the operating conditions of the test.

The Betz manometer measurement was recorded for completeness to ensure that the freestream windspeed was correctly measured. As will be demonstrated later, the calculation of windspeed is not specifically required for the calculation of the aerodynamic force coefficients, C_N and C_T, the manomter bank measurements of p_A and p_B were used for this calculation. Windspeed values were only required for the calculation of Reynolds Number.

Once the initial data had been recorded, the program NACATST would prompt for the static pressure measurements to be recorded. A total of twenty-two measurements were recorded; twenty static pressure measurements from the

surface of the test blade and the static pressures at the inlet and outlet of the contraction section. Since the microcomputer did not have a numeric keypad, these measurements were measured and recorded in units of 1/100ths of an inch, though it was only possible to measure the water column heights with an accuracy of ±2/100ths of an inch. In this way the recorded pressure measurement did not include a decimal point and therefore the keystrokes were restricted to the top row of the microcomputer keyboard. This proved to be a simple but effective means of decreasing the likelihood of keyboard error.

Immediately all twenty-two pressure measurements had been recorded, the computer displayed all the recorded data in the form of a bar chart. This display was used to mimic the visual appearance of the water columns in the manometer bank so that a visual comparison could be made to check the validity of the recorded data. If any of the recorded pressure measurements was seen to be in error then that single pressure value could be corrected without changing the others. The bar chart would be redisplayed and further ammendments to the data could be made until all measurements were correctly recorded to the satisfaction of the observer. Once the data had been successfully validated, the initial input data and all the pressure measurements in their raw form would be stored on floppy disk. The program would proceed to display the distribution of pressure coefficient, c_p, with respect to the chordwise position of the pressure tappings. If at this stage the recorded dataset was found to be in error, then the test procedure and recording of pressure measurements would have to be repeated from the start.

Once the test procedure was completed, the datafile would be 'LOCKED'; a software device for ensuring that a file

cannot accidently be erased from a floppy disk. The angle of attack of the test blade would be increased by 1° (5° for deep-stall measurements) and the data capture sequence repeated. It should be noted that all tests were carried out with the angle of attack *increasing* to ensure that the maximum aerodynamic forces were observed before the onset of stall. If the test procedure started with the blade at a high angle of attack and in a stalled condition, then if the angle of attack was gradually *decreased*, the maximum aerodynamic forces would not be observed since the air flow would not fully reattach until the angle of attack was well below the static stall angle. This phenomenon was observed during the test programme when the angle of attack of the blade was being reset to zero, however, no record of the angle of reattachment was made because it is dependent upon the rate of change of angle of attack, which can be observed from tests of oscillating aerofoils. For similar reasons, when the tests for a particular windspeed were complete, the angle of attack of the blade was reset to zero before the fan speed was changed.

A feature of the computer program NACATST was that on repeating the test procedure, the values of the initial variables became the default values for the subsequent test. Consequently it was usual to only modify the angle of attack and the Betz manometer measurement from the data of the previous test. This feature was included in the program to decrease the likelihood of input error.

The cycle time for completing a series of measurements was approximately five minutes. This ensured that a comprehensive range of operating conditions could be studied in short time that the wind tunnel was available. The analysis of the pressure measurements is discussed in length later, but as noted, all analysis was formally undertaken after the completion of all experiments.

6.6: The Measurement of Wind Speed in the Wake of the Blade using a Pitot-Static Traverse

The analysis of the static pressure measurements yield values of C_N and C_T which can be used to calculate the more familar aerodynamic coefficients of lift force, C_L, and drag force, C_D:

$$C_L = C_N\cos(\alpha) + C_T\sin(\alpha) \qquad (6.11a)$$

$$C_D = C_N\sin(\alpha) - C_T\cos(\alpha) \qquad (6.11b)$$

The drag of a body moving through a fluid is dependent upon the shape and position of that body. The total drag force is due to both pressure forces and friction forces acting on the body. The calculation of C_D for the test blade using the values of C_N and C_T derived from the pressure measurements will not include any friction drag component. At high angles of attack, where the aerofoil is fully stalled, the pressure drag force will be significantly greater than the friction drag force, so that the calculation of C_D using equation (6.11b) will be suitably accurate using the measured values of C_N and C_T alone. At low angles of attack this is not the case and a method of measuring both pressure and friction drag forces is required. The momentum traverse method is favoured for two-dimensional tests and is discussed at length below. This technique requires that the velocity in the wake downstream of the aerofoil be measured so that the rate of loss of momentum of the fluid can be determined. This loss is equal in magnitude to the total drag force acting on the aerofoil so that C_D may be determined directly using this method.

The momentum traverse method was used here to determine values of C_D for the various operating conditons to which the test aerofoil was exposed. The pitot-static tube was

used to measure total head and local static pressures at regular intervals across the wake of the aerofoil. The pitot-static tube should, ideally, be placed as close to the trailing edge of the aerofoil as possible. Unfortunately the pitot-static tube could be placed no nearer than nine chord lengths downstream of the aerofoil. In this position the velocity profile across the wake is not as pronounced as if observations were made close to the aerofoil because the wake dissipates into the downstream flow.

The BBC-B microcomputer was again used to record the measurements made during the momentum traverse using the program "MOMTRAV" which is similar to NACATST except that twenty-eight measurements of the total head across the wake were made and recorded for each traverse. The momentum method also requires that the static pressure be recorded in the wake for all measurement positions in practice, however, the variation of static pressure across the wake was found to be less than the resolution of the manometer bank grating so that only one measurement of local static pressure was made. The static pressures at inlet and outlet to the contraction were measured and recorded for determining the upstream flow conditions.

The pitot-static tube was mounted on traverse equipment which allowed the distance between measurement positions to be measured with a vernier scale. The program MOMTRAV prompted the input of the total head measurements by displaying the position that the pitot-static tube should be placed with respect to the measuring scale.

In the short time available to complete the experimental programme, it was only possible to perform wake velocity measurements for low angles of attack for all but the highest fan speed setting. Measurements across the wake

were made for angles of attack of 0°, 2°, 4°, 6°, 8° and 10° with the recorded data being stored in datafiles named with the prefix "MT". The analysis of the wake traverse measurements is detailed later, but involves taking the difference between measurements of similar pressures. Consequently the values of C_D determined using this method were subject to relatively large errors and required much manipulation before reliable values were obtained. This is discussed later.

6.7: The Calculation of the Coefficient of Normal Force

The primary objective of the experimental programme described here was to determine the variation of the aerodynamic force coefficients C_N and C_T with respect to angle of attack and Reynolds Number. The method used to determine C_T from the measurements of static pressure over the aerofoil surface is similar in principal to that used to determine C_N, however, it is more convenient to discuss the calculation of C_N first.

Since all pressure measurements were recorded on floppy disk, the procedure adopted to determine C_N was devised so that all calculations were performed using the BBC-B microcomputer. As will be demonstrated, the determination of C_N requires many calculations including the integration of surface pressure with respect to the chord of the aero-foil. The integration of pressure with respect to the chord cannot be successfully completed based upon twenty surface pressure measurements alone, consequently these measurements must be used to determine the static pressure at many more surface positions using interpolation techniques. Only then can the integration process be completed with confidence. These tasks are highly suited to the microcomputer provided the numerical methods used

for the interpolation and integration processes are sound and well founded.

All local static pressure measurements p can be described in terms of the far upstream static pressure p_∞, and the dynamic head $\frac{1}{2}\rho V_\infty^2$, to give the pressure coefficient C_p:

$$C_p = \frac{(p - p_\infty)}{\frac{1}{2}\rho V_\infty^2} \qquad (6.12)$$

The pressure coefficient is a non-dimensional quantity, and for comparative purposes the local chordwise position of the pressure tapping x, is described in terms of the aerofoil chord c.

Figure 6.2 shows the typical distribution of C_p with respect to x/c for an aerofoil at a low angle of attack. Note that the scale of the vertical axis is inverted so that negative (i.e. suction) pressure coefficients are plotted above the horizontal axis. The flow in this example is still fully attached with a high suction pressure apparent close to the leading edge on the upper aerofoil surface. At all chordwise positions the pressure on the upper surface is seen to be less than that on the lower surface except at the trailing edge where the pressure on both surfaces is the same. The value of C_N can be directly determined from calculating the area between the curves describing the pressure distribution on each surface. This is demonstrated below.

The coefficient of normal force acting on an aerofoil is given by:

$$C_N = \frac{N}{\frac{1}{2}\rho V_\infty^2 S} \qquad (6.13)$$

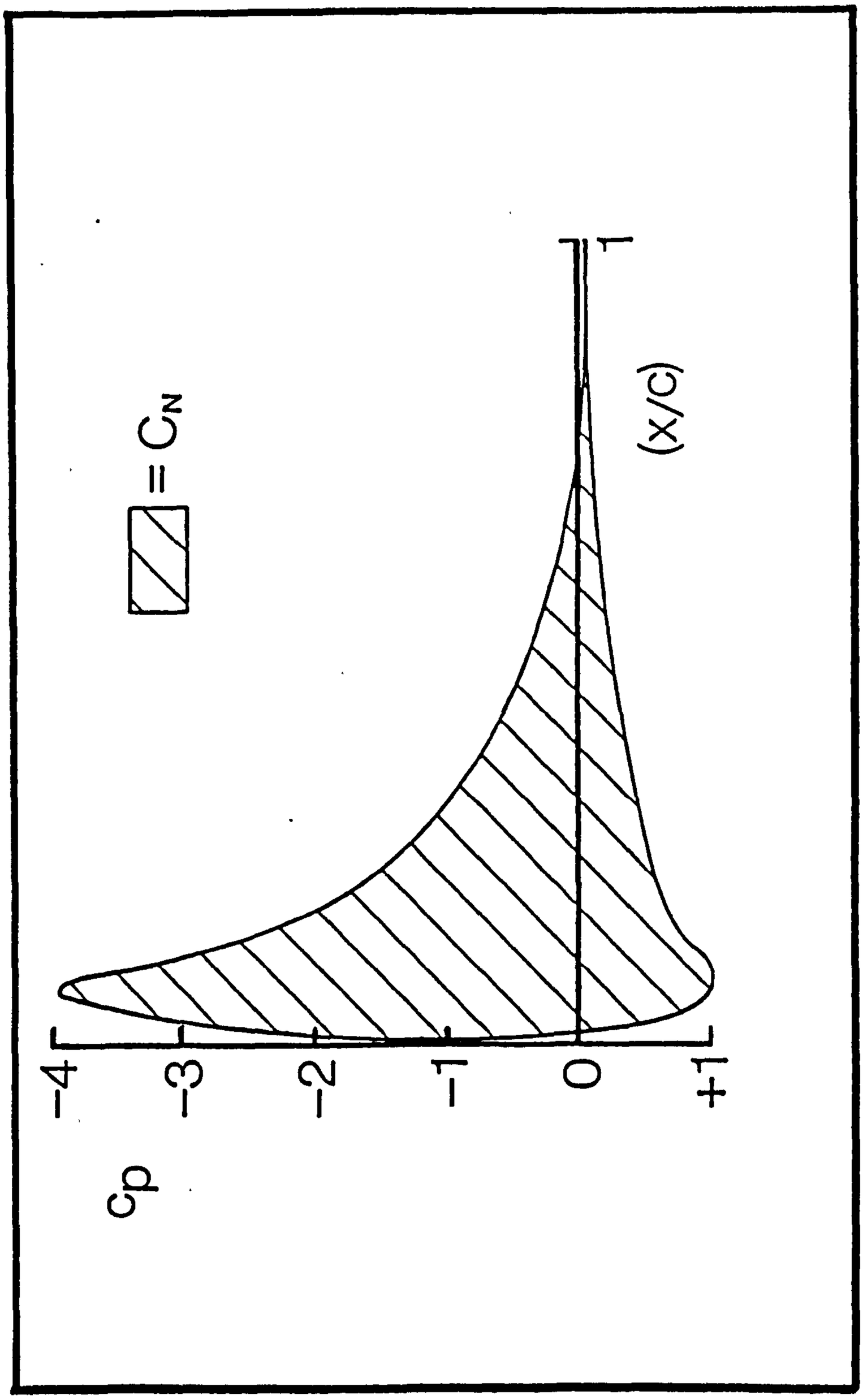

Figure 6.2: Chordwise distribution of pressure coefficient for aerofoil at a small angle of attack

where N is the total aerodynamic force acting normal to the aerofoil chord which is of area S, and V_∞ is the freestream windspeed. Figure 6.3 shows the shape parameters used to describe a blade section. If it is assumed that all flow is two-dimensional, that is there is no spanwise variation of the static pressure across the blade surface, then the blade section can be considered as being similar to the test aerofoil used for all experimental measurements.

Consider the chordwise element of area $b.\delta x$ on the upper surface of the blade. If the local static pressure acting on this element is p and the static pressure in the freestream is p_∞, then the elemental pressure force δN, acting normal to the chordwise axis is given by:

$$\delta N = -\Delta p b \delta x \qquad (6.14)$$

where

$$\Delta p = p - p_\infty. \qquad (6.15)$$

The force N_U, acting on the upper surface of the aerofoil in the normal direction, is given by:

$$N_U = \left[\int_{x=0}^{c} -\Delta p b dx\right]_{UPPER} \qquad (6.16)$$

whereas the force N_L, acting on the lower surface of the aerofoil in the normal direction, is given by:

$$N_L = \left[\int_{x=0}^{c} \Delta p b dx\right]_{LOWER} \qquad (6.17)$$

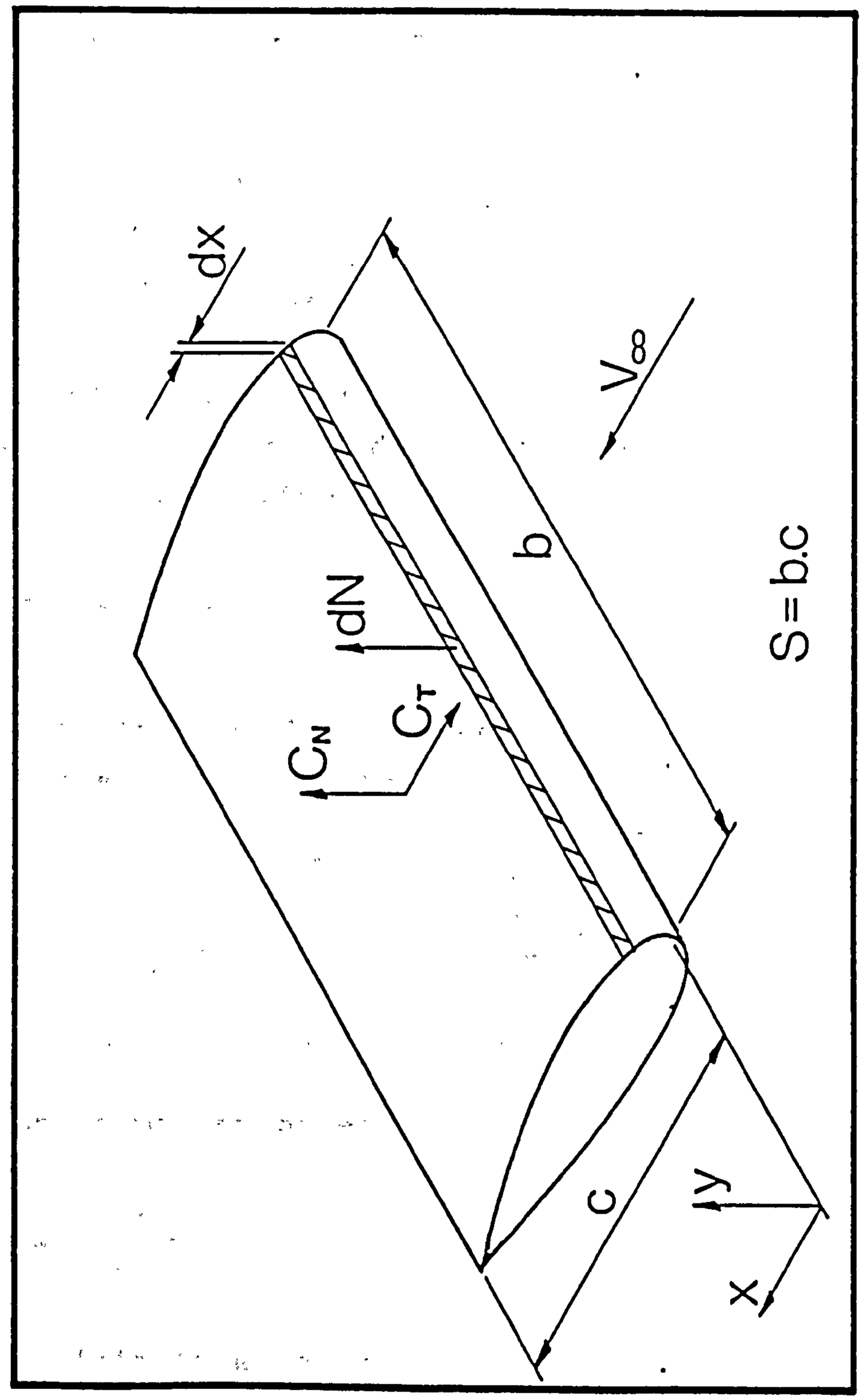

Figure 6.3: Shape parameters of aerofoil

The total force N, acting on the whole blade in the normal direction, is given by the sum of the forces N_{L} and N_{U}, which can be expanded using equations (6.16) and (6.17) to give:

$$N = \left[\int_{x=0}^{c} \Delta p b dx\right]_{LOWER} - \left[\int_{x=0}^{c} \Delta p b dx\right]_{UPPER} \quad (6.18)$$

The blade area S is equal to the product of the chord length c, and the blade width b, so substituting for S in equation (6.13) gives:

$$C_N = \frac{N}{\frac{1}{2}\rho V_\infty^2 bc} \quad (6.19)$$

Substituting for N using equation (6.18), and considering the blade width b to be unity, gives:

$$C_N = \left[\int_{0}^{1} \frac{\Delta p}{\frac{1}{2}\rho V_\infty^2} d(x/c)\right]_{LOWER} - \left[\int_{0}^{1} \frac{\Delta p}{\frac{1}{2}\rho V_\infty^2} d(x/c)\right]_{UPPER} \quad (6.20)$$

The Δp terms can be eliminated by condidering:

$$C_P = \frac{\Delta p}{\frac{1}{2}\rho V_\infty^2} \quad (6.21)$$

which simiplifies equation (6.20) to give:

$$C_N = \left[\int_{0}^{1} C_P \, d(x/c)\right]_{LOWER} - \left[\int_{0}^{1} C_P \, d(x/c)\right]_{UPPER} \quad (6.22)$$

In this way the coefficient of normal force can be calculated by integration of the pressure coefficient with

respect to chordwise position. Its value is equal to the shaded area of Figure 6.2.

The computer program "CALCCN2", written and developed by the author, uses this integration technique to calculate C_N from the measurements of static pressure. For integration calculations to be performed using a computer, a suitable numerical technique needs to be adopted that will ensure accurate calculation of C_N from only twenty surface pressure measurements. Popular numerical integration methods involve the use of either Simpson's Rule or the Trapezoidal Rule. In each case the integration calculation involves a finite number of data points which are equally distributed along the axis of integration. With the NACA0025 test aerofoil, the chordwise distance between pressure tappings is not constant so that neither Simpson's Rule nor the Trapezoidal Rule could use the raw pressure measurements alone.

In order that an accurate integration calculation could be performed, it was necessary to describe the pressure distribution (the pressure envelope) around the aerofoil in greater detail than twenty measurements could do alone. If the static pressure measurements were plotted on graph paper some form of manual curve fittng would be used to fully describe the pressure envelope. Such a technique would not be repeatable, especially with the large number of pressure plots that would be required for analysis of all the data. If the computer was to be used for analysis then some means of automatically generating the pressure envelope from the twenty measurements was required. The Least-Squares method of curve fitting was considered for generating the pressure envelope, however, the polynomial form of the fitted curve has to be assumed beforehand, and

the calculated pressure envelope would not necessarily pass through actual measured data points.

The method adopted to calculate the pressure distribution around the aerofoil was an interpolation technique known as Neville's Method [64]; interpolation being considered more appropriate. This particular technique is more sophisticated than simple linear interpolation, since the Neville's Method uses a higher order polynomial to calculate the value of the function at a particular position from a finite number of known function values. The order of the interpolating polynomial is dependent upon the number of data points used for the calculation. Interpolation techniques do not create best-fit curves, since the interpolating polynomial will pass through each of the measured values used for the calculation, nor do they require the raw data to be equally distributed along the axis of the independent variable. These features were considered worthy, because the pressure envelope would be generated using actual measured pressures, and unusual characteristics of the envelope would not be lost as would occur if a best-fit curve was used. Using this particular interpolation method the static pressure around the aerofoil can be calculated for many surface positions all equally distributed along the chordwise axis. The integration of the pressure envelope with respect to the chord can now be successfully completed using one of the numerical methods mentioned above. The program CALCCN2 embodies these principles to calculate C_N.

Once initiated, the program CALCCN2 requests the name of the datafile which is to be analysed. The data that is stored on floppy diskette is retrieved and stored in the computer memory. This data includes all the initialisation data and the twenty-two static pressure measurements. The program identifies the wind tunnel fan speed,

and utilises the appropriate value of the coefficient of discharge C_d. This is used to calculate the dynamic head of the working section using equation (6.7) during the test. The twenty surface pressure measurements are converted into non-dimensional values of C_p. Since C_p is a ratio of pressure differences, the water column height measurements do not need to be converted directly into units of pressure before being used to calculate C_p. Also note that the freestream pressure p_∞ in equation (6.12), is taken to be the static pressure at inlet to the working section p_A. The twenty static pressure tappings are distributed around the aerofoil surface as shown schematically in Figure 6.4. The (x, y) co-ordinates of each pressure tapping were carefully measured, allowing the measured distribution of C_p with respect to (x/c) to be plotted. The chord of the aerofoil c = 80.6 mm, and the maximum thickness t = 19.8 mm. The static pressure was not measured at the trailing edge of the aerofoil.

When all the static pressure measurements had been converted into non-dimensional values, the pressure envelope around the aerofoil surface was calculated. The variation of pressure coefficient with respect to chordwise position, Figure 6.2, is not a single valued function, because pressure coefficient is also dependent upon which of the surfaces the measurements are being made. So that the pressure distribution around the aerofoil surface can be calculated using Neville's Method, the pressure measurements had to be organised so that a single valued relationship between C_p and (x/c) could be calculated.

This was achieved by assigning the lower surface chordwise positions a negative value of (x/c). Thus the chordwise positions of the pressure tappings would all lie within the range $-1 \leq (x/c) \leq 1$ under such a mapping. It should be noted that if a pressure tapping had been made at the

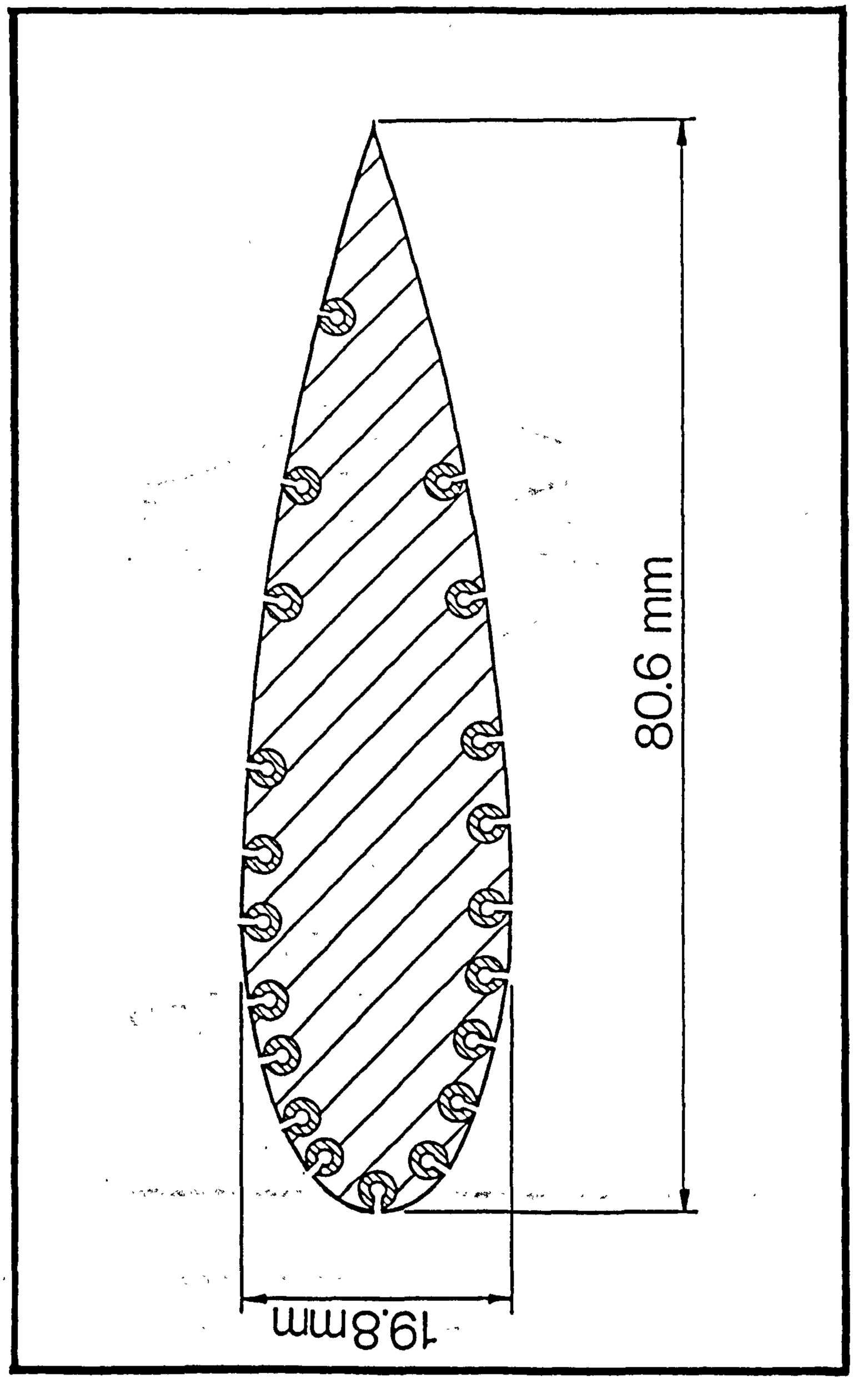

Figure 6.4: Positions of static pressure tappings around surface of NACA0025 aerofoil

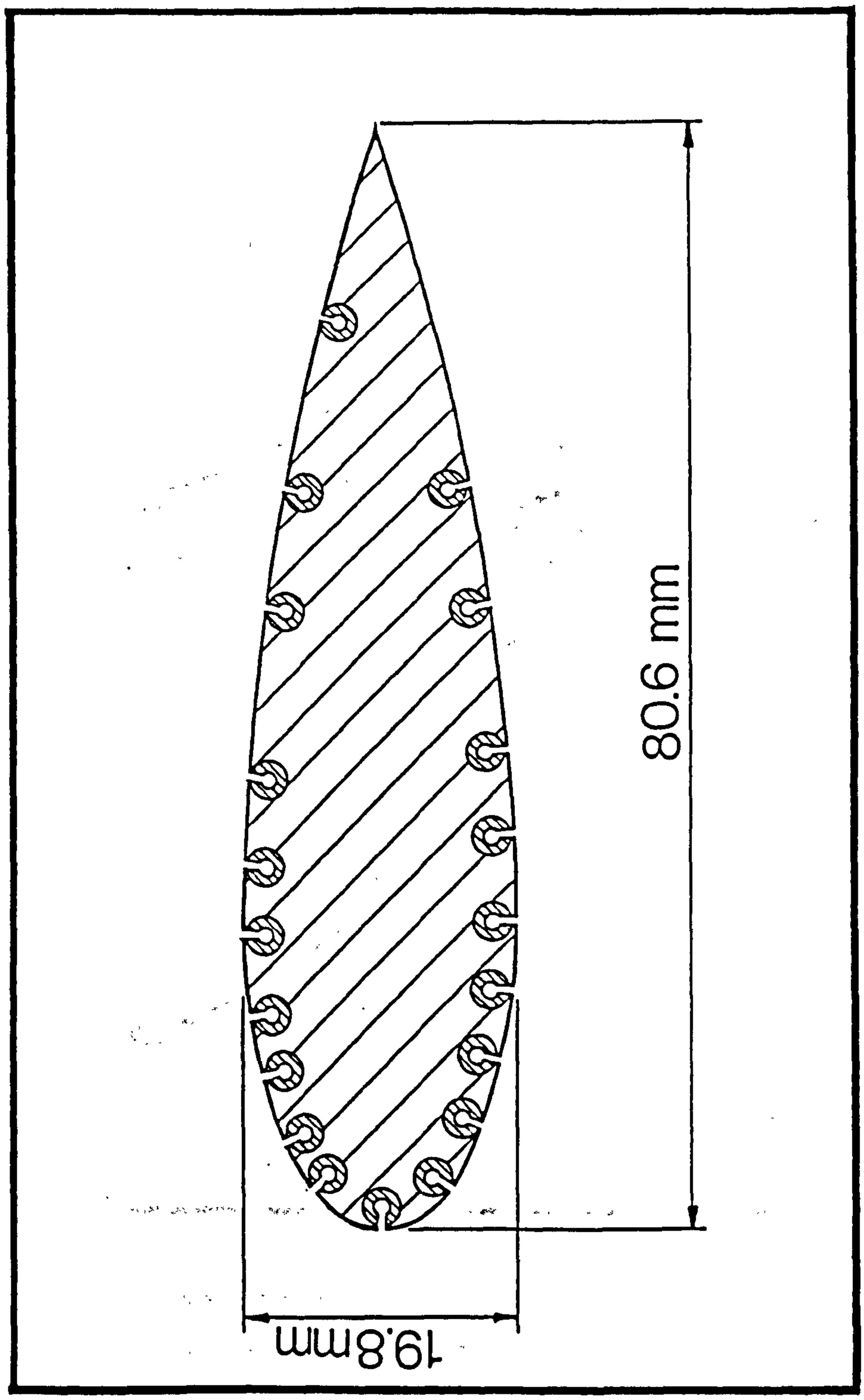

Figure 6.4: Positions of static pressure tappings around surface of NACA0025 aerofoil

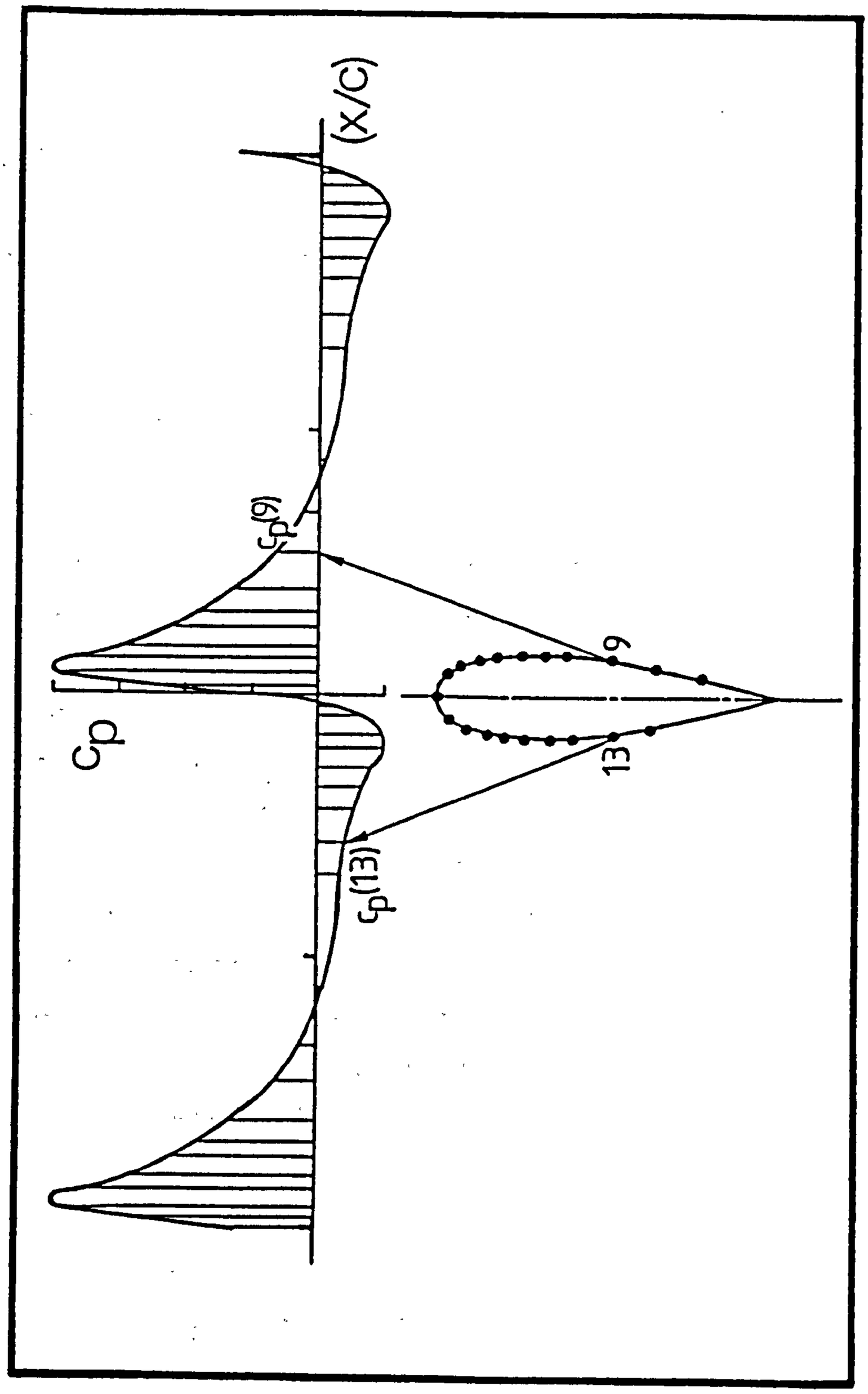

Figure 6.5: Mapping of pressure coefficient to an extended range of chordwise positions

trailing edge of the aerofoil, it would be mapped to both extremes of the (x/c) range, i.e. (x/c) = ±1.

If the mapping is extended outside the range of (x/c) = ±1, it can soon be shown that the leading edge pressure coefficient would be mapped to (x/c) = ±2n, and the trailing edge pressure coefficient to (x/c) = ±(2n+1), where n = 0, 1, 2,... This is shown in Figure 6.5.

The value of (x/c) can now be considered as the total distance travelled along the chordwise axis in travelling around the aerofoil surface. So, before any calculation is undertaken, the program CALCCN2 maps the twenty surface pressure measurements to forty pressure values as a function of (x/c) in the range $-2 \leq (x/c) < +2$. This was done to allow the interpolation calculation to be easily performed, and with accuracy at its range limits. However, the integration of C_p with respect to (x/c) is only carried out over the interval $-1 \leq (x/c) < +1$, this being equivalent to the integration of pressure over the complete surface area of the aerofoil.

With the pressure measurements mapped into an ordered manner, the variation of pressure with repsect to chordwise position could be calculated using interpolation. Neville's Method is best explained if the general case shown in Figure 6.6 is considered. Here the value of the function f(x) is to be estimated from four data points (x_0, f_0), (x_1, f_1), (x_2, f_2) and (x_3, f_3). The Neville's Method involves successive levels of interpolation to calculate the value of f(x) using a high order polynomial, each interpolation being an estimate of f(x) itself. The order of the polynomial that describes the function is dependent upon the number of data points used. Using only four points to estimate f(x), the first level interpolation gives the linear interpolating polynomials:

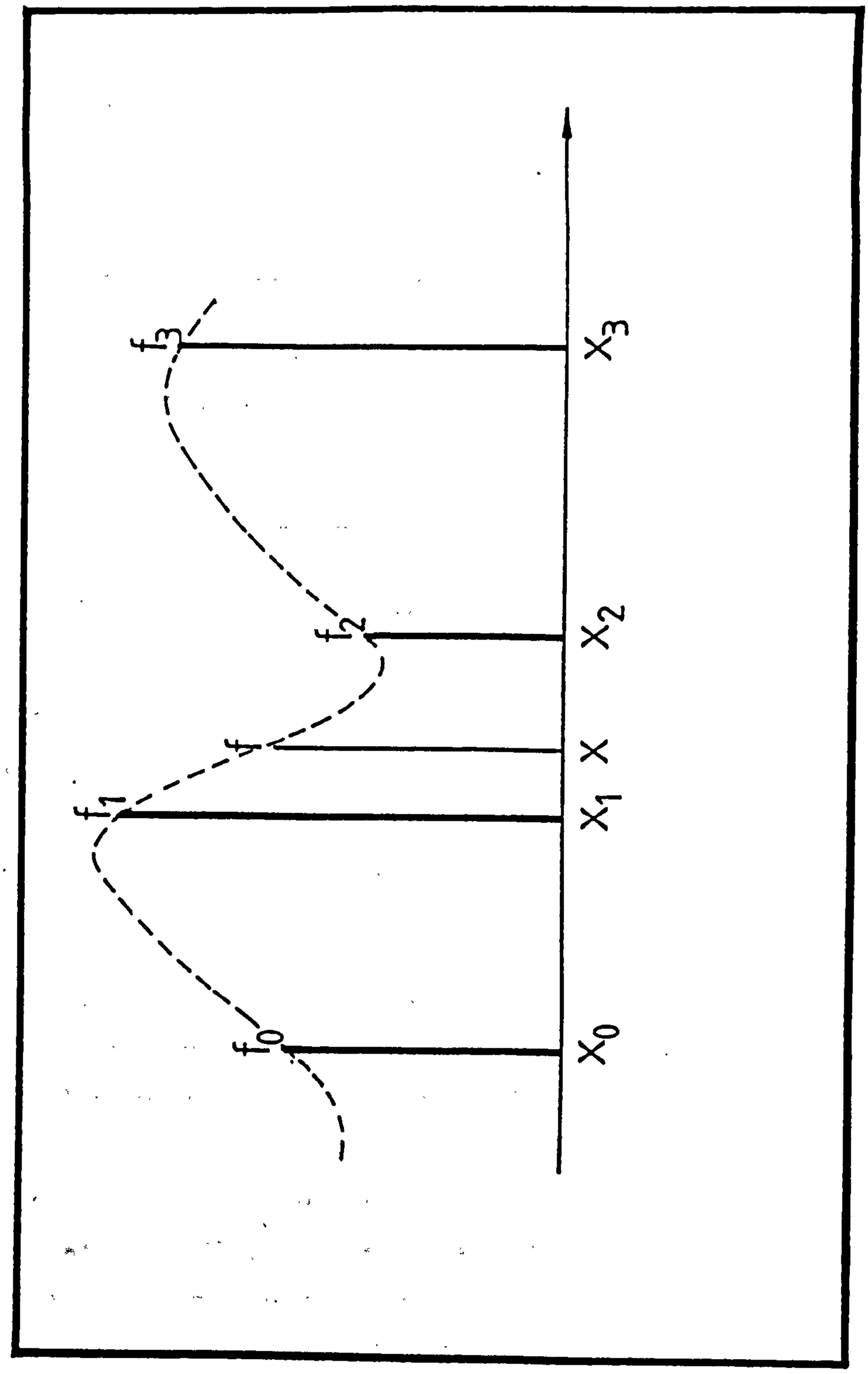

Figure 6.6: Interpolation using Neville's Method

$$p_{01} = \frac{(x-x_0)f_1 - (x-x_1)f_0}{x_1 - x_0} \qquad (6.23a)$$

$$p_{12} = \frac{(x-x_1)f_2 - (x-x_2)f_1}{x_2 - x_1} \qquad (6.23b)$$

$$p_{23} = \frac{(x-x_2)f_3 - (x-x_3)f_2}{x_3 - x_2} \qquad (6.23c)$$

The second level interpolation gives the quadratic interpolating polynomials:

$$p_{02} = \frac{(x-x_0)p_{12} - (x-x_2)p_{01}}{x_2 - x_0} \qquad (6.24a)$$

$$p_{13} = \frac{(x-x_1)p_{23} - (x-x_3)p_{12}}{x_3 - x_1} \qquad (6.24b)$$

and the third level gives the cubic interpolating polynomial:

$$p_{03} = \frac{(x-x_0)p_{13} - (x-x_3)p_{02}}{x_3 - x_0} \qquad (6.25)$$

The value of p_{03} is the best estimate of f(x) from the four known function values. Neville's Method is stable while the value of x lies within the bounds of x_0 and x_4. If the interpolation is extended beyond this range, then the estimated values of f(x) become unstable and highly inaccurate. Thus when CALCCN2 uses this technique to calculate C_p as a continuous function of (x/c), then the four measurements used for the estimation are selected such that (x/c) lies between the chordwise positions of the second and third measurements.

To calculate the pressure around the aerofoil and the coefficient of normal force, initially the value of (x/c) is set to that of the trailing edge, i.e. (x/c) = -1. The Neville's Method is used with four measured values to estimate the pressure coefficient at this position. The value of (x/c) is then incremented by a constant step

width, h = 0.005, and the new value of C_{p_m} is calculated. The C_{p_m} versus (x/c) characteristic is thus determined at a total of 400 chordwise positions using this method, these values all being used to calculate C_N. Since the chordwise stepwidth h is constant, either of the numerical integration techniques already mentioned can be used to calculate C_N. However, as with all numerical methods, both integration techniques incur a truncation error in calculating a finite integral. The magnitude of the truncation error for Simpsons Rule is proportional to h^5 whereas for the Trapezoidal Rule it is proportional to h^3, but the Trapezoidal Rule technique was adopted since it was the easier method to incorporate into the computer program. By calculating C_{p_m} at a large number of chordwise positions, thereby keeping h small, the truncation error is minimised, and a high degree of accuracy is maintained for the calculation of C_N.

The Trapezoidal Rule states:

$$\int_a^b f(x)dx = h[\tfrac{1}{2}f_0 + f_1 + f_2 + \ldots + f_{n-1} + \tfrac{1}{2}f_n] \qquad (6.26)$$

where the stepwidth h is given by:

$$h = \frac{b-a}{n} \qquad (6.27)$$

If the variation of pressure coefficient with respect to (x/c) is considered as a continuous function f(x/c), then equation (5.31) can be considered to be:

$$C_N = \int_{-1}^{0} f(x/c)\, d(x/c) \quad - \quad \int_{0}^{1} f(x/c)\, d(x/c) \qquad (6.28)$$

where f(x/c) is calculated using the Neville's Method as described above.

Equation (6.28) is further simplified by defining, within the integration interval, the step function φ such that:

$$\varphi = \begin{cases} 1 & -1 \leq (x/c) < 0 \\ -1 & 0 \leq (x/c) < 1 \end{cases} \qquad (6.29)$$

so that equation (6.28) becomes:

$$C_N = \int_{-1}^{1} \varphi f(x/c)\, d(x/c) \qquad (6.30)$$

In applying the Trapezoidal Rule to equation (6.30), it should be noted that the values of f_0 and f_n are, in both cases, the calculated values of preessure coefficient at the trailing edge, and are equal. If each of the calculated values of pressure coefficient, f_i, is calculated in turn and one of the end values ignored then:

$$C_N = h \sum_{i=1}^{400} \varphi f_i \qquad (6.31)$$

where:

$$h = \frac{1 - (-1)}{400} = 0.005 \qquad (6.32)$$

For simplicity, CALCCN2 summates the calculated values of pressure coefficient immediately it has been calculated, obviating the need to store all 400 values. When the summation is complete, the total is multiplied by the

stepwidth h to determine the final value of C_N. The value of C_N is displayed on the computer monitor but is not stored or recorded in any manner by the program CALCCN2.

The program CALCCN2 also takes advantage of the graphics facility of the microcomputer to display a plot of the pressure envelope as it is calculated using the Neville's Method algorithm. The plotting facility was a significant aid in developing the program CALCCN2, since it provided an immediate insight into the accuracy of the interpolation method. Initially more than four measured pressure values were being used to calculate the pressure at any chordwise position. However, the interpolating polynomial would greatly overshoot between ordinates were large pressure differences would occur, notably around the leading edge of the aerofoil. This effect was attenuated by using a cubic interpolating polynomial calculated from only four data points. The pressure envelope derived by this method is considered to be good. Moreover, the visualisation of pressure distribution has been invaluable in the subsequent intepretation of the measurements. The pressure plots were recorded by photographing the screen.

6.8: The Calculation of the Coefficient of Thrust Force

The calculation of the coefficient of thrust force, C_T, is essentially identical to the calculation of C_N except that the integration of static pressure is made with respect to the flapwise ordinates of the surface y. For simplicity all terms are converted to their appropriate non-dimensional units C_p and (y/c). Figure 6.7 shows the typical distribution of C_p with respect to (y/c) for an aerofoil at a low angle of attack. Again note that the scale of the vertical axis has been inverted so that negative pressure coefficients are plotted above the horizontal axis. The flow in this example is still fully attached

with a high suction pressure apparent close to the leading edge on the upper aerofoil surface. The C_{p_∞} against (y/c) curve is characterised by two loops, the enclosed areas of these loops being proportional to chordwise, thrust force acting on the aerofoil. However, the areas of these loops have opposite signs so that the thrust force is proportional to the difference between the areas of the two loops.

The coefficient of thrust force acting on the aerofoil is given by:

$$C_T = \frac{T}{\frac{1}{2}\rho V_\infty^2 S} \qquad (6.33)$$

where T is the net aerodynamic force acting on the aerofoil in the chordwise direction. For the NACA0025 aerofoil section it can be shown that:

$$C_T = \left[\int_{-0.125}^{0.125} C_p \, d(y/c)\right]_{\text{REARWARD}} - \left[\int_{-0.125}^{0.125} C_p \, d(y/c)\right]_{\text{FORWARD}} \qquad (6.34)$$

This expression is similar to equation (6.22), except that the limits of the finite integral are the surface ordinates of the position of maximum thickness, and the terms "Forward" and "Rearward" refer to the aerofoil surfaces either side of this position.

The computer program "CALCCT2", written and developed by the author, uses the same techniques as CALCCN2 to calculate C_T from the static pressure measurements. The Neville's Method is used to calculate a singled valued interpolating function of C_{p_∞} against (y/c). Here (y/c) can be considered as the total distance travelled in the y direction when travelling around the aerofoil surface such

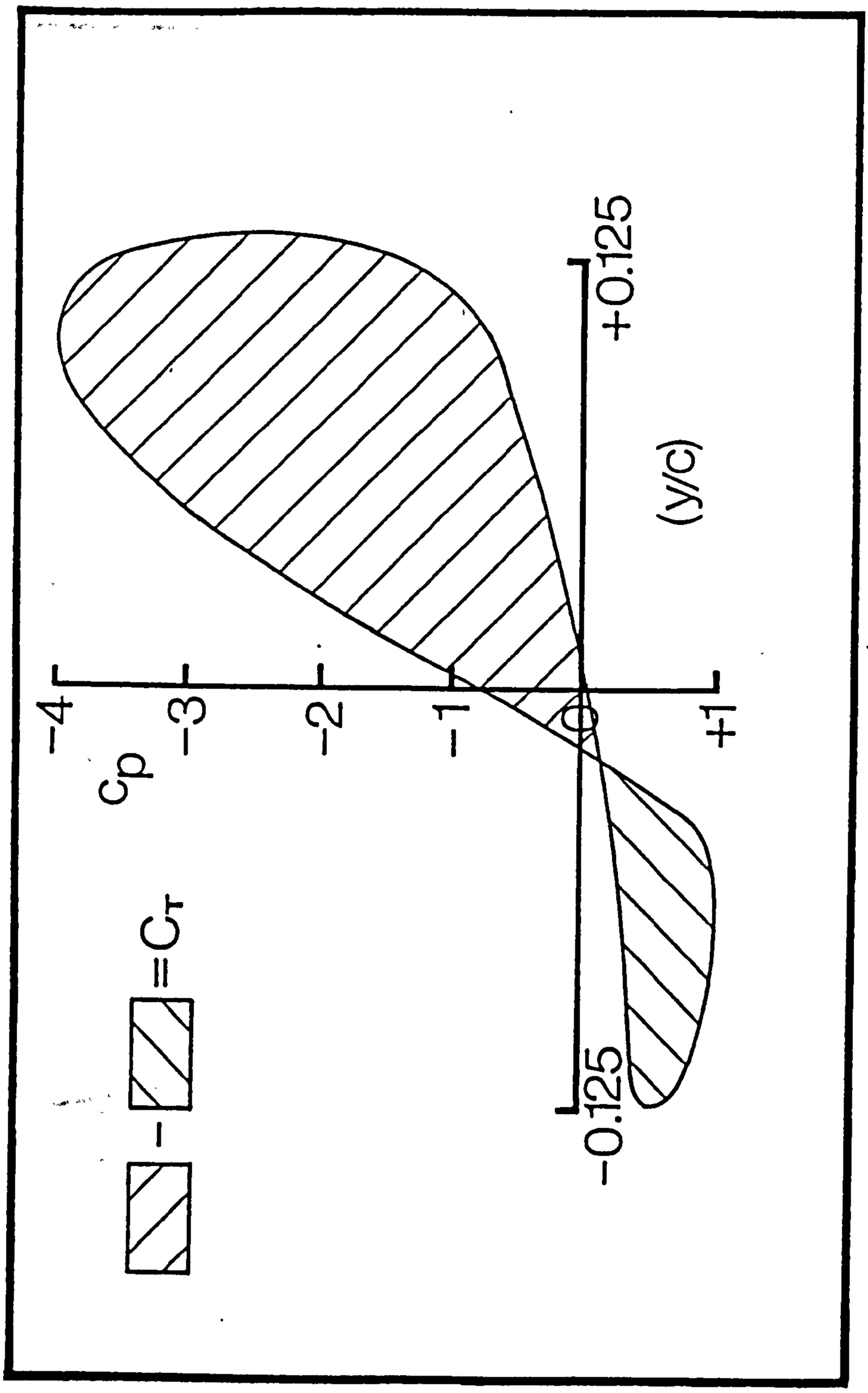

Figure 6.7: Plot of C_{p_w} vs (y/c) for aerofoil at a low angle of attack

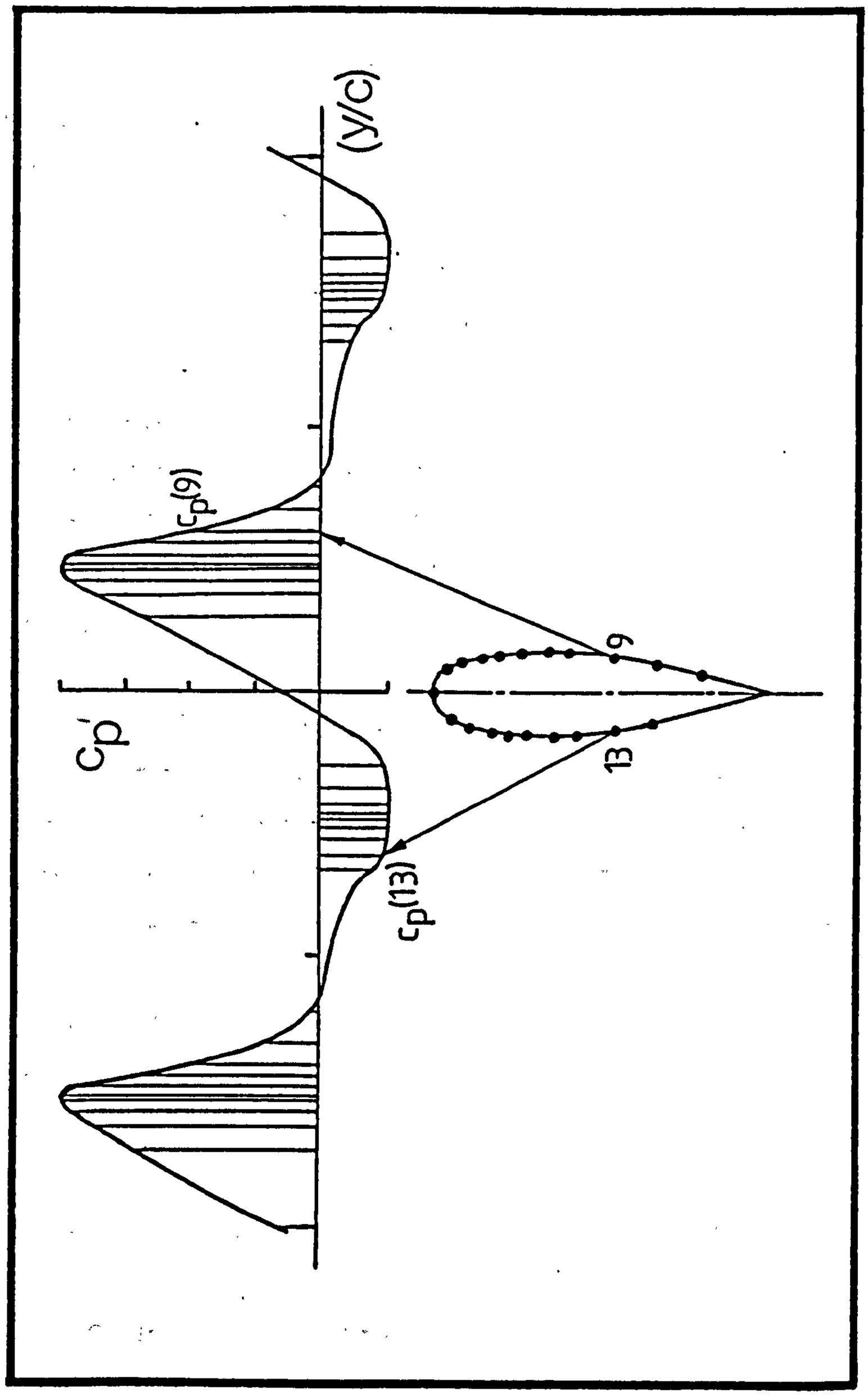

Figure 6.8: Mapping of $C_{P'}$ vs (y/c) to a single valued function

that the trailing edge ordinate becomes (y/c) = ±0.25. If the mapping is extended outside the range of (y/c) = ±0.25 then the leading edge pressure coefficient would be mapped to (y/c) = ±0.5n and the trailing edge pressure coefficient would be mapped to (y/c) = ±0.25(2n+1), where n = 0, 1, 2, ... This is illustrated in Figure 6.8.

A cubic interpolating polynomial was used to calculate the pressure distribution around the aerofoil surface at 400 surface positions. The value of (y/c) is incremented by a constant stepwidth, h=0.00125, and the new value of C_p calculated.

The Trapezoidal Rule was adopted as the most suitable integration technique and if the variation of pressure coefficient with respect to (y/c) is considered as a continuous, cyclically varying, single-valued function f(y/c), then eqn. (6.34) can be considered to be:

$$C_T = \int_{0.125}^{0.375} f(y/c)\, d(y/c) - \int_{-0.125}^{0.125} f(y/c)\, d(y/c) \qquad (6.35)$$

where f(y/c) is calculated using Neville's Method.

Equation (6.35) is further simplified by defining, within the integration interval, the step function φ given by:

$$\varphi = \begin{cases} 1 & 0.125 < (y/c) < 0.375 \\ -1 & -0.125 < (y/c) < 0.125 \end{cases} \qquad (6.36)$$

such that:

$$C_T = \int_{-0.125}^{0.375} \varphi f(y/c)\, d(y/c) \qquad (6.37)$$

When applying the Trapezoidal Rule to equation (6.37), note that the values of f(y/c) at the extremes of the integration interval are the same, so that f_{∞} and f_{n} of eqn. (6.26) are equal. If each of the calculated values of pressure coefficient f_i is calculated in turn, and one of the end values ignored, then:

$$C_T = h \sum_{i=1}^{400} \varphi f_i \qquad (6.38)$$

where:

$$h = \frac{0.375 - (-0.125)}{400} = 0.00125 \qquad (6.39)$$

For simplicity, CALCCT2 summates the calculated values of pressure coefficient immediately it has been calculated, obviating the need to store all 400 values. When the summation is complete, the total is multiplied by the stepwidth, h, to determine the final value of C_T. This value is displayed on the computer monitor, but is not recorded in anyway by this program.

As with CALCCN2, the graphics facility of the microcomputer is used to display a plot of the calculated pressure envelope as it is calculated.

6.9: The Calculation of the Coefficient of Drag Force

The wake traverse measurements described earlier are used to determine the true coefficient of drag force of the aerofoil at low angles of attack. Profile drag includes both friction force and pressure force components and therefore cannot be calculated from the measured values of C_N and C_T alone. The wake traverse method, initially developed by Jones, has been summarised by Petty [65]. With this technique the measurements of static pressure and total head across the wake of the aerofoil are used to determine the rate of loss of momentum of the fluid as it passes over the aerofoil, so allowing C_D to be determined. The analysis presented by Petty assumes that the measuring equipment is placed close to the trailing edge of aerofoil. Here the static pressure across the wake is considered to vary from the undisturbed freestream static pressure, p_∞. If:

H_w = Total head in the wake, m H_2O

p_1 = Static pressure in the wake, N/m^2

H_∞ = Total head in flow outside the wake, m H_2O

and defining:

$$g = 1 - \frac{(H_\infty - H_w)}{(H_\infty - p_\infty)} \qquad (6.40)$$

then for two-dimensional tests Petty shows that C_D can be calculated as follows:

$$C_D = \frac{1}{c} \int_{-d}^{+d} 2[1 - g^{0.5}] \left(g + \frac{(p_\infty - p_1)}{\frac{1}{2}\rho V_\infty^2} \right)^{0.5} dy \qquad (6.41a)$$

where the wake thickness is:

$$-d \leq y \leq +d \qquad (6.41b)$$

The computer program "CALCCD2", written and developed by the author, embodies the above calculation of C_D and uses the twenty-eight total head measurements across the wake to determine its value. It was noted that the wake traverse was not carried out close to the trailing edge of the aerofoil as assummed in the theory. The consequence was that the static pressure, p_1, was not observed to vary across the wake. For this particular condition equation (6.41) could be simplified, but since the program CALCCD2 can be considered for more general wind tunnel experimentation, the analysis detailed above was still used.

The measurements recorded using the computer program MOMTRAV are retrieved from the datafiles, and for each of the twenty-eight total head measurements the value of g is calculated using equation (6.40). This involves calculating the difference between similar values of total head H_w and H_∞, therefore, the error in g will be relatively large. For simplicity, numerical integration using the Trapezoidal Rule was used to calculate the value of C_D using equation (6.41). However, the accuracy of this coefficient will not be as good as the calculated values of C_T or C_N.

6.10: Wind Tunnel Interference Effects

The ultimate purpose of these tests was to produce a dataset of C_T and C_N values for variations of angle of attack and Reynolds Number which might be used with VAWTTAY to predict the behaviour of the model V-VAWT. In order that the test results might be used with confidence, it was

essential that the operating conditions experienced by the model aerofoil in the wind tunnel were dynamically similar to those that an aerofoil of similar shape would experience in the free-air. If the wind tunnel model is operating at the same Reynolds Number as its free-air counterpart, then the non-dimensional experimental results can be directlty applied to the free-air aerofoil. However, even though the wind tunnel tests are carried out at a Reynolds Number equal to the free-air conditions, the air flow around the model aerofoil will be disturbed by the limited cross-section of the tunnel itself. If these interference effects are not considered then it is not possible to ensure dynamic similarity has been maintained.

The evaluation of wind tunnel interference is approached by considering a number of independent interference effects. The overall interference effect imposed by the tunnel on the aerofoil is evaluated by the summation of the net effects of each of these interference types. Pankhurst and Holder [63] have considered wind tunnel interference at length, and of the effects discussed, the following are considered appropriate here:

(a) Solid blockage
(b) Wake blockage
(c) Lift effect

The corrections for interference are applied to the aerodynamic force coefficients calculated using uncorrected windspeed values. Consequently, the initial analysis of the measured data took no account of interference effects. The programs CALCCT2, CALCCN2 and CALCCT2 calculated uncorrected values of C_T, C_N and C_D respectively. The intereference corrections are calculated in terms of these uncorrected force coefficients and are applied directly to obtain the corrected coefficients.

6.10.1: Solid Blockage

Solid blockage is an inteference effect caused by the presence of the aerofoil itself in the closed working section of the wind tunnel. The continuity of mass flow throughout the tunnel causes the axial velocity in the locality of the aerofoil to be greater in magnitude than that measured at the entry to the working section. Solid blockage does not alter the transverse component of tunnel velocity and therefore only a change in axial velocity need be considered. This change requires corrections to be made to the measured tunnel speed, Reynolds Number, the dynamic head and all aerodynamic force coefficients.

To calculate the effect of solid blockage, Pankhurst and Holder considered a solid blockage correction ε_{sb}, which is used to calculate the true freestream velocity V_{F_∞}, in terms of the measured upstream velocity V_T, such that:

$$V_F = V_T(1 + \varepsilon_s). \tag{6.42}$$

The solid blockage correction is dependent upon the geometry of the wind tunnel, its height h, and the shape of the test aerofoil defined in terms of its cross-sectional area A, its chord c, and its maximum thickness t. The expression for ε_{sb} for two-dimensional flow in a wind tunnel with a rectangular working section is given as:

$$\varepsilon_s = \frac{2\tau A}{\pi h^2}(x_0 + x_1(t/c)) \tag{6.43}$$

where the values of x_0 and x_1 are generally considered for the two-dimensional case to be $x_0 = 1.0$, and $x_1 = 1.2$. For a closed tunnel, τ is given by:

$$\tau = \frac{\pi^2}{12} = 0.822 \qquad (6.44)$$

When the aerofoil is inclined to the flow, the solid blockage correction has to be increased by the amount $K_1\alpha^2$, where α is the angle of attack (in radians) and K_1 is a function of the thickness-chord ratio of the aerofoil. The value of K_1 was derived from Pankhurst and Holder's Fig. 240 and, for the NACA0025 aerofoil, determined to be $K_1 = 6.9$.

While the application of this angle of attack correction was not explicitly demonstrated, the calculation of solid blockage correction using equation (6.43) has been modified such that:

$$\varepsilon_s = \frac{2\tau A}{\pi h^2}(x_o + x_1(t/c))(1 + K_1\alpha^2) \qquad (6.45)$$

Vsing the measured dimensions of both the wind tunnel and aerofoil section with the values of the constants given above, equation (6.45) maybe used to determine a value of ε_s in terms of α alone:

$$\varepsilon_s = 0.00073(1 + 6.9\alpha^2) \qquad (6.46)$$

The solid blockage correction at low angles of attack is considered neglible and even at large angles of attack the difference between V_F and V_T is less than 1%.

6.10.2: Wake Blockage

The axial velocity of the fluid in the wake, downstream of the aerofoil trailing edge, is smaller than that of the fluid outside the wake; a phenomenon used to determine the

profile drag of the aerofoil as described in Section 6.9. In a closed wind tunnel, the continuity of mass flow must be satisfied, therefore the axial velocity of the fluid outside the wake must exceed that measured upstream of the aerofoil. In free-air these velocities would be equal. This interference effect is known as Wake Blockage.

As with solid blockage, the freestream velocity can be calculated in terms of the measured fluid velocity and a wake blockage correction, ε_w, such that:

$$V_F = V_T(1 + \varepsilon_w). \tag{6.47}$$

The wake blockage correction is dependent upon tunnel height, the aerofoil chord and the measured drag coefficient, C_{DT}, calculated using the uncorrected tunnel speed V_T, such that:

$$\varepsilon_w = \frac{1}{4}(c/h)C_{DT} \tag{6.48}$$

Using the known values of c and h, the wake blockage correction can be defined in terms of C_{DT} alone:

$$\varepsilon_w = 0.0197C_{DT} \tag{6.49}$$

At low angles of attack where C_{DT} is small, the wake blockage correction will be of similar magnitude to the solid blockage correction and could be ignored. At higher angles of attack, when the aerofoil is stalled, the rapid increase of C_{DT} with increasing angle of attack will ensure that wake blockage corrections cannot be ignored.

6.10.3: Lift Effect

In two-dimensional flow, the constraint imposed by the walls of the working section around the aerofoil induces a transverse velocity component to the fluid flow. This interference phenomenon introduces curvature to the flow around the aerofoil which effectively increases its camber and decreases the angle of attack of the flow to the aerofoil. This type of interference is termed "lift effect" and is considered here because [63]:

> "...lift effect is usually the most important correction at low speeds..."

Corrections for lift effect must in general be applied to both angle of attack and aerofoil camber. Such corrections have been throughly considered by Pankhurst and Holder, who subsequently developed a method of applying the camber correction directly to the measured lift force. It is these corrections that will be considered here.

In a closed wind tunnel the lift effect increases both the angle of attack of the flow and the aerofoil camber. The incremental changes are defined in terms of the uncorrected lift force C_{L_T}, and pitching moment C_{M_T} coefficients. However, the change in camber can be directly considered as a change in the lift coefficient. This change is given by:

$$C_{L_F} = C_{L_T}\left(1 - \frac{\pi^2}{48}(c/h)^2\right) \tag{6.50}$$

The change in angle of attack is given by:

$$\alpha_F - \alpha_T = \frac{\pi}{96}(c/h)^2(C_{L_T} + 2C_{M_T}) \tag{6.51}$$

Using the known values of c and h, lift effect corrections can be defined in terms of C_{L_T} and C_{M_T} alone:

$$C_{L_F} = 0.9987\ C_{L_T} \tag{6.52a}$$

$$\alpha_F - \alpha_T = 0.0002(C_{L_T} + 2C_{M_T}) \tag{6.52b}$$

As equation (6.52) clearly shows, the corrections for lift effect are not significant, and can be ignored for all angles of attack.

6.10.4: The Application of Wind Tunnel Interference Corrections

The discussion of tunnel interference corrections has shown that only solid blockage and wake blockage are worthy of further consideration, and then only at high angles of attack. The corrections that have been determined for these two interference effects can be used to calculate the freestream velocity V_F, in terms of the measured wind tunnel velocity V_T. The overall interference correction ε, can be calculated as the sum of the net corrections due to both blockage effects such that:

$$V_F = V_T(1 + \varepsilon) \tag{6.53}$$

where:

$$\varepsilon = \varepsilon_S + \varepsilon_W \tag{6.54}$$

Since a measured value of force coefficient C_{F_T} is calculated using the uncorrected wind tunnel velocity, its corrected value C_{F_T} can be determined by:

$$C_{F_F} = C_{F_T}\left(\frac{V_T}{V_F}\right)^2 = C_{F_T}\frac{1}{(1 + \varepsilon)^2} \tag{6.55}$$

which is simplied by ignoring ε^2 terms to give:

$$C_{FF} \propto C_{FT}(1 - 2\varepsilon) \tag{6.56}$$

In this way, all force coefficients can be corrected after they have been calculated using the uncorrected tunnel velocity. The computer programs CALCCN2, CALCCT2 and CALCCD2 did not include any interference correction algorithms, so that all the force coefficients derived from the experimental measurements are uncorrected.

6.11: The Presentation and Discussion of Measured Results

In this section the results of the experimental measurements are presented and discussed. The results will be presented in a number of ways, but in general they will show the variation of the force cofficients with respect to angle of attack at each Reynolds Number for which measurements were made. Since in all but the momentum traverse experiment the variation of static pressure around the aerofoil was observed, the force coefficients C_N and C_T as calculated using the programs CALCCN2 and CALCCT2 will form the major proportion of the results presented and considered here. The static pressure distribution around the aerofoil calculated by these programs is plotted on the computer monitor. These pressure plots are of great value when discussing the validity of the results and enable the behaviour of the aerofoil to be considered at all angles of attack and Reynolds Number for which observations were made.

When considering the results in detail, however, the author was always conscious of the need to produce a dataset of aerodynamic force coefficients suitable for use with the aerodynamic performance prediction program

VAWTTAY. Consequently, the overall behaviour of the NACA0025 aerofoil was constantly being compared to that of other four-digit NACA series aerofoils, especially those of smaller fineness ratios whose behaviour is well documented. It was considered that the characteristic behaviour of the test aerofoil should not be significantly different from those of the other aerofoils in this NACA aerofoil family. In developing the final force coefficient dataset for use with VAWTTAY, this has meant that many of the actual measured values of C_N and C_T have not been explicitly used, but they are recorded here for completeness.

In all, over 250 static pressure tests were conducted involving the observation and recording of some 5,500 static pressure measurements. Inevitably human error has meant that some of these measurements have been recorded incorrectly, despite the error checking routines incorporated into the data capture programs. In the short time the wind tunnel was available, it was not possible to validate measurements where they are considered to be in error, though the occurrences of bogus measurements were minimised by the checks in the data capture programs. During the tests, the stall angle at each Reynolds Number was observed and recorded. It is these observations alone that determined the range of angle of attack for which pressure tests were conducted at each fan speed. For presentation and discussion purposes, it is convenient to consider the pre-stall and early stall results for angles of attack less than 20° separately from those for the higher angles of attack where the aerofoil is generally in deep stall.

The momentum traverse observations are considered in isolation, since the C_D values determined using the computer program CALCCD2 are only of relevance when considering

tunnel interference effects and for the compilation of the final table of aerodynamic force coefficients.

Finally, the interference corrections are not applied until all uncorrected force coefficients have been satisfactorily determined. The corrected values will be used to form the NACA0025 dataset for use with VAWTTAY and to calculate the more familiar force coefficients C_L and C_D.

6.11.1: Results of Static Pressure Tests at Low Angles of Attack

The range of static pressure tests undertaken at each fan speed setting is shown in Table 6.2. This table also shows the static stall angle that was observed during the testing at each fan speed. At this angle the sudden collapse of suction pressure on the upper surface of the

Fan Speed Index Nº	Range of Angles of Attack	Observed Stall Angle	Reynolds Number
1	0° - 15°, 20°	8.9°	86,000
2	0° - 20°	9.9°	103,000
3	0° - 20°	11.8°	122,000
4	0° - 20°	12.4°	138,000
5	0° - 20°	12.9°	156,000
6	0° - 20°	13.9°	177,000
7	0° - 20°	14.7°	194,000
8	0° - 20°	15.6°	214,000
9	0° - 16°	16.9°	240,000

Table 6.2: Range of tests, observed stall angle and Reynolds Number for each fan speed setting

aerofoil could be detected by observation of the manometer bank. This change was observed as the angle of attack of the aerofoil was changed. All tests were conducted with the angle of attack increasing from the nominal zero-attack position, consequently all angles of attack are nominal and are as displayed by the trip counter. The average Reynolds Number of the tests conducted at each fan speed setting are also recorded in Table 6.2. The uncorrected values of C_N and C_T for low angles of attack, calculated using CALCCN2 and CALCCT2, are recorded in Tables 6.3a and 6.3b respectively. These results are also plotted in Figures 6.9 to 6.18, where each graph represents measurements taken at a single Reynolds Number.

Consider the results shown in Figure 6.17, which were observed at Re = 240,000. These results are the most reliable because the relative error of the pressure coeff-icients is at its smallest. The pressure distribution plots for this Reynolds Number setting are shown in Figure 6.18 for each of the seventeen angles of attack observed. Each plot has been photographed from the computer monitor and shows the output from the programs CALCCN2 and CALCCT2.

At angles of attack of 4° and less, the values of C_T are large in magnitude, and deviate from the solid curve as shown (the significant of the solid curves in all these graphs is discussed below). The low-α values of C_T must be held in doubt, since correction to fair profile drag values would require the addition of very large form drag values. A similar occurence was also noted by Pope [66] when pressure testing the NACA0018 aerofoil section at a Reynolds Number of 1,230,000. Pope considered that the accuracy of the pressure integration at low-α for calc-ulating chordwise forces to be poor, because it repre-sented a small difference between large areas. This

α	Reynolds Number 86000	103000	122000	138000	156000	177000	194000	214000	240000
0°	-0,286	-0,018	-0,001	0,007	-0,027	-0,019	-0,016	-0,026	-0,066
1°	-0,227	0,053	0,091	0,677	0,081	0,104	0,107	0,101	0,057
2°	0,036	0,138	0,145	0,189	0,190	0,227	0,229	0,216	0,169
3°	0,205	0,247	0,226	0,283	0,282	0,316	0,323	0,321	0,277
4°	0,314	0,354	0,341	0,393	0,365	0,404	0,411	0,404	0,371
5°	0,457	0,464	0,448	0,495	0,452	0,495	0,496	0,483	0,444
6°	0,661	0,592	0,553	0,583	0,570	0,587	0,586	0,571	0,525
7°	0,815	0,788	0,685	0,715	0,677	0,668	0,691	0,670	0,619
8°	0,927	0,930	0,849	0,871	0,801	0,824	0,808	0,780	0,720
9°	0,307	0,980	0,973	1,015	0,960	0,974	0,935	0,898	0,830
10°	0,065	0,088	0,988	1,023	1,040	1,022	1,014	0,981	0,947
11°	0,088	0,112	0,982	1,004	1,031	0,980	0,965	0,928	0,918
12°	0,115	0,136	0,152	1,049	1,012	0,972	0,951	0,927	0,900
13°	0,156	0,183	0,178	0,222	0,998	0,974	0,955	0,931	0,905
14°	0,240	0,277	0,224	0,266	0,240	0,267	0,964	0,938	0,893
15°	0,337	0,391	0,411	0,406	0,359	0,367	0,353	0,953	0,932
16°	-	0,464	0,479	0,495	0,476	0,487	0,484	0,464	0,938
17°	-	0,504	0,515	0,539	0,528	0,538	0,533	0,513	-
18°	-	0,524	0,545	0,582	0,566	0,575	0,566	0,555	-
19°	-	0,569	0,578	0,632	0,594	0,602	0,597	0,582	-
20°	0,551	0,596	0,605	0,634	0,622	0,632	0,632	0,616	-

Table 6.3a: Uncorrected values of C_N

α	Reynolds Number 86000	103000	122000	138000	156000	177000	194000	214000	240000
0°	-0,015	-0,015	0,036	0,033	0,026	0,030	0,018	0,017	0,017
1°	-0,030	-0,003	0,025	0,269	0,029	0,027	0,025	0,021	0,017
2°	-0,022	-0,008	0,006	0,016	0,024	0,026	0,027	0,028	0,022
3°	-0,003	-0,002	-0,002	0,004	0,012	0,021	0,026	0,031	0,030
4°	0,004	0,007	0,006	0,016	0,014	0,023	0,026	0,031	0,035
5°	0,014	0,024	0,023	0,032	0,058	0,037	0,039	0,040	0,038
6°	0,043	0,043	0,041	0,050	0,049	0,056	0,057	0,057	0,051
7°	0,069	0,075	0,064	0,075	0,071	0,106	0,079	0,079	0,071
8°	0,092	0,099	0,097	0,106	0,097	0,105	0,104	0,104	0,094
9°	-0,103	0,128	0,126	0,139	0,129	0,138	0,136	0,134	0,121
10°	-0,110	-0,111	0,145	0,160	0,157	0,164	0,164	0,162	0,154
11°	-0,120	-0,120	0,157	0,171	0,175	0,170	0,174	0,168	0,166
12°	-0,127	-0,132	-0,128	0,171	0,182	0,178	0,183	0,180	0,175
13°	-0,132	-0,137	-0,144	-0,151	0,187	0,190	0,194	0,191	0,186
14°	-0,147	-0,161	-0,159	-0,168	-0,160	-0,160	0,206	0,202	0,232
15°	-0,160	-0,167	-0,175	-0,180	-0,181	-0,176	-0,174	0,216	0,213
16°	-	-0,176	-0,181	-0,187	-0,185	-0,187	-0,187	-0,182	0,223
17°	-	-0,171	-0,181	-0,187	-0,188	-0,189	-0,188	-0,183	-
18°	-	-0,170	-0,181	-0,188	-0,188	-0,188	-0,189	-0,185	-
19°	-	-0,176	-0,180	-0,188	-0,188	-0,187	-0,189	-0,183	-
20°	-0,166	-0,175	-0,179	-0,185	-0,185	-0,186	-0,187	-0,183	-

Table 6.3b: Uncorrected values of C_r

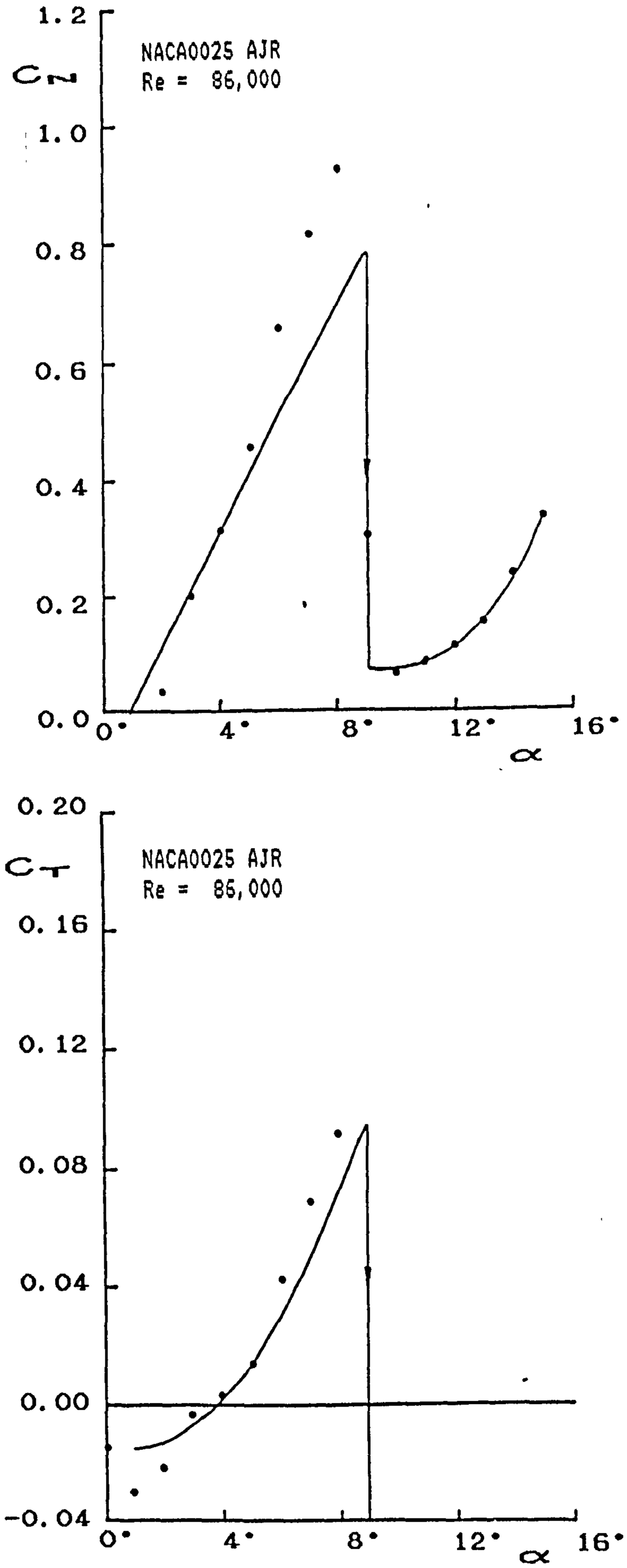

Figure 6.9: Uncorrected values of C_N and C_T at low angles of incidence for Re = 86,000

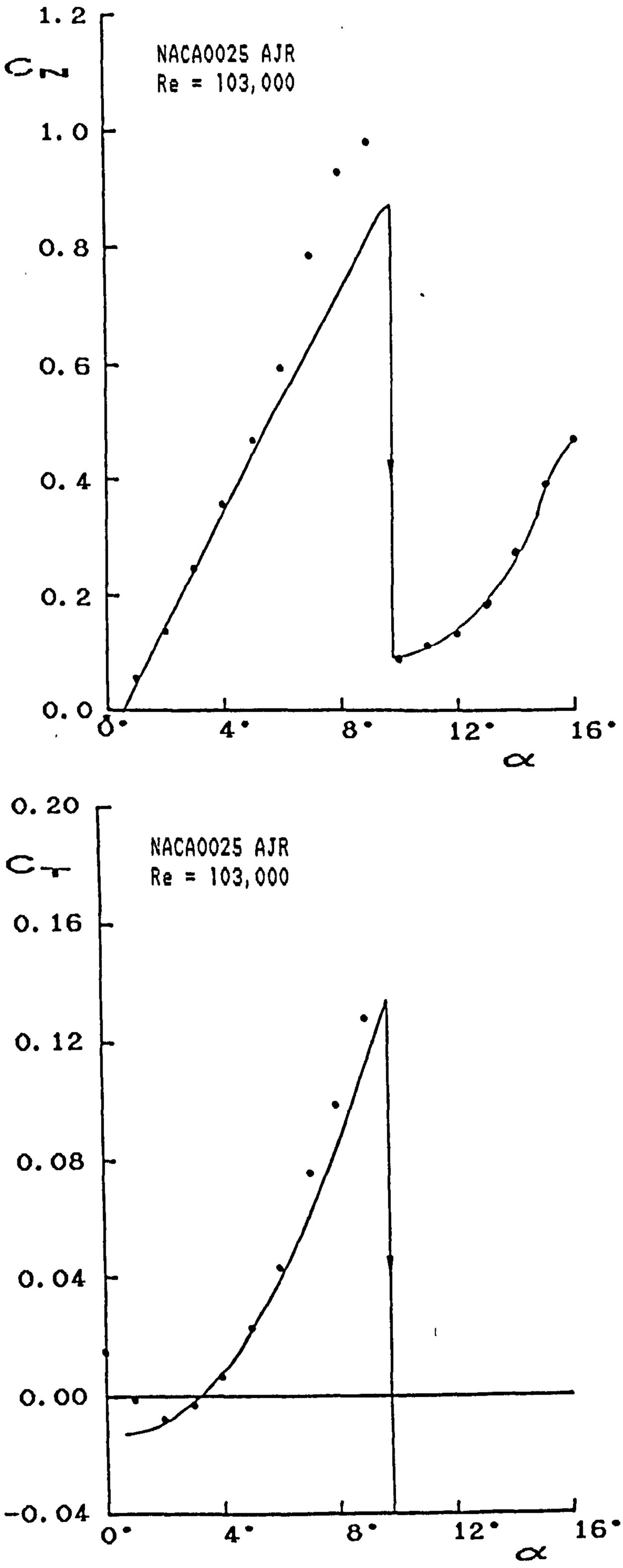

Figure 6.10: Uncorrected values of C_N and C_T at low angles of attack at Re = 103,000

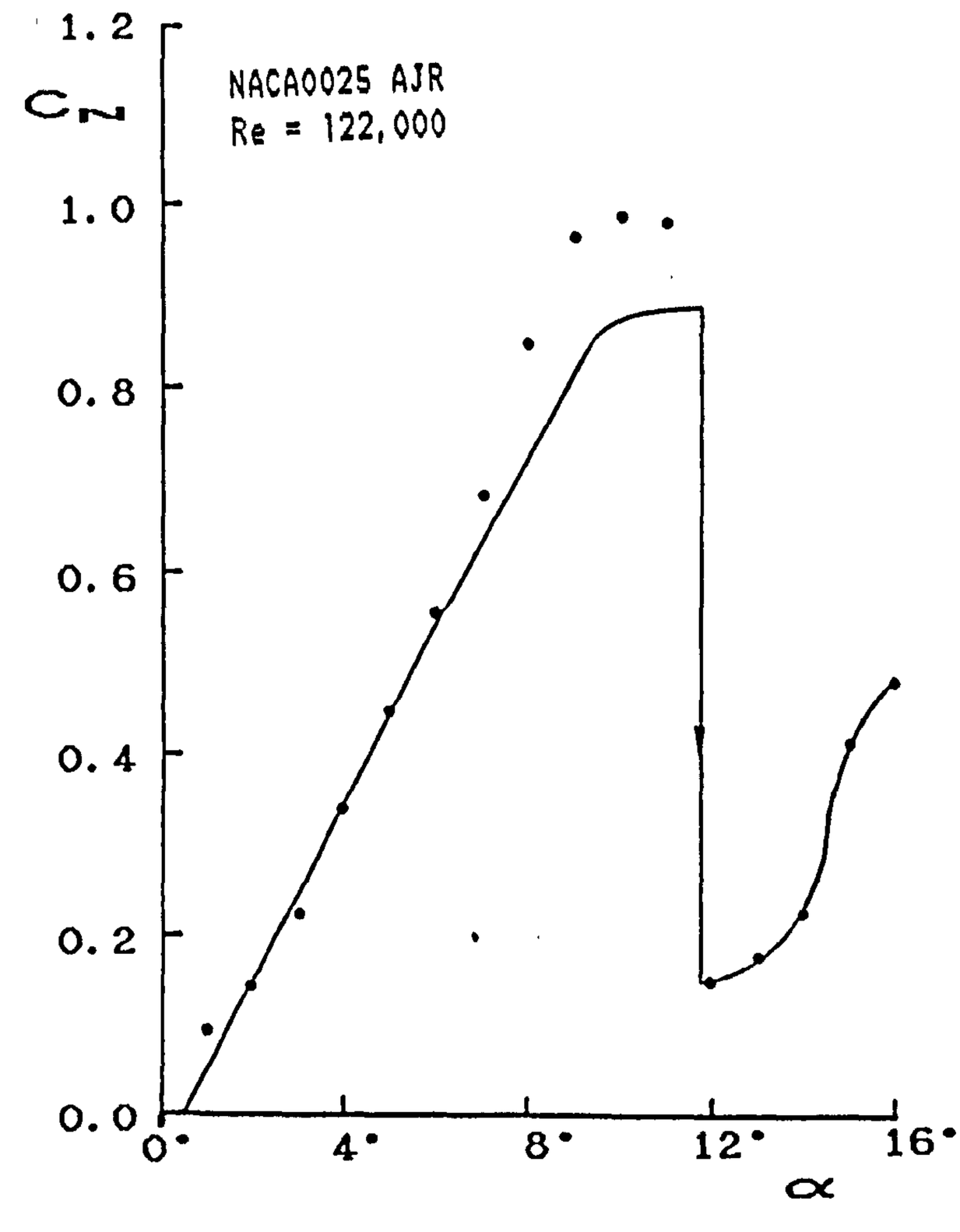

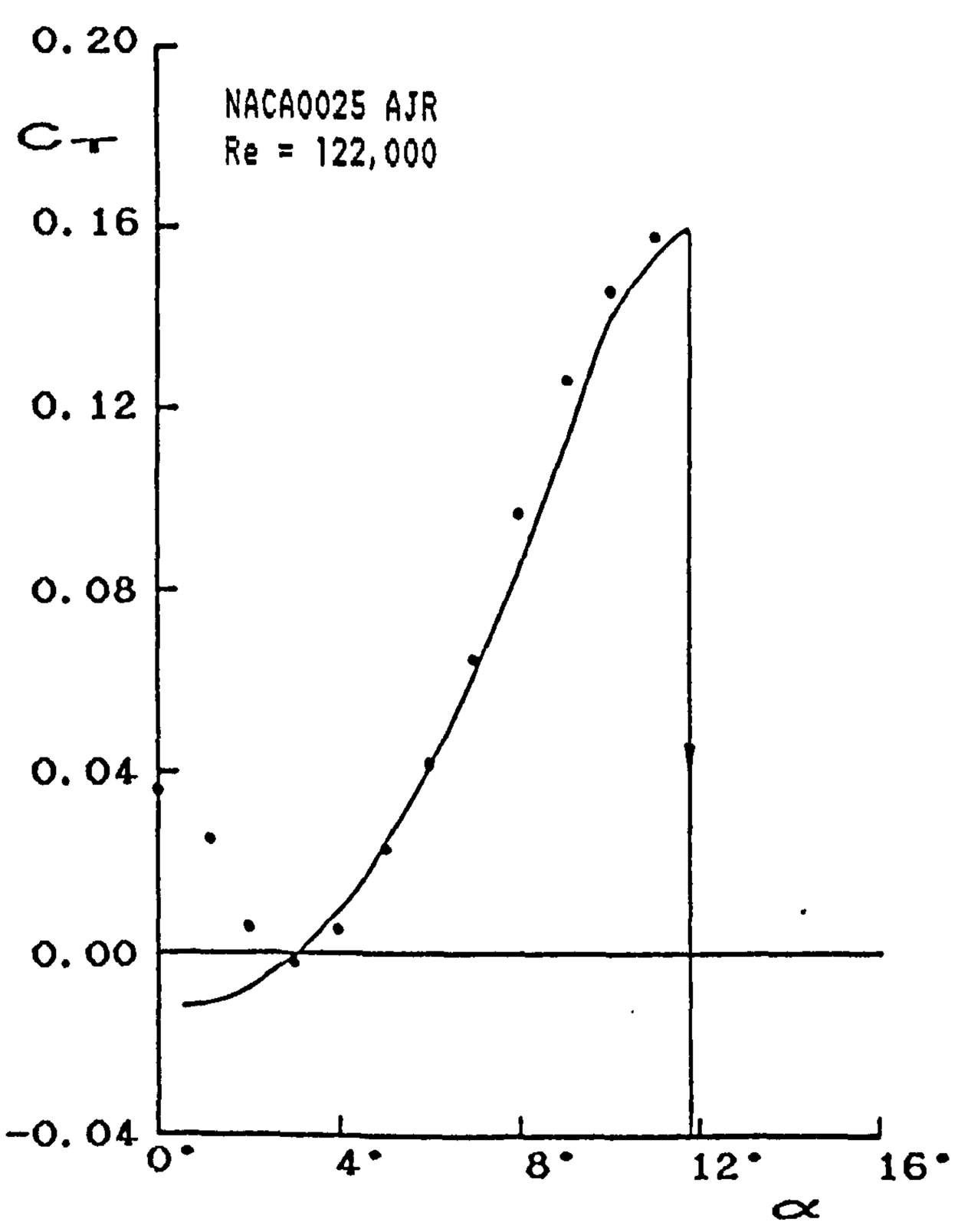

Figure 6.11: Uncorrected values of C_N and C_T at low angles of attack at Re = 122,000

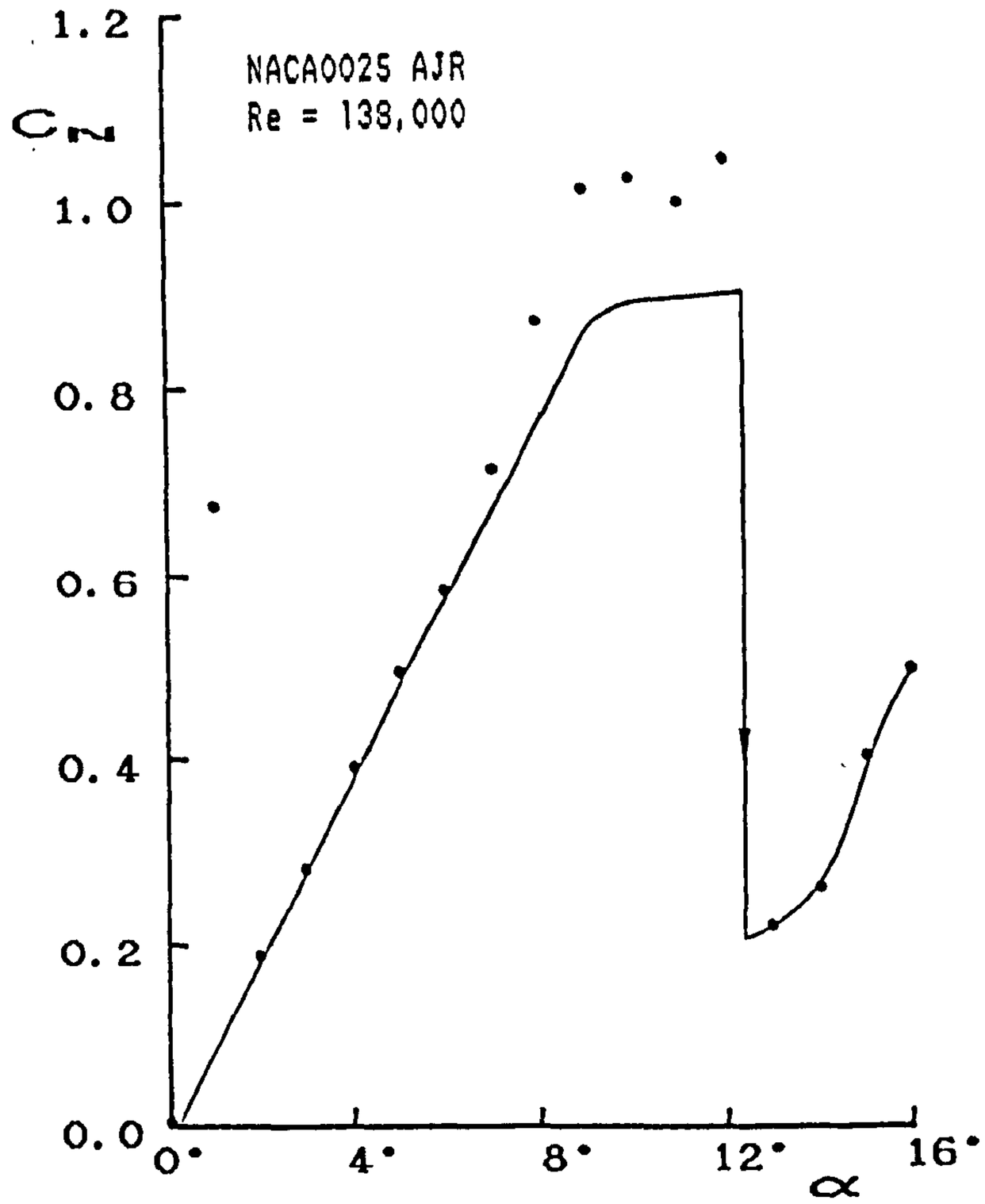

Figure 6.12: Uncorrected values of C_N and C_T at low angles of attack at Re = 138,000

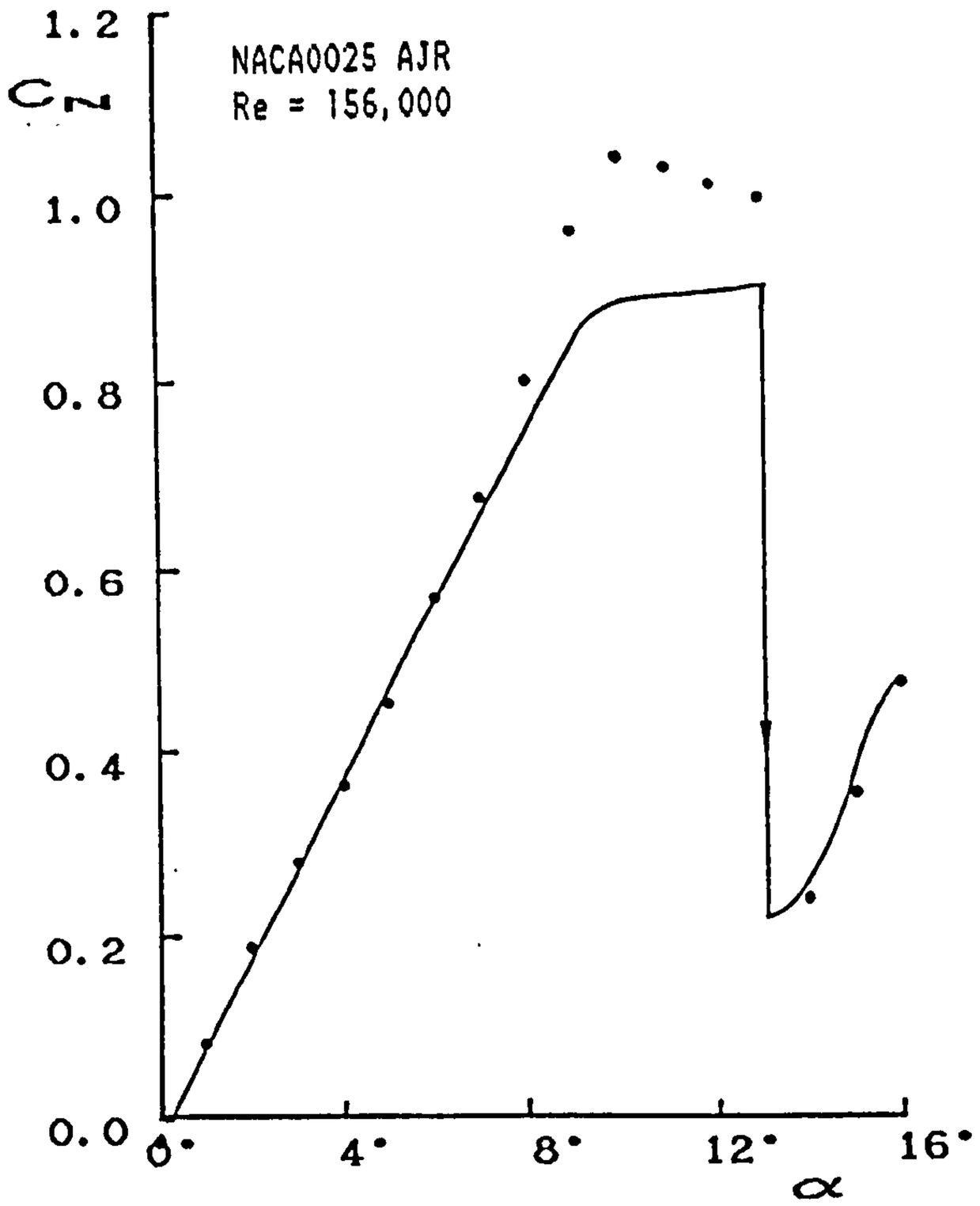

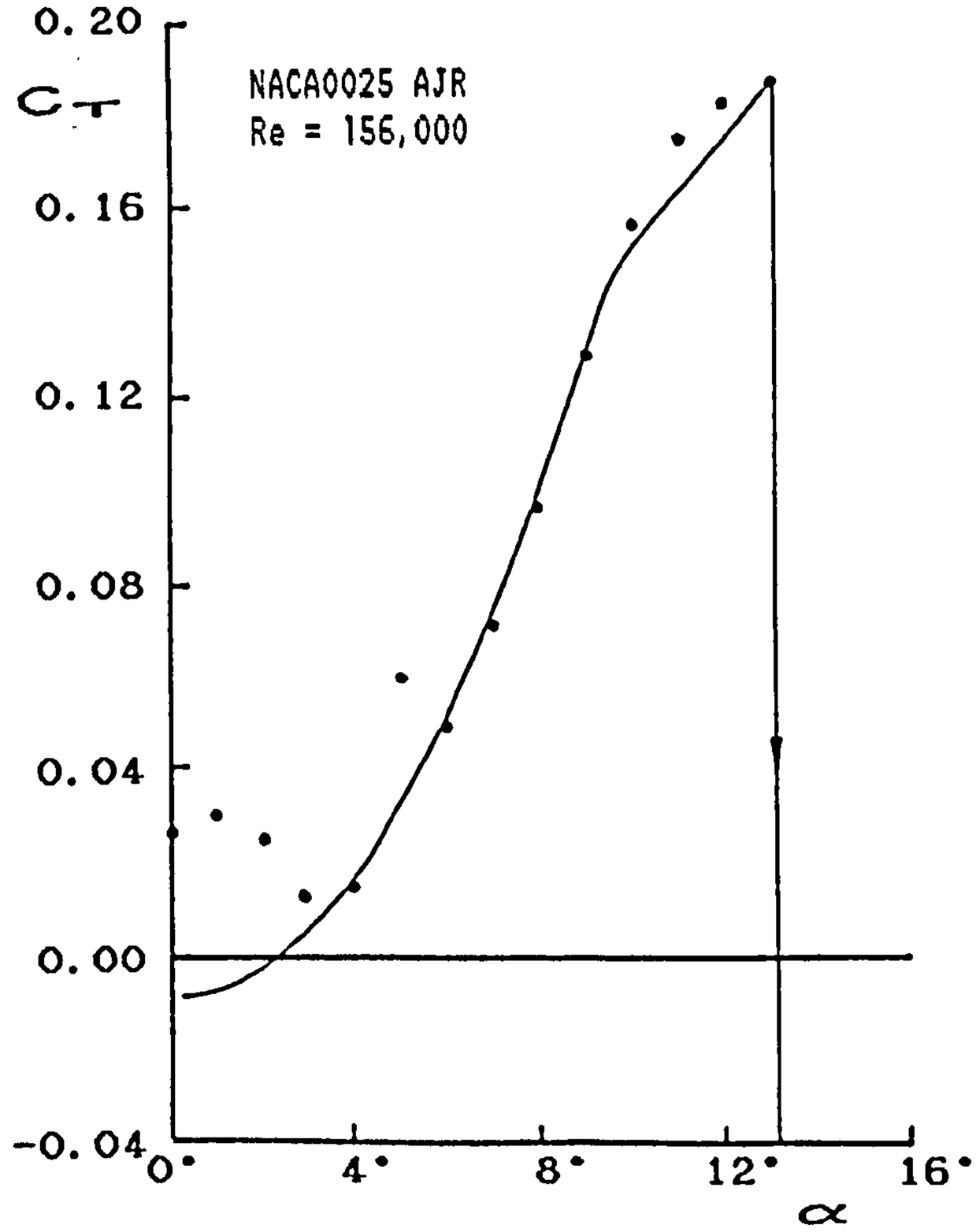

Figure 6.13: Uncorrected values of C_N and C_T at low angles of attack at Re = 156,000

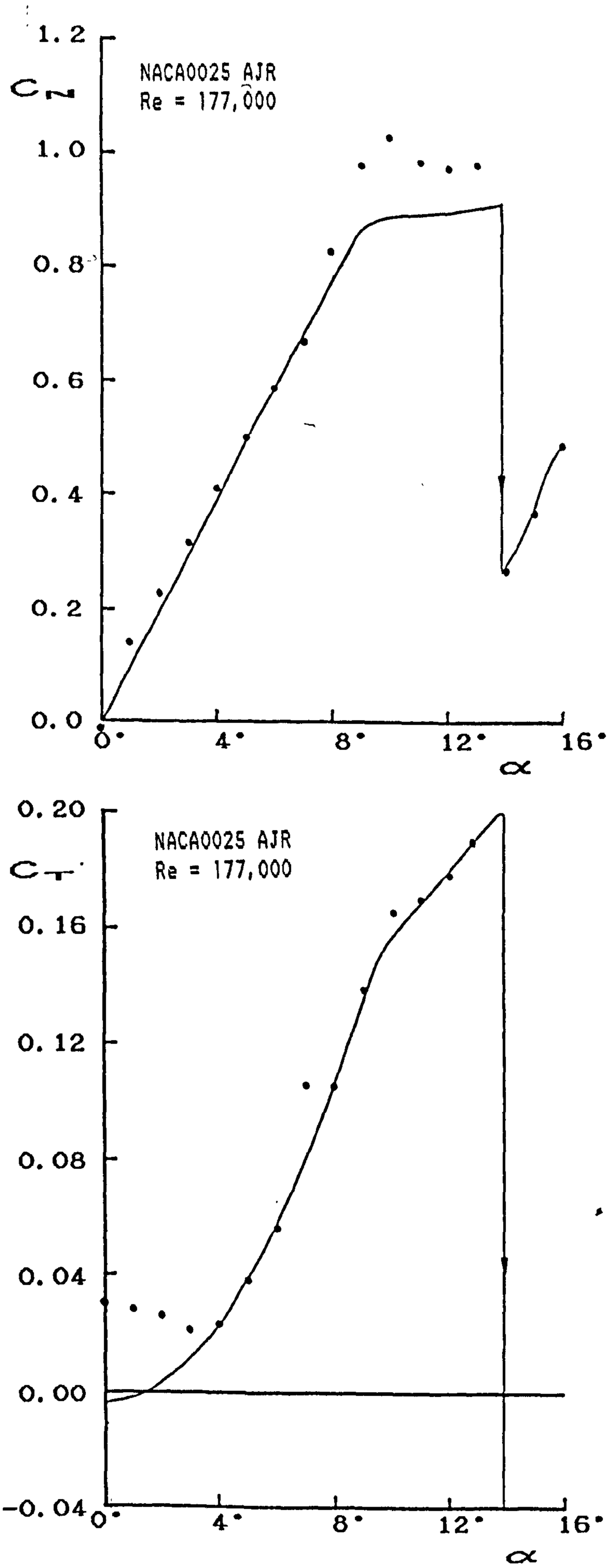

Figure 6.14: Uncorrected values of C_N and C_r at low angles of attack at Re = 177,000

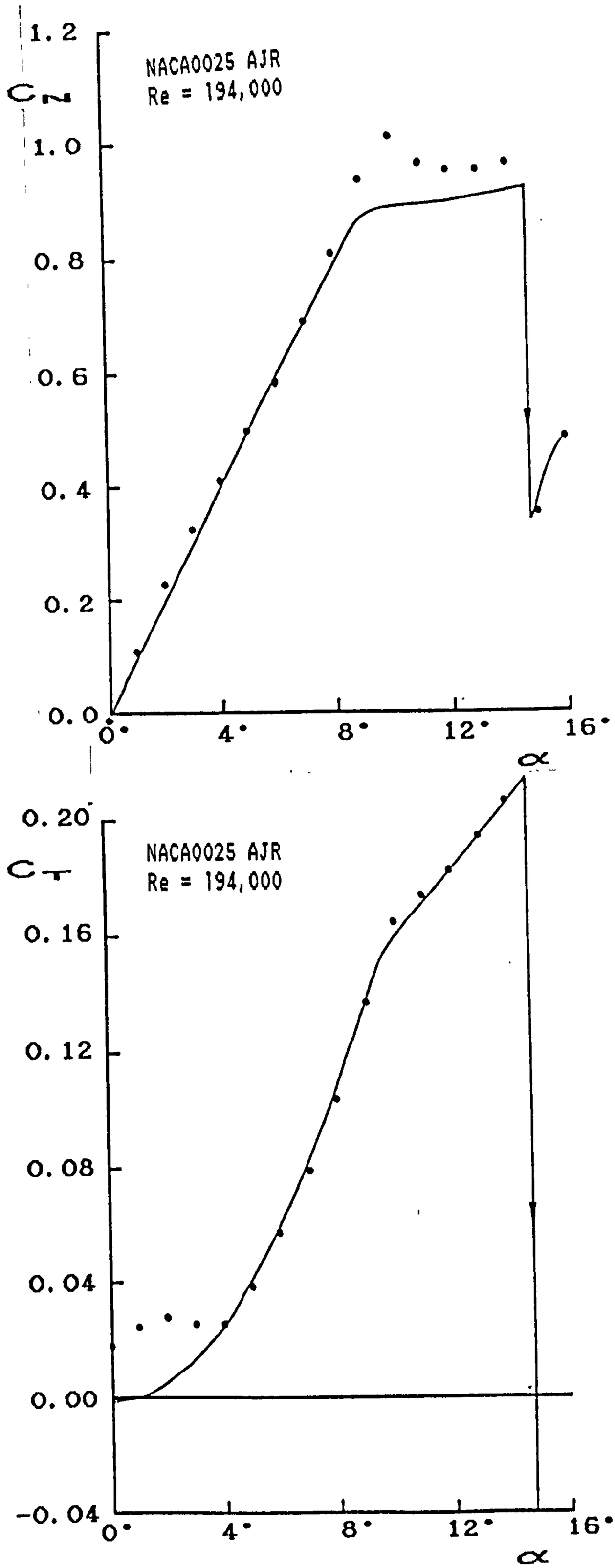

Figure 6.15: Uncorrected values of C_N and C_T at low angles of attack at Re = 194,000

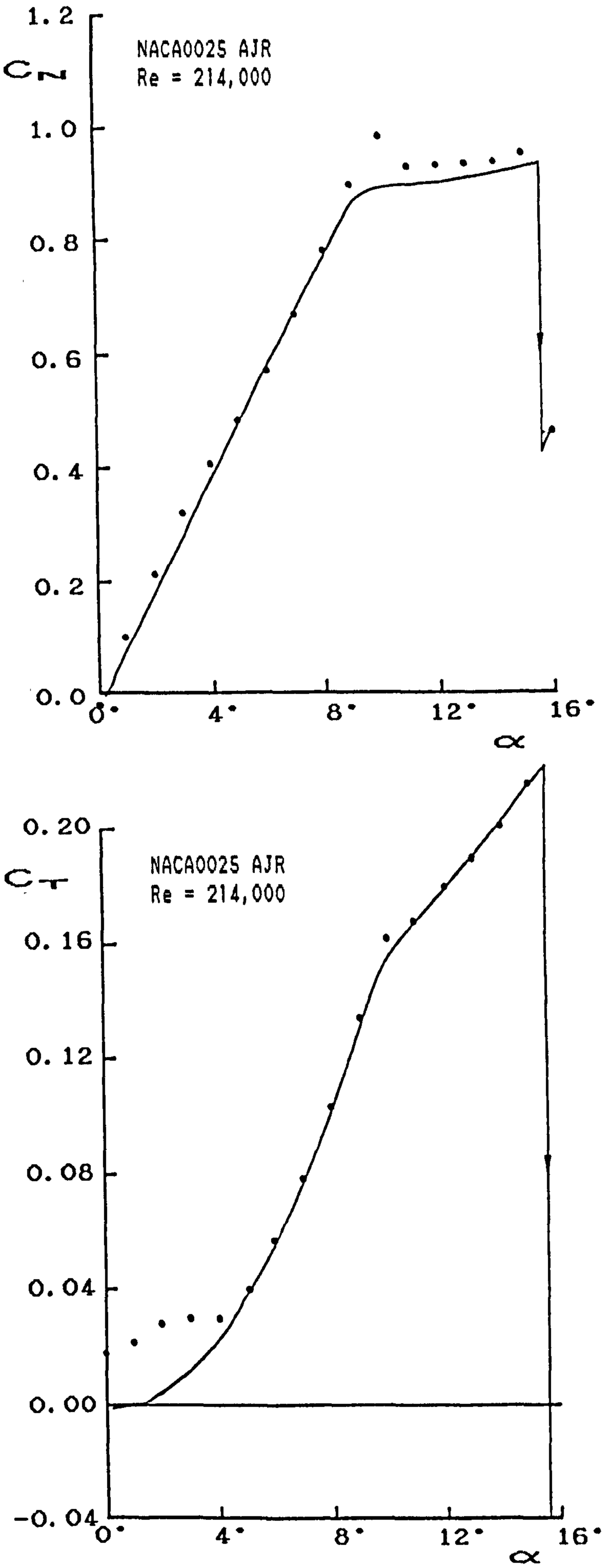

Figure 6.16: Uncorrected values of C_N and C_T at low angles of attack at Re = 214,000

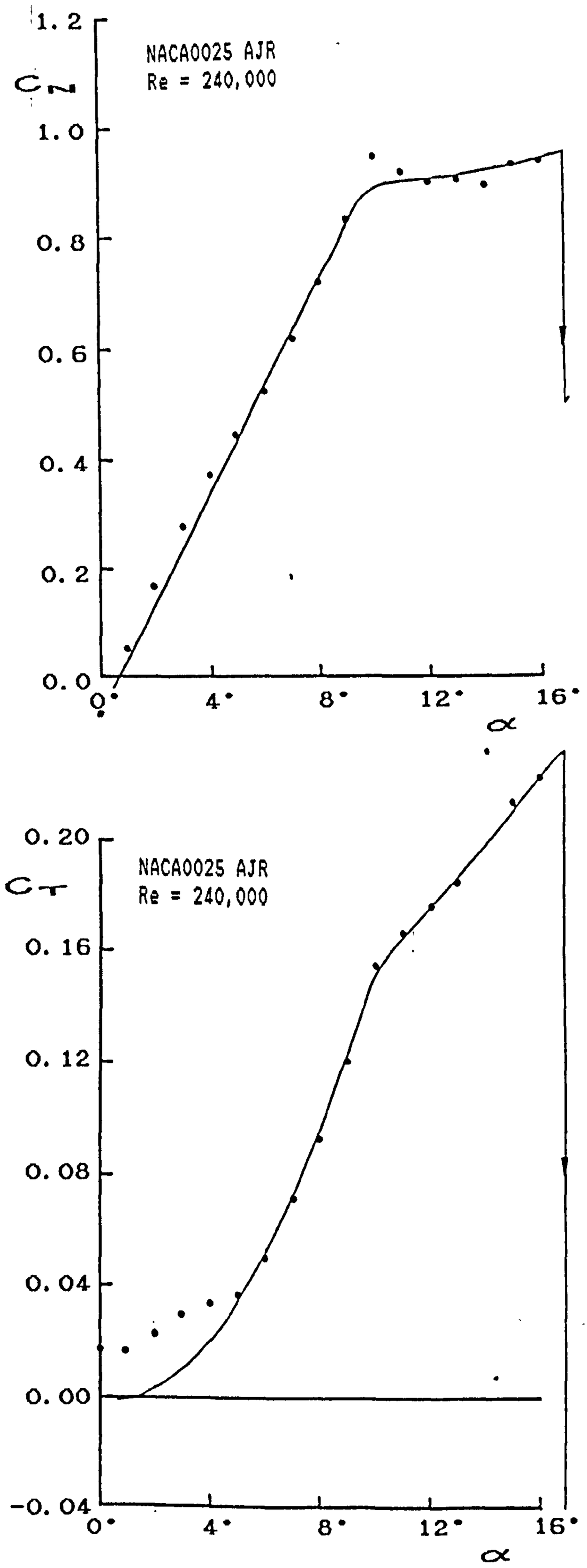

Figure 6.17: Uncorrected values of C_N and C_T at low angles of attack at Re = 240,000

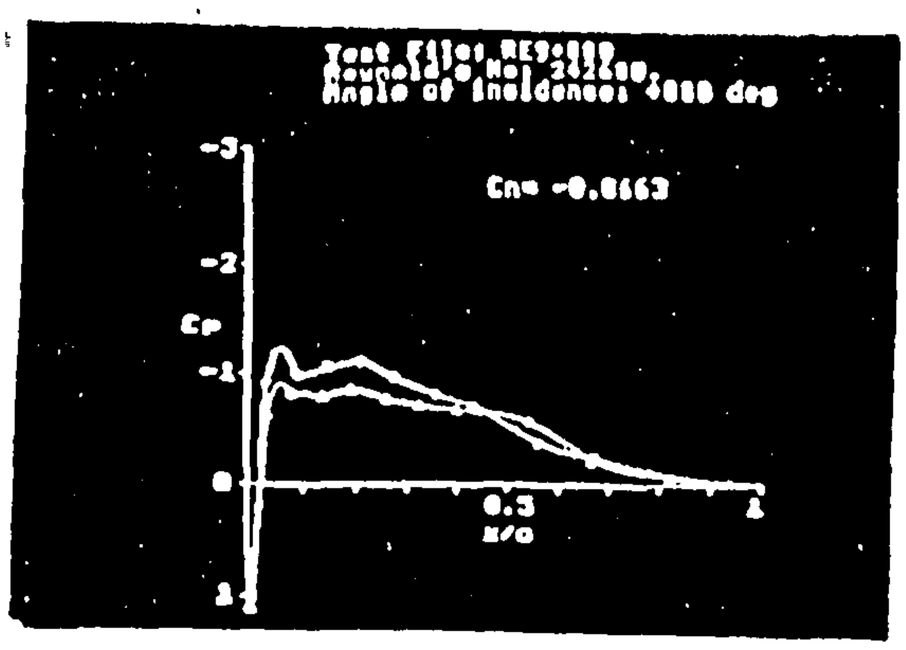

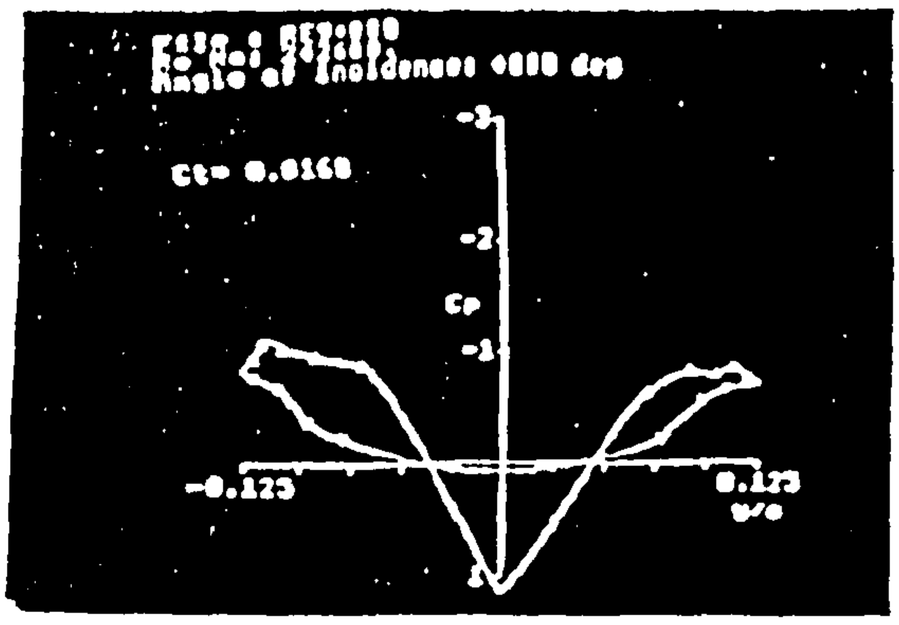

Figure 6.18a: C_{p_∞} plots at $\alpha = 0°$ for Re = 240,000

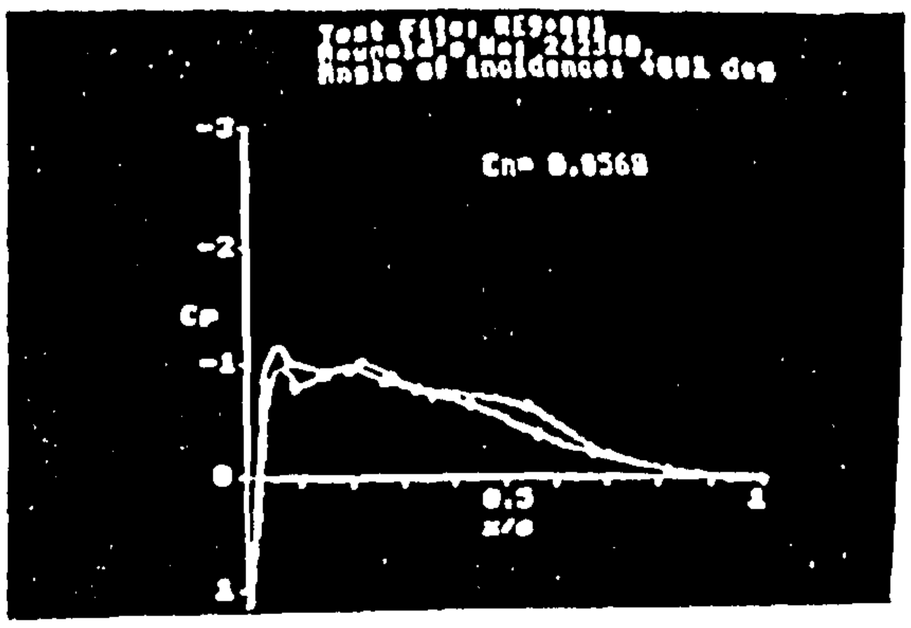

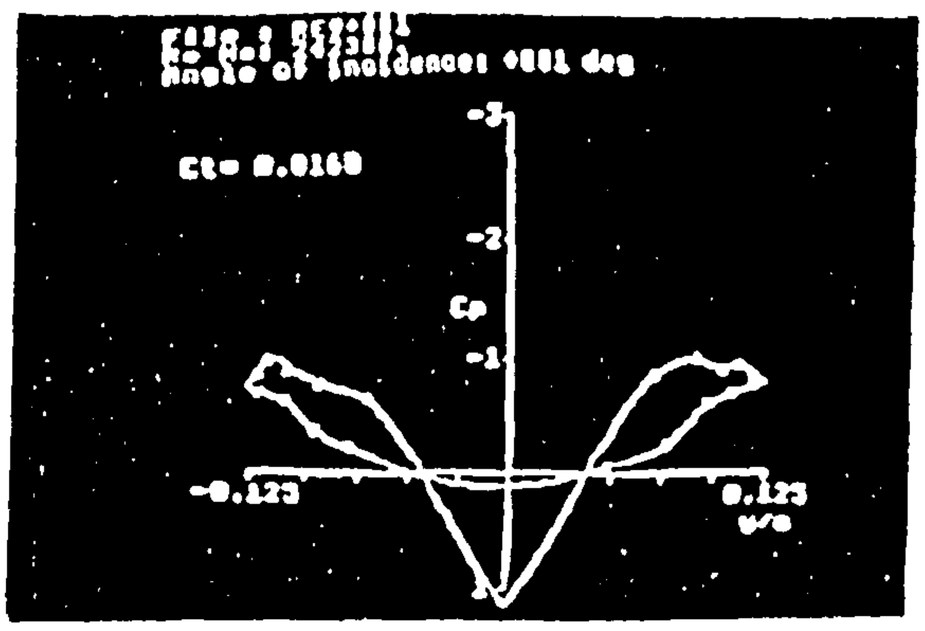

Figure 6.18b: C_{p_∞} plots at $\alpha = 1°$ for Re = 240,000

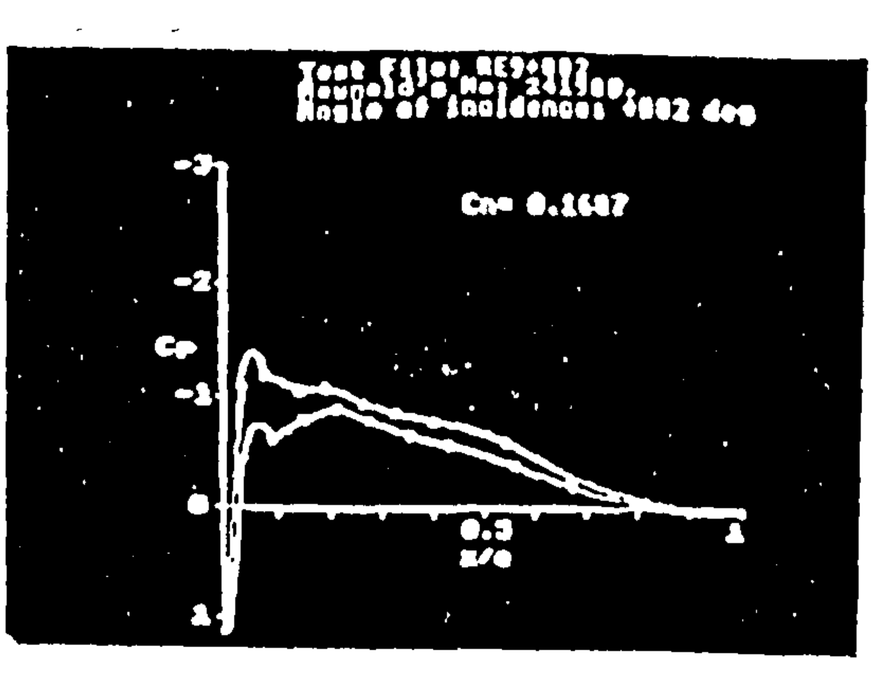

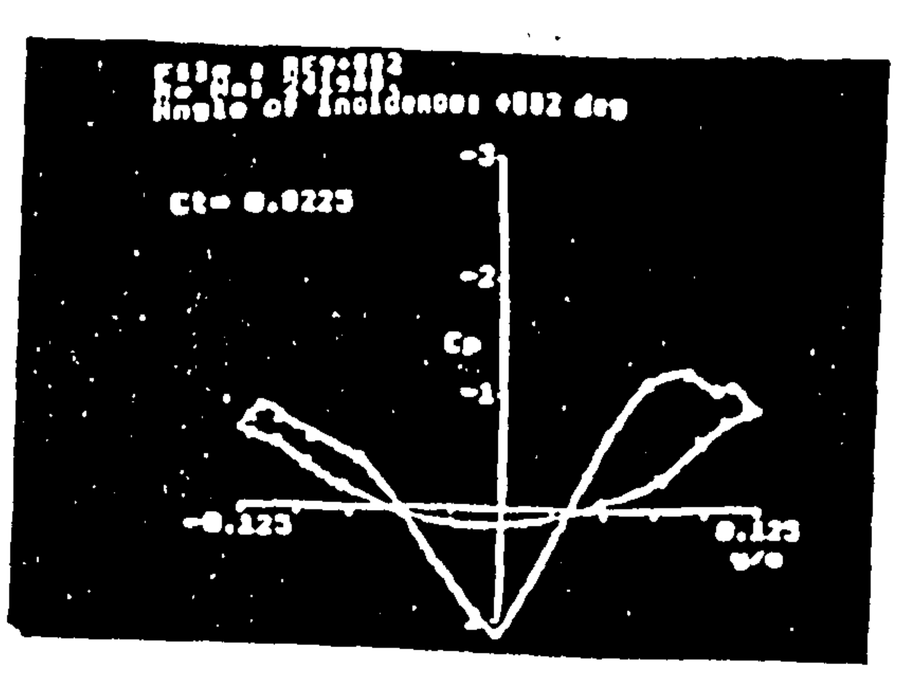

Figure 6.18c: C_{p_∞} plots at $\alpha = 2°$ for Re = 240,000

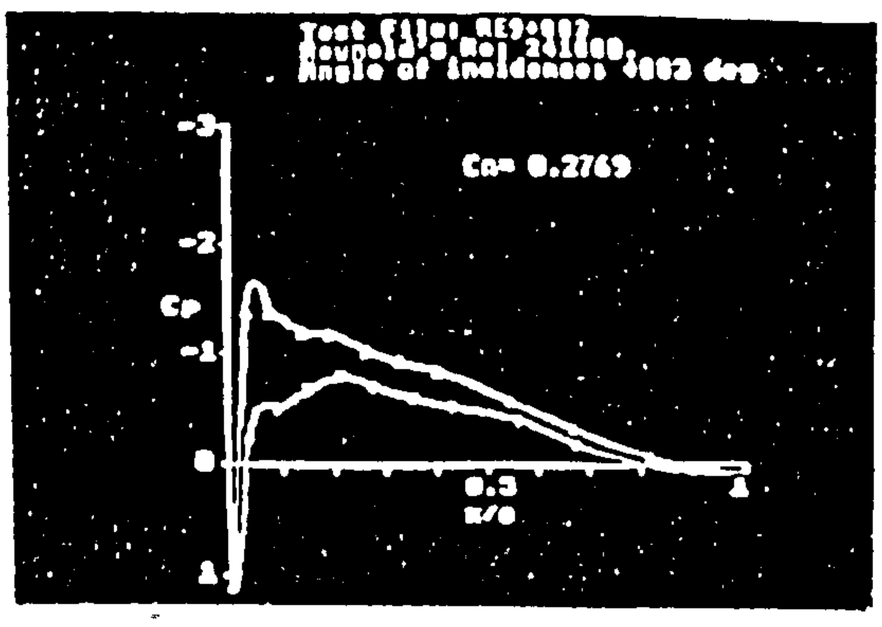

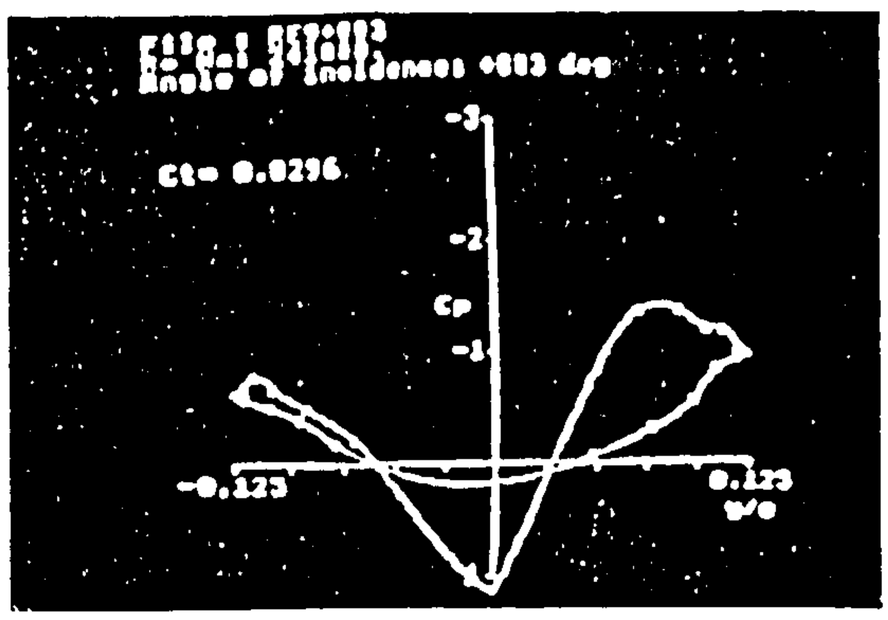

Figure 6.18d: $C_{p\infty}$ plots at $\alpha = 3°$ for Re = 240,000

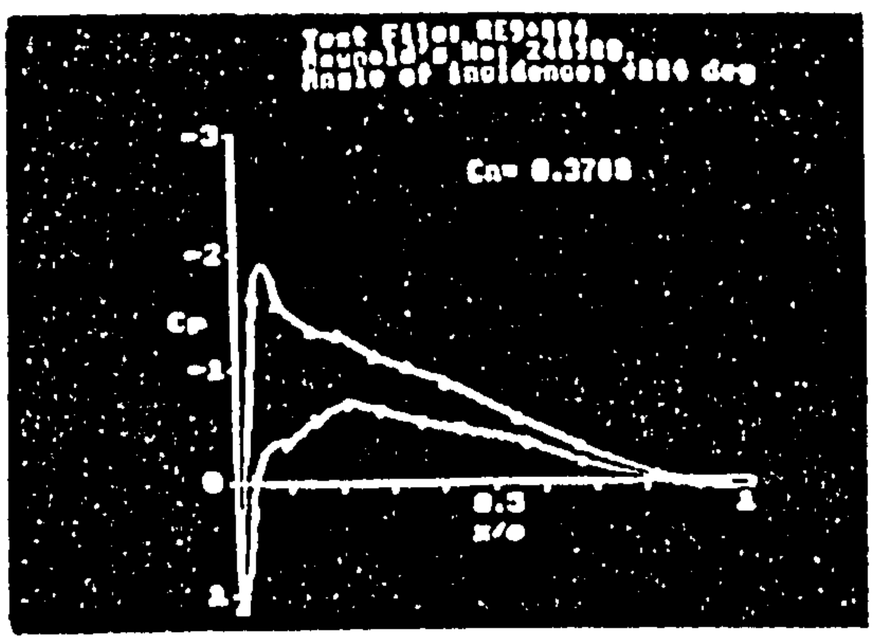

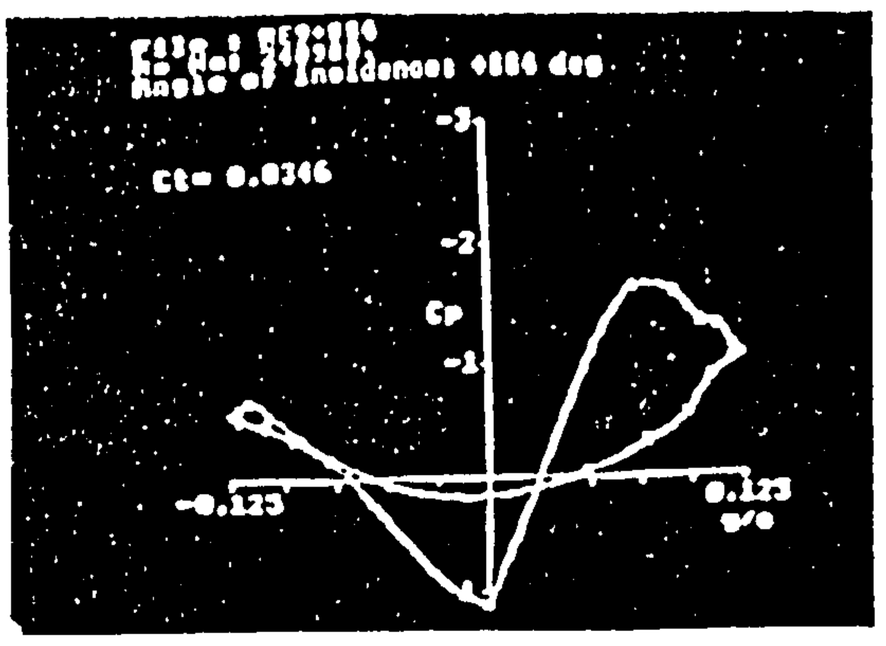

Figure 6.18e: $C_{p\infty}$ plots at $\alpha = 4°$ for Re = 240,000

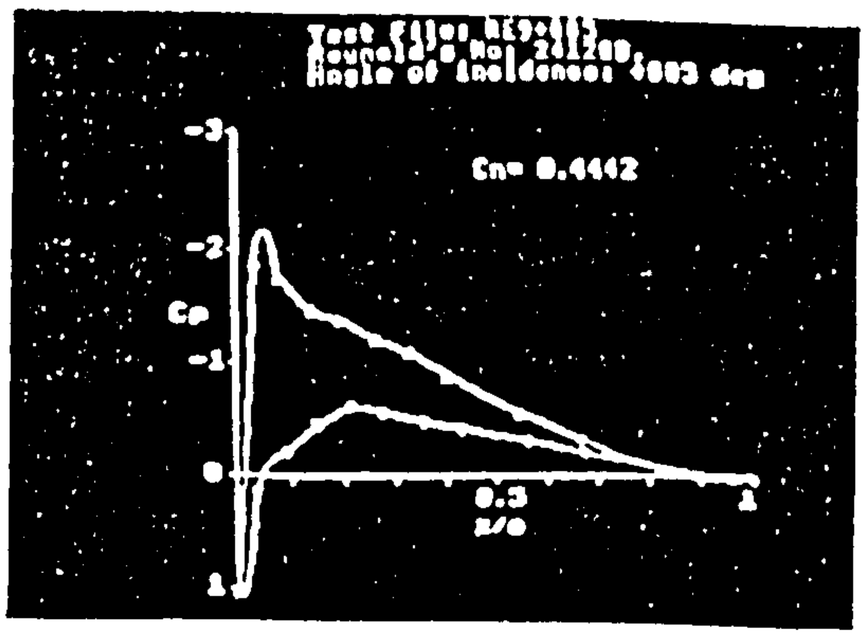

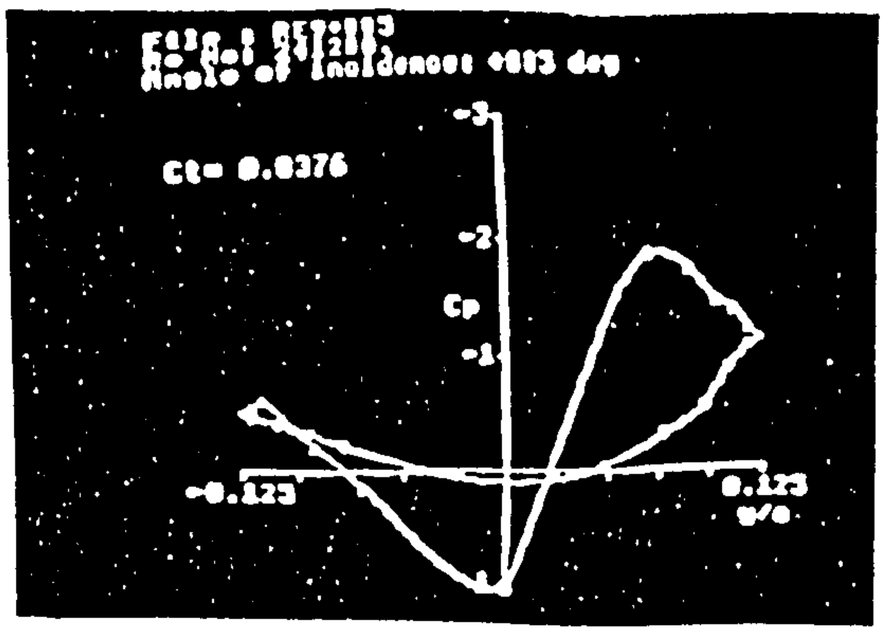

Figure 6.18f: $C_{p\infty}$ plots at $\alpha = 5°$ for Re = 240,000

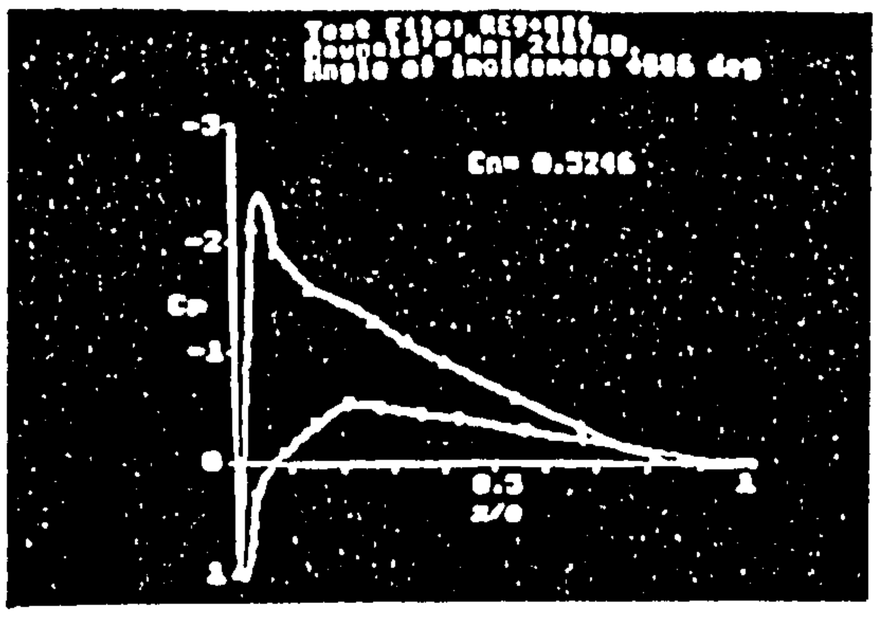

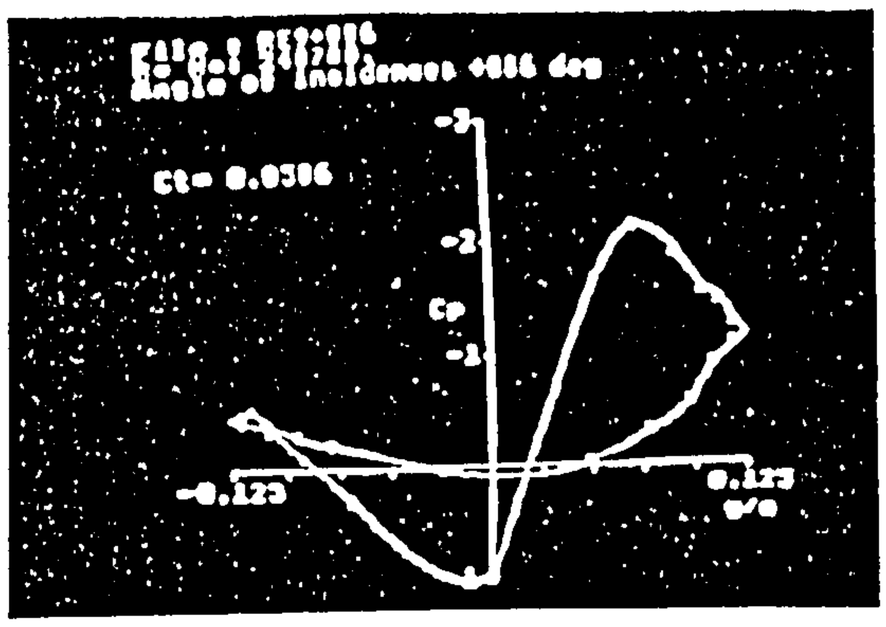

Figure 6.18g: C_{p_∞} plots at $\alpha = 6°$ for Re = 240,000

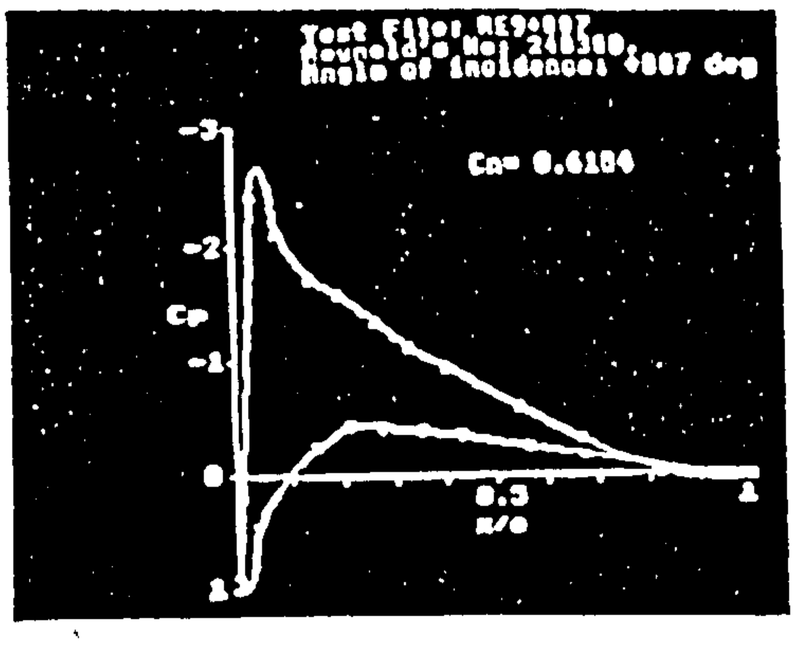

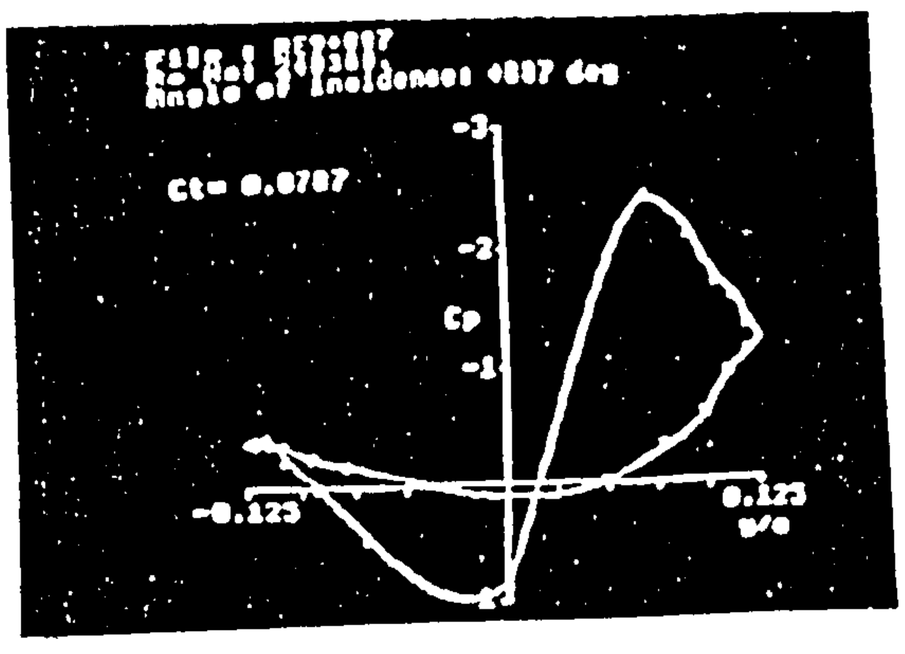

Figure 6.18h: C_{p_∞} plots at $\alpha = 7°$ for Re = 240,000

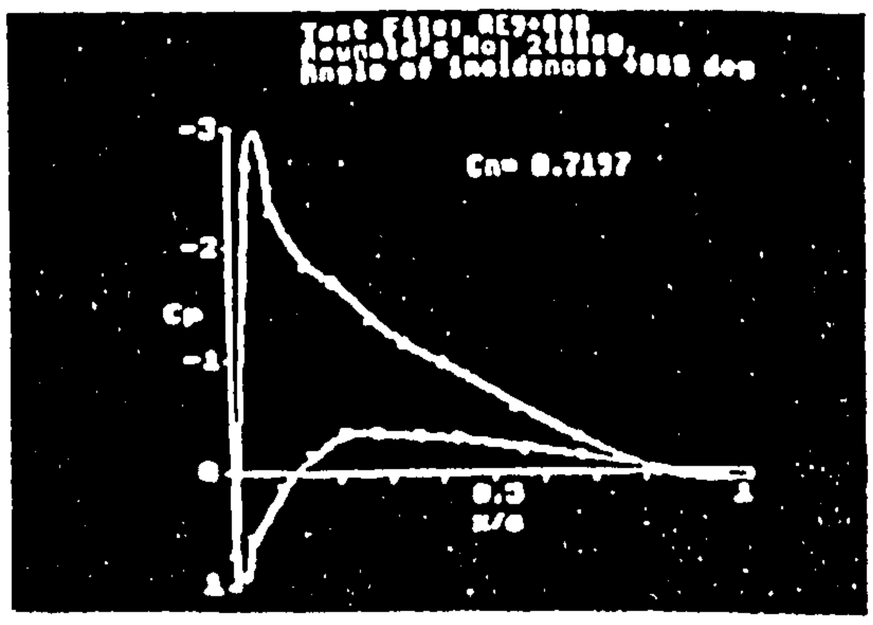

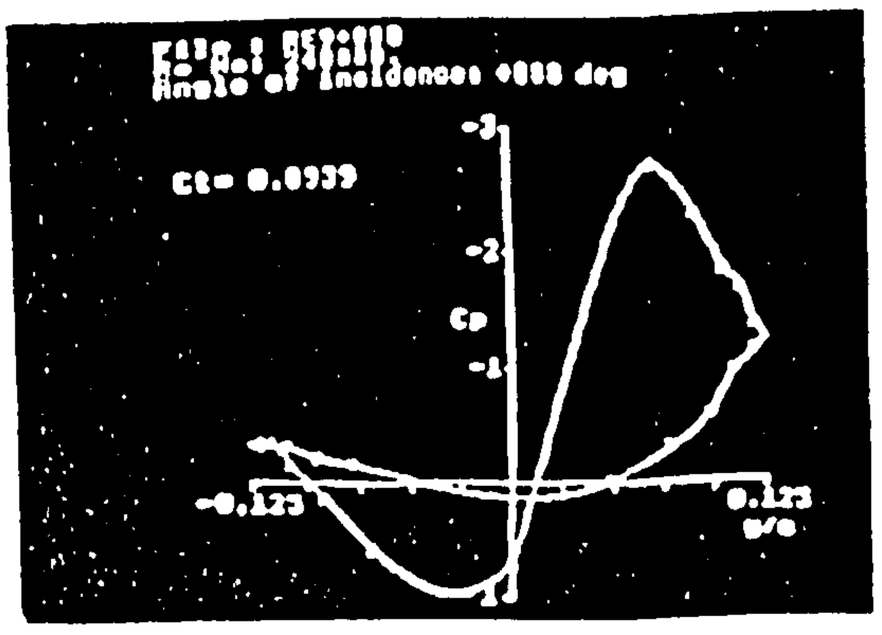

Figure 6.18i: C_{p_∞} plots at $\alpha = 8°$ for Re = 240,000

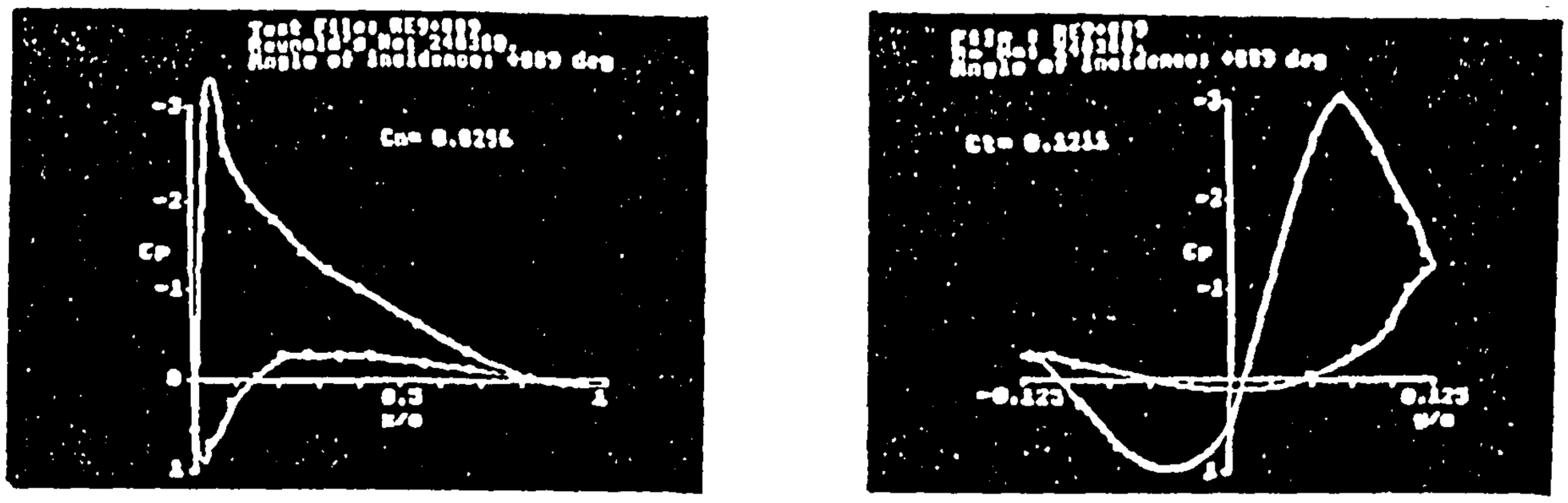

Figure 6.18j: C_{p_m} plots at $\alpha = 9°$ for Re = 240,000

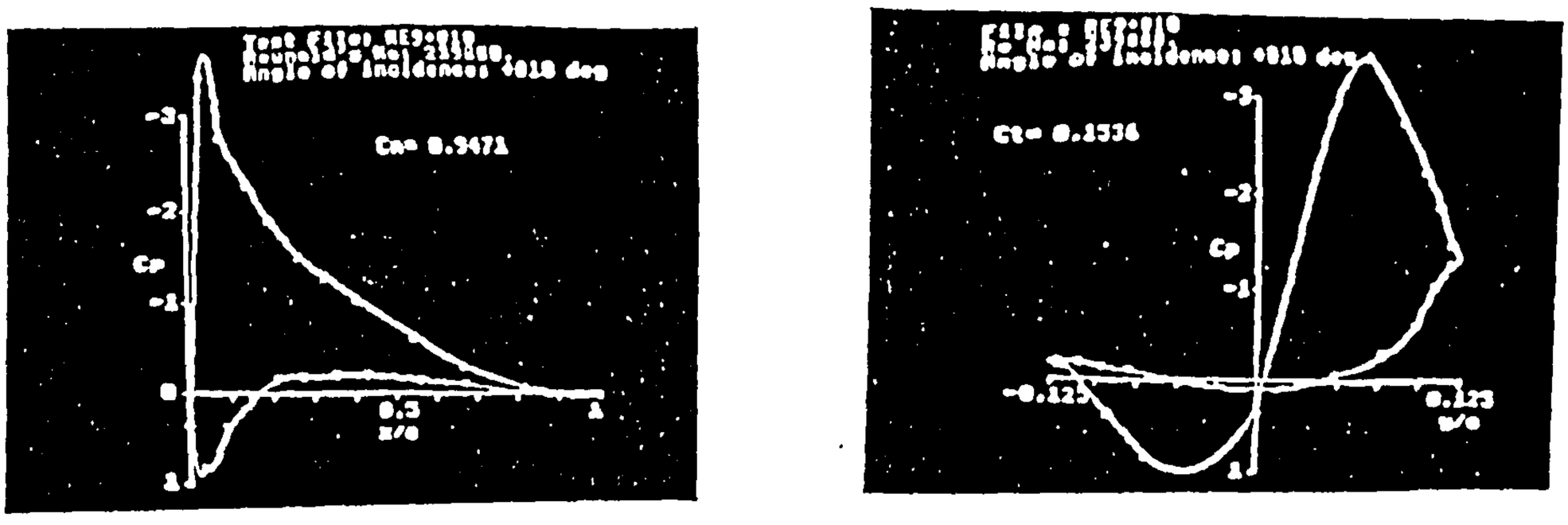

Figure 6.18k: C_{p_m} plots at $\alpha = 10°$ for Re = 240,000

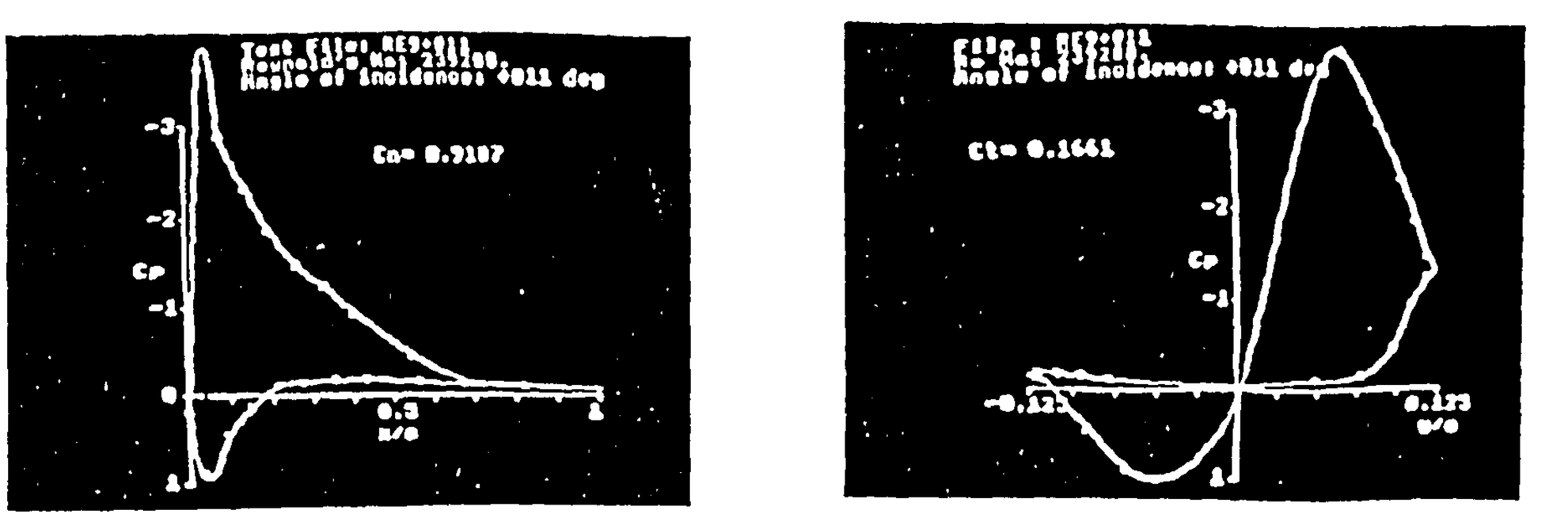

Figure 6.18l: C_{p_m} plots at $\alpha = 11°$ for Re = 240,000

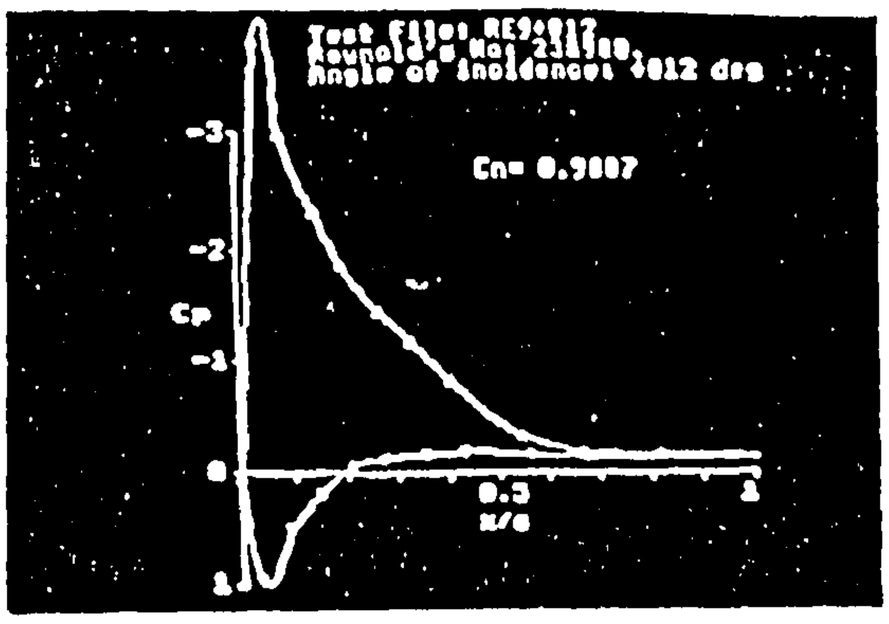

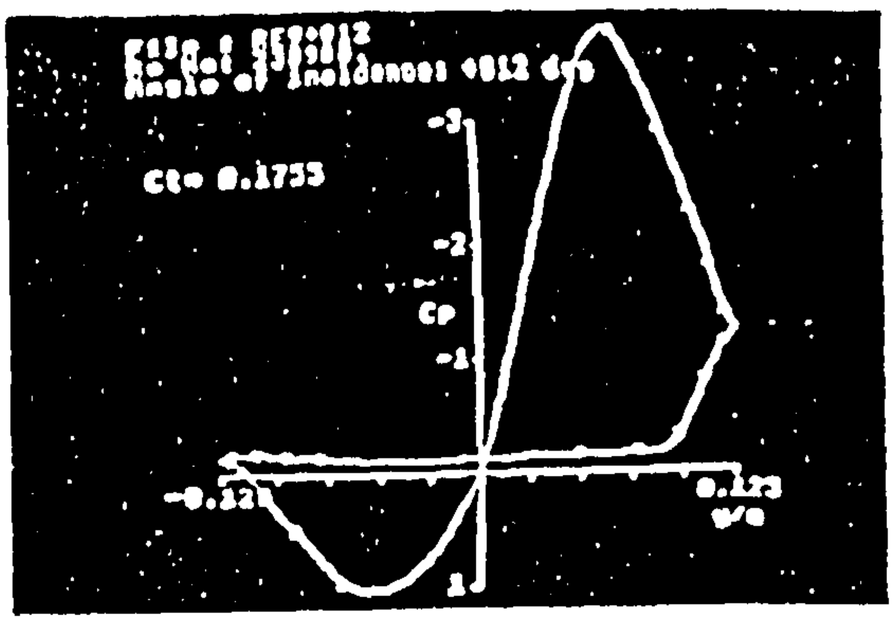

Figure 6.18m: $C_{f\infty}$ plots at $\alpha = 12^{\circ}$ for Re = 240,000

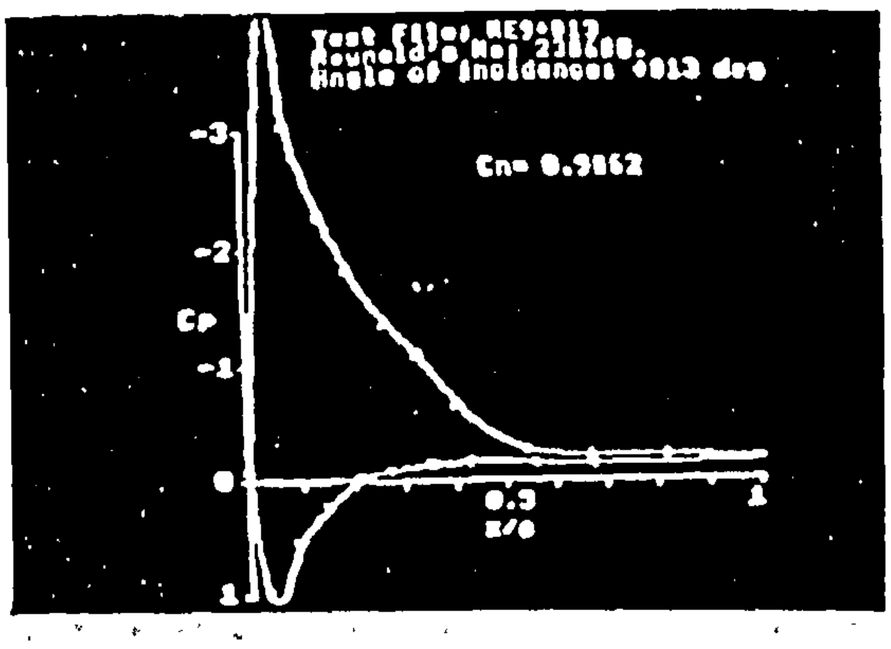

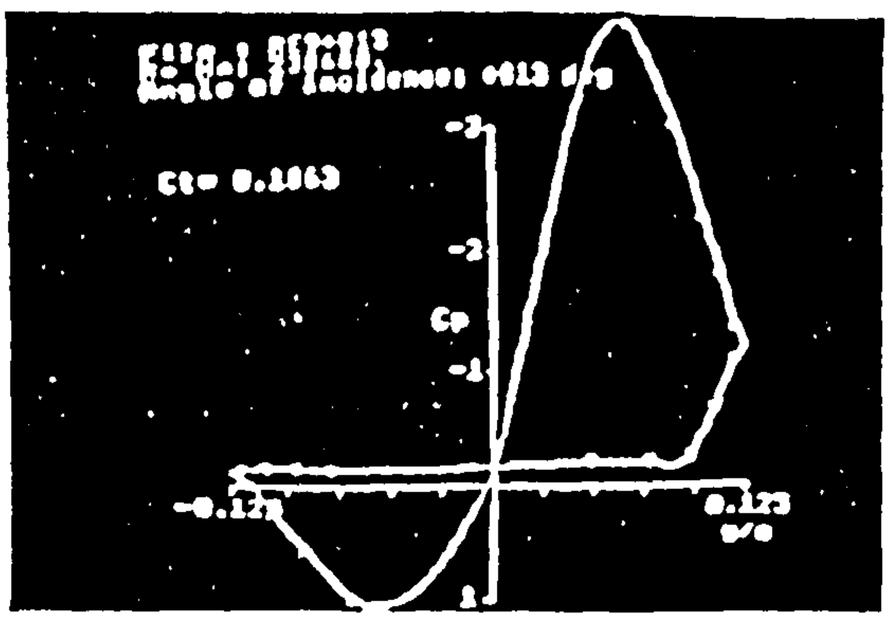

Figure 6.18n: $C_{f\infty}$ plots at $\alpha = 13^{\circ}$ for Re = 240,000

Figure 6.18o: $C_{f\infty}$ plots at $\alpha = 14^{\circ}$ for Re = 240,000

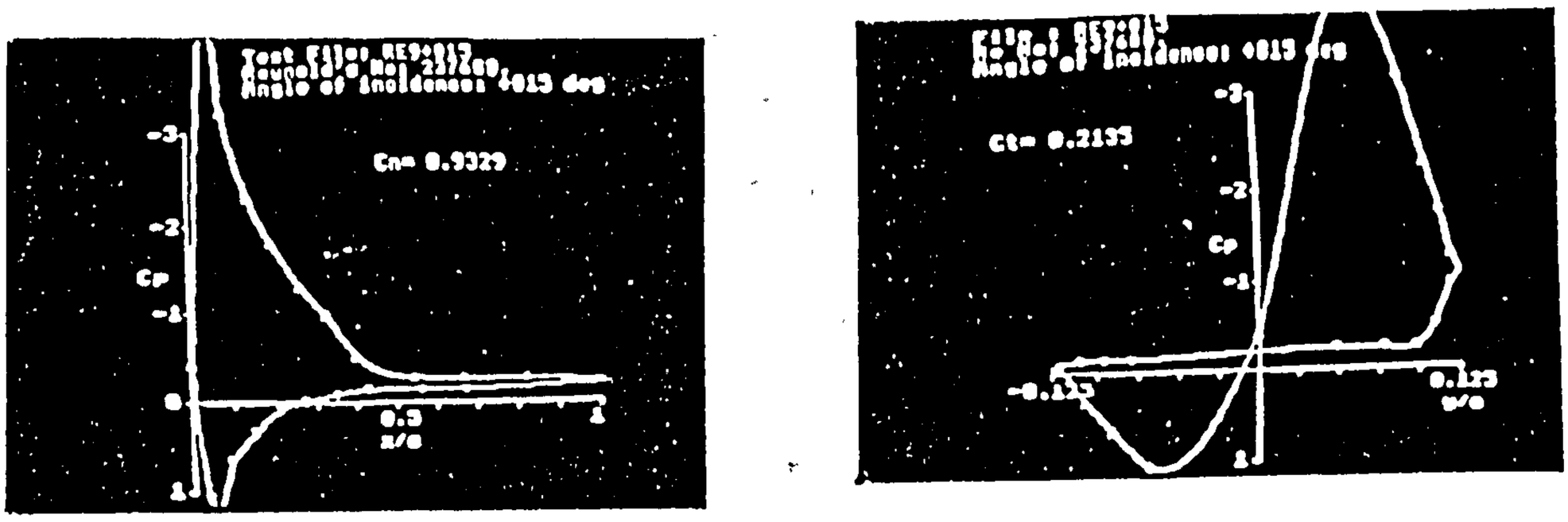

Figure 6.18p: C_{p_m} plots at $\alpha = 15°$ for Re = 240,000

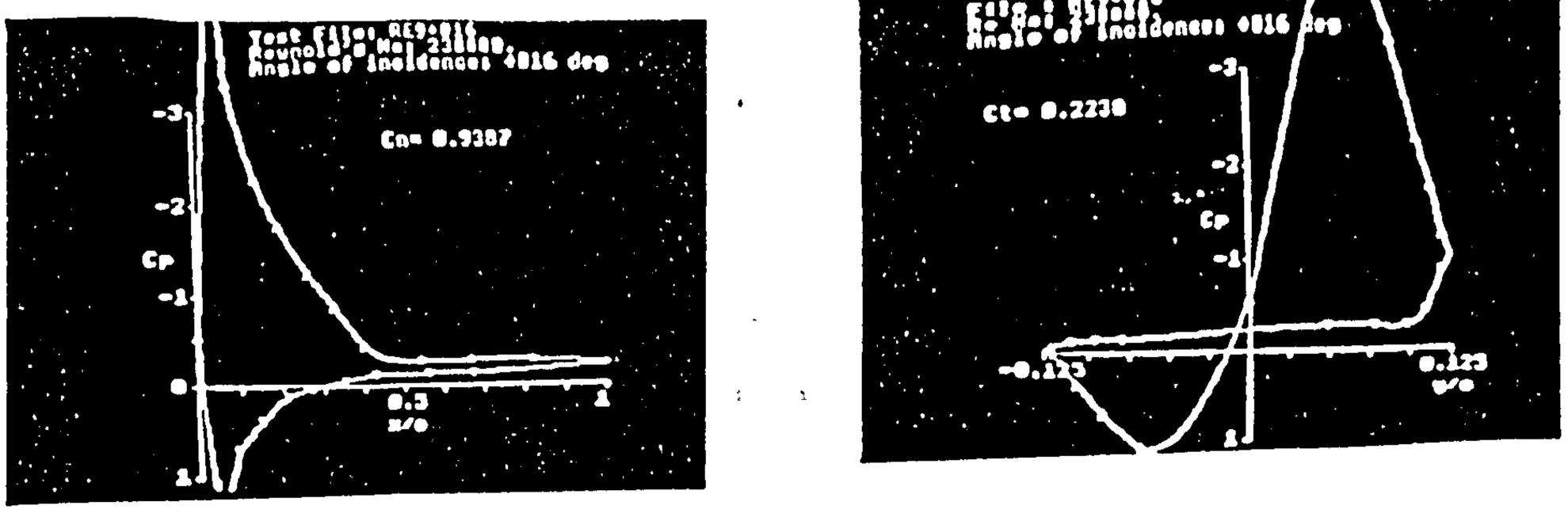

Figure 6.18q: C_{p_m} plots at $\alpha = 16°$ for Re = 240,000

explanation is not unreasonable here, especially since the pressure tappings are poorly distributed with respect to the normal of the chord. This enevitably means that the accuracy of the pressure envelope calculated by numerical interpolation around the leading edge is highly sensitive to the static pressures measured at the forward tappings. It is not possible to improve this calculation with the measurements made, but this does illustrate the need for a greater number of pressure tappings around the leading edge for chordwise force integrations. Pope did not rely upon his chordwise force measurements for angles of attack less than $\alpha = 13°$. Fortunately here the Reynolds Number is low and the measured thrust forces seem reasonable for $\alpha > 4°$. Only those close to $\alpha = 0°$ need be ignored.

The pressure integration at low-α for calculating normal forces is much better and the data here is considered good.

However, in order to determine the thrust forces at low-α it was necessary to consider ideal-fluid theory for thin aerofoils. If stalling is ignored, then the aerodynamic force coefficients can be expressed as follows:

$$C_N = a_0 \sin\alpha\cos\alpha \qquad (6.57a)$$

$$C_T = a_0 \sin^2\alpha \qquad (6.57b)$$

where a_0 is slope of the lift force curve at $\alpha = 0°$.

At low-α, $C_N \simeq C_L$ so that a_0 maybe determined from the normal force curve. By observation of the C_N curve of Figure 6.17, this value was determined to be $a_0 = 5.7$. Using this value of a_0, a curve that represents the normal force behaviour of the aerofoil can be drawn. At low-α the curve will generally satisfy equation (6.57a) and will fit the measured data. However, as α increases and the

aerofoil approaches stall, ideal-fluid theory breaks down. Here only measured values of C_N will truly represent the aerofoil behaviour at these angles of attack. The curve must pass through the measured values as stall approaches. The solid C_N curve shown in Figure 6.17 is just such a curve. At low-α it satifies equation (6.57a) but as stall approaches it is faired through the measured values of C_N. Notice that the nominal values of angle of attack have been ignored since it was not possible to accurately set the zero-attack condition in the wind tunnel.

A similar procedure can be adopted for representing the thrust force behaviour of the aerofoil. Here the low-α curve generally satifies equation (6.57b), and as stall approaches the curve is faired through the actual measured values of CT. The solid C_T curve shown in Figure 6.17 is just such a curve. Notice here that not only does the curve include an angle of attack offset, which is determined from the C_N graph, but that it includes a pressure drag component which the ideal-fluid theory ignores. Consequently, C_T will be negative at the true zero-attack condition.

The solid curves in both graphs of Figure 6.17 show the observed stall condition at the nominal angle of attack for this particular Reynolds Number.

In order to compare the aerofoil behaviour at different Reynolds Number, the solid curves of Figure 6.17 were used to make templates from which the solid curves in Figures 6.9 to 6.16 were constructed. At each Reynolds Number, the solid curve represents what is considered to be the best-fit through the measurements. The angle of attack offset is determined from the normal force graph and used on the thrust force graph to determine the pressure drag at zero-attack.

Looking at all the graphs, the measured values of C_N and C_T compare well at low-α to the solid curves if the measurements of C_T are ignored for $\alpha \leq 4°$. However as the aerofoil nears stall the measurements deviate away from the solid curves and the difference seems to progressively increases as the Reynolds Number decreases. Where deviation occurs, the measured values of C_N are seen to be larger than those followed by the solid line. This behaviour is curious since it suggests that the maximum value of C_L does not increase with increasing Reynolds Number as is usually observed of the four-digit NACA series of aerofoils. The author offers the following explanation for this behaviour.

Inspection of the pressure envelope calculated using CALCCN2, typically Figure 6.19, shows that for low Reynolds Number a suction "bubble" appears on the upper surface of the aerofoil. As Reynolds Number decreases the angle of attack at which the bubble first appears becomes smaller. The effect of the bubble is to increase the area bounded by the pressure envelope, so the measured values of C_N are larger than if the bubble did not exist. As the angle of attack increases, the bubble size increases so C_N continues to be larger than if the bubble did not exist. The large values of C_N at angles of attack near to stall result from the presence of the bubble. The influence of the bubble diminishes as Reynolds Number increases, and its presence is difficult to discern in the plots of Figure 6.18.

The bubble also affects the calculation of C_T, but its influence is less well defined. The bubble appears forward of the position of maximum thickness, so the forward suction pressures are slightly larger then if it did not exist. Consequently, C_T is calculated to be larger. However, the overall difference is small.

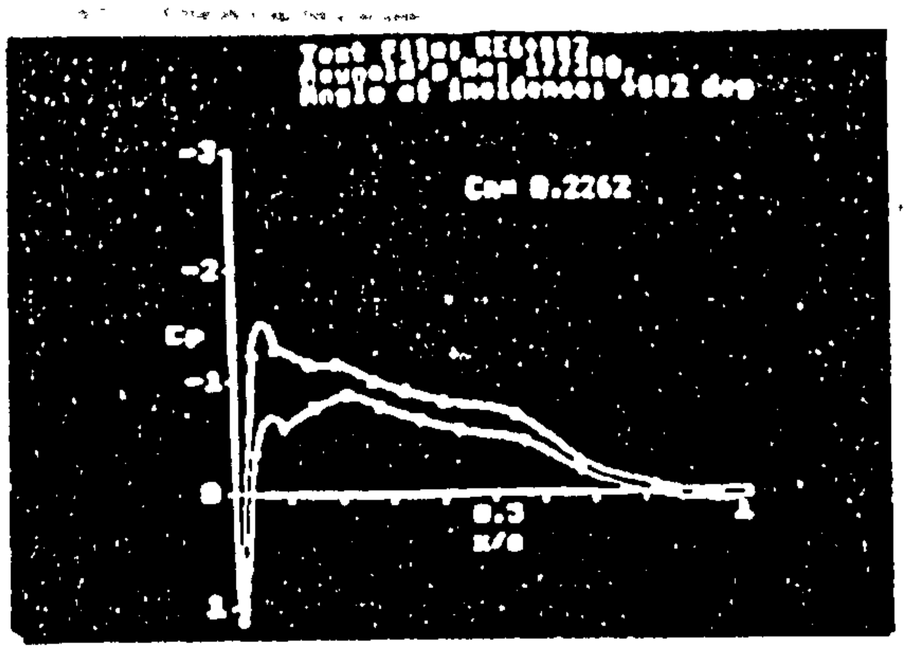

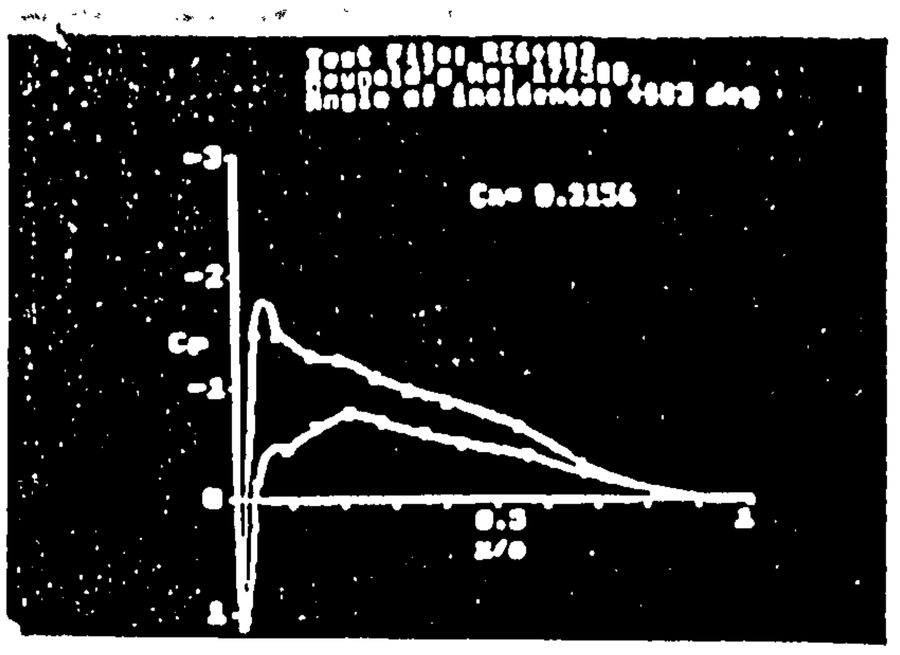

Figure 6.19a: C_p plots at α = 2° & 3° for Re = 177,000

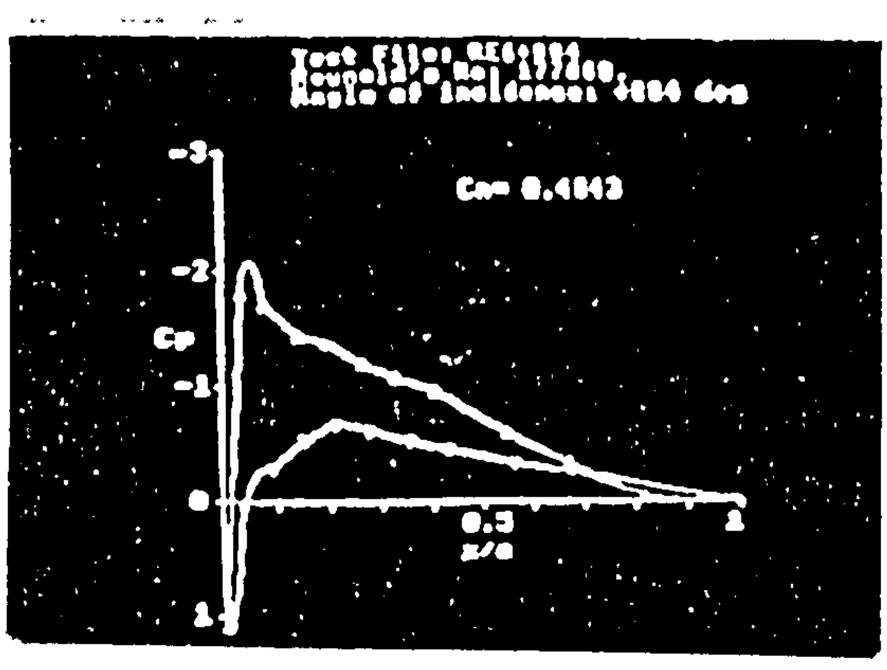

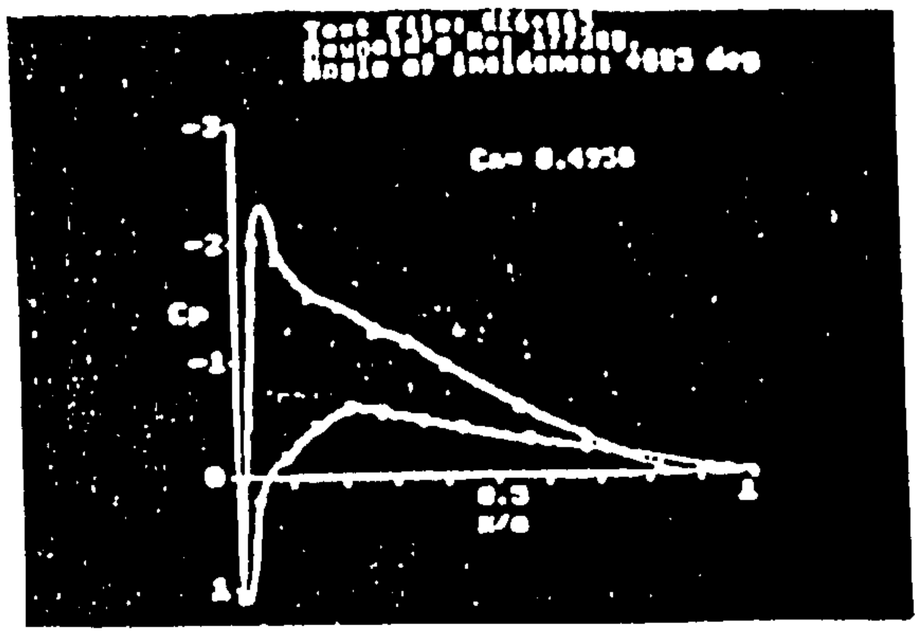

Figure 6.19b: C_p plots at α = 4° & 5° for Re = 177,000

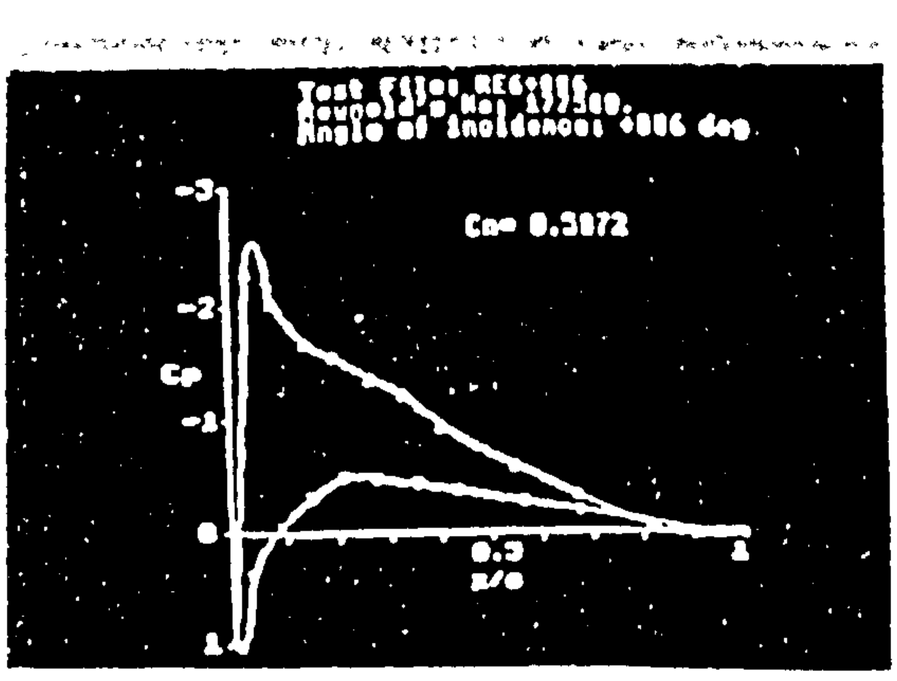

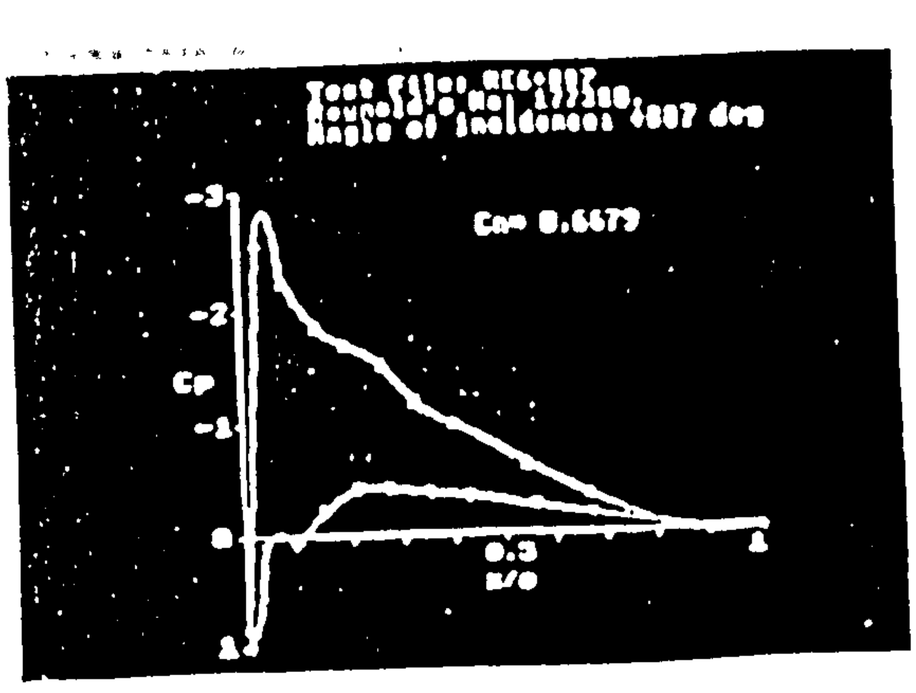

Figure 6.19c: C_p plots at α = 6° & 7° for Re = 177,000

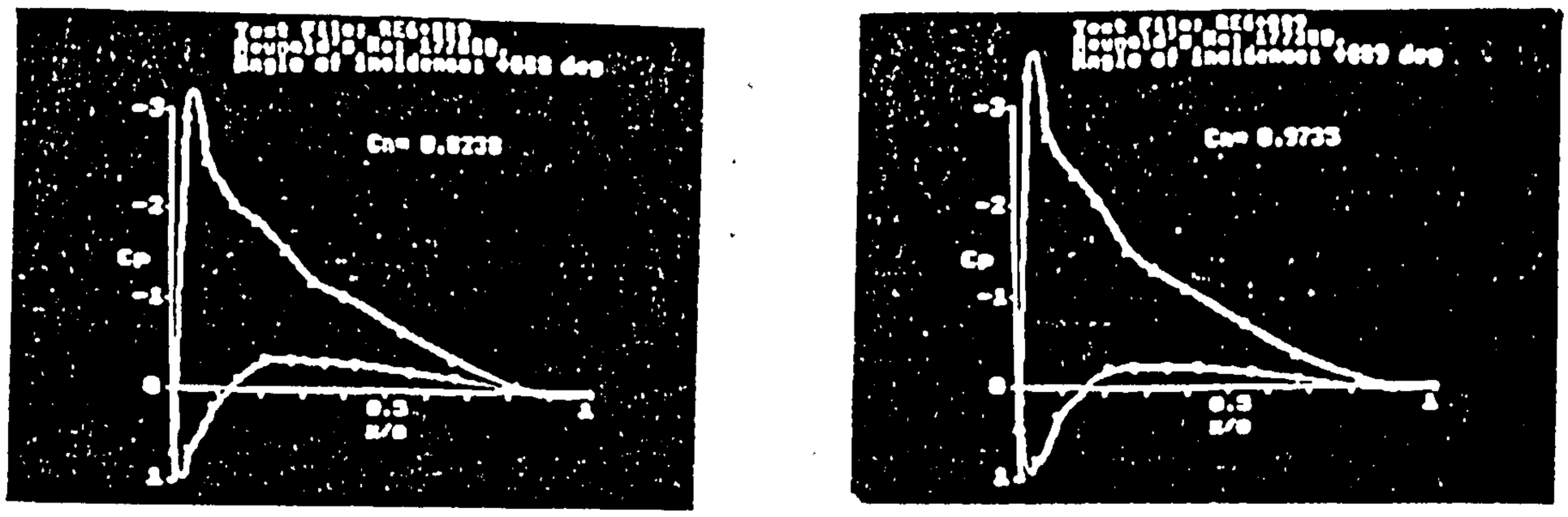

Figure 6.19d: C_{p_∞} plots at α = 8° & 9° for Re = 177,000

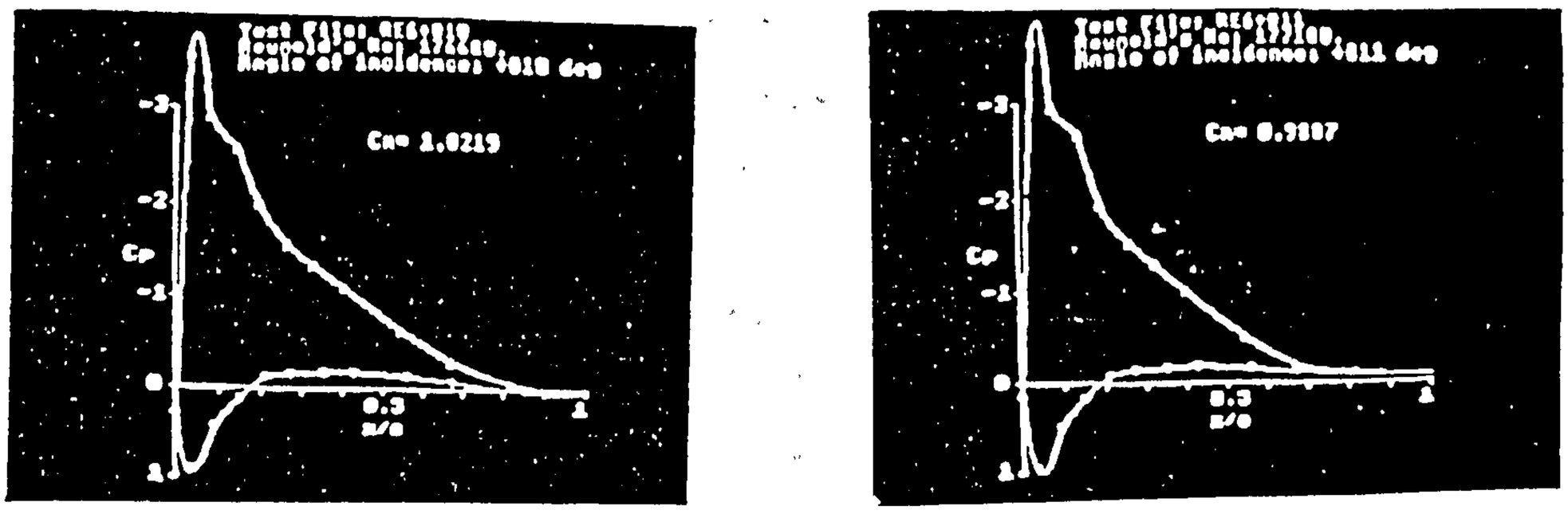

Figure 6.19e: C_{p_∞} plots at α = 10° & 11° for Re = 177,000

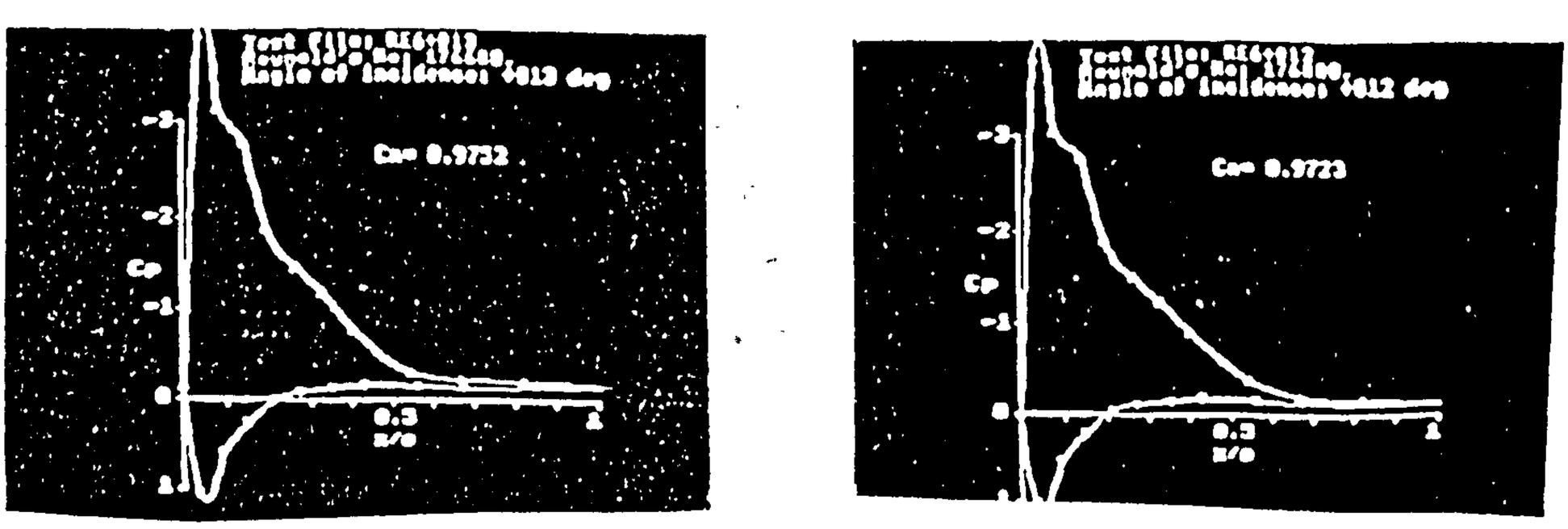

Figure 6.19f: C_{p_∞} plots at α = 12° & 13° for Re = 177,000

Whether the bubble is a feature of the NACA0025 aerofoil in general or whether it is peculiar to this particular test section is not known; the author considers the latter to be the more likely, since the sensitivity of the aerofoil behaviour to imperfections of manufacture will increase as Reynolds Number decreases. Since the influence of the bubble appears to decrease with increasing Reynolds Number, the author considers the behaviour of the aerofoil is more reliably described by the measurements made at the highest Reynolds Number of 240,000. Therefore the C_N-α and C_T-α curves are based upon the aerofoil characteristics observed at this Reynolds Number. These characteristics are represented by the solid curves.

Observation of Figures 6.9 to 6.17 shows that the author has chosen to ignore the large C_N results where the bubble effect is considered unreasonable. At the time of the analysis this seemed reasonable in order that a consistent set of results could be generated.

The early post-stall behaviour of the aerofoil is detailed in Figure 6.20. Here all post-stall measurements have been plotted on the same graph, though the nominal angle of attack has been corrected at each Reynolds Number using the offsets determined from Figures 6.9 to 6.17.

The normal force graph confirms the common held belief that post-stall behaviour of the aerofoil is independent of Reynolds Number. The solid curve indicates the best-fit considered by the author to be acceptble. The thrust force graph generally confirms the above observation, though the magnitude of the force does vary with Reynolds Number for angles of attack $\alpha > 14°$. Although no indication is made of the Reynolds Number of each measurement, the solid C_T curve of Figure 6.20 is faired through the higher Reynolds Number measurements.

The solid curves on both graphs have been faired into the deep-stall measurements to ensure continuity between datasets.

6.11.2: Results of Static Pressure Tests at High Angles of Incidence

The static pressure tests performed at high angles of attack were all conducted at a single Reynolds Number of Re ≃ 130,000. The early post-stall measurements conducted at different Reynolds Numbers confirmed the validty of assuming the post-stall behaviour of the aerofoil to be Reynolds Number independent. Measurements were made at five-degree intervals of angle of attack upto α=180°, when the aerofoil operates in reversed flow with the trailing-edge upwind of the leading-edge. The uncorrected measurements of normal and thrust force calculated using CALCCN2 and CALCCT2 are tabulated in Table 6.4.

The uncorrected measurements of normal and thrust force are shown in Figure 6.21; these are faired into the low-α results for the tests conducted at a similar Reynolds Number. The results are considered to be highly reliable and the solid curve represents the best-fit as considered by the author. There appears to be little need for correction except those required for interference effects.

6.11.3: Results of momentum traverse tests at low angles of attack

The primary objective of the momentum traverse tests was to determine the profile drag of the aerofoil section at low angles of attack. The measurements made here include both the friction drag and pressure drag components of the

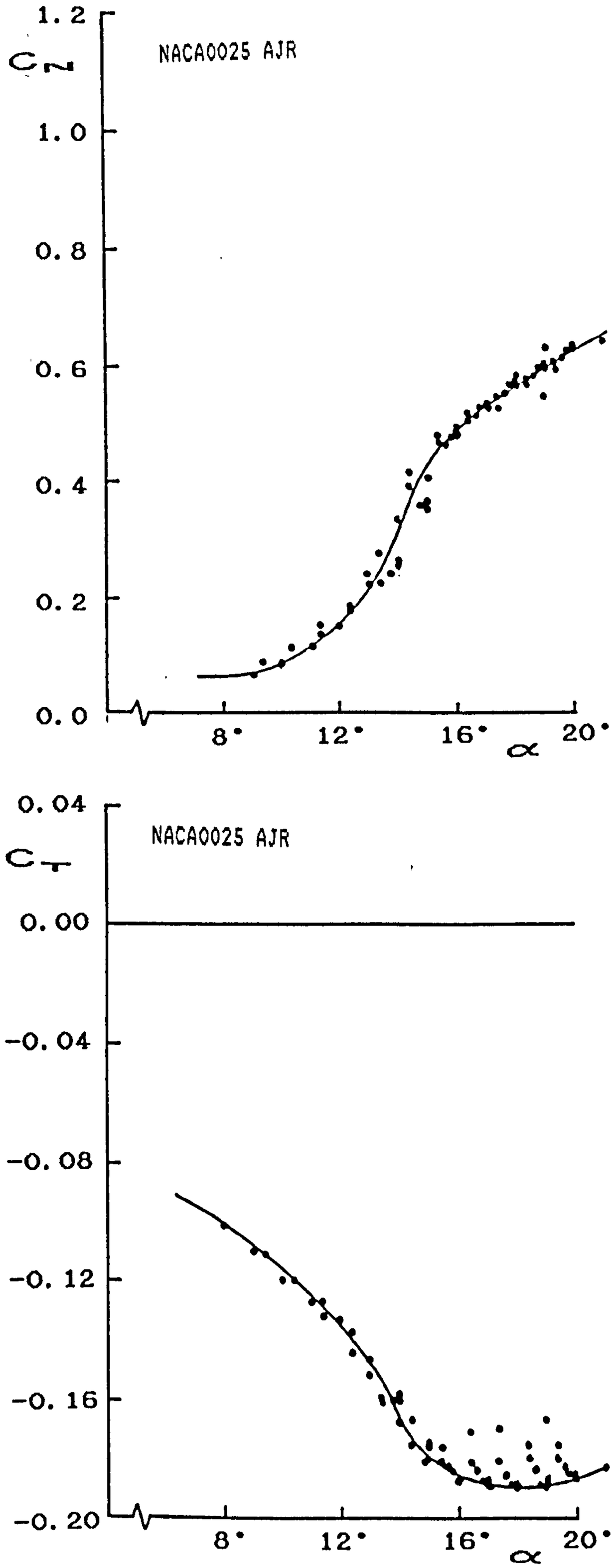

Figure 6.20: Uncorrected post-stall values of C_N and C_T at low angles of attack for all Reynolds Number

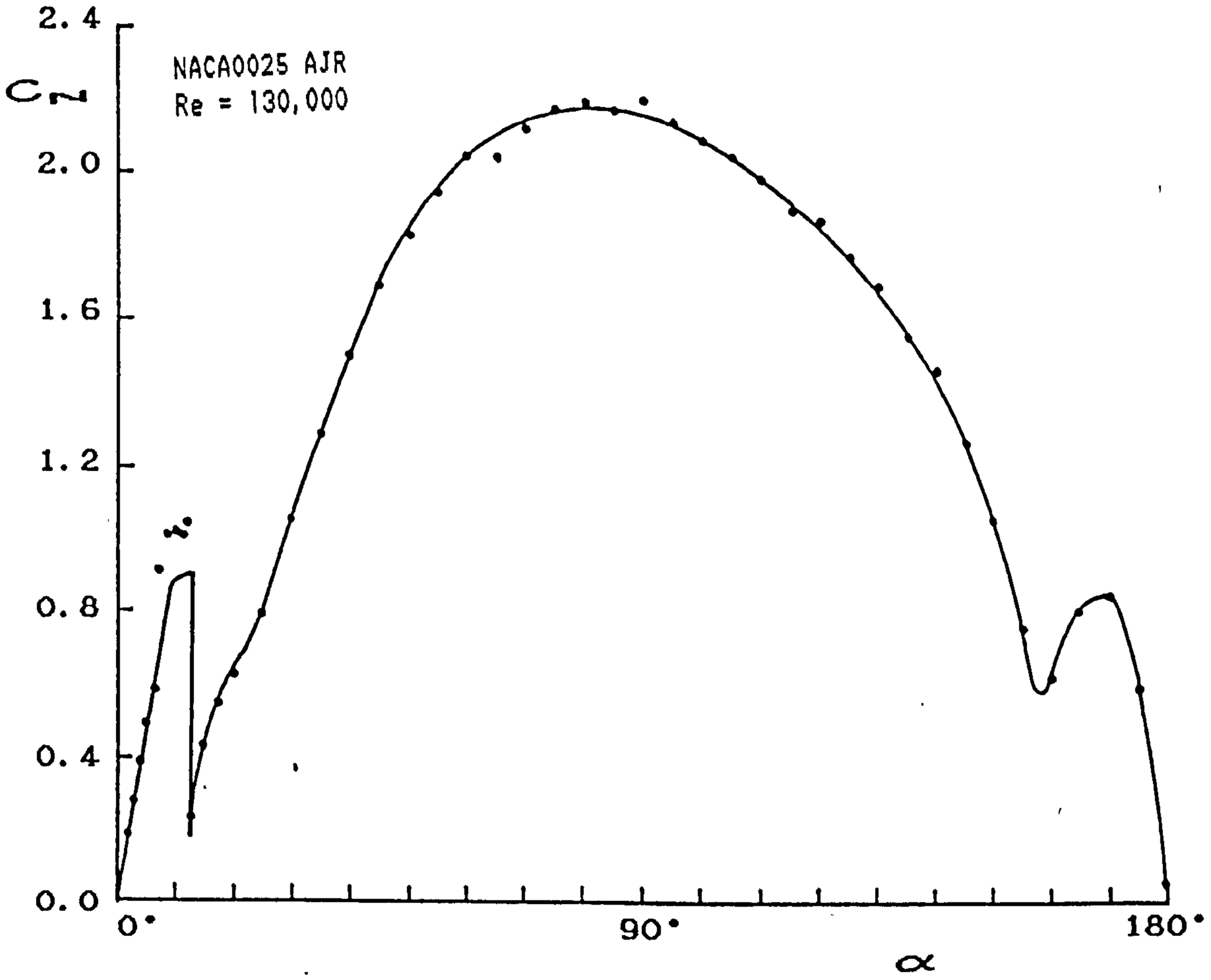

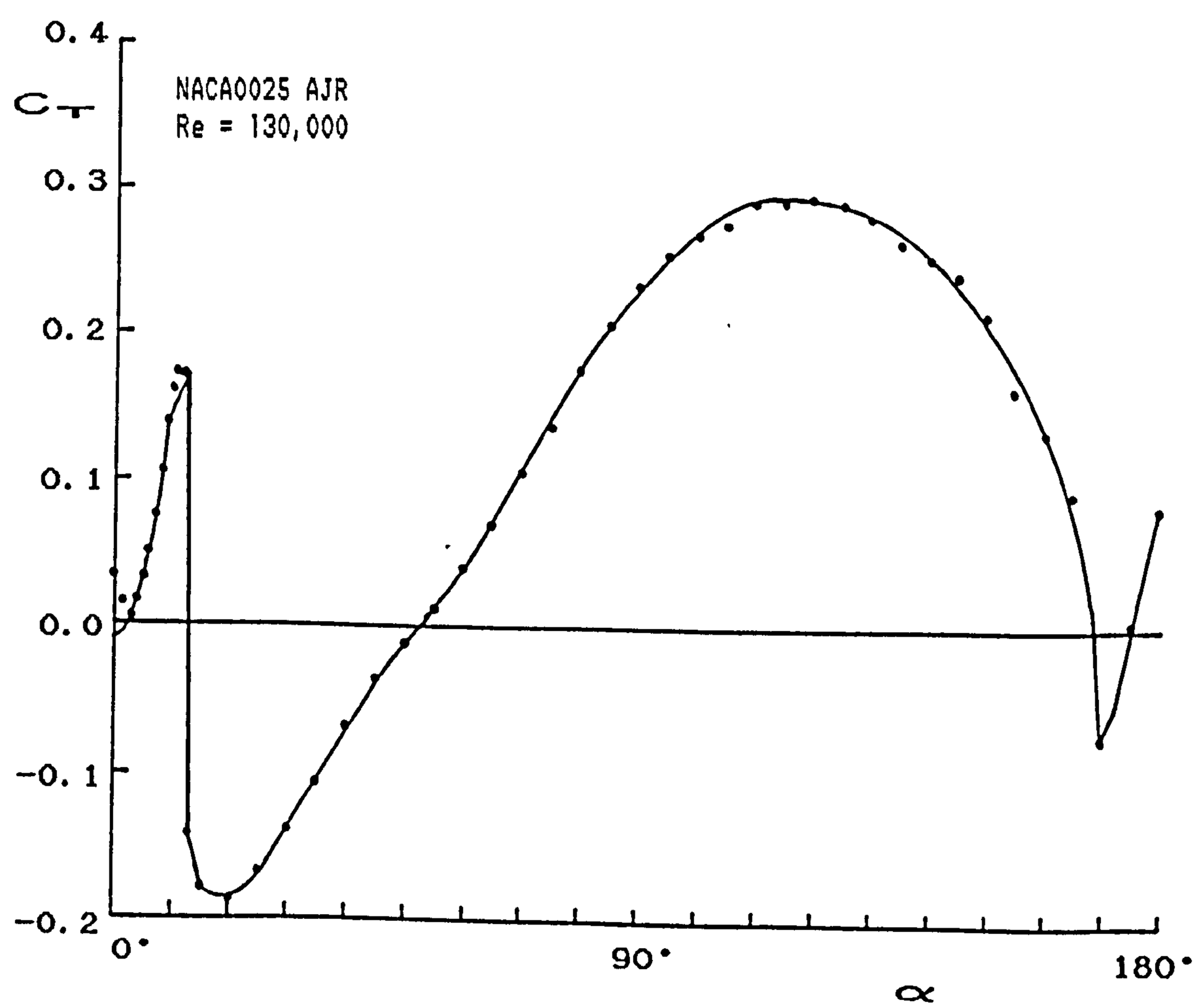

Figure 6.21: Uncorrected post-stall values of C_N and C_T at high angles of attack for Re ≈ 130,000

total drag force acting on the test section. The results of these tests would be used to modify the values of C_T to include friction drag.

A total of 48 momentum traverse tests were conducted at low angles of attack. The values of C_D determined using CALCCD2 are tabulated in Table 6.5. It should be noted that in practice the value of C_D was found to be highly sensitive to the value of the total head in the flow outside the wake, H_∞. As discussed previously, the calculation of C_D is subject to large relative errors, since the measurements of the total head inside and outside the wake are similar. This is reflected in the the scatter of the measured values of C_D at each Reynolds Number. From the measurements alone it is difficult to determine the influence of Reynolds Number or angle of attack on C_D. In order to gain a greater insight into the behaviour of the drag force, it was necessary to fit the measurements to the second order polynomial:

$$C_D = a + b\alpha^2 \qquad (6.58)$$

using a least-squared fitting routine. Of the two constants in equation (6.58), a is the most significant since it is equivalent to the profile drag at zero-attack C_{D0}. Determining C_{D0} alone would still enable the values of C_T to be modified to include friction drag.

Using the results of Table 6.5 and ignoring those measured when the aerofoil had stalled, the values of C_{D0} at each Reynolds was determined. These "synthesised" values of C_{D0} are given in Table 6.6, and plotted with respect to log(Re) in Figure 6.22. The variation of C_{D0} can be linearised over the range of the test Reynolds Numbers and a value of C_{D0} Re = 240,000 determined. It is, however,

α	C_N	α	C_N	α	C_N	α	C_N	α	C_N
21°	0,644	25°	0,789	30°	1,059	35°	1,294	40°	1,503
45°	1,689	50°	1,835	55°	1,943	60°	2,044	65°	2,032
70°	2,120	75°	2,169	80°	2,188	85°	2,166	90°	2,191
95°	2,136	100°	2,086	105°	2,041	110°	1,980	115°	1,901
120°	1,874	125°	1,777	130°	1,695	135°	1,551	140°	1,462
145°	1,275	150°	1,064	155°	0,758	160°	0,625	165°	0,804
170°	0,853	175°	0,597	180°	0,058				

Table 6.4a: Uncorrected post-stall values of C_N

α	C_T	α	C_T	α	C_T	α	C_T	α	C_T
21°	-0,183	25°	-0,169	30°	-0,140	35°	-0,106	40°	-0,068
45°	-0,035	50°	-0,010	55°	0,012	60°	0,040	65°	0,071
70°	0,108	75°	0,139	80°	0,176	85°	0,209	90°	0,234
95°	0,256	100°	0,270	105°	0,279	110°	0,292	115°	0,294
120°	0,297	125°	0,292	130°	0,284	135°	0,267	140°	0,256
145°	0,242	150°	0,216	155°	0,164	160°	0,135	165°	0,095
170°	-0,072	175°	0,047	180°	0,085				

Table 6.4b: Uncorrected post-stall values of C_T

	Reynolds Number							
α	86000	103000	122000	138000	156000	177000	194000	214000
0°	0,051	0,040	0,035	0,036	0,033	0,031	0,027	0,025
2°	0,043	0,040	0,034	0,032	0,030	0,027	0,028	0,025
4°	0,050	0,042	0,024	0,033	0,028	0,030	0,027	0,024
6°	0,039	0,032	0,021	0,032	0,026	0,025	0,025	0,022
8°	0,040	0,047	0,039	0,041	0,035	0,054	0,032	0,034
10°	0,101	0,084	0,060	0,039	0,036	0,041	0,041	0,035

Table 6.5: Uncorrected values of C_D

	Reynolds Number								
	86000	103000	122000	138000	156000	177000	194000	214000	240000
C_{Do}	0,048	0,038	0,026	0,033	0,029	0,028	0,025	0,023	----

Table 6.6: Values of zero-attack profile drag C_{Do} determined by least-squared fit

	Reynolds Number								
	86000	103000	122000	138000	156000	177000	194000	214000	240000
C_{Do}	0,043	0,039	0,035	0,033	0,030	0,027	0,025	0,023	0,021

Table 6.7: Variation of C_{Do} with Reynolds Number

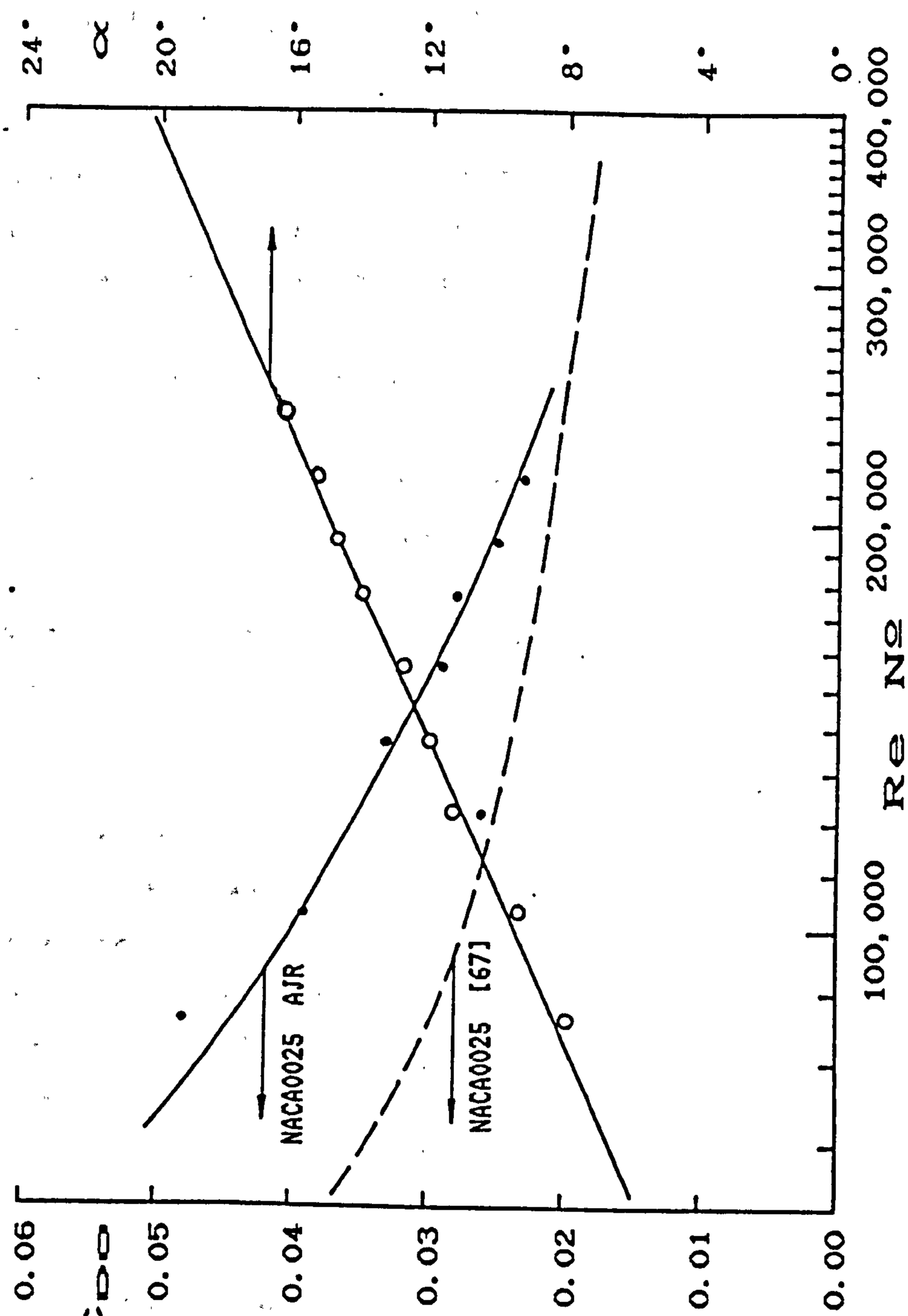

Figure 6.22: Variation of C_{DO} and stall angle with Reynolds Number

unreasonable to extrapolate much further beyond the synthesised values. The linearisation can be used to modify the values of C_{DO} at each Reynolds Number as appropriate; these new values are shown in Table 6.7. These values can be used to modifiy the measured values of C_T to include a friction drag component. The results of such a modification are not included here since the C_T values of the final dataset will include drag force components derived from another source.

Hoerner presents data for the section-drag coefficient, i.e. C_{DO}, of a number of 25% thick symmetrical sections over a range of Reynolds Number [67]. The results given extend well beyond the range of Reynolds Number for the tests conducted here. This data includes values of C_{DO} for a NACA0025 section, which have been superimposed onto Figure 6.22 for comparison. The sythesised values of C_{DO} show good correlation to those presented by Hoerner, and whilst they are larger in magnitude, this is not unreasonable considering the size and manner in which the test aerofoil has been manufactured. If values of C_{DO} are required at Reynolds Numbers higher than 240,000 for the purposes of generating a dataset for use with VAWTTAY, then the synthesised values show that the data presented by Hoerner should be used.

Since the overall drag force at zero-attack has been determined with some degree of confidence for each Reynolds Number, it is now possible to estimate the tunnel interference effects.

6.11.4: Applying the Tunnel Interference Corrections

As discussed previously, corrections for tunnel blockage effects must be considered, but the corrections for lift

effect will be neglible. At low angles of attack $C_{D_T} \approx C_{D_0}$; this implies that the wake blockage correction, ε_w, is of the same order of magnitude as the solid blockage correction, ε_w, so that the overall blockage correction, ε, is approximately one-fifth of one per-cent. It was therefore considered unecessary to modify the pre-stall measurements of C_N or C_T to account for interference effects.

When the aerofoil stalls, the drag force increases significantly, so wake blockage corrections cannot be ignored. The drag force is calculated using equation (6.11b). However, beyond stall, friction drag is less significant than pressure drag, so for simplicity all calculated values of C_{D_T} were determined from the pressure test measurements of C_{N_T} and C_{T_T} alone. The wake blockage correction is calculated using equation (6.49).

Also, as the angle of attack rises, the solid blockage correction increases to a maximum value at $\alpha = 90°$. Beyond this angle, the solid blockage correction decreases as the aerofoil moves towards the reversed flow condition. While solid blockage corrections are not as large as those for wake blockage, they cannot be ignored. The solid blockage correction is calculated using equation (6.46).

It was convenient to modify *all* post-stall measurements to include wake blockage and solid blockage corrections using equation (6.56). These modified force coefficents are used to create the single post-stall dataset tabulated in Table 6.9. All post-stall forces are considered to be independent of Reynolds Number.

6.12: The Creation of a NACA0025 dataset for use with VAWTTAY

In developing a normal force and thrust force dataset for use with VAWTTAY, the modified measurements have been used where considered appropriate. However, since the model V-VAWT operates at Reynolds Numbers in excess of 240,000, it has been necessary to extrapolate the pre-stall test data beyond this Reynolds Number. Linear extrapolation has been used to determine both the force coefficients and static stall angles at Reynolds Numbers upto 400,000. Such techniques have to be used with caution but are considered appropriate here. The modified post-stall data is considered Reynolds Number independent and therefore can be used without further modification, consequently the following discussion considers the pre-stall data alone.

As discussed previously, the solid curves shown in Figures 6.9 to 6.17 are considered to be representative of the true behaviour of the aerofoil given that the thrust force values are modified to include friction drag. The templates developed from these curves have been used to generate pre-stall forces over the range of Reynolds Number Re = 65,000 to 400,000. The thrust force has been modified to include a friction drag component of such magnitude that the zero-attack profile drag C_{DO}, is that given by Hoerner. While this effectively ignores the synthesised values of C_{DO}, the final dataset is probably more representative of the NACA0025 section in general.

It is worth noting that it is considered that the NACA0025 section would only be used for a free-air V-VAWT at the root of the blade where its superior structural properties would be more advantageous than those of a thinner aerofoil sections. While the chord would be significantly larger than the test aerofoil, close to the blade root the

local Reynolds Number would be similar to the higher Reynolds Number of this dataset. The blade profile drag would be that value given by Hoerner, since the quality of surface finish and profile shape would be much better than that of the test aerofoil. Consequently by developing a thrust force dataset based upon the C_{DO} values presented by Hoerner, predictions of the free-air section could be made with confidence provided the local Reynolds Number did not extend beyond the limits of the dataset.

The values of the normal force and thrust force coefficients are presented in Tables 6.8 and 6.9. This dataset is in a format suitable for use with VAWTTAY, and was transferred immediately to a suitable datafile by the author. The C_N-α and C_T-α characteristic curves are plotted in Figures 6.23 and 6.24.

6.13: Summary of Observations and Conclusions

The wind tunnel testing of a small NACA0025 aerofoil has enabled a dataset of normal and thrust force coefficients, suitable for use with the aerodynamic performance prediction program VAWTTAY, to be created. The C_N and C_T values calculated from the computer based integration of static pressure measurements have been comprehensively refined to ensure that a consistent dataset has been created. This dataset consists of pre-stall C_N and C_T values for a range of Reynolds Number upto Re = 400,000, and post-stall C_N and C_T values which are considered to be Reynolds Number independent.

In creating the pre-stall data, ideal-fluid theory was used to develop low-α C_N and C_T values for each Reynolds Number setting. These values were modified to include the friction drag effects noted by Hoerner for this aerofoil

α	Reynolds Number 65000	80000	100000	120000	145000	180000	220000	265000	325000	400000
0°	0,000	0,000	0,000	0,000	0,000	0,000	0,000	0,000	0,000	0,000
1°	0,099	0,099	0,099	0,099	0,099	0,099	0,099	0,099	0,099	0,099
2°	0,199	0,199	0,199	0,199	0,199	0,199	0,199	0,199	0,199	0,199
3°	0,297	0,297	0,297	0,297	0,297	0,297	0,297	0,297	0,297	0,297
4°	0,396	0,396	0,396	0,396	0,396	0,396	0,396	0,396	0,396	0,396
5°	0,494	0,494	0,494	0,494	0,494	0,494	0,494	0,494	0,494	0,494
6°	0,592	0,592	0,592	0,592	0,592	0,592	0,592	0,592	0,592	0,592
7°	0,059	0,689	0,689	0,689	0,689	0,689	0,689	0,689	0,689	0,689
8°	0,059	0,059	0,785	0,785	0,785	0,785	0,785	0,785	0,785	0,785
9°	0,064	0,064	0,870	0,870	0,870	0,870	0,870	0,870	0,870	0,870
10°	0,089	0,089	0,089	0,895	0,895	0,895	0,895	0,895	0,895	0,895
11°	0,119	0,119	0,119	0,119	0,900	0,900	0,900	0,900	0,900	0,900
12°	0,158	0,158	0,158	0,158	0,905	0,905	0,905	0,905	0,905	0,905
13°	0,217	0,217	0,217	0,217	0,217	0,910	0,910	0,910	0,910	0,910
14°	0,276	0,276	0,276	0,276	0,276	0,920	0,920	0,920	0,920	0,920
15°	0,365	0,365	0,365	0,365	0,365	0,365	0,930	0,930	0,930	0,930
16°	0,448	0,448	0,448	0,448	0,448	0,448	0,448	0,940	0,940	0,940
17°	0,507	0,507	0,507	0,507	0,507	0,507	0,507	0,950	0,950	0,950
18°	0,545	0,545	0,545	0,545	0,545	0,545	0,545	0,545	0,960	0,960
19°	0,579	0,579	0,579	0,579	0,579	0,579	0,579	0,579	0,579	0,970
20°	0,613	0,613	0,613	0,613	0,613	0,613	0,613	0,613	0,613	0,980

Table 6.8a: C_N at low angles of attack

α	Reynolds Number 65000	80000	100000	120000	145000	180000	220000	265000	325000	400000
0°	-0,036	-0,031	-0,026	-0,024	-0,022	-0,021	-0,020	-0,019	-0,018	-0,017
1°	-0,035	-0,030	-0,025	-0,023	-0,021	-0,020	-0,019	-0,018	-0,017	-0,016
2°	-0,029	-0,024	-0,019	-0,017	-0,015	-0,014	-0,013	-0,012	-0,011	-0,010
3°	-0,021	-0,016	-0,011	-0,009	-0,007	-0,006	-0,005	-0,004	-0,003	-0,002
4°	-0,009	-0,004	0,001	0,003	0,005	0,006	0,007	0,008	0,009	0,010
5°	0,007	0,012	0,017	0,019	0,021	0,022	0,023	0,024	0,025	0,026
6°	0,026	0,031	0,036	0,038	0,040	0,041	0,042	0,043	0,044	0,045
7°	-0,094	0,053	0,058	0,060	0,062	0,063	0,064	0,065	0,066	0,067
8°	-0,101	-0,101	0,084	0,086	0,088	0,089	0,090	0,091	0,092	0,093
9°	-0,108	-0,108	0,113	0,115	0,117	0,118	0,119	0,120	0,121	0,122
10°	-0,116	-0,116	-0,116	0,137	0,139	0,140	0,141	0,142	0,143	0,144
11°	-0,125	-0,125	-0,125	-0,125	0,150	0,151	0,152	0,153	0,154	0,155
12°	-0,134	-0,134	-0,134	-0,134	0,161	0,162	0,163	0,164	0,165	0,166
13°	-0,146	-0,146	-0,146	-0,146	-0,146	0,174	0,175	0,176	0,177	0,178
14°	-0,165	-0,165	-0,165	-0,165	-0,165	0,186	0,187	0,188	0,189	0,190
15°	-0,178	-0,178	-0,178	-0,178	-0,178	-0,178	0,197	0,198	0,199	0,200
16°	-0,183	-0,183	-0,183	-0,183	-0,183	-0,183	-0,183	0,209	0,210	0,211
17°	-0,185	-0,185	-0,185	-0,185	-0,185	-0,185	-0,185	0,221	0,222	0,223
18°	-0,185	-0,185	-0,185	-0,185	-0,185	-0,185	-0,185	-0,185	0,234	0,235
19°	-0,184	-0,184	-0,184	-0,184	-0,184	-0,184	-0,184	-0,184	-0,184	0,247
20°	-0,182	-0,182	-0,182	-0,182	-0,182	-0,182	-0,182	-0,182	-0,182	0,269

Table 6.8b: C_T at low angles of attack

α	C_N	α	C_N	α	C_N	α	C_N	α	C_N
21°	0,613	22°	0,676	23°	0,706	24°	0,737	25°	0,771
26°	0,819	27°	0,869	28°	0,922	29°	0,974	30°	1,027
31°	1,073	32°	1,118	33°	1,162	34°	1,204	35°	1,245
36°	1,284	37°	1,323	38°	1,361	39°	1,397	40°	1,433
41°	1,468	42°	1,501	43°	1,534	44°	1,565	45°	1,595
46°	1,622	47°	1,648	48°	1,672	49°	1,695	50°	1,716
51°	1,735	52°	1,752	53°	1,769	54°	1,785	55°	1,800
56°	1,819	57°	1,837	58°	1,853	59°	1,867	60°	1,877
61°	1,875	62°	1,871	63°	1,865	64°	1,860	65°	1,857
66°	1,867	67°	1,880	68°	1,893	69°	1,908	70°	1,921
71°	1,930	72°	1,937	73°	1,943	74°	1,948	75°	1,952
76°	1,956	77°	1,958	78°	1,959	79°	1,960	80°	1,959
81°	1,954	82°	1,948	83°	1,942	84°	1,937	85°	1,932
86°	1,935	87°	1,938	88°	1,941	89°	1,944	90°	1,944
91°	1,939	92°	1,932	93°	1,924	94°	1,914	95°	1,904
96°	1,897	97°	1,890	98°	1,883	99°	1,876	100°	1,869
101°	1,863	102°	1,857	103°	1,851	104°	1,845	105°	1,838
106°	1,831	107°	1,822	108°	1,813	109°	1,804	110°	1,794
111°	1,782	112°	1,769	113°	1,757	114°	1,745	115°	1,735
116°	1,732	117°	1,729	118°	1,727	119°	1,724	120°	1,719
121°	1,707	122°	1,693	123°	1,677	124°	1,660	125°	1,707
126°	1,632	127°	1,621	128°	1,609	129°	1,595	130°	1,580
131°	1,558	132°	1,533	133°	1,508	134°	1,484	135°	1,460
136°	1,446	137°	1,433	138°	1,419	139°	1,404	140°	1,387
141°	1,359	142°	1,328	143°	1,294	144°	1,259	145°	1,221
146°	1,187	147°	1,151	148°	1,113	149°	1,073	150°	1,029
151°	0,971	152°	0,911	153°	0,852	154°	0,794	155°	0,741
156°	0,698	157°	0,663	158°	0,636	159°	0,620	160°	0,614
161°	0,639	162°	0,673	163°	0,712	164°	0,753	165°	0,792
166°	0,819	167°	0,840	168°	0,852	169°	0,856	170°	0,848
171°	0,822	172°	0,783	173°	0,731	174°	0,669	175°	0,594
176°	0,509	177°	0,412	178°	0,304	179°	0,186	180°	0,057

Table 6.9a: C_N at high angles of attack

α	C_T	α	C_T	α	C_T	α	C_T	α	C_T
21°	-0,180	22°	-0,178	23°	-0,174	24°	-0,170	25°	-0,166
26°	-0,161	27°	-0,155	28°	-0,149	29°	-0,143	30°	-0,136
31°	-0,130	32°	-0,123	33°	-0,116	34°	-0,110	35°	-0,102
36°	-0,095	37°	-0,088	38°	-0,080	39°	-0,073	40°	-0,065
41°	-0,058	42°	-0,052	43°	-0,045	44°	-0,039	45°	-0,034
46°	-0,028	47°	-0,023	48°	-0,019	49°	-0,014	50°	-0,010
51°	-0,006	52°	-0,002	53°	0,002	54°	0,006	55°	0,011
56°	0,015	57°	0,020	58°	0,026	59°	0,031	60°	0,036
61°	0,042	62°	0,047	63°	0,053	64°	0,058	65°	0,064
66°	0,071	67°	0,078	68°	0,084	69°	0,091	70°	0,097
71°	0,103	72°	0,108	73°	0,114	74°	0,119	75°	0,125
76°	0,131	77°	0,137	78°	0,144	79°	0,151	80°	0,157
81°	0,163	82°	0,169	83°	0,175	84°	0,181	85°	0,186
86°	0,191	87°	0,195	88°	0,199	89°	0,203	90°	0,207
91°	0,212	92°	0,216	93°	0,220	94°	0,224	95°	0,228
96°	0,231	97°	0,234	98°	0,237	99°	0,239	100°	0,241
101°	0,243	102°	0,245	103°	0,247	104°	0,249	105°	0,251
106°	0,254	107°	0,256	108°	0,259	109°	0,262	110°	0,264
111°	0,265	112°	0,266	113°	0,267	114°	0,267	115°	0,268
116°	0,269	117°	0,269	118°	0,270	119°	0,271	120°	0,271
121°	0,271	122°	0,271	123°	0,271	124°	0,270	125°	0,270
126°	0,269	127°	0,268	128°	0,267	129°	0,266	130°	0,264
131°	0,262	132°	0,259	133°	0,256	134°	0,254	135°	0,251
136°	0,249	137°	0,247	138°	0,246	139°	0,244	140°	0,242
141°	0,241	142°	0,239	143°	0,237	144°	0,234	145°	0,231
146°	0,228	147°	0,224	148°	0,220	149°	0,215	150°	0,208
151°	0,199	152°	0,190	153°	0,180	154°	0,169	155°	0,160
156°	0,154	157°	0,148	158°	0,143	159°	0,138	160°	0,132
161°	0,129	162°	0,124	163°	0,117	164°	0,107	165°	0,093
166°	0,059	167°	0,022	168°	-0,014	169°	-0,046	170°	-0,072
171°	-0,069	172°	-0,057	173°	-0,040	174°	-0,019	175°	0,004
176°	0,028	177°	0,049	178°	0,067	179°	0,079	180°	0,084

Table 6.9b: C_T at high angles of attack

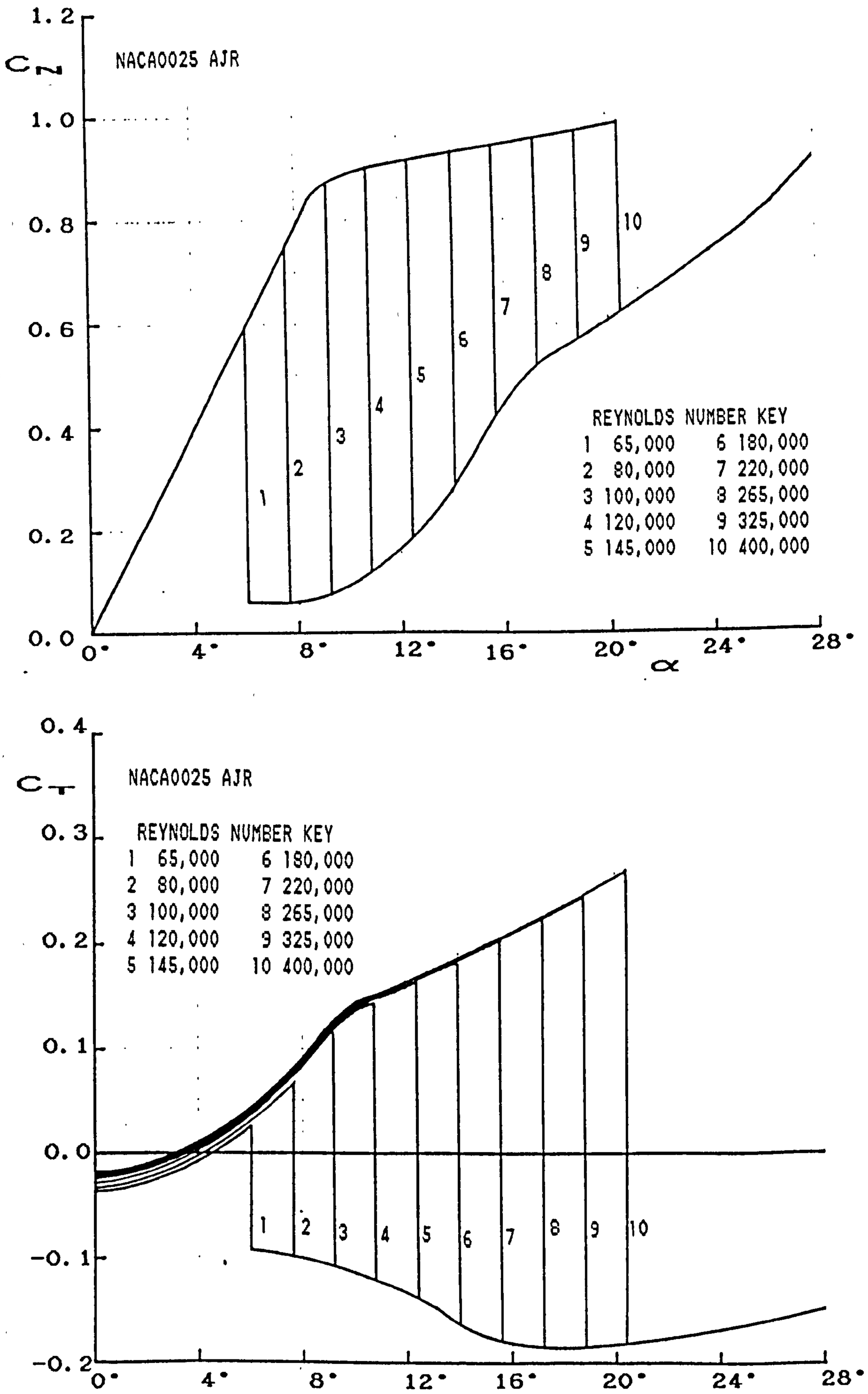

Figure 6.23: C_N-α and C_T-α at low angles of attack

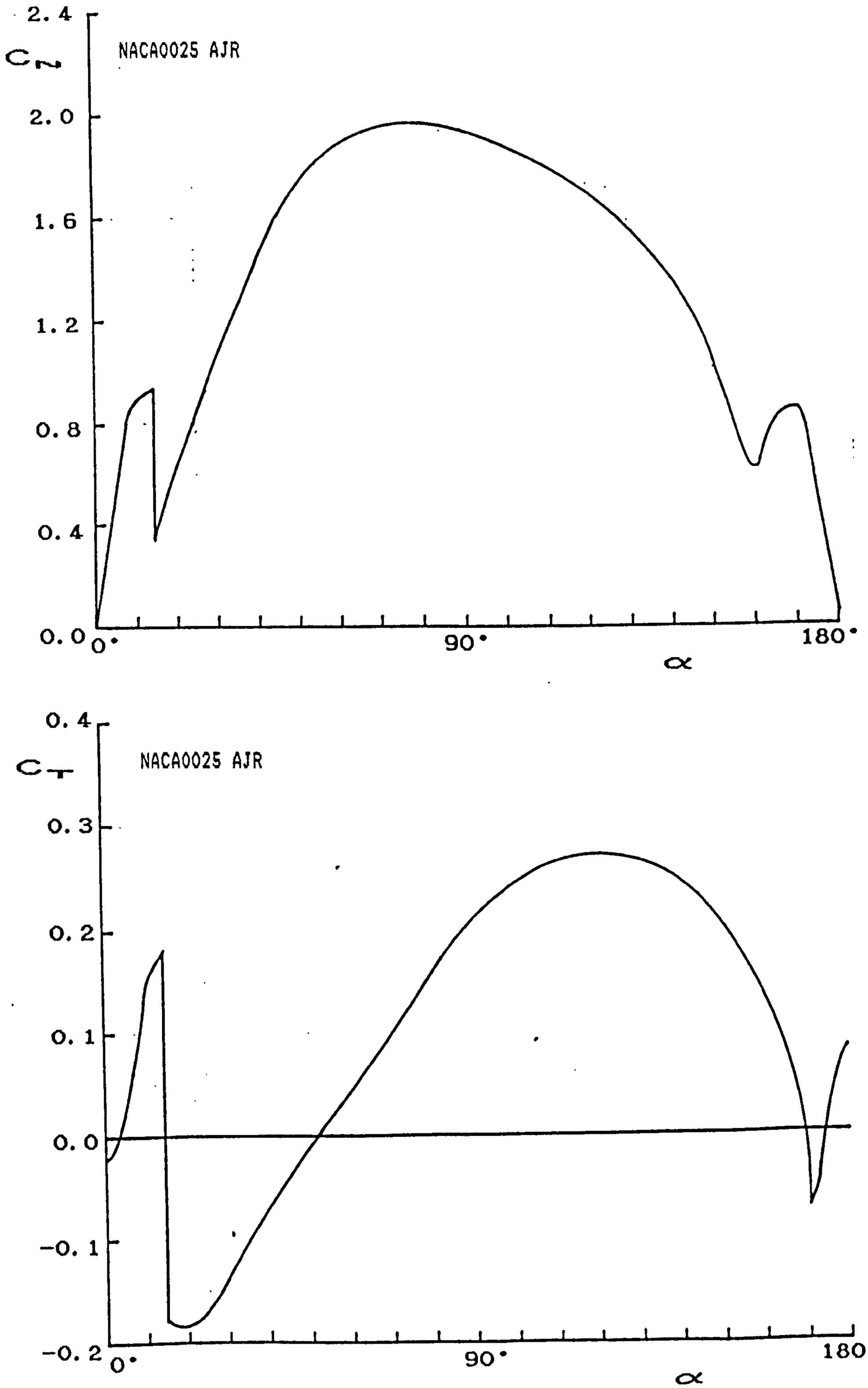

Figure 6.24: C_N-α and C_T-α at high angles of attack

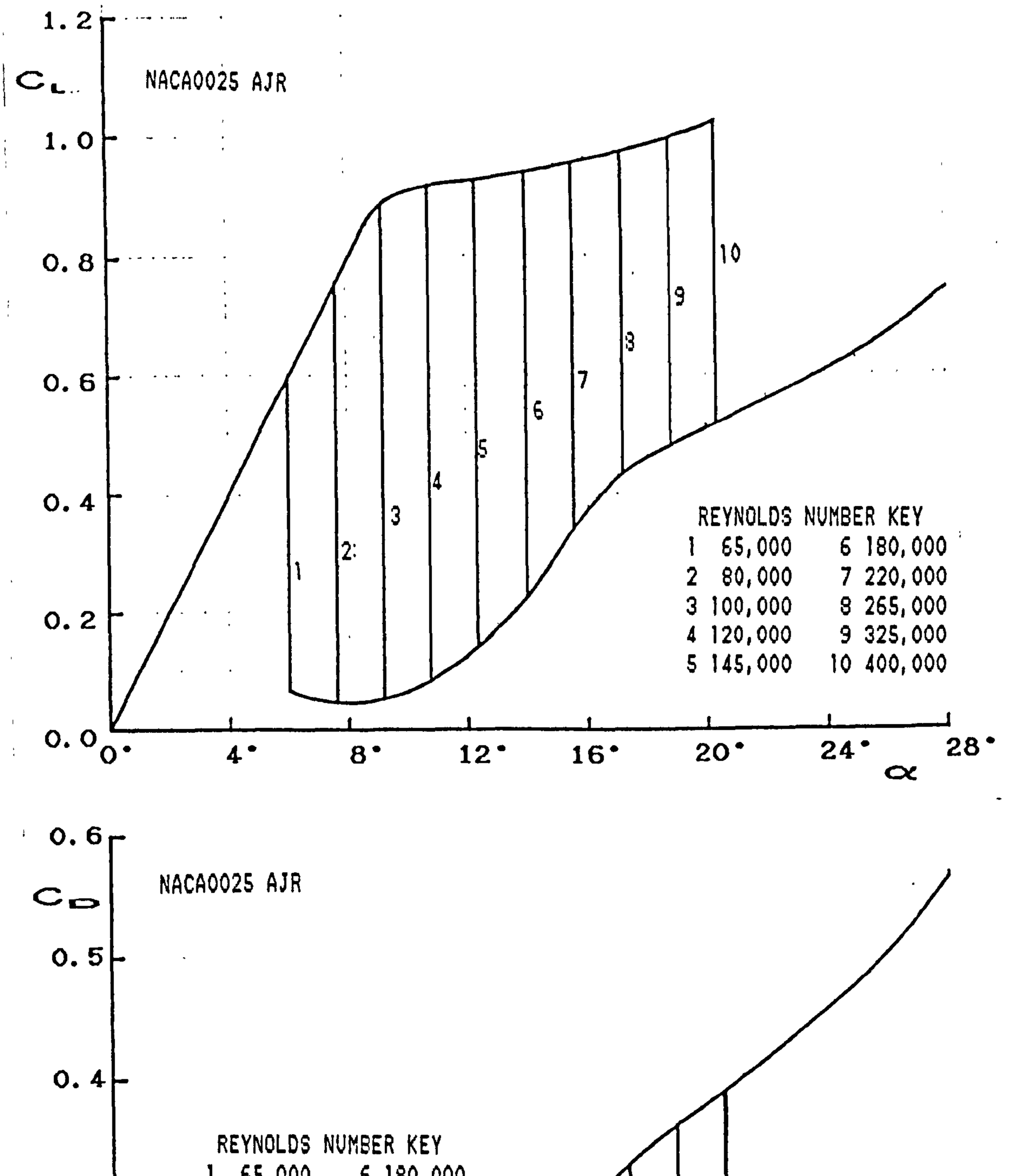

Figure 6.25: C_L-α and C_D-α at low angles of attack

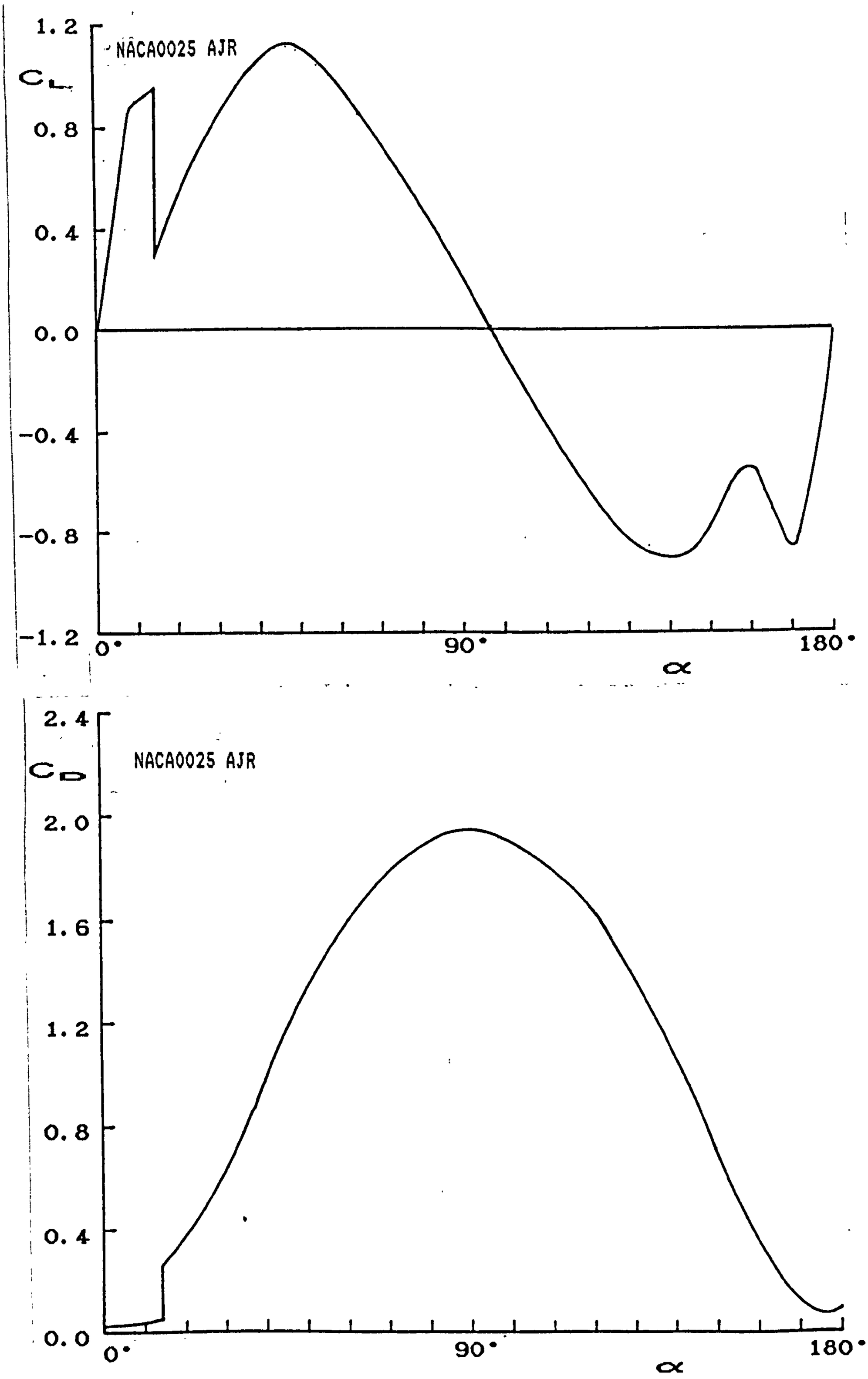

Figure 6.26: C_L-α and C_D-α at high angles of attack

section. Wind tunnel corrections were not applied to these coefficients. The Reynolds Number range of the dataset was extended using interpolation techniques.

The early post-stall data demonstrated that the behaviour of the aerofoil is Reynolds Number independent, allowing deep stall measurements to made at only one Reynolds Number setting. Measurements were made at 5° intervals of angle of incidence. The C_N and C_T values at intermediate angles were calculated using interpolation techniques. The coefficients were not modified for friction drag, but corrections for tunnel blockage were applied.

The characteristics of the aerofoil were continuously assessed and compared with the results of other NACA0025 tests or sections of the NACA four-digit family, to ensure the validity of the final dataset. To assist with the assessment, the normal and thrust force coefficients were used to calculate lift and drag force coefficients. These are plotted in Figures 6.25 and 6.26.

It is known that variations in lift curve slope caused by Reynolds Number increases are very small [66]. This slope provides a convenient method of comparing aerofoils, even if the data corresponds to different Reynolds Number measurements. Suprisingly, as Figure 6.27 shows, the behaviour of the test NACA0025 section is similar to that of sections with smaller fineness ratios. The slope of the lift curve at small angles of incidence from 0° to 6° is 0.099 per degree which compares favourably with that for the NACA0012, NACA0015 and NACA0018 sections [68], but it is significantly steeper than that of the NACA0025 data presented by Sheldahl and Klimas [26], or Bullivant [62].

The lift curve slope comparison demonstrates that the test aerofoil was as effective at generating lift as any other

four-digit NACA aerofoil, and that the low-α C_L data is reliable. Note that the C_N measurements required little modification, and since α is small $C_{L_{max}} \simeq C_{N_1}$, the measurements are therefore considered valid in this region.

At low-α, $C_D \simeq C_T$. Since ideal-fluid theory, using coefficients derived from the C_N data, and Hoerner's $C_{D_{SF}}$ values were used to modify the C_T measurements, the values of C_T and C_D can be considered reliable at low-α.

However, as α increases the similarity of the test aerofoil data with data from other sources diminishes.

Figure 6.28 shows the low-α lift and drag curves for a NACA0025 section over the same Reynolds Number range as the data presented here. These curves use data presented by Sheldahl and Klimas [26] that have be numerically generated at Sandia National Laboratories (SNL). This data does not show the sudden loss of lift observed in the tests reported here, though the shape of the pre-stall lift curves are similar. The onset of stall can only be judged from the drag curves, where a distinct rise in drag can be observed. The $C_{D_{SF}}$ values are smaller in magnitude, so that overall the drag is smaller; the stall angles are also much larger. The SNL data demonstrates that stall gradually occurs as the angle of incidence increases. Only small decreases in lift occur, and that increases in drag are the most notable change observed. The "gentle" stall characteristic of the Sandia data is more typical of the thicker symmetrical NACA four-digit symmetrical sections.

The post-stall characteristics observed here compare favourably with all other data sources, Figure 6.29, and therefore are considered to be a reliable and valid. The lift curve reaches a maximum $C_{L_{max}} = 1.11$ at $\alpha \simeq 45°$, and

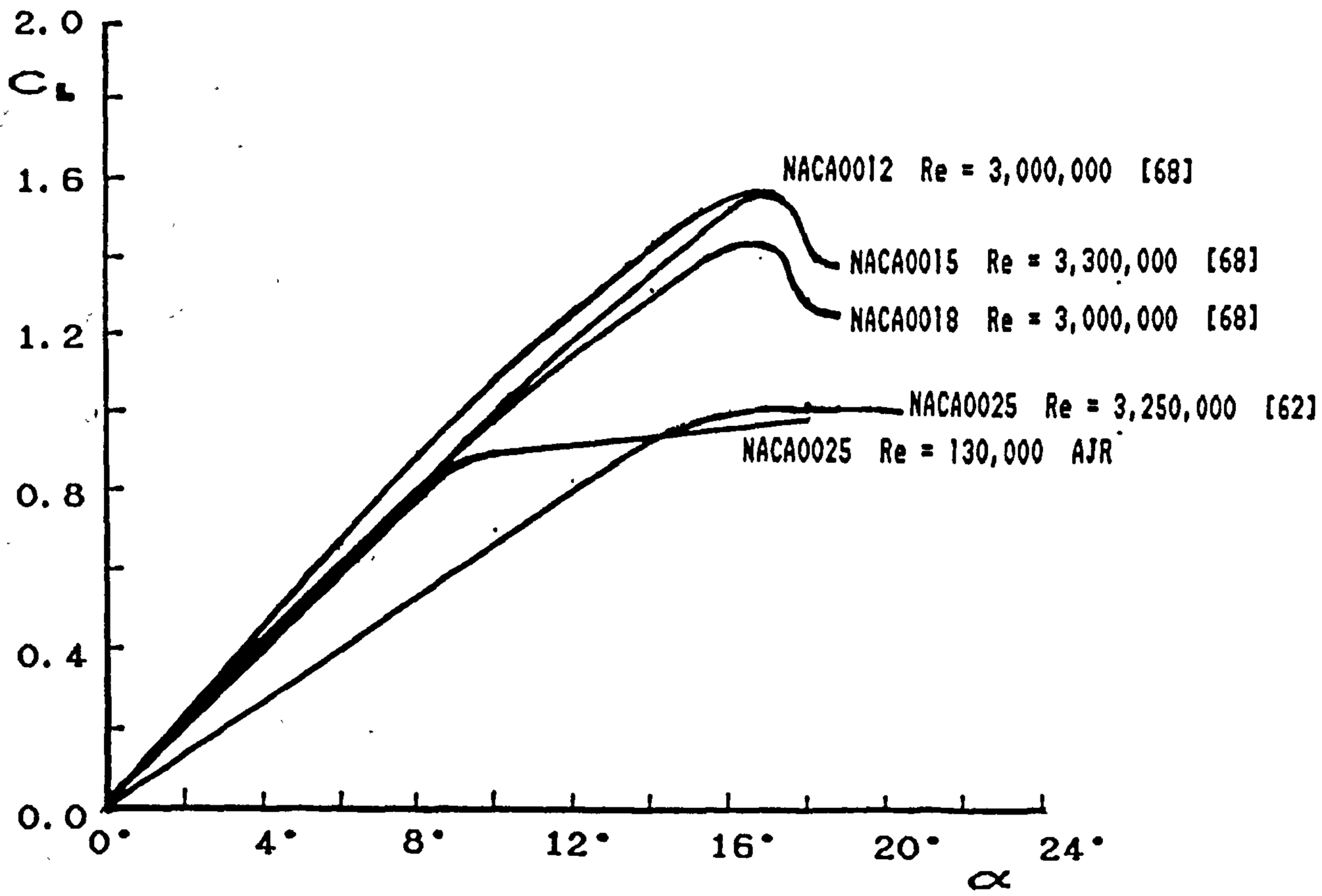

Figure 6.27: Comparison of C_L-α characteristics of NACA series aerofoils at low angles of attack

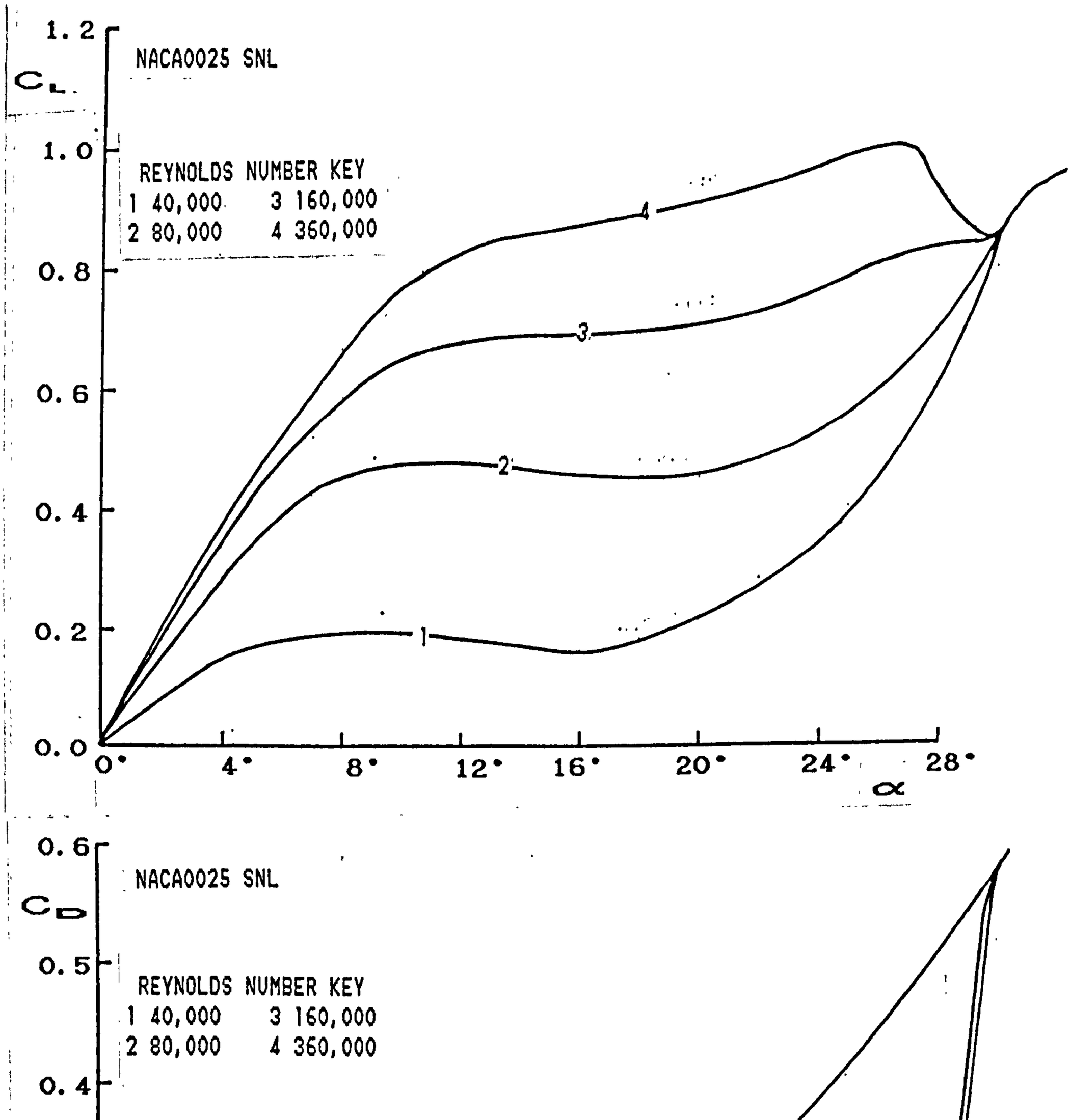

Figure 6.28: C_L-α and C_D-α at low angles of attack for SNL NACA0025 data [26]

$C_{L_{\alpha}} = 0$ at $\alpha \simeq 97°$. The drag curve continues to rise to a maximum $C_D = 1.94$ at $\alpha \simeq 90°$. These lift and drag characteristics are entirely consistent with the post-stall relationships given by Hoerner [67]:

$$C_L = (1.8 \text{ to } 2.0)\sin(\alpha)\cos(\alpha) \qquad (6.59a)$$

$$C_D = (1.8 \text{ to } 2.0)\sin^2(\alpha) \qquad (6.59b)$$

The most significant difference between the test data and the SNL data is the abrupt loss of lift at the observed stall angle. It is considered that the static pressure bubble observed from the pressure envelope plots, while increasing lift at low-α, eventually degrades the performance of the test aerofoil by prematurely invoking separation. The bubble has little effect on drag, but when the aerofoil is stalled the drag noticeably increases. The larger magnitude of the profile drag is apparent at low-α.

When using this data with VAWTTAY for aerodynamic performance predictions predictions of the model V-VAWT, it is anticipated that the predictions using the dataset developed here will be different from those using the Sandia data in two ways.

Firstly, since stall occurs at lower angles of incidence, and the test aerofoil exhibits a poor lift performance in its early-stall condition, performance predictions will be poor where the wind turbine operates in the early-stall condition, i.e. at low tip speed ratios. However, the very low tip speed ratio performance predictions should be similar because the deep-stall charcteristics of the two datasets are similar.

Secondly, since the profile drag of the test aerofoil is larger than that anticipated by the Sandia data, the

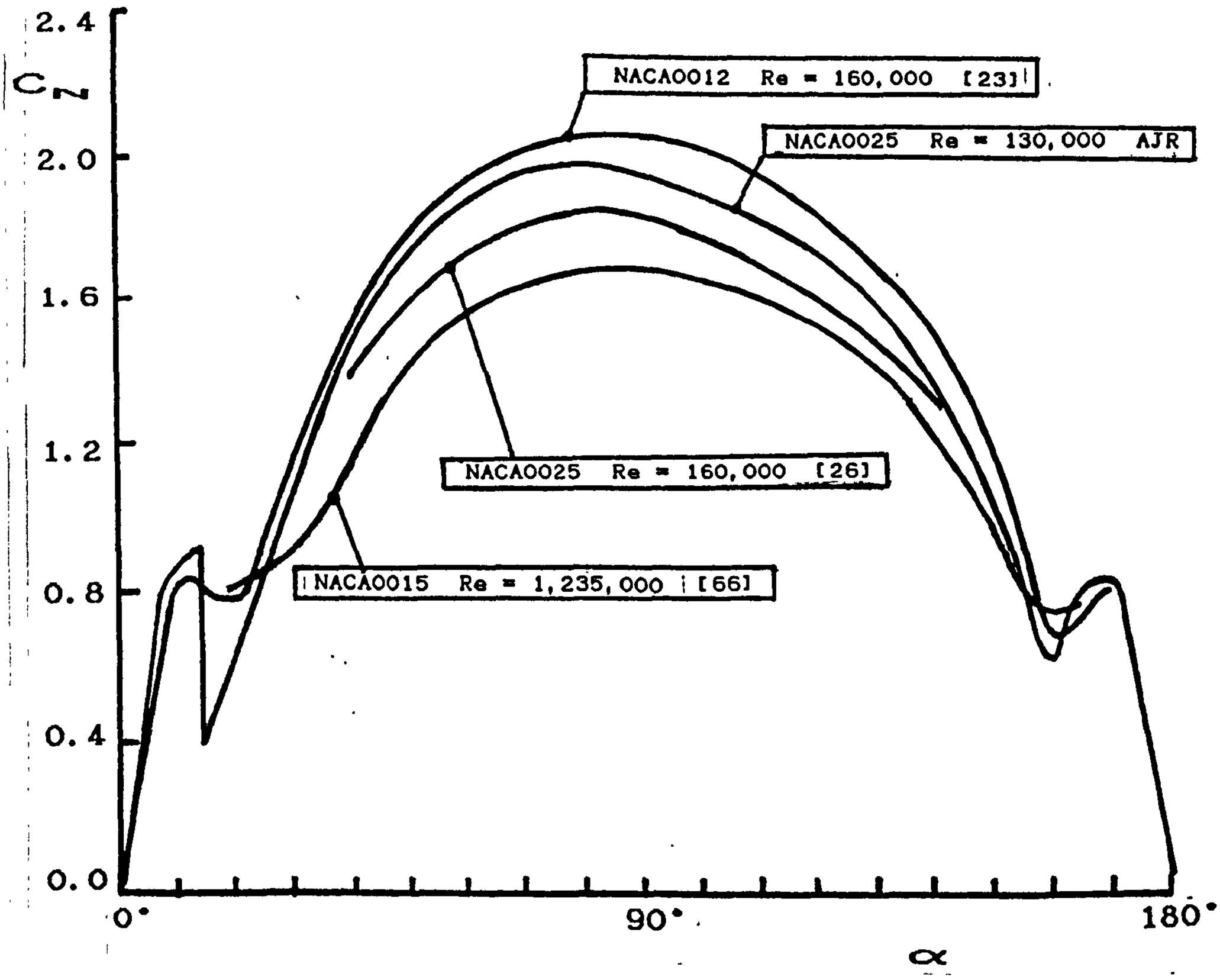

Figure 6.29: Comparison of C_N-α characteristics for NACA series aerofoils at high angles of attack

predicted runaway tip speed ratio will be smaller using the test data. At this condition, the V-VAWT blades are generally operating at small angles of incidence where the profile drag force dominates the driving force vector.

Predictions using the test data are presented and discussed in the next Chapter.

N.B. Note on bubble effect

Subsequent to the analysis of the NACA0025 measurements reported here, the observations of Willmer [69] came to the author's attention. During low Reynolds Number tests on the NACA0015 section, Willmer observed the presence of "bubble separation" at low angles of attack, and includes all the high lift results in his data, This suggests that the high C_N results observed here are valid and could be accepted as seen.

Chapter Seven: The Prediction of the Aerodynamic Characteristis of V-VAWT Configurations with Partial-span Pitch Control.

7.1: Introduction

In Section 2.2 the computer based aerodynamic prediction model VAWTTAY was briefly described. This computer model embodies the extended multiple streamtube theory that has been gradually developed by Sharpe [18] over a period of some ten .years. VAWTTAY, and its associated computer programs WRITEBLADE and READVAWTTAY were adapted by Sharpe for the V-type wind turbine configuration and were initially written in BASIC for the Commodore series of microcomputers. The predictions for the model V-VAWTs tested by Sharpe and Taylor (see Section 2.1) were made using the BASIC versions of these programs. The comparison between the theoretical results and the experimental results was considered good, so much so that Sharpe and Taylor are confident about using the prediction model for design studies of larger V-VAWT configurations.

In the work reported here, no attempt has been made to advance the theoretical development of the prediction model. The author has merely utilised Sharpe's BASIC programs for predicting the performance of the model V-VAWT, the design and testing of which is reported in previous chapters. The success of the prediction results was limited by the lack of suitable aerofoil data as discussed in Section 5.10, and the author has had to determine a suitable set of aerofoil characteristics for the NACA0025 section used for the wind tunnel model blades. Chapter Six discussed the experimental and analytical methods used to generate a suitable NACA0025 dataset for use with VAWTTAY. The performance predictions using this data are presented later in this chapter.

Notwithstanding the limitations of suitable aerofoil data, the author found using the VAWTTAY suite of programs in their original form both time consuming and inconvenient. The original WRITEBLADE and VAWTTAY programs had been developed by Sharpe to fully describe the shape and geometry of V-VAWT blade. The blade geometry can be defined to include the effects of taper, twist, root attachment axis offset, taper axis offset and twist axis offset. The describing parameters available allow almost any blade size or shape to be modelled and analysed. Linear variations of taper and twist are assumed between the blade root and tip, but the option to specify more precisely the spanwise variation of these describing parameters is available.

Unfortunately, the modelling of a blade with partial-span variable pitch could not be satisfactorily achieved using the computer programs in their original form. To generate the initial predictions for the model V-VAWT, the author had to resort to modelling the wind turbine blade as two discrete blades. The fixed pitch inboard portion and the variable pitch tip portion were described separately in different blade geometry files. The performance of each "blade" was analysed separately, and the results had to be numerically combined to give the overall performance of the V-VAWT rotor.

To investigate the effect of varying tip pitch required additional tip geometry files to be generated, each file describing a different pitch (twist) setting. Each file was analysed using VAWTTAY and the results numerically combined with the inboard blade results to give the overall performance characteristics of the rotor. This method yeilded the performance results reported in [57, 58, 59] and those discussed in Section 5.10.

Aside from the limitations of available aerofoil data, the method of generating the performance results was considered most inadequate by the author. Essentially two problems were identified:

(a) Speed of program execution
(b) Inconvenience of modelling approach for variable tip pitch

The modifications made by the author to the VAWTTAY suite of programs to overcome these problems are described in Section 7.2. The remainder of this chapter investigates the use of VAWTTAY for predicting the effect of partial-span pitch control on the performance of large, free-air V-VAWTs. Firstly, though, the NACA0025 dataset developed from the author's experimental measurements is used with the modified computer programs to evaluate the validity of the prediction model for predicting the effect of tip pitch. The theoretical predictions of performance for the model V-VAWT are compared with the results measured during the wind tunnel tests, and the significance of the discrepancies assessed. The suitability of the performance prediction model for determining the aerodynamic characteristics of a larger, free-air V-VAWT with variable tip pitch control is considered, rotor configurations evaluated, and possible control strategies defined.

7.2: Modifications to the VAWTTAY Suite of Computer Programs

The BASIC version of VAWTTAY was slow to execute, despite the structure of the program being optimised by Sharpe to ensure effective run-time operation. While some improvement in speed was seen by transferring the program from a Commodore PET to a Commodore 64, the calculation time was

still of the order of ten to twenty minutes for evaluating the rotor performance at a single tip speed ratio setting. To generate a complete C_{p_m}-λ characteristic with reasonable accuracy would take approximately two to three hours. This was not acceptable for parametric studies where optimisation of performance was being sought, and blade geometry modifications needed to be evaluated quickly.

To overcome the speed deficiency, the author decided that FORTRAN versions of the VAWTTAY suite of programs needed to be developed. The author undertook this task almost immediately the experimental measurements of the model V-VAWT had been completed. The programs were initially developed on a VAX 11/780 computer in standard FORTRAN 77 merely as copies of Sharpe's original BASIC programs. A limitation of Sharpe's BASIC programs was that variable names can only be identified uniquely by two characters. This did not allow Sharpe much scope to assign meaningful names to the program variables, so the author had great difficulty identifying the significance of some parts of the programs and how they related to the original stream-tube theory. However, the translation of the programs from BASIC to FORTRAN was successfully completed after many months effort and frustration! The author has continued to develop the programs further, and has optimised many of the routines used in the three programs. The structure of each program has been modified and the program listings contain many notes for user guidance. Error checking routines have been developed to ensure data entry is accurate and within the limits of the program. The author's FORTRAN version of the VAWTTAY suite currently runs on the VAX 11/750 computer in the Department of Mechanical Engineering at Portsmouth Polytechnic. Since it is written in standard FORTRAN 77, it is transportable.

The validation of the programs took a significant time, but comparison of the results of the BASIC and FORTRAN programs showed good correlation. The greater accuracy of the minicomputer ultimately means that the results of the latter program are more reliable, but most importantly they are generated much more quickly. Typically, the complete $C_{P_{max}}$-λ characteristic of the model V-VAWT takes approximately one minute (c.f. 2-3 hours) to analyse using the FORTRAN version of VAWTTAY. There is little or no time saving for the initialisation sequence, because it is the response and speed of the operator that determines the time taken to set up the operating conditions to be analysed. Similarly, the execution time of the WRITEBLADE and READVAWTTAY programs is little different, because these programs require more interaction with the operator. Data storage and retrieval is, however, quicker, and the size of the files and their management is easier to control on the minicomputer.

A great deal of time was spent writing and developing the FORTRAN versions of the VAWTTAY suite of programs. The author considers the time well spent because a faster and more flexible analytical tool has been developed.

Having developed a version of VAWTTAY that was both fast and reliable in its execution, the approach used to analyse the variation of tip pitch was reviewed. While considering the rotor as two separate blades and analysing the performance of each section separately was a suitable approach to initially adopt, it was clearly not appropriate for more extensive studies. Since the blade was modelled by two separate blade geometry files for each tip pitch variant, the overall rotor performance had to be determined by numerically combining the results of the separate VAWTTAY analyses of each blade file. Only the summary data generated by VAWTTAY could be combined in

this way, i.e. C_F and C_Q values. The post-processor program READVAWTTAY which utilises all the blade force data to generate other useful performance data such as azimuth torque variation, spanwise torque variation, blade loadings etc..., could not be used here. The results of the VAWTTAY analysis had to be combined without the aid of this program. This is clearly not suitable for more extensive design studies, where the detailed results output is vital for development purposes.

On a more practical note, the use of separate blade geometry files for each tip pitch variant not only requires good database management of the many files created, but a high proportion of computing time is spent generating the separate blade geometry files themselves. Repeated use of WRITEBLADE will require basic shape and size data to be entered time and time again as each tip pitch variant is created. The only difference between files being the pitch angle itself. Similarly, the VAWTTAY analysis will use the same range of operating conditions as each blade file is analysed. The initialisation of VAWTTAY often took longer than the analysis itself. Clearly a better approach was required.

The approach eventually adopted was in essence no different to that already used, in that the blade is considered as two separate parts that can be analysed independently of each other and the results combined. However, in the new approach all the blade data describing the tip pitch variants is generated automatically from within the WRITEBLADE program. The modified version of this program requires only the overall blade geometry to be defined as previously, but by defining the position of the spanwise transition point between the inner and outer blade sections, WRITEBLADE automatically generates the describing data for both blade sections. An additional data input

requires the operator to specify the range of tip pitch angles to be studied. From this input, WRITEBLADE automatically generates the tip data for all pitch angle variants. All the describing blade geometry data is stored in a single datafile.

The modus operandi of VAWTTAY had to be adapted to automatically analyse each tip variant and combine the results with the inner blade section to give overall performance characteristics. The modification did not affect the theoretical basis of VAWTTAY, but merely automated the analysis process to accommodate the modified structure of the new blade geometry files. Once initialised, VAWTTAY now analyses each tip pitch variant before proceeding to the next tip speed ratio. Table 7.1 shows a typical results summary generated by VAWTTAY at each tip speed ratio. In this way, the complete C_m-λ-β characteristic of a rotor can be generated by a single execution of the VAWTTAY program. The time taken to initialise the program is now only a small proportion of that time required to complete the full analysis.

The post-processor READVAWTTAY has been similarly modified, though little effort was directed to improving the presentation of the results, which now have a further "degree of freedom" to consider. However, since the various tip configurations have been analysed during the same VAWTTAY execution, all blade forces are saved in terms of the same base units. The detailed performance statistics, therefore, can now be generated by READVAWTTAY without modification, using the original analysis algorithms.

As Table 7.1 shows, the results summary generated at each tip speed ratio not only reports the variation of the non-dimensional quantities C_m and C_{Q}, but for convenience

Tip speed ratio = 6.19
Windspeed (m/s) = 12.00
Rotational speed (rpm) = 161.50

Pitch	Torque -(kNm)-	Power -(kW)-	CQ --	CP --	CD --
-5.0	0.366	6.186	0.0500	0.3095	0.6283
0.0	0.387	6.548	0.0529	0.3277	0.5962
5.0	0.354	5.992	0.0484	0.2998	0.5285
10.0	0.200	3.375	0.0273	0.1689	0.6019
15.0	-0.718	-12.143	-0.0982	-0.6076	0.4721
20.0	-1.614	-27.293	-0.2207	-1.3657	0.3963
25.0	-2.518	-42.592	-0.3444	-2.1313	0.3661
30.0	-3.361	-56.841	-0.4596	-2.8443	0.3679

Tip speed ratio = 5.30
Windspeed (m/s) = 14.00
Rotational speed (rpm) = 161.50

Pitch	Torque -(kNm)-	Power -(kW)-	CQ --	CP --	CD --
-5.0	0.566	9.578	0.0569	0.3018	0.5423
0.0	0.596	10.073	0.0598	0.3174	0.5315
5.0	0.553	9.356	0.0556	0.2948	0.4871
10.0	0.227	3.832	0.0228	0.1208	0.4298
15.0	-0.575	-9.720	-0.0577	-0.3063	0.3887
20.0	-1.465	-24.780	-0.1472	-0.7809	0.3512
25.0	-2.388	-40.387	-0.2399	-1.2727	0.3363
30.0	-3.209	-54.278	-0.3224	-1.7104	0.3427

Table 7.1: Typical results summary from author's modified version of VAWTTAY

calculates the real power and torque values for the particular rotor configuration being studied. The author finds this results format much more convenient for design studies. It is especially useful for the analysis of variable windspeed operation where the base units of the non-dimensional units change with windspeed.

The author again spent much time incorporating these changes into the FORTRAN versions of the VAWTTAY suite of programs. However, the resulting package is a highly developed and flexible suite of programs that allows the complete characteristics of a particular rotor and tip pitch control configuration to be easily described and quickly analysed. The author considers that only the post-processor program READVAWTTAY requires further development. The developments would include extending the range of information presented and, more importantly, creating plotting routines for the graphical display of results. The latter would greatly ease the interpretation of the vast quantity of data generated by the prediction model and serve to assist in the assessment of suitable design solutions.

7.3: Prediction of Performance of Model V-VAWT using Measured NACA0025 Dataset

To verify the accuracy and reliability of the performance prediction model VAWTTAY, the performance of the model V-VAWT was theoretically evaluated. Initial results were discussed in Section 5.10, where it was demonstrated that it was inappropriate to use the NACA0012 or SNL NACA0025 data for predicting the performance of the model V-VAWT. The wind tunnel testing of a NACA0025 section similar to that used on the model V-VAWT blades was described in the previous chapter, where the aerodynamic characteristics of

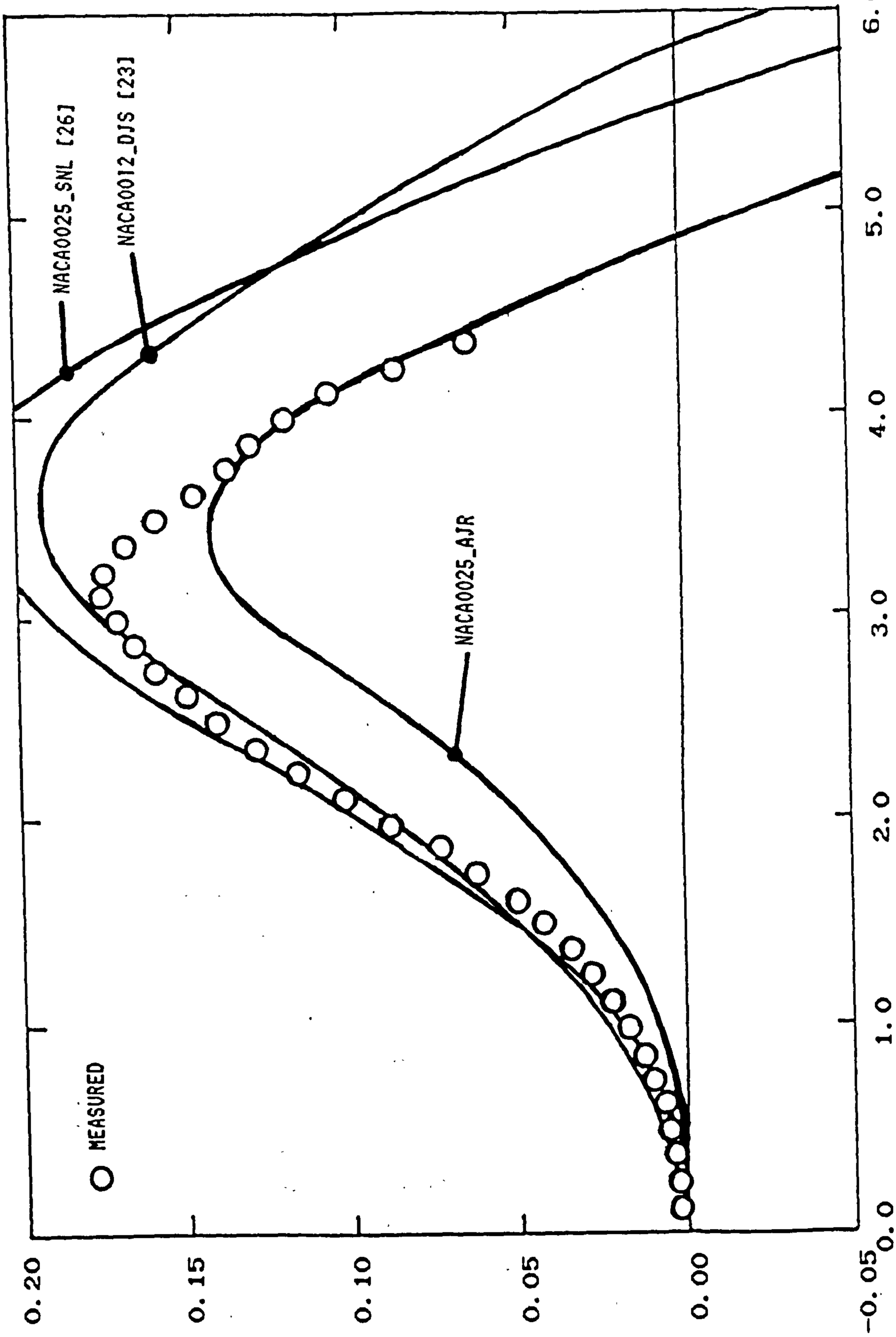

Figure 7.1: Comparison of predicted and measured performance of model V-VAWT

this section were developed into a format suitable for use with VAWTTAY. Using the force coefficients from the author's own NACA0025 dataset, the performance of the model V-VAWT has been predicted using VAWTTAY. The results of this evaluation are shown in Figure 7.1, which compares the measured results with the predicted results using all three aerofoil datasets available.

Figure 7.1 shows that there is still a discrepancy between the measured and theoretical predictions of the model V-VAWT even using the author's own NACA0025 dataset. However, the difference between the theoretical and experimental results no longer occurs at high tip speed ratios, where correlation is good, but rather at the lower tip speed ratios where the theory clearly under-predicts the rotor performance.

The theoretical predictions using the measured NACA0025 data rather than the SNL NACA0025 data, almost exactly correspond to the measurements made on the model V-VAWT at high tip speed ratios. This indicates that the profile drag of the model blades is more accurately represented by the author's own data than either of the other aerofoil sections. The runaway tip speed ratio is also clearly smaller and more representative of that of the model.

At the lower tip speed ratios the author's NACA0025 data clearly under-predicts the performance of the model. The predictions made using the other datasets provides good correspondence to the measured results at low tip speed ratios, though the peak C_P values are significantly larger than observed and occur at higher tip speed ratios. The author is suspicious of the good correspondence with the SNL NACA0025 and NACA0012 results and considers the correlation may be just co-incidence rather than accuracy of representation.

The author's suspicions about the apparent correlation of SNL NACA0025 and NACA0012 predictions at low tip speed ratios are aroused because at these speed ratios the rotor experiences the unsteady effects of dynamic stall. The author considers that his own NACA0025 data is valid over this operating range, and it is the prediction model VAWTTAY that is not sensitive enough to the effects of dynamic stall on this particular aerofoil section.

The phenomenon of dynamic stall is described in detail by McCroskey [70], but in simple terms an aerofoil operating in a flow regime where the angle of attack is increasing will experience a delay in the onset of stall, so extending its useful operating range beyond the static stall angle. The extent of the delay and the increase in lift force experienced during dynamic stall is the focus of attention of many investigators in the wind energy field. It is generally understood that predicting its effects in wind turbine applications is difficult, but mathematical models describing the effect have been developed but with limited success.

The aerodynamic performance prediction model VAWTTAY includes a number of features for predicting unsteady aerodynamic effects. Sharpe has devised suitable mathematical models to describe the effects of flow curvature, tip losses *and* dynamic stall [18]. All these models have been embodied into VAWTTAY, so the influence of these unsteady aerodynamic effects is already included in the theoretical results presented here. Sharpe's model of dynamic stall is based upon that of Gormont [71]. In this model, the modified angle of attack at which the aerofoil operates in its dynamic condition is a function of the pitch rate i.e. the rate of change of angle of attack. The lift and drag characteristics for this condition are determined from the static aerofoil characteristics.

The Gormont model was derived from empirical observations, and was adopted by Sharpe because it was simple to incorporate into the aerodynamic performance prediction model. When using this dynamic stall model with the multiple streamtube theory, Sharpe concluded [18]:

> "dynamic stalling should be applied only to blade normal force and only for the upwind blade pass."

Amongst others, Hales et al [72] have more recently summarised the evidence of dynamic stall effects on VAWT performance. They also discuss the problem of developing dynamic stall models suitable for predicting its effect and note that:

> "the laminar separation bubble described in the static case by Willmer, for Reynolds Numbers below about one million, plays an important role in the dynamic stall behaviour of these aerofoils....the dynamic stall behaviour of these sections cannot be defined solely in terms of a more precise experimental determination of static aerofoil characteristics versus Reynolds Number."

The laminar separation bubble observed by Willmer [69], was observed by the author in the tests of the NACA0025 section. It can be assumed, therefore, that the laminar bubble influences the dynamic stall characteristics of this section at low Reynolds Number in much the same way as it does the characteristics of the NACA0015 section.

While Hales et al acknowledge the common usage of the Gormont dynamic stall model in VAWT aerodynamic prediction theories, the use of the Westland time delay model is discussed. Both models utilise constants that have been determined empirically from tests on a limited number of aerofoils, and notwithstanding the advantages of each approach, it was concluded that:

> "the empirical constants should be determined on the appropriate aerofoil sections, rather than using the 'mean values' offered by the originators (of the models)."

The author is unaware of any dynamic stall investigations of the NACA0025 section, and therefore is unable to validate the results of applying the Gormont dynamic stall model to this section. It is the opinion of the author that the present dynamic stall model used in VAWTTAY is not suitable for predicting the dynamic stall effects of this thick aerofoil at the low Reynolds Numbers at which this phenomenon occurs. The theoretical predictions of the model V-VAWT are smaller in magnitude than actually measured in the low tip speed ratio region, and it is considered this to be entirely due to the uncertainty of the dynamic stall behaviour of this aerofoil. The author has been unable to justify this argument with any evidence other than that already presented.

An alternative reason for the poor correlation between the low tip speed ratio results may be due to the poor characteristics of the aerofoil section observed in the early-stall region, and that these observations are unrepresentative of the model V-VAWT blade. It was noted in Section 6.13 that the test aerofoil exhibits poor lift performance in the early-stall condition, and that the thrust force drops to large negative values immediately following separation. Stall is also observed to occur at low angles of attack in these low Reynolds Number conditions. The validity of these observations is, however, not doubted by the author because the repeatability of the measurements is demonstrated at all Reynolds Numbers. These characteristics will yield poorer aerodynamic performance predictions than the SNL NACA0025 data when the V-VAWT operates at low tip speed ratios, however, the overall characteristics of the aerofoil as measured is considered to be more representative of those

of the model V-VAWT blades. This is borne out by the higher tip speed ratio results, where correlation of results is good. Consequently, the author is confident that the early-stall aerofoil data is valid, and that it is the weakness of the dynamic stall model that accounts for the differences in the low tip speed ratio results.

Despite the speculation about the validity of the theoretical results generated using VAWTTAY, it is only for this particular model that such large discrepancies between theoretical and measured results have occured. From the discussion above, it is clear that it is the limitations of our knowledge of the behaviour of the NACA0025 section both statically and dynamically that limits the accuracy and reliability of the theoretical performance predictions. While the author considers that the dynamic stall model is unsuitable for predicting the behaviour of this 25% thick section, its use with the finer 12%, 15% and 18% sections is known to be more reliable. Therefore, when using these sections there is no reason to doubt the validity of the aerodynamic prediction theory or its embodiment into VAWTTAY.

The initial performance predictions using NAC0012 aerofoil data, Figures 5.8 to 5.11, show that VAWTTAY can be used to predict the effect of tip pitch. The modified versions of VAWTTAY were used to repeat these results to ensure that the new versions of the programs were valid theoretical tools. Repeatability was good, and therefore the author has no doubts about the suitability of VAWTTAY for predicting the effect of tip pitch control on larger V-VAWTs. It is this aspect of the work that will be discussed next.

7.4: Prediction of Performance of Large V-VAWTs with Variable Pitch Tips for Control

Satisfied that VAWTTAY was suitable for predicting tip pitch effects on the performance of V-VAWT rotors, it was now possible to undertake theoretical design studies of larger configurations.

The 5kW V-VAWT that will be considered here was first described by Sharpe and Taylor [19]; more recently the initial results of field trials at the Open University have been presented [22]. This machine was designed for research and development purposes, and since funds were limited, was adapted for use with equipment already in use on the Open University test facility [21].

The design of the rotor was completed by Sharpe and Taylor using the original version of VAWTTAY. The aerofoil used for the blades is the NACA0018. Their design studies with VAWTTAY were completed using characteristic aerofoil data for this section taken from reference [26]. The final rotor design, following the parametric studies described in reference [19], has blades that are 5.5 m in length and are tapered from the root (c = 460 mm) to the tip (c = 230 mm) with an aspect ratio of AR = 16. The tip radius is R = 4.39 m and the swept area is A = 19.03 m^2. Two- and three-bladed versions have been considered, but it is the two-bladed version that was first constructed and evaluated. For this version, the performance predictions using VAWTTAY showed $C_{P\ max} \simeq 0.32$ at $\lambda = 6.2$, which implied that at the rated windspeed of $V_{RAT} = 12$ m/s the maximum electrical power output of the system would be $P_{MAX} = 5.0$ kW, assuming an 80% transmission and conversion efficiency. The aerodynamic power output of the rotor is $P_{AERO} = 6.25$ kW at a rotor speed of N = 161.5 rpm.

The initial field trials of the 5kW V-VAWT have included the evaluation of the C_{P_m}-λ characteristic of this larger machine. The method adopted for these tests was a free-air variation of the acceleration method described in Section 5.3. The problems of using this method in the free-air environment has been demonstrated by Sharpe et al [22], but the initial performance results can be considered encouraging. The 5kW V-VAWT is not, at present, fitted with any aerodynamic control device, nor is it connected to an electrical generator of any kind. Thus evaluation of its performance as a controlled, grid-linked-wind turbine generator has not been possible.

The author's own studies of the 5 kW V-VAWT configuration were presented in reference [59]. These initial studies considered the use of tip pitch and 'T' brake options for control of this free-air machine. Based upon the findings of the experimental results presented in Chapter Five, the use of variable pitch tips and 'T' brakes with surface areas of only 5% of the total blade area was analysed using VAWTTAY. The results of this analysis showed that such small control surfaces would provide suitable power and speed regulation of this configuration. However, these theoretical studies of the 5kW V-VAWT were all carried out for constant windspeed operation, the wind-speed being V = 12 m/s. The effect of Reynolds Number is, therefore, not completely considered. Consequently, consideration of the C_{P_m}-λ characteristic for this type of operation alone, yields results that are misleading.

In developing aerodynamic control methods for the V-VAWT concept, the needs of electricity generation applications have always been considered to be the highest priority. If the V-VAWT is to succeed as a wind turbine generator, operating as part of a electricity distribution network, then power and speed control are necessary requirements.

Constant rotational speed operation poses the most difficult and challenging problems for the control of a wind turbine. Therefore, it is appropriate that this mode of operation be considered here for evaluation purposes. To maximise the effectiveness of the 5kW V-VAWT for electricity generation, the nominal operating speed of the two-bladed version should be N = 161.5 rpm. The speed step-up ratios of the transmission elements are chosen to ensure that when the rotor operates at its nominal speed, the electrical generator is operating at synchronous speed. In this way, the wind turbine will operate at its maximum efficiency when the windspeed is equal to the rated windspeed, V_{RAT} = 12 m/s.

When operating in windspeeds greater than rated, unless this particular configuration displays a natural stall characteristic, the "on-line" power output of the V-VAWT will have to be regulated to ensure that the rotor speed remains at synchronous speed and that the power output remains constant. Only by inspection of the constant rotor speed characteristic of the V-VAWT can the on-line power control effect of tip pitch be fully evaluated for this mode of operation.

While evaluation of constant speed operation will determine the on-line power control characteristics of the rotor, the evaluation of the rotor characteristics for constant windspeed operation is equally important. It is this mode of operation, that allows us to determine the "off-line" shutdown characteristics of the wind turbine in high windspeeds. While not specifically stated, it has been assumed that a suitable Cut-out windspeed for the 5kW V-VAWT would be V_{OUT} = 26 m/s. At this windspeed, a negative torque characteristic has to be demonstrated at all rotor speeds to ensure that full aerodynamic braking could be achieved during off-line operation.

To determine a suitable tip configuration for power and speed control of the 5kW V-VAWT, the effect of variable pitch tips with 5%, 10%, 15% and 20% surface areas were considered. The author's version of VAWTTAY has been used to theoretically evaluate the performance of the V-VAWT for each of these tip configurations. Constant rotational speed (N = 161.5 rpm) and constant windspeed (V = 26 m/s) performance evaluations have been carried out. The theoretical results of aerodynamic power versus windspeed and aerodynamic power versus rotational speed are presented in Figures 7.2 to 7.5. The results have been generated using NACA0018 data [26], but parasitic drag losses have been ignored. The rated aerodynamic power of the 5kW V-VAWT rotor is P_{AERO} = 6.25 kW at V_{RAT} = 12 m/s; this is clearly shown in each constant rotational speed plot. Tip pitch angles larger than $\beta = 30°$ are not shown.

The effect of tip pitch for angles larger than $\beta = 30°$ have been ignored because at these high pitch angles, the aerodynamic power output of the V-VAWT has been predicted to *increase* rather than reduce. The author has good reason to doubt the validity of these VAWTTAY results; clearly rotor power would continue to *decrease* with increasing tip pitch angle. Inspection of the VAWTTAY output does not show any computational errors, but the prediction model is clearly breaking down. After consulting David Sharpe, it is believed that the assumptions of the theory are being invalidated where the rotor operates in a region of high thrust; similar problems are known to occur when predicting HAWT performance. The author has been unable to modify VAWTTAY in the time available, since performnace tests at pitch angles greater than $\beta = 30°$ were not completed because of the limitations of the model itself. For control prediction purposes, the author has had to, therefore, limit the variation of tip pitch angle to $\beta_{Max} = 30°$.

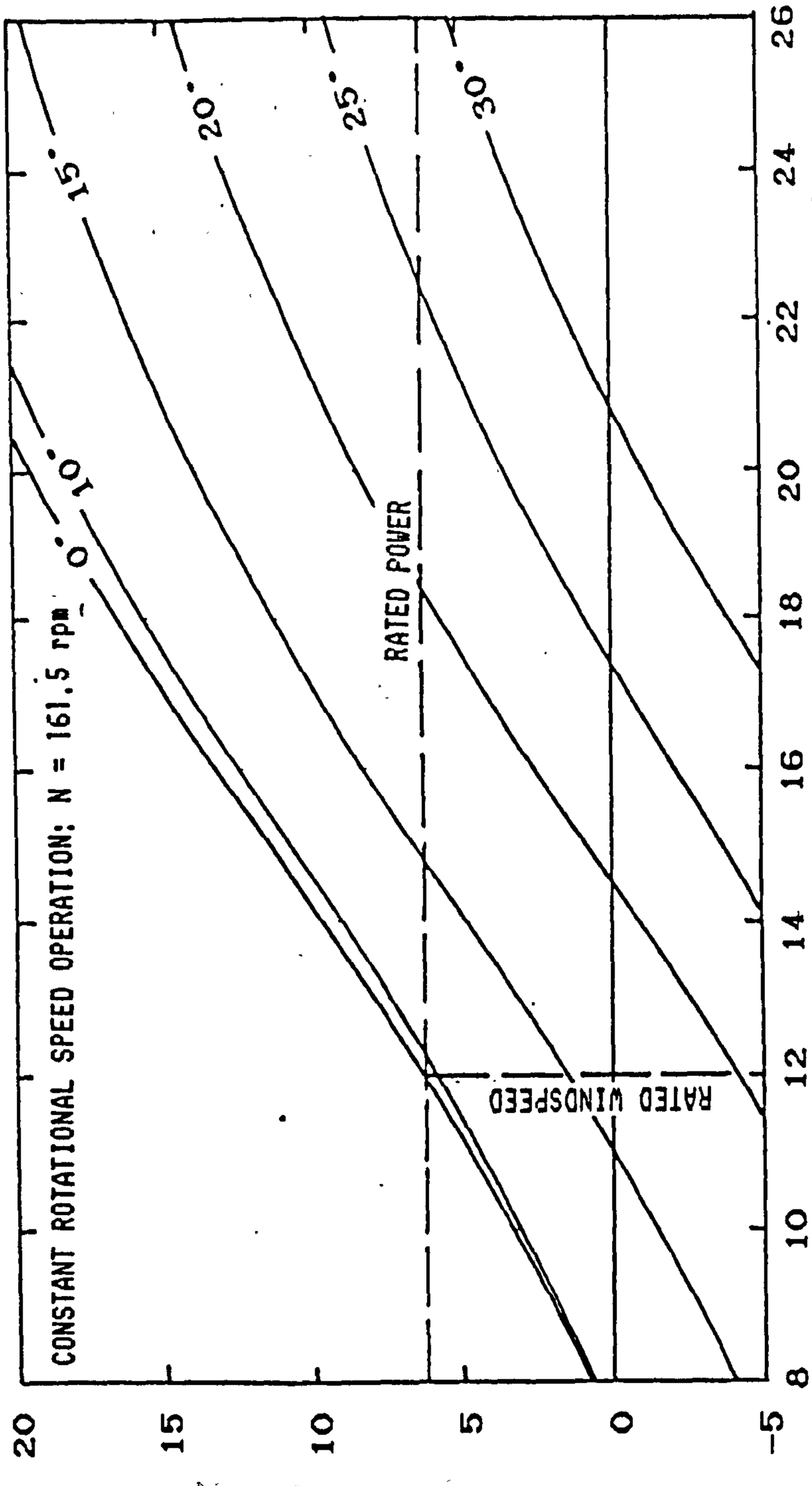

Figure 7.2a: Aerodynamic power versus windspeed for the 5kW V-VAWT with a 5% tip control surface

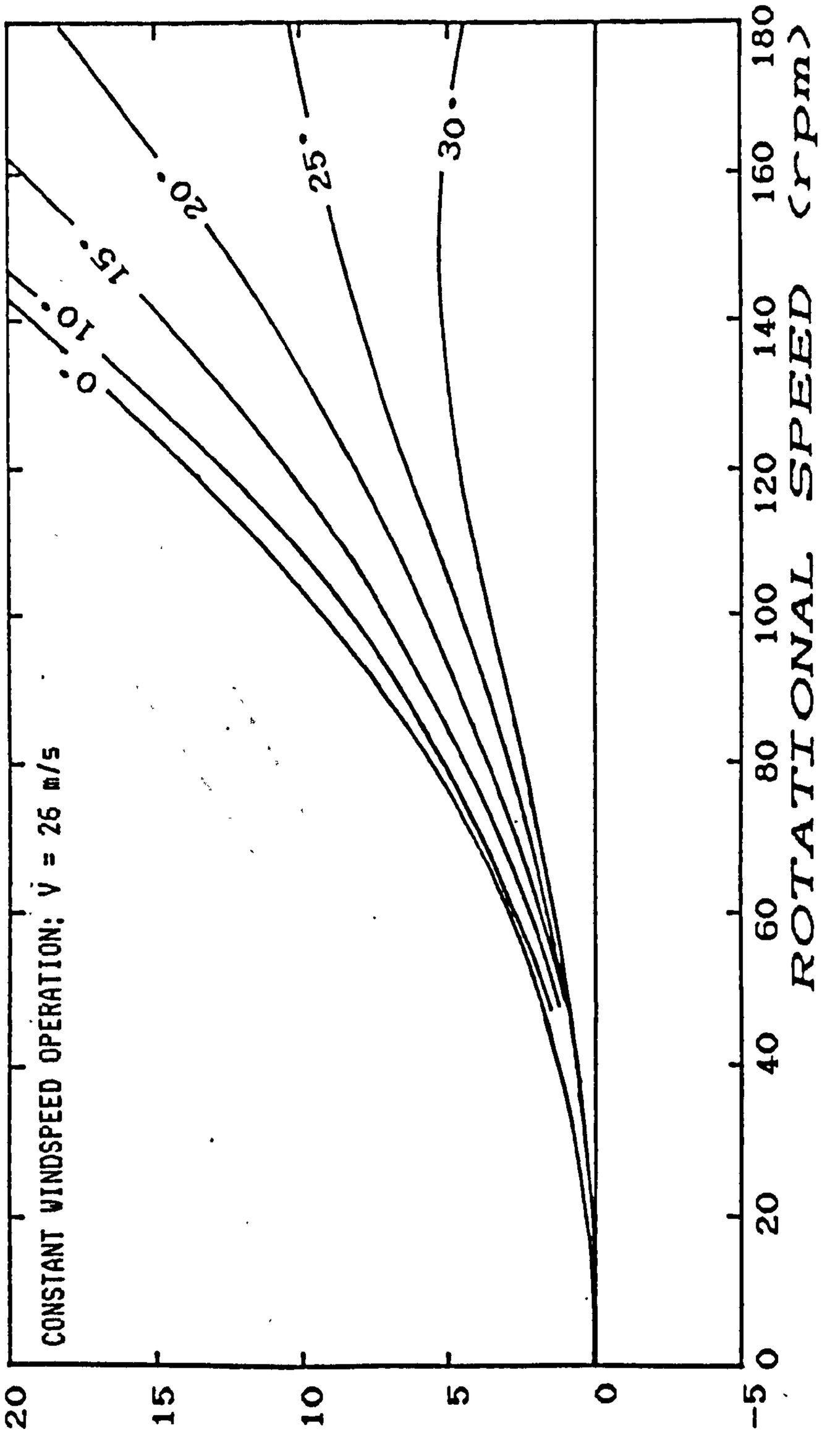

Figure 7.2b: Aerodynamic power versus rotor speed for the 5kW V-VAWT with a 5% tip control surface

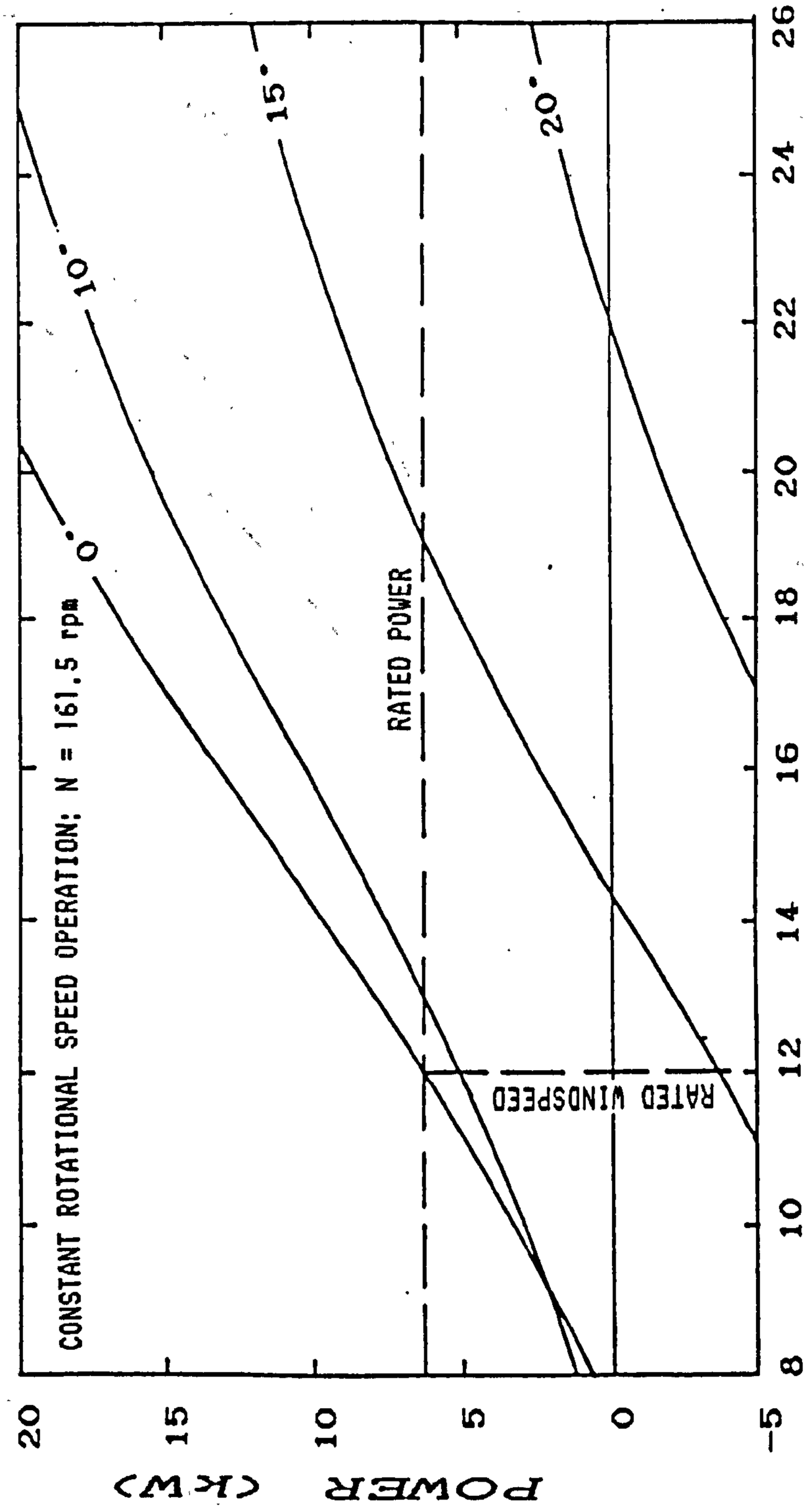

Figure 7.3a: Aerodynamic power versus windspeed for the 5kW V-VAWT with a 10% tip control surface

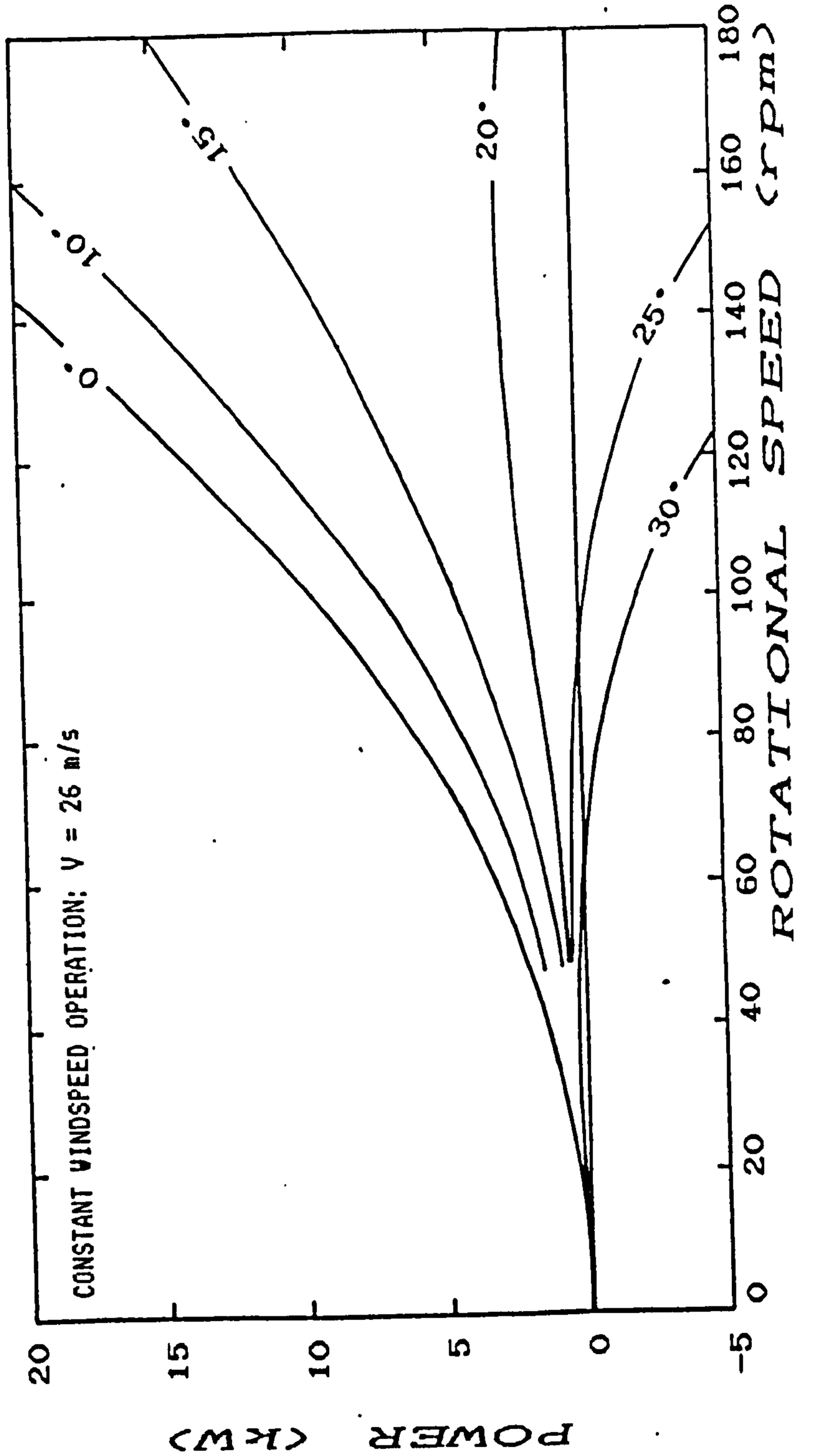

Figure 7.3b: Aerodynamic power versus rotor speed for the 5kW V-VAWT with a 10% tip control surface

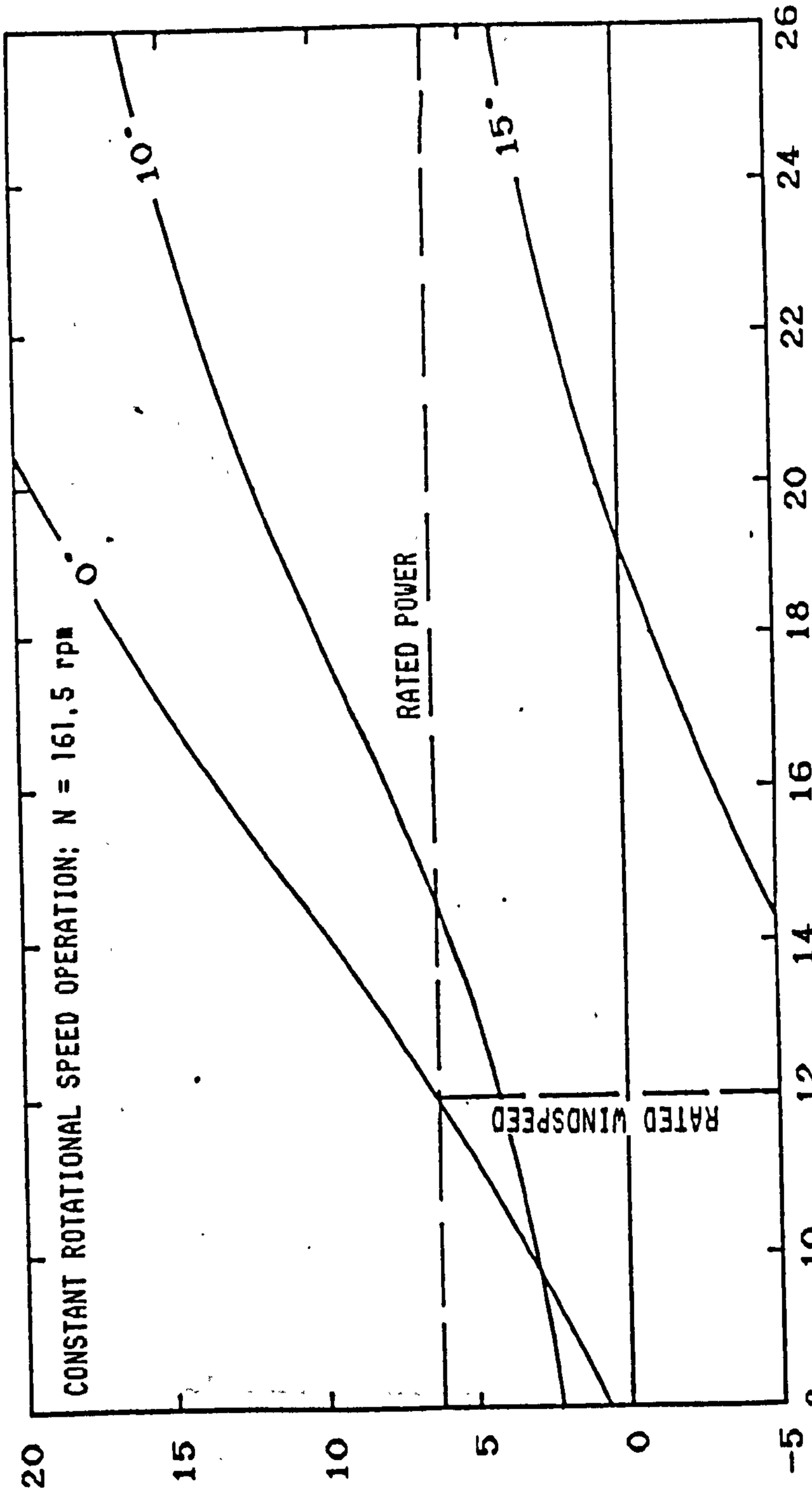

Figure 7.4a: Aerodynamic power versus windspeed for the 5kW V-VAWT with a 15% tip control surface

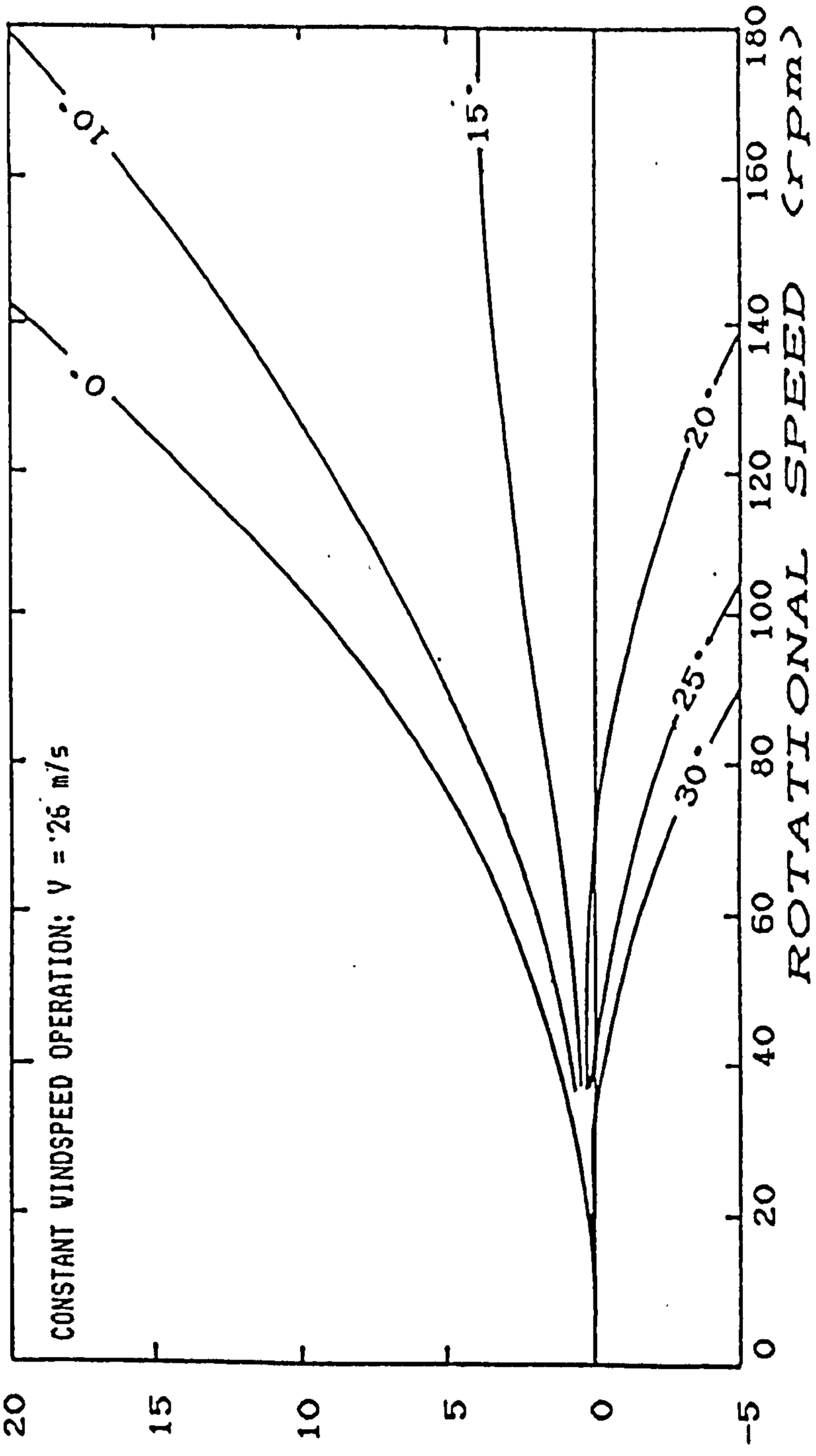

Figure 7.4b: Aerodynamic power versus rotor speed for the 5kW V-VAWT with a 15% tip control surface

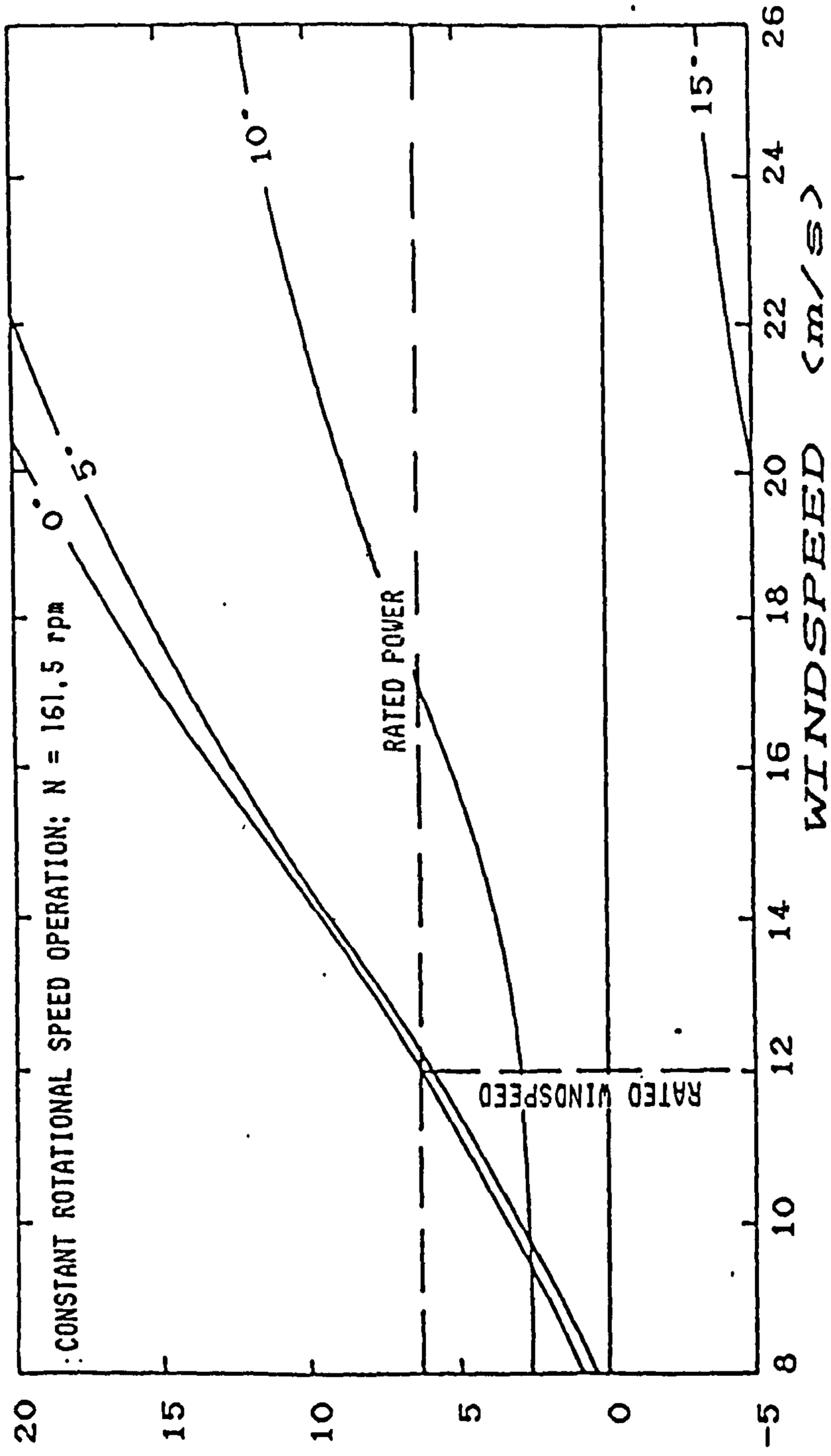

Figure 7.5a: Aerodynamic power versus windspeed for the 5kW V-VAWT with a 20% tip control surface

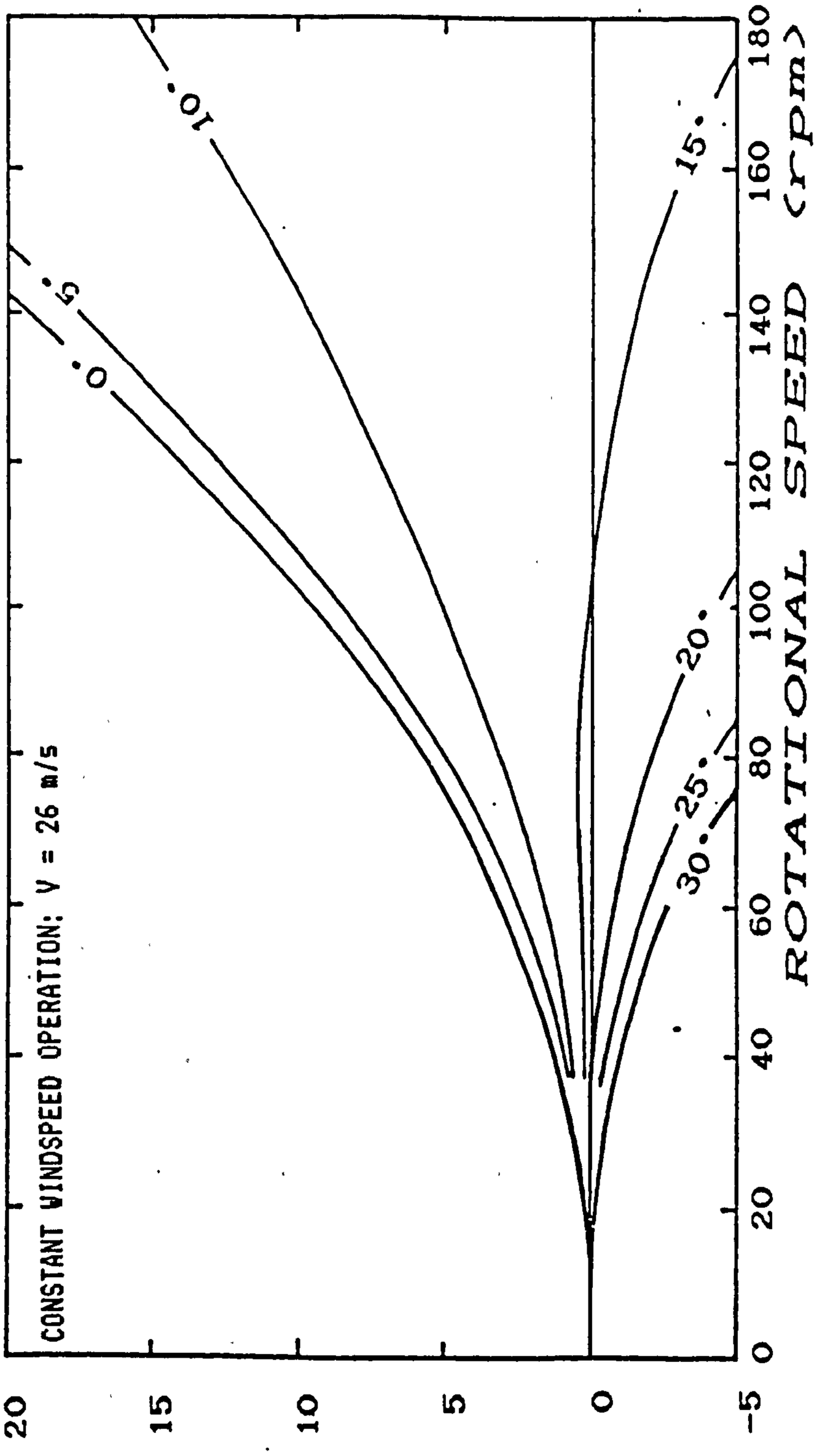

Figure 7.5b: Aerodynamic power versus rotor speed for the 5kW V-VAWT with a 20% tip control surface

Figure 7.2a shows that a 5% tip area would provide suitable power control for the 5kW V-VAWT for windspeeds upto V_{OUT} = 26 m/s. The power of the rotor can be regulated to remain within the rated power limit of P_{AERO} = 6.25 kW for all windspeeds using pitch angles upto β_{max} = 30°. As this plot shows, the rotor power achieves its rated output at the rated windspeed of V_{RAT} = 12 m/s. The change in power output is small for pitch angles upto β = 10° and little control effect is observed. However, the sensitivity of the rotor to pitch angle changes for β > 10° is apparent. The rate of change of power with respect to pitch angle change is reasonably constant for the larger pitch angles; a power gain of -1.0 kW per degree of pitch angle change is shown for β > 10°.

Figure 7.2b shows that a 5% tip is unable to develop negative power/torque when the windspeed is at the allowable operational maximum of V_{OUT} = 26 m/s. Even with the tip pitch angle at its maximum of β_{max} = 30°, positive power is developed for all rotational speeds. If or when the generator is disconnected from the electricity supply network, the unloaded rotor could not brought to a halt by aerodynamic means alone using a 5% tip area. As the mode of operation of the wind turbine changed from on-line to off-line, the rotor would tend to accelerate to a higher speed considerably in excess of N = 161.5 rpm.

While on-line power regulation can be achieved using only a 5% tip area, the author concludes that such a small control surface would not provide sufficient protection in high windspeeds during off-line operation.

Figures 7.3, 7.4 and 7.5 can be considered in the same way. The 10%, 15% and 20% tip areas are all capable of providing adequate on-line power regulation with observed power gains of -1.5, -2.3 and -2.8 kW per degree respect-

ively for pitch angles $\beta > 10°$. However, consideration of the constant windspeed results shows that better off-line speed regulation can be achieved using the tip areas larger than 5%. While the 10% and 15% tip areas are able to provide some aerodynamic braking at high windspeeds, the rotor still cannot be brought to a complete halt using aerodynamic means alone; off-line runaway rotor speeds of 62 rpm and 34 rpm can be observed for these two tip areas respectively. Only the 20% tip area provides complete aerodynamic braking at all rotational speeds.

The VAWTTAY predictions showed that of the four tip areas considered only the 20% tip had a negative "starting" torque with a pitch angle of $\beta = 30°$. Therefore, the 5kW V-VAWT rotor can be stopped completely only by using the largest of the control surfaces considered.

In reality, the 5kW V-VAWT is fitted with a shaft brake that is capable of providing over 1900 Nm of braking torque directly to the low speed rotor shaft. The rated torque of the 5kW V-VAWT rotor is only 370 Nm, but an uncontrolled rotor would develop 1570 Nm of torque at V = 26 m/s. The brake alone is, therefore, capable of retarding the rotor from its nominal speed to a stop without any assistance from an aerodynamic control surface. Here, though it is control by aerodynamic means that is considered most important.

The results of the theoretical performance evaluation of tip pitch control for the 5kW V-VAWT show that both power and speed regulation is clearly achievable using this control method. Whether full aerodynamic braking during shutdown is required or not is dependent entirely upon the needs of the wind turbine designer. It is the author's considered opinion that full aerodynamic braking is desirable. However, the larger control surfaces needed to

achieve this effect require more sensitive pitch angle control during on-line operation because the power gains characteristic of these control surfaces are much bigger. Inevitably, a compromise must be struck between these options, and provided the speed of the rotor and the power being transmitted through the system is maintained within the safe design limits of the machine, then the size of the tip area does not have to be closely controlled. It may be that a small control surface is required for on-line power regulation, while a larger control surface is required for shutdown procedures.

The analysis of the VAWTTAY predictions has so far only considered steady state operation. While it has been demonstrated that during on-line operation, the power output of the 5kW V-VAWT can be regulated using tip pitch control, the assumption has always been, that windspeed changes are small or slow to occur. In reality, gusting creates large and rapid fluctuations of windspeed that must be accommodated by any wind turbine control system. The slopes of the power versus windspeed curves show that power gains of 1.5 kW per m/s change in windspeed are typical of the this V-VAWT. Clearly, even small windspeed fluctuations will cause significant power output changes unless the control system is able to respond quickly and modify the pitch angle of the tip to an appropriate new setting. The transient response of the V-VAWT generator system to windspeed fluctuations, or any other external disturbances on the system, cannot be evaluated by consideration of the VAWTTAY predictions alone. Little more information can be gained by studying the aerodynamic performance data, and therefore a different approach is required. The dynamic behaviour of the 5kW V-VAWT is considered in the next chapter, and the suitability of tip pitch control for dynamic power and speed control considered.

7.5: Conclusions of Theoretical Studies

In this chapter, the modifications to VAWTTAY made by the author have been described. The modifications allow the evaluation of the theoretical performance of V-VAWT configurations with tip pitch control to be completed quickly and easily.

The VAWTTAY predictions using the author's own NACA0025 dataset correlate better to the measured high tip speed ratio results for the model V-VAWT than those predictions obtained using other datasets. However, the discrepancies that occur at low tip speed ratios demonstrate the need for the dynamic stall characteristics of the NACA0025 section to be more fully described.

The prediction model VAWTTAY is, however, considered a suitable tool for design studies of larger V-VAWT configurations, though the maximum pitch angle for which the predictions are valid must be restricted to $\beta_{max} = 30°$. The theoretical performance characteristics of the 5kW V-VAWT have been presented, and these results show that the power output of this wind turbine can be regulated with only a 5% tip area; if full aerodynamic braking during high windspeed shutdowns is required, then a 20% tip area must be used.

The theoretical results also show how sensitive the power output of the rotor is to both windspeed and pitch angle changes. For electricity generation purposes the dynamic response of the V-VAWT and its control system to external disturbances will determine the success of this wind turbine concept in this application. The response of the system cannot be evaluated by steady state analysis alone, so another approach is required.

Chapter Eight: The Dynamic Behaviour of a V-VAWT using Active Partial-span Tip Pitch Control

8.1: Introduction

Large electricity supply systems consist of a network of inter-connected synchronous generators. Each generator is driven at a constant speed by an independently controlled prime mover. The electrical power supplied by the network is distributed to various domestic and industrial users via a system of high voltage transmission lines. The "load" on the network fluctuates as the electrical power demanded by the users changes. The mechanical power developed by each prime mover, whether it be a diesel engine, steam turbine, gas turbine or water turbine, is actively controlled to ensure that the network is able to supply the power demanded. The control system is designed to ensure that the response of the prime mover to such changes does not adversely affect the quality of the electricity supply nor jeopardise the stability of the connection of the generator to the network.

The response of a generator system to small changes of mechanical power input can be anticipated by using power system stability analysis. Using this technique, the static power stability limit of a given generator system can be determined. Provided the power supplied to the synchronous generator does not exceed this limit, the steady state operation of the generator system will remain stable; the generator will continue to be synchronised with the network and provide useful electrical power. Yet if the power from the prime mover exceeds the static power stability limit, the generator system becomes unstable; the rotational speed of the generator will increase; synchronisation with the network will be lost and useful power cannot then be supplied to the network. The

generator system must be shut-down and a re-synchronisation procedure invoked, before it can supply electrical power to the network again. The static power stability limit indicates the maximum power, ignoring all losses, that the prime mover can constantly supply to the synchronous generator before the system becomes unstable and has to be disconnected from the network.

The static power stability limit of a generator system is solely dependent upon the electrical characteristics of the system. The characteristics of the prime mover and the coupling between it and the synchronous generator play no part in determining the value of this limit. Static stability analysis of the system only considers steady state operating conditions; the response of the generator system immediately following a disturbance cannot be anticipated using this technique alone.

In conventional generator systems, a large disturbance is considered to be either a large/sudden change in the mechanical power from the prime mover or a transitory loss of electrical load on the system due to a fault in the connection between the synchronous generator and the network. The transient response of the generator system to such disturbances is highly dependent upon the dynamic characteristics of all the components of the system. Even if the steady state response was statically stable, the transient response of the generator system may become unstable and loss of synchronisation of the generator with the network would occur. Alternatively, during the transient response of the system, if the static power stability limit is temporarily exceeded the steady state response might still remain stable. The stability of a generator system is most likely to be jeopardised when a fault occurs in the connection between the generator and the network. However, the critical time allowed for

clearing the fault can only be determined by transient stability analysis of the system.

The analysis of the transient stability of generator systems is not straightforward and a generalised solution cannot be formulated. The time response of the generator system to a large disturbance can be calculated using a step by step method. Such analysis requires a detailed knowledge of the dynamic characteristics of all the system components and lends itself to computer based solution.

The stability of a wind turbine generator that is connected to an electricity supply network can be assessed using the same static and transient stability analysis techniques. The response of the wind turbine driven system to the disturbances already described would be similar to that of a conventional generator system. However, an un-controlled wind turbine will provide a fluctuating mechanical power input to the generator system because of the continuous variation of the windspeed. Additionally, if a vertical-axis rotor is used, the aerodynamic power from the wind turbine will be cyclically varying even if the windspeed is constant. These power fluctuations will be transmitted to the synchronous generator and affect the state of its operation with the electricity supply network. Whether the system continues to remain stable depends upon the dynamic characteristics of the wind turbine system as a whole.

To ensure steady state stability when changes in the windspeed occur, the aerodynamic power developed by the wind turbine rotor must be regulated by its control system to ensure that the mechanical power delivered to the generator is within the static power stability limit. The experimental measurements presented in Section 5.3 demonstrate that changing the blade tip pitch angle offers

a suitable means of regulating the aerodynamic power output of a small V-VAWT rotor. The predictions of Section 7.4 also show that this control technique offers a suitable means of regulating the aerodynamic power output of larger V-VAWT rotors.

Clearly, it is possible to specify, at any instant, the optimum blade tip pitch angle for a given V-VAWT configuration that will ensure the generator system operates within the steady state stability limits of the system. However, since the windspeed is continuously varying, the optimum pitch angle will also need to vary. The transient response of both the blade tip pitch actuating system and the V-VAWT generator system to the constant fluctuations of windspeed may result in instability of the system.

The cyclic nature of the aerodynamic power output of the V-VAWT rotor cannot easily be actively controlled and the author considers that to try and do so will unreasonably complicate the design and construction of the machine. However, the magnitude of the power fluctuations can be damped by careful design and selection of the power transmitting components of the generator system. The degree of damping and the response of the V-VAWT generator system to cyclic aerodynamic power variations can only be evaluated by dynamic analysis of the whole system.

The response of a V-VAWT generator system to external disturbances such as windspeed variations, load changes or transmission faults will be crucially dependent upon the dynamic characteristics of the system components and the control system used. To date, all V-VAWT research activity has concentrated on the performance of the rotor in isolation. Experimental measurements have been used for the verification and the development of VAWTTAY. This

program has allowed various V-VAWT rotor configurations to be studied from which the 5kW free-air V-VAWT has been developed [19]. In all cases, the steady state operating characteristics of the wind turbine have been calculated and used to evaluate the performance of the rotor configuration. The experimental work and the analysis tools developed at The Open University and Queen Mary College do not provide any information about the dynamic behaviour of the V-VAWT; little or no consideration has been given to the interaction of the rotor with the other components of a whole wind turbine system. The V-VAWT rotor is only one part of a wind energy supply system, and if blade tip pitch control is to be rigourously evaluated, then it is essential that the dynamic behaviour of the whole system be considered here. Consequently, a necessary requirement for this project has been the development by the author of a mathematical model of a V-VAWT generator system for dynamic analysis and stability studies.

This chapter will describe the development of the computer program "DYNVAWT", which has subsequently been used to study the dynamic behaviour of the 5kW V-VAWT. A computer based solution method has been adopted since this allows greater flexibility in adapting the model to simulate the various operating conditions typically encountered by a wind turbine system. The computer program allows the power transmitting elements of a V-VAWT system to be modelled and the dynamic behaviour of the system simulated. The operational conditions influencing the behaviour of the system can be varied so that the effects of such changes can be studied. The mathematical model used as the basis of DYNVAWT only considers the power transmitting components of the wind turbine system; the structural behaviour of the wind turbine system is not considered nor structural elements included.

The primary function of the program is to allow the dynamic action of a blade tip pitch actuator to be simulated so that suitable control strategies can be developed. However, a V-VAWT generator system connected to an electricity supply network will have four basic modes of operation for which the suitability of blade tip pitch control must be considered:

(a) Off-line start-up and generator connection
(b) On-line power regulation
(c) Loss of load control
(d) Generator disconnection and rotor braking

The "on-line power regulation" and "loss of load" operating modes have been briefly discussed already since they are the most significant modes that need to be considered. However, the behaviour of the V-VAWT generator system in any of these operating modes will be crucially dependent upon the dynamic characteristics of the whole system and the control strategy that is adopted. Therefore, the computer program DYNVAWT has been developed to allow simulation of all four of these operating modes.

8.2: System Modelling and Methods of Analysis

The mathematical model of the V-VAWT generator system that will be developed here is a representation of the 5kW free-air V-VAWT currently sited at The Open University, Figure 8.1. The synchronous generator driven by this V-VAWT is not at present connected to the local electricity supply network nor is an active blade tip pitch control system fitted. However, the machine was designed to operate with the generator connected to the network, so all the power transmitting components have been suitably selected for this application. These

components can be accurately modelled since their dynamic characteristics can be readily evaluated. The mathematical models that will represent the synchronous generator and the blade tip pitch control system will have to take a generalised form, since the characteristics of these components cannot be based on actual hardware.

The overall system model could represent a generator system other than that driven by the 5kW V-VAWT. But it is convenient here to initially concentrate on this machine, because the dynamic characteristics of the system can be readily evaluated. Also, it is anticipated that future designs of larger V-VAWT generator systems will be based upon this machine, although the sizing and selection of individual components will differ.

Figure 8.2 is a schematic diagram of the drive train components of the 5kW V-VAWT generator system. The blades of the rotor are attached at their root to the stub tower which is free to rotate about the fixed internal tower. Each blade is supported at the 70% spanwise position by two cables which are fixed to the top of the stub tower. The cables are unable to transmit aerodynamic torque, so all rotor torque is transmitted through the blade root connection to the stub tower. This acts as a low-speed shaft and transmits the rotor torque to a V-belt pulley at its base. The parking/emergency brake is an electro-mechanical disc brake system which is attached to the internal tower. The brake disc is attached directly to the V-belt pulley, so the braking torque is applied directly to the V-VAWT rotor. The pulley is the driving pulley of the first stage of a two-stage, speed increasing drive system. The first-stage driven pulley and the second-stage driving pulley are fixed to a medium-speed layshaft, and the second-stage driven pulley is attached directly to the synchronous generator input shaft; the

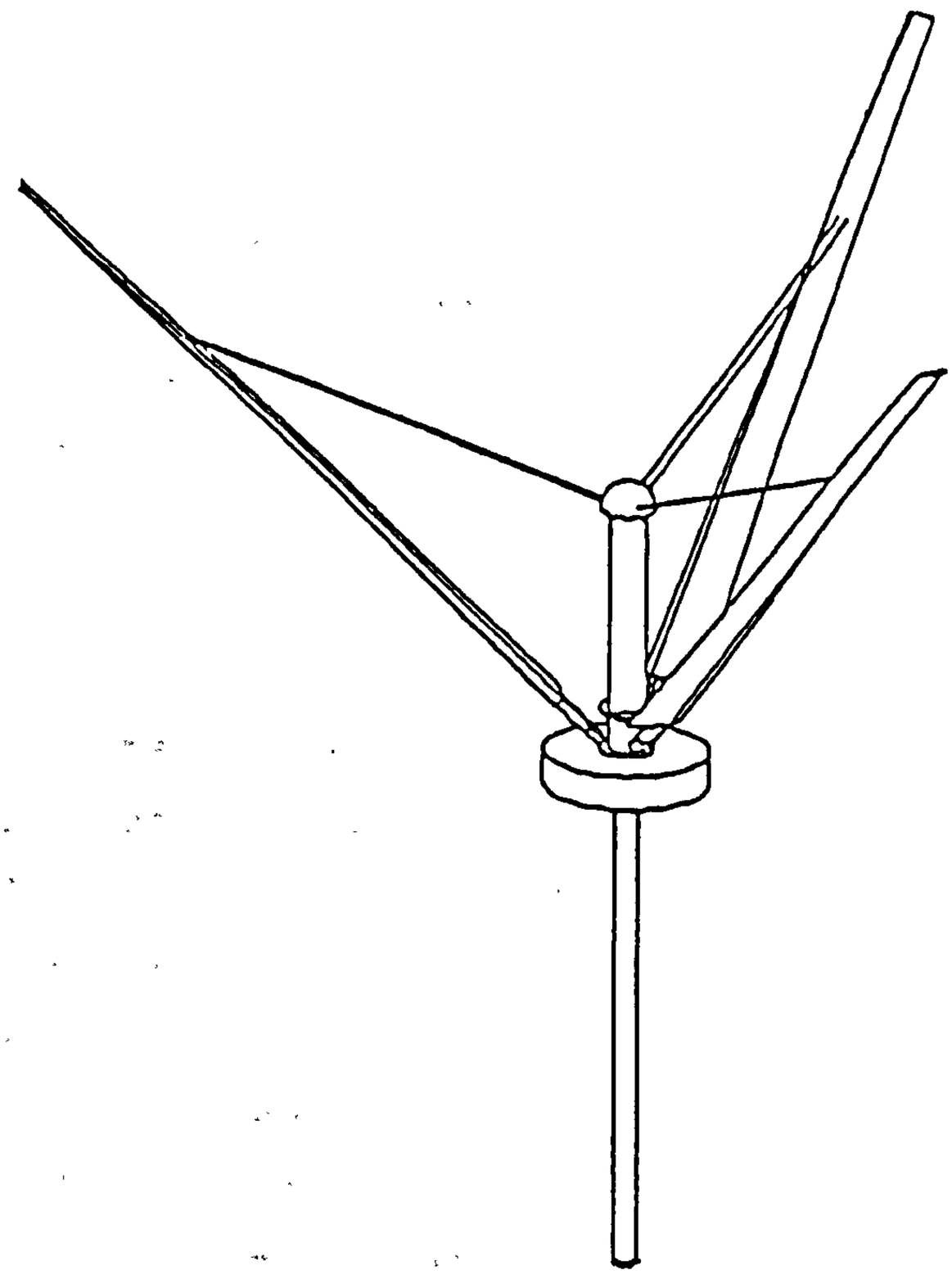

Figure 8.1: Three-bladed free-air 5kW V-VAWT

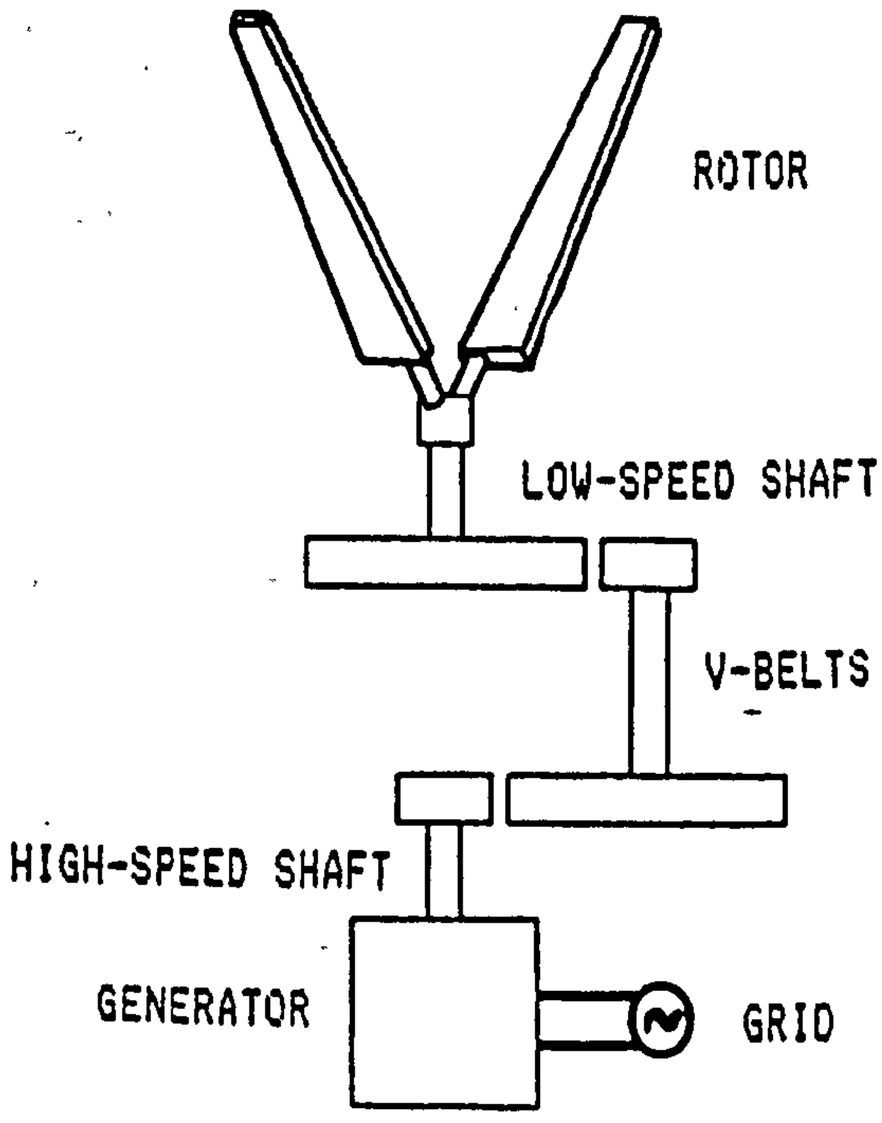

Figure 8.2: Schematic layout of drive train components of the 5kW V-VAWT generator system

high-speed shaft. The generator and layshaft are both supported by the internal tower. All the drive train components are rigidly attached to each other and only the V-belts provide any significant torsional flexibility in the system.

The drive train can be mathematically modelled if the most important mechanical components are considered as discrete, lumped inertia elements that are linked by torsional spring and damping elements. All the low-speed and medium-speed elements will be considered as high-speed equivalents for ease of analysis. The electrical connection between the generator and the supply network can be modelled as a torsional spring and damping element as will be demonstrated below. The lumped inertia approach allows the state of the drive train to be described by a finite number of state variables and its dynamic behaviour by a finite number of ordinary differential equations. The state of any one of the drive train components is dependent upon the state of all the other components in the system. Therefore it is convenient to consider the drive train as a sub-system of the whole V-VAWT generator system.

In addition to the drive train sub-system, the V-VAWT generator system has two other sub-systems which must be modelled. The blade tip pitch actuator and the disc brake system are both independent of the other, but each influences the state of the drive train sub-system. The state of these sub-systems can also be described by a finite number of state variables and their dynamic behaviour by a finite number of ordinary differential equations.

Since the state of the three sub-systems can be described by a number of state variables and ordinary differential

equations, the dynamic behaviour of the whole V-VAWT generator system can be completely modelled.

The V-VAWT generator system has two inputs which directly affect its state and which cannot be controlled:

(a) Windspeed
(b) Network voltage

These inputs must be modelled to represent typical forcing functions to which the V-VAWT generator system would have to respond. It is convenient that the windspeed and network voltage models should therefore take the form of the input forcing functions commonly used in control system analysis:

(a) step, ramp and impulse transient inputs
(b) sinusoidal input
(c) statistical input

There are only two outputs from the V-VAWT generator system to be controlled:

(a) Power (electrical)
(b) Frequency (electrical)

The control system can only use the inputs and the state variables of the V-VAWT generator system itself to determine a control strategy and set the control inputs to the sub-systems within the whole. The control strategy to be adopted has yet to be determined and it is a requirement of this project to establish a suitable control system design.

Having established the ordinary differential equations to describe the V-VAWT generator system, a method of solution

is required. The state space approach for system representation and analysis is considered to be the most suitable technique to use here. The ordinary differential equations that describe the system are replaced by difference equations that are more readily solved than the high-order equations that would be developed using classical system analysis techniques. The response of the system can be simulated in the time domain by a step-by-step solution of the difference equations. This technique is most suitable for multi-variable systems with non-linear characteristics, and lends itself to digital computer based solution.

The V-VAWT generator system is essentially a continuous time system, since all the inputs, state variables and outputs can be defined over a continuous period of time. A digital computer is a discrete time system, since its state is determined at distinct instances of time. If a digital computer is used to control the V-VAWT generator system then a hybrid system is formed, since the system contains both discrete and continuous time sub-systems.

A digital computer based analysis of the V-VAWT generator system will require a discrete-time model and the response of the system can only be observed at discrete time intervals. The observed response will be an approximation of the true response of the system and its accuracy will depend upon the interval of time between observations. In practice, there is a compromise to be made between the accuracy of the solution and the computing time required, but there are a number of numerical solution methods available that allow both fast and accurate solutions to be generated.

Simulating of the V-VAWT generator system in the time domain is not a convenient approach to adopt when

developing a control system design or evaluating its performance. The accuracy of the control system can be assessed visually by inspection of graphical traces of the output, or numerically by, say, evaluating the integral square error performance index. The steady state and transient stability of the system cannot be judged from the outcome of one simulation alone, since it is not possible to predict the degree of stability of the system; the simulated response will either be stable or unstable for a given set of conditions. However, the speed of the computer based solution allows a simulation study to be quickly repeated. Therefore, by adopting a trial and error approach, a satisfactory control system design will have to be developed by iteration.

The following sections discuss and describe the development of the mathematical models of the V-VAWT generator system sub-systems and forcing functions. As mentioned above, the behaviour of a synchronous generator can be satisfactorily modelled by torsional spring and damping elements. It is convenient that this model be developed first.

8.2.1: The Synchronous Generator Model

A synchronous generator may operate by itself supplying a single load or in parallel with other generators as part of a large electricity supply network. In a large system of generators each is connected to the network via the generator bus. Each generator will supply real and reactive power to the system and maintain the bus at a constant voltage. All the machines run at synchronous speed so that electricity is supplied by the system at a fixed frequency.

The output of each generator is controlled by the current exciting its field windings and the mechanical shaft torque supplied by its prime mover. When either one or both of these inputs change then the real power, reactive power, bus voltage and system frequency will all generally change. There is some cross-coupling between the inputs and outputs but for control purposes it is more desirable to have a single output controlled by a single input.

Where a synchronous generator acts in isolation, or with only a small number of other generators, the four outputs of the system will all vary in some respect when the generator experiences fluctuations in the mechanical shaft torque provided by its prime mover or the current supplied to its field windings. The sensitivity of the system to such fluctuations reduces as the size of the network increases. Very large networks are termed "infinitely strong" because a change in the input torque or field current of one generator has little effect upon the system frequency or the magnitude of the bus voltage. The change only affects the real and reactive power developed by the machine. Strong networks are able to accommodate fluctuations in input power without adversely effecting the quality of its output. A wind turbine driving a synchronous generator can only be successfully connected to a large electricity supply network if the turbulent nature of the wind does not create shaft torque fluctuations of such magnitude that the generator loses synchronisation and is disconnected from the network.

A synchronous generator that is connected to a large network behaves dynamically like a torsional spring that is connected between its input shaft and an imaginary reference that rotates at synchronous speed with the network. The large inertia of the rotor and low equivalent torsional stiffness of the drive train and generator connection

to the network mean that wind turbine generators generally have low fundamental torsional frequencies. A large proportion of the total energy in wind speed fluctuations is observed to occur at similarly low frequencies. Such turbulence will excite fluctuations in the power developed by a wind turbine generator and may provoke instability in the synchronisation of the generator with the network. The wind turbine control system must be able to attenuate these fluctuations to ensure that the generator is stable and the connection to the network is maintained. To simulate the dynamic behaviour of a grid-linked wind turbine generator, the operational characteristics of a synchronous generator connected to a large network must be mathematically modelled. The analogy of its behaviour to that of a torsional spring is a convenient one but an expression for the stiffness of the connection between the mechanical input shaft and the rotating reference must be established.

The Park-Blondel equations are used by electrical engineers to describe the dynamic behaviour of the synchronous machine and its electrical circuits. Some authors have used these equations for modelling generator behaviour in wind turbine studies [73, 74, 75, 76], however, these authors are simulating control strategies that rely upon control of the generator itself. The use of dynamic circuit theory is not applicable here because the state of the generator during any transient response is of little value in assessing the suitability of the tip pitch control. Like many of the system models used here, only input-output relationships are required. The Park-Blondel equations are the basis for all the generator power relationships presented in the texts considered for this exercise [77, 78, 79, 80].

A synchronous generator that is connected to a three-phase supply network is normally symmetrically loaded and the power delivered by each stator winding has three-phase symmetry. In such cases the behaviour of one winding need only be considered in detail. The power p developed by each winding pulsates around an average power value at the double radian frequency $2\omega_s$. During certain periods the winding is absorbing power from the grid and p is actually negative. A convenient form of the power equation is:

$$p = P_G(1 - \cos 2\omega_s t) - Q_G \sin 2\omega_s t \qquad (8.1)$$

where

P_G = Real power, W per phase

Q_G = Reactive power, VAr per phase

ω_s = synchronous frequency, rad/s

The real power P_G is the average power of p and is the useful power transmitted by each winding to the network. The reactive power Q_G is the peak value of a power component that is considered to travel back and forth between the generator and the network. This component has an average value of zero and therefore is capable of no useful work. While both P_G and Q_G have dimensions of Watts, it is usual to measure Q_G in Volt-amperes reactive, VAr, to emphasise that it is non active.

The phasor diagram, Figure 8.3, represents the steady state operating condition of a salient pole generator connected to a large network with a fixed bus voltage and constant field excitation voltage. The real power output equation is derived from Crary [79] as follows:

$$P_G = e_T i_T \cos\theta \qquad (8.2a)$$

or

$$P_g = i_D e_D + i_Q e_Q \tag{8.2b}$$

where

$$e_D = e_T \sin\delta \tag{8.3a}$$

$$e_Q = e_T \cos\delta \tag{8.3b}$$

but the phasor diagram shows that:

$$i_D = \frac{E_f - e_Q}{x_D} \tag{8.4a}$$

$$i_Q = \frac{e_D}{x_Q} \tag{8.4b}$$

thus the steady state real power equation is given by:

$$P_g = \frac{E_f e_T}{x_D} \sin\delta + \frac{e_T^2 (x_D - x_Q)}{2 x_D x_Q} \sin 2\delta \tag{8.5}$$

where

θ = angle by which terminal current lags terminal voltage, electrical radians

$\cos\theta$ = power factor

i_T = terminal current, A per phase

i_D = direct-axis current, A per phase

i_Q = quadrature-axis current, A per phase

e_T = terminal voltage, V per phase

e_D = direct-axis voltage, V per phase

e_Q = quadrature-axis voltage, V per phase

E_f = field excitation voltage, V per phase

x_D = direct-axis reactance, Ω per phase

x_Q = quadrature-axis reactance, Ω per phase

δ = power angle, electrical radians

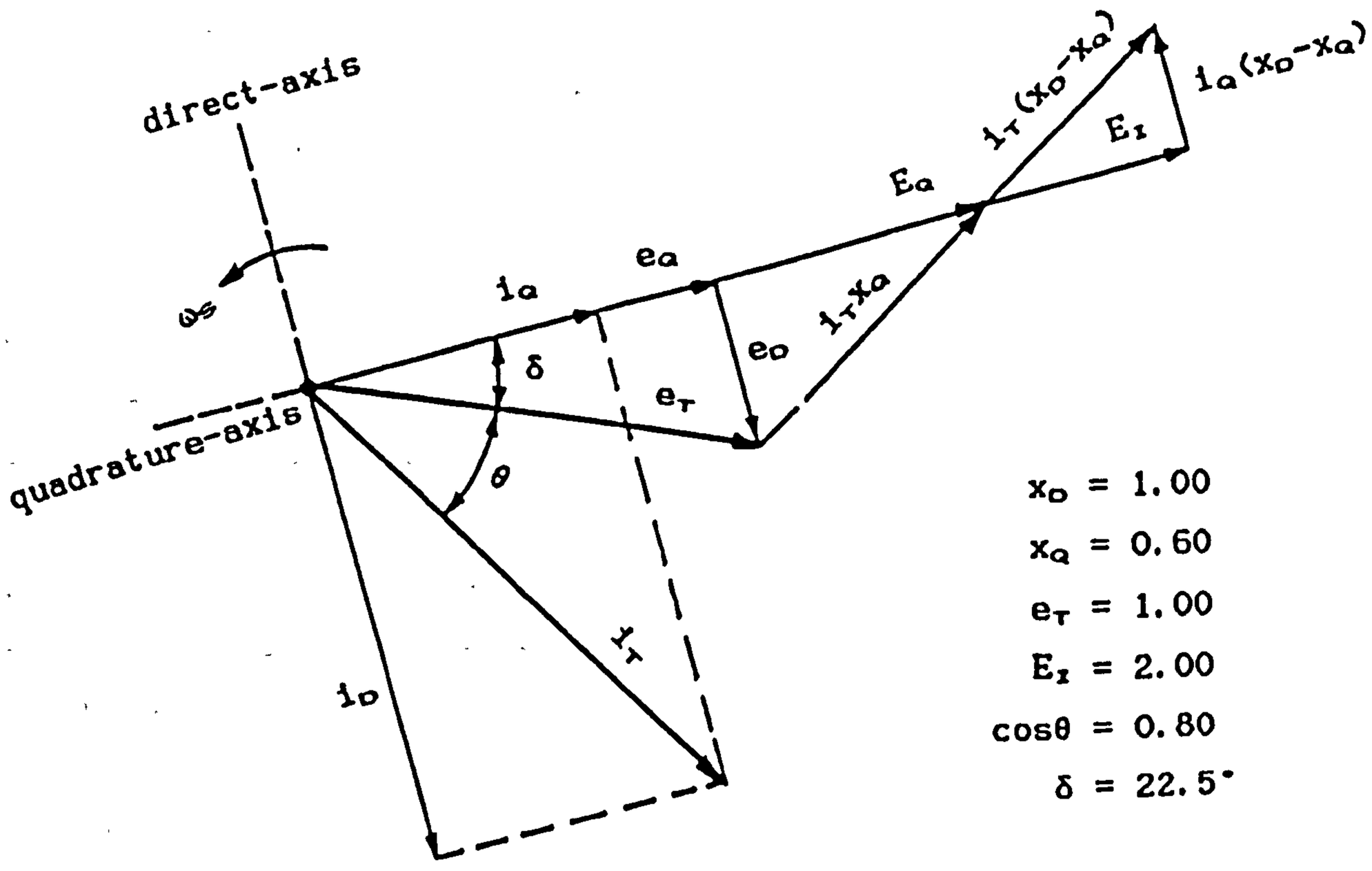

Figure 8.3: Phasor diagram for a salient pole generator connected directly to a large network.

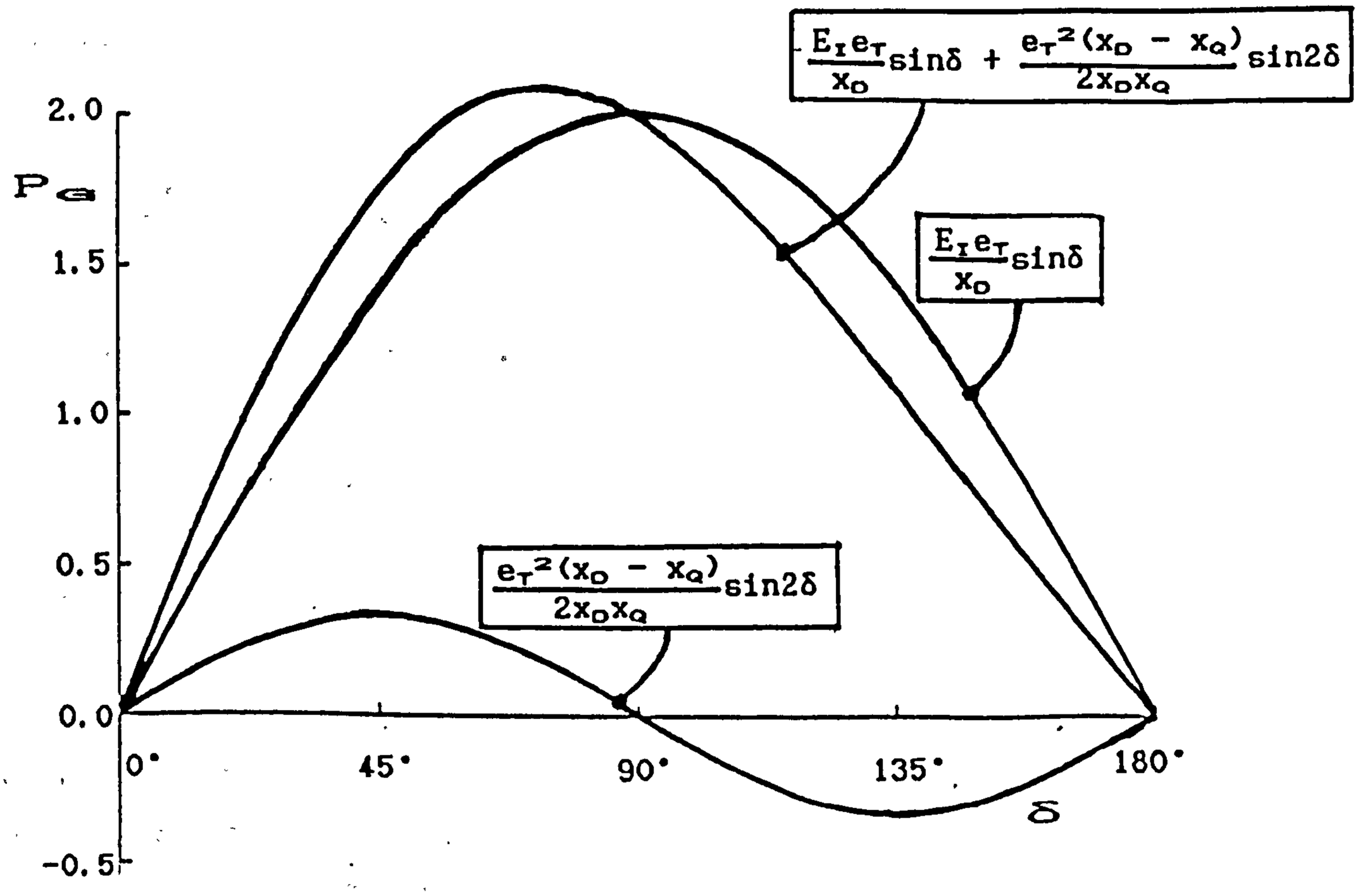

Figure 8.4: P_e-δ for a typical salient pole generator connected directly to a large network.

Of these parameters, the direct-axis and quadrature-axis reactances are fixed by design, and the terminal voltage is governed by the electricity supply network. Only the field excitation voltage can be controlled.

In order to evaluate the coefficients of the steady state power equation all parameters must be evaluated. A synchronous generator will be specified by its rated power output, the nominal power factor and the terminal voltage. If the direct-axis and quadrature-axis reactances are known, consideration of the nominal operating condition of the generator allows the magnitude of the nominal field excitation voltage to be determined.

The terminal current is found by rearranging (8.2a):

$$i_T = \frac{P_G}{e_T \cos\theta} \qquad (8.6)$$

Inspection of Fig. 8.3 shows the following relationships to be true::

$$E_Q = \sqrt{[(e_T + i_T x_Q \sin\theta)^2 + (i_T x_Q \cos\theta)^2]} \qquad (8.7)$$

$$\delta = \arctan \frac{i_T x_Q \cos\theta}{e_T + i_T x_Q \sin\theta} \qquad (8.8)$$

$$i_D = i_T \sin(\theta + \delta) \qquad (8.9)$$

$$E_I = E_Q + i_D(x_D - x_Q) \qquad (8.10)$$

Sequential solution of these equations will yield the value of the field excitation voltage at the rated operating condition of the generator. Provided the field excitation voltage remains constant, the coefficients of equation (8.5) will also remain constant. The variation

of P_G with respect to δ for a typical salient pole generator connected directly to a large network is shown in Figure 8.4.

The steady state reactive power equation can be similarly determined from:

$$Q_G = e_T i_T \sin\theta \qquad (8.11)$$

and is:

$$Q_G = \frac{E_I e_T}{x_D}\cos\delta - \frac{e_T^2(x_D + x_Q)}{2x_D x_Q} + \frac{e_T^2(x_D - x_Q)}{2x_D x_Q}\cos 2\delta \qquad (8.12)$$

Reactive power Q_G is of little interest when studying large networks since it is assumed that the system can adequately supply and absorb this component of the instantaneous power output of the generator. No further reference to reactive power will made here.

Per Unit analysis allows each value of power, voltage, current, reactance, frequency etc... to be expressed as a multiple of some base unit. The rated values of the actual synchronous generator are usually designated as the base units and all others quantities are expressed in per unit (p.u.) of these base values. When using per unit analysis, all the single phase power equations used above become representative of the machine as a whole. This technique is most convenient since it allows typical per unit values of E_I, e_T, x_D, x_Q, etc... to be used when actual values are not specifically known. The power equations can be used for any size of generator if the per unit form is used. Where real values are required, the per unit form can be multiplied by the base value to give the actual quantity in S.I. units.

The reactances x_D and x_Q depend upon the design of the machine and its operating state; they cannot be actively controlled. Typically x_D = 1.0 p.u. and x_Q = 0.6 p.u. [Crary], but for a round rotor generator the reactances of both axes are equal, so the final terms (known as the saliency or reluctance terms) of the equations for real and reactive power are zero.

If the network is infinitely strong then the terminal voltage e_T and the synchronous frequency ω_s will both be fixed i.e. e_T = 1.0 p.u. and ω_s = 1.0 p.u.

The power angle δ has dimensions of electrical radians and is the angle between the rotating magnetic axes of the rotor and stator windings. If E_I and e_T are constant then the real power output of the generator is a function of δ and, since the machine operates at a constant speed, it is directly proportional to the torque input to the generator from its prime mover.

If losses are neglected, then the mechanical driving torque must equal the electrodynamic torque of the generator. If the driving torque is increased then the electrodynamic torque and electrical power output will also increase. The power angle will increase to a new steady-state value that corresponds to the new power required to balance the increase in shaft torque.

The steady state synchronising power coefficient $\delta P_e/\delta\delta$ indicates the rate at which steady state power changes with changes in the power angle.

$$\frac{\delta P_e}{\delta\delta} = \frac{E_I e_T}{x_D}\cos\delta + \frac{e_T^2(x_D - x_Q)}{x_D x_Q}\cos 2\delta \qquad (8.13)$$

The maximum real power P_{max} that a salient pole machine can generate is delivered when $\delta = \delta_{max}$ and $\partial P_m / \partial \delta = 0$. At maximum power:

$$\delta_{max} = \arccos\left(\sqrt{[a^2 + 0.5]} - a\right) \qquad (8.14a)$$

where

$$a = \frac{E_f x_q}{4 e_T (x_d - x_q)} \qquad (8.14b)$$

The power angle δ will exceed δ_{max} if the prime mover tries to deliver more power than P_{max}. Increasing δ beyond δ_{max} results in less electrical power being generated. The generator will be operating beyond its steady-state stability limit and is statically unstable. The difference between mechanical input power and electrical output power will cause the speed of the rotor to increase, synchronisation will be lost and the generator will be disconnected from the network. The power P_{max} is often referred to as the "pull-out" power because it is the power at which synchronisation is lost.

The transient response of a synchronous generator to a sudden change in operating conditions may cause δ to temporarily exceed δ_{max}, even if the new operating point is within the static stability limit. Oscillations of the rotor will cause δ to fluctuate and the static stability limit may be exceeded, but if the oscillations diminish then the generator is stable and synchronisation with the network is maintained.

The field excitation voltage E_f does not affect the power being delivered to the generator by its prime mover and therefore cannot be used to control the power output of the generator. The reluctance terms are independent of

E_I, so a salient pole machine will generate power even if the field windings are not excited. However, if P_G is constant then increasing E_I will result in the steady state power angle being reduced. The value of P_{max} will be increased thereby increasing the steady-state stability limit. Increasing E_I also increases the magnitude of the synchronising power coefficient $\partial P_G/\partial\delta$.

Automatic Voltage Regulators (AVRs) are usually fitted to synchronous machines to control the output voltage by regulating the field excitation voltage. A very fast acting AVR could be used to increase E_I when a generator begins to operate beyond its steady-state stability limit. If E_I is increased so that $\partial P_G/\partial\delta$ remains positive, the machine will remain stable and synchronisation will be maintained. However, active field exciter control has been found to be unsuitable for wind turbine applications because the exciter response was slow [74]. For these studies, the field excitation voltage, E_I, will remain constant throughout the simulation period.

The synchronous generator may in reality be connected to the network via long transmission lines. In such cases the generator model must be modified to include the effects of an external reactance. The phasor diagram, Fig. 8.5, repreesents the state of a salient pole generator connected via an external reactance to a large network with a fixed bus voltage and constant field excitation voltage.

The real power output equation is derived by Crary in much the same way as before. The power delivered at the generator terminals is given by equation (8.2):

$$P_G = e_T i_T \cos\theta$$

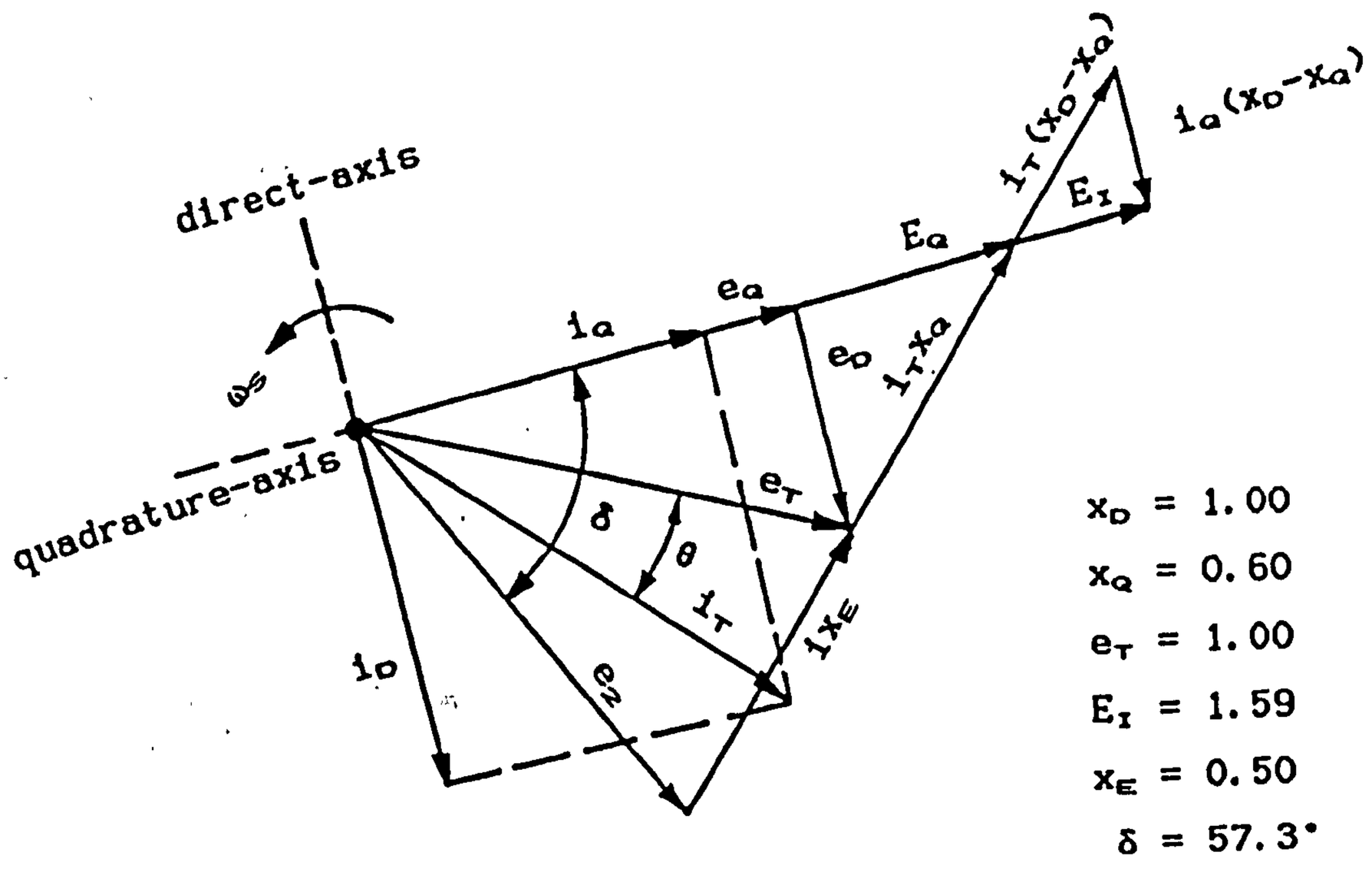

Figure 8.5: Phasor diagram representing a salient pole generator connected to a large network via an external reactance.

Figure 8.6: P_e-δ for a typical salient pole generator connected to a large network via an external reactance

but here the terminal voltage components are:

$$e_D = e_T \sin\delta_{12} \tag{8.15a}$$

$$e_Q = e_T \cos\delta_{12} \tag{8.15b}$$

The power delivered to the network via the external reactance is given by:

$$P_G = \frac{e_T e_2}{x_E} \sin 2\theta \tag{8.16}$$

Therefore, as Crary shows, the steady state real power output equation becomes:

$$P_G = \frac{E_I e_2}{(x_D + x_E)} \sin\delta + \frac{e_2^2 (x_D - x_Q)}{2(x_D + x_E)(x_Q + x_E)} \sin 2\delta \tag{8.17}$$

where

x_E = external reactance, Ω per phase

e_2 = infinite bus voltage, V per phase

The terminal current is calculated by first rearranging equation (8.16), so that:

$$\theta = \frac{1}{2} \arcsin \frac{P_G x_E}{e_T e_2} \tag{8.18}$$

and then substituting θ in equation (8.6) gives

$$i_T = \frac{P_G}{e_T \cos\theta}$$

Inspection of Figure 8.5 shows, that provided the generator remains stable, the following relationships hold true:

$$E_Q = \sqrt{[(e_T + i_T x_Q \sin\theta)^2 + (i_T x_Q \cos\theta)^2]}$$

$$\delta_{12} = \arctan \frac{i_T x_Q \cos\theta}{e_T + i_T x_Q \sin\theta} \qquad (8.19)$$

$$\delta = \delta_{12} + 2\theta \qquad (8.20)$$

$$i_D = i_T \sin(\theta + \delta_{12}) \qquad (8.21)$$

$$E_I = E_Q + i_D(x_D - x_Q)$$

Sequential solution of these equations will yield the value of the field excitation voltage at the rated operating condition of the generator. The field excitation voltage will remain constant, so the coefficients of equation (8.17) will also be constant. The relationship between P_G and δ for a typical salient pole generator connected to a large network via an external reactance is shown in Figure 8.6.

As before, the steady state synchronising power coefficient $\partial P_G/\partial\delta$ indicates the rate at which steady state power changes with changes in the power angle.

$$\frac{\partial P_G}{\partial\delta} = \frac{E_1 e_2}{(x_D + x_E)}\cos\delta + \frac{e_2^2(x_D - x_Q)}{(x_D + x_E)(x_Q + x_E)}\cos 2\delta \qquad (8.22)$$

The maximum real power P_{MAX} that a salient pole machine can generate is delivered when $\delta = \delta_{MAX}$ and $\partial P_G/\partial\delta = 0$. At maximum power:

$$\delta_{MAX} = \arccos(\sqrt{[a^2 + 0.5]} - a) \qquad (8.23a)$$

where

$$a = \frac{E_1(x_Q + x_E)}{4e_2(x_D - x_Q)} \qquad (8.23b)$$

The external reactance tends to weaken the link with the network and the power angle is much greater for a given power output than when it is directly linked. The generator therefore operates much closer to its steady state stability limit and is therefore more likely to become unstable if the operating conditions fluctuate.

Generally, it is these final equations that are used in the computer program DYNVAWT so that the influence of an external reactance on the behaviour of the system can be simulated if required. Clearly by setting $x_E = 0$, the above equations simplify to the form initially presented for case of a synchronous generator connected directly to the network.

The steady state torque Q_G (N.B. *not* reactive power) is simply:

$$Q_G = \frac{P_G}{\omega_S} \tag{8.24}$$

If the nominal synchronous speed $\omega_S = 1.0$ p.u., then the per unit equations for steady state power become per unit equations for steady state torque:

$$Q_G = \frac{E_1 e_2}{(x_D + x_E)}\sin\delta + \frac{e_2^2(x_D - x_Q)}{2(x_D + x_E)(x_Q + x_E)}\sin 2\delta \tag{8.25}$$

Similarly, the steady state synchronising torque coefficient $\partial Q_G/\partial\delta$ indicates the rate at which steady state torque changes with changes in the power angle. Let $T_S = \partial Q_G/\partial\delta$ so that

$$T_S = \frac{E_1 e_2}{(x_D + x_E)}\cos\delta + \frac{e_2^2(x_D - x_Q)}{(x_D + x_E)(x_Q + x_E)}\cos 2\delta \tag{8.26}$$

The behaviour of a synchronous generator is similar to that of a torsional spring with negligible inertia. If the spring stiffness is K_{EG}, and both ends are displaced θ_E and θ_G radians respectively, then the torque Q_{EG} Nm transmitted by the spring is:

$$Q_{EG} = K_{EG}(\theta_E - \theta_G) \qquad (8.27)$$

where

$$K_{EG} = \frac{\delta Q_{EG}}{\delta \theta} \qquad (8.28)$$

The spring stiffness is directly analogous to the steady state synchronising torque coefficient, however, the units need to be modified if the per unit expression for T_S is to be expressed in S.I. units for use with other drive train elements.

The power angle δ has real dimensions of electrical radians, but if θ_E is the angular displacement of the generator shaft and θ_G is the angular displacement of the rotating reference frame both wrt a datum on the generator frame, then:

$$\delta = \frac{N_P}{2}(\theta_E - \theta_G) \qquad (8.29)$$

where

N_P = number of generator poles

The nominal torque Q_R of a synchronous generator that has a rated power output of P_R and rated speed N_R is given by:

$$Q_R = \frac{30P_R}{\pi N_R} \qquad (8.30)$$

This is the base unit for all per unit values of torque. Therefore the torque transmitted by the spring is:

$$Q_{EG} = Q_G Q_K \tag{8.31}$$

Substituting for Q_{EG} and Q_K gives:

$$K_{EG}(\theta_E - \theta_G) = Q_G \frac{30P_R}{\pi N_R} \tag{8.32}$$

Rearranging (8.29) and (8.32) and substituting for $(\theta_E - \theta_G)$ gives

$$Q_G = K_{EG} \frac{2\pi N_R}{30P_R N_P} \delta \tag{8.33}$$

The steady state synchronising torque coefficient T_S is simply:

$$T_S = \frac{\delta Q_G}{\delta \delta} = K_{EG} \frac{2\pi N_R}{30P_R N_P} \tag{8.34}$$

therefore

$$K_{EG} = \frac{30P_R N_P}{2\pi N_R} T_S \tag{8.35}$$

which further simplifies to:

$$K_{EG} = 4.775 \frac{P_R N_P}{N_R} T_S \tag{8.36}$$

This expression for K_{EG} is similar to that presented without proof by Kos [81] except that his generator stiffness term is a slow-speed shaft equivalent. Note that while P_R, N_P and N_R are fixed, their values are determined by the rated characteristics of the machine, T_S varies with

the power angle, giving K_{eq} a non-linear characteristic. The stiffness, therefore, of the connection between the generator and the network varies with electrical power output. When $P_{eq} = P_{max}$ the steady state synchronising torque coefficient and the stiffness of the generator are *zero.*

The steady state response of an on-line synchronous generator to input power changes results in like changes of output power as discussed above. The response may or may not become unstable depending upon the characteristics of the generator and the severity of the change. In all cases it has been assumed that the deviation of the rotational speed of the rotor from synchronous speed (slip) is very small. However, when this deviation is larger, the acceleration of the rotor will be impeded by electrical damping forces. These forces are caused by currents that are induced in the amortisseur windings of the rotor due to its slip.

The time between opening and reclosing of the transmission line between a wind driven synchronous generator and the electrical network can only be short if synchronisation is to be maintained [75]. However, during such electrical disturbances the generator is temporarily unloaded, consequently the rotor will quickly accelerate in response to this condition. Electrically induced damping torque will act to oppose this acceleration and thereby needs to mathematically modelled if the effects of such disturbances are to be effectively simulated.

Of the references considered, only Crary [82] developed equations specifically for damping torque, and it is his model that is considered here. The equations describing damper action are only suitable for small changes of speed around synchronous speed and assume that some electrical

disturbance has occurred. Extensive knowledge of the transient behaviour of the generator is required and therefore the equations are of little value for general studies where much of the data required is unknown. However, Crary defines the per unit damping torque coefficient T_D as the negative of the per unit change in torque for per unit change in speed. This is a more convenient form of the damping equations since it is analogous to the action of a torsional damper. For this study, it is this damping term that will utilised.

The damping torque developed by a synchronous generator can be modelled by considering a torsional damper with negligible inertia. If the damping coefficient is C_{EG} and both ends have velocities ω_E and ω_G respectively, then the damping torque Q_{EG} is:

$$Q_{EG} = C_{EG}(\omega_E - \omega_G) \tag{8.37}$$

where

$$C_{EG} = \frac{\partial Q_{EG}}{\partial \omega} \tag{8.38}$$

The per unit slip ds is equal to the per unit change in synchronous speed, i.e. $ds = d\omega_S/\omega_S$, where:

$$d\omega_S = \frac{N_P}{2}(\omega_E - \omega_G) \tag{8.39}$$

The torque transmitted by the damper is:

$$Q_{EG} = Q_G Q_R \tag{8.40}$$

Substituting for Q_{EG} and Q_R gives:

$$C_{EG}(\omega_E - \omega_G) = Q_G \frac{30P_R}{\pi N_R} \tag{8.41}$$

Rearranging and substituting for $(\omega_E - \omega_G)$ gives

$$Q_G = C_{EG}\frac{2\pi N_R}{30P_R N_P} d\omega_S = C_{EG}\frac{2\pi N_R}{30P_R N_P} \omega_S ds \tag{8.42}$$

The damping torque coefficient T_D is simply:

$$T_D = \frac{\delta Q_G}{\delta s} = C_{EG}\frac{2\pi N_R}{30P_R N_P}\omega_S \tag{8.43}$$

therefore

$$C_{EG} = \frac{30P_R N_P}{2\pi N_R \omega_S} T_D \tag{8.44}$$

which further simplifies to:

$$C_{EG} = 4.775 \frac{P_R N_P}{\omega_S N_R} T_D \tag{8.45}$$

Again, this expression for C_{EG} is similar to that used by Kos [81]. Typical values of T_D = 3.15 - 23.10 p.u. and T_D = 2.00 - 20.00 p.u. are presented by Crary and Kos respectively. As will be demonstrated later, the damping action of the generator plays a vital role in controlling the transient stability of the wind turbine generator.

In summary, the torque Q_{EG} transmitted by a synchronous generator may be represented by a non-linear torsional spring with a stiffness K_{EG} and a damping element with a damping coefficient C_{EG} such that:

$$Q_{EG} = K_{EG}(\theta_E - \theta_G) + C_{EG}(\omega_E - \omega_G) \tag{8.46}$$

8.2.2: The Drive Train Model

The drive train model developed here uses a lumped inertia representation; the dynamic behaviour of each inertia being described by an ordinary differential equation. Initially a representation that modelled the six major drive train components of the 5kW V-VAWT generator system was considered suitable for this project. These six inertia elements were:

(a) V-VAWT rotor
(b) 1st stage driving pulley and brake disc
(c) 1st stage driven pulley
(d) 2nd stage driving pulley
(e) 2nd stage driven pulley
(f) Synchronous generator rotor

The low-speed, medium-speed and high-speed shafts and the first and second stage V-belts can be represented by torsional spring and damping elements. These elements are considered to have no inertia, so the inertial properties of the actual components must be included into the lumped inertia elements as appropriate. The speed changes at each stage of the V-belt transmission can be represented by ideal gear elements. Friction forces are applied directly to the inertia elements.

Mechanical torque acts on the system through the rotor and the brake. Electrical torque reacts on the system through the generator rotor.

The behaviour of the synchronous generator can be modelled by torsional spring and damping elements as described in the previous section. The electrical torque reaction on the generator rotor can be represented if the spring and damping elements connect the inertia element representing

the generator rotor to a seventh inertia element that represents the rotating magnetic field of the electricity supply network. Since this magnetic field rotates at a constant frequency, the inertia of this seventh element is considered to be infinite. This is a useful model to adopt, since the electrical torque reaction on the drive train system is modelled by a mechanical analogy.

The angular velocity and displacement of each inertia element must be measured with respect to a reference system. A suitable reference system is the rotating magnetic field of the electricity supply network. However, the author considers that a reference system external to the drive train system is more convenient to adopt, since all angular velocities and displacements would be those that could be observed on the actual machine. Adopting an external reference system allows the start-up and shut-down procedures, when the generator is disconnected from the network, to be readily simulated and the angular displacement of the rotor inertia would be directly equivalent to the azimuthal displacement of the V-VAWT rotor.

The representation of the V-VAWT generator system discussed so far is shown in Figure 8.7, where:

Q_i = torque applied to ith inertia element, Nm
J_i = ith inertia element, kg m^2
F_i = ith friction force, $Nm/rads^{-1}$
K_{ij} = torsional stiffness between ith and jth inertia elements, Nm/rad
C_{ij} = damping coefficient between ith and jth inertia elements, $Nm/rads^{-1}$
N_i = ith gear ratio
θ_i = angular displacement of ith inertia element, rad
ω_i = angular velocity of ith inertia element, $rads^{-1}$

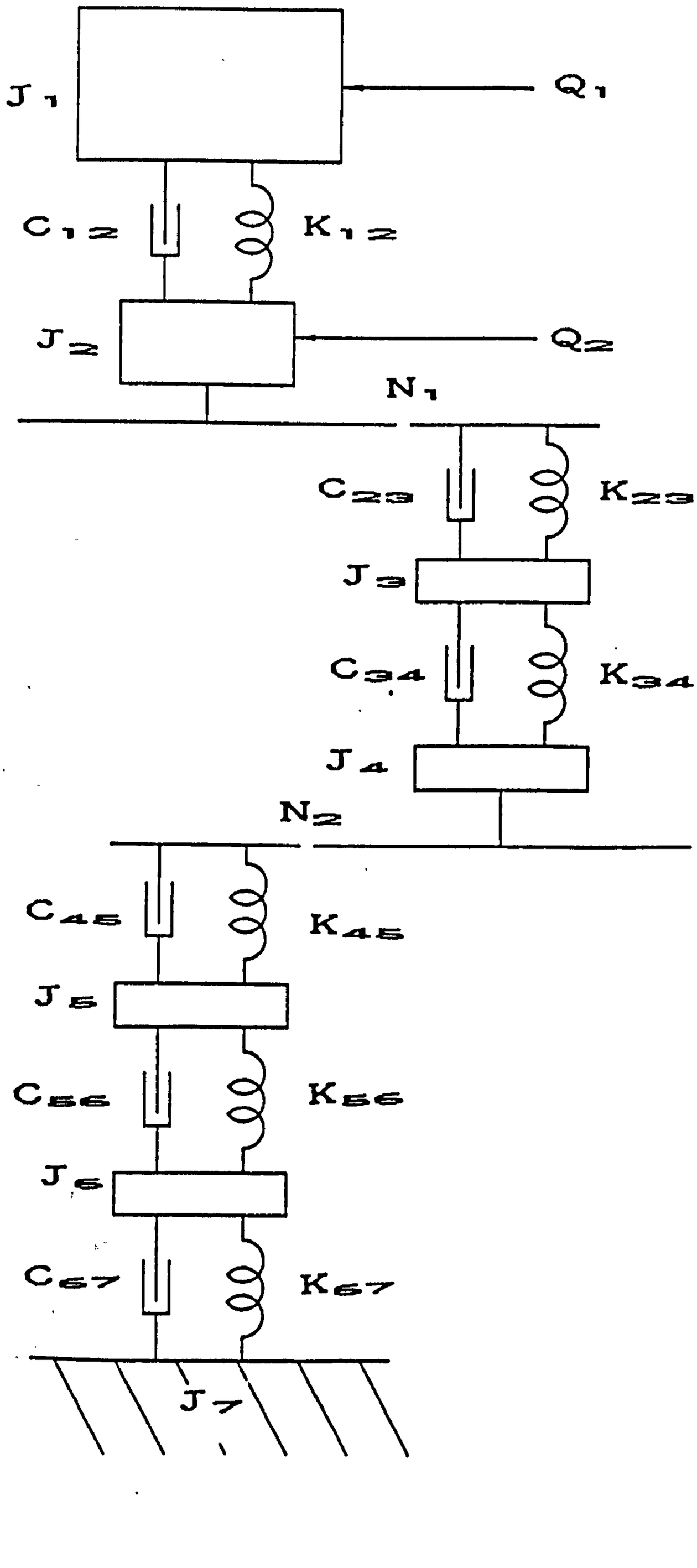

Figure 8.7: Lumped inertia model of V-VAWT drive train system

Where an ideal gear element of gear-up ratio N is included in the model, it is possible to modify the low-speed side parameters to high-speed side equivalents. The low-speed inertia, stiffness, damping and friction elements must be *reduced* by a factor N^2 to obtain their high-speed equivalents; applied torques must be *reduced* by a factor N; but angular velocities and displacements must be *increased* by a factor N. Using this approach here, requires the following modifications to be made to the model:

$$Q_1' = Q_1/(N_1N_2) \quad (8.47a)$$

$$Q_2' = Q_2/(N_1N_2) \quad (8.47b)$$

$$J_1' = J_1/(N_1N_2)^2 \quad (8.47c)$$

$$J_2' = J_2/(N_1N_2)^2 \quad (8.47d)$$

$$J_3' = J_3/(N_2)^2 \quad (8.47e)$$

$$J_4' = J_4/(N_2)^2 \quad (8.47f)$$

$$\theta_1' = \theta_1(N_1N_2) \quad (8.47g)$$

$$\theta_2' = \theta_2(N_1N_2) \quad (8.47h)$$

$$\theta_3' = \theta_3(N_2) \quad (8.47i)$$

$$\theta_4' = \theta_4(N_2) \quad (8.47j)$$

$$\omega_1' = \omega_1(N_1N_2) \quad (8.47k)$$

$$\omega_2' = \omega_2(N_1N_2) \quad (8.47l)$$

$$\omega_3' = \omega_3(N_2) \quad (8.47m)$$

$$\omega_4' = \omega_4(N_2) \quad (8.47n)$$

$$K_{12}' = K_{12}/(N_1N_2)^2 \quad (8.47o)$$

$$K_{23}' = K_{23}/(N_2)^2 \quad (8.47p)$$

$$K_{34}' = K_{34}/(N_2)^2 \quad (8.47q)$$

$$C_{12}' = C_{12}/(N_1N_2)^2 \quad (8.47r)$$

$$C_{23}' = C_{23}/(N_2)^2 \quad (8.47s)$$

$$C_{34}' = C_{34}/(N_2)^2 \quad (8.47t)$$

$$F_1' = F_1/(N_1N_2)^2 \quad (8.47c)$$

$$F_2' = F_2/(N_1N_2)^2 \quad (8.47v)$$

$$F_3' = F_3/(N_2)^2 \quad (8.47w)$$

$$F_4' = F_4/(N_2)^2 \quad (8.47x)$$

Using the modified model parameters, the ordinary differential equations that describe the motion of the drive train can be constructed by consideration of D'Alembert's Law at each inertia element. Thus:

$$Q_1' = J_1'\dot{\omega}_1' + K_{12}'(\theta_1'-\theta_2') + C_{12}'(\omega_1'-\omega_2') + F_1'\omega_1' \quad (8.48a)$$

$$Q_2' = J_2'\dot{\omega}_2' + K_{23}'(\theta_2'-\theta_3') + C_{23}'(\omega_2'-\omega_3') + F_2'\omega_2' - K_{12}'(\theta_1'-\theta_2') - C_{12}'(\omega_1'-\omega_2') \quad (8.48b)$$

$$0 = J_3'\dot{\omega}_3' + K_{34}'(\theta_3'-\theta_4') + C_{34}'(\omega_3'-\omega_4') + F_3'\omega_3' - K_{23}'(\theta_2'-\theta_3') - C_{23}'(\omega_2'-\omega_3') \quad (8.48c)$$

$$0 = J_4'\dot{\omega}_4' + K_{45}'(\theta_4'-\theta_5') + C_{45}'(\omega_4'-\omega_5') + F_4'\omega_4' - K_{34}'(\theta_3'-\theta_4') - C_{34}'(\omega_3'-\omega_4') \quad (8.48d)$$

$$0 = J_5\dot{\omega}_5 + K_{56}(\theta_5 - \theta_6) + C_{56}(\omega_5 - \omega_6) + F_5\omega_5 - K_{45}'(\theta_4'- \theta_5) - C_{45}'(\omega_4'- \omega_5) \quad (8.48e)$$

$$0 = J_6\dot{\omega}_6 + K_{67}(\theta_6 - \theta_7) + C_{67}(\omega_6 - \omega_7) + F_6\omega_6 - K_{56}(\theta_5 - \theta_6) - C_{56}(\omega_5 - \omega_6) \quad (8.48f)$$

$$0 = \dot{\omega}_7 \quad (8.48g)$$

and since the rotating magnetic field of the supply network rotates at synchronous speed ω_s, then:

$$\omega_7 = \omega_s \quad (8.49)$$

All the parameters describing the mechanical drive train components can be estimated from initial design data. The accuracy of these estimates is dependent upon the detail of the design data available at the time the dynamic modelling is to performed. For instance, a method for estimating the moment of inertia of the blades was developed on the assumption that only the overall controlling dimensions of the blade would be known. The dimensions of the blade are those used with the blade geometry preparation program WRITEBLADE. The internal form of the blade

is assumed to be solid and an equivalent material density is calculated from blades of similar construction and known mass. This method is considered to be appropriate here and the estimates of blade inertia to be sufficiently accurate for dynamic modelling purposes.

In this model the rotor inertia J_1 is the sum of the inertias of all the rotating components. The low-speed shaft stiffness $K_{1,2}$ and damping $D_{1,2}$ are representative of the torsional properties of the portion of the stub tower connecting the blade root attachments to the 1st stage driving pulley. This model, therefore, assumes that the blades are stiff in the edgewise plane and that the rotor is rigid.

Often the HAWT rotor has been modelled by other authors to include blade inertia, hub inertia and blade edgewise stiffness. Using such a model, introduces more flexibility into the drive train at the low-speed side of the rotor. However, to estimate the edgewise stiffness of the blade requires a detailed knowledge of its construction and the use of finite element analysis [81]. It is not possible to perform such analysis in the general case where the construction of the blade is unknown, therefore the refinement of the current rotor model to include edgewise stiffness effects is not considered appropriate. Where known and considered appropriate, the low-speed shaft stiffness term could be modified to include such effects.

Typical of Darrieus rotor models, Dubé [73] uses two lumped inertias connected via a torsional spring element. This model considers the upper and lower halves of the rotor blades to be separate and connected to each other by the central column. The column transmits the torque from the upper blade mounting points to the lower mounting

points at the rotor base. However, the blades of the V-VAWT rotor transmit torque to the stub tower only at their root, so it would be inappropriate to adopt this approach here.

All the mechanical components are considered to behave in a linear manner and that all the describing parameters do not vary with time. The electrical stiffness and damping terms are non-linear since their values are dependent upon the state of the connection with the supply network and state of drive train system itself; they must be evaluated at each step of the simulation process.

There are two applied torques acting on the system, Q_1 and Q_m, each independent of the other. Q_m is the torque applied by the brake system to disc on the low-speed shaft. The brake has only two states (on/off) and the so the steady state value Q_m is either the maximum rated value of the brake system or zero. Q_1 is the aerodynamic torque developed by the V-VAWT rotor and is very non-linear. For a given rotor configuration, Q_1 is a function of four parameters:

(a) Windspeed, V_ω
(b) Angular velocity of rotor, ω_1
(c) Azimuthal position of rotor, θ_1
(d) Blade tip pitch angle, β_A

The blade tip pitch angle is dependent upon the state of the actuator system and is the only parameter that can be actively controlled. Windspeed varies continually and the response of the rotor will be most sensitive to changes of this parameter. The angular velocity and azimuthal position of the rotor describe the state of the V-VAWT rotor and since their high-speed equivalents, ω_1' and θ_1' respectively, effectively appear on both sides of equation

(8.48a), this and the other differential equations cannot be explicitly solved. Introducing torque variations due to azimuth angle is indicative of the cyclic variation of the aerodynamic torque developed by VAWT rotors.

The V-VAWT performance predictions generated by VAWTTAY can be used as the basis of the aerodynamic torque model for calculating Q_1. In small perturbation analysis of the V-VAWT generator system, a simple aerodynamic torque model could be developed from linearisation of the performance predictions .about the operating point. However, such a model would not include cyclic torque variations nor would the non-linear characteristics of aerodynamic torque be accurately modelled where large perturbations about the operating point are excited. The aerodynamic torque model developed for this project calculates Q_1 from a look-up table of the performance predictions generated by VAWTTAY. This approach ensures that all the predicted characteristics of the particular V-VAWT configuration being analysed are included in the simulation. This model is described in greater detail in Section 8.2.7.

Both the applied torques depend upon the state of the V-VAWT generator system and its inputs, therefore they must be evaluated at each step of the simulation process.

The differential equations (8.48) cannot be solved explicitly nor are they in a form suitable for computer based solution. The state space approach allows an *n*th order differential equation to be replaced by *n* difference equations that are functions of the state variables describing the system. Each inertia element of the V-VAWT drive train system can be described by two state variables since a second order differential equation is used to describe the dynamic behaviour of the element. A total of fourteen state variables are required to satisfactorily

describe the drive train system, and it is convenient to choose the angular velocities and displacements of the inertia elements as these variables. Equation (8.48) can be rearranged in terms of the state variables and the fourteen state equations are defined as follows:

$$\dot{\omega}_1' = \frac{1}{J_1'}\left\{\begin{matrix} Q_1' - K_{12}'(\theta_1'-\theta_2') - C_{12}'(\omega_1'-\omega_2') - \\ F_1'\omega_1' \end{matrix}\right\} \quad (8.50a)$$

$$\dot{\omega}_2' = \frac{1}{J_2'}\left\{\begin{matrix} Q_2' - K_{23}'(\theta_2'-\theta_3') - C_{23}'(\omega_2'-\omega_3') - \\ F_2'\omega_2' + K_{12}'(\theta_1'-\theta_2') + C_{12}'(\omega_1'-\omega_2') \end{matrix}\right\} \quad (8.50b)$$

$$\dot{\omega}_3' = \frac{1}{J_3'}\left\{\begin{matrix} - K_{34}'(\theta_3'-\theta_4') - C_{34}'(\omega_3'-\omega_4') - \\ F_3'\omega_3' + K_{23}'(\theta_2'-\theta_3') + C_{23}'(\omega_2'-\omega_3') \end{matrix}\right\} \quad (8.50c)$$

$$\dot{\omega}_4' = \frac{1}{J_4'}\left\{\begin{matrix} - K_{45}'(\theta_4'-\theta_5') - C_{45}'(\omega_4'-\omega_5') - \\ F_4'\omega_4' + K_{34}'(\theta_3'-\theta_4') + C_{34}'(\omega_3'-\omega_4') \end{matrix}\right\} \quad (8.50d)$$

$$\dot{\omega}_5' = \frac{1}{J_5'}\left\{\begin{matrix} - K_{56}(\theta_5 - \theta_6) - C_{56}(\omega_5 - \omega_6) - \\ F_5\omega_5 + K_{45}'(\theta_4' - \theta_5) + C_{45}'(\omega_4' - \omega_5) \end{matrix}\right\} \quad (8.50e)$$

$$\dot{\omega}_6' = \frac{1}{J_6'}\left\{\begin{matrix} - K_{67}(\theta_6 - \theta_7) - C_{67}(\omega_6 - \omega_7) - \\ F_6\omega_6 + K_{56}(\theta_5 - \theta_6) + C_{56}(\omega_5 - \omega_6) \end{matrix}\right\} \quad (8.50f)$$

$$\dot{\omega}_7' = 0 \quad (8.50g)$$

$$\dot{\theta}_1' = \omega_1 \quad (8.50h)$$

$$\dot{\theta}_2' = \omega_2 \quad (8.50i)$$

$$\dot{\theta}_3' = \omega_3 \quad (8.50j)$$

$$\dot{\theta}_4' = \omega_4 \quad (8.50k)$$

$$\dot{\theta}_5' = \omega_5 \quad (8.50l)$$

$$\dot{\theta}_6' = \omega_6 \quad (8.50m)$$

$$\dot{\theta}_7' = \omega_7 = \omega_s \quad (8.50n)$$

It is often convenient to express the state equations using vector-matrix notation [83]

$$\dot{\underset{\sim}{x}} = \underset{\sim}{A}.\underset{\sim}{x} + \underset{\sim}{B}.\underset{\sim}{u} \quad (8.51)$$

where

$\underset{\sim}{x}$ = state vector

$\underset{\sim}{u}$ = input vector

$\underset{\sim}{A}$ = coefficient matrix of the process

$\underset{\sim}{B}$ = driving matrix

For this system, the coefficient matrix of the process would be a 14 x 14 square matrix and the driving matrix a 14 x 2 rectangular matrix. Both matricees would contain many zero entries and be considered sparse. Whilst the notation is convenient for computer based analysis of dynamic systems, the sparseness of the matrices suggests that it is not an efficient method for describing the state equations in this application. The form of the state equations presented in equation (8.50) can be readily adapted for computer based analysis and is considered to be more effective here.

Clearly, if all the system parameters are evaluated and the *initial* state of the drive train system is known then the *initial* state derivatives can be calculated using equation (8.50). If the time response of the system is to be simulated, the state derivatives and state variables must used to calculate the state of the system at the next discrete time step of the simulation. This calculation procedure is repeated for the duration of the simulation period.

The accuracy of the discrete time solution is dependent upon the numerical solution method adopted and the size of the time interval between calculation steps. Observation of the state equations shows that the state derivatives are sensitive to large stiffness values or small inertia

equivalent inertia	2-blades kgm²	3-blades kgm²
J_1'	2.771	2.567
J_2'	0.083	0.051
J_3'	0.004	0.003
J_4'	0.048	0.029
J_5'	0.010	0.010
J_6'	0.060	0.060
J_R	2.854	2.618
J_S	0.052	0.032
J_E	0.070	0.070

Table 8.1a: Estimated values of equivalent inertia for 5kW V-VAWT two and three bladed configurations

equivalent stiffness	2-blades Nm/rad	3-blades Nm/rad
K_{12}'	674 700	418 400
K_{23}'	456	283
K_{34}'	8 011	4 968
K_{45}'	1 908	1 908
K_{56}'	269 500	269 500
† K_{67}'	147	147
K_{R3}	456	283
K_{5E}	1 908	1 908
† K_{EG}	147	147
† K_{EG}	105	92

† Equivalent stiffness of synchronous generator calculated at nominal operating condition

Table 8.1b: Estimated values of equivalent stiffness for 5kW V-VAWT two and three bladed configurations

elements. The instantaneous angular accelerations of a small inertia elements will be relatively large, and if the time between calculation steps is too large then numerical instability will occur and poor solutions will be generated. Reducing the size of the time step incurs a computational time penalty, so a compromise step size and solution accuracy must be achieved if a useful dynamic analysis tool is to be developed. Critical appraisal of the drive train model shows that the number of inertia elements modelled can be reduced without affecting the validity of the dynamic simulation solution.

Table 8.1 lists the estimated values of the stiffness and inertia elements of the 5kW V-VAWT for both two-bladed and three-bladed configurations. The actual values of inertia and stiffness for each component have been estimated from design drawings, and modified to high-speed equivalents using equation (8.47). Clearly the equivalent inertia of the rotor is significantly larger than any other drive train component, thus making it the component of most interest. Also, note that the mechanical components of the V-VAWT drive train are very stiff compared to the V-belts and generator rotor. Usually, the low-speed shaft is the most compliant element of a wind turbine drive system, and it is the generator connection to the network that is considered to be stiff [81,84].

The drive train model can be modified if the mechanical components are considered to be rigid and their equivalent stiffness elements excluded from the model. This allows the system to be modelled with only three lumped inertia elements that are coupled to the electricity supply network via a series of stiffness and damping elements, Figure 8.9a. In this new model the V-VAWT rotor, 1st stage driving pulley and disc brake inertias are lumped together, as are the 1st stage driven and 2nd stage

driving pulley, and the generator rotor and the 2nd stage driven pulley. Thus:

$$J_R = J_1' + J_2' \tag{8.52a}$$

$$J_S = J_3' + J_4' \tag{8.52b}$$

$$J_E = J_5' + J_6' \tag{8.52c}$$

The stiffness element K_{RS} represents the 1st stage V-belts, K_{SE} the 2nd stage V-belts, and K_{EG} the synchronous generator stiffness. Of these elements, K_{RS} and K_{SE} are fixed by design but K_{EG} is dependent upon the state of the generator with respect to the electricity supply network. Thus:

$$K_{RS} = K_{23}' \tag{8.53a}$$

$$K_{SE} = K_{45}' \tag{8.53b}$$

$$K_{EG} = K_{67}' \tag{8.53c}$$

The synchronous generator is the only drive train component that has significant damping qualities, so it is convenient to exclude the damping effects of the mechanical components from the model. The response of the undamped mechanical system will more pessimistic than that of a lightly damped system, but this has the advantage that the control methods and strategies will be more severely tested. Thus:

$$C_{EG} = C_{67}' \tag{8.54}$$

The friction force coefficient F_{FR} can be used to include mechanical and electrical power losses into the drive train model. Its value has been initially evaluated at the nominal operating condition assuming the drive train has an overall power transmitting efficiency of 80%. Thus:

$$F_R = 0.2 \frac{Q_{Rnom}}{\omega_{Rnom}} \tag{8.55}$$

where

Q_{Rnom} = nominal torque of rotor, Nm

ω_{Rnom} = nominal angular velocity of rotor, rad/s

The torque Q_R applied to the inertia element J_R is the sum of the equivalent aerodynamic and braking torques applied to the drive train system. Thus:

$$Q_R = Q_1' + Q_2' \tag{8.56}$$

The state variables for the three inertia elements are the angular velocities ω_R, ω_G and ω_E and the angular displacements θ_R, θ_G and θ_E. The state of the rotating magnetic field of the electricity supply network is described by ω_S and θ_S.

The transient response of the modified model is dominated by the large inertia of the V-VAWT rotor, as the lumped inertias representing the intermediate drive train components and generator rotor are still significantly smaller than the rotor itself. The natural frequency of the smaller inertia elements is much higher than that of the rotor, therefore the transient response of these elements will decay in a much shorter time than the transient response of the rotor. If the transient response of these elements is to be accurately calculated, the time between the discrete steps of numerical solution must be chosen to be suitably small to avoid numerical instability of the solution. This necessarily increases the computation time for completing a simulation study. A further review and modification of the drive train model is required.

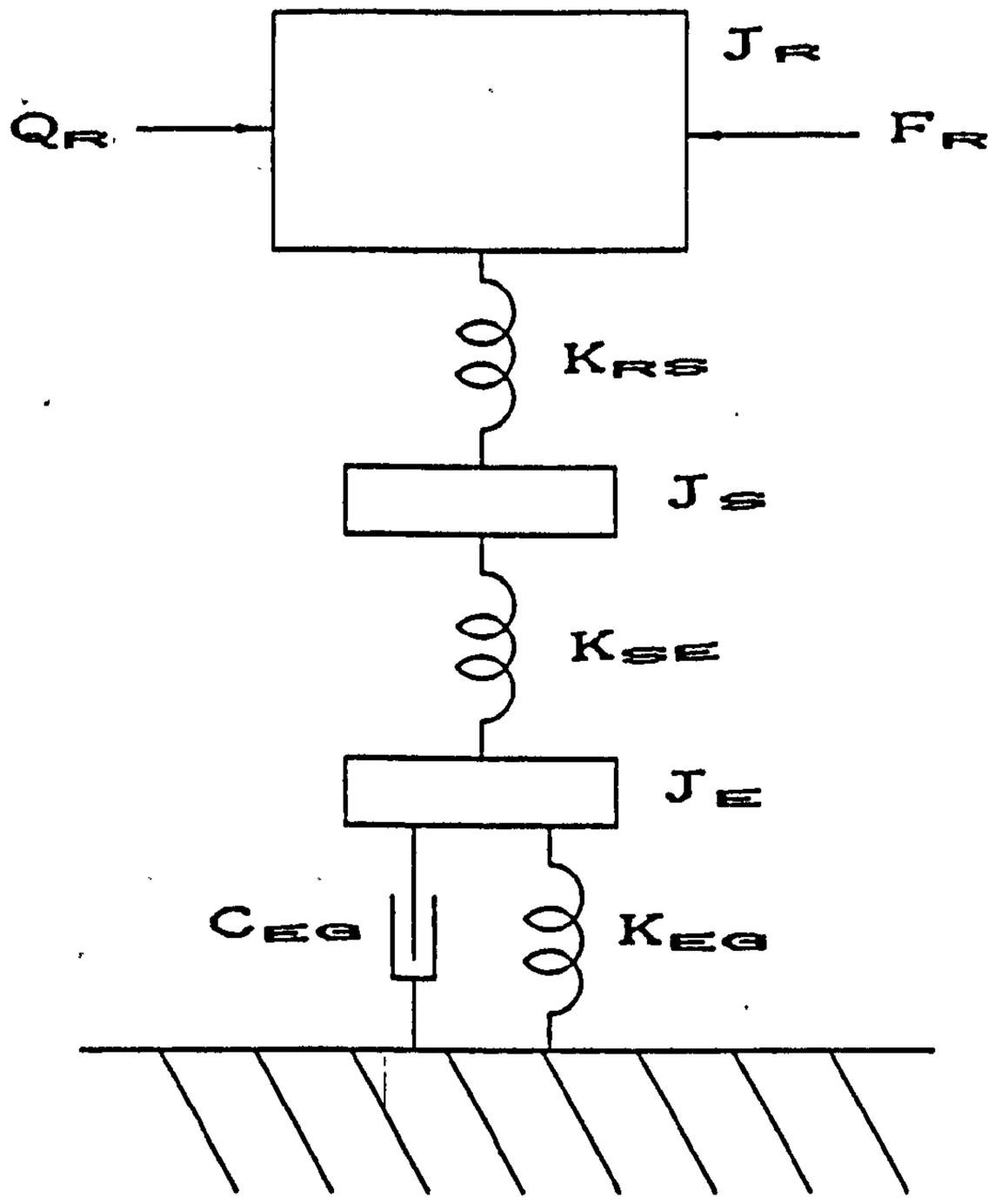

Fig. 8.9a: Modified dynamic model of 5kW V-VAWT drive train system with three inertia elements

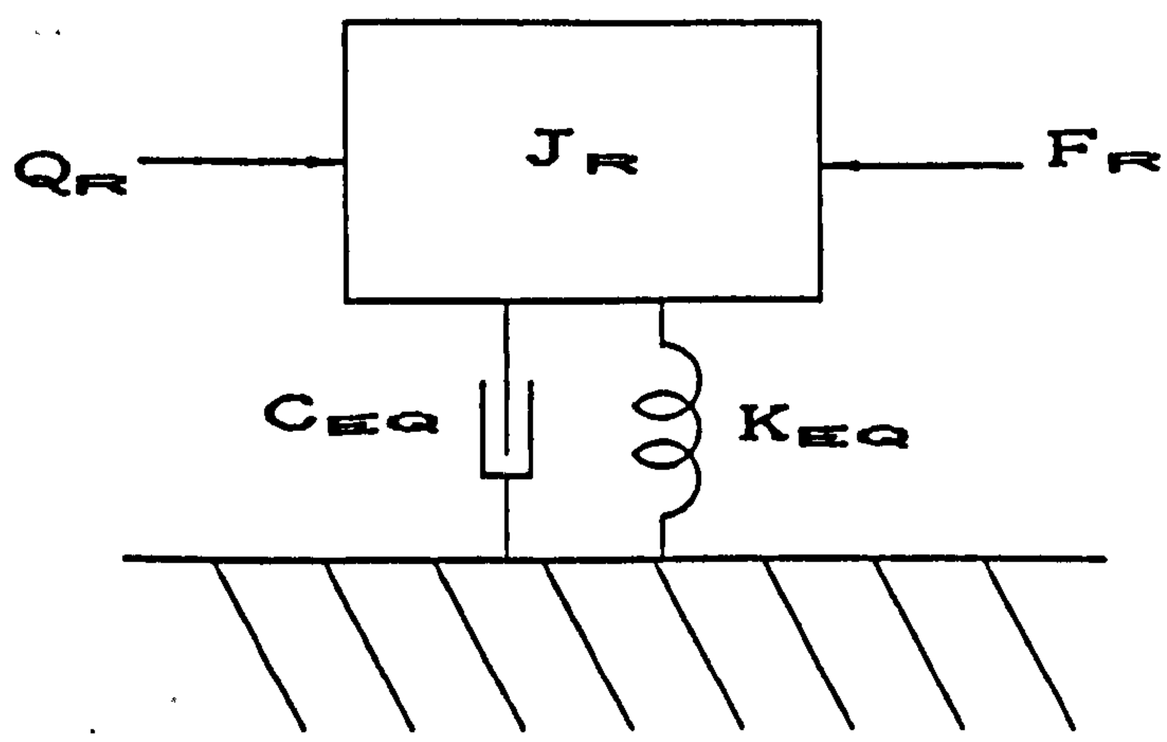

Fig. 8.9b: Simplified dynamic model of 5kW V-VAWT drive train system

The drive train model can be further simplified if the inertia of the V-belt pulleys and generator rotor are assumed to be negligible and that the behaviour of these components is not explicitly modelled by state equations. The drive train system can then be modelled by only a single inertia element, representing the V-VAWT rotor, that is coupled to the electricity supply network by a single stiffness element that represents the three stiffness elements acting in series, Figure 8.9b.

Using this simplified model, the state of the drive train system is completely described by only two ordinary differential equations:

$$Q_R = J_R\dot{\omega}_R + K_{EQ}(\theta_R - \theta_G) + C_{EQ}(\omega_R - \omega_G) + F_R\omega_R \qquad (8.57a)$$

$$0 = \dot{\omega}_G \qquad (8.57b)$$

where K_{EQ} is the equivalent stiffness of the coupling elements:

$$K_{EQ} = \frac{K_{RS}.K_{SE}.K_{EG}}{K_{RS}.K_{SE} + K_{SE}.K_{EG} + K_{EG}.K_{RS}} \qquad (8.58)$$

and C_{EQ} is the equivalent damping coefficient of the coupling elements:

$$C_{EQ} = C_{EG} \qquad (8.59)$$

Such a model does not allow the transient response of the V-belt pulleys or the generator rotor to be numerically simulated; only the transient response of the rotor itself can be explicitly modelled. However, the state of the V-belt pulleys is of little interest in these control studies, therefore excluding these components from the model is justified. The state of the generator rotor, though, must be evaluated so that the electrical power output and the generator stiff-

ness can be calculated. The state of the generator can only be evaluated if it is assumed that its transient response decays very rapidly and that its steady state response is in phase with that of the wind turbine rotor. Consequently, the angular velocity and displacement of the generator rotor with respect to the electricity supply network is assumed to be proportional to the velocity and displacement of the wind turbine rotor; the proportionality being dependent upon the stiffness of the interconnnecting elements.

The intermediate states of the V-belt pulleys and generator can be considered in terms of the stiffness elements and the state variables of the rotor and network, such that:

$$(\theta_E - \theta_G) = \frac{K_{RS}.K_{SE}}{K_{RS}.K_{SE} + K_{SE}.K_{EG} + K_{EG}.K_{RS}}(\theta_R - \theta_G) \qquad (8.60)$$

$$(\theta_S - \theta_E) = \frac{K_{RS}}{K_{RS} + K_{SE}}(\theta_R - \theta_E) \qquad (8.61)$$

$$(\omega_E - \omega_G) = \frac{K_{RS}.K_{SE}}{K_{RS}.K_{SE} + K_{SE}.K_{EG} + K_{EG}.K_{RS}}(\omega_R - \omega_G) \qquad (8.62)$$

$$(\omega_S - \omega_E) = \frac{K_{RS}}{K_{RS} + K_{SE}}(\omega_R - \omega_E) \qquad (8.63)$$

This simplified drive train model allows a numerical solution to be more rapidly completed because a smaller number of discrete time steps are required to accurately evaluate the transient response of the system for a given simulation time period.

The state differential equations are simply:

$$\dot{\omega}_R = \frac{1}{J_R}[Q_R - K_{EG}(\theta_R - \theta_G) - C_{EG}(\omega_R - \omega_G) - F_R\omega_R] \qquad (8.64a)$$

$$\dot{\theta}_R = \omega_R \tag{8.64b}$$

$$\dot{\omega}_G = 0 \tag{8.64c}$$

$$\dot{\theta}_G = \omega_G \tag{8.64d}$$

The above state equations and state variables only describe the drive train system, which is one sub-system of the whole V-VAWT generator system. The state of the V-VAWT generator can be described by a finite number of state variables which for convenience will be described by the variable x_i. The state equations for four of these variables are:

$$\dot{x}_1 = \frac{1}{J_R}[Q_R - K_{EQ}(x_2 - x_4) - C_{EQ}(x_1 - x_3) - F_{RM1}] \tag{8.65a}$$

$$\dot{x}_2 = x_1 \tag{8.65b}$$

$$\dot{x}_3 = 0 \tag{8.65c}$$

$$\dot{x}_4 = x_3 \tag{8.65d}$$

where

$$x_1 = \omega_R \tag{8.66a}$$

$$x_2 = \theta_R \tag{8.66b}$$

$$x_3 = \omega_G \tag{8.66c}$$

$$x_4 = \theta_G \tag{8.66d}$$

Although the drive train model has been considerably simplified, the representation of the coupling between the rotor and the electricity supply network as a series of stiffness elements allows the influence of different transmission characteristics to be studied. The present 5kW V-VAWT design is mechanically stiff and offers little damping to the fluctuations of torque developed by an

uncontrolled rotor. The synchronous generator offers the most compliance and damping. This is not ideal, because the largest angular displacements will be excited in the generator rotor and its stiffness is highly non-linear. The drive train design could be modified to show more compliance and damping in the mechanical components, but the current stiff design presents a greater challenge for the designer of an active aerodynamic power control system to overcome.

8.2.3: Tip Pitch Actuator Model

The actuator mechanism for changing the pitch angle of the V-VAWT blade tips has yet to be discussed. At present, an actuator mechanism specifically for the V-VAWT has not been designed in detail. The free-air 5kW V-VAWT has no mechanism for tip pitch control nor one for actuating the 'T' brake control device. The form that any such mechanism will take has not been specified, but for electricity generation applications of the wind turbine, it will be demonstrated that tip pitch must be actively controlled. In the simulation studies, it is the response of the actuator system to a pitch angle control command that is important. Therefore, only the input/output relationship of the actuator system is required; the detail design of the mechanism itself is of little significance.

The state of the actuating mechanism itself during wind turbine operation, like the states of the intermediate drive train components, bears little significance upon the behaviour of the wind turbine system as a whole. Operating boundaries have yet to be specified for the actuating mechanism; for instance, the maximum number of pitch change cycles has not been defined, nor have the load

limits that the actuator mechanism may impose upon each blade been specified. These and other design limitations will have to be considered at the detail design stage of the V-VAWT development. If an appropriate actuator system design existed, then a detailed model of the actuating mechanism could be developed. But knowledge of the operating states of each component of the mechanism would be of little value to this study, since it is not possible to test the acceptability of these states against any design criteria. Therefore, a simple mathematical model of the actuator mechanism that only describes the input/output relationship of the system is of greater value here. Such a model will be used to establish, and verify from simulation studies, the general performance requirements of any future V-VAWT tip pitch actuator design.

The simulation studies are concerned with the stability of the V-VAWT while generating electricity and so, as stated above, tip pitch must be actively controlled for such an application. The control strategy adopted is discussed in detail later, however, the input signal from the controller to the actuator system will invoke a response from the system which will be assumed to be equal for all blade tips. In reality, the response of each blade tip to the single pitch angle command will be slightly different due to differences in individual components and the local external forces acting on each device. However, such differences would add further complexity to the modelling process and are not considered to be relevant to the objectives of these simulation studies. Therefore, the assumption that each blade tip will respond in the same way and be in the same state as the other tips is considered reasonable here.

Cyclic variations of tip pitch are not considered because each blade tip would have to have its actuator system

described. The controller would also have to specify pitch angle commands to each actuator. Again this would lead to further complexity in modelling the wind turbine system and also calculation of the aerodynamic torque developed by the rotor would be significantly more difficult. Cyclic pitch control is considered too elaborate for power control purposes alone, but may be considered where the structural response of the rotor is significantly affected by changes of azimuthal position [85].

The tip pitch actuator is modelled as a second order system with unity proportional feedback for position control. In reality compensation in the form of either integral and/or derivative feedback may have to be used to enhance the speed, accuracy or stability of the actuating system in controlling the pitch angle of the blade tip. However, that is a matter of detail design to ensure that the response of the real actuator system will meet the performance criteria developed during this study. For simulation purposes, the characteristics of a second-order actuator system can be easily determined to ensure that a suitably fast, accurate and stable response is modelled.

The overall transfer function of a second-order system written in standard Laplace form is given by:

$$\frac{C(s)}{R(s)} = \frac{\omega_n^2}{s^2 + 2\zeta\omega_n s + \omega_n} \qquad (8.67)$$

where

ω_n = undamped natural frequency, rad/s

ζ = damping factor

The time response of a second-order positional control system to a step input is characterised by six performance indices [86]:

(a) Delay time, t_d
(b) Rise time, t_r
(c) Peak time, t_p
(d) Peak overshoot, M_p
(e) Settling time, t_s
(f) Steady-state error, e_{ss}

These indices are mutually dependent and can be defined in terms of ω_n and ζ alone. For modelling purposes values must be assigned to ω_n and ζ but it is more convenient to specify the desired behaviour of the actuator in terms of one or more of the performance indices. Only two of the indices need be specified to ensure unique values of ω_n and ζ are defined.

Accurate control of the wind turbine system as a whole will require the pitch angle control command to be continuously modified in response to windspeed fluctuations. Therefore the speed of response of the actuator system to the input command changes will be more important than necessarily its steady state positional error or the settling time. The performance of the actuator mechanism can best be defined in terms of:

(a) the maximum rate of change of pitch angle, deg/s
(b) the peak overshoot in response to a step input

since both of these performance indices can be quantified and are easily measured during dynamic testing.

The maximum rate of change of pitch angle is a limitation imposed by the components of the actuator mechanism, and

it is considered that a value of 15 deg/s should provide a suitable actuator response. Where shutdown procedures are invoked, the tip pitch angle will need to be set to 30°. In the worst case, the actuator will take approximately two seconds for the pitch angle to first reach the 30° position.

The peak overshoot of a system in response to a step input is an excellent measure of system damping since it is independent of ω_n. A 10% overshoot is considered to be acceptable, since this will ensure the actuator system is stable and yet underdamped to ensure a quick response to input changes.

Nagrath and Gopal [86] give the following expressions for rise time t_r and peak overshoot M_p in terms of ω_n and ζ:

$$t_r = \frac{\pi - \tan^{-1}\frac{\sqrt{(1 - \zeta^2)}}{\zeta}}{\omega_n\sqrt{(1 - \zeta^2)}} \qquad (8.68)$$

where for $0 < \zeta < 1$

$$0 < \tan^{-1}\frac{\sqrt{(1 - \zeta^2)}}{\zeta} < \frac{\pi}{2}$$

and

$$M_p = \frac{e^{-\pi\zeta}}{\sqrt{(1 - \zeta^2)}} \qquad (8.69)$$

However, it is more convenient to determine ζ from the graph of M_p versus ζ provided by Nagrath and Gopal, than to use equation (8.69). From this graph a value of ζ = 0.6 corresponds to a 10% peak overshoot. This value of ζ is used below to determine a suitable value of ω_n.

The rise time t_r is the time taken for the response of the underdamped system to a unit input to rise from 0% to 100% of the final output value. If it is assumed that the rate of change of pitch angle is constant during this initial period, then a value of t_r maybe estimated and a value of ω_n calculated by rearrangement of equation (8.68).

In determining a value of t_r, it was assumed that the maximum response of the tip pitch actuator system would be required for a 5° step input to the system and that the maximum pitch rate provided by the actuator is 15 deg/s. Using these values t_r has a value of 0.33 seconds and consequently ω_n = 8.3 rad/s.

When using this actuator model, it should be noted that the rise time is constant, regardless of the magnitude of the input. If only a 2° step input to the system is invoked, then it will take 0.33 seconds for the output of the system to first attain a value of 2°. The pitch rate during this response would not exceed its maximum value at any time. However, if an 8° step input was invoked, the output of the system model would still attain a value of 8° in 0.33 seconds, but in doing so the pitch rate would have to exceed its maximum value. This means that the current actuator model does not simulate the performance limitations that are considered to be typical of a real mechanism. This can be easily overcome with digital simulation by including a conditional statement .in the computer program; this ensures the magnitude of the pitch rate does not exceed its maximum value at any time. In this way the simple second order model is modified to ensure it accurately simulates the operating characteristics of a real actuator mechanism.

The differential equation that represents the behaviour of the actuator system is:

$$\omega_n^2\beta_{AC} = \ddot{\beta}_A + 2\zeta\omega_n\dot{\beta}_A + \omega_n^2\beta_A \qquad (8.70)$$

where

β_A = tip pitch actuator output angle, deg

β_{AC} = tip pitch actuator input angle, deg

A convenient state variable form of the characteristic equation is:

$$\dot{x}_5 = \omega_n^2\beta_{AC} - \omega_n^2 x_6 - 2\zeta\omega_n x_5 \qquad (8.71a)$$

$$\dot{x}_6 = x_5 \qquad (8.71b)$$

where

$x_5 = \dot{\beta}_A$ tip pitch rate, deg/s

$x_6 = \beta_A$ tip pitch angle, deg

The state equations can be arranged into matrix form but, as discussed previously, this form has not been adopted here because of the sparse nature of the process and driving matrices.

The values of ω_n and ζ determined above will ensure the actuator response will be fast, yet stable. However, to ensure the mathematical model is representative of a real mechanism, the pitch rate will be limited to a maximum value of 15 rad/s. The computer simulation program DYNVAWT checks and modifies as appropriate the magnitude of the state variable x_5 to ensure that this limiting condition is applied.

8.2.4: Disc Brake Model

The disc brake system currently fitted to the 5kW V-VAWT is a two-state device. The Twiflex AMR electric disc brake uses a spring-applied, electrically released actuator that is able to apply a maximum braking torque of 1950 Nm to the brake disc. The manufacturer's specified release time is 0.1 - 0.2 seconds and the application time is 0.15 - 0.4 seconds depending upon the adjustment and set-up of the system. The state of the brake system is controlled simply by switching on/off the electrical supply to the brake controller. The brake is only released when its electrical supply is connected. This mode of operation can be used to ensure that the wind turbine only operates when there is continuity of electrical supply to all control systems.

The magnitude of the braking torque cannot be controlled except by selecting different brake components. The wind turbine controller, therefore, need only specify the required state of the brake system i.e. whether the brake should be on or off. This braking system can be mathematically modelled by considering it as a first order system.

The overall transfer function of a first order system written in standard Laplace form is given by:

$$\frac{C(s)}{R(s)} = \frac{1}{1 + \tau s} \qquad (8.72)$$

where

τ = time constant, sec

The transient response of such a system to a step input is characterised by an exponential rise of the output from 0% to 100% of the input value. The initial rate of change of the output is equal to the inverse of the time constant. Thus the time constant is indicative of the speed of response of the system; a small time constant representing a fast response. The output of the system is within 2% of its final value when $t > 4\tau$. From the manufacturer's specification the time constant for the disc brake system would be $\tau = 0.025 - 0.100$ seconds depending upon whether the brake was being applied or released. A value of $\tau = 0.1$ seconds is used here for simulation purposes.

The differential equation that represents the behaviour of the disc brake system is:

$$\frac{1}{\tau}Q_{BC} = \dot{Q}_Z + \frac{1}{\tau}Q_Z \tag{8.73}$$

where

Q_Z = actual torque of disc brake system, Nm

Q_{BC} = required torque of disc brake system, Nm

A convenient state variable form of the characteristic equation is

$$\dot{x}_7 = \frac{1}{\tau}Q_{BC} - \frac{1}{\tau}x_7 \tag{8.74}$$

where

$x_7 = Q_Z$ disc brake torque, Nm

The disc brake has only two states, so the command signal from the wind turbine controller to the disc brake need

only be a digital equivalent of off or on i.e. 0 or 1. However, for convenience, the value assigned to Q_{brc} in the simulation program DYNVAWT is either 0 Nm or 1950 Nm. Such a form ensures that the state variable x_7 is always assigned a true value of disc brake torque. The magnitude of the actual torque developed by the brake system must be converted to a high-speed side equivalent, Q_{br}', using equation (8.47b) before if can be combined with the equivalent aerodynamic torque, Q_t', to give the rotor torque Q_r (N.B. Q_{br} is a *braking* torque and must be assigned a negative sign in the summation).

This simple mathematical model of the disc brake is easily implemented into the simulation program. The value of τ used here ensures that the braking torque is applied as slowly as the brake mechanism allows. The disc brake system responds to only one input, Q_{brc}, that is set by the wind turbine control system. The disc brake is not used to control the wind turbine while it is connected to the grid, and is only applied during shutdown procedures or when the wind turbine is stationary.

8.2.5: The Wind Model

The time-domain simulation of the V-VAWT must include a time varying model of the wind, otherwise the dynamic response of the wind turbine system to typical fluctuations in windspeed can not be studied. The wind model must allow the V-VAWT generator system to be disturbed by the common forcing functions used in control system analysis:

(a) step, ramp and impulse transient inputs
(b) sinusoidal input
(c) statistical input

The use of measured values of windspeed with respect to time would include all these forcing functions. The use of such data, however, is not convenient for simulation studies because the individual forcing components can not be readily separated from the overall wind characteristic. A mathematical based wind model was sought to allow the typical forcing function forms to be characterised individually or combined to give a realistic representation of the stochastic nature of the wind.

The wind model used is based upon those developed by Anderson and Bose [76], and Sundar and Sullivan [87], and the values assigned to the controlling parameters are typical of the values used by these authors. This mathematical wind model is ideally suited for computer based simulation studies, since the behaviour of the wind can be modelled to include gusting, rapid speed (ramp) changes and turbulent effects (noise). The wind model is only one-dimensional, since no variation of windspeed across the wind turbine rotor is considered.

The wind model consists of four wind velocity components and the computer program DYNVAWT allows any combination of these components to be used for simulation purposes. The upstream windspeed V_w at any given time, t, is given by:

$$V_w = V_{wB} + V_{wG} + V_{wR} + V_{wN} \qquad (8.75)$$

where

V_{wB} = base wind component, m/s
V_{wG} = gust wind component, m/s
V_{wR} = ramp wind component, m/s
V_{wN} = noise wind component, m/s

The base wind component is given by:

$$V_{WB} = K_B \tag{8.76}$$

where K_B is constant throughout the simulation period. The value of K_B can be varied between simulation runs and determines the initial operating conditions of the wind turbine system. Its value is not limited in any manner, though a positive, non-zero value is always assigned to K_B.

The gust wind component is given by:

$$V_{WG} = \begin{cases} 0 & t < T_{1G} \\ V_{COS} & T_{1G} < t < T_{2G} \\ 0 & t > T_{2G} \end{cases} \tag{8.77}$$

where

$$V_{COS} = \frac{MAXG}{2}\left(1 - \cos 2\pi\left(\frac{t - T_{1G}}{T_{2G} - T_{1G}}\right)\right) \tag{8.78}$$

and

MAXG = gust peak, m/s
T_{1G} = gust starting time, s
T_{2G} = gust finishing time, s

This is the NASA standard (1-cosine) gust that is generally used for simulation studies. The gust wind component is zero in magnitude at all times except during the gust period. When the time is greater than the gust start time, the magnitude of the gust wind component increases sinusoidally to its peak value at the mid-period time. It then decreases non-linearly to zero at a time equal to the gust finishing time. The severity of the gust is control-

led by the magnitude of its peak and the period of the gust.

The ramp wind component is given by:

$$V_{WR} = \begin{cases} 0 & t < T_{1R} \\ V_{RAMP} & T_{1R} < t < T_{2R} \\ MAXR & t > T_{2R} \end{cases} \qquad (8.79)$$

where

$$V_{RAMP} = MAXR\left(1 - \left(\frac{t - T_{1R}}{T_{2R} - T_{1R}}\right)\right) \qquad (8.80)$$

and

MAXR = ramp peak, m/s
T_{1R} = ramp starting time, s
T_{2R} = ramp finishing time, s

The ramp wind component allows the mean windspeed to increased or decreased about the base wind component during the simulation period. The ramp component is zero in magnitude when time is less than the ramp start time. When time is greater than the ramp start time, the magnitude of the ramp component increases linearly to its peak value at the ramp finish time. The ramp component then remains fixed at the peak value for the rest of the simulation period. A step change in windspeed can be simulated by making the ramp finish and start times all but equal.

The noise wind component is given by:

$$V_{WN} = \sum_{i=1}^{n} [2S(\omega_i)\Delta\omega]^{0.5} \cos(\omega_i t + \phi_i) \qquad (8.81)$$

where

$$S(\omega_i) = \frac{2C_T F^2 |\omega_i|}{\pi^2 \left[1 + (F\omega_i / \pi V_{M10})^2\right]^{4/3}} \qquad (8.82)$$

and

F = turbulence scale factor, m

C_T = ground roughness coefficient

$\Delta\omega = \omega_{cu}/n$, rad/s

ω_{cu} = upper cut-off frequency, rad/s

n = number of frequency components

$\omega_i = i\Delta\omega + \delta\omega$, rad/s

$\delta\omega$ = random frequency shift, rad/s $\quad \delta\omega < \Delta\omega/20$

ϕ_i = random phase angle, rad $\quad 0 < \phi_i < 2\pi$

V_{M10} = mean windspeed at 10m height above ground, m/s

The noise wind component is simulated by a series of cosine waves of various frequencies ω_i whose amplitudes are weighted according to the spectural density function $S(\omega_i)$. At frequencies above the upper cut-off frequency ω_{cu} the spectural energy density function is considered to be zero. Also, since a discrete-time simulation is being performed, frequencies above the simulation sampling frequency can be ignored because they will not contribute any variation to the noise wind component in the simulation studies.

The wave amplitudes are, in general, controlled by the turbulence scale factor F and the ground roughness coefficient C_T terms, while the overall form of the noise shape is controlled by the number of frequency components n and the upper cut-off frequency ω_{cu}. Each component frequency ω_i is a multiple of $\Delta\omega$, plus a random frequency shift $\delta\omega_i$ which ensures that ω_i is not periodically repeated. A random phase angle ϕ_i is, similarly, included in the cosine term of $V_{\omega N}$ to ensure that each component wave is out of phase with the others.

Values of F = 700m, C_r = 0.005, n = 50 and ω_{ll} = 100 rad/s have been assigned to these parameters based upon the values suggested by Anderson. There is little need to modify these values for the purposes of this study since no particular V-VAWT siting is being considered. The mean windspeed at the standard reference height of 10m above ground is varied since V_{M10} takes the value of the base wind component K_m. Thus a generalised noise wind component model is adopted.

The computer program DYNVAWT allows all the above parameters describing the four wind components to be varied between simulation runs, but they remain fixed for the duration of the simulation period. At each time interval, the four components V_{wB}, V_{wG}, V_{wR} and V_{wN} are calculated and summated to give the windspeed V_w. Any combination of the four components can be used in calculating V_w, so that simulation runs can be performed without including, for example, the ramp or noise wind components. This flexibility was the major advantage in favour of the mathematical wind model over the use of actual windspeed measurements for simulation studies. This wind model allows windspeed variations to be carefully controlled, yet the random fluctuations associated with free-air operation can be included if required.

8.2.6: Electricity Supply Network Connection Model

The dynamic characteristics of the synchronous generator depend upon the state of its connection with the electricity supply network. The infinite bus voltage, e_∞, is constant for a large network, but whether the generator sees this voltage or not depends upon the state of the connection.

A three-phase, symmetric fault in the transmission line will invoke the greatest disturbance to an on-line V-VAWT generator system. During a fault of this kind, the connection between the network and the generator will be temporarily open. For the duration of the fault, the bus voltage is zero and no electrical current will be induced in the stator windings. Consequently, the generator will not develop any power and the stiffness of the generator connection with the network, K_{eq}, will be zero. When the fault is cleared, the infinite bus voltage will be restored to that of the network and currents will once again be induced in the stator windings.

During a fault, the wind turbine system will be unloaded and an uncontrolled rotor will rapidly accelerate away from synchronous speed. When the fault is cleared, the angular displacement of the generator may be so far in advance of the rotating magnetic field of the electricity supply network that synchronisation will be lost. The critical clearing time for a fault is the longest time that the connection may be suspended before instability occurs and synchronisation lost when the fault is cleared.

A simple two state model of the electricity supply network connection to the generator is considered to be adequate for simulating these fault conditions. In this model, the variable JBUS has a value of unity unless a fault is invoked, in which case JBUS has a value of zero. The value of JBUS is therefore given by:

$$JBUS = \begin{cases} 1 & t < T_{1F} \\ 0 & T_{1F} < t < T_{2F} \\ 1 & t > T_{2F} \end{cases} \qquad (8.83)$$

where

JBUS = fault state

T_{1f} = fault starting time, s

T_{2f} = fault clearing time, s

During start-up and shut-down procedures the state of the generator connection to the network will be controlled by the wind turbine controller. As with the fault, the stiffness of the generator connection is zero until such time as the V-VAWT generator system is connected to the network. The off-line wind turbine system is unloaded so an uncontrolled rotor will rapidly accelerate. When the rotor is running at synchronous speed, the connection to the network may be closed and the generator will be synchronised with the network. The success of the synchronisation will depend upon the control strategy adopted for this procedure. If the connection is to remain stable the rotor must be controlled to ensure that synchronous speed is maintained; this will be discussed in more detail in Section 8.3.

The wind turbine controller can prescribe the state of the generator connection to the network by setting the value of the variable IBUS. IBUS can have either a value of unity or zero depending upon whether the contactor is closed or open, i.e.:

$$\text{IBUS} = \begin{cases} 0 & \text{generator contactor OPEN} \\ 1 & \text{generator contactor CLOSED} \end{cases} \qquad (8.84)$$

The two variables IBUS and JBUS can be considered to act like two switches acting in series; the connection between the generator and the electricity supply network is only fully closed when both variables have the value of unity. Using this analogy, the per unit value of the infinite bus voltage is the product of these two variables, i.e.:

$$e_x = IBUS.JBUS \qquad (8.85)$$

This is a simple technique for controlling the value of the infinite bus voltage and easily implemented into the computer simulation program DYNVAWT. Note that of the two variables controlling the state of the infinite bus voltage, one is controlled by the wind turbine controller itself and the other is externally controlled. The variable JBUS can be considered as an input from the environment to the V-VAWT generator system as a whole.

8.2.7: Aerodynamic Torque Model

The aerodynamic torque characteristics of a particular V-VAWT generator system depend upon blade design, rotor configuration and the size of the control surfaces. However, these rotor attributes are all fixed by design and, when studying the dynamic behaviour of a V-VAWT generator system, it is the variation of aerodynamic torque with windspeed and the state of the wind turbine itself that is of interest. An effective model of aerodynamic torque must allow the dynamic behaviour of different V-VAWT designs to be compared as well as effectively characterising torque variation with windspeed and wind turbine state.

Since the aerodynamic torque model must allow the dynamic behaviour of different V-VAWT designs to be compared, it was considered that this would be best achieved if the aerodynamic torque data used as the basis of the model was generated by the aerodynamic performance prediction program VAWTTAY. This allows the dynamic studies to be performed at an early stage of the design process so that the program DYNVAWT becomes a concept design analysis tool; this has always been one of the objectives of the exer-

cise. This approach has the advantage that accurate torque data may be readily generated that characterised an individual rotor design, thus allowing the influence of design modifications to be quickly compared. The data is also generated at the same time as overall aerodynamic performance characteristics are being calculated using VAWTTAY, therefore avoiding duplicity of calculation effort.

The aerodynamic torque model must also allow the torque variations due to windspeed changes and the state of the V-VAWT generator system to be accurately evaluated for all operating conditions. If the rotor design is fixed then:

$$Q_1 = f(\theta_R, \omega_R, \beta_A, V_w) \qquad (8.86)$$

In small perturbation analysis of HAWTs the aerodynamic torque characteristics of a wind turbine rotor are usually normalised about its operating point to give torque gains with respect to small changes of rotor speed, windspeed and blade pitch [81]. Where larger perturbations are to be studied the torque is characterised by a series of non-linear expressions based upon the C_q-λ characteristic of the rotor for different pitch angles of the control surface. While these methods are suitable for representing the general characteristics of HAWTs, the characteristic cyclical torque variation of VAWTs cannot be successfully incorporated into these models.

Since DYNVAWT is a digital computer based program, it was considered that the aerodynamic torque characteristics of a V-VAWT generator system would best modelled by a look-up table of C_q values that described the complete operating range of the system. The values of the table would be drawn from datafiles generated by VAWTTAY. In its most complete form the table would be four-dimensional, each

axis representing the range of operating conditions of the four independent variables θ_{PR}, ω_{PR}, β_{PA} and V_{ω}. However, this would not only require a large number of C_{TA} values to be calculated but also a large computer memory space to store the values for speedy retrieval during the execution of the program DYNVAWT. The size of the look-up table can be reduced by one dimension if the torque characteristic is considered to be given by:

$$Q_1 = f(\theta_{PR}, \beta_{PA}, \lambda_{PR}) \qquad (8.87)$$

where

λ_{PR} = tip speed ratio of the rotor

Note that the mean aerodynamic torque, Q_{1M}, developed by the rotor over a complete revolution is merely a function of tip pitch angle and tip speed ratio. The values of Q_{1M} are those normally output by VAWTTAY and so are already included in the datafiles generated by this program.

The manner in which the torque data for the table is generated using VAWTTAY will depend upon the operating condition that needs to be studied. For instance, for on-line studies the torque data should be generated at constant rotational speed for a range of windspeeds; the rotor speed being synchronous. Small changes of the rotational speed of the rotor will be equivalent to small tip speed ratio changes. Whereas for start-up and shut-down studies, the torque data should be generated at constant windspeed for a range of rotational speeds. In these studies small changes of windspeed would be equivalent to small tip speed ratio changes. Adapting the manner in which the data for the look-up table is generated to the type of simulation study to be performed, ensures economy of torque data calculation and prepar-

ation. More importantly, it also ensures that the data embodies the predicted effects of Reynolds Number on the performance of the V-VAWT rotor. This could not be satisfactorily achieved by using one set of data alone.

Since the look-up table consists of values of C_q calculated at discrete values of θ_{pc}, β_c and λ_{tc}, linear interpolation is used to calculate the value of C_q at intermediate operating points. The true value of the rotor torque is calculated in the usual way:

$$Q_t = \tfrac{1}{2}\rho A R V^2 C_q \qquad (8.88a)$$

where

$$V = V_w \qquad (8.88b)$$

This aerodynamic torque model uses data normally calculated when using VAWTTAY for performance predictions of V-VAWT configurations. No further refinement of the data is required for use with DYNVAWT. Therefore, dynamic simulation studies of the V-VAWT generator system can be readily performed at an early stage of a system development. The results of such studies would contribute to the overall evaluation of a particular design proposal in a way that the study of steady state aerodynamic performance predictions alone cannot.

8.2.8: A Summary of the V-VAWT System Model and Initialisation of the State Variables

The mathematical models of the three sub-systems of the V-VAWT generator system developed above may be combined to form a model of the whole system. The control system has yet to be developed, but the response of the uncontrolled

wind turbine system may now be evaluated in the time domain using the seven state differential equations:

$$\dot{x}_1 = \frac{1}{J_R}[Q_R - K_{EQ}(x_2 - x_4) - C_{EQ}(x_1 - x_3) - F_R x_1] \quad (8.89a)$$

$$\dot{x}_2 = x_1 \quad (8.89b)$$

$$\dot{x}_3 = 0 \quad (8.89c)$$

$$\dot{x}_4 = x_3 \quad (8.89d)$$

$$\dot{x}_5 = \omega_n^2 \beta_{AC} - \omega_n^2 x_5 - 2\zeta\omega_n x_5 \quad (8.89e)$$

$$\dot{x}_6 = x_5 \quad (8.89f)$$

$$\dot{x}_7 = \frac{1}{\tau} Q_{BC} - \frac{1}{\tau} x_7 \quad (8.89g)$$

where the state variables are:

$x_1 = \omega_R$ angular velocity of V-VAWT rotor, rad/s
$x_2 = \theta_R$ angular displacement of V-VAWT rotor, rad
$x_3 = \omega_G$ angular velocity of generator rotor, rad/s
$x_4 = \theta_G$ angular displacement of generator rotor, rad
$x_5 = \dot{\beta}_A$ tip pitching rate, deg/s
$x_6 = \beta_A$ tip pitch angle, deg
$x_7 = Q_B$ disc brake torque, Nm

and

Q_R = equivalent torque applied to rotor
β_{AC} = required tip pitch angle, deg
Q_{BC} = required disc brake torque, Nm

Only β_{AC} and Q_{BC} can be directly controlled by the wind turbine controller. The torque, Q_R, developed by the rotor is the sum of both aerodynamic torque and the applied brake torque. The coefficients of the difference equations are dependent upon the design of the V-VAWT generator system. The coefficients are all time invariant

with the exception of K_{mech}. This coefficient is system state dependent and therefore its characteristics vary in time. The infinite bus voltage, e_∞, is an external input to the system and is dependent upon the connection between the generator and the electricity supply network whose state is determined by the variables IBUS and JBUS. The state of IBUS is controlled by the wind turbine controller, but JBUS is externally controlled.

The initial state of the system must be evaluated before numerical solution of the system equations can commence. Given that all the component characteristics have been determined, the initial values of the state variables will depend upon the operating mode that is to be simulated. Equilibrium of the system is implicit during the initialisation procedure.

If a start-up operation is to be simulated, the initial angular displacements and the rotor velocity will be set to zero. The angular velocity of the rotating magnetic field of the electricity supply network will be set at synchronous speed. The pitch angle and brake states will be determined by the V-VAWT controller. All state differentials will be zero.

If a shutdown operation is to be simulated, the V-VAWT generator system will be considered to be initially operating on-line. The external disturbances must be designed to invoke a shut-down procedure during the simulation period.

The initialisation of on-line operation is not straightforward, however, the following approach has been successfully adopted. The initial angular displacement of the rotating magnetic field is set to zero, and both angular velocities of the system are set to synchronous speed.

The pitch angle and brake states will be determined by the V-VAWT controller. All state differentials will be zero. The initial state of the rotor is not completely defined as its angular displacement must be determined. Since the system is considered to be in equilibrium, the initial rotor torque will be considered to be equal to the mean aerodynamic torque, Q_{1M}, calculated using the initial tip pitch angle and tip speed ratio values. Subtraction of the friction loss torque from the value of rotor torque will yield the value of mechanical torque transmitted to the generator. Thus the power input to the generator is determined. In order to determine the power angle at which the generator system is initially operating, the value of δ is set to zero and its value gradually increased in discrete increments. At each increment the output power of the generator is calculated. The procedure is repeated, until the calculated power output of the generator equals that transmitted from the wind turbine drive train. In this way the initial value of δ can be determined. The initial stiffness of the drive train system can now be evaluated and the angular displacement between the rotor and the network calculated. The initial value of all the state variables are now all determined.

Since the mean torque, Q_{1M}, is used to determine the initial state of the on-line V-VAWT generator system, the system can only be considered to be in a state of quasi-equilibrium. The actual rotor torque developed by the rotor will differ from the mean value because of the cyclic nature of V-VAWT torque. The difference immediately imposes a disturbance on the system which will invoke a transient response, even when the system inputs remain constant. Once, however, a steady state operating condition has been achieved, then excitation of the system with external disturbances may be simulated as required.

8.2.9: Numerical Solution of the State Differential Equations

Equation (8.89) defines the seven state differentials of the V-VAWT generator system solely in terms of the system inputs, control outputs, component characteristics and the state variables themselves. These equations can be evaluated provided the initial state of the system has been defined and all the equation coefficients have been calculated. The numerical simulation of the V-VAWT generator system requires that these state differentials are used to evaluate the state of the system at the next discrete time step. Repetition of this process will yield the solution of the state equations for the complete simulation period. The numerical solution technique described below is one of many solution methods considered for use in the simulation program DYNVAWT.. The superior accuracy and self-starting attributes of the Fourth Order Runge-Kutta technique, however, weighed heavily in its favour over the other methods, and the author considers the choice of this solution technique to be most important factor in ensuring that the computer program DYNVAWT is a reliable and quick dynamic analysis tool.

The basis of the Fourth Order Runge-Kutta numerical solution method comes from the consideration of a first-order system that has a single state variable $x(t)$ and a single input $u(t)$. It is assumed that the initial value of $x(t)$ is known at time t_o and $u(t)$ is known for all $t \geq t_o$. The discrete time based solution requires the state of the system to be evaluated at each discrete step. It is assumed that the time T between each step is constant for the duration of the simulation period. As will be demonstrated the accuracy of the solution is highly dependent upon the choice of step size.

The state differential equation is assumed to be of the form:

$$\dot{x}(t) = f[x, u, t] \tag{8.90}$$

If the initial state $x(t_o)$ is known, then the next state to be evaluated is at $t = t_o + T$. Taylor's expansion about t_o gives:

$$x(t_o + T) = x(t_o) + T\dot{x}(t_o) + \frac{T^2}{2!}\ddot{x}(t_o) + \ldots \tag{8.91}$$

The Taylor's expansion would allow an exact value of $x(t_o + T)$ to be calculated if all the derivatives of $x(t_o)$ could be evaluated and if the infinite series could be summated. However, in the general case this cannot be done and therefore only an approximate solution can be evaluated.

Since the initial state of the system is known, the state differential equation (8.90) allows the first derivative of $x(t_o)$ to be evaluated. If the step size is chosen to be suitably small, the higher order derivatives can be neglected and an approximate solution of equation (8.91) can be found, such that:

$$x(t_o + T) = x(t_o) + Tf[x(t_o), u(t_o), t_o] \tag{8.92}$$

The state of the system at $t = t_o + 2T$ can now be evaluated:

$$x(t_o + 2T) = x(t_o + T) + Tf[x(t_o + T), u(t_o + T), t_o + T] \tag{8.93}$$

The process can be continued so that:

$$x(t_o + (k+1)T) = x(t_o + kT) + Tf[x(t_o + kT), u(t_o + kT), t_o + kT] \tag{8.94}$$

A simpler form of equation (8.94) often used is:

$$x^{k+1} = x^k + Tf[x^k, u^k, k] \tag{8.95}$$

This solution method is known as Euler's Method and is the simplest numerical solution technique of those considered. The method is classed as a single-step technique, since the *k*th step of the simulation must be evaluated before the *k+1*th step can be evaluated. It is also self-starting, since only the initial state of the system need be known for the complete solution to be generated. However, the solution is not exact because the higher order derivatives are ignored. The truncation error, e(t), for Euler's Method is:

$$e(t) = \frac{T^2}{2}\ddot{x}(t_o + \tau) \qquad 0 < \tau < T \tag{8.96}$$

In a higher order system with n state variables and m inputs the generalised state differential equation takes the form:

$$\dot{x}_i(t) = f_i[x_1, x_2, \ldots, x_n, u_1, u_2, \ldots, u_m, t] \tag{8.97}$$

so that:

$$x_i^{k+1} = x_i^k + Tf_i[x_1^k, x_2^k, \ldots, x_n^k, u_1^k, u_2^k, \ldots, u_m^k, k] \tag{8.98}$$

As with the first order system, all the state variables must be evaluated at each discrete step before proceeding to the next step of the simulation.

The Runge-Kutta solution methods are based upon Euler's Method, but are more refined to increase the accuracy of the solution. The order of a Runge-Kutta method refers to the number of state derivative evaluations made for each state variable at each step of the simulation. The Fourth Order Runge-Kutta solution method requires four state derivatives to be calculated for each state at each time step. The form of the algorithm used is:

$$x_i^{k+1} = x_i^k + \frac{T}{6}[A_1 + 2A_2 + 2A_3 + A_4] \tag{8.99a}$$

where

$$A_1 = f_i[x_1^k, \ldots, x_n^k, u_1^k, \ldots, u_m^k, k] \tag{8.99b}$$

$$A_2 = f_i[x_1^k + \tfrac{1}{2}TA_1, \ldots, x_n^k + \tfrac{1}{2}TA_1, u_1^{k+0.5}, \ldots, u_m^{k+0.5}, k + \tfrac{1}{2}] \tag{8.99c}$$

$$A_3 = f_i[x_1^k + \tfrac{1}{2}TA_2, \ldots, x_n^k + \tfrac{1}{2}TA_2, u_1^{k+0.5}, \ldots, u_m^{k+0.5}, k + \tfrac{1}{2}] \tag{8.99d}$$

$$A_4 = f_i[x_1^k + TA_3, \ldots, x_n^k + TA_3, u_1^{k+1}, \ldots, u_m^{k+1}, k + 1] \tag{8.99e}$$

This method involves evaluation of four state derivatives; one at the start of the time interval, two at the mid-point of the time interval and one at the end of the time interval. All four state derivatives are weighted and used to calculate an average value across the whole interval. Finally, the average value of the state derivative is used to calculate the state variable at the end of the interval.

Although the Fourth Order Runge-Kutta method requires four derivative evaluations at each step, the accuracy of the solution is greatly improved since the truncation error is only of the order T^5. This allows the time step to be significantly larger than that required by Euler's Method to maintain the same accuracy of solution. Adopting a larger time step enables the numerical solutions to be generated more quickly for a given simulation time period.

Multistep numerical solution methods such as the Fourth Order Adams-Bashford method and the Adams-Moulton predictor-corrector method offer similar solution accuracy to the Fourth Order Runge-Kutta method, but only require one state derivative to be calculated at each step of the solution. This obviously reduces the number of calculations to be performed at each step, so numerical solutions can be generated more rapidly than with the single step method. However, these techniques use the state derivatives from the previous three steps to calculate an average value of the state derivative at the current step. Multistep methods, therefore, are not self-starting since knowledge of the initial state of the system alone is not sufficient to commence a simulation study. Single step methods must be used to evaluate the first few steps, after which the multistep method can be used to continue the calculation.

All these methods require the step time to be suitably chosen to ensure that the solution remains stable. It is not possible to explicitly determine the critical time interval for the dynamic model of the V-VAWT generator system. However, the simplified drive train model that avoids stiff transmission elements and small inertia elements was developed with numerical solution stability always in mind. These elements would typically have a high frequency transient response that could only be satisfactorily evaluated if very small time steps were used. The simplified model allows relatively large time steps to be made and consequently numerical solutions can be generated quickly. Graphical display of the simulation has been a great aid in indentifying likely instabilities due to the limitations of the numerical solution technique and for determining by trial-and-error suitable time steps for the systems modelled.

The Fourth Order Runge-Kutta solution method was adopted for use in DYNVAWT since it is accurate and self-starting. The additional complexity of using a Multistep solution method to decrease calculation time was considered to offer little benefit when solutions can be generated quickly using the Runge-Kutta method alone.

8.3: The Computer Program DYNVAWT

The dynamic model of the V-VAWT generator system is now complete and all mathematical models have been fully described and documented. The control strategy devised for this system is discussed in the next section, since it can be treated separately from the dynamic model of the wind turbine system. All the mathematical models and solution methods discussed have been developed specifically for numerical solution using a digital computer; this was considered the most convenient analysis tool available for simulating the dynamic behaviour of the V-VAWT generator system in the time domain. The program must allow the various operating conditions to be simulated, and while the digital computer solutions are not exact, the response of the system to be quickly evaluated and easily observed; these needs necessarily outweigh the need for precise solutions of the general case. The use of the Fourth Order Runge-Kutta solution method allows numerical solutions to be quickly and accurately calculated, and computer graphics allows these solutions to be easily interpretated without having to resort to additional numerical analysis. Trial-and-error modifications to the system design can be easily implemented and their effect quickly observed, essential where new system designs are being evaluated.

8.3.1: Program Structure and Development

The computer program DYNVAWT has been written and developed by the author at Portsmouth Polytechnic. The program embodies all the mathematical models developed for simulating the dynamic behaviour of the V-VAWT generator system. The program runs on a VAX 11/750 computer and is written in standard ANSI FORTRAN 77; this allows it to be run on other computer systems if required. Computer graphics have been included by using standard GINO-F graphics routines. The program has been written in a modular form, therefore allowing future modifications and or extensions to be easily included. Where alphanumeric data is required, DYNVAWT prompts the user with clear messages. Thorough error checks are made of all user defined data. The rigorous use of error checking routines and facilities was considered essential to ensure reliability of both program execution and simulation results. Figure 8.10 shows a program flowchart outlining the basic phases through which the program proceeds. The sequence of events is briefly discussed below.

An initial welcome message is followed by a prompt for the name of the aerodynamic torque datafile from which the look-up table of C_Q values is to be constructed. The program uses aerodynamic torque data generated by the prediction program VAWTTAY, which operates on the same computer facility. The datafile must be created before execution of DYNVAWT because the interaction with VAWTTAY is weak. The program neither activates VAWTTAY nor checks that the aerodynamic data is representative of the system being modelled; only the format of the data is checked. The program user must ensure that the correct aerodynamic torque datafile is retrieved when using DYNVAWT. The author has adopted a simple notation that enables the datafiles to be easily identified and correctly selected

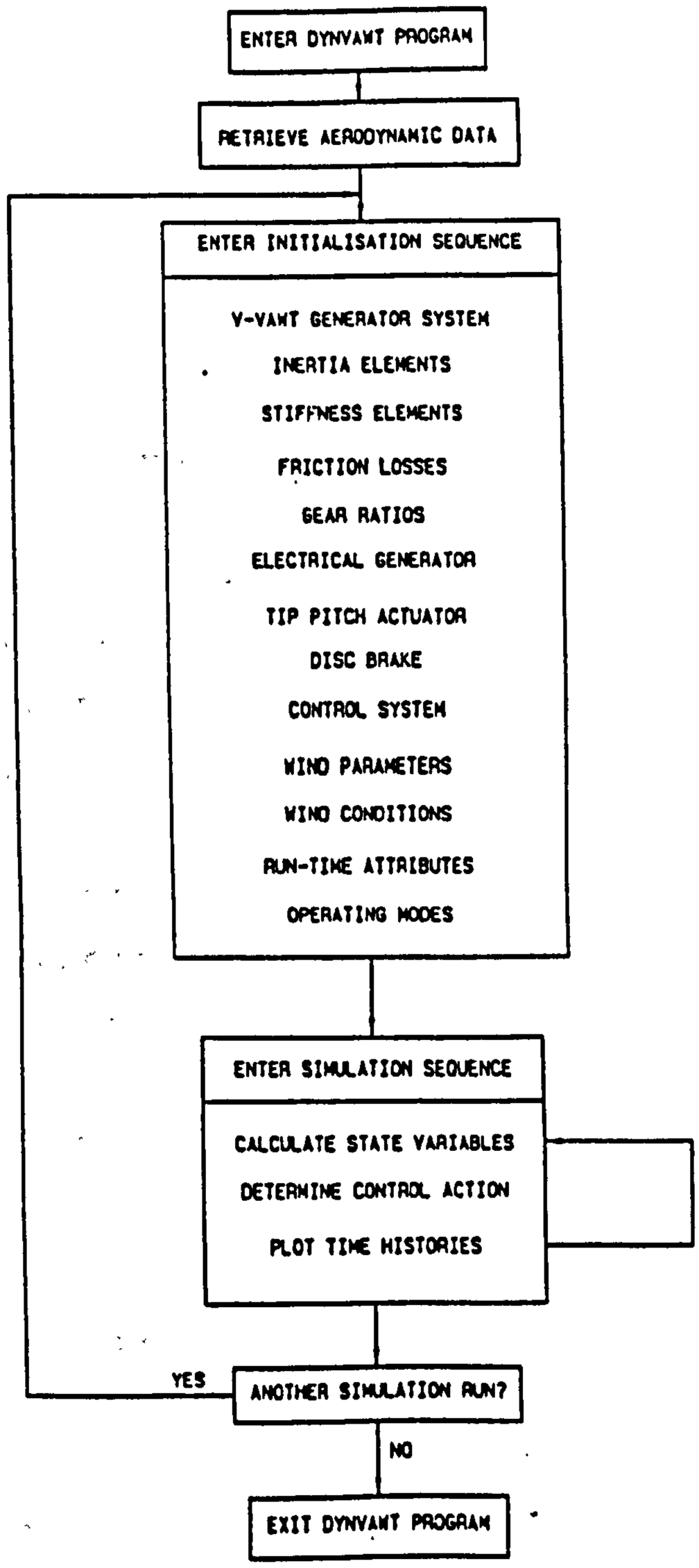

Figure 8.10: Flowchart showing basic phases of DYNVAWT

for the appropriate simulation study. As discussed in Section 8.2.7, the aerodynamic torque data must be generated either at constant rotational speed or at constant windspeed to ensure the look-up table embodies Reynolds Number effects for tip speed ratio changes. The geometric characteristics of the V-VAWT rotor are fixed and correspond to geometry initiated when using VAWTTAY.

The initialisation of the aerodynamic torque look-up table takes approximately five minute, since the datafile will typically hold 36,000 entries. It is the only phase of the program that cannot be returned to once complete. If another torque datafile is required, then the user must exit from the program and start again. However, the large table size does allow the behaviour of the wind turbine system to simulated at the extremes of its specified operating range. For instance, with on-line operation, the look-up table will typically include C_m values covering the range of windspeeds 10-36 m/s, tip pitch angles 0-30 degrees and 40 azimuthal positions of the rotor. Such detail ensures that the aerodynamic torque developed by each V-VAWT rotor configuration is as accurately modelled by DYNVAWT as the prediction program VAWTTAY allows.

Once the aerodynamic torque look-up table has been created, the program enters an initialisation sequence in which all the *independent* system parameters are defined. In order to simplify this activity, all these parameters have been assigned default values. The default values correspond to those of the two-bladed, 5kW V-VAWT rotor driving a salient pole synchronous generator at a speed of 1500 rpm. For each aspect of the system model, whether it be the generator characteristics or the parameters describing the ramp component of windspeed, the default values are displayed in a table. If a controlling

parameter is required to be changed, its index number is selected and a new value can be entered. The modified table is re-displayed and this process can be repeated until the user is happy that the controlling parameters have been assigned their correct values. When the escape index number is selected, the sequence moves into the next initialisation phase. The thirteen phases of this sequence are briefly described below:

1) V-VAWT Generator System Characteristics: The rated characteristics of the system are set here. The parameters evaluated include power output; rated rotational speed of the V-VAWT rotor; cut-in, rated and cut-out windspeeds; minimum and maximum brake application speeds. All these parameters are either control set points or out-of-limits conditions. Although their values may be changed, they are not inputs to the system because their values remain fixed for a particular V-VAWT configuration or control strategy design. The parameters are used by the controller to evaluate the condition of the system and determine the control action required.

2) Inertia Elements: The true values of the inertia elements are entered here. These values are later converted to high-speed equivalents when all the characteristics of the system have been defined.

3) Stiffness Elements: The true values of the mechanical stiffness elements are entered here. These values are converted to high-speed equivalents as appropriate. The mechanical stiffnesses are subsequently combined with the electrical generator stiffness to define the equivalent stiffness of the system.

4) Friction Loss: The friction loss coefficient is defined here and converted to a high-speed equivalent as appropriate.

5) Gear Ratios: The ratios of the two-stage speed increasing V-belt system are defined here. Once these ratios have been defined, the conversion to high-speed equivalents of all mechanical drive train parameters is possible.

6) Generator Characteristics: The rated characteristics of the synchronous generator defined here are rated power output, number of poles, rated frequency, infinite bus and terminal voltages (pu); quadrature-axis, direct-axis and external reactances (pu); power factor (pu); and damping coefficient (pu). These are used to calculate the synchronous speed of the electricity supply network and determine the coefficients of the equations for calculating electrical stiffness and damping.

7) Tip Pitch Actuator: The minimum and maximum pitch angle; maximum pitching rate; undamped natural frequency; damping factor; and initial pitch angle are defined here.

8) Disc Brake: The maximum brake torque; time constant; and initial brake state are defined here.

9) Control System: Although the control system has not been discussed yet, the parameters used to determine the control action are defined here.

10) Wind Parameters: Here all the parameters that the describe the characteristics of the four components of the wind model are defined.

11) Wind Conditions: Here the components of the wind model which are to be active during the simulation period are selected. The program DYNVAWT only calculates the values of the active wind components during the simulation period.

12) Run-time attributes: The start time, finish time and size of the time step for the simulation period; and the network fault start and clearing times are defined here. The nature of the aerodynamic torque model, a choice between cyclic torque or mean torque values, can also be selected at this stage and an option for saving the numerical solution is given.

13) Operating Modes: This simply selects the initial operating mode of the V-VAWT generator system. There are three modes available start-up and synchronisation; on-line operation; and on-line operation with network fault. As discussed previously, the shutdown sequence is simulated by invoking a large disturbance that ensures the system will be shutdown by the controller.

Once all the user-defined data has been correctly entered, the program enters a further initialisation sequence. During this sequence all the *dependent* system parameters are calculated. The initialisation procedure described in Section 8.2.8 is followed to determine the initial state of the system. A summary table that shows the initial values of the state variables is displayed before the simulation process is commenced. If the numerical solution is to be saved, all system parameters and state variables are written to an external datafile.

At the start of the simulation sequence, the program activates the computer graphics facility. The terminal

screen is cleared and the axes of six graphs are drawn on the screen. Scales and appropriate labels are shown on all axes. The independent variable in each case is time. The dependent variables are windspeed, mean aerodynamic torque, tip pitch angle, network contactor state, brake state and generator output power. The program DYNVAWT only displays these six quantities, since these were considered to be the most useful for evaluating the suitability of the control device and strategy. Since it is possible to save the results of a simulation study into an external datafile, it is considered that a post-processing program could be developed for further examination of a simulation solution. Such a program has yet to be developed by the author, but it is envisaged that the program would allow "replays" of a simulation study, using the data in the external datafile, to be carried out. This would give the opportunity for the variation with time of other quantities to be graphically displayed. However, the six graphs utilised in DYNVAWT give a sufficient insight into the behaviour of the V-VAWT generator system to enable an appraisal of the control system to be made.

Immediately on entry to the calculation loop, all system outputs are calculated. The system outputs and state variables at this calculation stage represent the state of the system at the beginning of the time interval; it is these quantities that would be observed at this point in time and measured by appropriate transducers, if fitted. It is these quantities that the control system will use to decide its next control action(s) at the end of the interval. The state of the system may be stored in an external datafile at this phase of the calculation sequence, if required. The values of windspeed, mean aerodynamic torque, tip pitch angle,, network contactor state, brake

state and generator power are all plotted on the time history graphs.

The program then proceeds into the Fourth Order Runge-Kutta calculation loop. This involves four repeated calculations of the state differentials over the interval period. The state variable notation of Section 8.2.9 is used to ensure that the state variables at the start of the interval are not over-written by the temporary state variables calculated in this phase. At the end of this sequence, an average value of each state differential is calculated and used to determine the value of the state variables at the end of the interval period.

Before the calculation enters the next time interval, the system outputs calculated at the beginning of the interval are used by the control system routine to determine the next control action(s). The inputs to the tip pitch actuator, the disc brake and the generator to network connection are all set at this point in the calculation sequence.

One cycle of the calculation sequence is now complete, and the procedure is repeated for the duration of the simulation period. Once the simulation has been completed, the screen will show six complete time history graphs. The program pauses at this point to allow the user time to evaluate the outcome of the simulation. A hard-copy of the graphs can be simply obtained by invoking the screen dump facility of the graphics terminal. This will generate a dot-matrix printer record of the screen image. Alternatively, photographing the graphics terminal will enable the detail of a high-resolution screen image to be fully recorded. Once a record of the graphs has been made, the program user is given the option to exit the program or to continue with another simulation study.

If another simulation study is required, the initialisation sequence must be invoked once again. However, on the second and subsequent passes through this part of the program, it is not necessary to initialise *all* the system parameters. A selection table is displayed in which each of the thirteen initialisation phases described above are numbered. Selecting the phase number enables the user to modify the parameters of that phase. For instance, selecting phase Nº 11 allows the active components of the wind model to be changed. The parameters describing the characteristics of each wind component will not be changed, unless phase Nº 10 is subsequently selected. Any number of changes to the system parameters may be made before the simulation sequence is invoked again. Thus, many simulation studies may be completed without having to re-start the program and initialise the aerodynamic torque table again.

The program DYNVAWT was written over a long period of time and required far more planning and development than any other computer program written by the author for this project. The modular programming approach has allowed each module of the program to be developed and tested in isolation before being used with the main program. The control system described in the next section was the last module of the program to be developed. However, the uncontrolled behaviour of the V-VAWT generator system could be modelled without the control routines being included into the program. This allowed the validity of the numerical solutions generated by DYNVAWT to be evaluated before the program was fully complete. The graphical output was a great aid in assessing and identifying programming errors or bugs in the solution routines. The VAX computer system also offers the computer programmer many runtime debugging facilities. These were extensively used by the author to check the validity of the whole

program in all its phases. The values of any program variable could be interrogated as it was calculated, or recalled from memory, and checked with hand calculations. The exhaustive use of error trapping routines ensures that all user-defined data is valid and is within the limits of the system model. The author is satisfied that a reliable and accurate analysis tool has been created which correctly embodies all the mathematical models developed in the previous sections. The program allows a wide scope of simulation studies to be made of the V-VAWT generator system, and the graphical display of output time histories allows the results to be easily interpreted.

8.3.2: Initial Results from DYNVAWT of an Uncontrolled 5kW V-VAWT Generator System

The program DYNVAWT can be used to simulate the behaviour of uncontrolled V-VAWTs. In its early development stage, this behaviour was used to verify the output generated by the program. Subsequent to the inclusion into the software of the control strategies discussed in the next section, the uncontrolled operating mode is an option in the present version of DYNVAWT. The results presented in Figures 8.11 and 8.12 show the simulated behaviour of a two-bladed 5kW V-VAWT operating without any on-line controller. The characteristics of the system are the same as those for the V-VAWT generator system considered in the case studies presented later in this chapter.

In the first case, Figure 8.11, the windspeed V = 10 m/s and is below rated. It remains constant throughout the simulation period; the gust, ramp and noise effects are not included. The simulation clearly shows the power output of the system is increasing towards the static stability limit of the generator, and the connection to

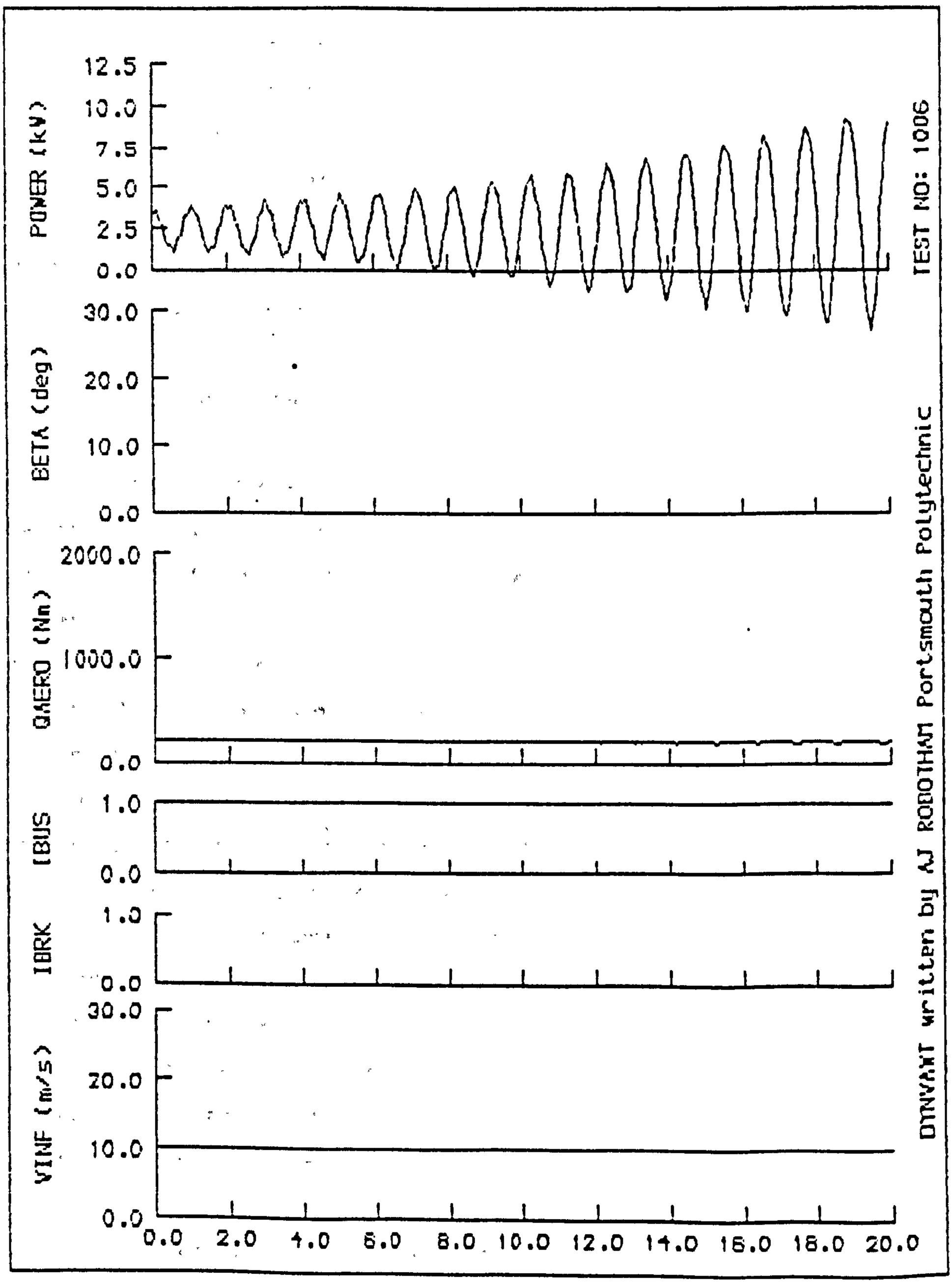

Figure 8.11: Response of uncontrolled 5kW V-VAWT when operating in windspeeds below rated.

the network would become unstable if the simulation had been continued. The cyclic nature of the electrical power output is caused by the uncontrolled wind turbine rotor oscillating with respect to the rotating reference frame of the electricity supply network. The oscillation is invoked by the inability of the initialisation sequence to accurately determine the initial values of the state variables and their derivatives. The small errors involved in evaluating the initial state of the system has invoked an unstable steady state response, even though the windspeed remained below rated.

In the second case, Figure 8.12, the windspeed is initially set to V = 10 m/s. But here, the windspeed is steadily increased to V = 14 m/s over a period of twelve seconds starting from T_{1R} = 4.0 s; the response of the system to this change is clearly shown. The electrical power output of the uncontrolled wind turbine increases with increasing windspeed. However, once the static stability limit of generator power is exceeded, the system becomes unstable, synchronisation is lost, and a shutdown procedure is invoked. The shutdown procedure is characteristic of the program DYNVAWT. If a wind turbine was truly uncontrolled during a period of rising windspeed, the rotor speed would tend to increase until a new equilibrium operating condition was achieved. The program DYNVAWT only allows the on-line behaviour of the wind turbine to be uncontrolled; once the V-VAWT operates off-line, the simulation program automatically invokes the shutdown procedure.

The uncontrolled V-VAWT exhibits an unstable response during its on-line operation, even if the windspeed is below the rated windspeed of the system. The need for active control of the V-VAWT generator system is apparent considering the poor response shown in these two cases.

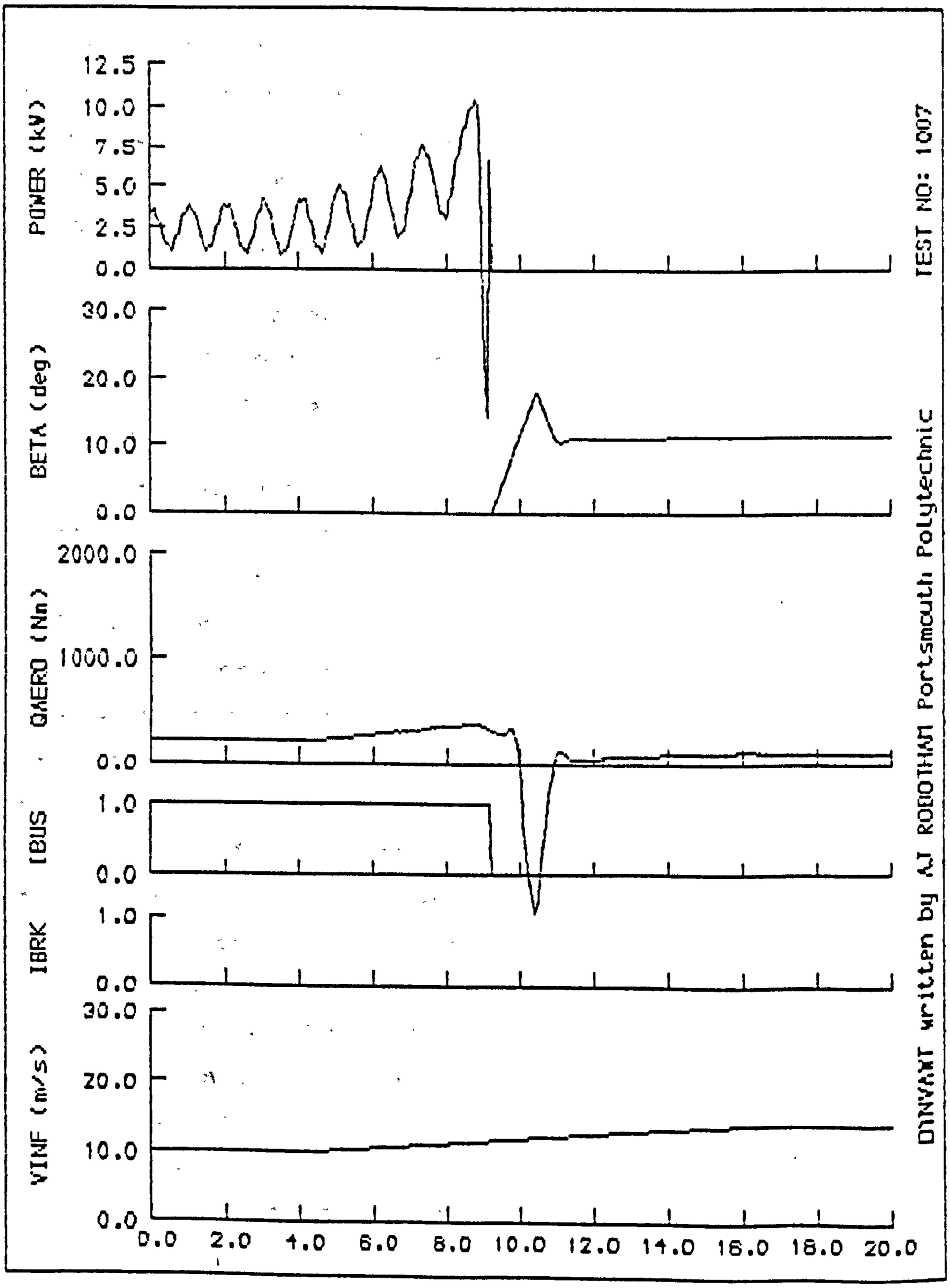

Figure 8.12: Response of uncontrolled 5kW V-VAWT when operating in windspeeds above rated.

8.4: V-VAWT Generator System Control Strategy

In this section, the active control system developed for the on-line and off-line control of the V-VAWT generator system is discussed. This control system has been devised merely to demonstrate the viability of tip pitch control as being a suitable means of actively controlling the aerodynamic power of the V-VAWT rotor in the following operating modes:

(a) Start-up and generator synchronisation
(b) On-line power regulation
(c) Shutdown and rotor braking

This control system is not, however, a complete wind turbine management system. A management system, in addition to controlling the power output of the system, would utilise various monitoring devices to check for out-of-limits operation of any components of the machine. In this way, the onset of potentially dangerous or damaging working conditions would be detected. These condition indicators are used to ensure the wind turbine system operates within its specified safety limits, and detection of any out-of-limits operation would generally invoke the control system to shutdown the wind turbine. The monitoring and checking of out-of-limits conditions, other than those specifically concerned with off-line or on-line power regulation, is not considered further, because they make no significant contribution to the aims of this particular exercise. Such checks are therefore not included in the control system devised here.

The control of the wind turbine during each operating mode can be considered separately, and often it is convenient to consider and analyse the strategies for each mode in isolation. However, the control system here has been

developed to allow the transition between operating modes to be successfully executed and simulated using DYNVAWT. The computer model of the control system can automatically identify the appropriate mode of operation required, and the sequence of V-VAWT start-up, synchronisation, on-line power regulation and shutdown can be simulated during a single study.

The use of a computer to control the wind turbine is implicit in the strategy that has been devised. While it may be possible to devise hardwire, analogue control systems to, say, control the on-line power output of the wind turbine operating at rated windspeed, the author believes that these systems do not provide the flexibility required to control the wind turbine in all its operating modes. The overall management of the wind turbine system must be computer based where precise control of the system output is required. The non-linear behaviour of the wind turbine system will necessarily require adaptive control techniques to be used, as appropriate, to ensure that the wind turbine system is operating effectively in all working conditions.

Since the purpose of this exercise is to demonstrate the viability of blade tip pitch control, the V-VAWT generator system is considered to be disturbed by only *two* external inputs:

(a) Windspeed

(b) Fault in network to generator connection

These system inputs both directly influence the dynamic behaviour of the wind turbine drive train system. Windspeed affects the aerodynamic torque developed by the rotor, and the state of the network to generator connection affects the electrical load on the machine. Both of

these inputs are modelled in DYNVAWT, thus allowing their effect on the V-VAWT generator system to be studied.

The control system developed for the V-VAWT generator system uses open loop rotor power control with compensated rotor speed control to determine blade tip pitch angle. This strategy enables the rotor speed to be accurately controlled while the average power developed by the system does not grossly deviate from its rated performance. The pitch angle specified by these two control systems, however, will be overidden if out-of-limits operation with respect to windspeed or rotor speed is detected. The disc brake and generator contactor are controlled independently. The justification for this system is given below, but the control strategy has been designed to minimise the disturbance on the system caused by these two inputs, and where appropriate, strives to maintain continuity of electricity power supply to the network.

Judging the success of any one particular strategy is not straightforward, and at this stage of the development of V-VAWT concept, it is only possible to compare the simulated performances of the different control strategies with each other. It has not been possible to test the control system or validate the simulation results using the free-air 5kW machine at The Open University. Therefore the results of the DYNVAWT simulation studies are the only means available to assess its suitability or success.

The control system is a sub-system of the whole, and its outputs are dependent upon the its inputs and the control strategy which it embodies. The control system inputs must be observable, so that they can be measured directly by suitable transducers. They have been selected in the knowledge that they can be simply and accurately measured, and are quantities that would be normally monitored by a

commercial wind turbine management system. The control system has internally defined setpoints of power output and rotor speed. These setpoints act as reference inputs to the power control and speed control systems, and are used to determine their controlling outputs. The values assigned to the setpoints are characteristic of the V-VAWT generator system being modelled. In striving to maintain the safe and reliable operation of the system, the control system has only the blade tip pitch actuator, the disc brake actuator and generator contactor to control. The strategy used to control these devices is described below. This strategy was developed for the 5kW V-VAWT generator system after repeated use of DYNVAWT.

Since the control system is computer based, the state of the system will be observed at discrete intervals of time. During the period between observations, the control system must seek and determine the most appropriate control action for the wind turbine system, and set the state of the control system outputs. The state of these outputs will be determined solely by the observations made at the beginning of each control cycle and the strategy embodied in the control system.

The control strategy that has been developed for the V-VAWT generator system, has three distinct phases:

(a) Identify current operating mode
(b) Identify current state of V-VAWT generator system
(c) Determine control system outputs

The state of the current operating mode is identified in the control system software by the variable IMOD. This variable can take four values:

$$IMOD = \begin{cases} 1 & \text{start-up and synchronisation} \\ 2 & \text{on-line power regulation} \\ 3 & \text{on-line power regulation with network fault} \\ 4 & \text{shutdown and rotor braking} \end{cases} \qquad (8.100)$$

The state of the current operating mode determines the initial path followed in the logic of the control strategy. The state of V-VAWT generator system is used to determine subsequent step in the control strategy, which may include changing the current operating mode.

The state of the V-VAWT generator system was initially determined using just *two* control system inputs. A third input was, though, considered necessary for identification of a fault in the connection to the electricity supply network; infinite bus voltage was used as this input. The three control system inputs selected are:

(a) Windspeed
(b) Rotor speed
(c) Infinite bus voltage

These quantities can be measured directly and do not require modification of any standard system components. The windspeed would be measured by an anemometer, rotor speed by a tachogenerator driven by the V-VAWT rotor, and infinite bus voltage would be measured by suitable transducers that would convert the bus voltage to a level suitable for use by the low-voltage control system.

Measurements of windspeed and rotor speed allow the actual state of the V-VAWT generator system to be determined, and then compared to the following rated operating characteristics of the system:

(a) Cut-in windspeed

(b) Rated windspeed

(c) Cut-out windspeed

(d) Minimum rotational speed

(e) Rated rotational speed

(f) Maximum rotational speed

The method used to determine the subsequent strategy is best illustrated by Figure 8.13. Each diagram shows a "condition matrix" of control options for each operating mode. The limits of the condition matrix are defined by the six system characteristics shown above. The state of the current operating mode determines which of the three condition matrices is initially used. The control strategy is then determined by where the state of the V-VAWT generator system is positioned in that condition matrix. Where the state of the system is positioned within the working range of the condition matrix, the reference values to the open loop rotor power control and rotor speed control systems are set, and the disc brake, blade tip and the generator contactor states all defined. Where the state of the system is positioned outside the working range of the condition matrix, the operating mode is changed and the control strategy must be determined using the condition matrix of the new current operating mode.

Note that knowledge of the state of the V-VAWT generator system alone is not sufficient to determine the control strategy to be adopted. The state of the current operating mode determines the initial range of control options available, though the operating mode may change once the state of the system is considered, and a new range of control options would become available.

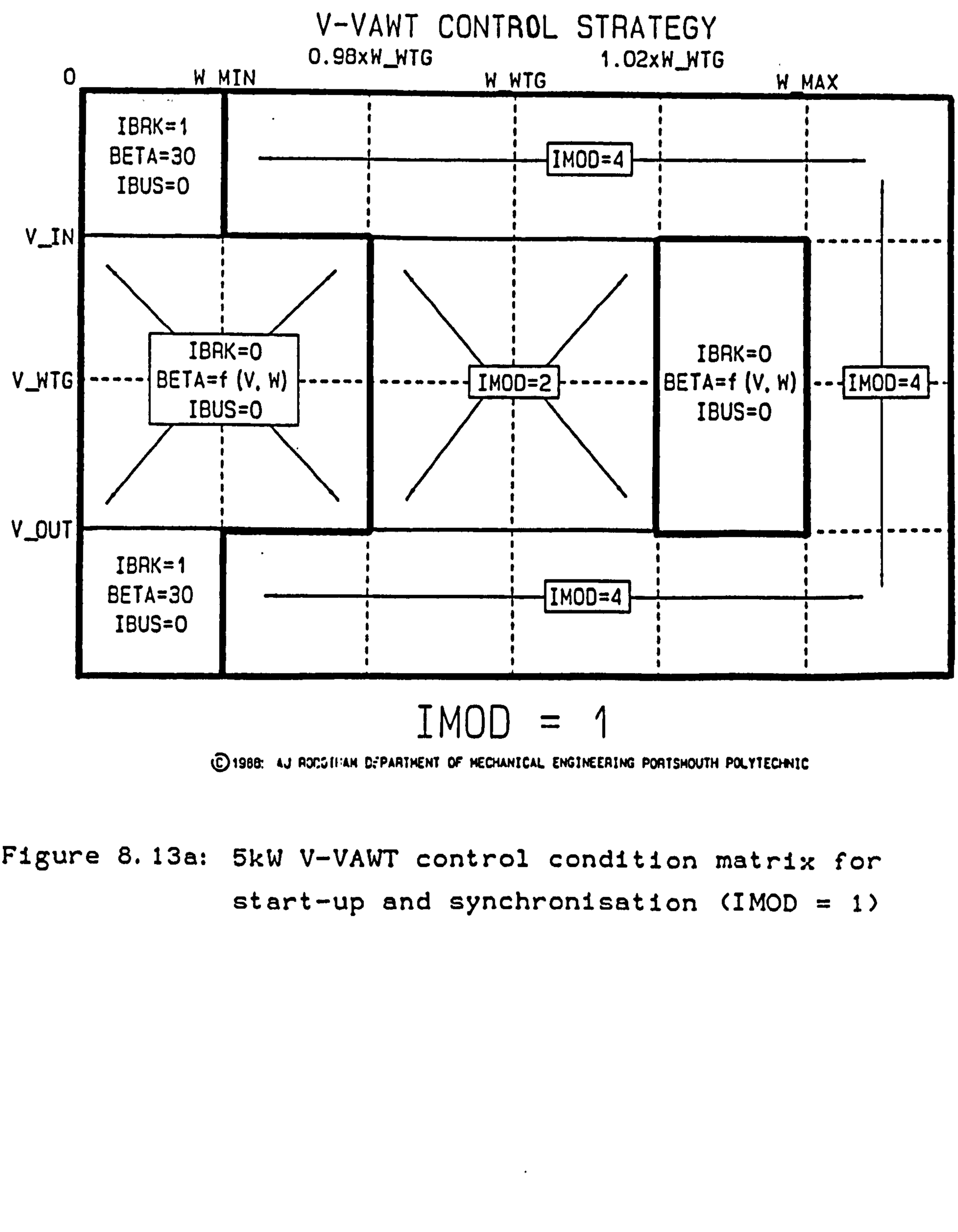

Figure 8.13a: 5kW V-VAWT control condition matrix for start-up and synchronisation (IMOD = 1)

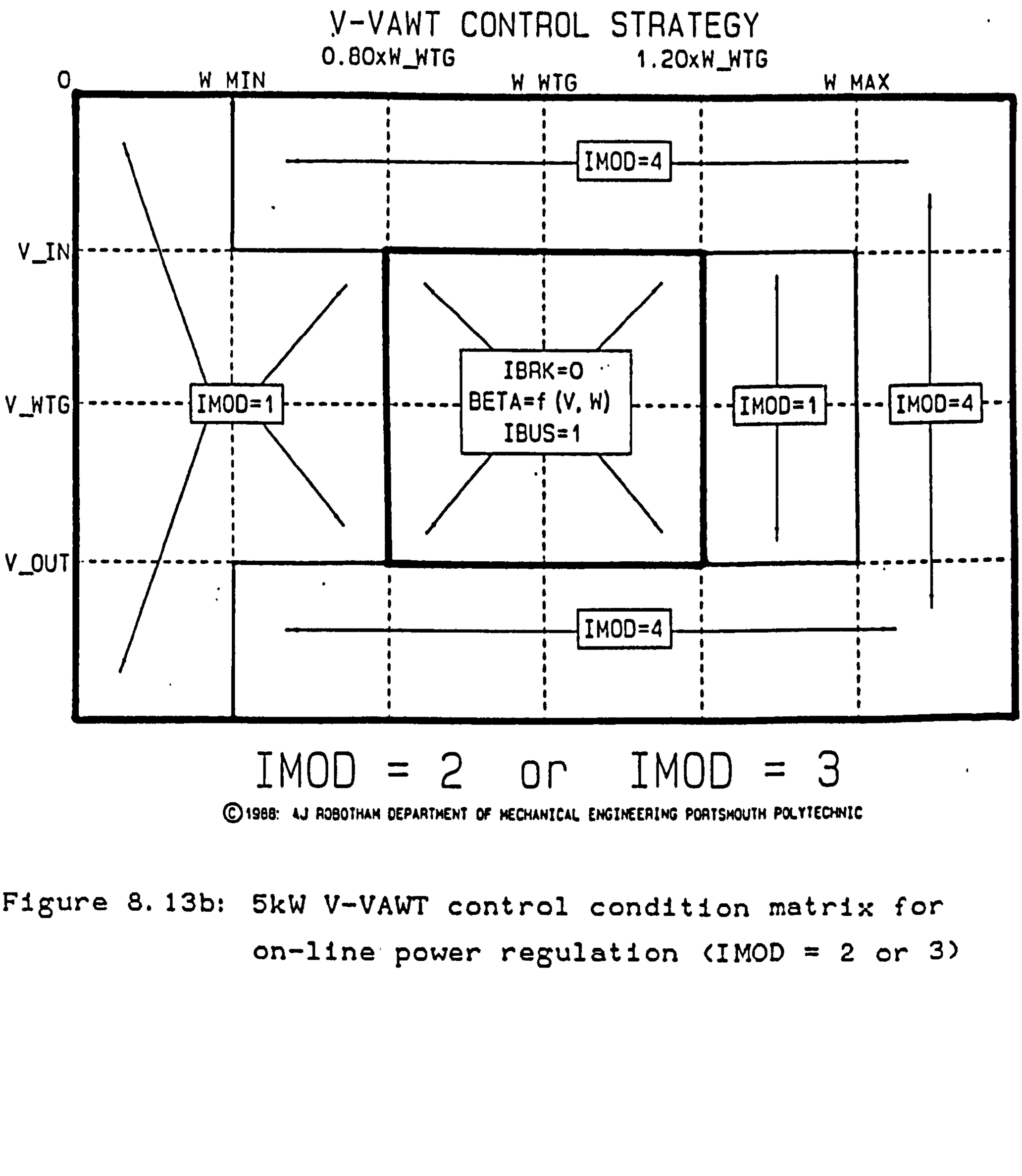

Figure 8.13b: 5kW V-VAWT control condition matrix for on-line power regulation (IMOD = 2 or 3)

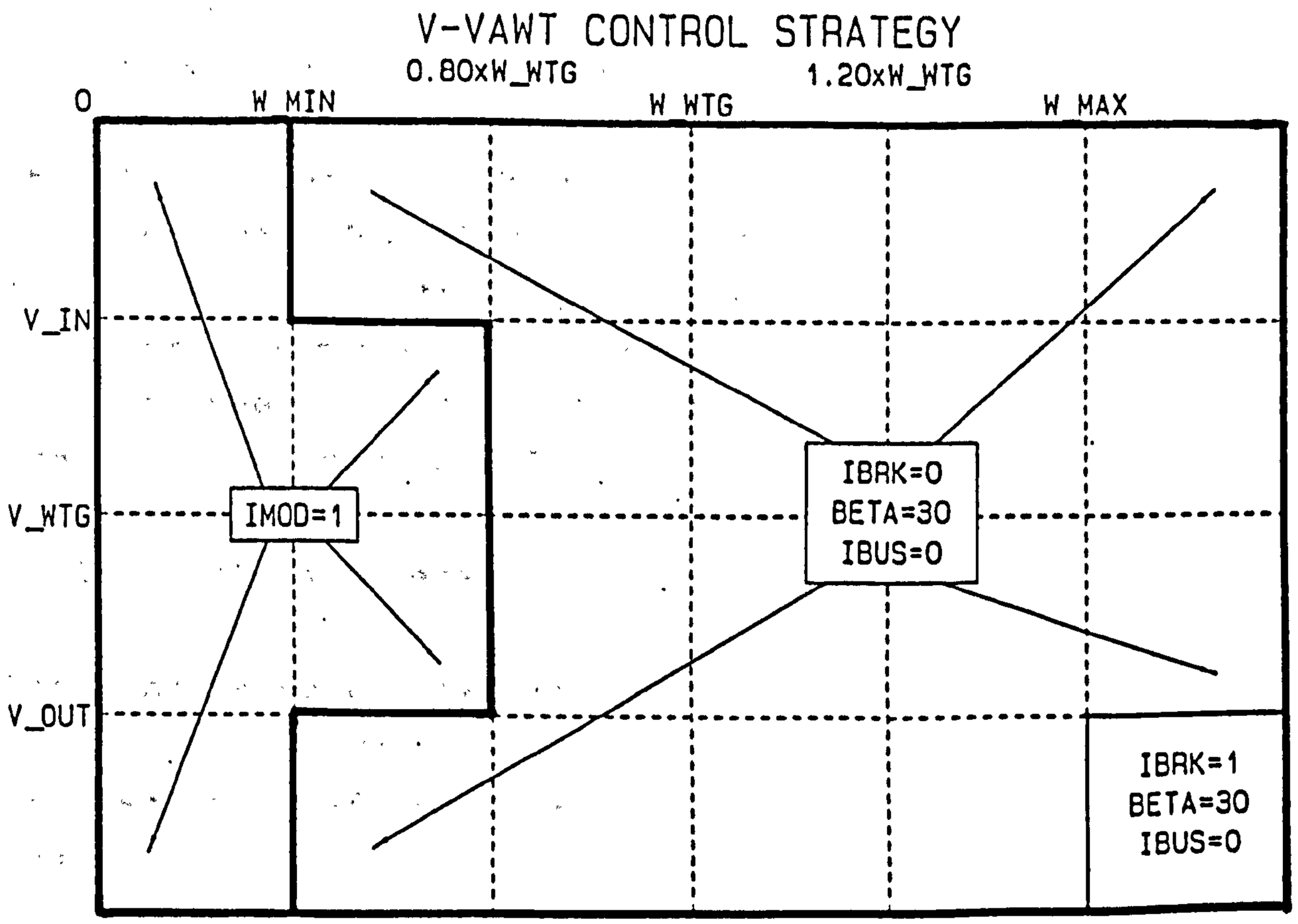

Figure 8.13c: 5kW V-VAWT control condition matrix for shutdown and rotor braking (IMOD = 4)

The operating regime of particular interest here is bound by the cut-in and cut-out windspeed limits and the maximum allowable rotor speed limit. Within these limits, the wind turbine system will be either in the start-up and synchronisation mode, or else in the on-line operation mode. Outside these limits, the shutdown and braking mode is invoked. The control strategies devised for each operating mode are described in detail below.

The start-up and synchronisation operating mode (IMOD = 1) considers the V-VAWT generator system to be disconnected from the electricity supply network, the disc brake to be off, and the rotor to be at rest or rotating slowly. If the windspeed is above cut-in and below cut-out, the start sequence may commence. The blade tip is set to its minimum pitch angle, and since the system is unloaded, the rotor will quickly accelerate.

When the speed of the rotor exceeds 80% of the rated rotor speed, the rotor power and speed control systems are invoked, and reference values set. The reference speed is the rated rotor speed, and the reference power is 40% of rated system power. The reduced power reference ensures the rotor speed continues to increase towards synchronous speed, but the acceleration of the rotor is reduced. The power and speed control systems determine the appropriate blade tip pitch angle.

When the speed of the rotor is within ±2% of the rated speed, the synchronisation of the generator with the electricity supply commences. However, rather than close the contactor immediately the rotor speed reaches synchronous speed, a delay has been included in the control algorithm. The reference speed and power values remain unchanged, and the rotor should maintain its speed at or very near to synchronous speed. If the rotor continues to

rotate at or near synchronous speed, the control system will eventually close the contactor and synchronous operation with the network will begin. The delay allows the rotor speed to settle close to synchronous speed after the initial acceleration period. Once synchronisation is complete, the operating mode is changed to on-line operation (IMOD =2).

Immediately after synchronisation is complete, and the operating mode is changed, the reference value to the rotor power control system is slowly ramped from 40% to 100% of rated power. Ramping the power control reference value to the maximum, ensures the synchronisation with the network is not lost during the initial period of connection when the connection transients are still decaying.

If the system is disturbed such that synchronisation with the grid is lost, the unloaded wind turbine rotor will tend to accelerate, or decelerate, to a stable speed, the runaway speed, appropriate to the windspeed and blade tip pitch angle. If the rotor speed increases by 20% above the rated rotor speed, the shutdown and braking operation mode is invoked. If the rotor speed decreases by 20% below the rated rotor speed, the start-up and synchronisation operation mode is invoked. The 20% speed error has been arbitrally set at present, and could be reduced if required.

If during on-line operation, a network to generator fault is detected (IMOD =3), the reference value to the rotor power control system is reduced to 40% of rated power. The reference value to rotor speed control remains as rated rotor speed. If when the network connection is restored, the V-VAWT generator system is still synchronised with the network, the reference value to the rotor

power control system is slowly ramped from 40% to 100% of rated power, and normal on-line operation continues.

When the V-VAWT generator system operates in either the start-up and synchronisation mode, or the on-line operating modes, if the windspeed should deviate outside the cut-in or cut-out limits, the shutdown and braking mode is automatically invoked. Similarly, if the rotor speed should rise more than 20% above the rated rotor speed, the shutdown and braking mode is invoked once again.

In the shutdown and braking mode (IMOD = 4), the power control and speed control systems are overidden, the generator contactor is automatically opened, and the blade tip pitch angle set to a maximum. This control action will immediately retard the rotor and avoid overspeeding above the specified maximum rotor speed. The disc brake is only applied when the rotor speed falls below the specified minimum rotor speed. If the windspeed is between cut-in and cut-out windspeeds and the rotor speed is less than 20% below the rated rotor speed, the start-up and synchronisation mode is once more invoked. In this way, the rotor need not be brought to a standstill before re-synchronisation is attempted, provided the windspeed remains within the specified limits of the system.

The condition matrices of Figure 8.13, best illustrate the limits of operation for each operating mode, and show the circumstances required for control to pass between different modes.

The open loop power control and compensated rotor speed control systems can be considered separately, since their sole function is to determine a suitable pitch angle for the blade tips.

The open loop power control system has the following inputs:

(a) Windspeed
(b) Reference rotor speed
(c) Reference rotor power

These inputs are used to determine the most suitable blade tip pitch angle from a look-up table of such values stored in the control system software. The look-up table is created from the mean values of torque calculated for the V-VAWT generator system using VAWTTAY. Cyclic values of rotor power are not used. The power control system does not compare the actual and reference power outputs of the V-VAWT generator system. Thus, no power error compensation is included in this system at present.

In HAWT control systems, the error signal of either electrical power output or rotor shaft torque measurements is often used to modify the power control signal to the system. However, two characteristics of the 5kW V-VAWT generator system at present prevent power error feedback being adopted here.

The stiff nature of the V-VAWT generator drive train system, means that the cyclical variation of aerodynamic torque is transmitted through the drive train, and manifests itself as a cyclic variation of electrical output power. The magnitude of the variation depends upon the dynamic characteristics of the rotor and drive train system, and while its effects may be damped out to a large degree by component design and selection, the cyclic shaft torque effects are never completely vanquished; a small instantaneous power output error, therefore, will be observed at all times.

When connected to the network, the relative angular displacement of the rotor with respect to the rotating reference frame of the electricity supply network, tends to oscillate. The frequency of oscillation corresponds to the approximate natural frequency of the system at its rated operating point. This oscillation may or may not become unstable. Since the oscillation causes the generator power angle to exhibit a periodic variation, a periodic variation of power output error can be observed.

The response of the uncontrolled V-VAWT generator systems shown in Figures 8.11 and 8.12, clearly demonstrate these effects. In both cases, the average power output of the system remains constant. If the power control system had error feedback, the system would be responding to power errors caused by problems inherent in the dynamic characteristics of the V-VAWT generator system, and not to deviations of the average power output from rated.

The compensated rotor speed control system has the following system inputs:

(a) Rotor speed
(b) Reference rotor speed

From these two inputs, proportional and derivative speed error compensation is used to calculate a blade tip pitch angle correction. The proportional error is computed by direct comparison of the two system inputs. The derivative error is computed by comparing the present value of rotor speed to that rotor speed measured in the previous control cycle. These two values are used to calculate an instantaneous rate of change of rotor speed. The values of the proportional and derivative gains were established after repeated simulation trials using DYNVAWT. The rotor speed blade tip pitch angle correction is summated to the

the rotor is N = 161.5 rpm, which will drive the 4-pole generator at its synchronous speed of 1500 rpm. The rotor is controlled using 20% blade tips with a pitch angle range of $0° \leq \beta \leq 30°$, and a maximum pitch rate of 15°/s. An electrically released, spring applied disc brake acts directly onto the rotor; the maximum braking torque of 1950 Nm can be applied in 0.1 seconds.

The generator is a four-pole synchronous type rated at 5.0 kVA. It is considered to be connected directly to the supply network, operating with a 0.8 power factor at 50 Hz frequency. The direct and quadrature axis reactances are $x_d = 1.0$ and $x_q = 0.6$ respectively.

The values of the *independent* parameters that describe the mechanical and electrical characteristics of this system are tabulated in Table 8.1. These values remained constant for all the case studies presented here; only the effect of changes to the external inputs to the system were considered. The describing parameters of the mechanical and electrical components of the system can only be changed by design, and therefore the values were chosen to be representative of the free-air machine itself.

The aerodynamic performance of the 5kW V-VAWT, predicted using VAWTTAY, was discussed in Section 7.4. The rotor is controlled using a 20% blade tip area since this size of control surface gives full aerodynamic braking during high windspeed shutdown. Where the case study involves on-line operation, the performance data has been generated for constant rotational speed operation, but where start-up or shutdown operation is simulated, the aerodynamic data has been generated for constant windspeed operation. The datafiles are "VAWT_5KW_20_2S" and "VAWT_5KW_20_2W" respectively.

WIND TURBINE GEOMETRY

1	Rotor Radius	4.39 metres
2	Swept Area	19.0 m2

WIND TURBINE GENERATOR CHARACTERISTICS

1	Rated WTG power (kW)	5.00
2	Rated windspeed (m/s)	12.00
3	Cut-in windspeed (m/s)	4.00
4	Cut-out windspeed (m/s)	26.00
5	Rated rotor rpm	161.50
6	Minimum brake-speed rpm	40.00
7	Maximum overspeed rpm	180.00

INERTIAL ELEMENTS

1	V-VAWT rotor, l.s. shaft	239.01 kg.m2
2	disc brake, 1st stage l.s. pulley	7.15 kg.m2
3	1st stage m.s. pulley, m.s. shaft	0.04 kg.m2
4	2nd stage m.s. pulley, m.s. shaft	0.42 kg.m2
5	2nd stage h.s. pulley, h.s. shaft	0.01 kg.m2
6	coupling, generator rotor	0.06 kg.m2

V-BELT STIFFNESSES

1	1st stage V-belts	4035.00 Nm/rad
2	2nd stage V-belts	1908.00 Nm/rad

GEAR RATIOS

1	1st stage ratio	3.125
2	2nd stage ratio	2.972

ROTOR FRICTION

1	Rotor friction	0.04 Nm.sec/rad

GENERATOR CHARACTERISTICS

1	Terminal voltage	1.000	p.u.
2	Direct-axis reactance	1.000	p.u.
3	Quadrature-axis reactance	0.600	p.u.
4	Number of poles	4	
5	Grid frequency	50.000	Hz
6	Rated POWER	5.000	kVA
7	Connected DIRECTLY to bus		
8	POWER factor	0.800	p.u.
9	Damping coefficient	2.620	p.u.

DISC BRAKE CHARACTERISTICS

1	Maximum brake torque	1950.00	Nm
2	Time constant	0.10	
3	Brake is OFF		

ACTUATOR CHARACTERISTICS

1	Minimum pitch angle	0.0	deg
2	Maximum pitch angle	30.0	deg
3	Maximum pitch rate	15.0	deg/sec
4	Damping Factor	0.6	
5	Natural Frequency	8.3	rad/sec
6	Initial pitch angle	0.0	deg

PID CONTROL GAINS

1	Proportional SPEED gain	0.40000
2	Differential SPEED gain	0.80000
3	Proportional TORQUE gain	0.00020
4	Differential TORQUE gain	0.00020

Table 8.1: Describing parameters of two-bladed 5kW V-VAWT generator system

Case Study № 1015

VAWT configuration:	two-bladed, 5kW V-VAWT with 20% blade tip pitch control, open-loop power and compensated rotor speed control strategy.
VAWTTAY datafile:	VAWT_5KW_20_2S
Operating mode:	On-line (IMOD = 2)
Base windspeed:	V_{WB} = 10.0 m/s
Ramp component:	MAXR = 4.0 m/s T_{1R} = 4.0 s T_{2R} = 16.0 s
Results plot:	Figure 8.14

Observations and Comments

The 5kW V-VAWT is initially operating in a windspeed below rated, and the electrical power output is observed to be oscillatory. The period of oscillation corresponds to the nominal natural frequency of the V-VAWT generator system. The power control is not sufficiently sensitive to damp out the power variation stimulated at start-up.

As windspeed increases to above rated, the pitch angle of the tips is quickly adjusted to ensure the power output of the system remains constant. The transient fluctuations of power output are damped by the control system and a stable power output is achieved. Small fluctuations are observed, the frequency of which corresponds to the blade passing frequency of the rotor. The cyclic variation of rotor torque, though, has been considerably damped at the electrical end of the drive train system.

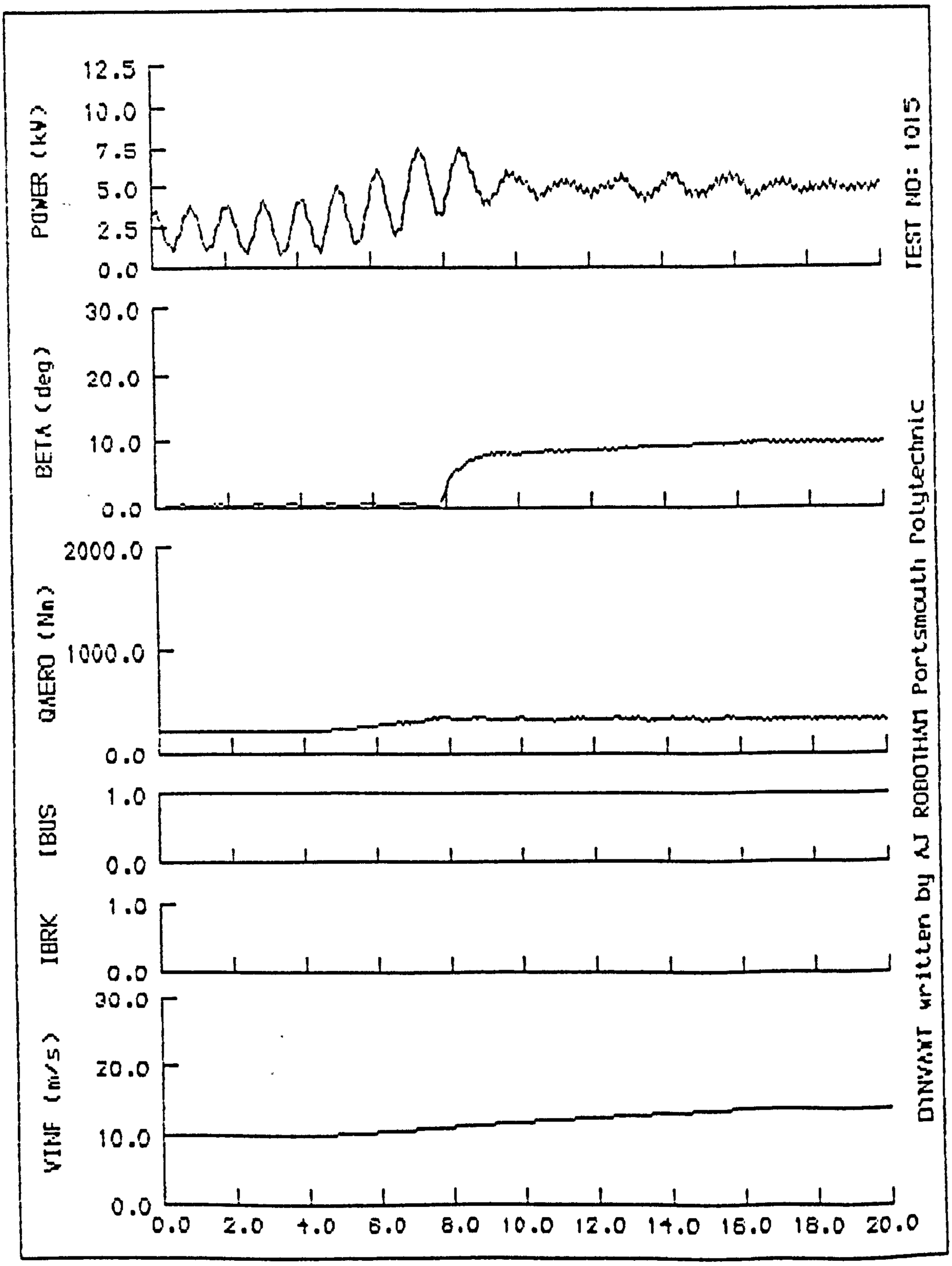

Figure 8.14: Simulation case study № 1015

Case Study Nº 1016

VAWT configuration: two-bladed, 5kW V-VAWT with 20% blade tip pitch control, open-loop power and compensated rotor speed control strategy.

VAWTTAY datafile: VAWT_5KW_20_2S

Operating mode: On-line (IMOD = 2)

Base windspeed: V_{WB} = 14.0 m/s

Results plot: Figure 8.15

Observations and Comments

Here the 5kW V-VAWT is operating in a windspeed above rated. The initial transient response at the start of the simulation period is due to the small error in the initialisation of the state variables during this sequence of the program DYNVAWT. As can be seen, however, the control system damps out the transient response and a stable power output is achieved. The state variables at the end of this simulation sequence could be used to initialise other case studies where the base windspeed is V_{WB} = 14.0 m/s. However, the author has not included this option in the computer program, therefore all the case studies presented here will show a similar transient response at the start of each simulation period. The transients decay quickly, and are negligible for t > 3.0 s, so all disturbances to the system are invoked at t = 4.0 s to avoid accumulation of the transient responses in the initial period of the simulation.

Small cyclic variations of power output are observed in the steady state response. The frequency of the variation equals the blade passing frequency, showing that the cyclic variation of rotor torque has not been completely damped by the drive train elements or control system.

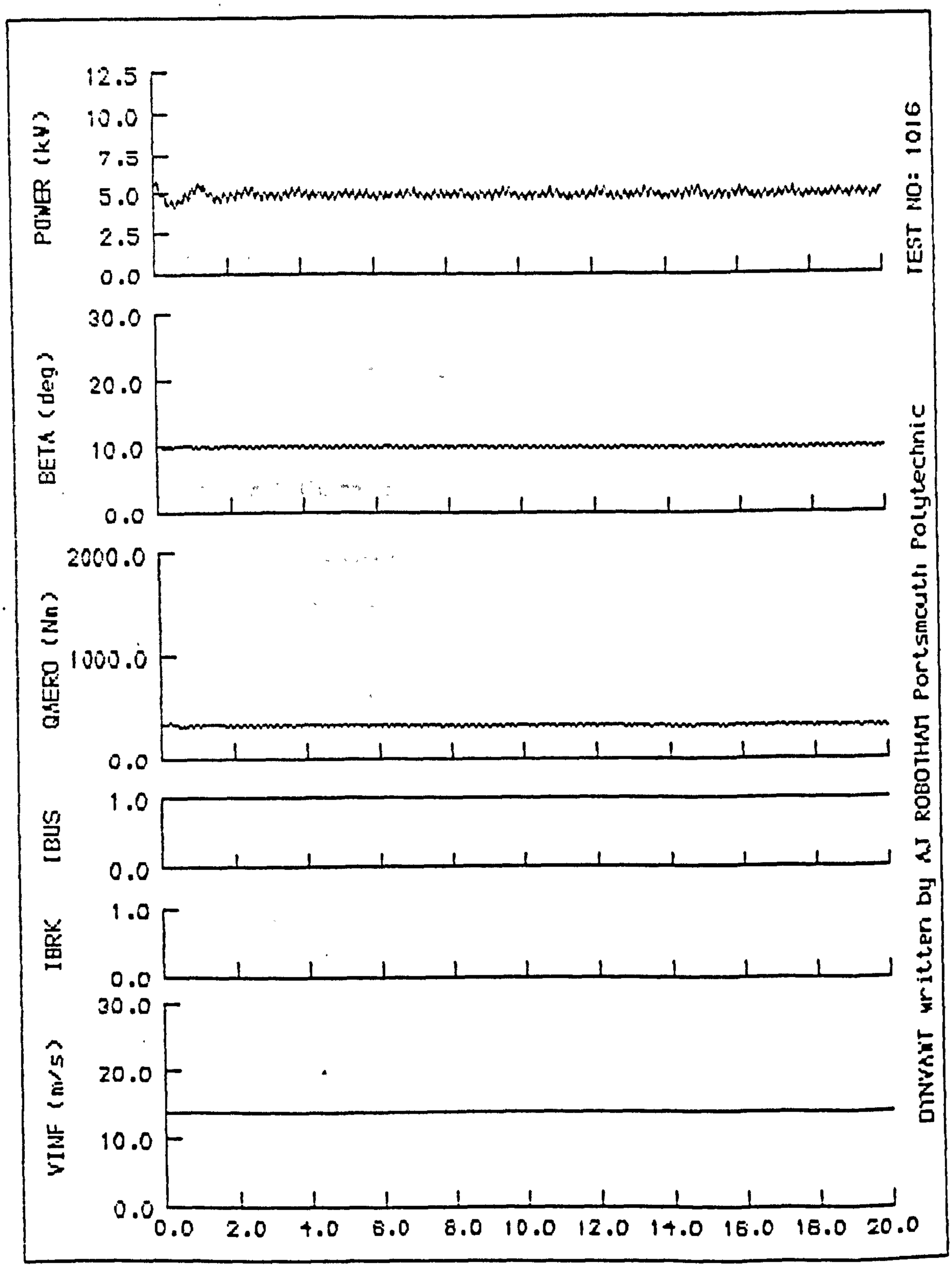

Figure 8.15: Simulation case study № 1016

Case Study № 1019

VAWT configuration: two-bladed, 5kW V-VAWT with 20% blade tip pitch control, open-loop power and compensated rotor speed control strategy.

VAWTTAY datafile: VAWT_5KW_20_2S

Operating mode: On-line (IMOD = 2)

Base windspeed: V_{web} = 14.0 m/s

Noise component: F = 700.0 m
C_T = 0.005
ω_{cf} = 100.0 rad/s

Results plot: Figure 8.16

Observations and Comments

The gusty wind conditions simulated here provoke large fluctuations in the power output of the system. The tip pitch controller is continually adjusting the pitch angle to accommodate the rapid changes of windspeed seen by the rotor. The result, however, shows that the static stability limit of the generator is exceeded and synchronisation with network is lost at t ≈ 19 s. The contactor is opened, and useful power is no longer being delivered by the V-VAWT generator.

The tip pitch controller is unable to cope with the rapid windspeed changes simulated here. The "measured" windspeed used in DYNVAWT for control purposes is observed at the same time as it acts on the rotor; anticipation of the windspeed using feed-forward control has not been considered. The stiff nature of the drive train elements ensures that mean rotor torque fluctuations are transmitted to the electrical generator, yet cyclic variations which are larger in magnitude are not.

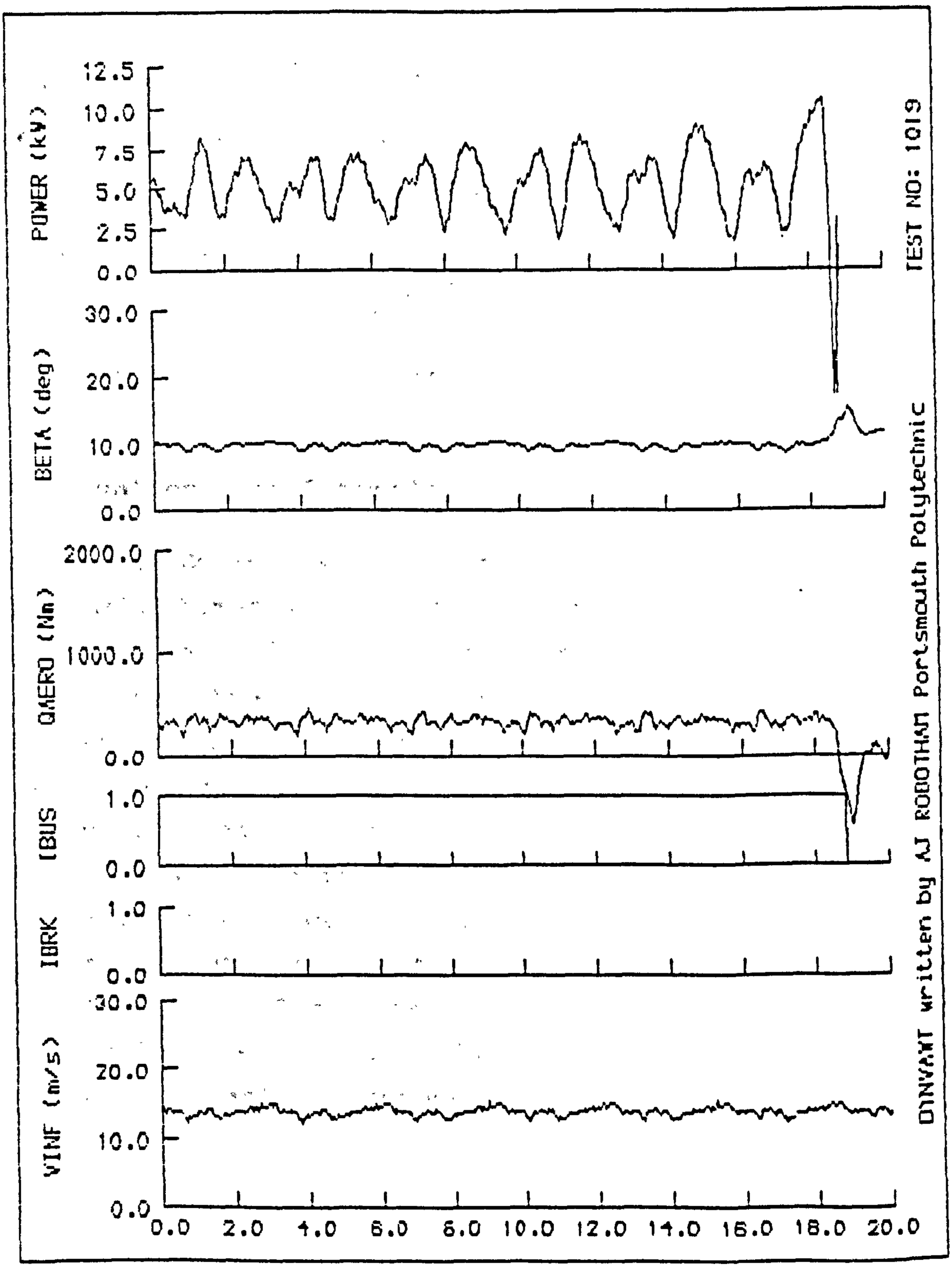

Figure 8.16: Simulation case study Nº 1019

Case Study № 1020

VAWT configuration:	two-bladed, 5kW V-VAWT with 20% blade tip pitch control, open-loop power and compensated rotor speed control strategy.
VAWTTAY datafile:	VAWT_5KW_20_2S
Operating mode:	On-line (IMOD = 2)
Base windspeed:	V_{WB} = 14.0 m/s
Gust component:	MAXG = 5.0 m/s T_{1G} = 4.0 s T_{2G} = 6.0 s
Results plot:	Figure 8.17

Observations and Comments

At the peak of the gust, the wind energy available is two and half times greater than when the windspeed is at its base value. If all this energy is transmitted to the generator, the static stability limit would be exceeded, and an unstable response would be observed. The transient response of the system following a discrete gust is, however, seen to be stable, with the electrical power output being suitably attenuated by the controller. Although the power output fluctuates during the gust, power output transients are seen to have decayed by $t \simeq 10.0$ s. The rate of change of windspeed in this particular case is clearly not so fast that the control system is unable to respond in a suitable manner.

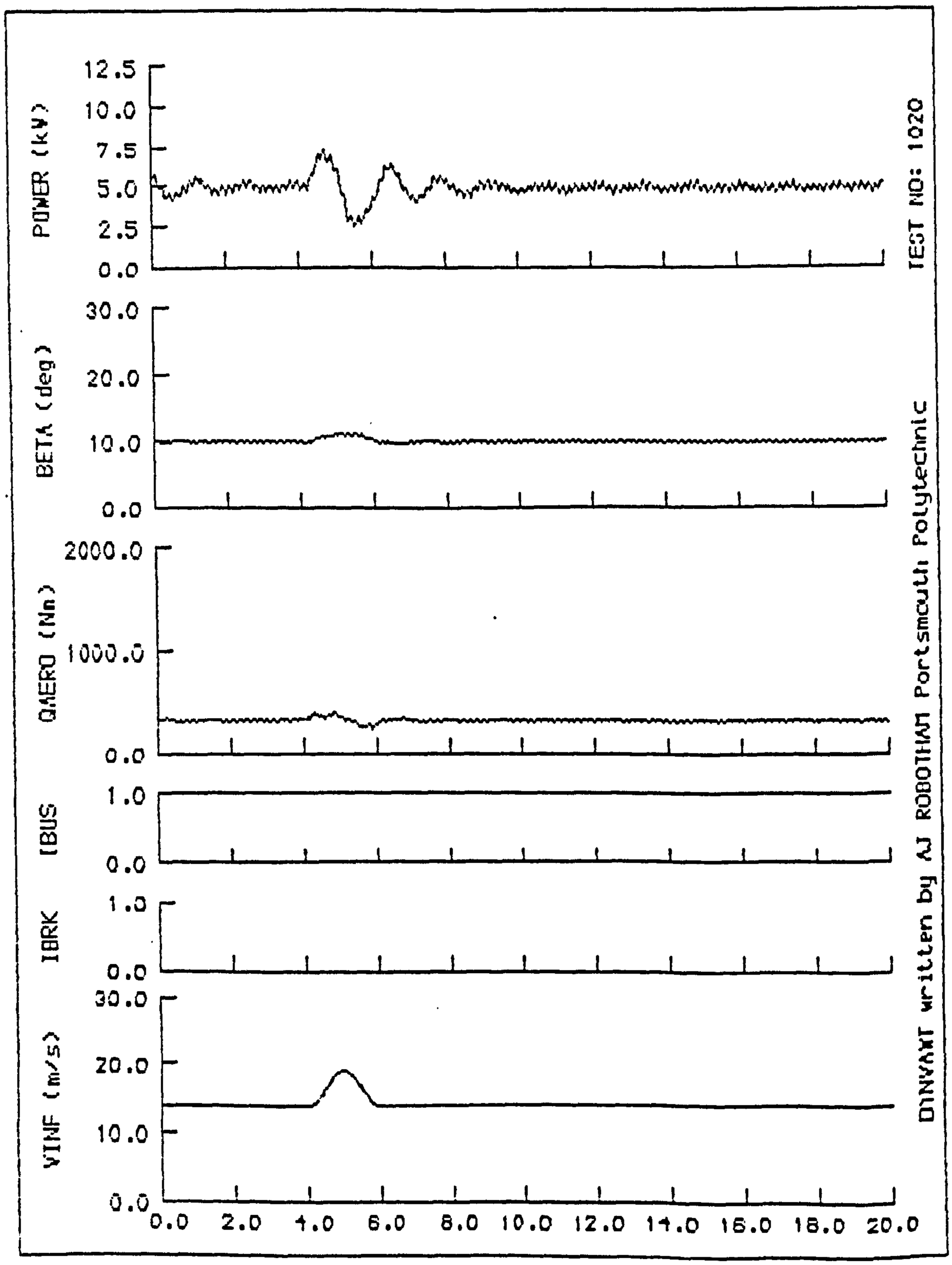

Figure 8.17: Simulation case study № 1020

Case Study № 1021

VAWT configuration:	two-bladed, 5kW V-VAWT with 20% blade tip pitch control, open-loop power and compensated rotor speed control strategy.
VAWTTAY datafile:	VAWT_5KW_20_2S
Operating mode:	On-line with fault (IMOD = 3)
Base windspeed:	V_{wB} = 14.0 m/s
Fault conditions:	T_{1F} = 4.0 s T_{2F} = 4.2 s
Results plot:	Figure 8.18

Observations and Comments

The fault clearing time is only 0.2 s, and during this period the power of the rotor is reduced to 40% of rated. When the fault clears, the V-VAWT generator system is still synchronised with the network, so the power output is slowly increased upto 100% of rated. In this particular case, the V-VAWT generator system has remained stable, and useful power is produced immediately the fault is cleared.

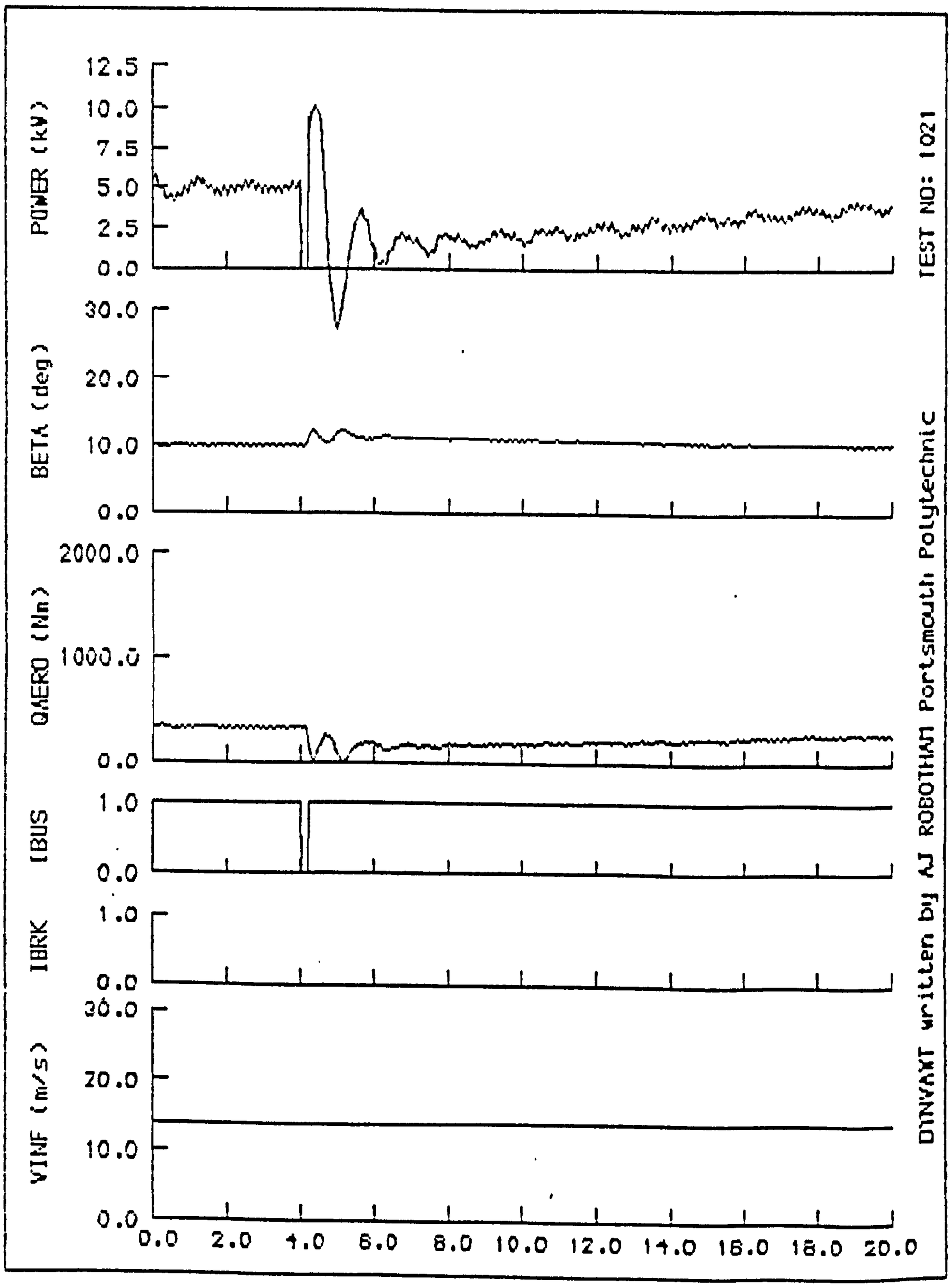

Figure 8.18: Simulation case study Nº 1021

Case Study Nº 1022

VAWT configuration:	two-bladed, 5kW V-VAWT with 20% blade tip pitch control, open-loop power and compensated rotor speed control strategy.
VAWTTAY datafile:	VAWT_5KW_20_2S
Operating mode:	On-line with fault (IMOD = 3)
Base windspeed:	V_{web} = 14.0 m/s
Fault conditions:	T_{1f} = 4.0 s T_{2f} = 4.4 s
Results plot:	Figure 8.19

Observations and Comments

The fault clearing time is now 0.4 s, and during this period the power of the rotor is reduced to 40% of rated. When the fault clears, the V-VAWT generator system is still synchronised with the network; useful power is produced immediately. The control system is, however, unable to stabilize the reconnection of the V-VAWT generator system to the network. Within a second of the fault clearing, the contactor is re-opened and the re-synchronisation procedure invoked.

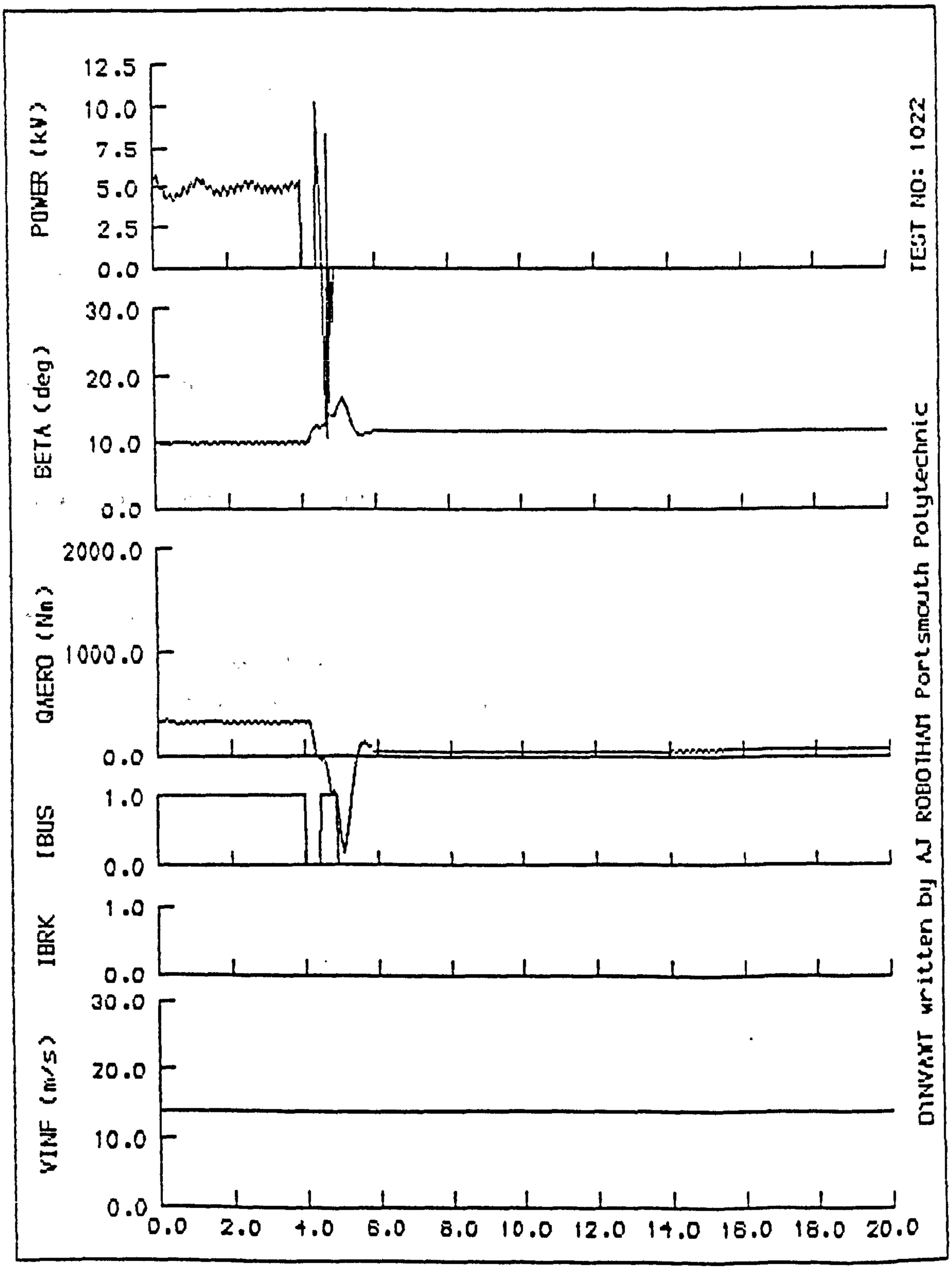

Figure 8.19: Simulation case study Nº 1022

Case Study № 1023

VAWT configuration: two-bladed, 5kW V-VAWT with 20% blade tip pitch control, open-loop power and compensated rotor speed control strategy.

VAWTTAY datafile: VAWT_5KW_20_2S

Operating mode: On-line (IMOD = 2)

Base windspeed: V_{WB} = 14.0 m/s

Ramp component: MAXR = 4.0 m/s
T_{1R} = 4.0 s
T_{2R} = 16.0 s

Results plot: Figure 8.20

Observations and Comments

In this particular case, the windspeed slowly rises over the simulation period. The power output clearly remains stable as the windspeed at all times remains within the operating limits of the system.

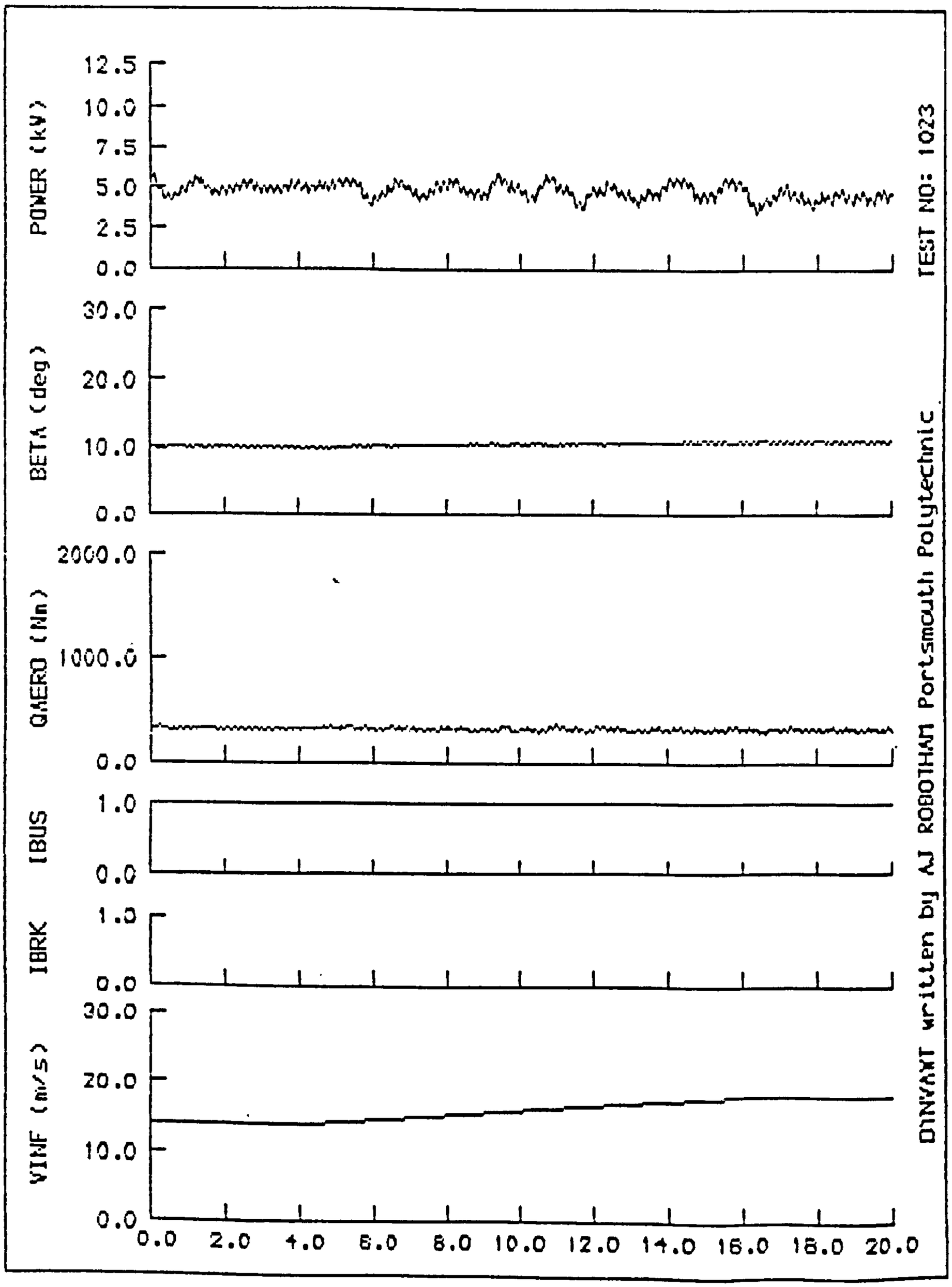

Figure 8.20: Simulation case study Nº 1023

Case Study № 1024

VAWT configuration: two-bladed, 5kW V-VAWT with 20% blade tip pitch control, open-loop power and compensated rotor speed control strategy.

VAWTTAY datafile: VAWT_5KW_20_2S

Operating mode: On-line (IMOD = 2)

Base windspeed: V_{WB} = 24.0 m/s

Results plot: Figure 8.21

Observations and Comments

Here the 5kW V-VAWT is operating in a windspeed above rated. The initial transient response at the start of the simulation period is similar to that observed in Case Study № 1019. The control system, however, damps out the transient response and a stable power output is achieved. The transients decay quickly, and are negligible for t > 3.0 s.

Small cyclic variations of power output are observed in the steady state response. The frequency of the variation equals the blade passing frequency, showing that the cyclic variation of rotor torque has not been completely damped by the drive train elements or control system.

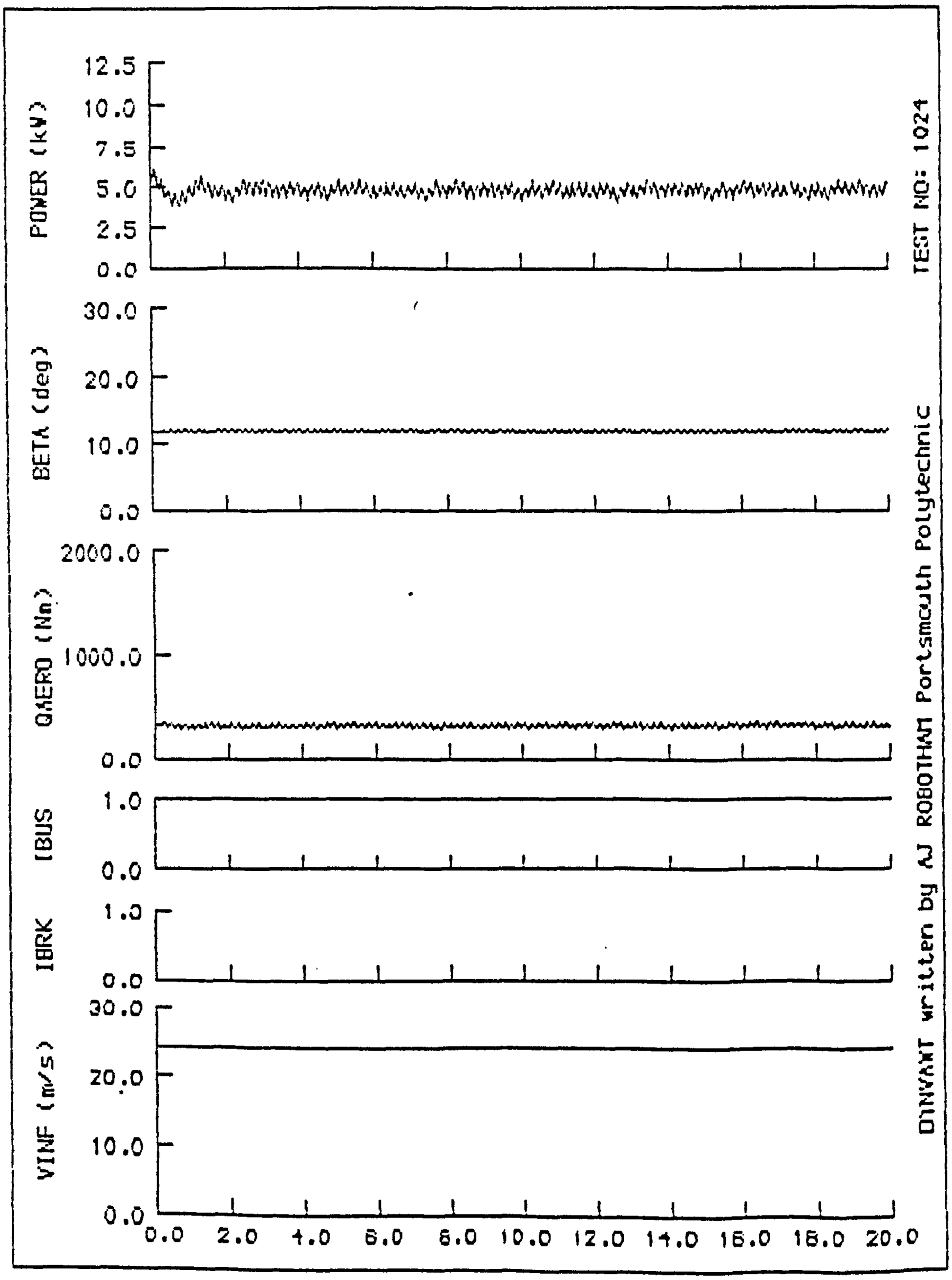

Figure 8.21: Simulation case study № 1024

Case Study Nº 1025

VAWT configuration: two-bladed, 5kW V-VAWT with 20% blade tip pitch control, open-loop power and compensated rotor speed control strategy.

VAWTTAY datafile: VAWT_5KW_20_2S

Operating mode: On-line (IMOD = 2)

Base windspeed: V_{WB} = 24.0 m/s

Noise component: F = 700.0 m
C_T = 0.005
ω_U = 100.0 rad/s

Results plot: Figure 8.22

Observations and Comments

The gusty wind conditions simulated here provoke large fluctuations in the power output of the system. The tip pitch controller is continually adjusting the pitch angle to accommodate the rapid changes of windspeed seen by the rotor. During the simulation period, the windspeed exceeds the upper operating windspeed limit. A high windspeed shutdown is invoked, the contactor is opened, and useful power is no longer being delivered by the V-VAWT generator. Since the windspeed is continuously varying, the controller attempts to reconnect the V-VAWT generator to the network. Once again the windspeed is seen to exceed the safe upper limit of the system and a shutdown procedure is invoked. This cycle repeats itself throughout the simulation period.

A limitation of the control condition matrix approach is seen here where the short-term crossing of the upper windspeed limit has the effect of invoking a shutdown, even though the mean windspeed is still within safe operating limits.

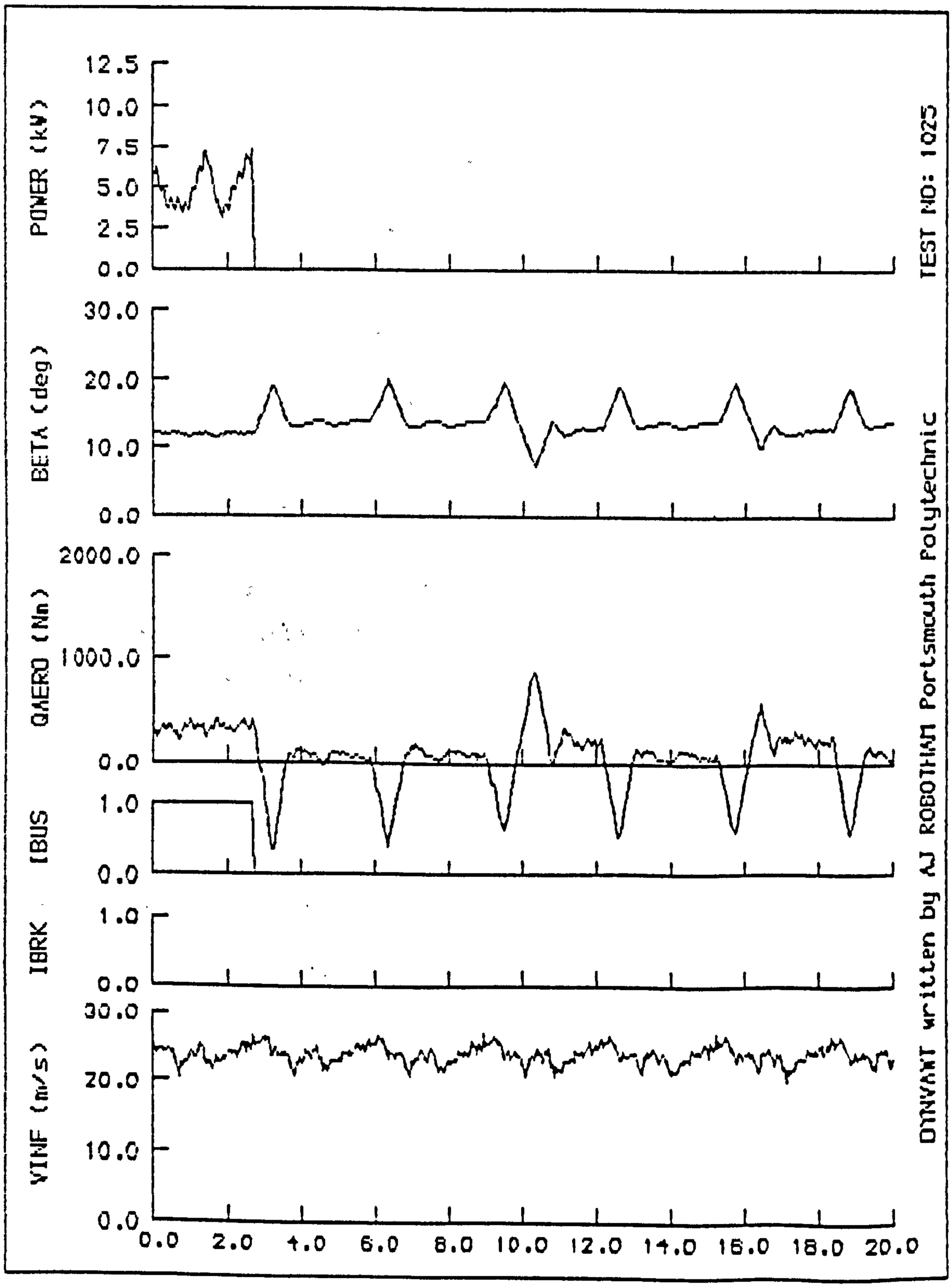

Figure 8.22: Simulation case study № 1025

Case Study № 1026

VAWT configuration: two-bladed, 5kW V-VAWT with 20% blade tip pitch control, open-loop power and compensated rotor speed control strategy.

VAWTTAY datafile: VAWT_5KW_20_2S

Operating mode: On-line (IMOD = 2)

Base windspeed: V_{wB} = 24.0 m/s

Gust component: MAXG = 5.0 m/s
T_{1G} = 4.0 s
T_{2G} = 6.0 s

Results plot: Figure 8.23

Observations and Comments

The discrete gust invokes a shutdown procedure because the windspeed exceeds the upper windspeed limit for about one second of its duration. However, the windspeed returns to a mean value within the operating limits of the system, so the start-up and synchronisation procedure is invoked. Within six seconds of the V-VAWT generator system being disconnected from the network, it is once again synchronised, connected, and delivering useful power. The power output is slowing increased from 40% of rated to 100% of rated to allow the transients of reconnection to fully decay.

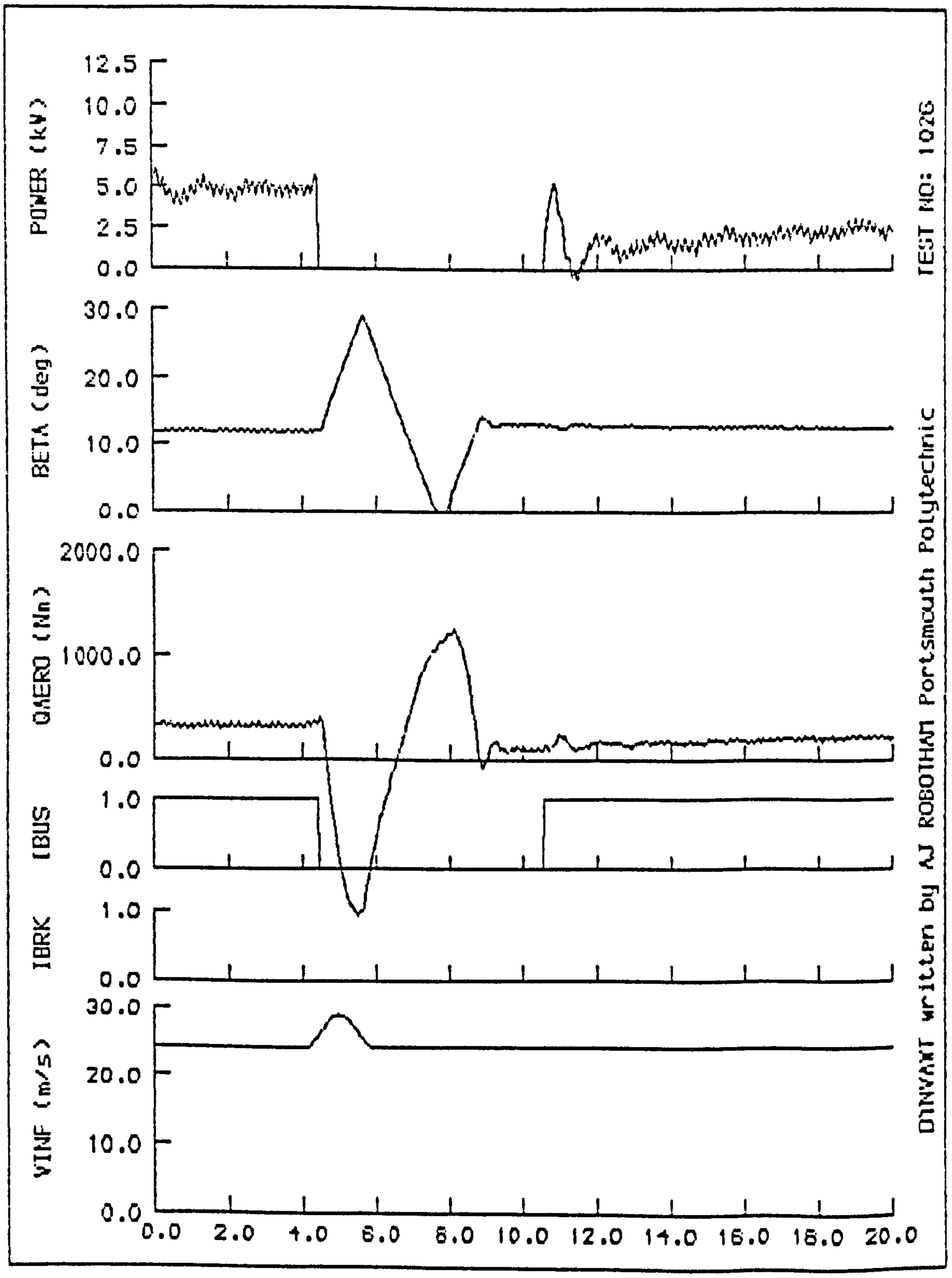

Figure 8.23: Simulation case study № 1026

Case Study Nº 1027

VAWT configuration:	two-bladed, 5kW V-VAWT with 20% blade tip pitch control, open-loop power and compensated rotor speed control strategy.
VAWTTAY datafile:	VAWT_5KW_20_2S
Operating mode:	On-line with fault (IMOD = 3)
Base windspeed:	V_{wB} = 24.0 m/s
Fault conditions:	T_{1F} = 4.0 s T_{2F} = 4.2 s
Results plot:	Figure 8.24

Observations and Comments

The fault clearing time is only 0.2 s, and during this period the power of the rotor is reduced to 40% of rated. When the fault clears, the V-VAWT generator system is still synchronised with the network, so the power output is slowly increased to 100% of rated. In this particular case, the V-VAWT generator system has remained stable, and useful power is produced immediately the fault is cleared.

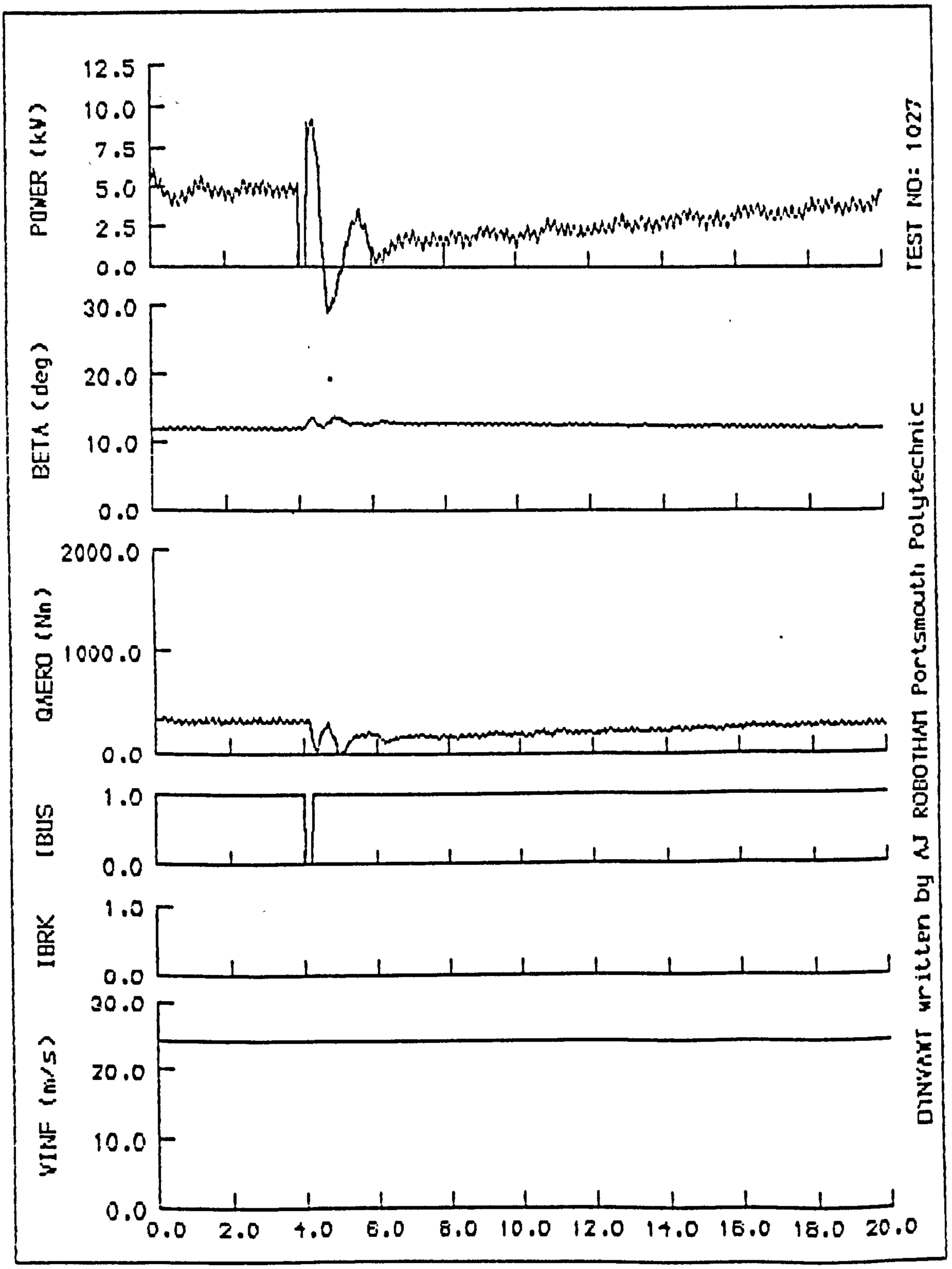

Figure 8.24: Simulation case study № 1027

Case Study Nº 1028

VAWT configuration:	two-bladed, 5kW V-VAWT with 20% blade tip pitch control, open-loop power and compensated rotor speed control strategy.
VAWTTAY datafile:	VAWT_5KW_20_2S
Operating mode:	On-line with fault (IMOD = 3)
Base windspeed:	V_{web} = 24.0 m/s
Fault conditions:	T_{1F} = 4.0 s T_{2F} = 4.4 s
Results plot:	Figure 8.25

Observations and Comments

The fault clearing time is now 0.4 s, and during this period the power of the rotor is reduced to 40% of rated. When the fault clears, the V-VAWT generator system is still synchronised with the network; useful power is produced immediately. The control system is, however, unable to stabilize the reconnection of the V-VAWT generator system to the network. Within two seconds of the fault clearing, the contactor is re-opened and the synchronisation procedure invoked.

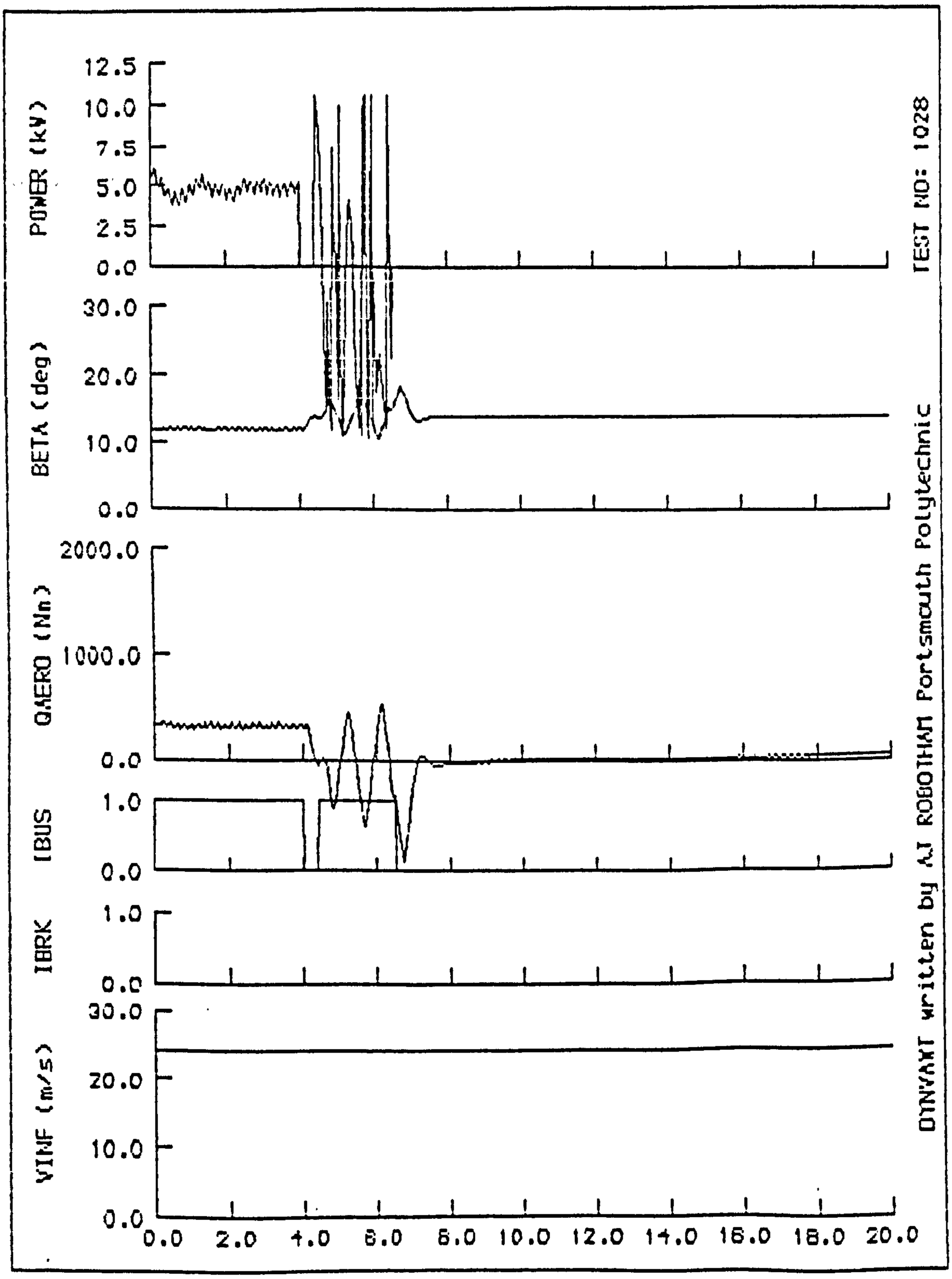

Figure 8.25: Simulation case study № 1028

Case Study Nº 1029

VAWT configuration:	two-bladed, 5kW V-VAWT with 20% blade tip pitch control, open-loop power and compensated rotor speed control strategy.
VAWTTAY datafile:	VAWT_5KW_20_2S
Operating mode:	On-line (IMOD = 2)
Base windspeed:	V_{wB} = 24.0 m/s
Ramp component:	MAXR = 4.0 m/s T_{1R} = 4.0 s T_{2R} = 16.0 s
Results plot:	Figure 8.26

Observations and Comments

In this particular case, the windspeed slowly rises over the simulation period. At t = 10.0 s the windspeed exceeds the upper windspeed limit and a shutdown procedure is invoked. Since the windspeed remains above the upper limit for the rest of the simulation period, no attempt is made to reconnect the V-VAWT generator to the network.

Although it is not visible here, the shutdown procedure is not fully simulated in this example. The constant rotational speed performance data used in this case study, does not allow variable speed operation to be accurately modelled, especially where the speed of the rotor is significantly different from its nominal speed. Reynolds Number effects are not completely satisfied by one set of data, so for start-up and shutdown simulations the constant windspeed performance data should be used to give a more accurate simulation of the behaviour of the V-VAWT generator system.

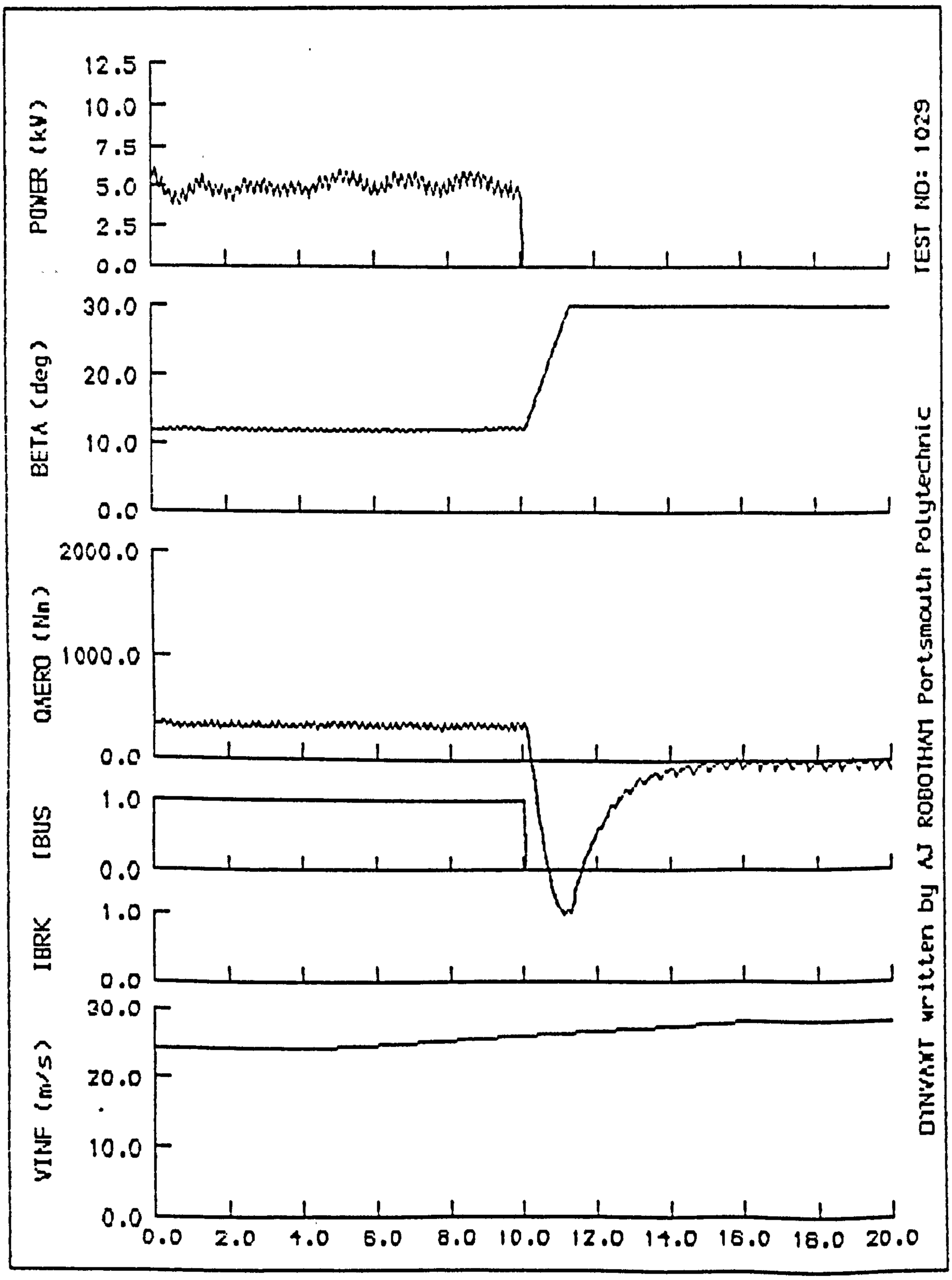

Figure 8.26: Simulation case study № 1029

Case Study Nº 1030

VAWT configuration:	two-bladed, 5kW V-VAWT with 20% blade tip pitch control, open-loop power and compensated rotor speed control strategy.
VAWTTAY datafile:	VAWT_5KW_20_2W
Operating mode:	Start-up and synchronisation (IMOD = 1)
Base windspeed:	V_{WB} = 4.0 m/s
Ramp component:	MAXR = 10.0 m/s T_{1R} = 1.0 s T_{2R} = 1.1 s
Results plot:	Figure 8.27

Observations and Comments

The start-up sequence is best simulated with the mean windspeed starting below cut-in windspeed, and then being increased rapidly to a suitable operating windspeed. The simulation shows the rotor self-starting and accelerating towards its nominal rotational speed. When the rotational speed of the rotor exceeds 80% of nominal, the synchronisation procedure commences. The rotor power is set to 40% of rated, allowing the rotor to continue accelerating to synchronous speed. The rotor speed is maintained within limits of ±2% of synchronous speed before the contactor is closed, and the V-VAWT generator is connected to the network. Once connected, the power output of the system is slowly increased to 100% of rated over a period of twenty seconds; this ensures all the transients of synchronisation fully decay before full power is achieved. The whole procedure takes about fifty-five seconds in this example.

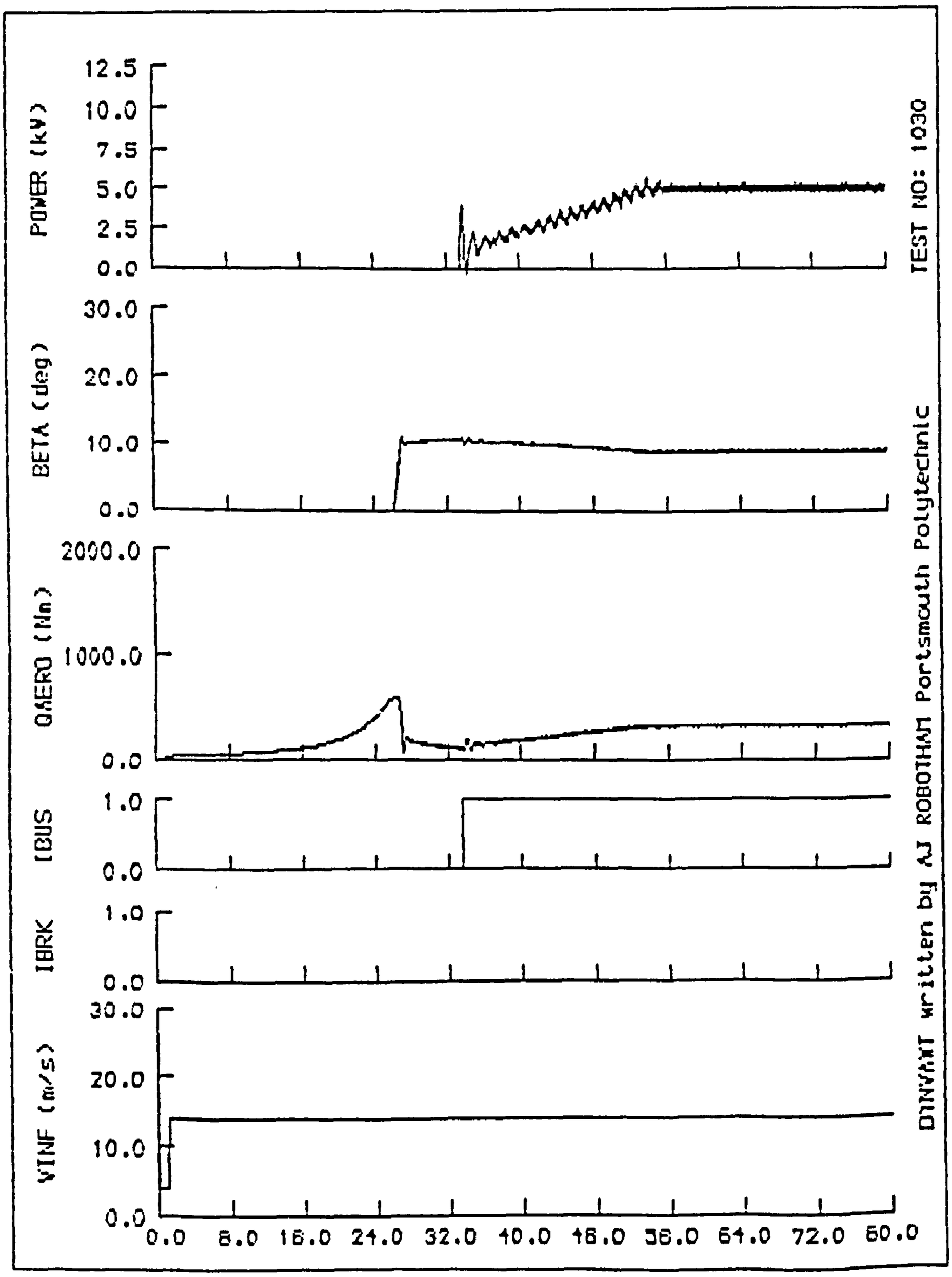

Figure 8.27: Simulation case study Nº 1030

Case Study Nº 1034

VAWT configuration: two-bladed, 5kW V-VAWT with 20% blade tip pitch control, open-loop power and compensated rotor speed control strategy.

VAWTTAY datafile: VAWT_5KW_20_2W

Operating mode: On-line (IMOD = 2)

Base windspeed: V_{WB} = 24.0 m/s

Ramp component: MAXR = 4.0 m/s
T_{1R} = 4.0 s
T_{2R} = 16.0 s

Results plot: Figure 8.28

Observations and Comments

In this particular case, the windspeed slowly rises over the simulation period. At t = 10.0 s the windspeed exceeds the upper windspeed limit and a shutdown procedure is invoked. Since the windspeed remains above the upper limit for the rest of the simulation period, no attempt is made to reconnect the V-VAWT generator to the network. When the rotational speed of rotor falls below the brake cut-in speed, the brake is activated and the rotor is rapidly brought to a standstill.

Unlike Case Study Nº 1029, the shutdown procedure is simulated correctly because constant windspeed performance data is used for the simulation.

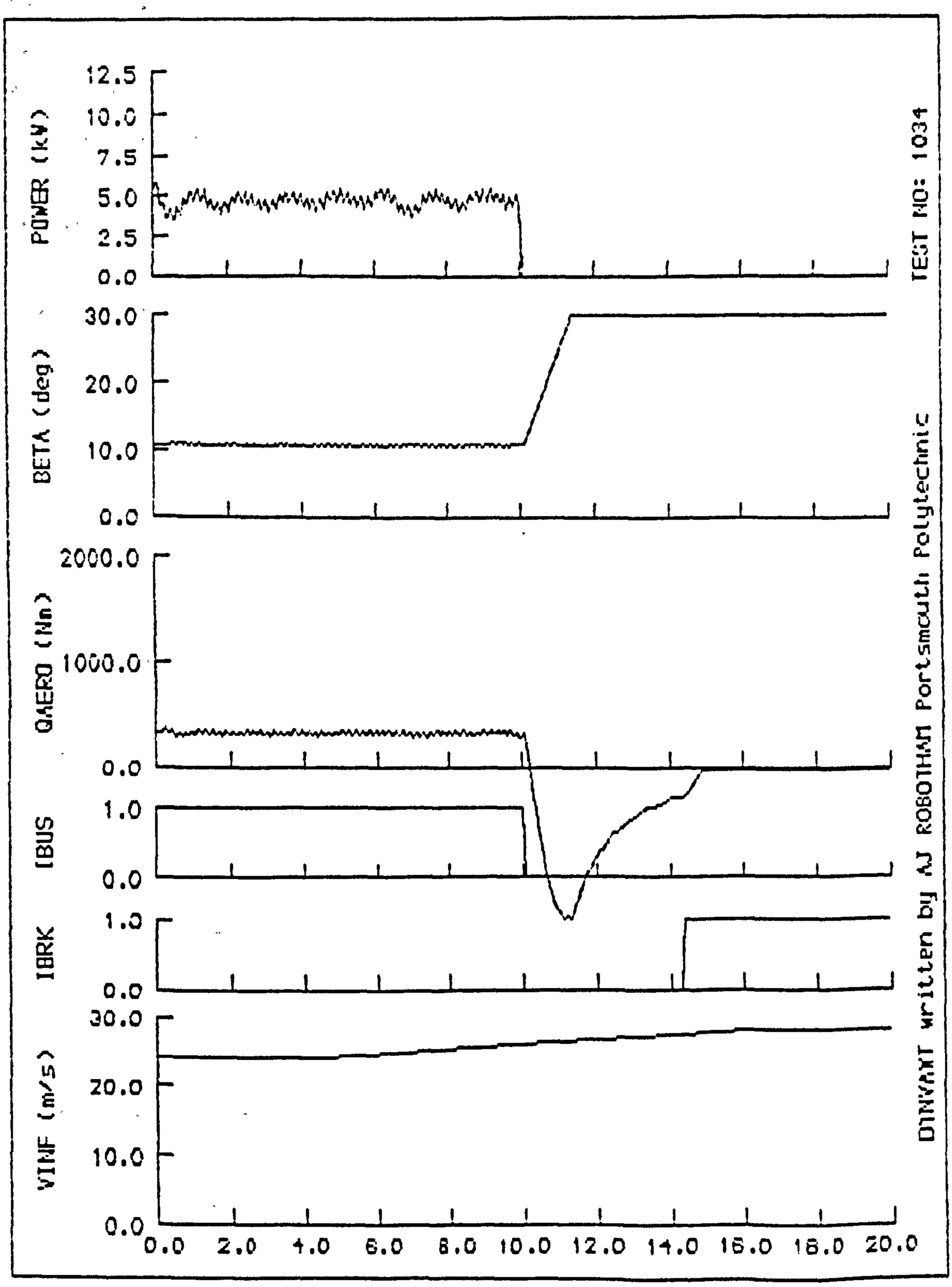

Figure 8.28: Simulation case study NΩ 1034

8.6: Conclusions from Dynamic Behaviour Case Studies

The dynamic behaviour of the 5kW V-VAWT generator system has been mathematically modelled and a control strategy developed. The computer program DYNVAWT embodies the state variable descriptions that characterise this wind turbine configuration and, using this program, the dynamic behaviour of the wind turbine generator and control system have been evaluated. In the case studies presented here, the characteristics of the two-bladed V-VAWT generator system that are fixed by design remained fixed; only the external inputs to the system were varied. The results, therefore, do not show how the response of the system can be controlled by design, but merely serve to demonstrate the typical responses that can be expected of this wind turbine generator and control system. The practicality and cost of linking such a small machine to the network would be of little commercial value, however, for the purposes of assessing the performance of tip pitch control it was a convenient scenario to consider.

The case study results demonstrate that, in theory, an actively controlled partial-span pitch control system would enable the V-VAWT generator to operate as an integral part of any electrical supply network with reasonable success. The computer results have yet to be verified by field tests, but the author is confident that, by variation of tip pitch, full control of the rotor can be achieved in all operating conditions. However, this overall impression needs to be qualified by consideration of the practicality of the system modelled.

The two-bladed 5kW V-VAWT generator system was modelled with a 20% blade tip control surface. This tip area was chosen, because it was the minimum tip size for which full aerodynamic braking during a high windspeed shutdown was

predicted. Smaller tip areas were considered, but with a pitch angle limit of $\beta = 30°$, full aerodynamic braking was not predicted using VAWTTAY. Predictions for larger pitch angles showed an *increase* in power output, but since the wind tunnel results of the model V-VAWT did not include any measurements for pitch angles of $\beta > 30°$, the author has no means of verifying any modifications of the prediction model required to correct the VAWTTAY results for the larger pitch angles. It was, therefore, considered necessary to restrict the maximum pitch angle to $\beta_{max} = 30°$, because the reliability of the aerodynamic performance results predicted using VAWTTAY for pitch angles upto this limit is known to be good.

Using a 20% tip area ensures that full aerodynamic braking is achieved during a high windspeed shutdown, but during on-line operation the power output of the V-VAWT generator system is highly sensitive to small pitch angle changes. The author is sceptical of whether the fineness of pitch angle position control simulated using DYNVAWT can be achieved in reality. In the computer program, the pitch angle set point is defined by the control system with an accuracy of ±0.05°. The 20% tip area has a power gain of -2.8 kW per degree of pitch i.e. -0.28 kW for each incremental pitch angle change that can be made using this pitch angle resolution. Small pitch angle changes are observed using this size of control surface, which if required in a real machine, would require a responsive tip pitch actuator mechanism to be designed to achieve this sensitivity of control.

The need for sensitive on-line control and full aerodynamic braking off-line enevitably requires a compromise solution to be considered. The author considers that the on-line control needs are the most important and that the specification for the control system should be derived

from the needs for this operating condition. The 5% tip area may prove to be dynamically suitable, though, high windspeed shutdown using this size tip would not be possible, unless a positive braking effect is actually observed for pitch angles $\beta > 30°$. Clearly, there is a need to determine the reductions in power output that might be achieved when operating at large pitch angles, and modifications made to VAWTTAY to allow performance predictions to be made of V-VAWTs with large pitch angle settings. The author is unwilling to speculate at this stage about the outcome of such investigations, and considers this to be the next step to take in developing a control system for the V-VAWT.

The condition matrix control strategy in essence works very well, however, the boundaries that define the various operating modes and control actions are "hard". That is to say, crossing to a different operating mode is instantaneous; the state of the system either invokes, say, an IMOD = 2 response, or not; the windspeed and rotational speed boundaries ensure that the control state is exactly defined at any one time. In most cases this approach is satisfactory, but when a boundary is crossed, abrupt changes in control action can occur. Case studies Nº 1025 and Nº 1026 are good examples of this occurrence. In both cases the cut-out windspeed in temporarily exceeded because of windspeed gusting. The base windspeed is only $V_{B} = 24$ m/s, yet because the windspeed temporarily rises above the cut-out windspeed, shutdown procedures are invoked. This is unsatisfactory because synchronisation with the network must be achieved once again before any useful power can be delivered by the system.

If the condition matrix system is to be adopted, then the windspeed and rotational speed boundaries should be "softened" to accommodate short term excursions outside a

"control area" without affecting the current control mode. This might be best achieved by introducing time delays on the more sensitive boundaries, or by defining the state of the system using long term average conditions of windspeed and rotational speed; instantaneous conditions would then be used to define the subsequent control action.

The open-loop power and compensated rotor speed control strategy gives highly satisfactory results. Not only is it suitable for ensuring good on-line power control, but allows start-up and synchronisation to be successfully completed. The values of the control gains have been determined by trial-and-error, so it is not possible to comment upon whether the quality of the system output can be further improved. As said before, this dynamic modelling approach only demonstrates the behaviour that is typical of this V-VAWT generator system. In most cases, the control system was able to maintain a stable connection between the generator system and the electricity supply network. Where this was not possible, shutdown and synchronisation procedures have been successfully invoked. However, this approach does not allow any assessment to be made of how good the stability of the response is. Classical control system analysis allows such assessment, but the time domain approach only enables the stability of the system to observed as either "stable" or "unstable".

In this particular wind turbine generator system, the generator connection to the network is seen to be the most flexible transmission element. Therefore the characteristics of the generator and the network connection crucially affect the behaviour of the system as a whole. One way of improving the stability of the system studied involves increasing the rating of the generator. The generator rating was 5 kVA, and although design characteristics were not changed, if this rating was increased, the

static power stability limit of the system would be similarly increased. The author notes that the generator rating of most commercial machines is often 25% larger than the rating of the wind turbine generator system itself. Excess generator capacity would allow larger fluctuations in rotor power to be tolerated before synchronisation with the network was lost.

Similarly; using a round rotor generator rather than a salient pole generator would increase the static power stability limit of the system. However, a generator that is connected to the network via long transmission cables will have a weaker link with the grid and therefore have a lower static power stability limit. These options have not been evaluated here but (i) the program DYNVAWT has the flexibility for such case studies to be evaluated.

An inherent quality of the V-VAWT design is the stiff nature of the mechanical drive train elements. Whilst the v-belt transmission allows some flexibility, it is the electrical connection to the network that is the most compliant transmission element. This characteristic is unlike any other wind turbine, where compliance is built into the mechanical transmission elements, and by comparison the electrical connection is considered stiff. The quality of the electrical output is improved in these systems because rotor torque fluctuations are dissipated by the flexibility and damping of the mechanical elements. Mechanical damping has not been simulated here. The author considers that attention should be directed to improving the compliance and damping properties of the mechanical elements of the V-VAWT drive train so that power output quality can be similarly improved.

The validity of the computer program DYNVAWT has yet to be verified, and to do this simulation results will have to

be compared to actual performance results. However, the author considers both the theoretical model of the V-VAWT generator system to be good, and its embodiment into the computer program DYNVAWT accurate. Consequently, the author considers that he has developed a useful and flexible tool for assessing the dynamic behaviour of V-VAWT generator systems. The control strategy and use of condition matrices has been demonstrated as a simple means of providing adaptive control. However, the modular programming style allows the control system to be easily enhanced or replaced in DYNVAWT. The flexibility of the program allows countless case study scenarios to be set-up and evaluated, and it is the intention of the author to use the program to assess possible alternative drive train and control system designs, and investigate how the quality of the power output may be improved. To date the program DYNVAWT has been used merely to demonstrate that partial-span pitch control is a viable method for actively controlling the dynamic behaviour of a network linked V-VAWT generator system.

Chapter Nine: Project Summary, Final Conclusions and Recommendations for Future Work

9.1: Summary of Work Completed and Observations Made

The project reported here has required the author to undertake many theoretical and laboratory based studies. The author has read widely around the subjects of concern, but only where specific observations or conclusions have been drawn from other authors have they been referenced here. During the period of study, the author attended a number of wind energy conferences and seminars, and prepared in collaboration with Messrs Taylor, Sharpe and Boyle technical papers that were presented at some of these events; three papers can be found in Appendix 3. A number of computer programs have been developed by the author to assist in the numerous data analysis tasks that have been completed. These programs have been written for use on a variety of machines, and all embody mathematical models developed solely by the author as reported here. Only the performance prediction model VAWTTAY has its origins elsewhere, the author's contribution being to extend the scope of its functions and shorten its execution time. At all times the author was aware of the need to develop practical solutions and design aids for the development of the V-VAWT concept.

The project brief required the author to investigate control methods for the V-type vertical axis wind turbine. Initial theoretical and experimental work carried out by Taylor and Sharpe had established the V-VAWT as a promising wind turbine configuration with many features that were considered would make it a cost-effective machine. The author reviewed this work and that reported by many other wind energy investigators. The literature search provided valuable background information and data,

allowing the necessary requirements of a suitable control method to be defined. It was concluded from this preliminary study that the control needs of electricity generating applications were the most demanding. For such applications, the V-VAWT requires good speed and power regulation over a wide range of operating windspeeds. When driving synchronous generators, start-up and synchronisation, on-line speed and power control, and high windspeed shutdown are modes of operation that must be considered when selecting suitable control methods to investigate.

The review of control methods considered many control alternatives, but it was partial-span pitch control that the author considered to be the most promising option for V-VAWT applications. The author was unaware of any research or development work on VAWTs that had systematically investigated this control option. Whilst some experimental and theoretical work on full-span pitch control had been carried out on H-VAWTs, no previous study had been made of the effectiveness of partial-span pitch as a control method for the H-VAWTs or, more specifically, for the V-VAWT concept. It was, therefore, necessary to systematically investigate this control option for V-VAWT applications; experimental and theoretical studies were planned and subsequently executed by the author.

The experimental work required a small wind tunnel sized model V-VAWT to be designed and manufactured. To assist with the structural design of this model, a computer program was developed to analyse the steady state loads acting on the wind turbine blade when operating at various rotational speeds. This program embodies a simple beam bending theory that accounts for centrifugal and gravitational loads; aerodynamic loads were ignored. Since the model was to be designed to operate in a laboratory

environment, a strict code of design was imposed upon the author. This code required the model to be designed to survive rotational speeds upto 2500 rpm, at which speed centrifugal loads are significantly larger than gravitational loads which, for simplicity, can be excluded from the analysis. Using this computer analysis tool, the author was able to derive a satisfactory blade design for the model V-VAWT.

To test the effect of partial-span pitch control on the performance of the model V-VAWT, each blade was fitted with three moveable tip portions. These three separate tip portions allowed a variety of tip area and pitch angle combinations to be evaluated. The model V-VAWT was tested in a wind tunnel at Queen Mary College, London using equipment developed by Sharpe and used for previous tests on model V-VAWTs. The performance of the wind turbine was measured using the acceleration technique, a simple and quick method for determining the complete $C_{p\omega}$-λ characteristic of a wind turbine. The blade tips could not be moved during testing, so the measurement procedure was repeated with the tips preset with known pitch angle offsets. In this way, the author was able to derive results for some 40 tip pitch angle and tip area combinations.

The experimental measurements were analysed using numerical methods; these methods were considered in depth by the author to ensure the accuracy and quality of the results were good. Measurements of bearing friction and cable drag were made separately, and corrections applied to all results; the final results were effectively measurements of the aerodynamic power of the rotor. The results of these wind tunnel tests were published in the conference papers presented in Appendix 3.

The limited range of rotational speeds over which the cable drag measurements had been made required the corrections for this effect at high rotational speeds to be interpolated from measurements made at low rotational speeds. This was considered unsatisfactory, so a mathematical model of cable drag was developed by the author. Good correlation of the low rotational speed cable drag measurements and predicted results enabled the author to use the prediction model with confidence at all rotational speeds. Predicted cable drag results were used to modify the cable drag corrections previously used, so the wind tunnel results presented here are considered to be more representative of the true aerodynamic performance of the model V-VAWT.

The results clearly showed that the aerodynamic power of the model V-VAWT can be regulated using partial span tip control. The results for 5%, 10% and 15% tip areas all showed that the power of the model wind turbine could be completely "killed" using nose-in pitch angle offsets, and that small nose-out pitch angle offsets actually *increased* the power output of the rotor. The high starting torque that is characteristic of this wind turbine configuration was observed for all but the largest tip pitch angle offsets. Although the wind tunnel measurements were made at low Reynolds Number, the results were considered encouraging and it was concluded that partial-span pitch control would be suitable for larger V-VAWT applications.

The computer program VAWTTAY allows the aerodynamic performance of the V-VAWT to be predicted and is based upon Sharpe's extended multiple streamtube theory. Original versions of this program were microcomputer based and had been validated by the Sharpe's earlier theoretical experimental work. The author, however, spent much time and effort translating the BASIC version of the program into a

FORTRAN version for use on minicomputers. The new version of VAWTTAY allows a full aerodynamic appraisal of a V-VAWT configuration to be completed in significantly shorter times than previously achieved. The author has not made any significant changes to the prediction theory that the program embodies, but has derived a thorough understanding of its principles in the meantime.

To test the validity of the FORTRAN version of VAWTTAY, prediction results were compared to those obtained beforehand using the BASIC version. Satisfied that the program was accurate and correct, the author used the program to predict the performance of the model V-VAWT and the effect of partial-span pitch control. While the characteristic shape of each C_P-λ curve was predicted fairly well, the numerical correlation of the results was not good. The difference between measured and predicted results was considered due to the lack of accurate aerofoil data to adequately described the characteristics of the NACA0025 aerofoil used to construct the blades of the model V-VAWT. If the predicted results were to show better correlation, then suitable NACA0025 data was required for use with VAWTTAY. Despite searching for such data, none could be found for the low Reynolds Number required which could be considered reliable or suitable for use with VAWTTAY. The author, therefore, decided to determine the aerofoil characteristics of the model blades by experimentation.

A NACA0025 aerofoil section was constructed to the same dimensions as the model V-VAWT blades, and static pressure tappings were made around its surface. The aerofoil was tested in a closed-return wind tunnel at Queen Mary College, London. Pressure measurements were made for angles of attack upto 20° in increments of 1° over a range of low Reynolds Number, and for angles of attack upto to 180° in increments of 5° for one Reynolds Number.

The static pressure measurements were read directly from a water manometer bank, and entered into a data capture program written and developed by the author on a microcomputer. Once the measurements were verified, they were stored on floppy diskette. Similar tests for profile drag were carried out, but verification of the results using force balance techniques could not be completed in the time available.

To analyse the pressure measurements, the author developed two computer programs for calculating normal and thrust force coefficients. The fundamentals of each program are similar, requiring a pressure envelope around the aerofoil to be calculated by interpolation of the twenty static pressure measurements. The generation of the pressure envelope allows the pressure distribution around the aerofoil to be integrated with respect to the chord and cross-chord axes, yielding the normal and thrust force coefficients respectively. Using these computer programs, the aerodynamic characteristics of the aerofoil was completely determined from the measurements made. The profile drag measurements were found to be inconsistent and were not considered reliable, but the author found suitable low Reynolds Number values of profile drag coefficient from another source, and it is these values that have been used here to modify the measured thrust coefficient results.

The pre-stall aerodynamic characteristics of the NACA0025 section were developed into a dataset suitable for use with VAWTTAY by smoothing the force coefficient versus angle of attack curves, and by extending the Reynolds Number range using extrapolation to Re = 400,000. The post-stall aerodynamic characteristics were developed into a single dataset that is Reynolds Number independent.

The author considers the NACA0025 dataset to be good, though the "bubble" effect observed at low angles of attack has been ignored, and immediately following stall, the thrust coefficient takes large negative values not observed in other four-digit NACA aerofoils.

Using the author's NACA0025 dataset, the aerodynamic performance of the model V-VAWT was predicted using VAWTTAY. The results using this data show much better correlation between predicted and measured rotor power outputs at large tip speed ratios, but the predictions clearly under-estimate the power developed by the rotor at low tip speed ratios. Despite the large negative thrust force coefficients observed immediately following stall, the author considers the poor correlation of results at low tip speed ratios is due to a limitation of the dynamic stall model used in VAWTTAY. The dynamic stall characteristics of the NACA0025 section are unknown, therefore it is not possible to determine whether the Gormont dynamic stall model is accurate for this section.

Although it has not been possible to accurately predict the performance of the model V-VAWT using a single aerofoil dataset, the author considers VAWTTAY to be an accurate and valid tool for determining the behaviour of larger V-VAWT configurations with partial-span pitch control.

The computer program has been used to determine the performance of the 5kW V-VAWT with 5%, 10%, 15% and 20% tip areas for various pitch angle offsets. One notable feature of the predictions for this machine which had not been previously observed, was that for pitch angles in excess of $\beta = 30°$, the power output of the rotor has been predicted to *increase*. The maximum pitch angle offset of the tips on the model V-VAWT was limited to $\beta = 30°$,

therefore, it was not possible to confirm the validity of these predicted results. The author considers that the assumptions of the prediction model VAWTTAY are breaking down at these large pitch angles, and that such results are invalid. Therefore, it was necessary to limit the maximum tip pitch angle of the 5kW V-VAWT to β_{max} = 30° if the rotor power was to be continually reduced as the tip pitch angle was increased.

The electricity generation application of the 5kW V-VAWT demands power and speed control during start-up and synchronisation, on-line operation, and high windspeed shutdown. While a 5% tip area would be suitable for regulating the power output of the rotor during on-line operation, the VAWTTAY predictions showed that a 20% tip area was required if full aerodynamic braking was to be achieved during a high windspeed shutdown. Using such a large tip area would ensure that the rotor could be brought to a standstill by aerodynamic means alone, but for on-line power and speed regulation, the control of the rotor would be highly sensitive to small pitch angle changes. Inevitably a compromise between the needs of full aerodynamic braking and sensitivity of on-line control must be made. If full aerodynamic braking cannot be achieved, an additional rotor braking device would be required to ensure the rotor can be brought to a standstill during a high windspeed shutdown.

The use of the V-VAWT for electricity generation is most demanding, especially since the energy source of a wind turbine cannot be regulated. Unlike other electrical generator prime movers, wind turbine generators have an energy source that is continually varying. The wind turbine control system must be capable of reacting to the variations of windspeed typically encountered by a free-air machine, while striving to maintain the stability of

the connection between the electricity network and the generator itself. To assess the success with which this can be achieved with a V-VAWT generator system using partial-span pitch control requires the dynamic behaviour of the wind turbine system to modelled and evaluated.

The computer program DYNVAWT was written and developed by the author and embodies a state variable description of a V-VAWT generator system. This program allows time domain studies of the dynamic behaviour of such a system to be simulated, enabling the characteristic behaviour of the system to be observed. The program allows the characteristics of the component parts of the system to be described, and the external forcing functions varied as required. In this way, start-up and synchronisation, on-line operation, and high windspeed shutdown modes of operation can all be simulated. The control strategy developed for simulation purposes uses a condition matrix approach, in which the control strategy is adapted to the current operating state of the wind turbine system. The only devices that can directly controlled are the tip pitch actuator mechanism, the rotor brake, and the electrical generator/network contactor. An open-loop power and compensated rotor speed control system has been built into the control system to ensure that a constant power and constant frequency power supply is maintained to the network.

The computer program DYNVAWT was used for many case studies based upon the 5kW V-VAWT generator system, but none of the results have been validated by experimental observations. A variety of changes to the external inputs to the V-VAWT generator system were studied and, in general, the partial-span pitch control was able to respond in a manner that maintained the stability of the network connection. Where this was not the case, shutdown

or re-synchronisation procedures were invoked. The principles of the condition matrix control strategy were thoroughly tested and proved to be a successful control approach. The limitations of the approach were identified, but the computer program has been developed on a modular basis, so modification or replacement of the control strategy is simply done.

The case studies evaluated using DYNVAWT were based upon the present 5kW V-VAWT design. Only the external forcing functions were varied in the case studies presented here; no attempt has been made to optimise the behaviour of the system by changing the design of the system itself. Using a 20% tip area for control, start-up and synchronisation, on-line operation, and high windspeed shutdown were all successfully simulated. The mechanical components of the 5kW V-VAWT generator system are torsionally stiff, yet in each case, rotor power and speed was regulated using tip pitch. It is clear from these studies that a large tip area requires fine tip pitch positional control to ensure a good quality and stable power supply is maintained, but future system designs must include more compliance and damping in the mechanical drive train elements to assist in alleviating the large torque variations that must be accommodated by the system.

The author considers that a valuable analysis tool has been developed for future evaluation work of V-VAWT generator systems. The flexibility of the programming approach will allow the design of the mechanical components of such systems to be modified to ensure the behaviour of the system as a whole is stable, reliable and provides a good quality power output to the electricity network.

It can be concluded from the work reported here that:

(a) partial-span pitch control is highly suitable for controlling the on-line operation of the V-type wind turbine in electricity generation applications. The size of the tip area crucially affects the sensitivity of the control that can be achieved, and it is unlikely that full aerodynamic braking can be achieved during high windspeed shutdowns if small tip areas are used. A compromise must be struck between these two needs.

(b) the aerodynamic performance prediction program VAWTTAY is suitable for predicting the steady state behaviour of the V-VAWT using blade geometries with small partial-span pitch angle offsets. The accuracy of the predictions relies upon the accuracy of the static aerofoil dataset used for the analysis, and the validity of the dynamic stall model that is embodied in the program. The theory appears to break down where the configuration includes large pitch angle offsets.

(c) the dynamic behaviour of an actively controlled V-VAWT generator system can be simulated using the author's own computer program, DYNVAWT. The time domain simulations provide valuable information about the effectiveness of the V-VAWT generator system and its control system in maintaining a stable and good quality power supply to the electricity supply network. DYNVAWT enables the dynamic behaviour of system designs to be be evaluated at an early stage of their development. Suitable modifications or alternatives can be tried before the design is finalised.

9.2: Recommendations for Future Work

The author recommends that the following additional work should be undertaken as a result of the observations and findings of this work:

(a) field trials of 5kW V-VAWT to be conducted using partial-span pitch control to determine validity of simulation program DYNVAWT.

(b) performance evaluations of V-VAWT configurations with large tip pitch offsets ($\beta > 30°$) required to validate the modifications that must be made to VAWTTAY for these large pitch angle predictions.

(c) further investigation of NACA0025 aerofoil section required to confirm author's own characteristic aerodynamic data, and observe its dynamic stall behaviour at low Reynolds Number.

(d) design studies to be made of large V-VAWT configurations with special attention being paid to increasing the compliance and damping attributes of the mechanical elements of the drive train, so reducing the torque variations that must be accommodated by the electrical generator.

(e) development of adaptive control strategy, based upon condition matrix approach, with "softer" boundaries defined between control action changes.

9.3: Closing Remarks

The work reported here has stretched over many years, but the author has never doubted the validity of the approach taken, nor the need that each task be undertaken, nor even how the results of each compliment the conclusions of the whole. The experimental and analysis techniques adopted are not necessarily original or new, however, the author

has always considered that simplicity of approach is more worthy where the problems being considered and the solutions methods being developed are in fact new to the author himself. By its very nature, the V-VAWT is a wind turbine configuration of simple construction and design. The control methods used for this particular machine need to be similarly simple if this machine is to be cost effective in electricity generation applications. The work reported here shows, in theory, that partial-span pitch control satisfies all the control needs of this V-VAWT application. Further work is clearly required to verify some of the findings reported here, before larger V-VAWT configurations can be built using this control technique. On this basis, and using the Department of Energy's terminology, the author considers that partial-span pitch control should be classified as a "promising, but uncertain" V-VAWT control option.

References

1 DEPARTMENT OF ENERGY: "Harnessing the wind: wind energy technology". Dept. of Energy pamphlet, U.K., 1987.

2 BRITISH WIND ENERGY ASSOCIATION: "Wind power for the U.K.". British Wind Energy Association position paper, U.K., January 1987.

3 "Tvind celebrate tenth anniversary". Windirections, Vol VIII, Nº 1, pp 11-13, Summer 1988.

4 "U.K. wind farm programme announced". Windirections, Vol VII, Nº 4, pp 22-23, Spring 1988.

5 "Wind turbine technology development". Windirections, Vol VII, Nº 4, p 28, Spring 1988.

6 "U.S. wind energy after seven years". Windirections, Vol VIII, Nº 1, pp 19-21, Summer 1988.

7 LYNETTE, R.: "Status of the U.S. wind power industry". Proc. 10th British Wind Energy Association Conference, London, U.K., March 1988.

8 DEPARTMENT OF ENERGY: "Renewable energy in the UK: the way forward". Energy Paper 55, HMSO, U.K., June 1988.

9 SHARPE, D.J. and TAYLOR, D.A.: "Preliminary investigations into an innovative vertical axis wind turbine". Proc. World Solar Energy Congress, Perth, Australia, 1983.

10 GOLDING, E.W.: "The generation of electricity by wind power". E. & F.N. Spon, London, U.K., 1955.

11 NITTEBERG, J., de Boer, A.A. and SIMPSON, P.: "Estimation of cost of energy from wind energy conversion systems". IEA Expert Group Report, Paris, France, 1983.

12 GUO, A. and PALUTIKOF, J.P.: "A comparison of two simple mesoscale models to predict windspeeds in the lower boundary layer". Proc. 10th British Wind Energy Association Conference, London, U.K., March 1988.

13 LYSEN, E.H.: "Introduction to wind energy". CWD 82-1, Consultancy Services Wind Energy Developing Countries, Amersfoort, Netherlands, May 1983.

14 SWIFT-HOOK, D.T: "Describing wind data". Wind Engineering, Vol. 3, p167, 1979.

15 MUSGROVE, P.J.: "The economics of existing wind turbines in the size range 10 to 100 metres diameter". Proc. 5th British Wind Energy Association Conference, Reading, U.K., March 1983.

16 PARK, J.: "Simplified wind power systems for experimenters". Helion, U.S.A., 1976.

17 LJUNGSTROM, O.: "Advanced vertical axis rotor concepts". Proc. Advanced Wind Energy Systems Workshop, Stockholm, Sweden, 1974.

18 SHARPE, D.J.: "Refinements and developments of the multiple streamtube theory for the aerodynamic performance of vertical axis wind turbines". Proc. 6th British Wind Energy Association Conference, Reading, U.K., March 1984.

19 SHARPE, D.J. and TAYLOR, D.A.: "The aerodynamic performance of the vee type vertical axis wind turbine". Proc. 7th British Wind Energy Association Conference, Oxford, U.K., March 1985.

20 SHARPE, D.J.: "Wind tunnel data for Darrieus rotor". Queen Mary College, University of London, London, U.K., unpublished.

21 TAYLOR, D.A.: "ATG wind turbine field test facility". Appropriate Technology Group, Open University, Milton Keynes, U.K., May 1983.

22 SHARPE, D.J., TAYLOR, D.A. and BOYLE, G.A.: "Developments with the "V" type vertical axis wind turbine". Proc. 9th British Wind Energy Association Conference, Edinburgh, U.K., March 1987.

23 SHARPE, D.J.: "Theoretical and experimental study of the Darrieus vertical axis wind turbine". Kingston Polytechnic, Kingston, U.K., 1977.

24 READ, S. and SHARPE, D.J.: "An extended multiple streamtube for vertical axis wind turbines". Proc. 2nd British Wind Energy Association Workshop, Cranfield, U.K., April 1980.

25 READ, S. and SHARPE, D.J.: "A critical analysis of the extended multiple streamtube for the aerodynamics of a vertical axis wind turbine". Proc. Wind and Solar Energy Technology Conference, Kansas City, U.S.A., 1982.

26 SHELDAHL, R.E. and KLIMAS, P.C.: "Aerodynamic characteristics of seven symmetrical airfoil sections through 180-degree angle of attack for use in aerodynamic

analysis of vertical axis wind turbines". SAND80-2114, Sandia National Laboratories, Albuquerque, New Mexico, U.S.A., 1980.

27 KLIMAS, P.C.: "Tailored airfoils for vertical axis wind turbines". SAND84-1062, Sandia National Laboratories, Albuquerque, New Mexico, U.S.A., 1984.

28 COOPER, B.J and LAW, H.: "A review of control system options for wecs". Proc. 4th International Conference on Energy Options, IEE, London, U.K., 1984.

29 BOSSANYI, E.A. and ANDERSON, M.B.: "A comparison of techniques for evaluating the frequency of wind turbine shut-downs". Proc 6th British Wind Energy Association Conference, Reading, U.K., March 1984.

30 METS, V. and HERMANSSON, O.: "Status and experience with the 2MW WTS75 at Nasudden, Gotland". Proc. IEE Vol. 130, Pt. A, Nº 9, 1983.

31 FRERIS, L.L.: "A plain man's guide to electrical aspects of WECs". Proc 7th British Wind Energy Association Conference, Oxford, U.K., March 1984.

32 ROBOTHAM, A.J.: "A review of wind turbine control methods". ATG Working Paper, The Open University, U.K., May 1985.

33 KETLEY, G.R. and QUARTON, D.C.: "Aerodynamic aspects of HAWTG design": Proc. of BWEA-DEn Workshop on Aerodynamics and Control of Wind Turbines, ETSU-N-1/86, Harwell, U.K., February 1986.

34 JACOBS, J.H.: "Wind driven unit". U.S. Patent 1930390, U.S.A., 1933.

35 SPIERINGS, P.A.M. and CHENEY, M.C.: "Self-regulating composite bearingless wind turbine". United Technologies Research Report R76-912185-2, U.S.A., June 1976.

36 BERGEY, K.H.: "Development of high-performance, high-reliablity windpower generators". Bergey Windpower Cº Inc., Oklahoma, U.S.A.

37 "FDO/Holec/Fokker produce new wec design". Windirections, Vol III, Nº 4, pp 1-2, April 1984.

38 KLIMAS, P.C.: "Aerodynamics and performance testing of the VAWT". Sandia National Laboratories, Albuquerque, New Mexico, U.S.A.

39 STACEY, G. and MUSGROVE, P.J.: "The effect of fixed pitch offset on a high solidity vertical axis windmill". Proc. 3rd British Wind Energy Association Workshop, Cranfield, U.K., 1981.

40 GRYLLS, W., DALE, B. and SARRE, P.E.: "A theoretical and experimental investigation into the variable pitch vertical axis wind turbine". Proc. 2nd International Symposium on Wind Energy Systems, Amsterdam, Netherlands, October 1978.

41 SHARPE, D.J.: "A survey of aerodynamic control methods for VAWTGs". Proc. of BWEA-DEn Workshop on Aerodynamics and Control of Wind Turbines, ETSU-N-1/86, Harwell, U.K., February 1986.

42 TEMPLIN, R.J. and RANGI, R.S.: "Vertical-axis wind turbine development in Canada". IEE Proc. Vol. 130, Pt. A, Nº 9, December 1983.

43 MUSGROVE, P.J.: "The variable geometry vertical axis windmill". Proc. 1st International Symposium on Wind Energy Systems, Cambridge, U.K., September 1976.

44 STACEY, G.: "Experimental and theoretical developments of the variable geometry vertical axis wind turbine". University of Reading PhD Thesis, U.K., 1983.

45 MAYS, I.D., MUSGROVE, P.J., MORGAN, C.A. and HANCOCK, G.: "The evolution of the straight bladed vertical axis wind turbine". Proc. 10th British Wind Energy Association Conference, London, U.K., March 1988.

46 BANNISTER, W.S.: "An investigation into the use of boundary layer control as a method of overspeed prevention for vertical axis wind turbines". Proc. 7th British Wind Energy Association Conference, Oxford, U.K., March 1985.

47 KLIMAS, P.C. and SLADKY, J.F.: "Pumped spoiling VAWT control" Sandia National Laboratories, Albuquerque, New Mexico, U.S.A.

48 McCORMICK, B.W: "Aerodynamics, aeronautics, and flight mechanics". John Wiley & Sons, New York, U.S.A.,

49 ABBOTT, I.H. and Von DOENHOFF, A.E.: "Theory of wing sections". Dover Publications Inc., New York, U.S.A., 1958.

50 WENTZ, W.H., SYNDER, M.H. and CALHOUN, J.T.: "Feasibility study of aileron and spoiler control systems

for large horizontal axis wind turbines". Wichita State University, Wichita, Kansas, U.S.A., May 1980.

51 MILLER, D.R. and SIROCKY, P.J.: "Summary of NASA/DOE aileron control development program for wind turbines". Proc. Windpower 85, San Francisco, U.S.A., August 1985.

52 WILMSHURST, S.M.B.: "The use of spoilers to control a horizontal axis wind turbine". Proc. 8th British Wind Energy Association Conference, Cambridge, U.K., March 1986.

53 PEDERSEN, T.F.: "Air brakes on stall regulated windmills". Proc. 6th British Wind Energy Association Conference, Reading, U.K., March 1985.

54 TEMPLIN, R.J and SOUTH, P.: "Some design aspects of high-speed vertical axis wind turbines". Proc. 1st International Symposium on Wind Energy Systems, Cambridge, U.K., September 1976.

55 ROBOTHAM, A.J: "The design of a V-VAWT wind tunnel model with pitching tips". ATG Working Paper, The Open University, U.K., 1985.

56 HOERNER, S.F.: "Fluid-dynamic lift". Published by author, Brick Town, New Jersey, U.S.A.

57 ROBOTHAM, A.J., SHARPE, D.J., TAYLOR, D.A. and BOYLE, G.A.: "Further developments in the Taylor 'V' type VAWT concept". Proc. Intersol 85 World Solar Energy Congress, Montreal, Canada, June 1985.

58 BOYLE, G.A., ROBOTHAM, A.J., SHARPE, D.J. and TAYLOR, D.A.: "The Taylor 'V' type vertical axis wind turbine: current status". Proc. Windpower 85, San Francisco, U.S.A., August 1985.

59 ROBOTHAM, A.J. and SHARPE, D.J.: "The aerodynamic control of the 'V' type vertical axis wind turbine by blade tip control". Proc. 8th British Wind Energy Association Conference, Cambridge, U.K., March 1986.

60 SARRE, P.E.: "Wind energy project". Dept. of Chemical Engineering, University of Exeter, U.K., WEP 1, May 1977.

61 JACOBS, E.N. and SHERMAN, A.: "Aerofoil section characteristics as affected by variations of Reynolds Number". NACA Report Nº 586, U.S.A., 1937.

62 BULLIVANT, W.K.: "Tests of the NACA 0025 and 0035 airfoils in the full-scale wind tunnel". NACA Report Nº 708., U.S.A.

63 PANKHURST, R.C. and HOLDER, D.W.:" Wind tunnel technique: an account of experimental methods in low- and high-speed wind tunnels". Pitman, London, U.K., 1952.

64 JAMES, K.R. and RIHA, W.: "Lecture notes on numerical methods". Department of Computer Studies, University of Leeds, Leeds, U.K.

65 PETTY, D.: "Drag estimation by the method of pitot traverse". Laboratory notes, Department of Aeronautical Engineering, Queen Mary College, London, U.K.

66 POPE, A.: "The forces and pressures over an NACA0015 airfoil through 180 degrees angle of attack". Aero Digest, February 1947.

67 HOERNER, S.F. "Fluid-dynamic drag". Published by author, Brick Town, New Jersey, U.S.A., 1965.

68 JACOBS, E.N., WARD and PINKERTON: "The characteristics of 78 related aerofoil sections from tests in the variable density wind tunnel". NACA Report Nº 460, U.S.A., 1936.

69 WILLMER, A.C.: "Low Reynolds Number tests on the NACA0015 section". Proc. 1st British Wind Energy Association Conference, Cranfield, U.K., April 1979.

70 McCROSKEY, W.J.: "The phenomenon of dynamic stall". NASA Technical Memo 81264, U.S.A., March 1981.

71 GORMONT, R.E.: "A mathematical model of unsteady aerodynamics and radial flow for application to helicopter rotors". USAAMRDL Technical report 72-67, U.S.A., 1973.

72 HALES, R.L., ORAM, C.E. and GARSIDE, A.J.: "Unsteady aerodynamics of vertical axis wind turbines". Proc 7th British Wind Energy Conference, Oxford, U.K., March 1985.

73 DUBE, B. and PEROCHEAU, A.: "Mathematical models used for digital simulation of wind turbine generators". Internal report Institut de recherche d'Hydro-Québec, Varennes, Canada, December 1983.

74 SEIDEL, R.C., GOLD, H. and WNESEL, L.M.: "Power-train analysis for the DOE/NASA 100kW wind turbine generator". DOE/NASA/1028-78/19, U.S.A., October 1978.

75 KRAUSE, P.C. and MAN, D.T: "Transient behaviour of a class of wind turbine generators during electrical disturbances". IEEE Transactions Power Apparatus and Systems, Vol PAS 100, pp 2204-2210, 1981.

76 ANDERSON, P.M. and BOSE, A.: "Stability simulation of wind turbine systems". IEEE Transactions on Power Appparatus and Systems, Vol PAS-102, Nº 12, pp 3791-3795, December 1983.

77 ELGERD, O.I.: "Basic electric power engineering". Addison-Wesley, London, U.K., 1977.

78 HUGHES, E.: "Electrical technlogy". Longmans, London, U.K.

79 CRARY, S.B.: "Power system stability Volume 1: steady state stability". Wiley, New York, U.S.A., 1945.

80 WEEDY, B.M.: "Electric power systems". John Wiley & Sons, New York, U.S.A., 1979.

81 KOS, J.M.: "On-line control of a large horizontal axis wind energy conversion system and its performance in a turbulent wind environment". Proc 13th Intersociety Energy Conversion Engineering Conference, pp 2064-2073, August, 1978.

82 CRARY, S.B.: "Power system stability Volume 2: transient state stability". Wiley, New York, U.S.A., 1947.

83 SCHWARZENBACH, J. and GILL, K.F.: "System modelling and control". Edward Arnold, London, U.K., 1978.

84 GARRAD, A.D.: "Wind turbine transmission systems". Proc 3rd British Wind Energy Conference, Cranfield, U.K., March 1981.

85 LIEBST, B.S.: "A pitch control system for the KaMeWa wind turbine". Transactions of the ASME, Journal of Dynamic Systems, Measurement and Control, Vol 107, pp 47-52, March 1985.

86 NAGRATH, I.J. and GOPAL, M.: "Control system engineering". John Wiley & Sons, New York, U.S.A., 1982.

87 SUNDAR, R.M. and SULLIVAN, J.P.: "Performance of wind turbines in a turbulent atmosphere". Solar Energy, Vol 31, Nº 6, pp 567-575, 1983.

Appendix One: Structural Analysis of Model V-VAWT

A1.1: Glossary of Symbols and Subscripts

Symbols

m	Total mass of blade (kg)
L	Total length of blade (m)
a	Spanwise distance of cable attachment point from blade root (m)
ω	Angular velocity of rotor (rad/s)
w	Mass of blade per unit length (kg/m)
r	Radial co-ordinate (m)
z	Spanwise co-ordinate (m)
θ	Angle of blade inclination to rotation axis (°)
g	Gravitational acceleration (m/s^2)
F	Shear force (N)
M	Bending moment (Nm)
P	Axial force (N)
R	Shear force reaction (N)
M	Bending moment (N)
P	Axial force (N)
Φ	Step function
v	Flapwise displacement
E	Young's modulus (N/m^2)
I	Second moment of area(m^4)
σ	Stress (N/m^2)
y	Maximum thickness of material from neutral axis (m)
A	Cross-sectional area (m^2)
b	width of spar (m)
d	height of spar (m)
t	thickness of spar (m)
D_o	Outer diameter of spar (m)
D_i	Inner diameter of spar (m)
ρ	density of material (kg/m^3)

Subscripts

A	Root attachment
B	Cable attachment
W	Skin section
S	Spar section
F	Blade section
C	Compressive
T	Tensile
Z	Spanwise direction
V	Flapwise direction
c	Centrifugal component
g	Gravitational component

A1.2: Derivation of General Equations for Shear Force, Bending Moment, Axial Force and Flapwise Displacement

The analysis of the V-VAWT blade developed here is only suitable for a straight, constant chord blade that attached to the rotating shaft at its root and by a cable near to the blade tip. The following assumptions are made:

(a) Blade considered to act like a beam
(b) Mass of blade is evenly distributed along its span
(c) Blade root either simply supported or built-in
(d) Cable attachment is a simple support
(e) Cable acts perpendicular to plane of blade
(f) Aerodynamic forces ignored

Figure A1.1 is a schematic diagram of the V-VAWT blade in its simplest form. If the total mass of the blade is m, and the total length of the blade is L, then the mass per unit length w is given by:

$$w = \frac{m}{L} \qquad (A1.1)$$

Consider a small element of the blade at a spanwise co-ordinate z of length dz. If the blade is inclined at an angle θ to the vertical, the radial co-ordinate of the element r is given by:

$$r = z\sin\theta \qquad (A1.2)$$

The elemental mass dm is given by:

$$dm = wdz \qquad (A1.3)$$

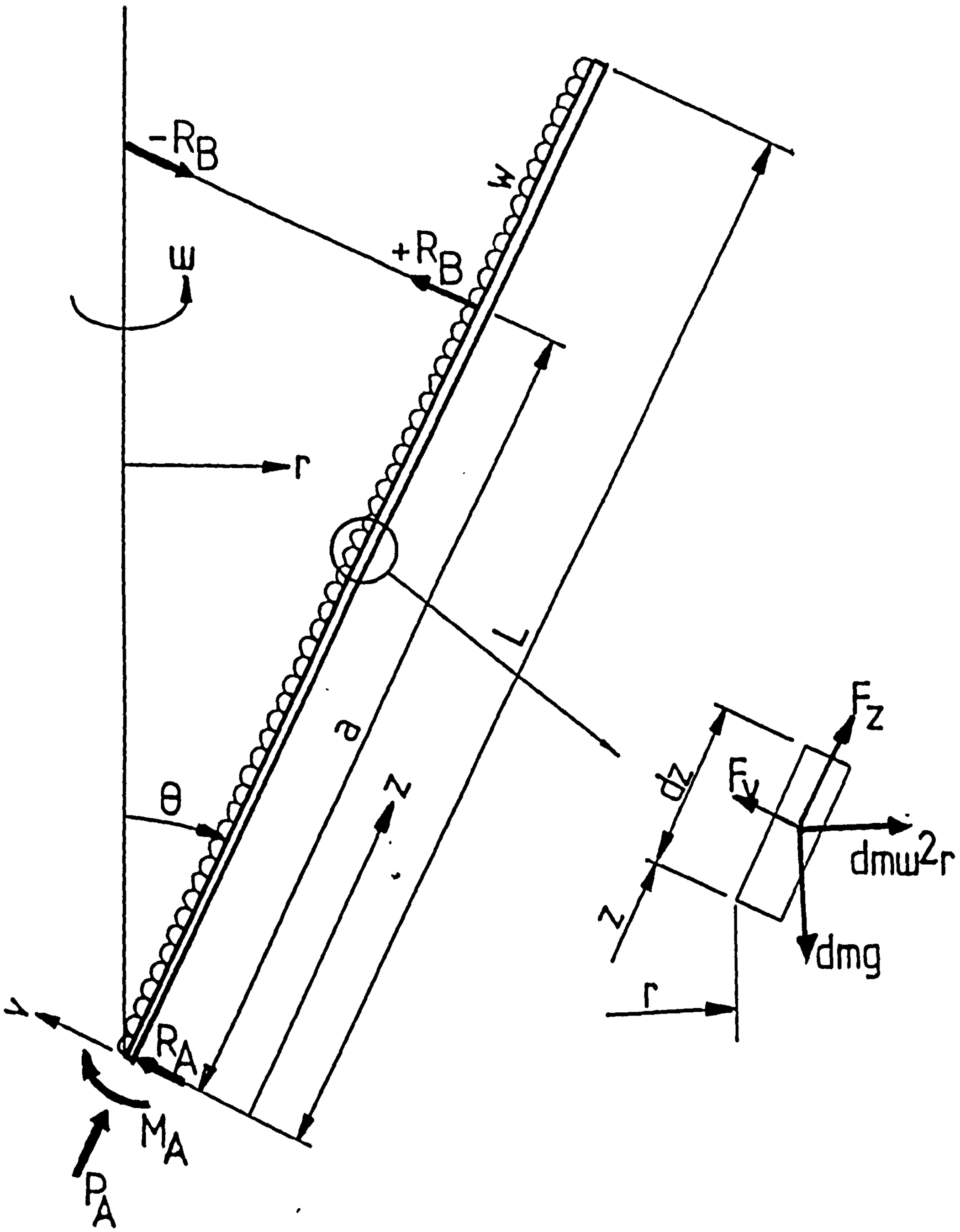

Figure A1.1: Schematic diagram of V-VAWT blade showing structural loads

The *per unit mass* centrifugal F_c and gravitational F_g body forces are given by:

$$F_c = \omega^2 r \qquad \text{(A1.4)}$$

$$F_g = g \qquad \text{(A1.5)}$$

Resolving these forces in the z and v directions gives:

$$F_v = -F_c\cos\theta - F_g\sin\theta \qquad \text{(A1.6)}$$

$$F_z = F_c\sin\theta - F_g\cos\theta \qquad \text{(A1.7)}$$

and substitution of F_c, F_g and r leads to:

$$F_v = -\tfrac{1}{2}\omega^2 z\sin 2\theta - g\sin\theta \qquad \text{(A1.8)}$$

$$F_z = \omega^2 z\sin^2\theta - g\cos\theta \qquad \text{(A1.9)}$$

It is convenient here to define the step function Φ:

$$\Phi = \begin{cases} 0 & 0 \leq z \leq a \\ 1 & a < z \leq L \end{cases} \qquad \text{(A1.10)}$$

which can be used to define expressions for shear force F, bending moment M and axial force P as functions of the spanwise co-ordinate z:

$$F(z) = R_A + \int_0^z wF_v dz + \Phi[R_B] \qquad \text{(A1.11)}$$

$$M(z) = M_A + R_A z + \int_0^z\int_0^z wF_v dz dz + \Phi[R_B(z - a)] \qquad \text{(A1.12)}$$

$$P(z) = P_A + \int_0^z wF_z dz \qquad \text{(A1.13)}$$

Substituting for F_v and F_z, and integrating with respect to z gives:

$$F(z) = R_A - w\omega^2 \sin 2\theta \frac{z^2}{4} + wg\sin\theta z + \Phi[R_B] \qquad (A1.14)$$

$$M(z) = M_A + R_A z + w\omega^2 \sin 2\theta \frac{z^3}{12} + wg\sin\theta \frac{z^2}{2} + \Phi[R_B(z - a)] \qquad (A1.15)$$

$$P(z) = P_A + w\omega^2 \sin^2\theta \frac{z^2}{2} - wg\cos\theta z \qquad (A1.16)$$

The further solution of these expressions depends upon the boundary limits imposed at the blade root, cable attachment point and blade tip. However, for the case of the model V-VAWT these expressions may be simplified if gravitational force terms are ignored. The gravitational force terms are very much smaller than the centrifugal force terms because, for design purposes, the rotational speed of the rotor is set at 2500 rpm. The simplified expressions become:

$$F(z) = R_A - w\omega^2 \sin 2\theta \frac{z^2}{4} + \Phi[R_B] \qquad (A1.17)$$

$$M(z) = M_A + R_A z - w\omega^2 \sin 2\theta \frac{z^3}{12} + \Phi[R_B(z - a)] \qquad (A1.18)$$

$$P(z) = P_A + w\omega^2 \sin^2\theta \frac{z^2}{2} \qquad (A1.19)$$

The flapwise deflection v(z) is given by:

$$EI\frac{d^2v}{dz^2} = -M(z) \qquad (A1.20)$$

which means:

$$-EI\frac{d^2v}{dz^2} = M_A + R_A z - w\omega^2 \sin 2\theta \frac{z^3}{12} + \Phi[R_B(z - a)] \qquad (A1.21)$$

Integrating with respect to z gives:

$$-EI\frac{dv}{dz} = M_A z + R_A\frac{z^2}{2} - w\omega^2 \sin 2\theta \frac{z^4}{48} + \Phi\, R_B\frac{(z - a)^2}{2} + A \qquad (A1.22)$$

Integrating with respect to z once again gives:

$$-EIv(z) = M_A\frac{z^2}{2} + R_A\frac{z^3}{6} - w\omega^2 \sin 2\theta \frac{z^5}{240} + \Phi\, R_B\frac{(z - a)^3}{6} + Az + B \qquad (A1.23)$$

where the A and B are constants of integration.

The general expressions for shear force, bending moment, axial force and flapwise displacement are the basis of the solutions for the two loading cases considered below. Expressions for R_A, M_A, P_A, R_B, A and B are developed in each case by the application of appropriate boundary conditions.

A1.3: Solution for a V-VAWT Blade Simply Supported at both its Root and Cable Attachment

In this case, the V-VAWT blade is considered to be simply supported at its root and at its cable attachment. The following boundary conditions apply:

$$M(0) = 0 \qquad (A1.24a)$$

$$v(0) = 0 \qquad (A1.24b)$$

$$v(a) = 0 \qquad (A1.24c)$$

$$F(L) = 0 \qquad (A1.24d)$$

$$M(L) = 0 \qquad (A1.24e)$$

$$P(L) = 0 \qquad (A1.24f)$$

Substitution of these boundary conditions into the general equations developed above yield the following solutions:

$$R_A = m\omega^2 \sin 2\theta \left(\frac{L}{4} - \frac{L^2}{6a}\right) \qquad \text{(A1.25)}$$

$$M_A = 0 \qquad \text{(A1.26)}$$

$$P_A = -m\omega^2 \sin^2\theta \frac{L}{2} \qquad \text{(A1.27)}$$

$$R_B = m\omega^2 \sin 2\theta \frac{L^2}{6a} \qquad \text{(A1.28)}$$

$$A = m\omega^2 \sin 2\theta \left(\frac{L^2 a}{36} + \frac{a^4}{240L} - \frac{La^2}{24}\right) \qquad \text{(A1.29)}$$

$$B = 0 \qquad \text{(A1.30)}$$

A1.4: Solution for a V-VAWT Blade Simply Supported at its Cable Attachment and Built-In at its Root.

In this case, the V-VAWT blade is considered to be simply supported at its cable attachment and built-in at its root. The following boundary conditions apply:

$$\frac{dv(0)}{dz} = 0 \qquad \text{(A1.31a)}$$

$$v(0) = 0 \qquad \text{(A1.31b)}$$

$$v(a) = 0 \qquad \text{(A1.31c)}$$

$$F(L) = 0 \qquad \text{(A1.31d)}$$

$$M(L) = 0 \qquad \text{(A1.31e)}$$

$$P(L) = 0 \qquad \text{(A1.31f)}$$

Substitution of these boundary conditions into the general equations developed above yield the following solutions:

$$R_A = m\omega^2 \sin 2\theta \left(\frac{3L}{8} - \frac{a^2}{80L} - \frac{L^2}{4a} \right) \qquad \text{(A1.32)}$$

$$M_A = m\omega^2 \sin 2\theta \left(\frac{L^2}{12} - \frac{aL}{8} + \frac{a^3}{80L} \right) \qquad \text{(A1.33)}$$

$$P_A = -m\omega^2 \sin^2\theta \frac{L}{2} \qquad \text{(A1.34)}$$

$$R_B = m\omega^2 \sin 2\theta \left(\frac{a^2}{80L} - \frac{L}{8} + \frac{L^2}{4a} \right) \qquad \text{(A1.35)}$$

$$A = 0 \qquad \text{(A1.36)}$$

$$B = 0 \qquad \text{(A1.37)}$$

A1.5: Tensile and Bending Stresses in Composite Blade

In a composite blade, the tensile stress in the two materials is given by:

$$\sigma_s(z) = \frac{P(z)E_s}{A_sE_s + A_wE_w} \qquad \text{(A1.38a)}$$

$$\sigma_w(z) = \frac{P(z)E_w}{A_sE_s + A_wE_w} \qquad \text{(A1.38b)}$$

In a composite blade, the maximum bending stress in the two materials is given by:

$$\sigma_s(z) = \frac{M(z)y_sE_s}{I_sE_s + I_wE_w} \qquad \text{(A1.39a)}$$

$$\sigma_w(z) = \frac{M(z)y_wE_w}{I_sE_s + I_wE_w} \qquad \text{(A1.39b)}$$

The cumulative stress in the two materials is given by:

$$\sigma_s(z) = \frac{P(z)E_s}{A_sE_s + A_wE_w} + \frac{M(z)y_sE_s}{I_sE_s + I_wE_w} \qquad \text{(A1.40a)}$$

$$\sigma_w(z) = \frac{P(z)E_w}{A_sE_s + A_wE_w} + \frac{M(z)y_wE_w}{I_sE_s + I_wE_w} \qquad \text{(A1.40b)}$$

A1.6: Cross-Sectional Areas and Second Moments of Area

The V-VAWT model blades are largely a composite of wood and aluminium alloy. A number of blade spar geometries were considered, but the skin of the blade was always considered solid. The basic dimensions of the spar and the cross-sectional area of blade profile provide sufficient information from which all geometrical properties of the blade section can be determined.

Three cross-sectional geometries were considered for the blade spar:

(a) Circular tube
(b) Rectangular box
(c) Rectangular tube

The cross-sectional area and second moment of area of the two blade materials differs according to the choice of spar section. The rectangular tube was eventually selected for the V-VAWT model giving:

$$A_s = bd - \frac{\pi D_i^2}{4} \qquad \text{(A1.41)}$$

$$I_s = \frac{bd^3}{12} - \frac{\pi D_i^4}{64} \qquad \text{(A1.42)}$$

$$A_w = A_{fr} - bd \qquad \text{(A1.43)}$$

$$I_w = I_{fr} - \frac{bd^3}{12} \qquad \text{(A1.44)}$$

where the cross-sectional area A_{fr} and second moment of area I_{fr} of the aerofoil section have been determined beforehand.

The mass of the blade is calculated as follows:

$$m = m_s + m_w \qquad \text{(A1.45)}$$

where

$$m_s = \rho_s A_s L \qquad \text{(A1.46a)}$$

$$m_w = \rho_w A_w L \qquad \text{(A1.46b)}$$

A1.7: The Computer Programs TAYVAWT and STAVAWT

The computer programs TAYVAWT and STAVAWT were written and developed by the author as an aid for evaluation of the structural performance of any given V-VAWT model blade design. The programs were written in BASIC and are run on the BBC-B microcomputer. The programs have greatly assisted the author in evolving the final blade design, by allowing design modifications to be quickly evaluated and compared with other design solutions.

TAYVAWT is a pre-processing program in which all the independent blade dimensions and material properties are entered by the program user. To assist this process, a number of default dimensions and material property values are written into the program software. The loading case required, i.e. simply supported or built-in at blade root,

and the cross-sectional geometry of the blade spar are both specified in this program. The dependent dimensions and properties of the blade ~~the blade~~ are then calculated.

All the dimensions and properties of the blade design are stored in a blade geometry datafile on a floppy diskette. This datafile contains all the pertinent information about the blade required ~~of~~ by the analysis program STAVAWT.

The analysis program STAVAWT is automatically invoked when the blade geometry datafile has been created. The values stored in the datafile are immediately retrieved from the diskette to initialise the blade dimensions and material properties of the analysis program. Before analysis commences, the method of presenting results is selected. Results may be displayed either in a numerical or graphical form. A hard copy of the results may also be created if a suitable printer is connected to the computer. With the program initialisation complete, the analysis of the blade commences. The program enters two repetitive calculation routines.

The first routine is a rotational speed loop, in which the analysis of the blade is performed at different rotational speeds. Generally, only a couple of rotational speeds are considered, these being 2000 rpm and 2500 rpm. Comparing the results at these two speeds, has allowed the author to check the validity of the program, because all forces, moments, displacements and stresses should be 56% larger at 2500 rpm than those calculated at 2000 rpm.

At each rotational speed, the values of $R_{(n)}$, $M_{(n)}$, $P_{(n)}$, $R_{(n)}$, A and B are evaluated. These values are used in the algorithms to calculate the shear force, bending moment, axial force and flapwise displacement distribution of the blade. This is done in the second routine, in which the values of

F(z), M(z), P(z) and v(z) are evaluated at various spanwise ordinates, including the cable attachment point. The maximum material stresses are likewise evaluated. The results of these calculations are displayed or printed directly into a tabular form, if this option has been selected. When this routine is completed, the values of R_A, M_A, P_A, R_B, A and B are themselves displayed. If graphical output of the results was selected, the screen is cleared and the shear force, bending moment and flapwise displacement distributions are plotted on the screen. A second display shows axial force and material stress distributions.

When this routine is completed, the program repeats the analysis of the blade at the next required rotational speed. When the analysis of the blade design has been completed at all rotational speeds, the program user is given the option to exit from the program, or to repeat the analysis using an alternative blade geometry datafile.

Appendix Two: The Calculation of Angular Acceleration using Numerical Methods

A2.1: The Calculation of Angular Acceleration using Numerical Differentiation

The acceleration method is a simple method for determining the torque developed by a rotating body. If the net torque acting on the body is positive, the rotational speed will increase; if it is negative the rotational speed will decrease. By measuring the rate of change of rotational speed of the body, the net torque acting on the body can be calculated using equation (5.1).

The acceleration method is used throughout the performance test programme to measure the shaft torque developed by the model V-VAWT, the friction torque of the bearings and the aerodynamic drag torque of the blade support cables. In all cases, measurements of angular velocity with respect to time have been made. No direct measurement of angular acceleration, or retardation, was possible, so the instantaneous angular acceleration must be calculated using numerical differentiation.

The test facility at Queen Mary College uses a Commodore PET microcomputer to record measurements of angular velocity and time. The angular velocity of the shaft is measured by a low voltage d.c. tachogenerator that is directly coupled to the rotating shaft. The output voltage from the tachogenerator is continuously converted to a 12-bit digital signal by an analogue to digital converter. The A to D converter is directly coupled to the User Port of the microcomputer, enabling the rapid sampling of the angular velocity measurements. A sampling frequency of 10 Hertz is achievable with this system.

The tachogenerator was calibrated during previous experimental work using a stroboscope, and a calibration factor was established to convert the digital output signal to a revolutions per minute value. The r.p.m. value is further converted to a radians per second value for the torque measurement tests.

Measurements of time are made using the internal clock of the microcomputer. The internal clock measurements are in 'giffies', where one giffy is one sixtieth of a second. The measured value of time is converted into a value in units of one second.

The data logging programs record measurements of angular velocity and time. These measurements are immediately converted into their respective units and stored in the internal memory of the computer. The measurements are made continuously during the test period until either recording is stopped manually or a maximum of 500 measurements have been made. Once the recording sequence has stopped, the stored values of angular velocity and time are permanently stored on magnetic disk and the analysis sequence commences.

It should be noted that the A to D converter output value of angular velocity and the value of time in giffies are both integer, binary values and are therefore discrete in range, yet the quantities being measured are continuous. The conversion of these measurements to their appropriate units creates real values, but their range is still discrete. The values of angular velocity and time recorded during all tests are multiples of the following Base Units:

Base Unit of angular velocity:	0.1277581 $rads^{-1}$
Base Unit of time:	0.0166667 sec

Index No. i	Angular Velocity (rad/s)	f_i (p.u.)	Time (s)	x_i (p.u.)
0	60.9406143	477	0.366667	52
1	61.4516467	481	0.966667	58
2	61.5794048	482	1.050000	63
3	61.8349210	484	1.150000	69
4	62.2181953	487	1.250000	75
5	62.4737115	489	1.316667	79
6	62.7292277	491	1.416667	85
7	62.9847439	493	1.500000	90
8	63.2402601	495	1.600000	96
9	63.6235345	498	1.700000	102
10	63.8790506	500	1.783334	107
11	64.1345668	502	1.883334	113
12	64.5178411	505	1.966667	118
13	64.7733574	507	2.066667	124
14	65.4121478	512	2.150000	129
15	65.4121478	512	2.250000	135
16	65.9231802	516	2.350000	141
17	65.9231802	516	2.400000	144
18	66.1786964	518	2.500000	150
19	66.4342127	520	2.583334	155
20	66.6897288	522	2.683333	161
21	66.9452451	524	2.766667	166
22	67.2007612	526	2.866667	172
23	67.5840356	529	2.966667	178
24	67.8395518	531	3.050000	183
25	68.0950679	533	3.150000	189
26	68.3505842	535	3.233334	194
27	68.7338585	538	3.333334	200
28	69.2448908	542	3.433333	206
29	69.3726489	543	3.500000	210
30	69.6281653	545	3.600000	216

Table A2.1: Typical Recorded Values of Angular Velocity and Time

The absolute error for any of these digital measurements is heavisided due to the manner in which analogue measurements are truncated during digital conversion.

The figures in Table A2.1 are typical of the measurements made during the performance testing of the model V-VAWT, and will be used to illustrate the calculations that are made during the numerical differentiation process.

The value of a function $f(x_o+h)$ and $f(x_o-h)$ can be estimated, given the values $f(x_o)$, $f'(x_o)$, $f''(x_o)$, $f'''(x_o)$ etc.., using the Taylor's Series:

$$f_1 = f(x_o+h) = f(x_o) + hf'(x_o) + \frac{h^2f''(x_o)}{2!} + \frac{h^3f'''(\varepsilon_1)}{3!} \qquad (A2.1)$$

$$f_{-1} = f(x_o-h) = f(x_o) - hf'(x_o) + \frac{h^2f''(x_o)}{2!} - \frac{h^3f'''(\varepsilon_2)}{3!} \qquad (A2.2)$$

Rearrangement of these two equations yields:

$$f_o' = \frac{f_1 - f_{-1}}{2h} - \frac{h^2f'''(\varepsilon)}{6} \qquad x_o-h < \varepsilon < x_o+h \qquad (A2.3)$$

Thus the rate of change of $f(x)$ with respect to x at x_o can be approximated by:

$$f'(x_o) = \frac{f(x_o+h) - f(x_o-h)}{2h} \qquad (A2.4)$$

where the truncation error is:

$$\frac{-h^2f'''(\varepsilon)}{6} \qquad x_o-h < \varepsilon < x_o+h \qquad (A2.5)$$

From the measurements of angular velocity and time, the rate of change of angular velocity with respect to time,

at a particular time, can be estimated using equation (A2.4). The equation is slightly modified for use with the measurements stored in the computer so that:

$$\omega = \frac{f_i - f_{i-n}}{x_i - x_{i-n}} \qquad \text{(A2.6)}$$

where:

$$\omega = \frac{f_i + f_{i-n}}{2} \qquad \text{(A2.7)}$$

The calculation of ω and ω using equations (A2.6) and (A2.7) respectively is easily performed using the microcomputer, however the accuracy of these calculated values is crucially dependent upon the stepwidth h. The truncation error is given by (A2.5) where:

$$h = \frac{x_i - x_{i-n}}{2} \qquad \text{(A2.8)}$$

The smaller h is, the smaller the truncation error. However, when using the digitally stored measurements of angular velocity and time for the numerical calculation of angular acceleration, rounding error must be considered. If h is small, f_i and f_{i-n} are almost equal and the rounding error in calculating $(f_i - f_{i-n})$ may be comparable with the size of $(f_i - f_{i-n})$. Similarly, x_i and x_{i-n} are almost equal and the rounding error in calculating $(x_i - x_{i-n})$ may be comparable with the size of $(x_i - x_{i-n})$. Consequently a large relative error will result when calculating ω using equation (A2.6).

Table A2.2 illustrate how the relative error changes with stepwidth using the measurements given in Table A2.1. Note that the rounding error on all 'per unit' values is +1, so the rounding error in $(f_i - f_{i-n})$ and $(x_i - x_{i-n})$ will

Let i = 30, let the index number stepwidth n be varied as shown, and let:

δ_f ≡ relative error in $(f_i - f_{i-n})$

δ_x ≡ relative error in $(x_i - x_{i-n})$

δ_ω ≡ relative error in calculation of ω

n	f_i	x_i	f_{i-n}	x_{i-n}	$f_i - f_{i-n}$	$x_i - x_{i-n}$	relative errors δ_f	δ_x	δ_ω
1	545	216	543	210	2	6	±50%	±17%	±67%
5	545	216	533	189	12	27	±8%	±4%	±12%
10	545	216	522	161	23	45	±4%	±2%	±6%
20	545	216	500	107	45	109	±2%	±1%	±3%
30	545	216	477	52	68	164	±1%	±½%	±1½%

Table A2.2: The Variation of Relative Errors with Stepwidth Size

be ±1. Also note that in calculating ω the computer program uses a constant value of n, the index number stepwidth, and in reality the stepwidth h varies with each calculation.

The data used for this analysis illustrates clearly the need to use a large index number stepwidth to ensure accurate calculation of the instantaneous angular acceleration. The acceleration of the rotor is small at both low rotational speeds and where the rotor speed is nearing the equilibrium speed where the magnitude of the aero-

dynamic torque is equal to the magnitude of the parasitic torque losses. At small angular accelerations it is even more necessary to use a large index number stepwidth, to the ensure accuracy of calculation. The truncation error, however, using equation (A2.6) is proportional to h^n and $f'''(\varepsilon)$. While increasing the stepwidth n from 10 to 30 units reduces the relative error in ω by a factor of four, the truncation error in increased by a factor of nine!. However, $f'''(\varepsilon)$ is the rate of change of the rate of change of angular acceleration with respect to time, within the time interval $(x_i - x_{i-n})$, and in real terms can be considered insignificant. Therefore the truncation error can be considered to be insignificant, even though its magnitude is increased with increasing stepwidth size.

The angular velocity, ω, is calculated by simple linear interpolation using equation (A2.7), and is the velocity at which the angular acceleration of the rotor is ω. The relative error in calculating ω is small, typically less than ±1%, however, with what confidence can linear interpolation be used over large stepwidth intervals?

The confidence with which linear interpolation can be applied to calculating ω is dependent upon the change in angular acceleration over the time interval $(x_i - x_{i-n})$. Where the angular acceleration of the rotor increases over the time interval, the calculated value of ω will tend to be larger than actual, and where angular acceleration decreases over the time interval, ω will be smaller than actual.

The difference between actual and calculated values of ω will increase with increasing stepwidth. However, with an index number stepwidth of n = 30 and letting i = 30, then $f_i = 545$, and $f_{i-n} = 477$. Using equation (A2.7) gives $\omega = 511 \pm 1$, which compares favourably with the half-

interval measurement of angular velocity, f_{res} = 512. Therefore, there appears to be no need to use a more complex interpolating equation to calculate instantaneous angular velocity than that of equation (A2.7).

A2.2: Conclusions and Recommendations

Initially the index number stepwidth was set at n = 10, but for the post-experimental analysis the stepwidth was increased to n = 30, and all results presented in Chapter Five are calculated with this larger stepwidth. Each test run was limited to maximum of 500 measurements, but often this limit was not reached before the run was stopped. With a stepwidth of n = 10 the number of calculations of ω possible was 490, but this is reduced to 470 when the stepwidth is increased to n = 30. The calculation of ω is therefore restricted to the midvalues of the recorded dataset. No calculations were possible at the extremes of the dataset without changing the index number stepwidth but, for simplicity, the stepwidth remained constant for all calculations. A future modification to the computer program might allow the stepwidth to be dynamically altered to ensure the range of calculations and the accuracy of each calculation is maximised.

The sensitivity of the angular velocity measurements would be increased if the input speed of tachogenerator were increased. It is recommended that, for future experimentation, the Queen Mary College test facility be modified to include a step-up gearbox or belt drive between the rotor shaft and the tachogenerator shaft. A 4:1 step-up ratio would maintain an accuracy of ±1½% for ω with a stepwidth of only n = 10, while ensuring greater confidence in the interpolated value of ω and increasing the number of possible calculations derived from the maximum dataset of 500 measurements for each test run.

Appendix Three: Published Papers Presented at Wind Energy Conferences

The initial results of the experimental performance measurements of the model V-VAWT with pitching tips were presented at three wind energy conferences. The papers were subsequently published in the proceedings of these events, and are reproduced here for completeness.

Each paper was jointly written with other members of the V-VAWT development team, but those for the Intersol 85 and BWEA 8 conferences were presented and read by the author himself. The Intersol 85 and Windpower 85 conferences also required poster presentations to be prepared.

The three technical papers are reproduced in the chronological order of presentation:

ROBOTHAM, A.J., SHARPE, D.J., TAYLOR, D.A. and BOYLE, G.A.: "Further developments in the Taylor 'V' type VAWT concept". Proc. Intersol 85 World Solar Energy Congress, Montreal, Canada, June 1985.

BOYLE, G.A., ROBOTHAM, A.J., SHARPE, D.J. and TAYLOR, D.A.: "The Taylor 'V' type vertical axis wind turbine: current status". Proc. Windpower 85, San Francisco, U.S.A., August 1985.

ROBOTHAM, A.J. and SHARPE, D.J.: "The aerodynamic control of the 'V' type vertical axis wind turbine by blade tip control". Proc. 8th British Wind Energy Association Conference, Cambridge, U.K., March 1986.

The author has also prepared two internal reports at The Open University in which the review of wind turbine control methods [32] and the design of the model V-VAWT [55] have been reported.

FURTHER DEVELOPMENTS IN THE TAYLOR 'V' TYPE VAWT CONCEPT

by

A.J. Robotham*, D.J. Sharpe**, D.A. Taylor* and G.A. Boyle*

A paper presented at Intersol 85, Montreal, Canada in June 1985

*Appropriate Technology Group, The Open University,
Walton Hall, Milton Keynes, MK7 6AA, U.K.

**Dept. of Aeronautical Engineering, Queen Mary College,
London University, Mile End Road, London, E1 4NS, U.K.

FURTHER DEVELOPMENTS IN THE TAYLOR 'V' TYPE VAWT CONCEPT

A.J. Robotham*, D.J. Sharpe**, D.A. Taylor* and G.A. Boyle*

*Appropriate Technology Group, The Open University,
Walton Hall, Milton Keynes, MK7 6AA, U.K.
**Dept. of Aeronautical Engineering, Queen Mary College,
London University, Mile End Road, London, E1 4NS, U.K.

ABSTRACT

This paper describes the development of the Taylor 'V' Type Vertical Axis Wind Turbine (V-VAWT) which was first described at the 1983 ISES Solar Energy Congress in Perth, Australia.

The aerodynamic performance prediction model VAWTTAY has been enhanced in VAWTTAY6, and further wind tunnel tests have been carried out using two-bladed models, two of which are described. These tests have produced results which are close to the values predicted by VAWTTAY6, and which have demonstrated that power control of the V-VAWT can be achieved by varying the pitch of the blade tips.

The design of a prototype 5kW machine, that utilises lightweight, composite blades, and the continued development of the V-VAWT concept is discussed.

KEYWORDS

'V' type Vertical Axis Wind Turbine; Double Actuator Disc Theory; Dynamic Stall; VAWTTAY6 Aerodynamic Performance Model; Tip Pitch Control; Wind Tunnel Tests; Wind Energy; Taylor V-VAWT.

INTRODUCTION

Wind energy promises to be one of the first renewable energy sources to be cost-competitive with conventional fuels, but to fufill this promise wind turbines will need to be reliable and low in cost.

The 'V' type vertical axis wind turbine (V-VAWT) was conceived by Derek Taylor at The Open University, and first described by Sharpe and Taylor [1]. The turbine has an inherent simplicity which could lead to an inexpensive machine that is easy to maintain and highly reliable, Fig. 1.

As well as the usual advantages of VAWTs over horizontal axis wind turbines, the V-VAWT has some additional favourable features. The rotor uses two, or three, straight blades mounted in the form of a 'V' on a short tower (just 3 or 4 metres high), and supported by bracing cables from a central pylon. The blades are straight, untwisted and the planform may be tapered or untapered. The turbine is self starting, which is unusual for vertical axis machines.

Aerodynamic control devices such as spoilers, flaps or variable pitch tips can be used to regulate power. This simple arrangement avoids the use of heavy cross arms, a tall tower or curved blades, and allows easy access to the generator, transmission and the rotor itself.

AERODYNAMIC PERFORMANCE

The prediction of the aerodynamic performance of the V-VAWT uses the computer program VAWTTAY [1], which embodies Sharpe's extended multiple streamtube theory and dynamic stall effects [2]. This computer model has been enhanced with VAWTTAY6 to take account of blade inclination, blade shape, blade taper, blade pitch (and twist) and blade tangential offset. A study of the effects of these features on overall performance has been made by Sharpe and Taylor [3] to establish the optimum aerodynamic configuration.

WIND TUNNEL TESTS

A number of model V-VAWTs have been tested in the exit of a straight through, blowdown wind tunnel at Queen Mary College, London. One of these models has been used to check the aerodynamic performance predictions of VAWTTAY6, and one to investigate the variation of tip pitch on overall turbine performance.

The well established acceleration method [4] was used to derive values of rotor torque and power from measurements of rotational velocity in constant wind speed conditions. The test results presented here have been corrected for cable drag, bearing friction and tunnel blockage. Cable drag was the most significant of these corrections and was measured separately.

The first of these recent models (model-A) had two blades of uniform 60mm chord and were 500mm in length, giving an aspect ratio of nine. Each blade was held at an inclination of 45 degrees to the vertical by a pair of cables attached 120mm from the tip. The blades had a NACA0018 aerofoil cross section.

The wind tunnel test results for model-A at a wind speed of 13.7 m/s are shown in Fig. 2. These are compared with theoretical predictions based on NACA0012 aerofoil data (data for the NACA0018 section has not yet been compiled for use with VAWTTAY6). The small difference between the theoretical and experimental results is due, in part, to the different aerofoil sections. The superior post-stall behaviour at the lower tip speed ratios and the higher profile drag at the higher tip speed ratios of the 18% section is clearly illustrated. A similar difference has been demonstrated by Sharpe and Taylor [3].

These test results were regarded as encouraging and established the aerodynamic prediction model as a useful design tool. Predictions for 5kW and 100kW V-VAWTs using VAWTTAY6, Fig. 2, show that Power Coefficients in excess of 0.3 can be achieved. The difference between the three theoretical predictions shown in Fig. 2 is due primarily to Reynold's Number effects.

The second model (model-B), Fig. 3, was constructed with two blades of

uniform, 80mm chord and a length of 665mm. Each blade was held at an inclination of 45 degrees to the vertical by a pair of cables attached 115mm from the tip. For strength the blades had a NACA0025 aerofoil cross section. Additionally, each blade had a moveable tip portion measuring either 5%, 10% or 15% of the blade area. The pitch angle of each tip portion was adjustable and could be pre-set with either positive, 'nose-in' pitch or negative, 'nose-out' pitch. Using this model it was possible to study the effect of the variation of both tip pitch and tip area on overall performance.

The results of the wind tunnel tests are plotted in Fig. 4, and show how tip pitch for tip to blade area ratios of 5%, 10% and 15% affects the performance of the turbine. The results clearly show that 'nose-in' pitch encourages the stall condition, thereby decreasing the developed power of the turbine. Figure 5 shows how the loss of developed power increases as the tip area increases, for a +5 degrees nose-in pitch position.

It appears that developed power can be increased by small nose-out pitch settings, since in such positions the stall condition is delayed at low tip speed ratios, and drag decreased at high tip speed ratios. From the results for all three tip areas (though not all reproduced here), a nose-out pitch of -5 degrees seems maximise the developed power. These nose-out results are compared to those for nose-in pitch settings in Fig. 4.

Predictions of turbine performance for different tip pitch positions have been derived from the theoretical model using NACA0012 aerofoil data (data for the NACA0025 section has not yet been compiled for use with VAWTTAY6). While it is not possible to match these predictions to the test results because of the different aerofoil sections, the effects of nose-in pitch, nose-out pitch and tip area are demonstrated, Fig. 6.

The high starting torque developed by the V-VAWT has been predicted by the theory and confirmed by the results of the wind tunnel tests, Fig. 7. Also it seems an increase in starting torque is possible with small negative, nose-out pitch positions.

FIVE KILOWATT V-VAWT

A 5kW prototype, Fig. 8, has been designed and is scheduled for erection in October 1985. The 5.5 metre blades for this machine are being manufactured by Gifford Technology Limited, at their own cost, from composite materials. The predicted performance of this machine is shown in Fig. 2.

CONCLUSIONS

Recent wind tunnel tests of the Taylor 'V' type vertical axis wind turbine have shown the aerodynamic performance prediction model to be a useful and valid design tool, and that further tests have demonstrated that both overspeed control and power regulation can be achieved by variation of tip pitch. These results are being used for the further development of this VAWT concept, which includes the design and erection of a 5kW prototype V-VAWT.

ACKNOWLEDGEMENTS

The authors wish to express thanks to the technical staff of the Open University and Queen Mary College, Scott Forrest and Neville Kolb who made the wind tunnel models, Gifford Technology Limited and The Science and Engineering Research Council.

REFERENCES

1. D. J. Sharpe and D. A. Taylor, Preliminary investigations into an innovative vertical axis wind turbine. Presented at the World Solar Energy Congress, Perth, Australia, 1983.
2. D. J. Sharpe, Refinements and developments of the multiple streamtube theory for the aerodynamic performance of vertical axis wind turbines. Proc., Sixth BWEA Wind Energy Conference, Reading, 1984.
3. D. J. Sharpe and D. A. Taylor, The aerodynamic performance of the vee type vertical axis wind turbine. Seventh BWEA Wind Energy Conference, Oxford, 1985.
4. D. J. Sharpe, A theoretical and experimental study of the Darrieus vertical axis wind turbine. Research report, School of Mech., Aero. and Prod. Eng., Kingston Polytechnic, October, 1977.

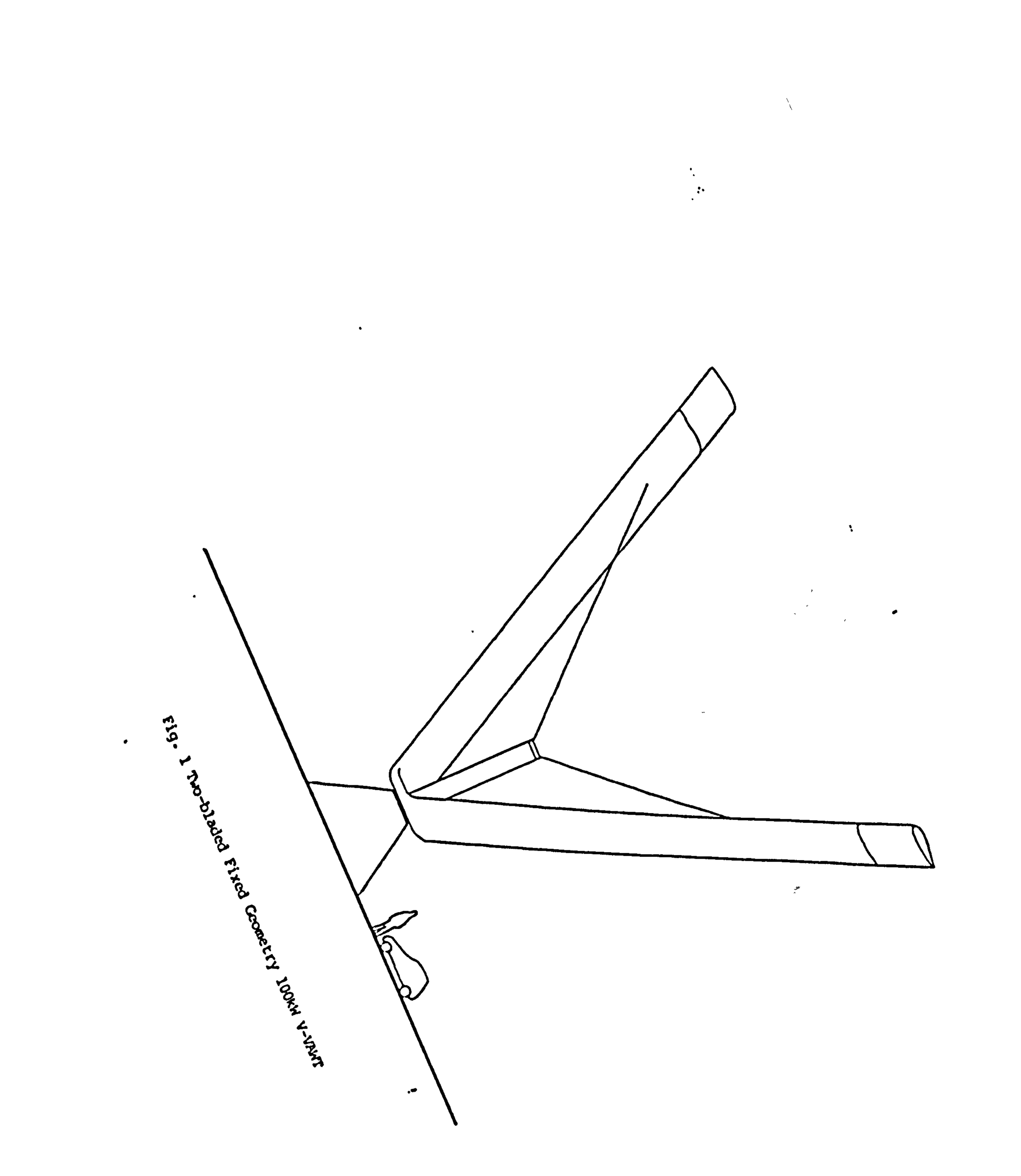

Fig. 1 Two-bladed Fixed Geometry 100kW V-VAWT

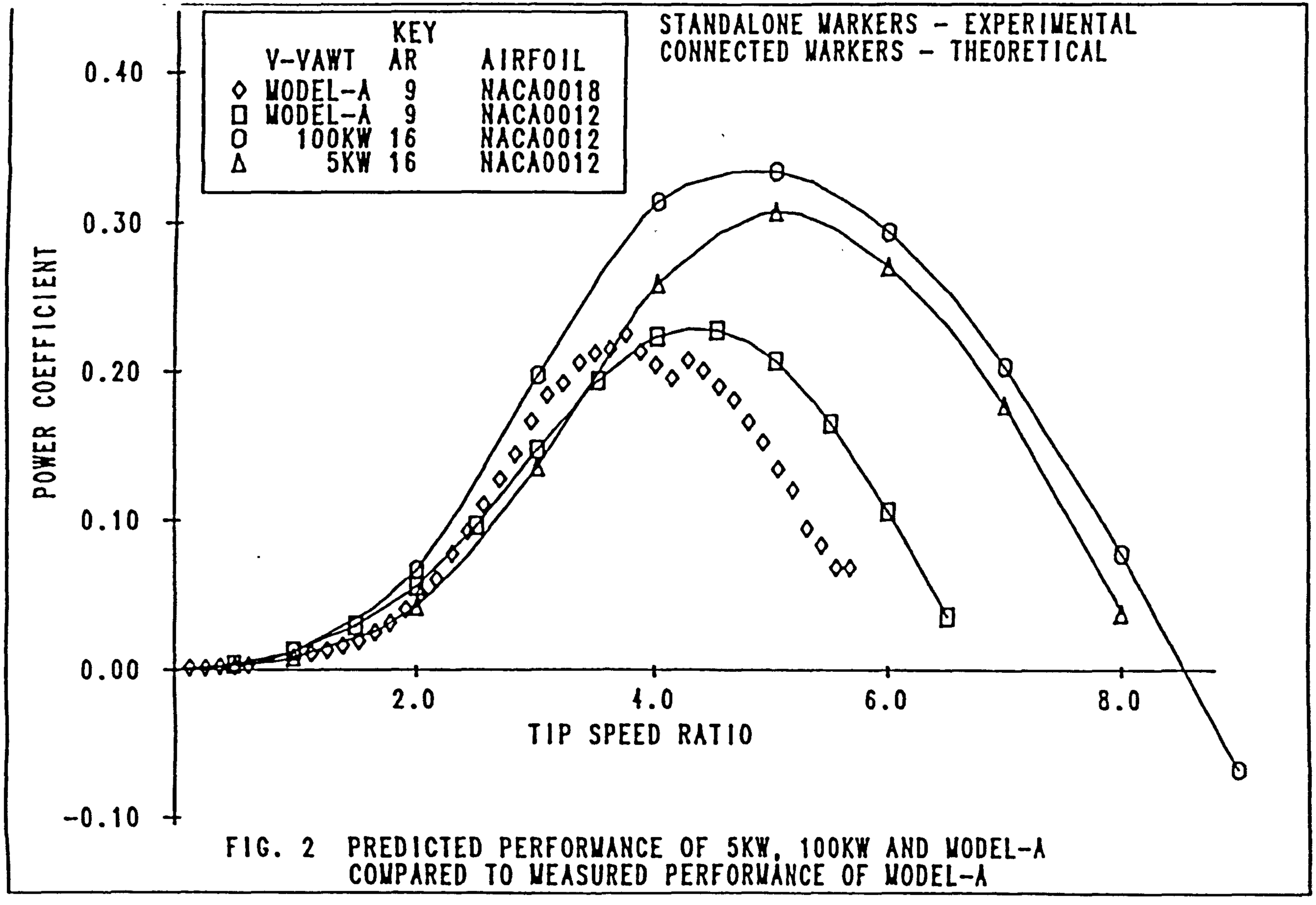

FIG. 2 PREDICTED PERFORMANCE OF 5KW, 100KW AND MODEL-A COMPARED TO MEASURED PERFORMANCE OF MODEL-A

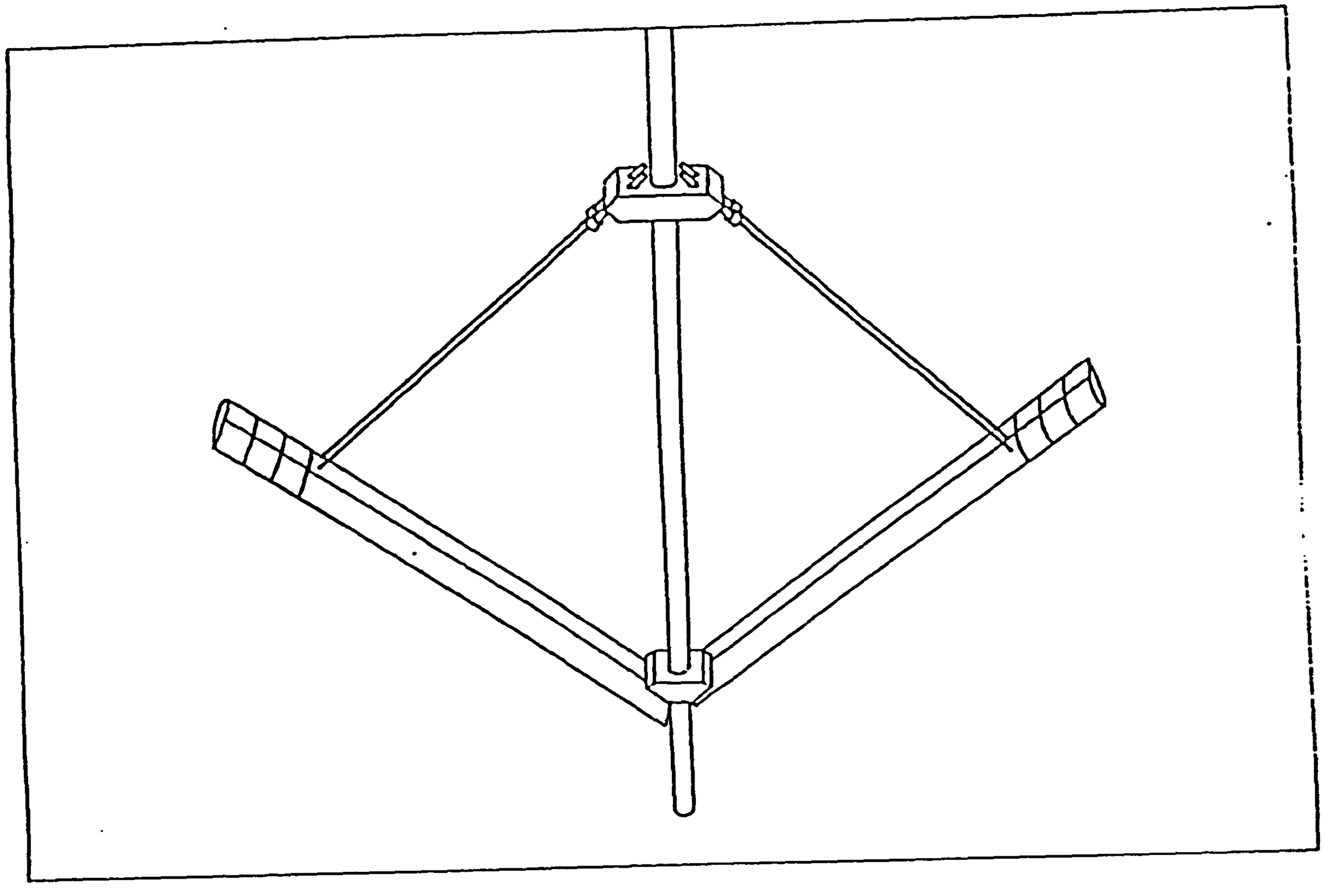

Fig. 3 Model-B: Wind tunnel V-VAWT with pitching tips

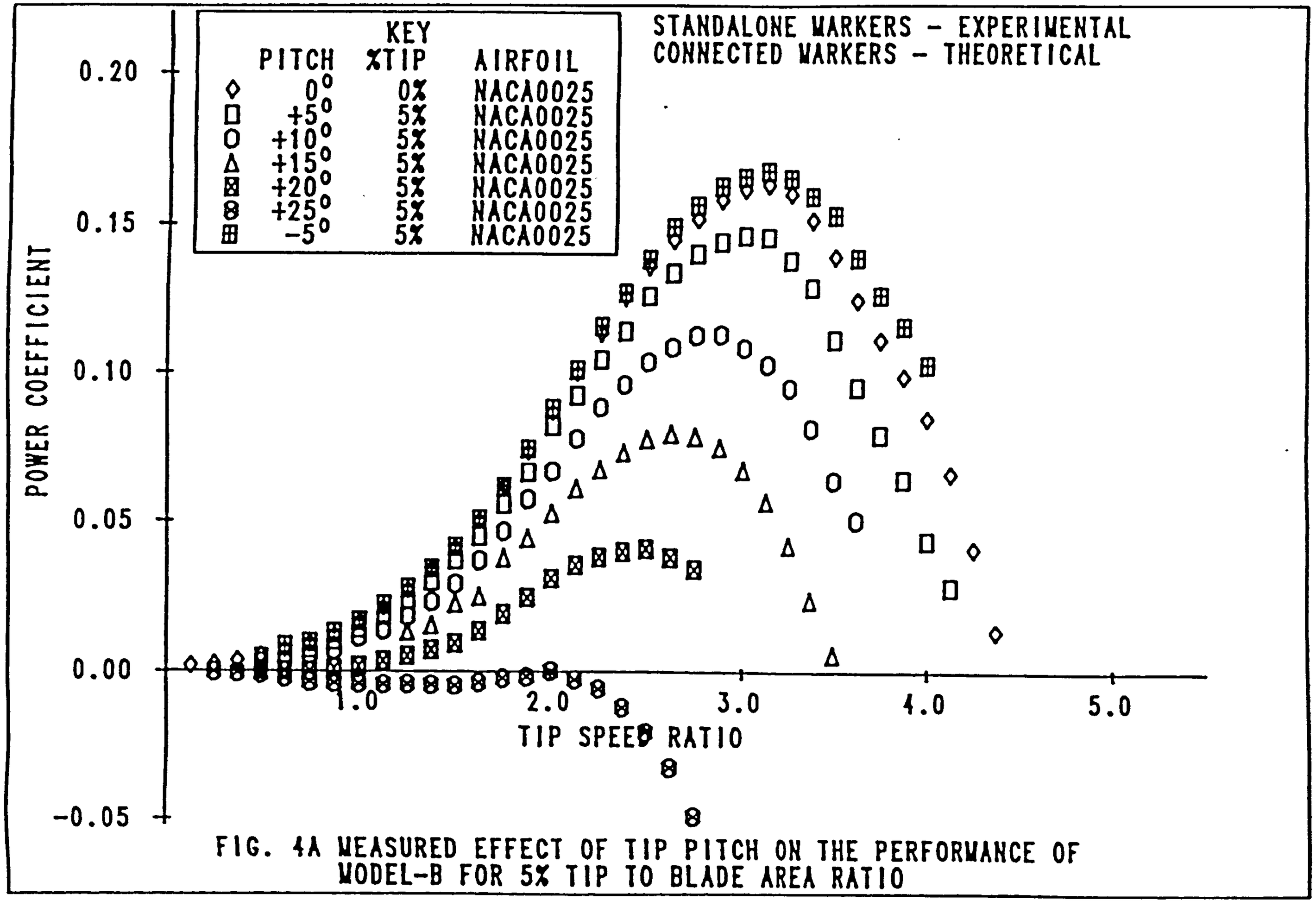

FIG. 4A MEASURED EFFECT OF TIP PITCH ON THE PERFORMANCE OF MODEL-B FOR 5% TIP TO BLADE AREA RATIO

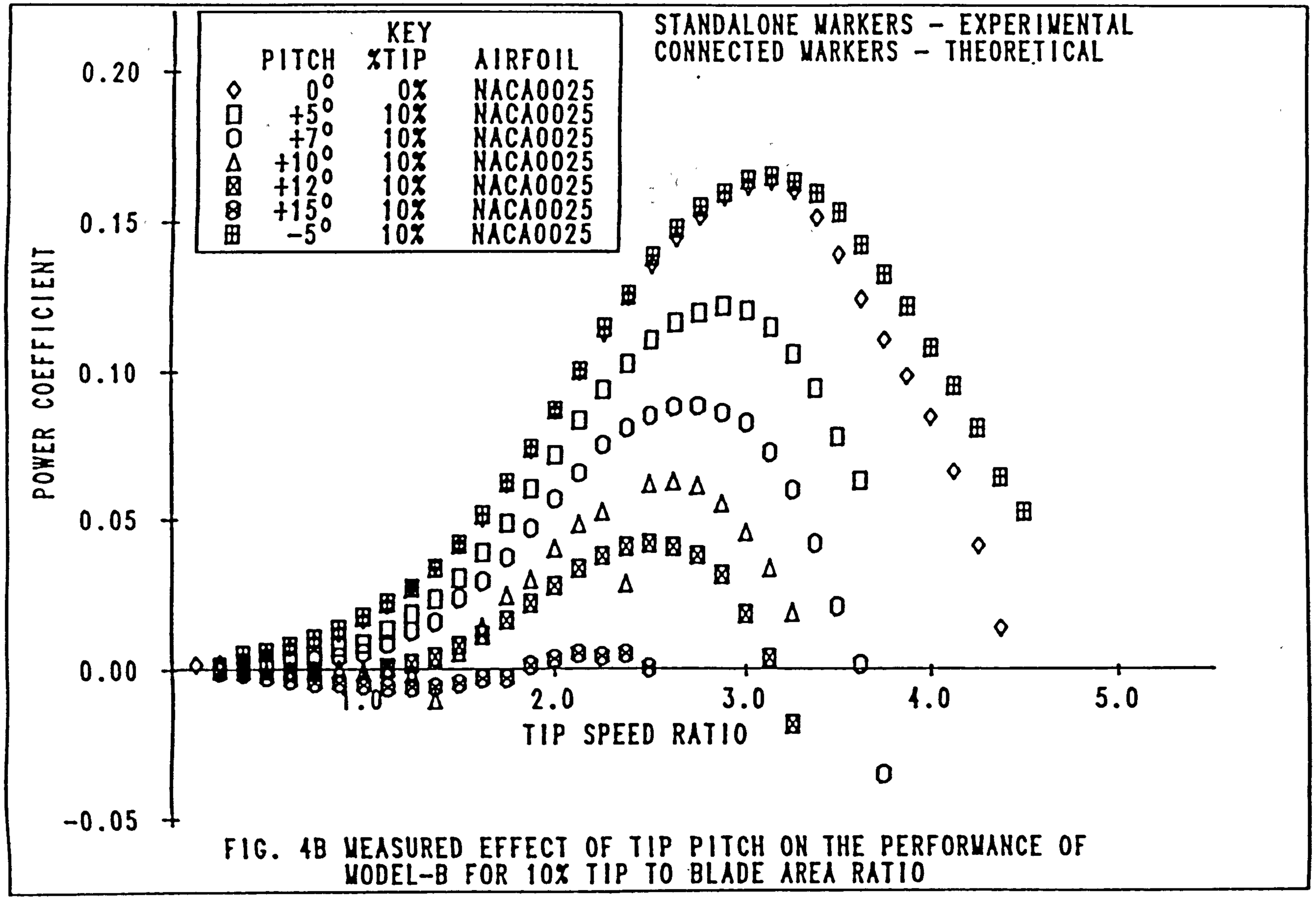

FIG. 4B MEASURED EFFECT OF TIP PITCH ON THE PERFORMANCE OF MODEL-B FOR 10% TIP TO BLADE AREA RATIO

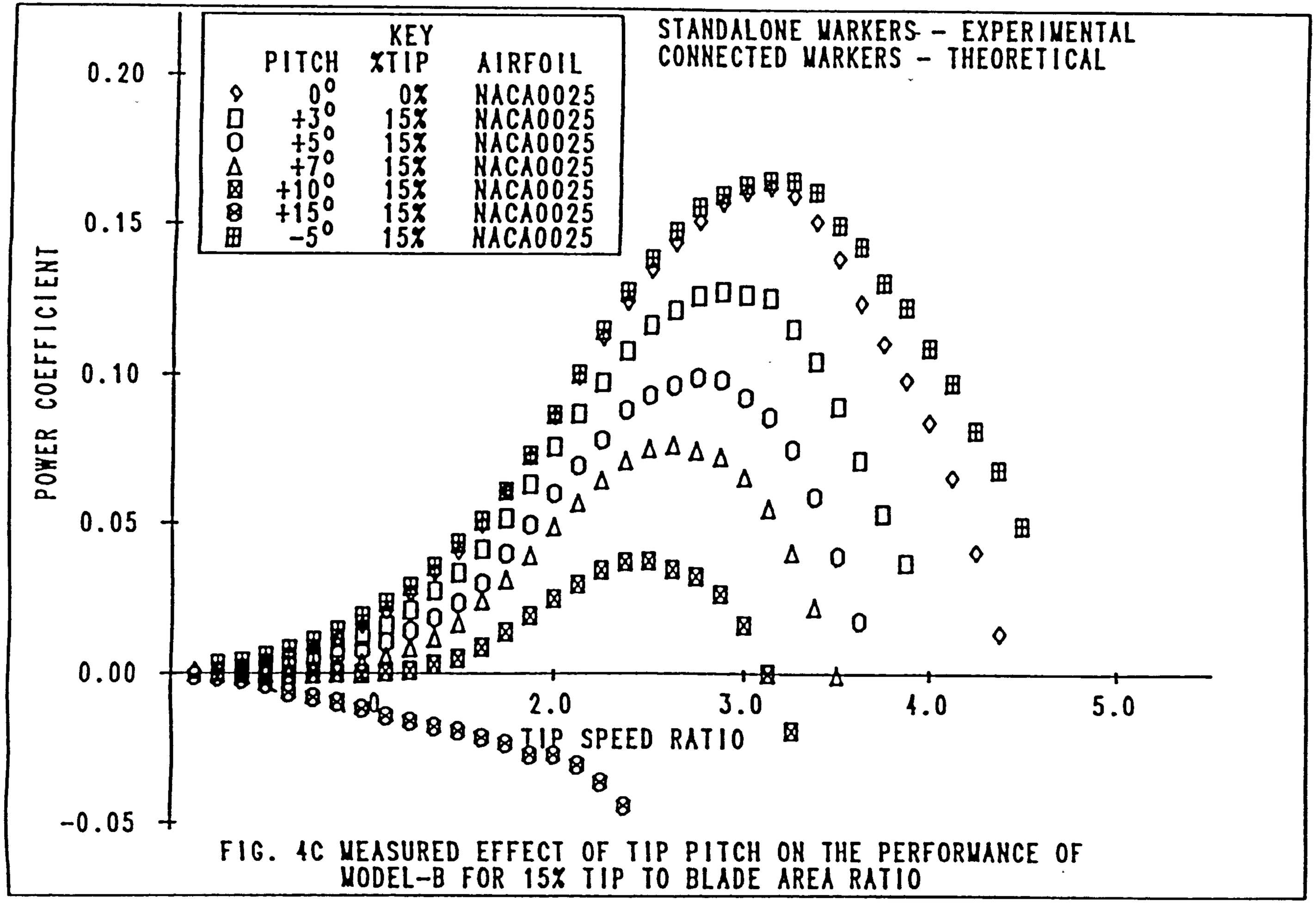

FIG. 4C MEASURED EFFECT OF TIP PITCH ON THE PERFORMANCE OF MODEL-B FOR 15% TIP TO BLADE AREA RATIO

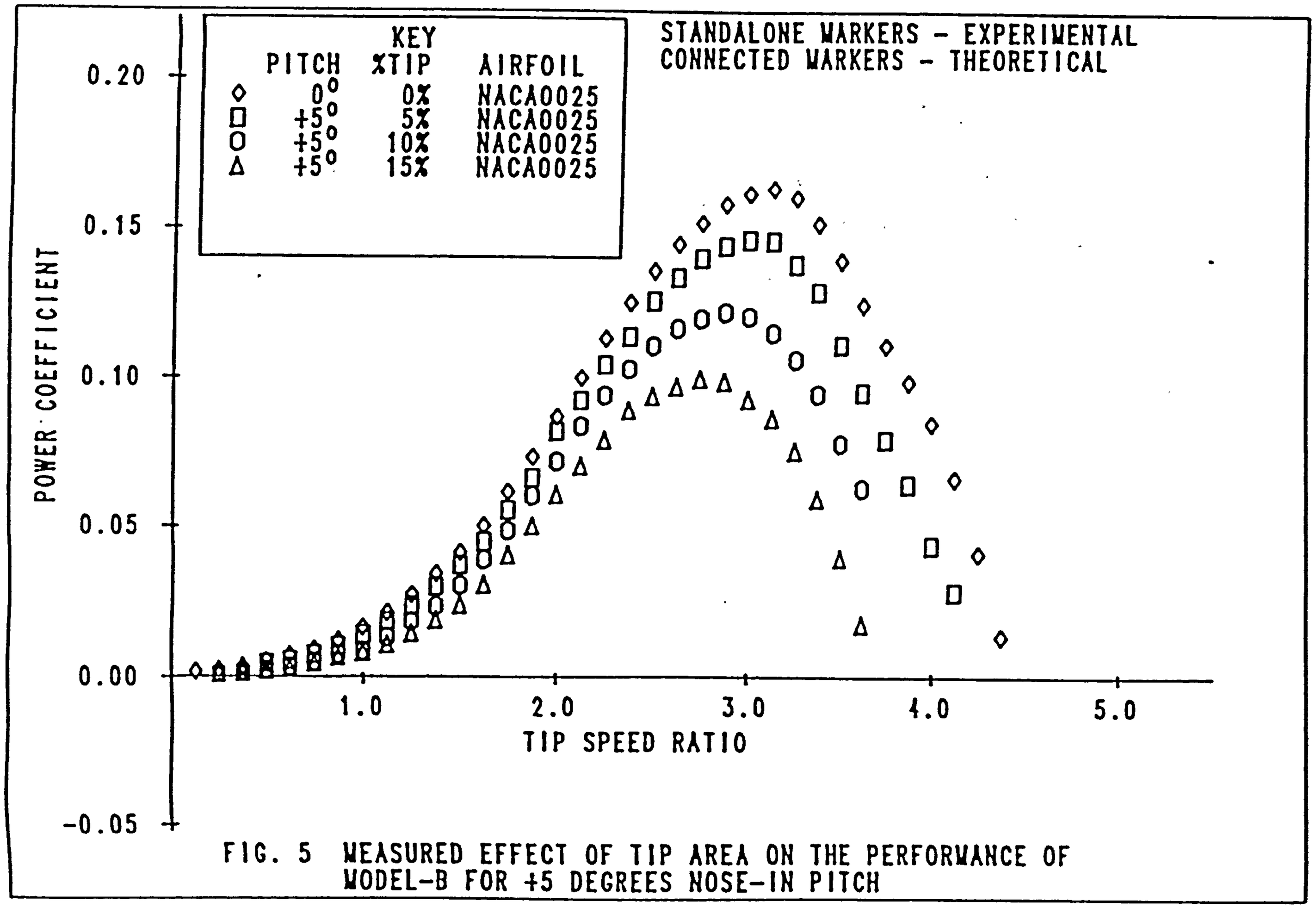

FIG. 5 MEASURED EFFECT OF TIP AREA ON THE PERFORMANCE OF MODEL-B FOR +5 DEGREES NOSE-IN PITCH

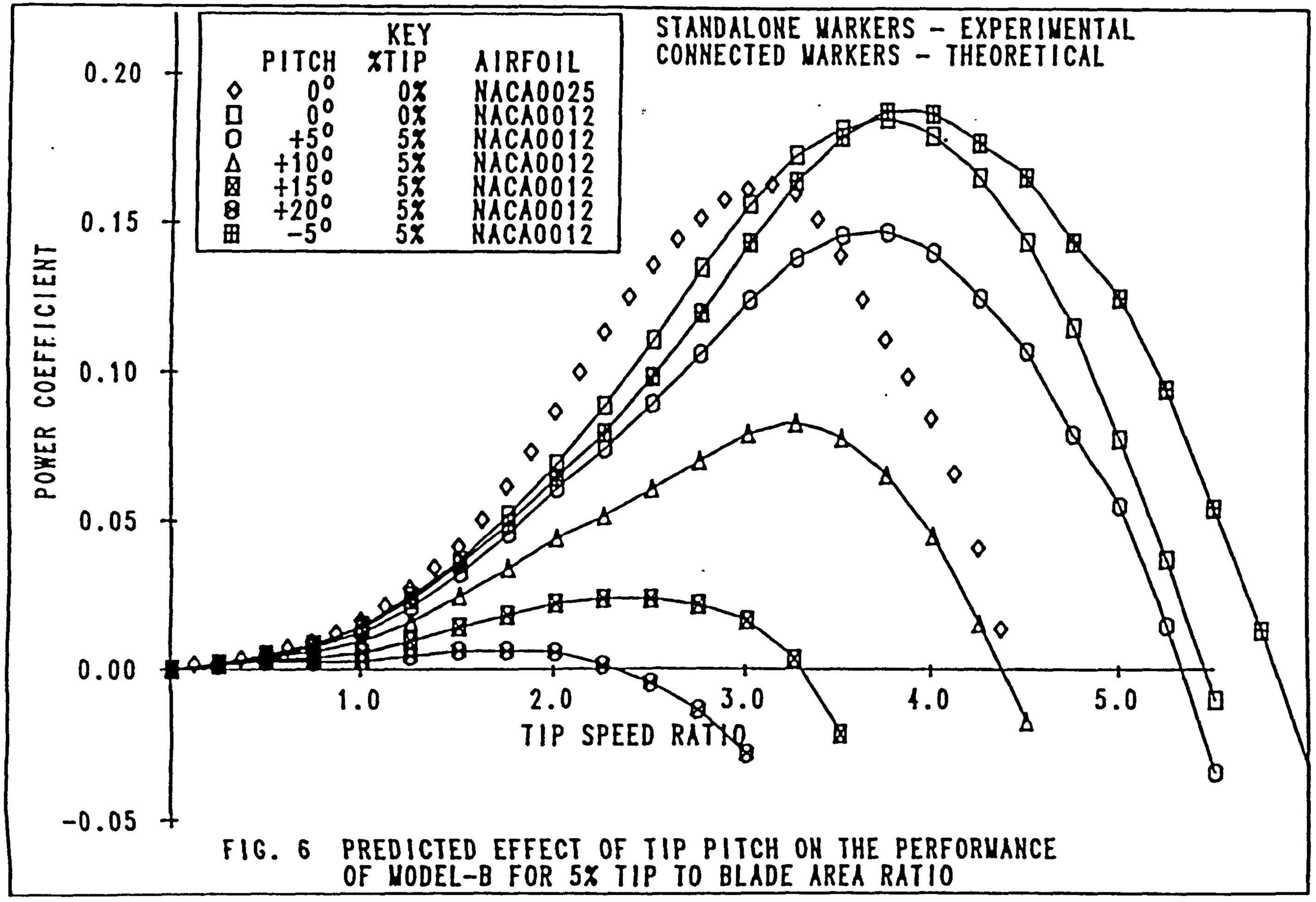

FIG. 6 PREDICTED EFFECT OF TIP PITCH ON THE PERFORMANCE OF MODEL-B FOR 5% TIP TO BLADE AREA RATIO

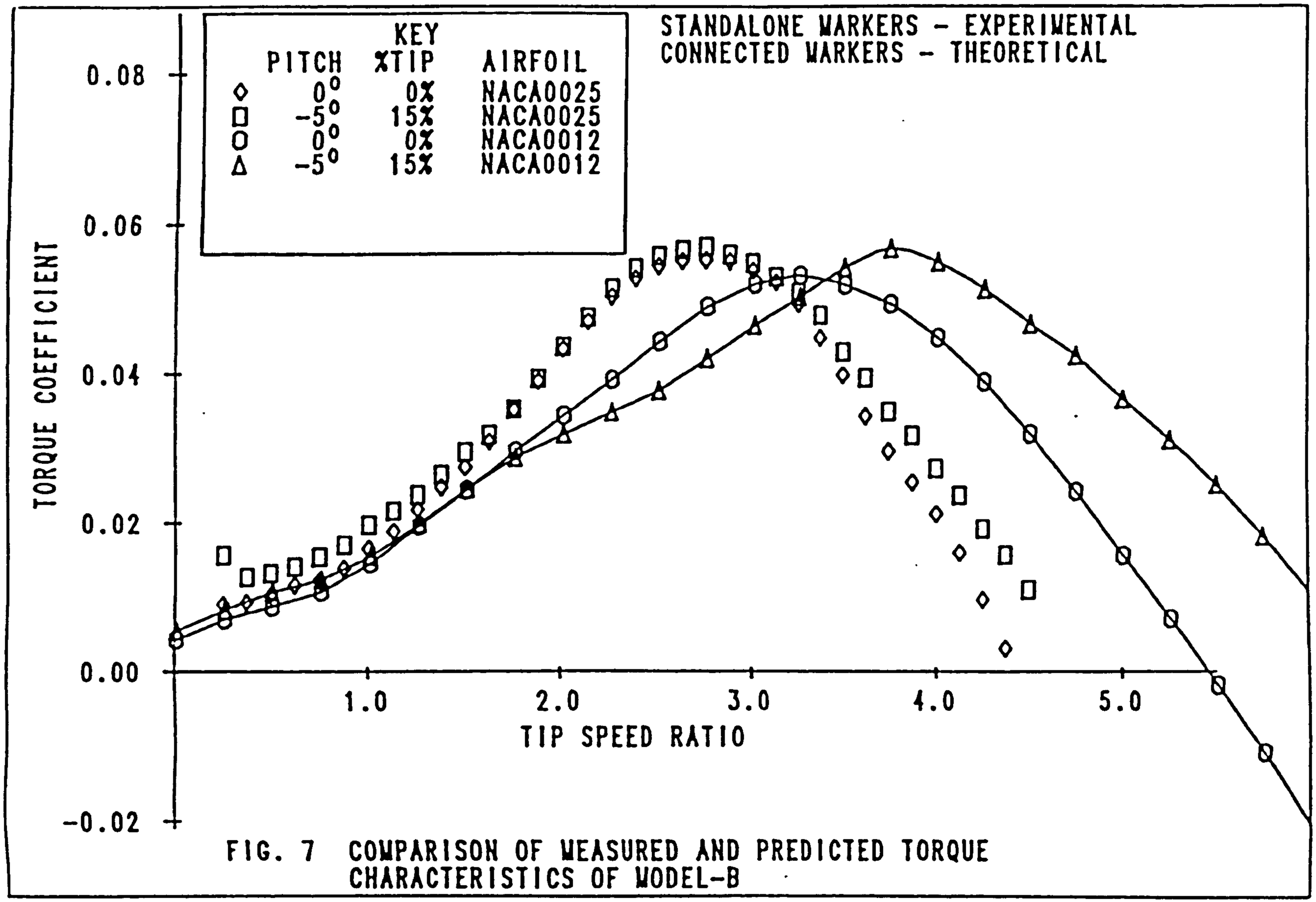

FIG. 7 COMPARISON OF MEASURED AND PREDICTED TORQUE CHARACTERISTICS OF MODEL-B

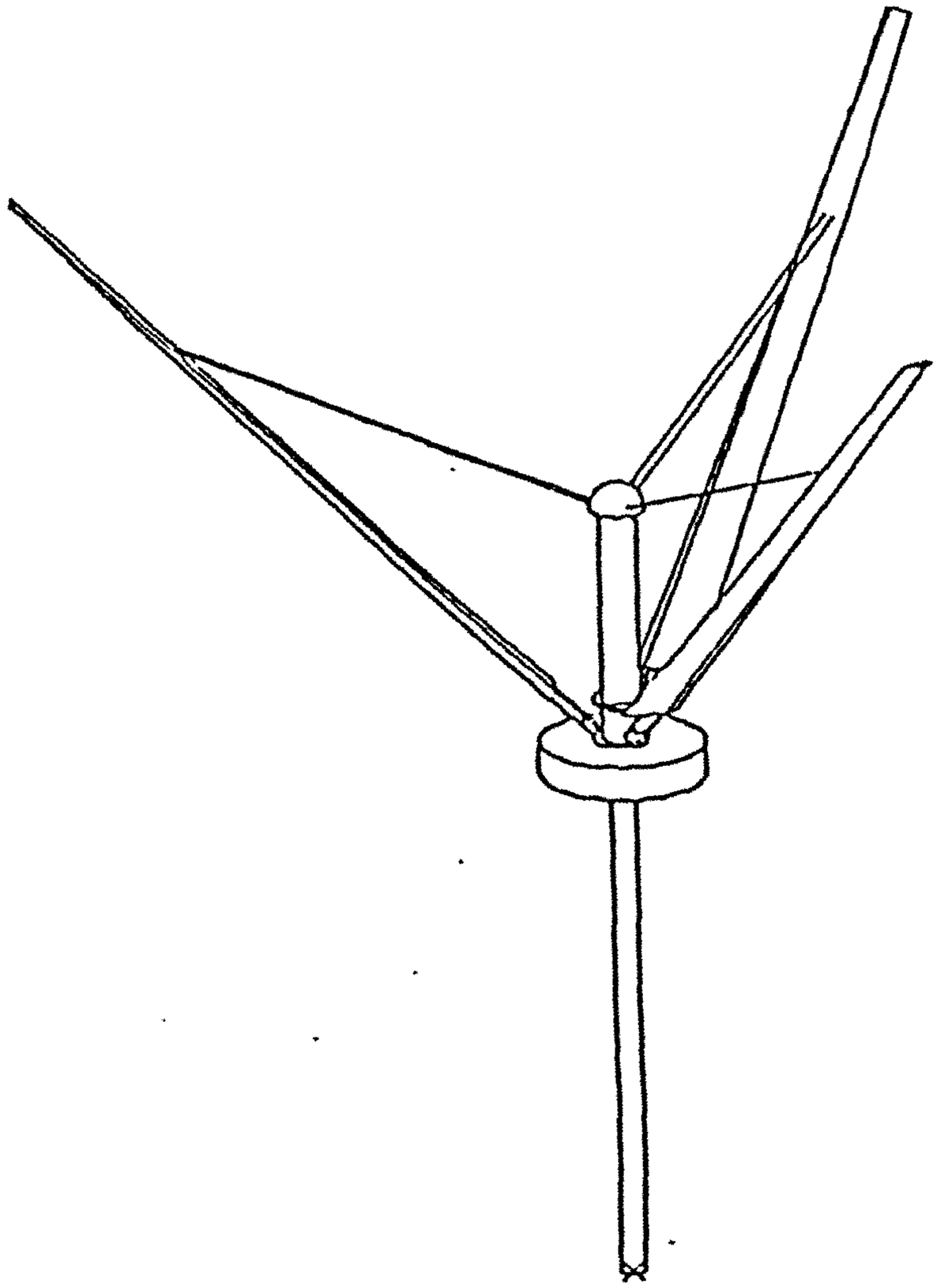

Fig. 8 General view of three-bladed 5kW prototype V-VAWT

THE TAYLOR "V" TYPE VERTICAL AXIS WIND TURBINE:

CURRENT STATUS

G.A. Boyle* A.J. Robotham* D.J.Sharpe+ D.A. Taylor*

Paper presented at the Windpower 85 Conference

27 - 30 August 1985

San Francisco, California

+ Department of Aeronautical Engineering, Queen Mary College, University of London, Mile End Road, London EC1 : tel. 01 980 4811

* Alternative Technology Group, Open University, Walton Hall, Milton Keynes, Buckinghamshire, MK7 6AA, UK : tel. 0908 653387

THE TAYLOR 'V' TYPE VERTICAL AXIS WIND TURBINE: CURRENT STATUS

G.A. Boyle, A.J. Robotham*, D.J. Sharpe#, D.A. Taylor*

*Alternative Technology Group, Open University, Milton Keynes, MK7 6AA, UK
#Dept. of Aeronautical Engineering, Queen Mary College, London University, London, UK

ABSTRACT

The paper describes the current status of the Taylor 'V' Type Vertical Axis Wind Turbine (VAWT), which was first described at the 1983 ISES Solar World Congress in Perth, Australia. The turbine which resembles the letter "V", has an inherent simplicity and a number of innovative features which could lead to an inexpensive machine, both in terms of capital and maintenance costs.

An aerodynamic performance prediction model, VAWTTAY6, for this wind turbine has been developed and enhanced, and the effects of certain parameter changes on overall machine performance are compared. The results show that power coefficients in excess of 0.30 are achievable. The turbine is also self-starting even at relatively low solidities.

Wind tunnel test results are presented for models with two blades, which match closely the values predicted by VAWTTAY6. Experiments on a V-VAWT model with blades which have variable pitch tips have also been carried out and their effects on performance is discussed. An experimental 8.8 metres diameter prototype is being designed and is described.

INTRODUCTION

Wind energy promises to be one of the first of the renewable energy sources to be cost-competitive with conventional fuels, but to fulfill this promise, wind turbines will need to be reliable and low in cost. The turbine that forms the basis of this paper has been developed with these factors very much in mind.

Figure 1 shows a number of cross-flow vertical axis wind turbine (VAWT) configurations conceived by Derek Taylor at the Open University, and for which international patents are pending. The configurations are broadly similar and the common feature is that the rotor consists of straight blades, inclined at angle θ, from the vertical and attached by one end to the vertical shaft. Each of the configurations operates in the same manner as a conventional Darrieus VAWT, and when rotating resemble a cone, (or twin cones point to point, in the case of "X" VAWTs).

However, whilst all these turbines are under consideration, research has so far centred on the "V" type VAWT (Figure 1b) with two or three blades. The innovative V-VAWT (Fig. 2) consists of a rotor comprising two or three blades in the form of a "V", supported by bracing cables from a central pylon, is mounted on a short, stocky sub-tower which need be no more than about 3-4 metres in height whatever the size of the turbine. The blades are straight and untwisted, but they can be tapered. Aerodynamic control devices such as spoilers and rotatable tips can be easily employed. This simple arrangement avoids the use of heavy cross arms or curved blades and a tall tower, yet retaining all the advantages of vertical axis wind

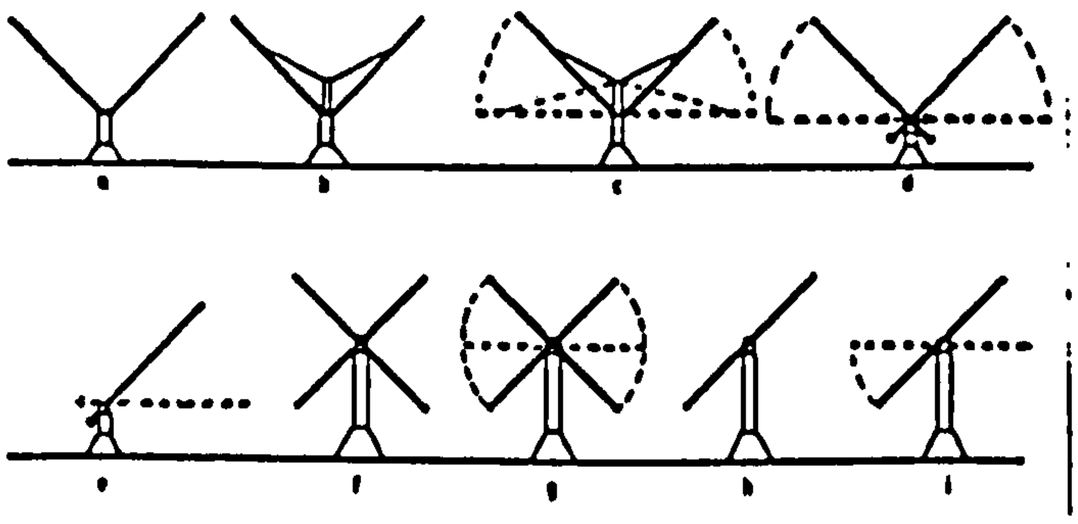

FIG. 1 VARIOUS "V" AND "X" TYPE CONFIGURATIONS UNDER CONSIDERATION.

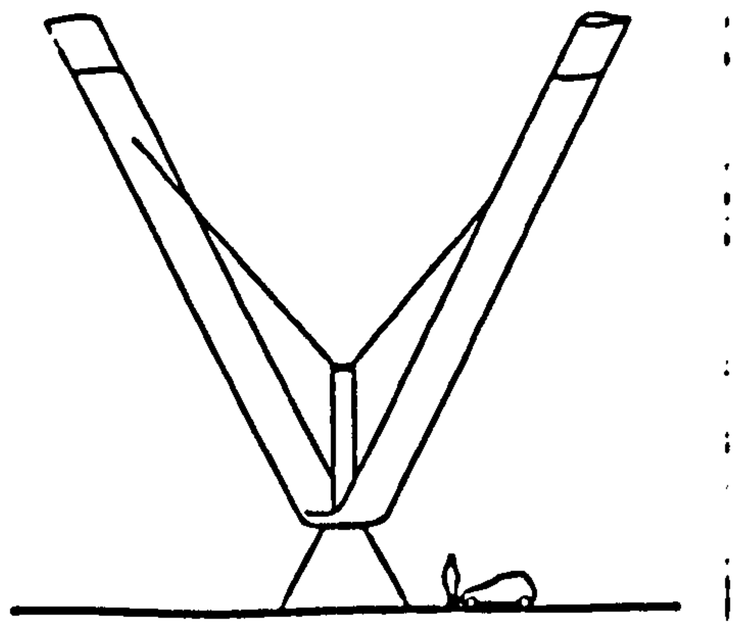

FIG. 2 V-VAWT WITH 2 BRACED BLADES.

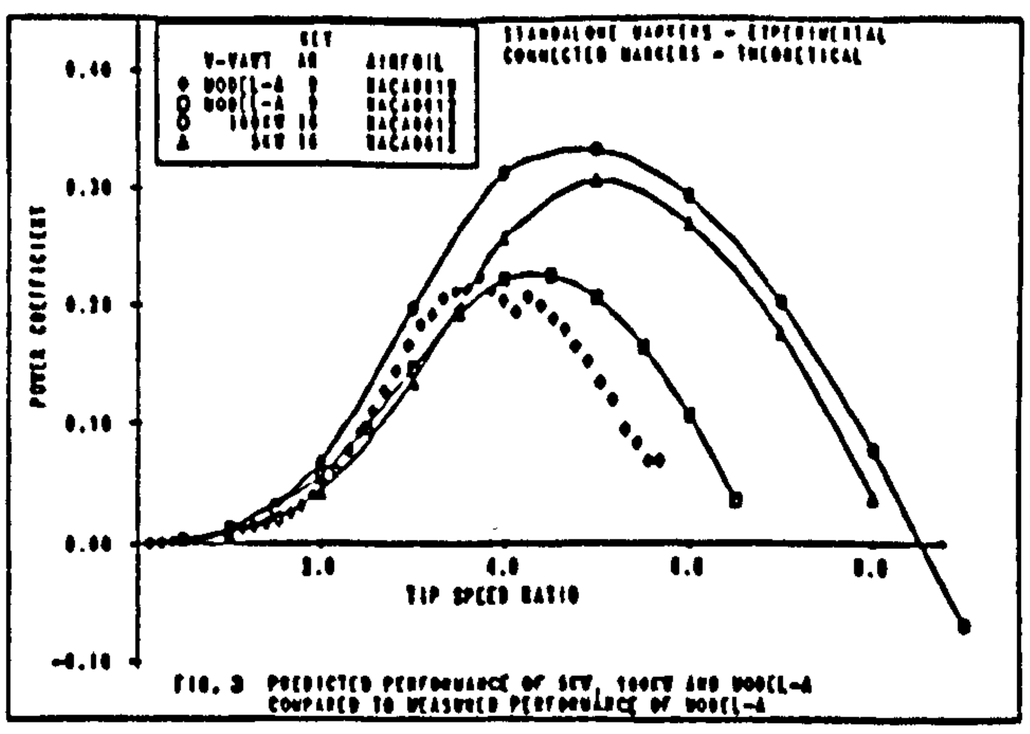

.FIG. 3 PREDICTED PERFORMANCE OF 5kW, 100kW AND MODEL-A COMPARED TO MEASURED PERFORMANCE OF MODEL-A.

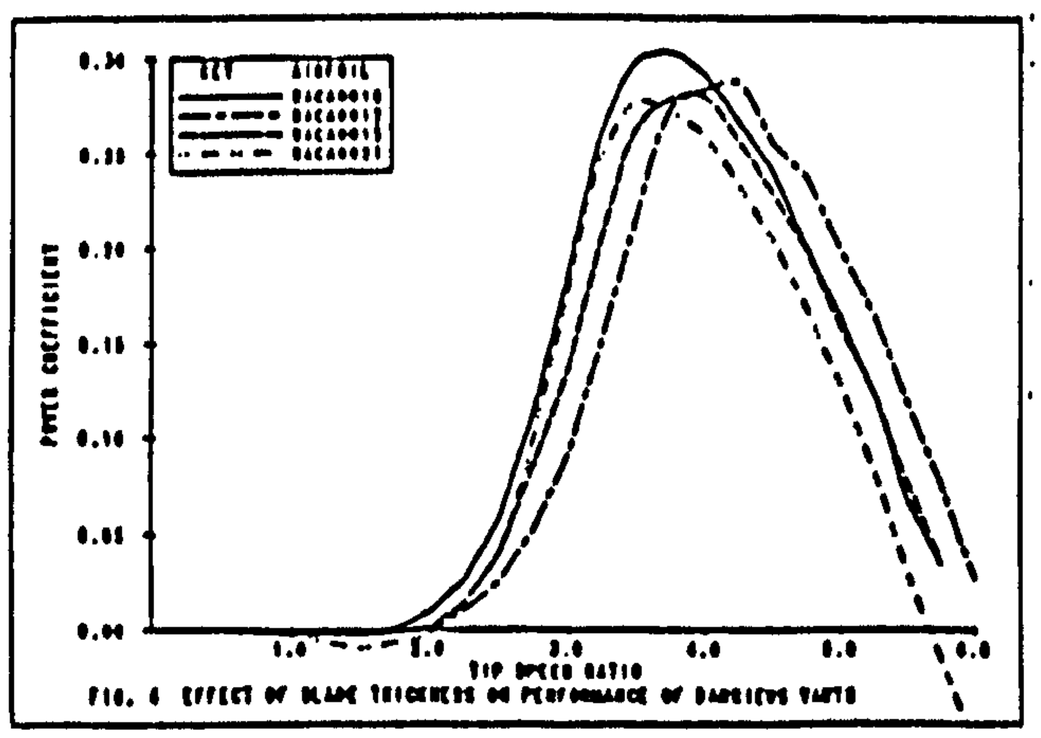

FIG. 4 EFFECT OF BLADE THICKNESS ON PERFORMANCE OF DARRIEUS VAWTs (MEASURED).

turbines, such as ground mounted transmission and generator, and the lack of need for a yawing mechanism. Blades can be raised and lowered from hinges at the root making erection, inspection and maintenance relatively simple. The bulk of the rotor swept area is located in the higher wind speed zone and the turbine produces a high starting torque.

For a given swept area the V-VAWT has longer blades than horizontal axis wind turbines (HAWTs) (though shorter than for a Darrieus), but the blades of a horizontal axis wind turbine system account for only a small proportion of overall cost and it is expected that the cost of the longer blades in the V-VAWT will be more than offset by savings in the tower design. Blade weights on the other hand need be no heavier because of the method of support. Blade manufacturing techniques are similar to, but simpler than those employed on HAWTs because of the lack of twist.

For small machines the ability to fold the blades like an umbrella will allow the whole rotor to be assembled in the factory complete and later unfolded on site. For the largest machines the blades may be constructed and transported in sections for assembly at the site. This is feasible because the bracing cables put the blades into compression which greatly simplifies the form of the required joint.

AERODYNAMIC PERFORMANCE

To determine the aerodynamic performance of the V-VAWT a theoretical computer model, VAWTTAY6[1] has been developed and enhanced. This model is based on the author's extended multiple streamtube theory [2].

The theory is a Double Actuator Disc Model, which includes a dynamic stall analysis, flow curvature effects and flow expansion. It uses aerofoil data for the NACA 0012 aerofoil profile spread over a range of Reynolds Numbers from 40000 to 3 million. For each blade element the Reynolds Number is calculated and suitable aerofoil data is chosen.

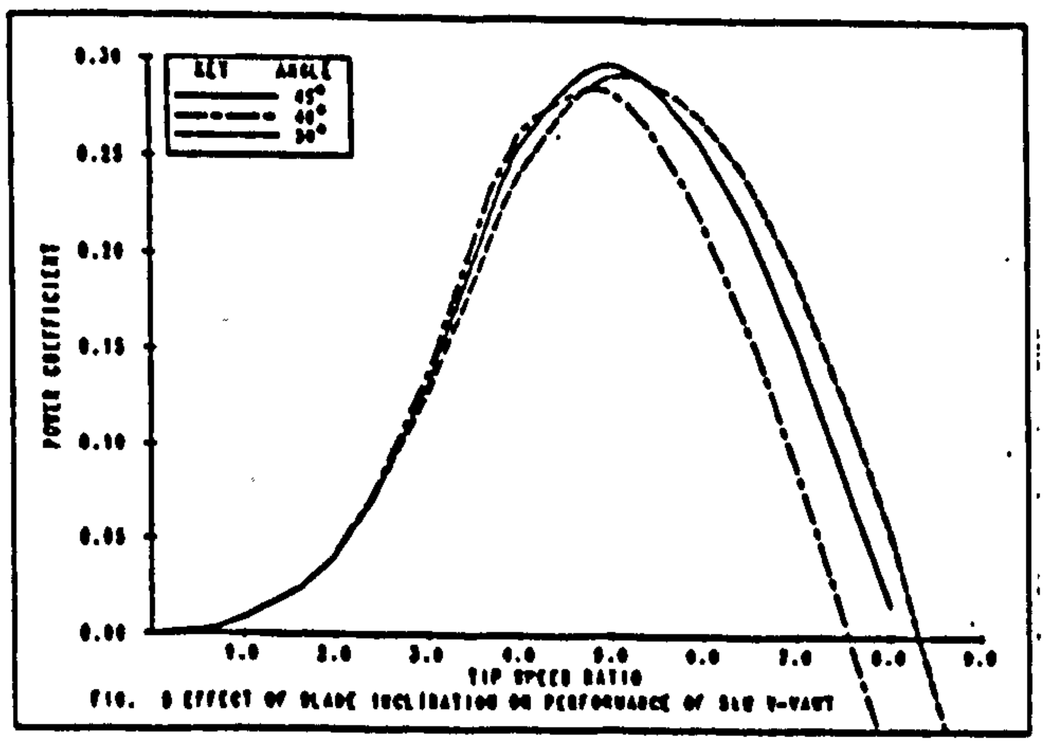

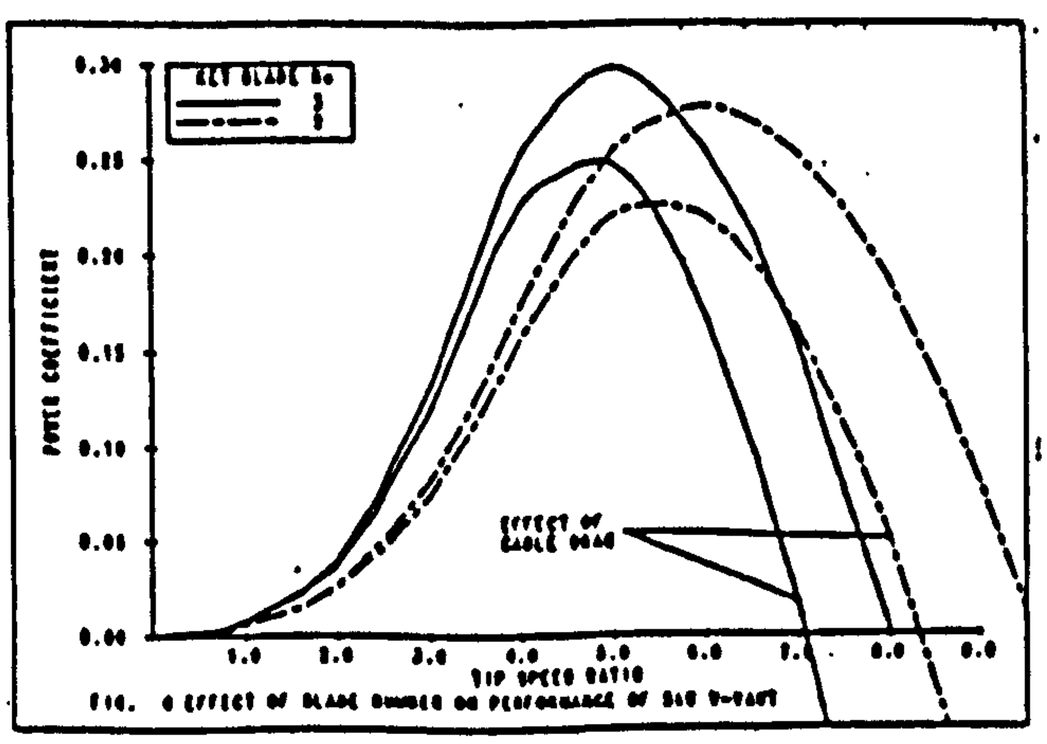

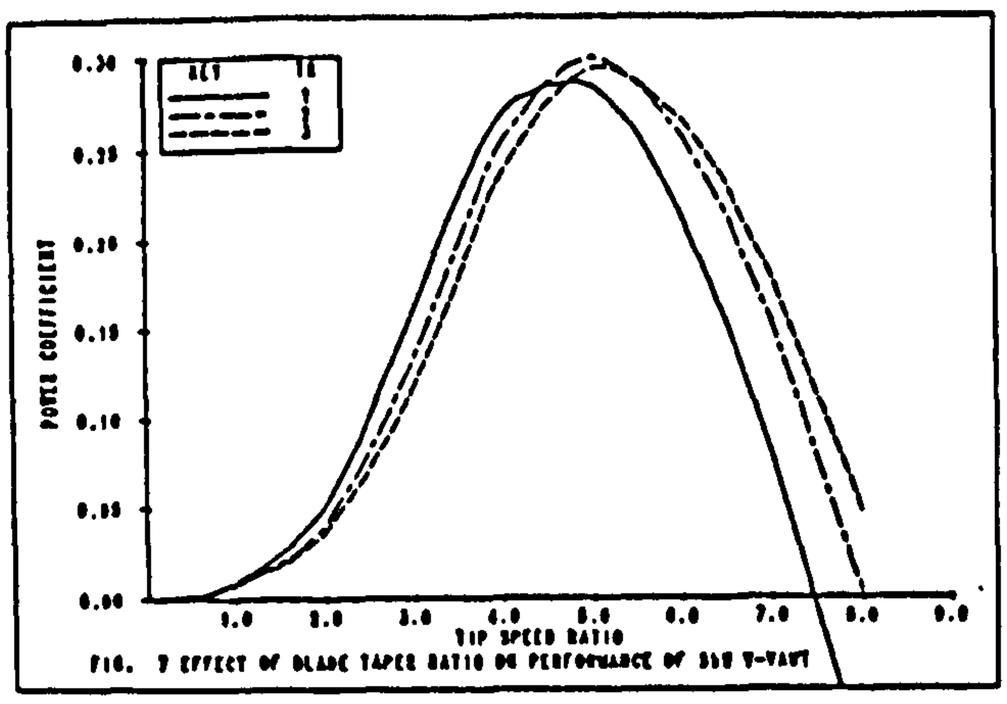

FIG. 7 EFFECT OF BLADE TAPER RATIO ON PERFORMANCE OF 5kW V-VAWT.

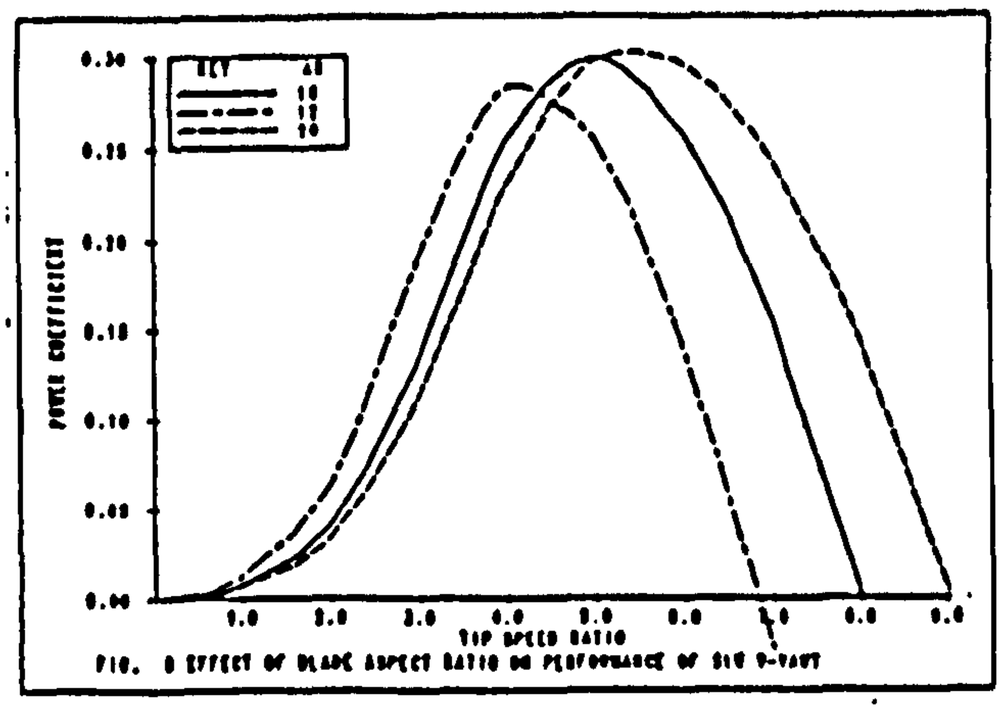

FIG. 8 EFFECT OF BLADE ASPECT RATIO ON PERFORMANCE OF 5kW V-VAWT.

The computer model allows for variations of blade inclination, blade taper, full and partial span blade pitch angle (and twist) and tangential offset. The program was used to predict the performance characteristics of a wind tunnel model V-VAWT (Model A). Model A had two 500mm long untapered blades of 60mm chord and an aspect ratio of nine. Each blade was held at an inclination of 45 degrees from the vertical by a pair of cables attached 120mm from the tip. The blades had a NACA 0018 aerofoil cross section for both structural and aerodynamic reasons. Figure 3 compares the theoretical and experimental power coefficient curves for Model A.

The difference between the two curves is due primarily to the different thickness of the aerofoils used on the physical and theoretical models. The effect of aerofoil thickness on the CP-λ curve of VAWTs was previously observed during experiments with Darrieus VAWTs [1] and [3] and shown in Figure 4. NACA 0018 aerofoil data is currently being compiled into the format suitable for VAWTTAY6.

The well established acceleration technique was used to measure rotation speed, torque and power. The model V-VAWT was tested in a wind speed of 13 m/s at the end of a blow-down wind tunnel at Queen Mary College and the test results were corrected for cable drag bearing friction and tunnel blockage.

The wind tunnel test results were regarded as encouraging and confirmed the use of the model as a design tool. During these wind tunnel tests the V-VAWT demonstrated a high starting torque. This was predicted by VAWTTAY6 and represents a major advantage over existing low solidity VAWTs, enabling stand-alone operation in remote sites.

PARAMETRIC STUDY

In order to obtain an idea of the optimum parameters for the V-VAWT, a study was undertaken with the VAWTTAY6 model to establish the effects on performance of changing the blade inclination angle, number of blades, blade taper, tangential offset and aspect ratio. Figures 5 to 8 show the effects of these parameter changes on the performance of a V-VAWT with 5.5 metre long blades.

AERODYNAMIC CONTROL

As with other wind turbines the V-VAWT requires some means of aerodynamic control for power or overspeed regulation. The V-VAWT can however utilise existing aerodynamic control mechanisms currently employed on HAWTs, and one such device that is being examined for utilisation on the V-VAWT is that of partial span pitch control [4].

A further wind tunnel model (Model B), Figure 9, was constructed with two untapered 665mm long blades of 80mm chord. Each blade was held at an inclination angle of 45 degrees by a pair of cables attached 115mm from the tip. For strength, the blades had a NACA 0025 aerofoil cross section. Additionally, each blade had a moveable tip portion measuring either 5%, 10% or 15% of the blade area. The pitch angle of each portion was adjustable and could be pre-set with either positive, 'nose-in' pitch or negative 'nose-out' pitch. Using this model it was possible to study the effect of the variation of both tip pitch and area on overall performance.

The results of some of these wind tunnel tests are plotted in Figures 10 and 11, and show the manner in which the performance is affected by tip pitch and blade area ratios of the moveable tip portion.

Predictions of turbine performance for different tip pitch positions have been derived from VAWTTAY6 using NACA 0012 aerofoil data (data for the NACA 0025 section has not yet been compiled for use with VAWTTAY6). Whilst it is not possible to match these predictions to the test results because of the different aerofoil sections, VAWTTAY6 has demonstrated the effect of tip pitch and area on the performance of Model B.

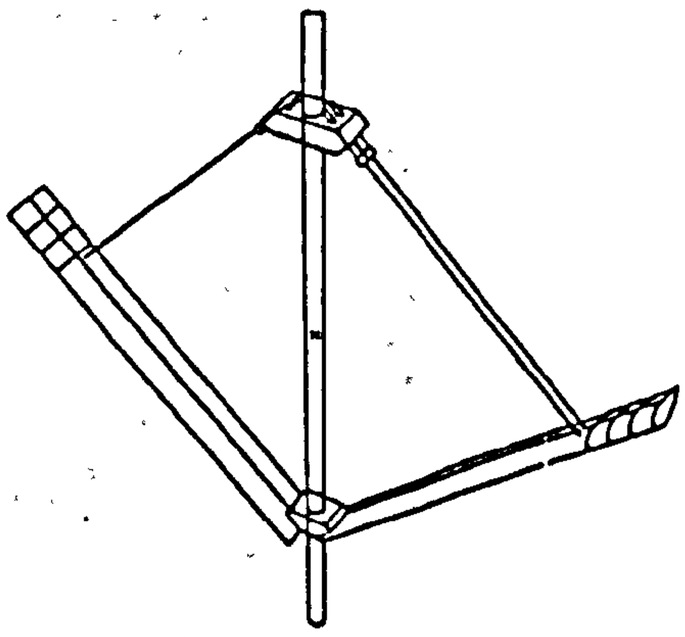

FIG. 9 MODEL-B: WIND TUNNEL MODEL WITH PITCHING TIPS.

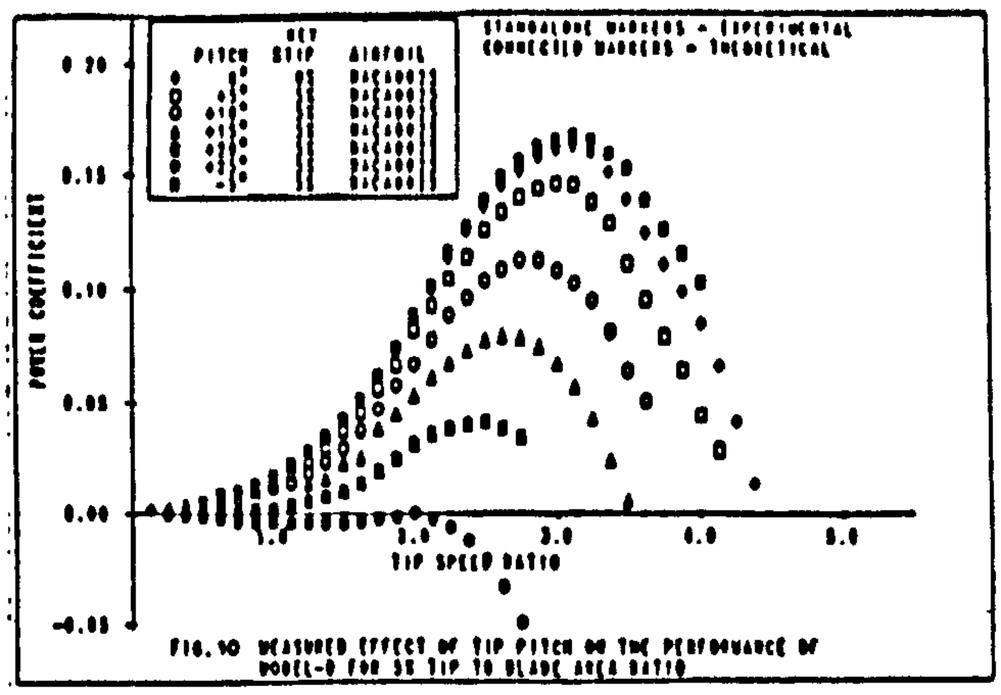

FIG. 10 MEASURED EFFECT OF TIP PITCH ON THE PERFORMANCE OF MODEL-B FOR 5% TIP TO BLADE AREA RATIO.

As can be seen, a moveable tip of just 5% blade area with a positive pitch of 25 degrees, seems to be suitable for overspeed control. It is also possible to achieve a small increase in starting torque with small negative pitch of the tip portion.

T-BRAKE

In addition to the partial span study, another somewhat simpler means of aerodynamic control, which avoids discontinuities in the structural integrity of the blades is being investigated. This consists of a control surface set across the tip of the blade like a letter 'T', and has been dubbed the 'T'-brake. This control device, shown in Figure 12, is capable of acting in both passive and active modes of operation and is the subject of patent applications.

Under normal operation the control surface is maintained in line with the chord of the blade, and in the control mode the surface rotates about an axis set at 90 degrees to the blade surface. In order to avoid the possibility of stall flutter, the T-brake control surface has a slender body planform, allowing deployment angles approaching 40 degrees without stall occurring. A number of planforms, including slender delta are being evaluated.

The T-brake is to be employed on a free air prototype, initially as a passive overspeed control device activated by centrifugal force acting against a spring located at the hub, and connected to the T-brake via a cable linkage.

FREE AIR PROTOTYPE V-VAWT

An experimental prototype, with a swept area of 19 square metres and 5.5 metre long blades, has been designed initially in a two bladed configuration for variable speed operation (Figure 13). It is to be tested on the Alternative Technology Group's wind turbine field test facility later this year. These blades have been designed in collaboration with Gifford Technology Ltd and are being manufactured at their own cost.

Each composite blade, illustrated in Fig. 14, has a taper ratio of 2 and an aspect ratio of 16 and utilises a novel spar-less form of construction. This has resulted in a very lightweight type of blade, each with a mass of 18 kilogrammes.

The root end of each blade is attached via a pivot joint to the rotor hub, and the blade angle is locked via a pin joint between hub/blade struts and the blade root. This pin is removable, allowing the blade to be tilted down for inspection, removal or installation. It also allows the blade to be folded up like an umbrella to facilitate transportation. Each rotor blade is supported at the 70% spanwise position by a pair of cables, which are attached to a central pylon.

The design of this prototype is based around an existing guyed mast and incorporates an internal tower spindle with an external shaft tube. A bearing is located at the top of the internal tower spindle and at the rotor hub. Shaft power is transmitted by a 2 stage belt drive to a 5 kilowatt alternator.

The predicted performance of the free air prototype is shown in Figure 3 together with that for a 100kW sized V-VAWT, and as can be seen, power coefficients in excess of 0.3 are anticipated for full scale machines.

CONCLUSION

Recent wind tunnel tests of the Taylor 'V' type vertical axis wind turbine have shown the aerodynamic performance model to be a useful and valid design tool, and that further tests have demonstrated that both overspeed control and power regulation can be achieved by variation of tip pitch.

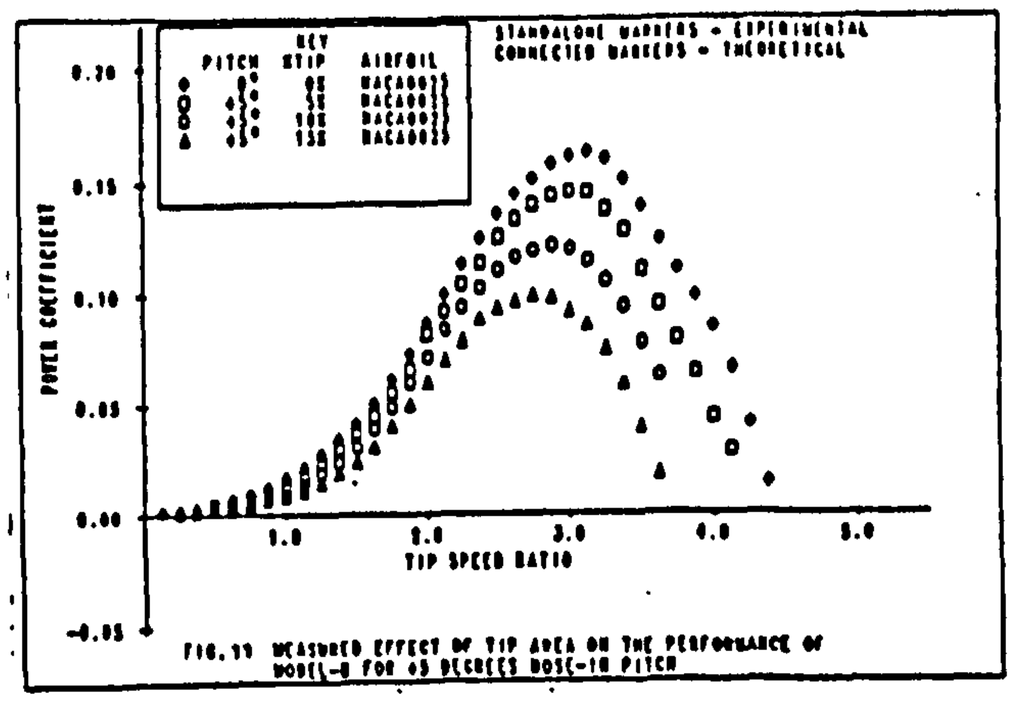

FIG. 11 MEASURED EFFECT OF TIP AREA IN THE PERFORMANCE OF MODEL-B FOR +5% NOSE-IN PITCH.

The concept is continually being refined and the free air research prototype will be used as a test bed to develop the turbine further.

ACKNOWLEDGEMENTS

The authors wish to express their thanks to the technical staff of the Open University and Queen Mary College, Scott Forrest and Neville Kolb who made the wind tunnel models, Sally Boyle and Richard Hearne for graphic support in preparing the poster, Gifford Technology for a refreshingly open minded and generous approach to this project, also to Jim Frederickson and Liz Hainstock of the Open University, the Open University Research Committee and the Science and Engineering Research Council.

REFERENCES

1. Sharpe D.J. and Taylor D.A.: The Aerodynamic Performance of the Vee type Vertical Axis Wind Turbine. 7th BWEA Wind Conference, Oxford, 1985.

2. Sharpe, D.J.: Refinements and developments of the multiple streamtube theory for the aero-dynamic performance of vertical axis wind turbines. 6th BWEA Wind Energy Conference, Reading, 1984.

3. Sharpe, D.A.: Wind Tunnel Performance Tests on Small Darrieus Wind Turbine Models. Windpower '85 Conference, August, 1985.

4. Robotham, A.J., Sharpe, D.J., Taylor, D.A. and Boyle, G.A.: Further Developments in the Taylor Type VAWT Concept. INTERSOL85, Montreal, 1985.

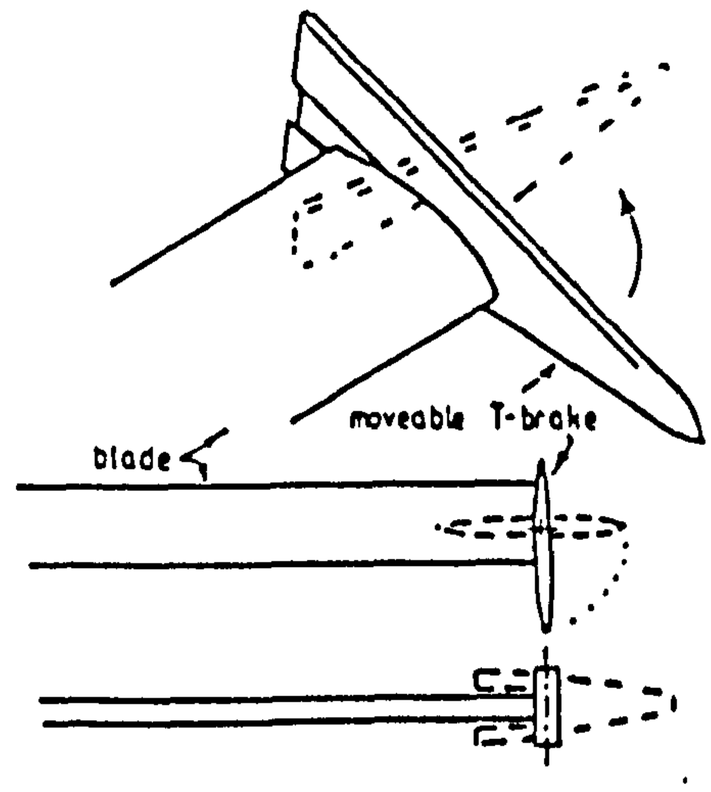

FIG. 12 T-BRAKE AERODYNAMIC CONTROL DEVICE

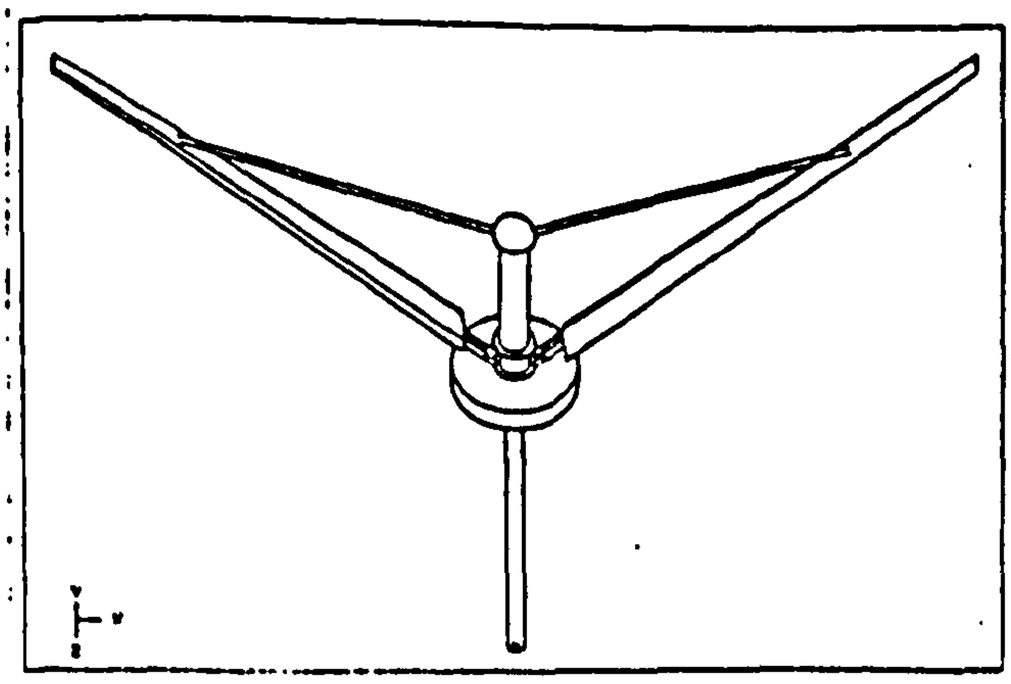

FIG. 13 DESIGN FOR EXPERIMENTAL FREE AIR V-VAWT

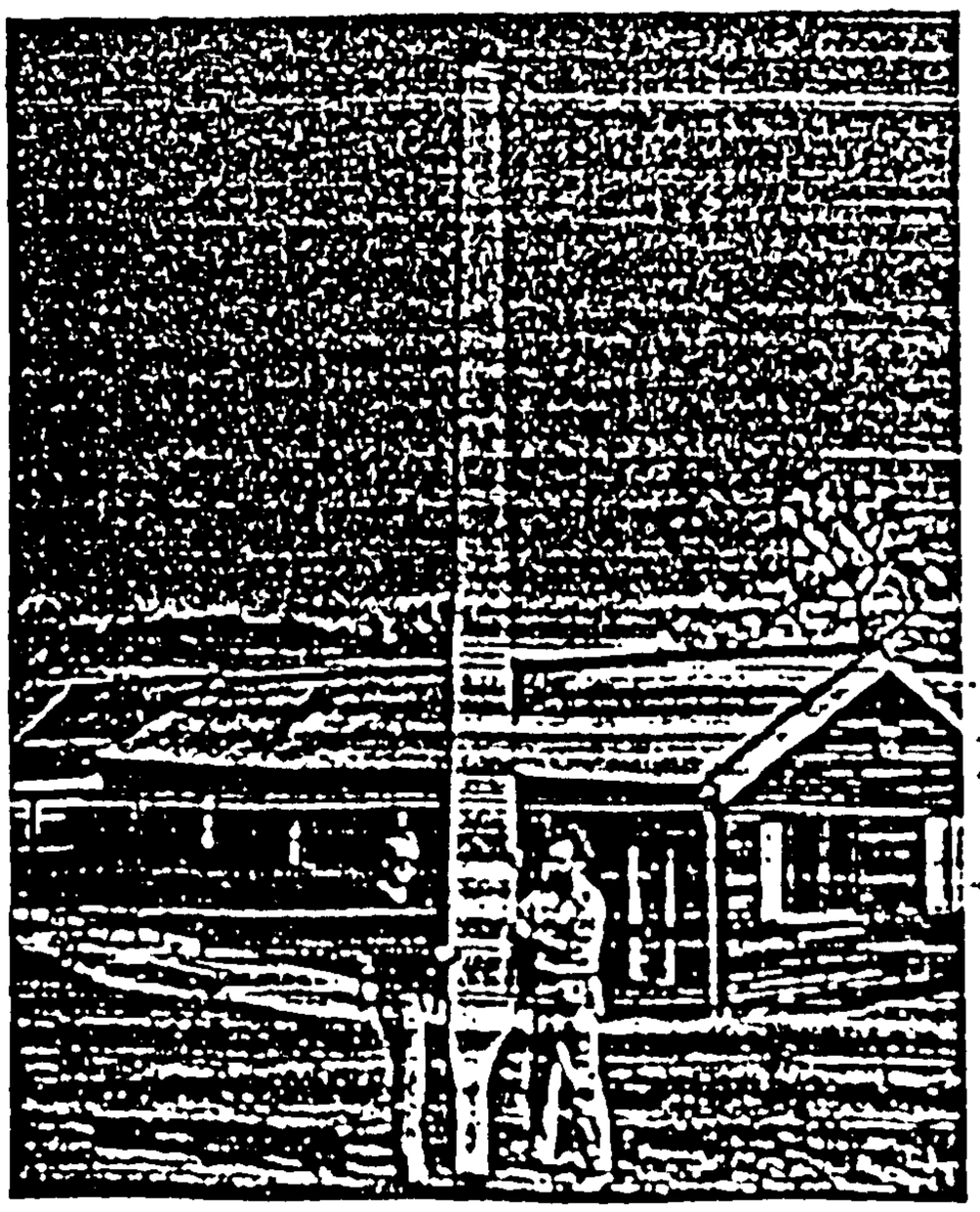

FIG. 14 5.5 METRE V-VAWT BLADE MANUFACTURED BY GIFFORD TECHNOLOGY

THE AERODYNAMIC CONTROL OF THE 'V' TYPE VERTICAL AXIS WIND TURBINE BY BLADE TIP CONTROL

by

A.J. Robotham+ and D.J. Sharpe++

+Appropriate Technology Group, The Open University,
Walton Hall, Milton Keynes, MK7 6AA, U.K.

++Dept. of Aeronautical Engineering, Queen Mary College,
London University, Mile End Road, London, E1 4NS, U.K.

Presented at the Eighth BWEA Conference, Cambridge, March 1986.

SYNOPSIS

This paper presents results of wind tunnel tests carried out on a small V-type Vertical Axis Wind Turbine (V-VAWT). This model wind turbine was specifically designed to study the effect of tip area and tip pitch on the performance of this novel vawt. The results have demonstrated that tip pitch is highly suitable for overall control of the V-VAWT and that tip areas as little as 5% of the total blade area could provide both power regulation and overspeed control. While it has not been possible to match the predicted performance data directly to these tests results, the computer model VAWTTAY6 can be used with some confidence to predict the performance of larger sized V-VAWTs.

1 INTRODUCTION

The V-type Vertical Axis Wind Turbine, conceived by Derek Taylor at The Open University, has been described at a number of international wind energy and solar energy conferences [1-4].

The development of the V-VAWT concept has concentrated on the enhancement of Sharpe's aerodynamic performance prediction model VAWTTAY6, the verification of this model with data from wind tunnel tests of small V-VAWTs and the design and construction of a 5kW free-air wind turbine. The 5kW V-VAWT has recently been erected on the Appropriate Technology Group's field test facility at The Open University, but only preliminary evaluation of the performance of this machine has been conducted.

This paper will consider the aerodynamic control methods that have been perceived as suitable for rotor power control and overspeed protection of a medium sized V-VAWT, and will compare the predicted performance and measured performance of a small V-VAWT with pitchable blade tips, Fig 1.

2 AERODYNAMIC PERFORMANCE PREDICTION

The aerodynamic performance of the V-VAWT is modelled using the computer program VAWTTAY6, which embodies Sharpe's extended multiple streamtube theory [5]. The predictions using VAWTTAY6 have been verified by wind tunnel tests with model V-VAWTs undertaken at Queen Mary College, London [2].

3 POWER REGULATION AND OVERSPEED CONTROL

All wind turbines, whether they be of horizontal axis or vertical axis configuration, require some form of power regulation and overspeed protection, either actively or passively activated and the V-VAWT is

no exception.

Blade tip control has been extensively used on horizontal axis wind turbines of all sizes and has proven to provide power regulation and overspeed control. However the only vertical axis machine known to the authors employing such control is the recently developed Westwind 75kW wind turbine; an 'H'-type VAWT with two blades of fixed pitch but with moveable tips at both ends of each blade.

Blade tip control is also considered highly suitable for the V-VAWT, but the tip device known as the T-brake [4] has a number of structural advantages and because of its simplicity is favoured for the 5kW free-air V-VAWT. However, in order to assess the potential of tip pitch control, a wind tunnel sized V-VAWT with moveable tip portions was constructed and its performance evaluated at Queen Mary College.

3.1 Wind tunnel test model and testing technique

A two-bladed model V-VAWT of tip diameter 940mm was constructed to assess the potential of tip pitch control. Each blade was 615mm in length, with a uniform chord of 80mm. For strength the blades were of a NACA0025 aerofoil cross section and were made from English Ash encapuslating a high tensile aluminium spar for rigidity. Each blade was held to the hub at the 30% chord, inclined at 45 degrees to the vertical and supported by a pair of cables attached 115mm from the tip.

Additionally, each blade had three moveable tip portions, the area of each measuring 5% of the total blade area. The pitch angle of each tip portion was adjustable and could be pre-set with either positive, 'nose-in' pitch or negative, 'nose-out' pitch. The position of each tip portion was locked by two grubscrews that were accessible through the leading edge. During tests, the access holes were filled with plasticene and covered with vinyl tape to restore the leading edge profile. Using this model, the effect of variation of tip pitch on overall performance for tip areas of 5%, 10% and 15% of the total blade area on overall turbine performance has been studied.

The model V-VAWT was tested in the blowdown wind tunnel at Queen Mary College using the acceleration method [6], which is a simple and quick method for determining the complete Cp-lamda characteristic of the turbine.

The test results have been corrected for cable drag and bearing friction, both of which were measured separately. Cable drag is the most significant of these parasitic losses and was measured in a manner previously described [2]. Corrections for wind tunnel blockage have not been included because the experiments were conducted in an open jet tunnel.

The rotor would only accelerate to a rotational speed where the torque being developed by the turbine was equal in magnitude to the parasitic

drag losses from the cables and the bearings. In order to obtain performance data for rotational speeds greater than this equilibrium speed, it was necessary to drive the turbine via a friction contact with an electric motor. When the motive power was released, the deceleration of the turbine was measured. This technique allowed measurement of rotor torque over a greater range of tip speed ratios and tip pitch settings.

All tests were conducted at an average Reynold's Number of approximately 2-300000 which is much lower than the operating Reynold's Numbers of larger-sized, free-air machines. The consequence of testing at such low Reynold's Numbers is discussed below.

3.2 Wind tunnel test results

Some of the results from this series of tests are presented in figures 2-6. Figures 2-4 show how Power Coefficient is affected by changes in tip pitch angle for tip areas of 5%, 10% & 15% of the total blade area. Figure 5 compares the effect of tip area for a pitch setting of +5 degrees.

These results illustrate the effectiveness of tip pitch control as a means of power modulation and overspeed protection. Even a 5% tip area, at pitch angles in excess of +25 degrees, can effectively 'kill' all the power developed by this model wind turbine at all but the lowest tip speed ratios.

Looking again at figures 2-4, it is seen that Power Coefficient is enhanced with small negative (nose-out) pitch angles. From the test results available, a pitch angle of -5 degrees appears to optimise this enhancement. Enhancement of power with small, full-span pitch offsets was noted by Stacey and Musgrove [7] for the 'H'-VAWT, so a similar effect was not unexpected with the V-VAWT.

Figure 6 shows how Torque Coefficient varies with pitch angle for a 5% tip area. It shows the high starting torque that is a feature of the V-VAWT, and illustrates how a small negative pitch offset enhances the turbine performance. Note that the enhancement of developed torque is apparent at all tip speed ratios for a -5 degree pitch angle even at starting.

3.3 Predictions of tip pitch effects

The computer program VAWTTAY6 can be used to predict the effect of tip pitch on the performance of the model V-VAWT. However, it is not possible for these predictions to be matched directly with the wind tunnel results because at present VAWTTAY6 uses NACA0012 static aerofoil data, whereas the wind tunnel model was constructed using the thicker NACA0025 section.

Published aerofoil data for the NACA0025 aerofoil section is scarce, though Sandia Laboratories have published data for this section that has been generated using the Eppler computer code [8]. Despite the fact that this data covers angles of incidence upto 180 degrees for a range of Reynold's Numbers, none of the data presented for this section has been verified by wind tunnel tests. Consequently the authors have not used this aerofoil data for predicting the performance of the model V-VAWT. Low Reynold's Number static aerofoil tests of a NACA0025 section are planned for later this year so that more accurate predictions of performance of can be made using VAWTTAY6.

However, the predictions of Power Coefficient using the NACA0012 aerofoil data show tip pitch effects that are similar to those demonstrated by the wind tunnel tests, Fig 7. The high starting torque developed by the model V-VAWT and the enhancement of torque with small negative, nose-out pitch positions is also predicted by the theory, Fig 8.

As a result of these tests, the performance of larger V-VAWTs using tip pitch control can be predicted with some confidence. Figure 9 shows the predicted performance of the 5kW 3-bladed free-air V-VAWT, that has been described previously [2-4], and the predicted effect of tip pitch for a 5% tip area.

These predictions have been made for operational Reynold's Number of approximately 1500000, and show how the developed power can be destroyed for pitch angles as little as +30 degrees. The effectiveness of a blade tip deployed at a large pitch angle is largely Reynold's Number independent, though the lift, and hence torque, generated by the fixed portion of the blade will generally increase with Reynold's Number. Consequently as the operating Reynold's Number increases, the tip must be deployed at a larger pitch angle to obtain the same net braking effect. The choice of tip size and the pitch angle range through which it is deployed will be crucially dependent upon the operating conditions and the control criterion specified for the machine. At this stage of the V-VAWT development however, blade tip areas of approximately 5% of the total blade area seem appropriate for both power regulation and overspeed control.

3.4 The T-Brake as a control device

The T-Brake offers a number of advantages over pitching tip control: it can be simply mounted at the blade tip without creating any discontinuity in the blade structure; actuation can be of a push-pull nature as opposed to pitching, and the swept area of the turbine is increased by the additional aerofoil surfaces. However, the effect on performance of the T-Brake control surface is very similar to that of the pitching the blade tip and can be predicted with some confidence using VAWTTAY6, Fig 10.

These predictions should be treated with caution though, since they do not account for any flow interaction between the T-Brake and the fixed blade. In its pitched position the trailing edge of the T-Brake will spoil the flow over the outer portion of the fixed blade. It is therefore likely that these predictions may underestimate the braking effect of the T-Brake, but at present it is not possible to quantify this underestimation. The T-Brake should also act as an end plate thus reducing the blade tip losses and so increasing the lift developed by the fixed blade.

4. CONCLUSIONS

Recent wind tunnel tests of a model V-VAWT have shown that the aerodynamic performance of this wind turbine can be modulated with tip pitch control. These tests have demonstrated that both overspeed control and power regulation can be achieved with tip areas as little as 5% of the total blade area. Some enhancement of torque at all operating speeds has been demonstrated by small negative pitch settings. While it has not been possible to match the results exactly to predicted data, the use of the aerodynamic prediction model VAWTTAY6 for development of larger sized V-VAWTs with tip control seems reasonable.

ACKNOWLEDGEMENTS

The authors wish to express thanks to Derek Taylor and Godfrey Boyle of the Open University, Scott Forrest who made the wind tunnel model and the technical staff at Queen Mary College for assistance during testing. Tony Robotham is sponsored by the Science and Engineering Research Council.

REFERENCES

1. D. J. Sharpe and D. A. Taylor, Preliminary investigations into an innovative vertical axis wind turbine. Proc. World Solar Energy Congress, Perth, Australia, 1983.
2. D. J. Sharpe and D. A. Taylor, The aerodynamic performance of the vee type vertical axis wind turbine. Proc. Seventh BWEA Wind Energy Conference, Oxford, 1985.
3. A. J. Robotham, D. J. Sharpe, D. A. Taylor and G. A. Boyle, Further developments in the Taylor 'V' type VAWT concept. Proc. Intersol 85 World Solar Energy Congress, Montreal, Canada, June 1985.
4. G. A. Boyle, A. J. Robotham, D. J. Sharpe and D. A. Taylor, The Taylor 'V' type vertical axis wind turbine: current status. Proc. Windpower 85 Conference, San Francisco, U.S.A., August 1985.
5. D. J. Sharpe, Refinements and developments of the multiple streamtube theory for the aerodynamic performance of vertical axis wind turbines. Proc., Sixth BWEA Wind Energy Conference,

Reading, 1984.
6. D. J. Sharpe, A theoretical and experimental study of the Darrieus vertical axis wind turbine. Research report, School of Mech., Aero. and Prod. Eng., Kingston Polytechnic, October, 1977.
7. G. Stacey and P. J. Musgrove, The effect of fixed pitch offset on a high solidity vertical axis windmill. Proc., Third BWEA Wind Energy Conference, Cranfield, 1981.
8. R. E. Sheldahl and P. C. Klimas, Aerodynamic characteristics of seven symmetrical airfoil sections through 180-degree angle of attack for use in aerodynamic analysis of vertical axis wind turbines. Sandia Laboratories Report, SAND80-2114, 1981.

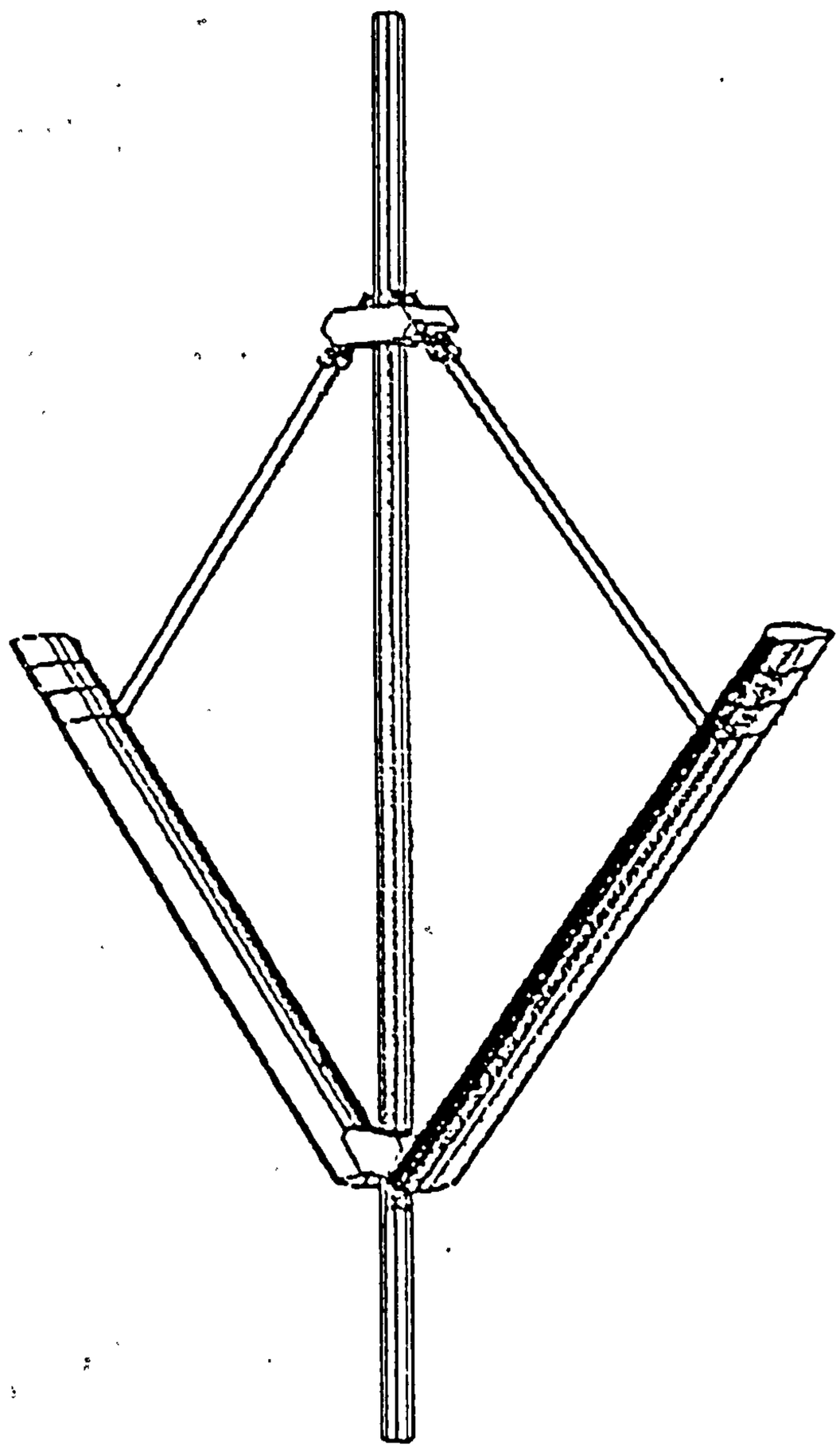

Figure 1: General view of model V-VAWT with pitching tips

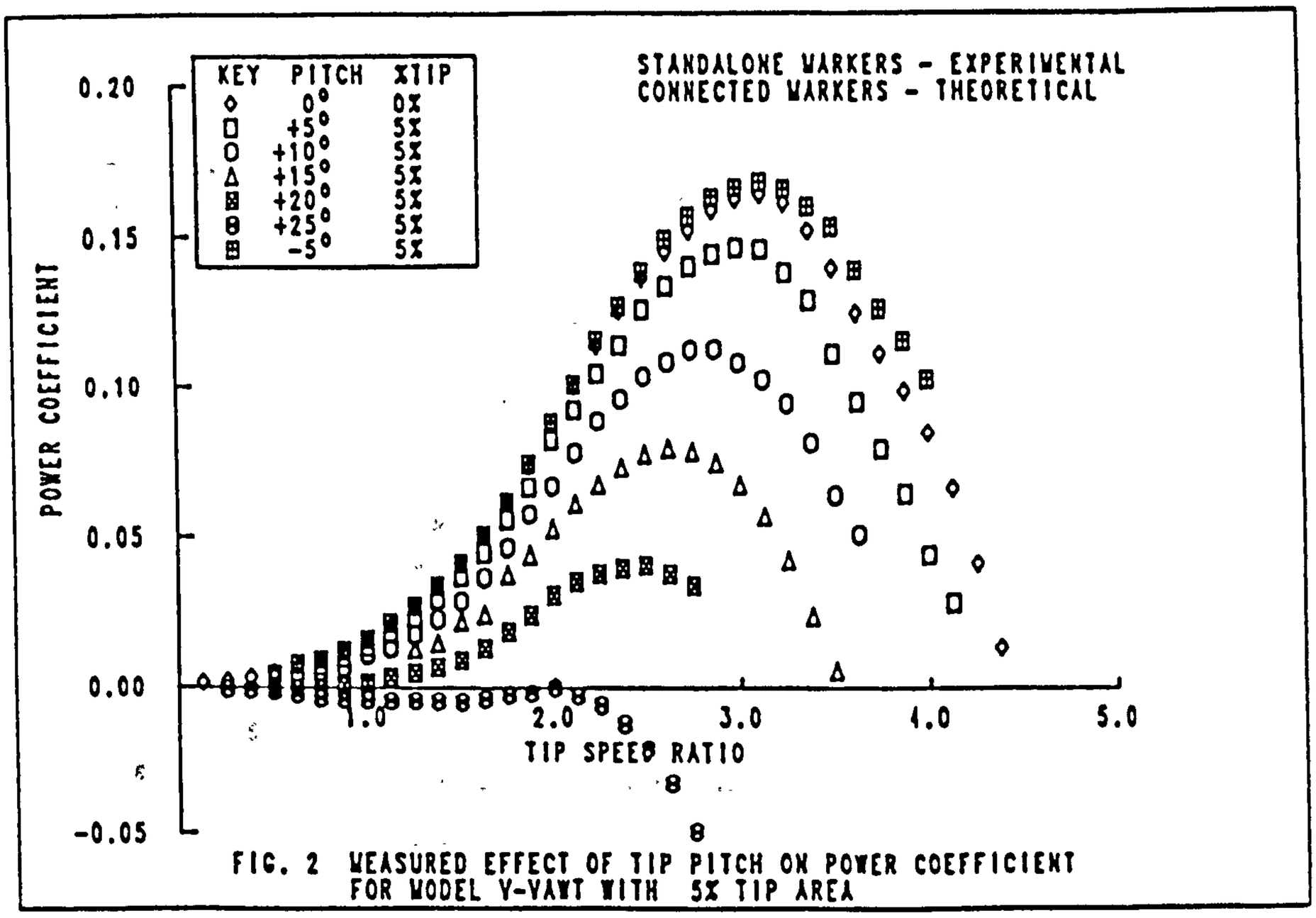

FIG. 2 MEASURED EFFECT OF TIP PITCH ON POWER COEFFICIENT FOR MODEL V-VAWT WITH 5% TIP AREA

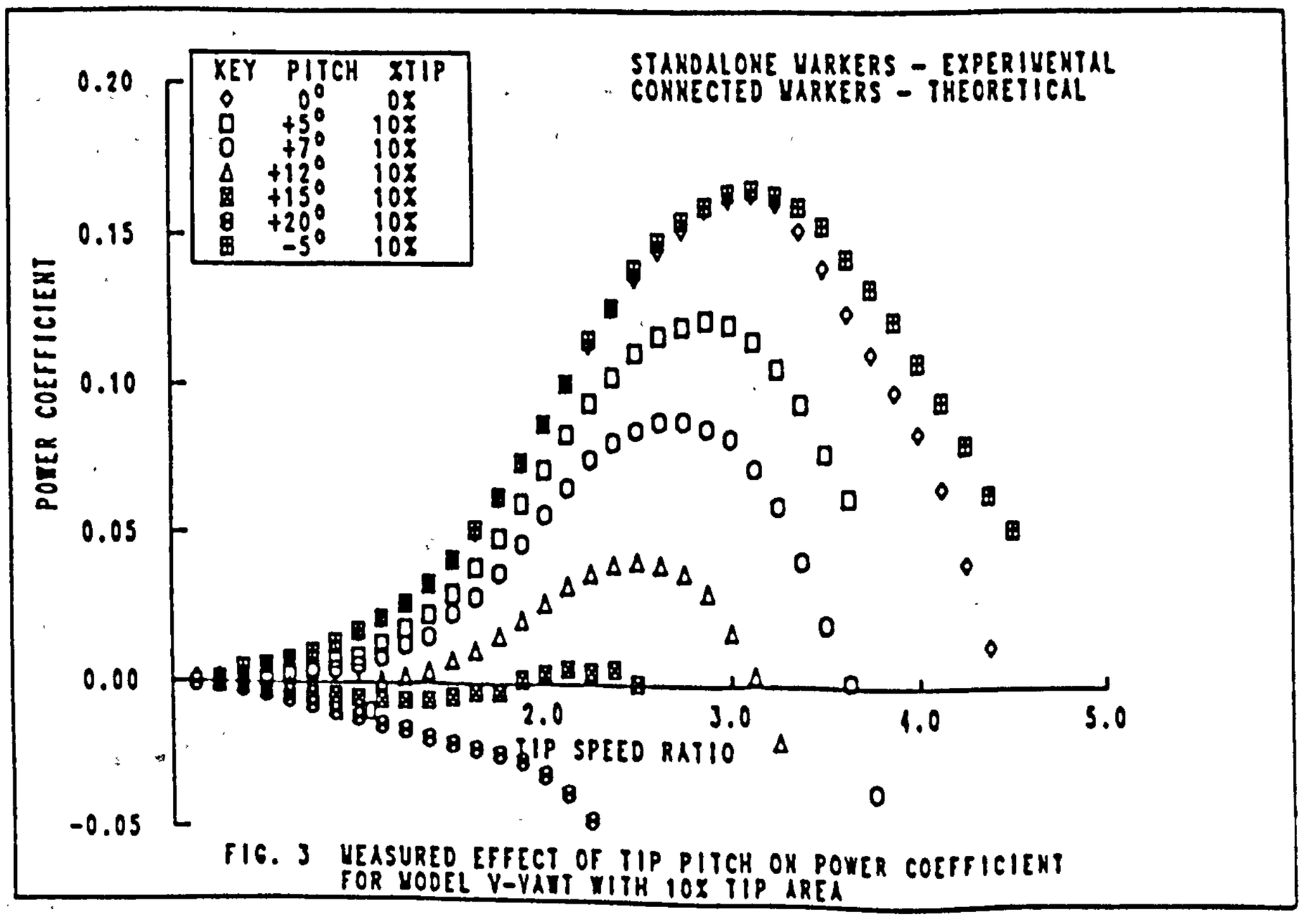

FIG. 3 MEASURED EFFECT OF TIP PITCH ON POWER COEFFICIENT FOR MODEL V-VAWT WITH 10% TIP AREA

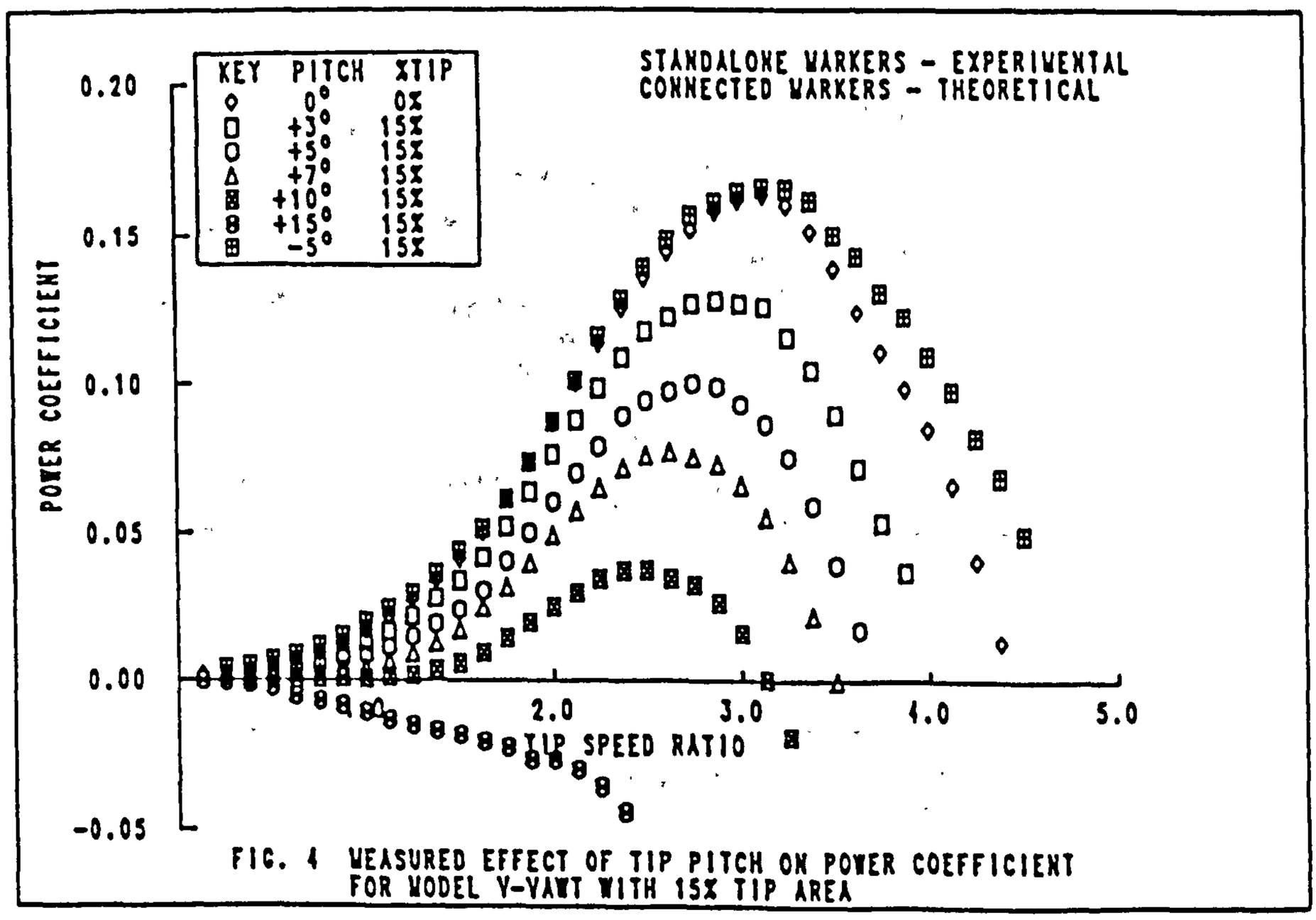

FIG. 4 MEASURED EFFECT OF TIP PITCH ON POWER COEFFICIENT FOR MODEL V-VAWT WITH 15% TIP AREA

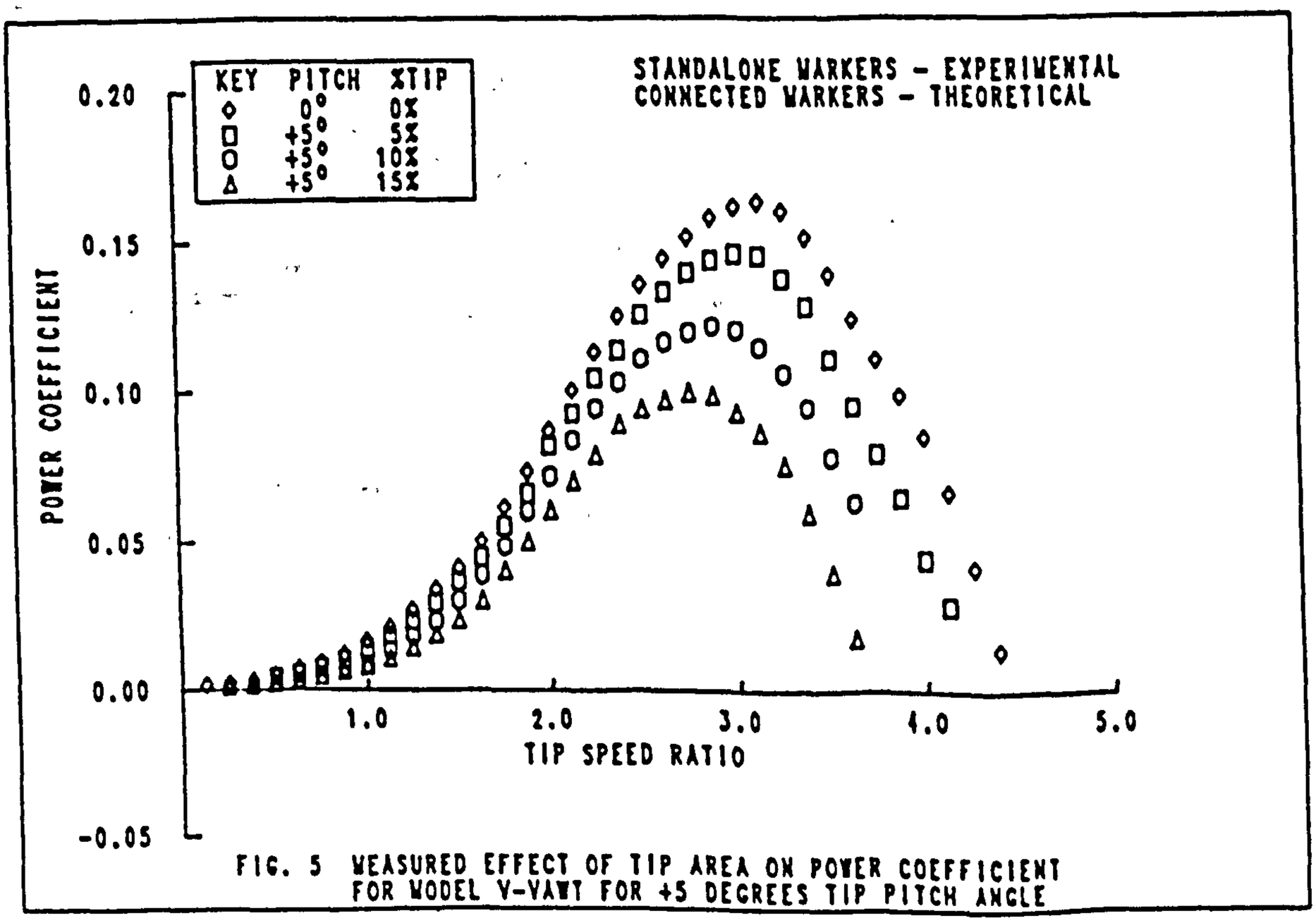

FIG. 5 MEASURED EFFECT OF TIP AREA ON POWER COEFFICIENT FOR MODEL V-VAWT FOR +5 DEGREES TIP PITCH ANGLE

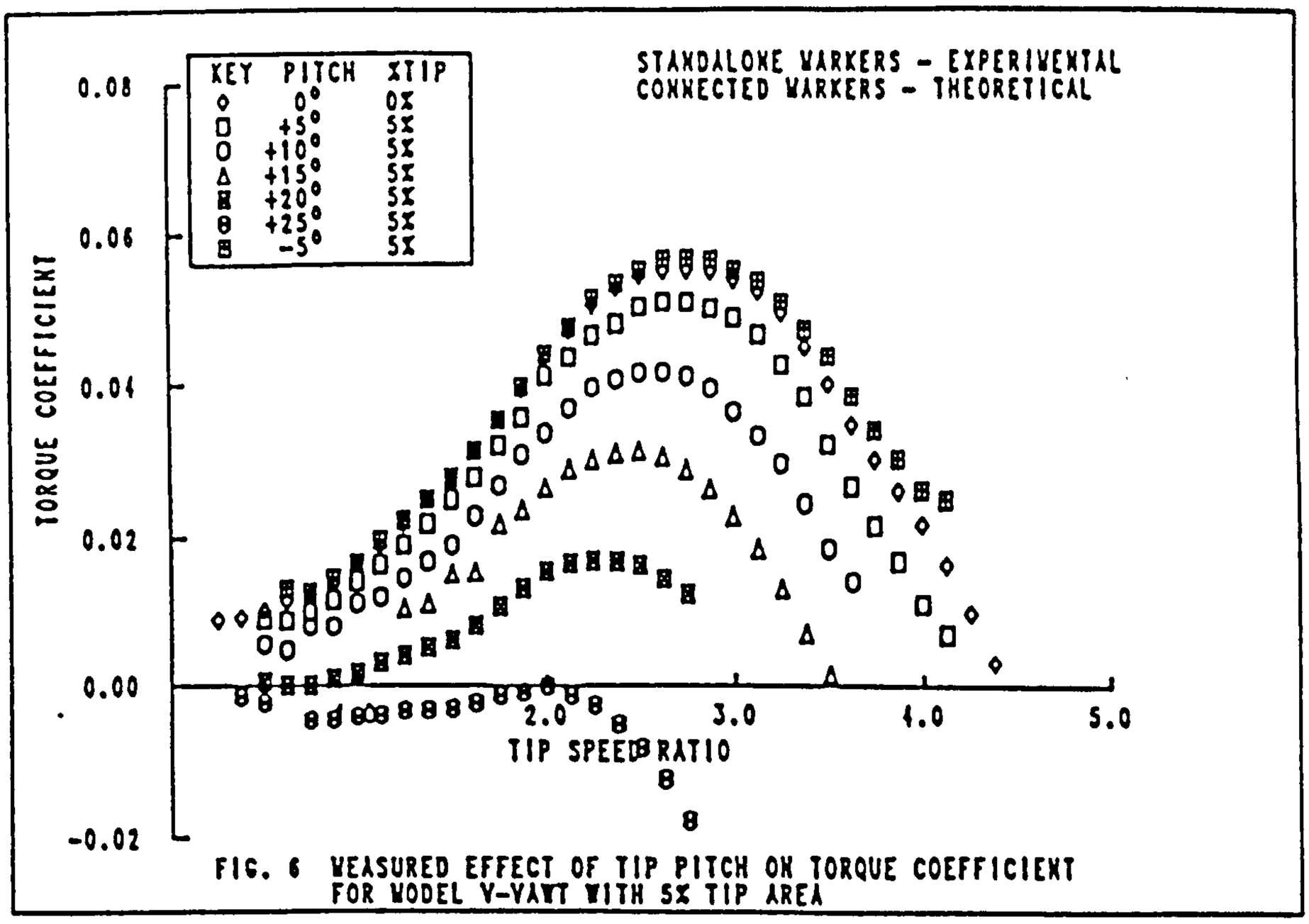

FIG. 6 MEASURED EFFECT OF TIP PITCH ON TORQUE COEFFICIENT FOR MODEL V-VAWT WITH 5% TIP AREA

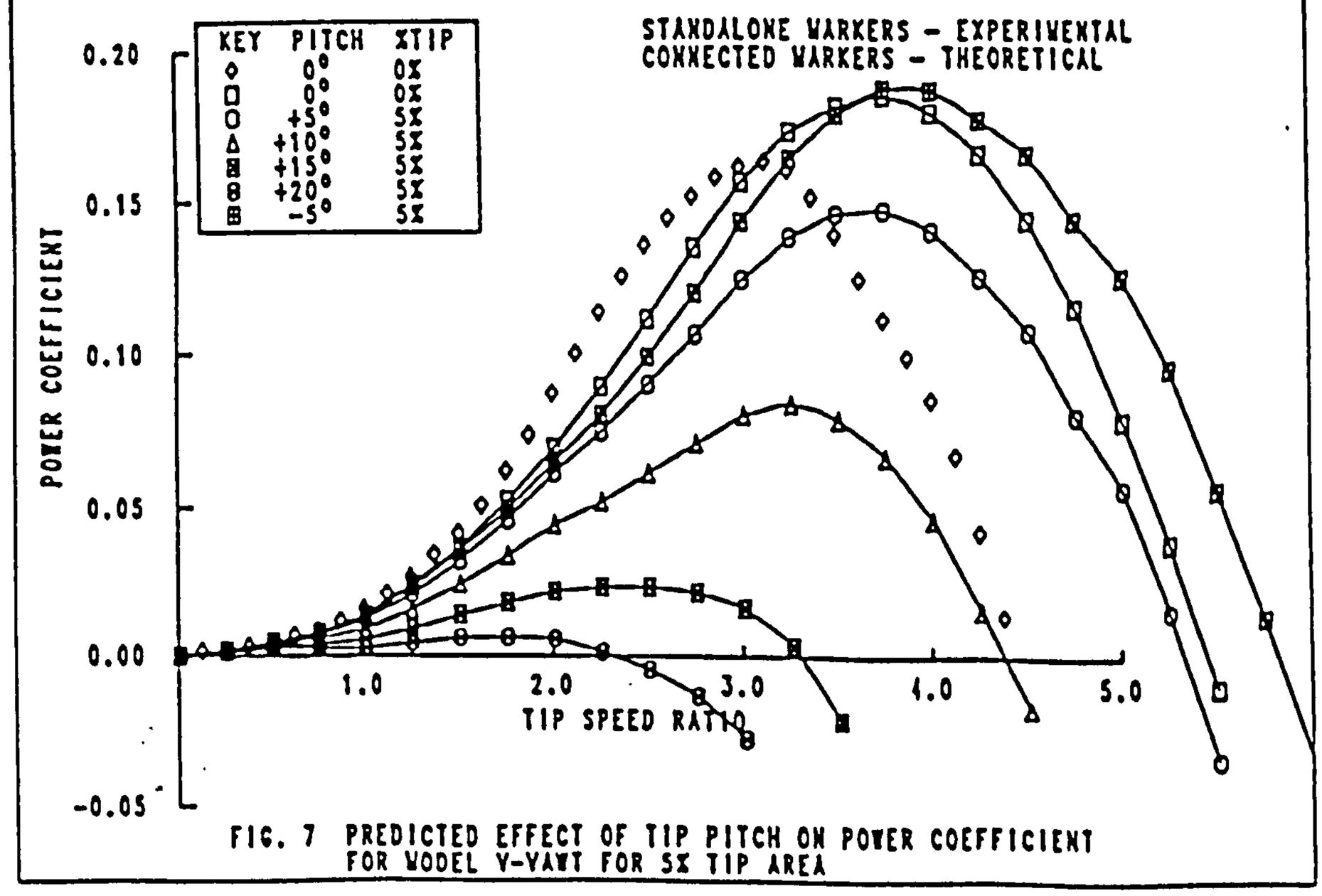

FIG. 7 PREDICTED EFFECT OF TIP PITCH ON POWER COEFFICIENT FOR MODEL V-VAWT FOR 5% TIP AREA

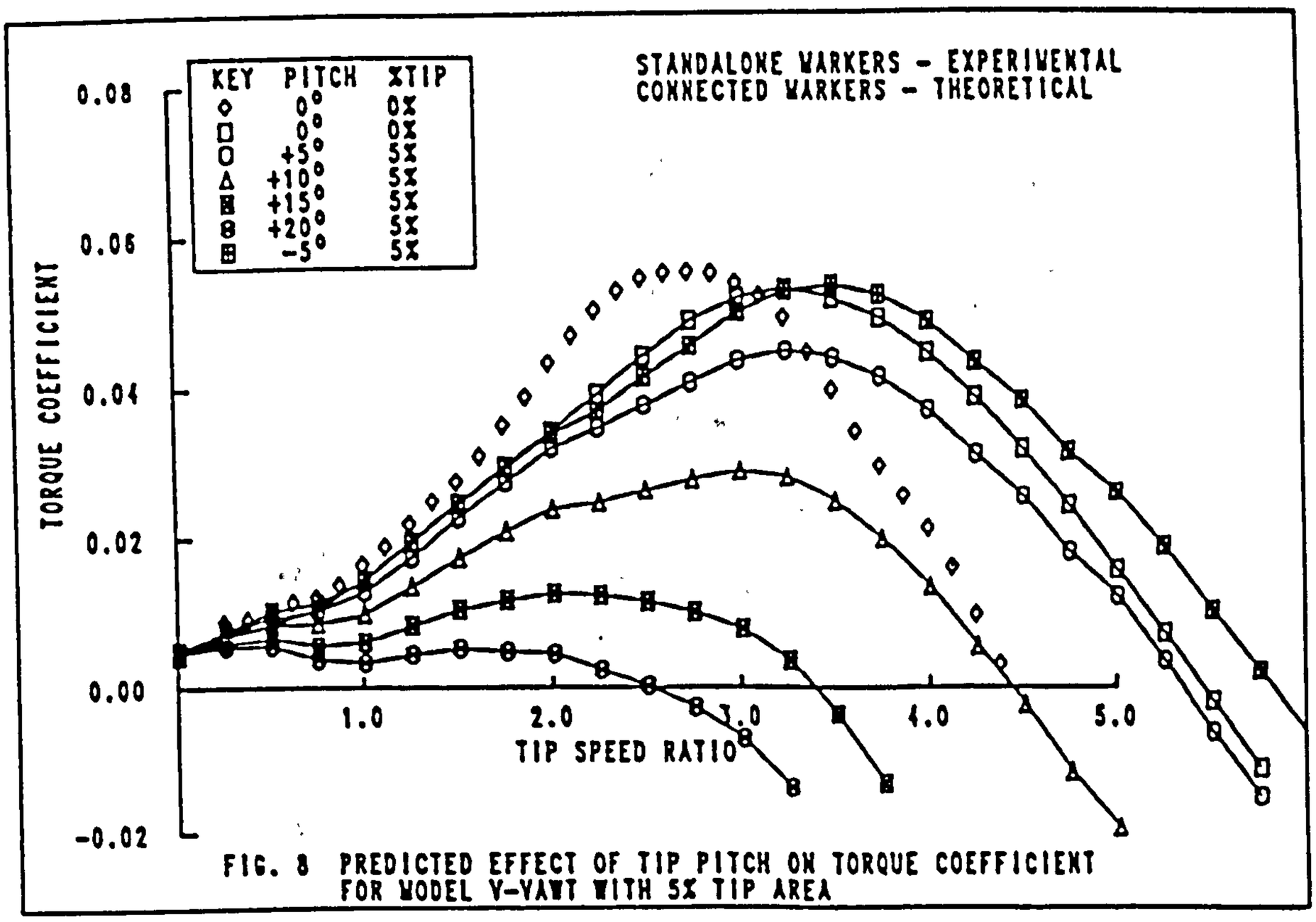

FIG. 8 PREDICTED EFFECT OF TIP PITCH ON TORQUE COEFFICIENT FOR MODEL V-VAWT WITH 5% TIP AREA

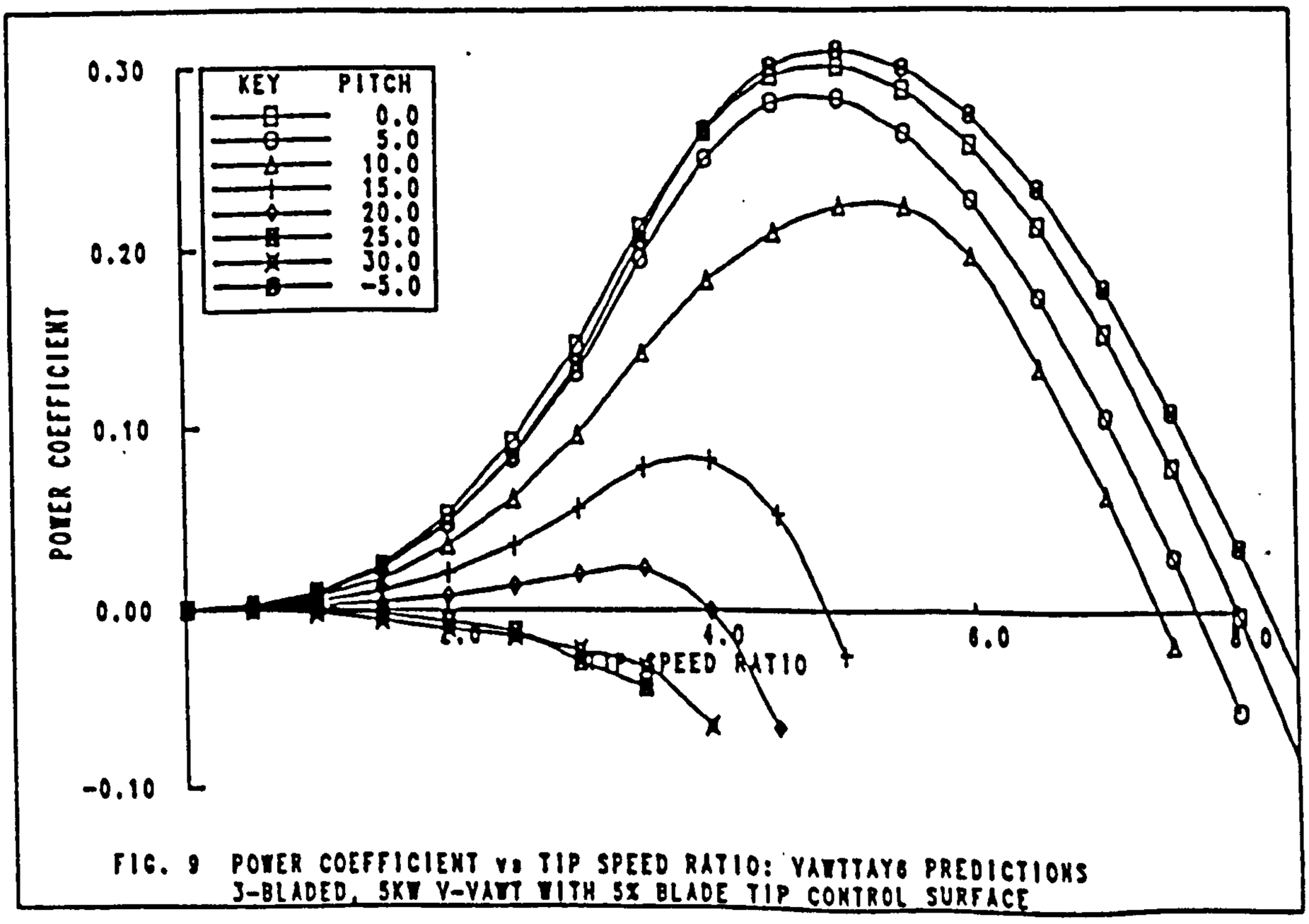

FIG. 9 POWER COEFFICIENT vs TIP SPEED RATIO: VAWTTAY6 PREDICTIONS 3-BLADED, 5KW V-VAWT WITH 5% BLADE TIP CONTROL SURFACE

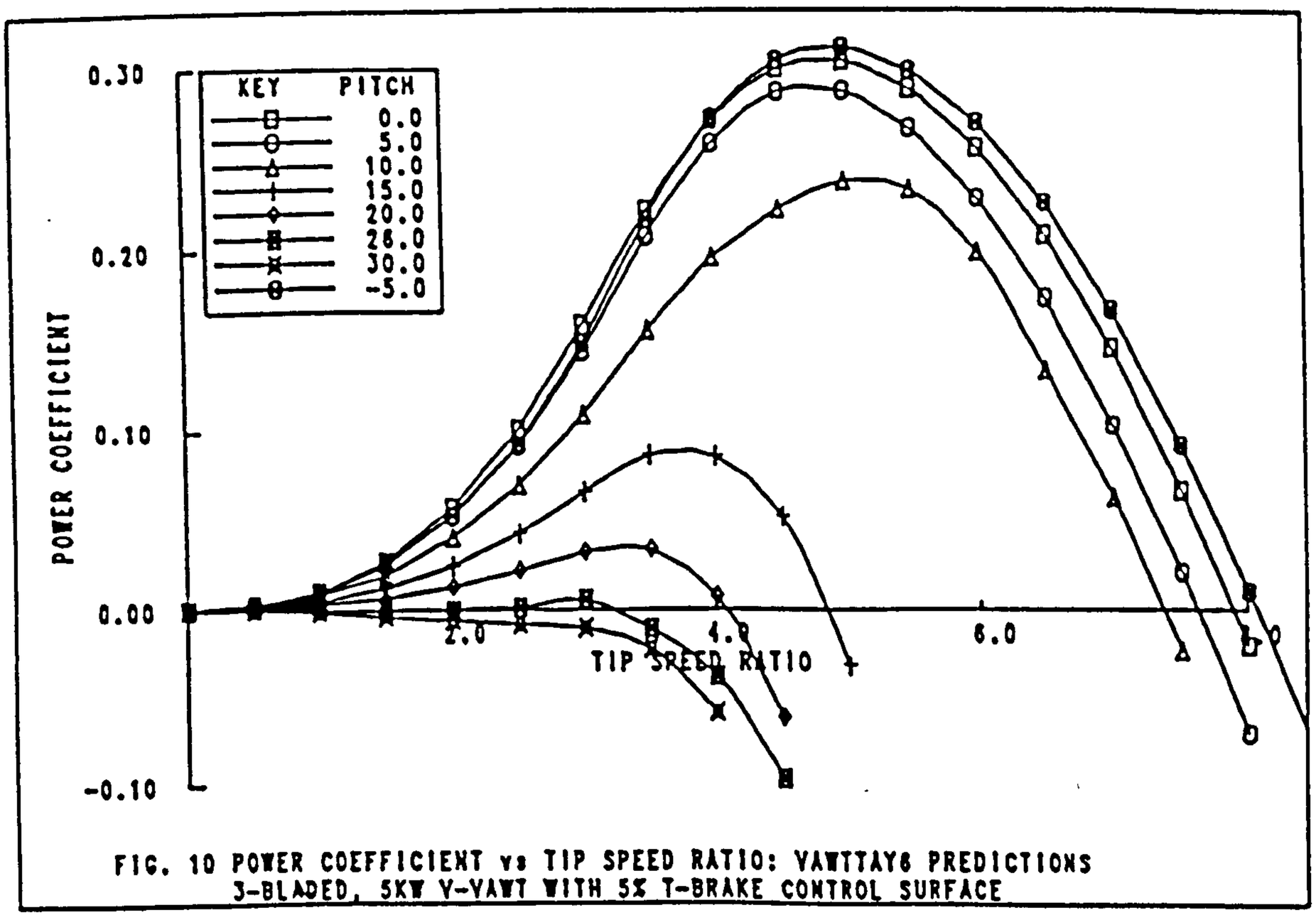

FIG. 10 POWER COEFFICIENT vs TIP SPEED RATIO: VAWTTAY6 PREDICTIONS
3-BLADED, 5KW V-VAWT WITH 5% T-BRAKE CONTROL SURFACE